Development and application of novel analytical methods for molecularly targeted cancer therapeutics

Sandra Roche

Ph.D. Thesis 2011

Development and application of novel analytical methods for molecularly targeted cancer therapeutics

A thesis submitted of the degree of Ph.D.

By

Sandra Roche B.Sc. (Hons)

The research work described in this thesis was carried out under the supervision of

Dr Robert O' Connor

and

Prof. Martin Clynes

National Institute for Cellular Biotechnology

Dublin City University

January 2011

I hereby certify that this material, which I now submit for assessment on the programme of study leading to the award of Ph.D is entirely my own work, that I have exercised reasonable care to ensure that the work is original, and does not to the best of my knowledge breach any law of copyright, and has not been taken from the work of others save and to the extent that such work has been cited and acknowledged within the text of my work.

Signed: _____

ID No.: 96539461

Date: _____

Acknowledgement

However, a very special thanks to Mark, for everything too vast to mention, for knowing the difference in when to drag me away and when to make me work, for essentially supporting me endlessly with patience, cups of tea and your own unique humour and perspective – Thank you.

Abbreviations

%	Percentage
5-Fu	5-Fluorouracil
ABC	ATP Binding Cassette
ADP	Adenosine Diphosphate
ADR	Adriamycin
ATCC	American Tissue Culture Collection
ATP	Adenosine Triphosphate
AUC	Area under the curve
BBB	Blood Brain Barrier
BCRP	Breast Cancer Resistance Protein
BSA	Bovine Serum Albumin
CB	Chloro-4-butane
DMEM	Dublecco's Minimum Essential Medium
DMSO	Dimethyl Sulfoxide
DNA	Deoxyribonucleic Acid
DOX	Doxorubicin (adriamycin)
EA	Ethyl Acetate
ECACC	European Collection of Animal Cell Culture
ED	Effective dose
EDTA	Ethylene Diamine Tetra-acetic Acid
EGF	Epidermal Growth Factor
EGFR	Epidermal Growth Factor Receptor
erbB2	HER2
FCS	Foetal Calf Serum
HBSS	Hanks Balanced Salt Solution
HCl	Hydrochloric Acid
HPLC	High Performance Liquid Chromatography
IC_{50}	Inhibitory Concentration at 50%
ICH	International Conference for Harmonisation
IS	Internal Standard
kDa	Kilo Daltons
LC	Liquid Chromatogram

LLE	Liquid-Liquid Extraction
MDR	Multi-Drug Resistance
min	Minutes
Mitox	Mitoxantrone
MRM	Multiple reaction monitoring
MRP	Multidrug Resistance-associated Protein
MS	Mass Spectrometry
MS/MS	Tandem mass spectrometry
MW	Molecular Weight
NaCl	Sodium Chloride
NaOH	Sodium Hydroxide
NSCLC	Non-Small Cell Lung Cancer
PBS	Phosphate Buffered Saline
P-gp	P-glycoprotein
PPT	Protein Precipitation
QQQ	Triple Quadrupole MS
R.S.D.	Relative Standard Deviation
RT	Room temperature
SD	Standard Deviation
SIM	Selected Ion monitoring
SPE	Solid Phase Extraction
t-BME	*tert* Butyl Methyl Ether
TDM	Therpuetic Drug Monitoring
TI	Theraputic Index
TIC	Total Ion Chromatogram
TKI	Tyrosine Kinase Inhibitor
TLDA	TaqMan Low Density Array
UHP	Ultra High Pure Water
v/v	volume/volume
VAD	Vincristine-Doxorubicin -Dexamethasone

Table of Contents

Abstract

Abstract

A detailed understanding of correlations of drug levels with drug action is an important aspect of the pre-clinical, clinical development and routine use of anti-cancer drugs.

In furtherance of this important aim, the research in this thesis sought to develop and apply novel, highly sensitive, analytical methods to examine and understand correlations of drug levels with drug resistance mechanisms, therapeutic efficacy and side effects.

LC-MS/MS is a state of the art analytical technique used to characterise and quantify both bio-molecules and pharmaceutical agents. Based on LC-MS/MS techniques, novel sensitive analytical methods were developed for the quantification of 1) tyrosine kinase inhibitor anti-cancer drugs to examine the interaction of these agents with drug resistance mechanisms, and 2) the multiple myeloma drug thalidomide as a pilot study to identify potential correlations between serum drug levels and toxicity/efficacy.

Acquired resistance to chemotherapeutics through the over-expression of ABC transport proteins has presented a significant clinical challenge. The up-regulation of ABC transporters such as P-glycoprotein (P-gp), Breast Cancer Resistant Protein (BCRP) and Multidrug Resistance-associated Protein (MRP-1) is an important cellular mechanism of resistance *in vivo* and *in vitro*. Using cell-line models and the developed LC-MS/MS quantification method it was established that dasatinib, an agent used in treatment of chronic myelogenous leukaemia, is a substrate of ABC transporters P-gp and BCRP but not of MRP-1, and that dasatinib does not inhibit these transporters at clinically relevant concentrations. Another Tyrosine Kinase Inhibitor (TKI) being used in breast cancer, Lapatinib, was shown to be an inhibitor of P-gp but not a substrate of this resistance mechanism. Levels of other TKIs were also found to vary in their uptake in primary models of brain cancer.

Using LC-MS/MS, the circulating serum levels of thalidomide in multiple myeloma patients were studied. A clear correlation between dosing regime and serum level was seen; however, the research also unearthed evidence of a significant incidence of non-compliance which could have far reaching consequences for patient treatment.

Overall, LC-MS/MS methods for the quantification of chemotherapeutic agents in complex biological matrices produced sensitive and accurate data which we successfully exploited to characterise resistance to new drugs and examine correlations between serum levels and treatment variables.

SECTION 1.0 Introduction

1. Introduction

Cancer as a disease affects millions of people through the world either directly or indirectly. Three main approaches are used to treat cancer; surgery, radiotherapy and chemotherapy. Different approaches or combinations of modes of treatment are indicated depending on the type of cancer, its location, degree of progression and/or level of invasion and metastasis.

In brief, surgery is used to excise tumours or the affected organ if the tumour is small and localised. Surgery is also used to determine the extent of the disease and whether it has metastasised to other locations. Radiation therapy or radio-therapy, administered internally or externally, works by destroying both cancerous and normal cells in a targeted area. Most normal cells can recover while the cancerous cells may be more sensitive and die. Chemotherapy is the administration of drugs to treat cancer. These can be classic chemotherapy drugs such as anthracyclines and taxanes, or targeted therapies, such as monoclonal antibodies and small molecule tyrosine kinase inhibitors. One of the challenges of cancer chemotherapy is resistance, be that acquired or inherent resistance. The goal of this research was to develop analytical methods that could be used to examine treatment efficacy and model processes important in resistance.

1.1. Treatment of cancer

The conventional chemotherapy drugs, used in the treatment of many forms of advanced cancer, attack proliferating healthy and cancerous cells leading to potentially serious side effects including myelosuppression, hair loss and gastrointestinal problems. The emerging goal of cancer pharmacology research is the development and optimal application of targeted therapies. Advances in molecular targeted therapies have yielded various anticancer agents[1]. These targeted therapies are specifically active in cancer cells, thereby giving increased activity while having reduced incidence and severity of toxicity and side effects. Optimal targets for such individualised treatment schemes are targets that are only present in the cancer cell and are involved in carcinogenesis and tumour survival. Characterised examples of targets of such include; the BCR-ABL protein which is considered causative in many cases of CML; the human epidermal growth factor receptor (EGFR) family, associated with tumourigenesis and disease progression; mammalian target of rapamycin (mTOR) which regulates protein synthesis; the Raf/MEK/ERK pathway is which is implicated in a variety of cellular

functions including proliferation, cell-cycle arrest, terminal differentiation and apoptosis; the ubiquitin proteasome pathway which plays a role in cell cycle control and tumour growth; the overexpression of cyclin-dependent kinases (cdk) or absence of cdk inhibitors which provides tumour cells with a selective growth advantage and vascular endothelial growth factor (VEGF) and its receptors (VEGFR) which are a target of antiangiogenic treatments[2]. Therapies which target such mechanisms include monoclonal antibodies such as Herceptin and cetuximab and tyrosine kinase inhibitors such as dasatinib, imatinib and lapatinib.

1.2. Resistance to treatments

Resistance to chemotherapeutic agents in cancer can be an acquired phenomenon or intrinsic to the patient. Inherent or intrinsic resistance simply means that the cells already possess mechanisms which make the drug ineffective, while acquired resistance occurs after exposure to treatment and the cells respond/develop/enhance specific characteristics to overcome the toxicity of the agent. Multi drug resistance is the development of resistance simultaneously to many structural and mechanically diverse antineoplastic agents. Overcoming multi drug resistance (MDR) is one of the greatest challenges of cancer care and cancer treatment[3].

A tumour is defined as clinically resistant to the maximum tolerated dose (MTD) of a chemotherapeutic agent if the dosage of the drug in the tumour does not achieve complete response (CR) or partial response (PR). This may be due to different physiological mechanisms, including[4]:

- inappropriate application of the drug, for example inadequate infusion
- low metabolic activation in the case of the use of a prodrug
- pharmacokinetic alterations in the plasma for example the metabolism, excretion or drug clearance rates of the drug may change
- tumour microenvironment; this would take into account the vasculature of a tumour and the delivery of the agent to the tumour
- tumour availability – i.e. the architecture of the barriers, for example the blood brain barrier

However, it is the cellular mechanisms of resistance that are more commonly focussed on in the laboratory and translational research setting.

The cellular mechanism of resistance can be attributed to many factors including:

- ATP-binding cassette (ABC) transporters
- modulations of the cell death pathways
- alterations in DNA repair pathways
- decreased DNA topoisomerase II activity

However, perhaps the most commonly studied mechanism of resistance is the active efflux of chemotherapeutic agents by ABC transporters. It is the ABC transporters, which will be examined in more detail, to expand on the breadth of information already gathered within this research group[5-8].

1.3. ABC transporters

The ATP-binding cassette (ABC) transporters are a large family of transmembrane pump proteins which are responsible for the classic MDR profile of resistance to many substrates. Using the energy of adenosine triphosphate (ATP) hydrolysis these proteins transport a variety of substrates across membranes, as well as being involved in various other biological processes. ATP hydrolysis involves the cleavage of the phosphoanhydridic bonds to yield high energy inorganic phosphate (Pi) and Adenosine diphosphate (ADP). The exact mechanism of this energy dependent transportation is not fully understood, as reviewed by Seeger and Van Veen[9] and Ambudkar et al[10].

This protein super-family is known to include 48 ABC proteins [11]. The family has been organised into seven groups with the nomenclature A-G.

All designated ABC transporters have a common structural element[12], principally an ATP-binding domain of 200-250 amino acids. This amino acid sequence is the nucleotide-binding domain (NBD). The NBD unit includes two short conserved peptide motifs known as Walker A and Walker B[13]. Glycine rich Walker A and hydrophobic Walker B are involved in ATP binding. A third conserved sequence called the ABC signature [14], located between Walker A and Walker B, is unique to the NBD unit.

ABC transporters are NBD containing proteins associated with hydrophobic, membrane embedded, transmembrane domain (TMD). The TMD usually comprises six transmembrane α helices and it is the TMD that is believed to convey substrate specificity for transportation. To be functionally/biologically active, ABC transporters

require a minimum of two TMDs and two NBDs. In "full transporters" the two TMD-NBD units are part of the same polypeptide chains where as "half transporters" comprise of only one TMD-NBD module. The activity of half transporters requires the aggregation of multi-protein complexes. Full transporters are usually in the plasma membrane and half transporters in the intracellular membrane with the Breast Cancer Resistant Protein (BCRP, ABCG2) being the exception[15]. Figure 1-1 outlines the structures of these three ABC transport proteins.

Figure 1-1: Schematic representation of MDR proteins[16].
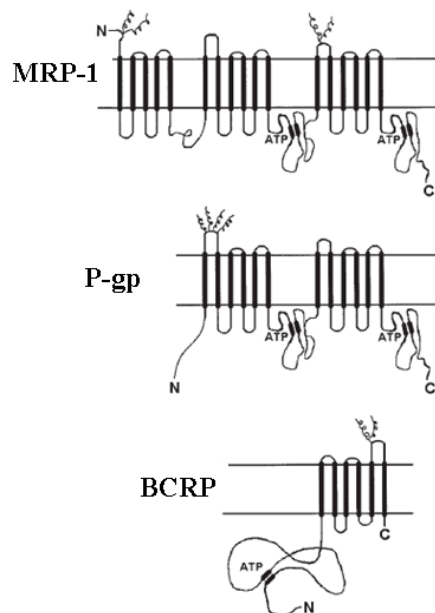
Illustration taken from Litman *et al[16].*

Models for the predicted structures of MRP-1, MDR1 and BCRP. The transmembrane helixes, the ATP-binding fold (filled bars) and glycosylation sites (ξ) are indicated. Note that the orientation of MXR is 'reverse' to that of P-gp and MRP-1. The latter proteins are oriented in the order TMD-NBD-TMD-NBD, whereas the orientation of MXR is NBD-TMB. It should be noted that these figures are highly schematic, and that the transmembrane segments probably form some kind of a pore in the membrane [17]

1.3.1. ABC transporter evolution

The expression and action of ABC transporters is not solely a response to cancer therapy. ABC transporters are more likely an evolutionary response to the need to remove toxins, both naturally occurring physiological toxins as well as xenotoxins from the body. However, as a large number of current/traditional chemotherapeutics are based on naturally occurring compounds[18], ABC transporters play a significant role in resistance to these therapies.

In the taxane family of compounds, paclitaxel (taxol) is isolated from the pacific yew tree (*Taxus brevifolia*), while docetaxel (taxotere) is a semi-synthetic product of the needle of the European yew tree (*Taxus baccata).*

Vinca alkaloids, used in the treatment of leukaemia, were the first plant based chemotherapeutic agent. These were isolated from the Madagascan periwinkle plant.

Anthracycline chemotherapy agents are also naturally derived products, though not plant based, with doxorubicin being isolated from the fermentation broth of *Streptomyces peucetius*. Epirubicin is a semi synthetic derivative of doxorubicin. It is largely unsurprising then that these naturally occurring compounds and their analogues suffer reduced efficacy due to transport by ABC proteins.

Table 1-1, adapted from Lage *et al.*[4]*,* lists the ABC transporters known to be involved in multi drug resistance, including some of their chemotherapeutic substrates as well as their physiological substrates. The classical MDR spectrum of drugs referred to in Table 1-1 is expanded upon in Table 1-2.

Table 1-1: ABC-Transporters associated with drug resistance[4]

ABC Transporter HUGO[1] Name	Common Name	Drugs	Physiological Substrates	Ref
ABCA2	ABC2	Estramustine, mitoxantrone	Steroids	[19-22]
ABCA3	ABC3	Doxorubicin	Surfactant productions	[23]
ABCB1	MDR-1, P-gp, P-170, PGY1	"Classical" MDR spectrum[2]	Phospholipids, neutral & cationic organic compounds	[24-28]
ABCB2	TAP1	Mitoxantrone,	Peptides	[24, 29, 30]
ABCB3	TAP2	Mitoxantrone,	Peptides	[24, 29, 30]
ABCB4	MDR3-P-gp, MDR3, PGY3	Paclitaxel, vinca alkaloids	Phosphatidylcholine	[31, 32]
ABCB5		Doxorubicin, camptothecin, 5-fluorouracil	Pigment transport?	[33-35]
ABCB6	MTABC3	Cisplatin, camptothecin	Mitochondrial porphyrin uptake	[36, 37]
ABCB11	BSEP, SPGP, ABC16, PGY4	Paclitaxel	Bile salts	[25, 38, 39]
ABCC1	MRP, MRP-1	Anthracyclines, vinca alkaloids, methotrexate	Glutathione-, and other conjugates organic anions, leukotriene	[40-42]
ABCC2	MRP2, cMOAT[3]	Platin-drugs, Anthracyclines, vinca alkaloids, camptothecins, methotrexate	Glutathione-, and other conjugates organic anions, leukotriene C_4	[41, 43-46]
ABCC3	MRP3, MOAT-D, MLP2	vinca alkaloids, methotrexate, cisplatin	Glucuronides, bile salts, peptides	[47-50]
ABCC4	MRP4, MOAT-B	Nucleotide analogues, methotrexate,	Organic anions	[47, 51-53]
ABCC5	MRP5, MOAT-C	Nucleotide analogues	Organic anions, cyclic nucleotides	[47, 54, 55]
ABCC6	MRP6	Anthracyclines, cisplatin	Glutathione conjugates	[25, 56]
ABCC10	MRP7	Taxanes, vinca alkaloids	Organic anions, cyclic nucleotides, bile salts, leukotriene C_4	[57, 58]
ABCC11	MRP8	5-Fluorouracil	Organic anions, cyclic nucleotides, leukotriene C_4	[57, 59]
ABCG2	BCRP, MXR, ABCP	Mitoxantrone, anthracyclines, camptothecins, topotecan	Prazosin	[60-64]

Table 1-1: list of ABC transporters associated with drug resistance and their substrates, physiologically and chemotherapeutic[24]. Yellow denotes transporters of further interest.

---

[1] Human Genome Organisation
[2] See Table 1-2
[3] Canalicular multispecfic organic anion transporter

1.3.2. P-glycoprotein

The mechanism of multi-drug resistance was originally described in the 1970s when cells selected with just one agent, showed resistance to the cytotoxic effects of multiple unrelated agents. The cells were treated with actinomycin D and showed resistance to mithramycin, vinblastine, vincristine, puromycin, daunomycin, demecolcine and mitomycin C[65]. The protein responsible was identified as P-glycoprotein or P-gp, a 170kDa plasma membrane glycoprotein[66]. In addition to the cross-resistance of agents, a decreased intracellular concentration of the target drugs was also noted[65]. This was attributed to the active efflux of the agent from the cells[67-69]. Gottesman *et al.*[70], showed that P-gp is an ATP-dependent drug pump involved in the transport of a broad range of structurally unrelated compounds. Bellamy[71] identified that P-gp also confers taxane resistance and can cause intracellular redistribution of the drug.

The precise molecular mechanism of drug transport by P-gp is not entirely understood. However, it is known that P-gp possesses a central pore which appears conical in resting phase with the apex of the cone, at the cytoplasmic end, appearing practically closed. The P-gp substrate binding site is located within the pore. Using QSAR (quantitative structure-activity relationship) studies, Garrigues *et al.*[72], identified two pharmacophores (distinct P-gp regions that bind certain types of substrates). However, more recently, Pleban *et al.*[73], identified the drug binding pocket at the interface of TMD1 and TMD2. Interaction with the binding site in the presence of ATP induces ATP hydrolysis. This hydrolysis is essential for drug transport[10]. It appears as though ATP binding and substrate binding causes the closure of the drug binding pocket while ATP hydrolysis causes the TM rearrangement. Results from Omote & Al Shawi[74] suggest that the substrate is actively transported out of the lipid bi-layer whereas, alternative researchers propose that P-gp acts as an outwardly directional flippase[75, 76]. Ultimately the substrate is either pushed or flipped out. Figure 1-2 shows a schematic depiction of the structure of P-pg.

Figure 1-2: Schematic models of P-gp

Illustration and figure legend taken from Loo & Clarke[77].
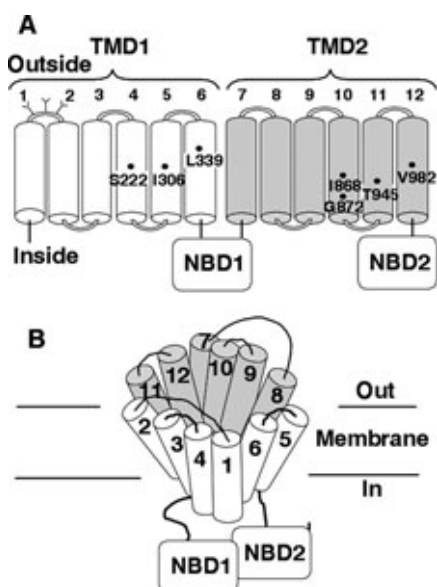
A): White cylinders represent the TM segment in TMD1, while the grey cylinders represent TM segments with TMD2. The branched lines represent the glycosylation sites and the rounded rectangles represent the NBDs. The residues shown in the TM segments are predicted to be part of the drug binding pocket because cysteines introduced at these positions in TMD1 can be cross-linked to cysteines introduced at the indicated positions in TMD2 with MXM cross-linkers that are substrates of P-gp[78].

B): Model of the organisation of the TM segments base on cross-linking and cysteine-scanning mutagenesis studies. The common drug binding pocket is at the interface between the TMDs.

1.3.3. MRP-1

The *ABCC1* gene encodes for the ABCC1 transporter protein which was the 2nd ABC cancer resistance transporter to be discovered. This gene was identified in 1992 by Cole *et al.*[40], in small cell lung carcinoma cell line NCI-H69. MRP-1 or ABCC1, is considered the founding member of the C subfamily of ABC transporters. The ABCC family of proteins have 12 members labelled ABCC1 to ABCC12. Members MRP-1 to MRP8 (ABCC1-ABCC6, ABCC10 and ABCC11) have been shown to be able to transport anticancer agents. MRP-1 has a broad range of substrates, including therapeutic agents such as anthracyclines, vinca-alkaloids and methotrexate a substrate profile similar to P-gp. However, MRP-1 also transports glucuronate, sulphate and glutathione conjugates [79, 80].

MRP-1 overexpression is found in various cancers including breast[81], ovarian[82], renal cell carcinoma[83] and melanoma[84]. However, studies carried out have both confirmed and rejected a correlation between clinical outcome and MRP-1 expression, suggesting that the clinical role of MRP-1 in relation to multi-drug resistance may benefit from further investigation [4].

Structurally MRP-1 is similar to P-gp with the $[TMD-NBD]_2$ core, however, MRP-1 has an additional N-terminal transmembrane domain (TMD0) which is linked to the core region by an intracellular linker region (L0), see Figure 1-3.

Figure 1-3: Schematic of MRP-1[85]
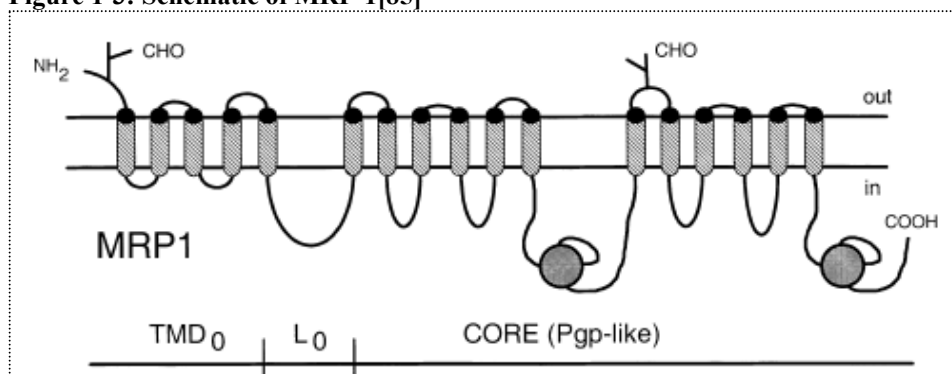
Illustration from Borst et al., showing schematic model of MRP1 indicating the transmembrane segments adenosine triphosphate binding sequences, and the location of carbohydrate (CHO) chains.

1.3.4. BCRP

The third most investigated member of the ABC transport family is Breast Cancer Resistant Protein (BCRP), also called ABCG2, MXR (mitoxantrone resistance protein) or ABCP (placental ABC protein). The BCRP protein is a half transporter identified simultaneously by three separate studies[60-62].

This 72kDa protein, arranged in the format of [NBD-TMD] with ABC domains located towards the N terminus of the polypeptide chain, has been thought to function as a homodimer though recent studies have suggested a tetramer bridge[86]. It is interesting that the conserved ABC domain is in a reverse arrangement in BCRP as compared to ABCB or ABCC groups and the membrane insertion pattern and topology indicates 6 transmembrane helices[87].

The expression of BCRP in various normal tissues (including the placenta, colon, large and small intestine, sebaceous glands, islets and acinar cells of the pancreas) suggests a physiologically protective role. Jonker *et al*.[88, 89], have suggested that the protein may be responsible for either the transport of compounds in the foetal blood supply or the removal of toxic metabolites.

However, BCRP has been detected in various *in vitro* cancer models, particularly following exposure to mitoxantrone. While the P-gp substrates vinblastine, paclitaxel and verapamil are not substrates of BCRP, BCRP does transport a variety of dyes (e.g. Hoechst 33462), chemotherapeutics such as flavopiridol topotecan, irinotecan and its active metabolite SN-38 as well tyrosine kinase inhibitors erlotinib, imatinib and gefitinib[90]. The BCRP variants R482T and R482G have been found to be expressed in drug selected cell-lines MCF7/AdVp3000 and S1-M1-80[91]. These functional variants are associated with an amino acid substitution. In the wild type BCRP position 482 is the amino acid arginine (R), whereas in variant R482T position 482 is occupied by threonine (T) and in the variant R482G position 482 is occupied by the amino acid glycine (G). This results in a loss of methotrexate transport activity but increased methotrexate resistance[92]. Figure 1-3 illustrates the substrate specificity of BCRP and the R482G variant[93].

Figure 1-4: Differences in substrate of BCRP and R482G Variant[93]

Wild-type BCRP   *R482G variant*

Methotrexate

Hoechst, Flavopiridol, Phenophorbide, Mitoxantrone, Topotecan, TKIs,

Doxorubicin, Daunorubicin, Epirubicin, Rhodamine 123

Illustration adapted from Sarkadi *et al.,* 2004[93]
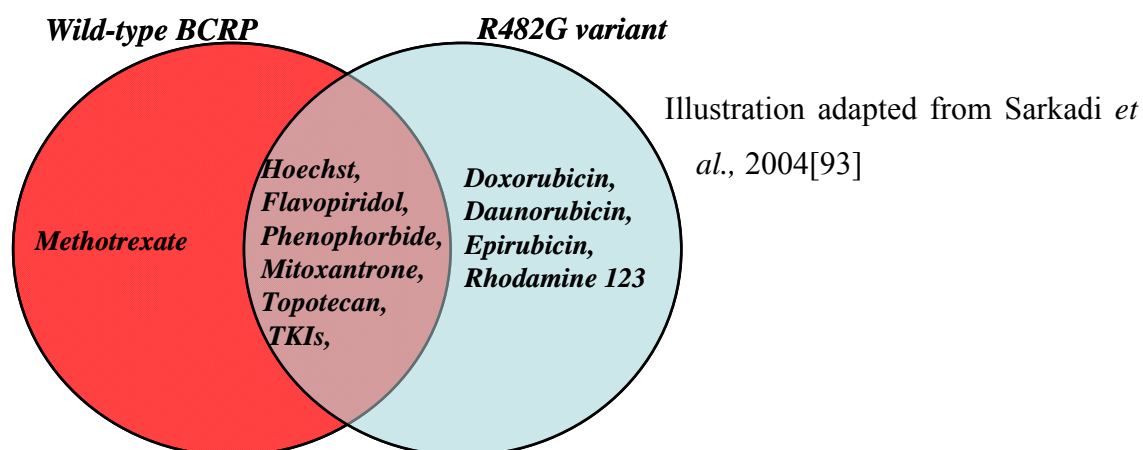
Table 1-2: A summary table of the substrates of P-gp, BCPR and MRP-1[4, 94]

P-gp Substrates	BCRP Substrates	MRP-1 Substrates
Anticancer		
Anthracyclines – doxorubicin, daunorubicin	Anthracyclines – doxorubicin, daunorubicin (R482T)	Anthracyclines – doxorubicin, daunorubicin
Epipodophyllotoxins- etoposide, teniposide	Epipodophyllotoxins- etoposide, teniposide	Epipodophyllotoxins- etoposide, teniposide
Vinca Alkaloids – vinblastine, vincristine		Vinca Alkaloids – vinblastine, vincristine
Taxanes – paclitaxel, docetaxel		Taxanes – paclitaxel, docetaxel
Campothecans - Topotecan	Campothecans - topotecan, irinotecan	Campothecans - topotecan, irinotecan
	Methotrexate	Methotrexate
Anathracenes – bisantrene	Bisantrene (R482T form)	
	Mitoxantrone	
Fluorescent Compounds		
Hoescht 33342	Hoescht 33342	Calcein
Calcein-AM	BODIPY-prazosin	Fluor-3
Rhodamine 123	Rhodamine 123 (R482T/G)	BCECF

Selected substrates of P-gp, BCRP and MRP-1

1.4. MDR Inhibitors

Given that multi drug resistance is mediated through the over-expression of cell efflux proteins and has such an impact on treatment and the efficacy of therapy, it is hardly surprising that inhibiting or reversing this activity to restore sensitivity is of key importance. Some work has been carried out at a transcriptional level to control the activity of ABC transporter but with limited success[95]. The majority of research in this area involves the use of small molecule agents to inhibit the function of the MDR protein, see Table 1-3.

With the focus primarily on the inhibition of P-gp, the first inhibitor was discovered in the 1980's. The calcium channel blocker, verapamil, restored vincristine sensitivity to resistant leukaemia cells[96]. Cyclosporin A (CsA) was also shown to restore sensitivity of vincristine and daunorubicin in leukaemia cells and as well as showing efficacy in solid tumours[97]. However, clinical trials of combination of these agents with chemotherapy drugs proved unsuccessful[98]. For verapamil the tolerable drug levels were less than those which inhibited vinblastine *in vitro*[99]. CsA when administered with doxorubicin did increase the area under the curve (AUC) of doxorubicin by 55% and was shown to inhibit the clearance of doxorubicin and its metabolite (doxorubicinol)[100]. However, such doses of CsA had high levels of serious side effects.

Second generation inhibitors of P-gp include SDZ PSC833 (Valspodar) and S9788. SDZ PSC833 is a derivative of CsA, and S9788, a triazine, was based on the chemical structure of verapamil[101, 102]. However, combinations of these with P-pg substrates also failed to improve treatment.

GF120918 (Elacridar), OC144-093 (Ontogen), XR9576 (Tariquidar) and LY335979 (Zosuquidar) are 3rd generation P-gp inhibitors. These agents are more selective than the second generation molecules and effective at nanomolar concentrations. Elacridar and tariquidar also inhibits BCRP. Phase I/II trials of these inhibitors are underway in combination with a range of chemotherapeutics[103-106]. Investigation into the inhibition of P-gp is not limited to these molecules. In a comprehensive review, Baumert & Hilgeroth[107] describes, in detail, the variety of compound classes that

effect the action of P-gp. These include isoquinoline and quinoline derivatives, quinazolin and indole derivative (such as gefitinib, lapatinib and erlotinib), pyridine derivative (nifedipine), oxygen heterocycles (such a coumarin compound furanocoumarin cnidian), cannaboids, terpenes (such as non-cytotoxic taxane derivatives) and others.

Less information is reported on specific MRP-1 inhibitors. Gekeler *et al.,* reported MK-571 to inhibit MRP-1 without any effects on P-gp[108]. Sulindac sulphide, the active metabolite of Non-Steroidal Anti-Inflammatory Drug (NSAID) sulindac has been shown to inhibit MRP-1 efflux[109].

A fungal toxin Fumitremorgin C (FTC), was shown to inhibit ABCG2-mediated transport[110]. Ko143 is a more potent, specific and less toxic an analogue of FTC[111].

However, despite the array of compounds and other methods (antibodies, siRNA, plasma membrane alterations) of ABC inhibition available, the modulation of ABC proteins is not simple. Translation of effective combination *in vitro* to *in vivo* is complicated by non uniform MDR expression levels in patients but more critically by the unpredictable drug interactions. Also, it is important to bear in mind that MDR proteins are expressed naturally in the body and not only in the tumour cells. Table 1-3 outlines some the classic MDR inhibitors.

Table 1-3: Classic MDR Inhibitors[94, 109, 110]

P-gp	MRP-1	BCRP
First Generation	VX-710 (biricodar)	GF120918 (elacridar)
Verapamil	Sulindac Sulphide	Ko143
Cyclosporin A		Pantoprazole
Tamoxifen		XR9576 (tariquidar)
Second Generation		VX-710 (biricodar)
PSC833 (valspodar)		Fumitremorgin C (FTC)
VX-710 (biricodar)		
Third Generation		
LY335979 (zosuquidar)		
XR9576 (tariquidar)		
GF120918 (elacridar)		
OC144-093 (ontogen)		

1.5. Tyrosine kinase inhibitors

Tyrosine kinases are enzymes that catalyze the transfer of the γ phosphate of ATP to the tyrosine hydroxyl groups on target proteins [112]. Strict control of the tyrosine kinase activity in the cell regulates important processes such as cell cycle, proliferation and cell death. In many cases, the abnormal proliferation characteristics of cancer are driven by growth factor receptor-mediated signalling. In tumour cells, it is often the failure of the control mechanism that leads to excessive phosphorylation, and pathways sustained in an activated state [113, 114]. The characterisation of the role of these enzymes has led to the development of pharmaceutical inhibitors of such kinases. Such inhibitors are now emerging with some success from oncology clinical trials into mainstream cancer treatment [115, 116]. Table 1-4 details some of the current tyrosine kinase inhibitors approved for use in patients. These small molecule inhibitors compete with ATP binding at the tyrosine kinase domain. This negates the catalytic activity of the receptor[117].

The focus of this thesis is the tyrosine kinase inhibitors lapatinib and dasatinib. Dasatinib is administered in response to imatinib-intolerance and imatinib resistance in patients. These TKIs will be expanded upon in greater detail.

Table 1-4: Overview of Approved Tyrosine Kinase Inhibitors[118, 119]

Name	Trade Name	Research Name	Target	Approval Date
Imatinib	Gleevec[4] / Glivec[5]	STI571	Bcr-Abl, PDGFRα, - β, c-KIT	2001
Gefitinib	Iressa	ZD1839	EGFR	2003
Erlotinib	Tarceva	OSI774	EGFR	2004
Sorafenib	Nexavar	BAY 43-9006	C-RAF, B-RAF, c-KIT, FLT3, VEGFR2, -3, PDGFR-β	2005
Dasatinib	Sprycel	BMS354825	Bcr-Abl, SRC-family kinases, PDGRFβ, c-KIT, ephrin (EPH) receptor kinases	2006
Sunitinib	Sutent	SU11248	PDGFRα, - β, VEGFR1, -2, -3, c-KIT, RET, CSF-1R, FLT3	2006
Lapatinib	Tykerb	GW572016	EGFR(HER-1), HER-2	2007
Nilotinib	Tasigna	AMN107	Bcr-Abl, c-KIT, PDGFRα, - β,	2007
Pazopanib	Votrient	GW786034	VEGFR-1, VEGFR-2, VEGFR-3, PDGFR-a/β, and c-kit	2009

[4] USA
[5] Europe/ Australia

1.5.1. Imatinib

Imatinib (*STI-571,* Gleevec (US) Glivec (Europe)) was the first commercially available small molecule tyrosine kinase inhibitor, rationally designed against the *BCR-ABL* oncogene. The *BCR-ABL* gene encodes for the 210kDa Bcr-Abl protein which is involved in the main signal transduction pathways including Raf/Ras, MAPK, P13-K, Src kinase family. Imatinib was approved for the treatment of chronic myeloid leukaemia (CML) in 2001[120] and at the time was the first treatment of its type. Bcr-Abl made an excellent target as it is present in 95% of CML patients and the Bcr-Abl tyrosine kinase is, by itself, sufficient for the development of leukaemia[121]. Imatinib also inhibits the tyrosine kinase activity of the c-kit receptor in c-kit positive gastrointestinal stromal tumours (GIST)[122]. The main mechanisms of imatinib resistance include alterations of Bcr-Abl, c-kit mutations, P-glycoprotein up-regulation and alpha acid glycoprotein binding.

Resistance to imatinib has been seen to have been attributed to mutations at 17 amino acid positions within the Bcr-Abl kinase domain[115, 123]. Imatinib resistance *in vivo* and in patients has also been identified as being due to both Bcr-Abl under-expression[124] and Bcr-Abl over-expression and gene amplification[125, 126].

Mahon *et al.*[127], showed that cells cross resistant to imatinib, from treatment with doxorubicin, could have imatinib sensitivity restored in the presence of a P-gp inhibiting compound. Additional studies have confirmed that imatinib is a substrate for P-gp[128] and BCRP[129]. However, Gardner *et al.*[130], suggest that, though P-gp and BCRP affects the distribution and excretion of imatinib, inhibition does not improve clinical outcome.

The resistance mechanism associated with alpha1 acid glycoprotein (AGP) is attributed to AGP binding to imatinib and blocking imatinib inhibition of Bcr-Abl[131]. The role of AGP has been investigated in Ph+ cells and K562 leukaemia cell-line and shown that a combination of AGP and imatinib does not influence the growth[132]. A study by le Coutre *et al.*[133], showed that elevated levels of AGP in patients corresponded with slower response rates to imatinib treatment, though no correlation was shown between resistance and AGP levels.

1.5.2. Dasatinib

Dasatinib (BMS-354825, Sprycel™), is a thiazole-based ATP-competitive, dual Src/Abl kinase inhibitor[134], approved for the treatment of imatinib resistant and imatinib-intolerant patients across all phases of chronic myelogenous leukaemia (CML)[135]. Dasatinib is effective in treating imatinib-resistant CML as dasatinib is insensitive to the activation state of Bcr-Abl. Imatinib is effective in sustaining the Bcr-Abl protein in its inactive conformation, however, mutations at 17 amino acid positions render imatinib ineffective by "locking" Bcr-Abl in its active conformation. Dasatinib is less selective in its binding requirements and binds to the active form of the Abl kinase thus overcoming 14 imatinib resistant mutations[136].

Dasatinib also targets the Src kinase pathway. Dasatinib inhibits the action of Src family kinases (SFKs) Lyn and Src at nanomolar concentrations in prostate cancer as well as inhibiting FAK and CAS kinases[137]. The Src-family kinases are non-receptor signalling tyrosine kinases that are involved in cell differentiation, proliferation and survival, see Figure 1-5. Originally identified as the viral (v-Src) cancer causing protein in Rous sarcoma virus, a chicken tumour, discovered in 1911[138], there has since been 11 members of the Src family kinases identified in humans[139]. As a proto-oncogene, it is the disruption or alteration in the levels of Src activity which modulates signal transduction through several oncogenic pathways. Elevated levels of Src activity has been identified in colon cancer and breast and other epithelial cancers including pancreatic, ovarian, lung and head and neck cancers, as reviewed by Frame[140].

Figure 1-5: Src mediated pathways in tumour progression[141]
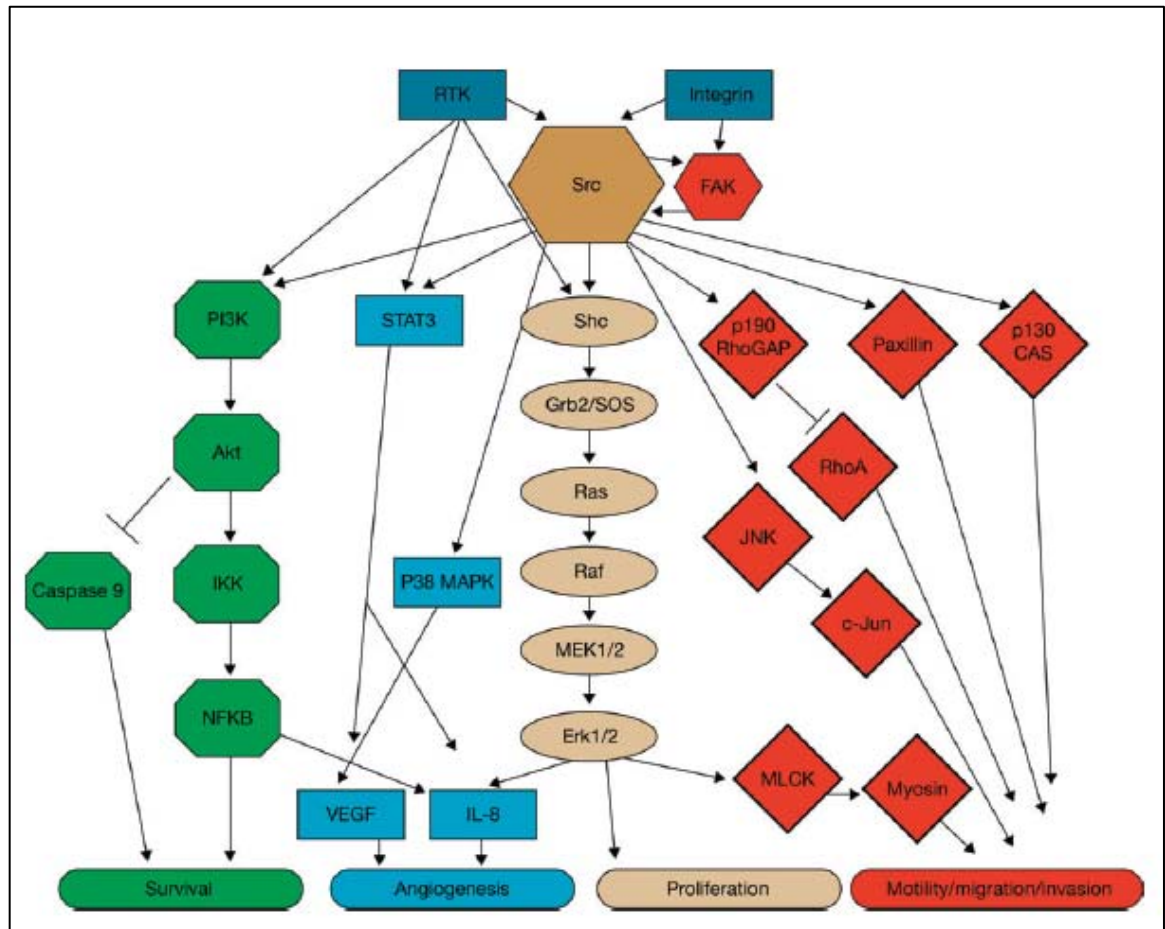
Illustration taken from Fizazi[141], based on work by Summy & Gallick[142].

Figure 1-5 shows Src-mediated pathways that may contribute to tumour progression. Abbreviations used: CAS, Crk-associated substrate; ERK, extracellular signal-regulated kinase; FAK, focal adhesion kinase; IKK, IkB kinase; IL-8, interleukin 8; JNK, Jun N-terminal kinase; MAPK, mitogen-activated protein kinase; MEK, mitogen-activated protein kinase MAPK/ERK kinase; MLCK, myosin light chain kinase; NFKB, nuclear factor kB; PI3K, phosphatidylinositol 3-kinase; RhoGAP Rho GTPase-activating protein; RTK, receptor tyrosine kinase; SOS, son of sevenless; STAT3, signal transducer and activator of transcription 3; VEGF, vascular endothelial growth factor.

1.5.3. Lapatinib

Lapatinib (GW572016, Tykerb™), a 4-anilinoquinazoline compound, is a small molecule dual inhibitor of the tyrosine kinase functionality of the epidermal growth factor receptor (EGFR or ErbB1) and HER-2/*neu* (erbB2) receptors of the epidermal growth factor (EGF) family[143] approved for use in breast cancer treatment[144].

There are four Erb proteins, ErbB-1 also called EGFR (epidermal growth factor receptor) or HER1 (human epidermal receptor), ErbB-2, also called HER2, ErbB-3, also called HER3 and ErbB-4, also called HER4. All four have a typical extracellular ligand binding region, a membrane spanning region and a cytoplasmic region containing the tyrosine kinase domain[145]. Typically the binding of the ligand causes the phosphorylation of the tyrosine kinase in the tail region, which then initiates downstream signalling. Ligand binding stimulates dimerisation of the receptors, which can form homo or hetero-dimers. HER2 has no known ligand and preferentially combines with HER3 or HER4 forming a heterodimer[146].

HER2 and EGFR has been the focus of targeted treatments in the form of both small molecules and antibodies. These two members of the ErbB family have been focussed on for a number of reasons including being commonly over-expressed in several common cancer types. Also, erbB3 has an inactive kinase domain and needs to dimerise with HER2 to promote downstream signalling. There is no clear link between erbB4 and cancer progression. However, signalling of the erbB family in cancer cells has been linked to proliferation, adhesion, migration and decreased apoptosis[147], as illustrated in Figure 1-5. Overexpression of erbB1 and erbB2 correlates with poor clinical outcome in breast[148], lung, pancreatic, head and neck, prostate and renal cancers, as summarized by Carter *et al*.[149]. Lapatinib reversibly inhibits erbB1 and Her2 by binding to the kinase domain thus inhibiting substrate phosphorylation. This prevents downstream signalling pathways, preventing proliferation and survival mechanisms[150, 151].

Figure 1-6: Ligand binding on erbB receptors and the downstream signalling[149]
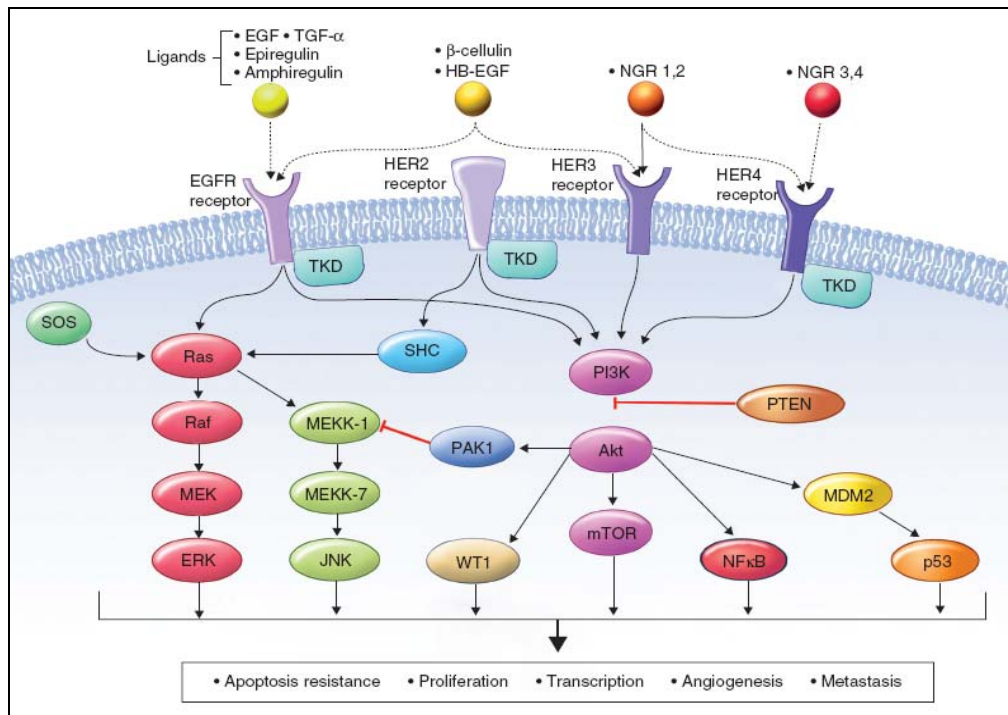
The signalling pathway for erbB receptors

Abbreviations used:; ERK, extracellular signal-regulated kinase; MEK, mitogen-activated protein kinase; PI3K, phosphatidylinositol 3-kinase; TKD, tyrosine kinase domain NGR, neuregulin, JNK, Jun N-terminal kinase; mTOR, mammalian target of rapamycin; PTEN, phosphatase and tensin homolog;

1.5.4. Erlotinib

Erlotinib (Tarceva^{TM}, OSI-774), a quinazolinamine derivative is an EGFR targeting small molecule anti-cancer drug, approved for the treatment of non small cell lung cancer (NCSLC) and in combination with gemcitabine for the treatment of pancreatic cancer. Erlotinib was initially approved, in 2004, for the treatment of locally advanced or metastatic NSCLC after failures of other regimes and in 2005, approval was given for the treatment of pancreatic cancer in combination with gemcitabine in patients with locally advanced, unresectable or metastatic pancreatic carcinoma[120]. Erlotinib is a selective and reversible inhibitor of EGFR.

The primary causation of resistance to erlotinib is the mutation of the EGFR target, specifically a secondary mutation of the target called T790M.[152]

1.5.5. Gefitinib

Gefitinib (Iressa^{TM}) is also a small molecule reversible EGFR inhibitor. Similar in structure to erlotinib, gefitinib is also a quinazolinamine derivative. Gefitinib was approved by the FDA in 2003 for the treatment of patients with NSCLC who had failed a platinium based and docetaxel based treatment [120]. Gefitinib was re-examined following the results of a large study (ISEL) of which showed that there was no survival benefit in a randomised trial of gefitinib vs a placebo[153]. Though the results of the trial were negative, analyses showed improvement in the gefitinib arm of the study in patients who had never smoked and in patients of Asian origins[154]. Evidence suggests that gefitinib may have a role in the treatment of patients with specific EGFR mutations[155]. Lynch *et al.,* identified somatic mutations in 8 out 9 lung cancer responders to gefitinib based therapy[156].

Gefitinib is also susceptible to T790M mutation of the EGFR target as a mechanism of acquired resistance[157]. Further information of the mechanism of resistance of erlotinib and gefitinib are detailed in Bianco *et al.[158]*

1.5.6. Sorafenib

Sorafenib (BAY 43-9006, Nexavar) is a dual Raf kinase/VEGFR inhibitor that effects tumour cell proliferation and angiogenesis. Sorafenib has shown increased activity in

five tumour types – renal, colon, pancreatic, lung and ovarian[159] and was approved for the treatment of advanced renal cell carcinoma in 2005 and the treatment of inoperable hepatocellular carcinoma in 2007[120].

1.6. Interaction of TKIs and ABC transporters

Though targeted therapies such as tyrosine kinase inhibitors were heralded as the magic bullet to cancer, they are not without their limitations. Acquired resistance to lapatinib as a monotherapy or in combination with chemotherapy usually occurs within 12 months[160]. Acquired resistance to imatinib is seen in 45% of cases of CML, according to a study of the usage of imatinib in the clinic[161]. Acquired resistance to tyrosine kinases inhibitors can be through mutations in the targets or changes in signalling pathways. However, ABC transporters have been shown to have an important relationship with tyrosine kinase inhibitors[87]. Table 1-5 summarises the interaction of P-gp, BCRP and MRP-1 with tyrosine kinase inhibitors.

1.6.1. Imatinib and ABC transporters

A variety of mechanisms are responsible for patient relapse on imatinib including drug efflux, Bcr-Abl amplification and kinase mutations. Gorre *et al.*[162], identified an amino acid substitution at position 315 (threonine – isoleucine) which led to resistance in 6 out of 9 patients. This amino acid substitution prevents the formation of a hydrogen bond with the drug. Druker *et al.*[163], focussed on ascertaining why Bcr-Abl remains inhibited and, using x-ray crystallographic analysis of mutated proteins, established the effect of point mutations, by x-ray crystallography, on imatinib activity[164].

However, molecular aberrations of the target alone are not solely responsible for resistance. Mahon *et al.*[165], showed an interaction, in Bcr-Abl expressing cell-lines, between imatinib and P-glycoprotein and that inhibition of P-gp led to an increased uptake of imatinib in the LAMA84-r cell-line. Using 5mM glutathione-conjugate stimulated MRP-1, Hegedús *et al.*[166], demonstrated that imatinib inhibited MRP-1 but only marginally and at high concentration, 50% inhibition at higher than 100 µM. Mukai *et al.*[167], has also shown that imatinib does not inhibit MRP-1 at up to 200µM.

The relationship between BCRP and imatinib is more convoluted. The role of imatinib as a BCRP inhibitor has been shown in CML cells as imatinib reduces the efflux of 200nM BODIPY-Prazosin in a dose dependant manner[168]. This study also stated that imatinib was not a substrate of BCRP as inhibition of BCRP did not alter response of the CML CD34$^+$ cells to imatinib. This was in agreement with a previous study which showed that imatinib increased the accumulation of BCRP substrate, topotecan, but that imatinib itself was not transported by BCRP[169].

However, other groups have found imatinib to be a BCRP substrate by comparing the level of imatinib accumulated in BCRP over expressing cells when compared to parental cell-lines[170]. Brendel et al.[171], also showed that a CML cell model, K562, which was transduced with the *BCRP* gene was 2-3 fold resistant to imatinib and that BCRP inhibition reversed the resistance. This group also showed that less imatinib was accumulated in the BCRP-transduced cells and that imatinib interacts directly with BCRP at the substrate binding pocket. This implies that imatinib is both a substrate and inhibitor of BCRP.

1.6.2. Dasatinib and ABC transporters

As dasatinib is used as a treatment for imatinib resistant and imatinib intolerant patients it is clear that dasatinib overcomes some of the molecular causes of imatinib resistance in CML. Specifically, dasatinib's lack of specificity for the activation state of Bcr/Abl overcomes mutations of Bcr/Abl that lock the kinase in the active conformation[136]. However, given that imatinib is a substrate of BCRP and an inhibitor of P-gp, it is important, if dasatinib is to truly treat imatinib resistant patients, to establish the effect of ABC transporters on dasatinib.

Caco-2, an intestinal epithelial cell line model, is routinely cultivated as monolayers on permeable filters for studies of the transepithelial transport of drugs[172]. In 2008 Kamath et al.[173], showed using Caco-2 cell model, that dasatinib had a 2-fold efflux ratio indicating that dasatinib maybe a substrate for P-gp, however, when assessed in P-gp knock-out mice, there was no difference in the amount of unabsorbed dasatinib, suggesting that dasatinib may not be cleared by P-gp.

Further work published in 2008 by Hiwase *et al.*[174], showed, through the use of ^{14}C labelled dasatinib, that the intracellular uptake and retention (IUR) of dasatinib was significantly lower in P-gp over-expressing cells (K562-DOX) compared to parental cell-line(K562). Similarly the IUR of dasatinib in BCRP over expressing cells was lower compared to the parental cell-lines, and the use of a BCRP inhibitor (Ko143) significantly increased the IUR of dasatinib in BCRP resistant cells. Also Lagas *et al.*[175], identified that dasatinib was a substrate for P-gp and BCRP. Looking at polarized canine cells, transformed to express P-gp (ACBCB1), MRP2 (ABCC2) and murine BCRP (ABCG2), dasatinib was seen to be transported in the P-gp and BCRP models but not the MRP2 model. This group also examined the oral uptake of dasatinib *in vivo* with wild type and P-gp and BCRP knock-out mice, and concluded that P-gp but not BCRP, restricts oral absorption of dasatinib.

As an interesting side note, one mechanism of cellular uptake that dasatinib has overcome is transport with OCT-1. OCT-1, an organic cation transport, is an influx transporter. OCT-1 has been shown to increase the intracellular level of imatinib[176]. Differential expression or function of OCT-1 appears to be a significant determinant of patient response to imatinib mesylate. Dasatinib is not a substrate for OCT1 and thus is not susceptible to alteration intracellular concentrations of this transporter protein[174].

1.6.3. Lapatinib and ABC transporters

Lapatinib has been found both in-house and in the literature to interact with P-gp. Polli *et al.,* showed that lapatinib is a substrate of P-gp and BCRP while also inhibiting the P-gp transport of digoxin by 74%, and the BCRP transport of cimetidine by 82% [177]. Lapatinib increased the accumulation of P-gp and BCRP substrates in P-gp and BCRP over-expressing cell-lines[178]. Collins *et al.*[179], showed lapatinib to have an inhibitory affect on the action of P-gp and suggests that lapatinib has a high affinity for the binding site of P-gp, affecting P-gp's ability to transport substrates. Lapatinib has also been shown to increase the expression of P-gp[7, 180] and to inhibit the action of MRP7 (ACBC10)[181].

1.6.4. Gefitinib and ABC transporters

In-vitro studies by Ozvegy-Laczka *et al.,* found gefitinib to be a transport substrate of P-gp and an inhibitor of MRP-1[123]. Similarly Kitazaki *et al.*[182], and Nakamura *et al.*[183], have shown gefitinib to be an inhibitor of P-gp and BCRP respectively. However, a more recent study suggests that gefitinib may act as a transport substrate for BCRP as gefitinib competed with ^{3}H mitoxantrone transport and depleted cellular levels of ATP[184].

Table 1-5: Tyrosine Kinase Inhibitors and their interactions with ABC transport proteins

Agent	P-gp	BCRP	MRP-1
Imatinib	Substrate [165]	Substrate[170]/inhibitor[169]	Marginally inhibitory [166]
Dasatinib	Substrate	Substrate	Unknown
Lapatinib	Inhibitor[178]	Inhibitor[178]	Unknown
Erlotinib	Substrate[185] Inhibitor at high concentrations[186]	Inhibitor at high concentrations [187] Substrate at low concentrations[186]	
Gefitinib	Substrate [123]	Possible substrate[184]	Inhibitor[123]

1.7. Therapeutic drug monitoring of cancer drug levels

Therapeutic drug monitoring (TDM) involves the quantification and interpretation of drug concentrations in biological fluid with the view to adjusting the drug dosage or scheduling of a patient to maximise benefit. Therapeutic monitoring of drug levels is carried out in a range of disease classes, and agents monitored include cardiovascular agents, antiepileptic medication, antibiotics and anti-inflammatory agents, immunosuppressant, anti depressants and some anti-cancer medication[188]. Therapeutic drug monitoring is most suited to drugs that [189]:

1) have a large degree of inter-patient variability at a given dosage
2) can be measured in biological fluids
3) have a narrow therapeutic index (TI)
4) show a correlation between exposure and response
5) have a sensitive robust method of analysis and quantification
6) have a specific target

Cancer, as a disease type, does not lend itself well to the therapeutic monitoring of an agent as frequently the drug plasma concentration is not representative of the drug concentration at the site of action. The target site may be distant from intravascular spaces and solid tumours frequently have their own blood supply. Patients who have been heavily pre-treated with other chemotherapy regimes may have a differing response. Similarly, many agents are given in combinations, complicating the evaluation of therapeutic effect by altering dose or scheduling of one agent.

However, some of the characteristics of chemotherapy agents that do align with the requirements for TDM are that they (a) have a narrow therapeutic index (TI) (b) can be measured in biological fluids, and (c) display a large degree of inter-patient variability.

Also, there are a vast number of quantification methods for anti-cancer agents available, some of which have been developed to quantify drug pharmacokinetics in animal studies[190]. Part of the difficulty of therapeutically monitoring cancer agents in patients is determining an appropriate outcome. If the desired outcome is "improvement in cure rate" this requires a minimum of five years follow-up.

It is clear, however, that there are many potential benefits to TDM for cancer chemotherapy. Personalising patient care has become a focus in cancer research in recent years[191]. However, the individualisation of patient care should maximise chemotherapy intensities by administering concentrations, within the TI, that are at the upper end of the nontoxic range. Clinical trials have shown the benefits of avoiding sub-optimal drug concentration or drug concentration in the toxic range by achieving maximum chemotherapy intensity[192]. Alnaim[188], and Rosseau & Marquet[193] comprehensively reviewed systems for evaluating response in cancer TDM including methods for dose individualisation such as

1) *a priori* method - where the dose is calculated based on several factors including age, gender, body weight, and where the formula designed, must have a close relationship between the estimated parameter and pre-treatment factors. However, no concentration data is used to influence the concentration profile.

2) test-dose methods – a two stage process where a large dose of a moderate concentration of the agent is given and multiple blood samples are taken to evaluate pharmacokinetic parameters. These parameters are used to calculate the full dose necessary.

3) *posteriori* methods – are adaptive methods, convenient for repetitive administration or long continuous infusion. Nomograms, multi-linear regression or Bayesian estimation are frequently used for these methods.

1.8. Quantification techniques

The accurate quantification of agents in biological matrices such as blood, serum, urine and tissue samples is the cornerstone of TDM. Clinical decisions and further treatment options for patients can only be based on accurate validated analytical methods. Likewise when determining the efficacy, dose limiting toxicity or pharmacokinetics of new agents or new combinations of agents, accurate and precise quantification methods are required. The predominant quantification techniques used are spectrometric based instruments such as ultraviolet radiation (UV) or mass spectrometry (MS).

The use of UV is prolific in analytical laboratories as instrument costs have decreased significantly in recent years. UV is suitable for quantification purposes as, in UV, analyte concentration is related to detected absorbance by the Beer-Lambert Law ($A_\lambda = \varepsilon_\lambda c l$). A_λ =absorbance at defined wavelength, ε_λ =excitation coefficient at a defined wavelength, c=concentration and l=pathlength. In reality this means that when the pathlength (l) and the excitation coefficient (ε_λ) remain constant, as they do during most experiments, the absorbance detected is proportional to the concentration[194].

Mass spectrometry is based on the generation of ions in a gaseous state and separating them according to their mass to charge ratio (m/z) detection is based on their m/z. Though the instrumentation is significantly more expensive than UV instruments, MS instruments are attractive to an analyst as (a) they provide chemical and structural information about the molecules from their molecular weights and fragmentation pattern and (b) they are extremely sensitive with detection limits typically in 10^{-12} to 10^{-15} molar range[194].

The separation of molecules and introduction into an MS system is usually through on-line coupling to a chromatography system. The most common front-end separation techniques for MS are Gas Chromatography (GC) or High Pressure Liquid Chromatography (HPLC/ LC) system. Chromatography is the process of separating the components of mixtures between a stationary phase and a flowing mobile phase. The concept of chromatography was originally conceived by a Russian botanist, Mikhail Tswett, for the separation of plant pigments. On a glass tube packed by chalk powder, Tswett loaded plant leaf extract and petroleum ether as saw a separation of brightly

coloured bands[195]. The term chromatography comes from the Greek terms from "colour" and "writing", though interestingly, Tswett is also the Russian word for colour.

1.8.1. GC-MS

Gas chromatography is a technique for the separation of volatile components of mixtures by differential migration through a column containing a liquid or solid stationary phase. In GC, the mobile phase is an inert carrier gas and does not contribute to the separation. There are two types of GC columns, capillary columns and packed columns. The stationary phase can be thin layers of high boiling point liquids, oils or waxes (GLC), or solid sorbents and polymers (GSC)[195].

The advent of coupling separation methods to high-end detection methods began with the union of gas chromatography (GC) with mass spectrometry (MS). This link in techniques was, in part, a natural analytical evolution as the requirements of compounds for GC separation are the same as the requirements to produce a mass spectra i.e. both volatile and thermally stable at the temperatures used to achieve separation [188, 196]. However, GC-MS is limited to a range of analytes which are volatile and vaporise easily, most anticancer agents display neither of these properties.

1.8.2. LC-MS

HPLC is the separation of components of mixtures by differential migration through a column containing microparticulate solid stationary phase. Solutes are transported through the column by pressurised flow of liquid mobile phase[195]. HPLC is a complementary technique to GC, as HPLC is recommended for a wide range of sample types which are unsuitable to GC.

The coupling of the LC to MS allows for the identification of analytes across a broad mass range, enabling the detection of low mass drugs and metabolites up to large biomolecules. However, coupling HPLC with mass spectrometry is less straight forward as it is not possible to simply connect one to the other without the use of an interface. The role of the interface is primarily the removal of chromatographic mobile phase.

In HPLC the component being analysed are frequently in complex mixtures. Identification and quantification by HPLC relies on the retention characteristics of the analyte. Even with accurate reference compounds it is not always possible to either achieve complete separation or to confidently identify and quantify the analytes of interest in complex mixtures. However, MS detection primarily identifies the molecular mass of the analyte, with more sophisticated instruments providing further information such as the product ions, providing increased specificity and selectivity.

It is the diverse utility of HPLC and the specificity of MS that make LC-MS one of the most used hyphenated techniques in an analytical lab.

LC-MS/MS or tandem MS in its simplest form, is the combination of two mass analyzers. The first MS isolates the ion(s) of interest from the other ions. The ions(s) then get fragmented and travel on to the 2nd MS where the mass of each fragment is detected. There are two main types of MS/MS instruments used for analysis and quantification of small molecules, the ion trap and the triple quad. The instrument used throughout this project was an Agilent 6410 triple quadrupole mass analyser, and will be discussed in more detail here.

1.8.3. LC-MS – Triple Quad

A triple quad MS is a tandem MS system consisting of three sections with distinct applications. Despite being called a triple quadrupole, the instrument actually consists of 2 quadrupoles and a hexapole. A quadrupole consists of four charged rods which run parallel to the flight path of the ion. The quadrupole determines the selectivity of the ions trajectory to the detector by creating oscillating electric fields. As seen in Figure 1-12, the quadrupoles are the first (MS1) and last sections (MS2) of the instrument, the middle section, the collision cell, is a hexapole. In the collision cell, ions collide with nitrogen gas atoms to give rise to product ions. This process is known as collision induced dissociation (CID). The resulting fragment ions travel to the last quadrupole (MS2) where the mass to charge ratio (m/z) is detected. Additionally, there is an octopole ion guide before the first quadrupole to focus ions.

In each scan mode, the instrument operates is a subtly different manner. The difference in the MS modes used are outlined below.

1.8.3.1. *MS2Scan*

MS2Scan detects all ions in their precursor form (barring in-source fragmentation). As the ions enter the MS, they pass through MS1 and through the collision cell unchanged and without fragmentation to the detector in the final quadrupole, as shown in Figure 1-7.

Figure 1-7: Schematic of MS2Scan
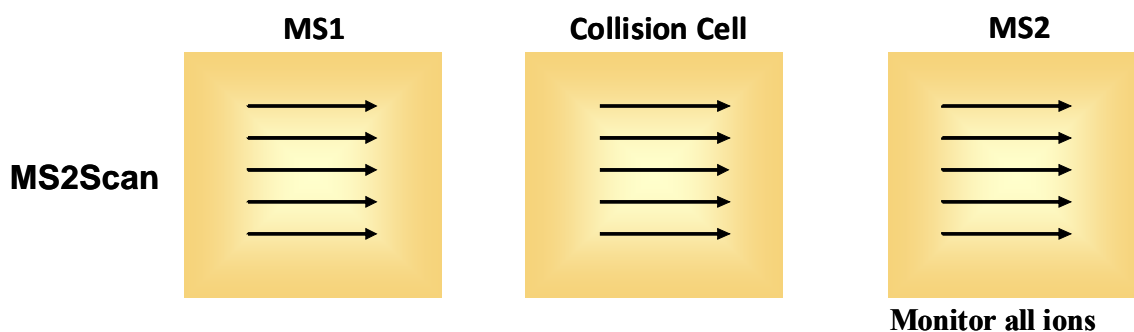
Schematic diagram of mode of action for each quad in MS2Scan mode.

1.8.3.2. *SIM*

SIM is an acronym for selected ion monitoring. SIM is the scan mode discussed in the optimisation of the fragmentor voltage (Section 3.3.2). In selected ion monitoring the precursor ion is detected without collision in MS2. MS1 filters the ions so that only the ions of a particular m/z ratio are permitted into the system. The detector continues to monitor the same single m/z value over the entire scan period, as shown in Figure 1-8.

Figure 1-8: Schematic of SIM
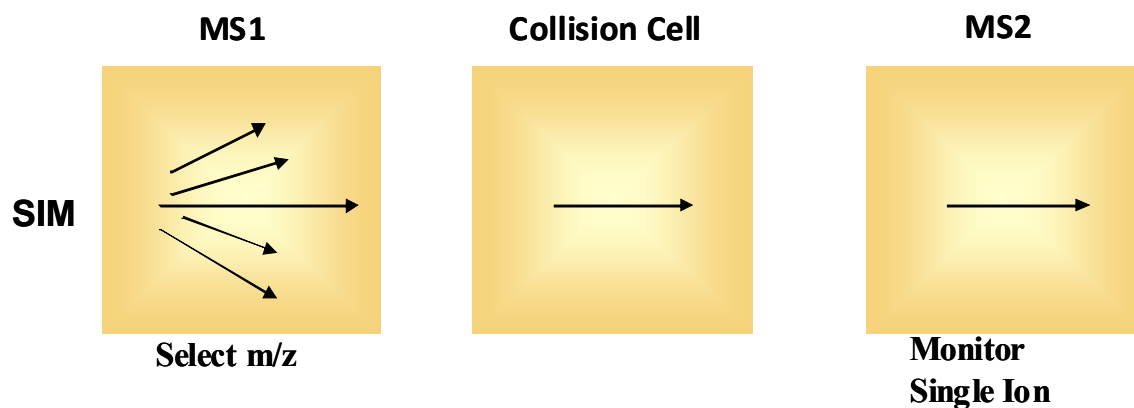
Schematic diagram of mode of action for each quad in SIM Scan mode.

1.8.3.3. Product Ion Scan

Product ion scan is used to determine the product ions. The ions enter MS1 where only the ions of interested are filtered in and sent to the collision cell. Through collision with nitrogen gas, at operator controlled voltages, the precursor ion is broken into the product ion(s). In this way it is possible to identify the product ions, as shown in Figure 1-9.

Figure 1-9: Schematic of Product Ion Scan
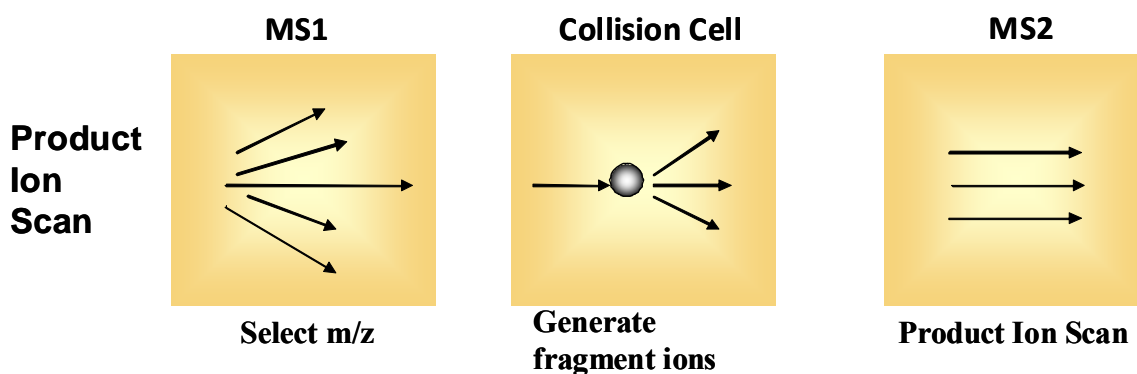
Schematic diagram of mode of action for each quad in Product Ion Scan mode.

1.8.3.4. MRM

It is this process for monitoring for a known precursor ion, fragmenting the precursor ion in the collision cell and monitoring the known product ions that is called multiple reaction monitoring (MRM). Outlined in Figure 1-10 is a schematic of the three quads and there operation during MRM analysis.

Figure 1-10: Schematic of MRM
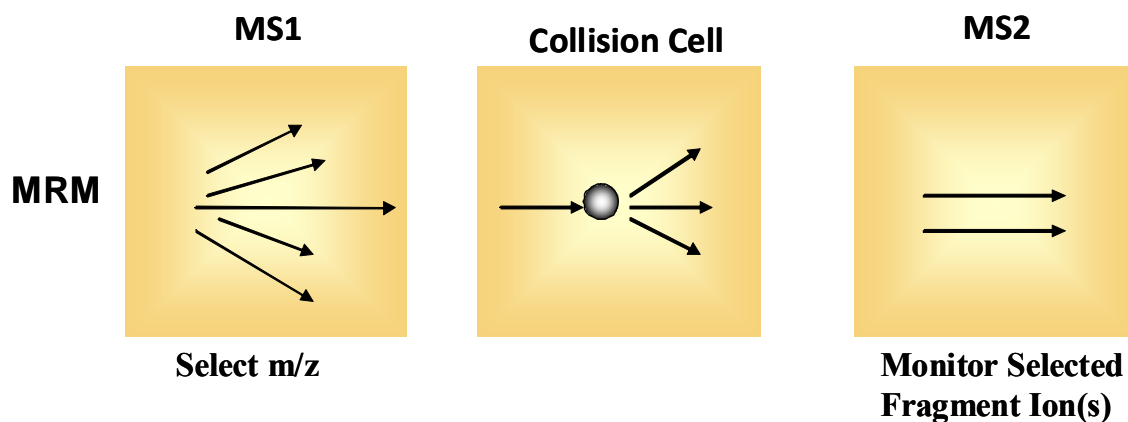
Schematic diagram of mode of action for each quad in MRM Scan mode.

1.8.3.5.   *Ionisation*

One of the other key components of any MS is the ion source. The ion source is where the sample is ionised (with either a positive or negative charge) and converted into a gas phase. The main ion sources interfacing with LC are electrospray ionisation (ESI) and Atmospheric Pressure Chemical Ionisation (APCI). ESI is a soft ionisation technique, meaning that normally the analyte ions remain intact and do not undergo a large degree of in source fragmentation. The inlet of sample, either from an LC or infusion pump system enters the source chamber as a mist, where it is mixed with high temperature drying gas (N_2)[6]. This rapid solvent evaporation causes the droplet to shrink to the point that surface tension can no longer sustain the charge. This is the Rayleigh limit. At this point the surface tension is pulled apart and the droplet, or analyte molecule receives the charge. This is called Coulombic explosion[197].

The analyte spray can be in an "in-line" or "orthogonal" position. The Agilent Triple Quad instrument used in this thesis employs an orthogonal spray position system. This allows for uncharged molecules and unionised mobile phase to flow straight to waste. Figure 1-11 shows a schematic of the source orientation in the Agilent Triple Quad.

Figure 1-11: Schematic of Agilent 6410 Triple Quad Ionisation Source [198]
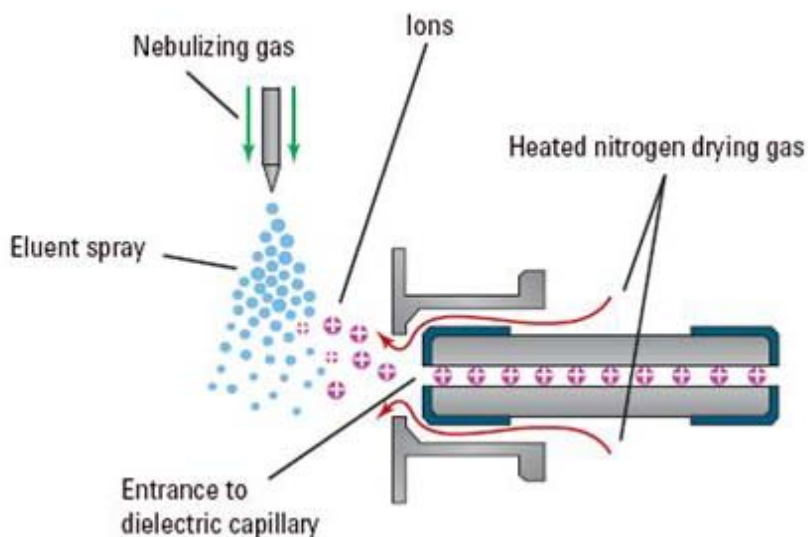
Schematic diagram of the ESI ion source, demonstrating the orthogonal positioning of the nebuliser to the MS

---

[6] In the case of the Agilent 6410 Triple Quad the dry gas is nitrogen, though other systems may use other gases.

Figure 1-12: Schematic of Agilent 6410 Triple Quad [198]

Octopole ion guide
Better ion transmission over a wider mass range

Hyperbolic quadrupole
Enhanced ion transmission and spectral resolution

Hyperbolic quadrupole
Enhanced ion transmission and spectral resolution

Thin skimmer & short capillary-to-skimmer distance
Reduced beam broadening

Patented lenses
Enhanced high-mass ion transmission and increased sensitivity

High-pressure hexapole collision cell with linear acceleration
Optimized MS/MS fragmentation without cross-experiment memory effects

Off-axis, high-energy dynode detector
High gain with rapid polarity switching, long life, and low noise

MS1　　　　　**Collision Cell**　　　　　**MS2**

Schematic diagram of 6410 triple quad, taken from the Agilent Technologies website[198]

1.9. Extraction procedures

Sample preparation in bio-analytical analysis is necessary to remove the analyte of interest from the biological matrix. In general bio-analytical chemistry, the biological matrix can be blood[199] or plasma[200], the most common in pharmacokinetic studies, but biological matrices may also comprise of saliva[201], hair[202], urine[203] and others. Blood, serum and plasma contain approximately 10,000 different proteins with a total concentration of 6–8 g/dL, and urine contains 50–100mg of protein/dL. Plasma also contains approximately 3mg/mL of sodium, 0.2mg/mL of potassium, 15–38.5 mg/dL of urea, and many other organic and inorganic compounds[204]. With such complex mixtures and the dynamic ranges of proteins, fatty acids, lipids and salts, it is clear that it is important to remove these components from the analysis, as these factors could confound the analysis and flood the detector with irrelevant ions.

1.9.1. Solid phase extraction

Solid phase extraction (SPE) is one of the most common bio-analytical extraction methods in publication literature, a search of journal articles using the sciencedirect search engine for the term "SPE" yielded 151,017 hits, with 4,657 hits for the year 2010 alone. SPE involves a solid-liquid phase separation of the analytes from the biological sample, by the selective transfer between a liquid and solid state[195]. The analyte is physically separated from the biological matrix by the differential interacting with a solid phase sorbent material. These sorbents, packed primarily into either disposable cartridges or discs, can be polar, non-polar or ionic depending on the experimental requirements. Solid phase extraction is based on four distinct protocol steps (1) sorbent conditioning, (2) sample loading, (3) washing and (4) analyte elution, as illustrated in Figure 1-12.

The availability of commercially available solid phase extraction material, cartridges or sorbents, has led to uniformity in analysis and makes method replication and transfer from one lab to another more straightforward. SPE is also frequently used in on-line extraction. Automation of sample clean-up is advantageous as it decreases the high level of manual handling and error associated with manual extraction procedures. Though on-line SPE is faster and allows for increased through-put injections and offers

high recoveries, extensive method development is required to optimise many experimental variables[205].

The commercialisation of solid phase extraction cartridge material has led to a lack of specificity, though some groups overcome this through the evolution of molecularly imprinted polymers (MIPs) as a SPE material[206, 207]. For example Anderson *et al.*[208], details the application of MIPs as SPE material for the detection of low levels of benzodiazepines in hair samples.

Figure 1-13: Schematic of solid phase extraction procedure

Sorbent Conditioning	Sample Loading	Washing	Target Elution

Solid phase sorbent is pre-conditioned prior to sample is loaded

Sample is loaded

Analyte of interest is adsorbed to the solid phase packing material and the interfering components of the sample are eluted

Analyte of interest is eluted and collected
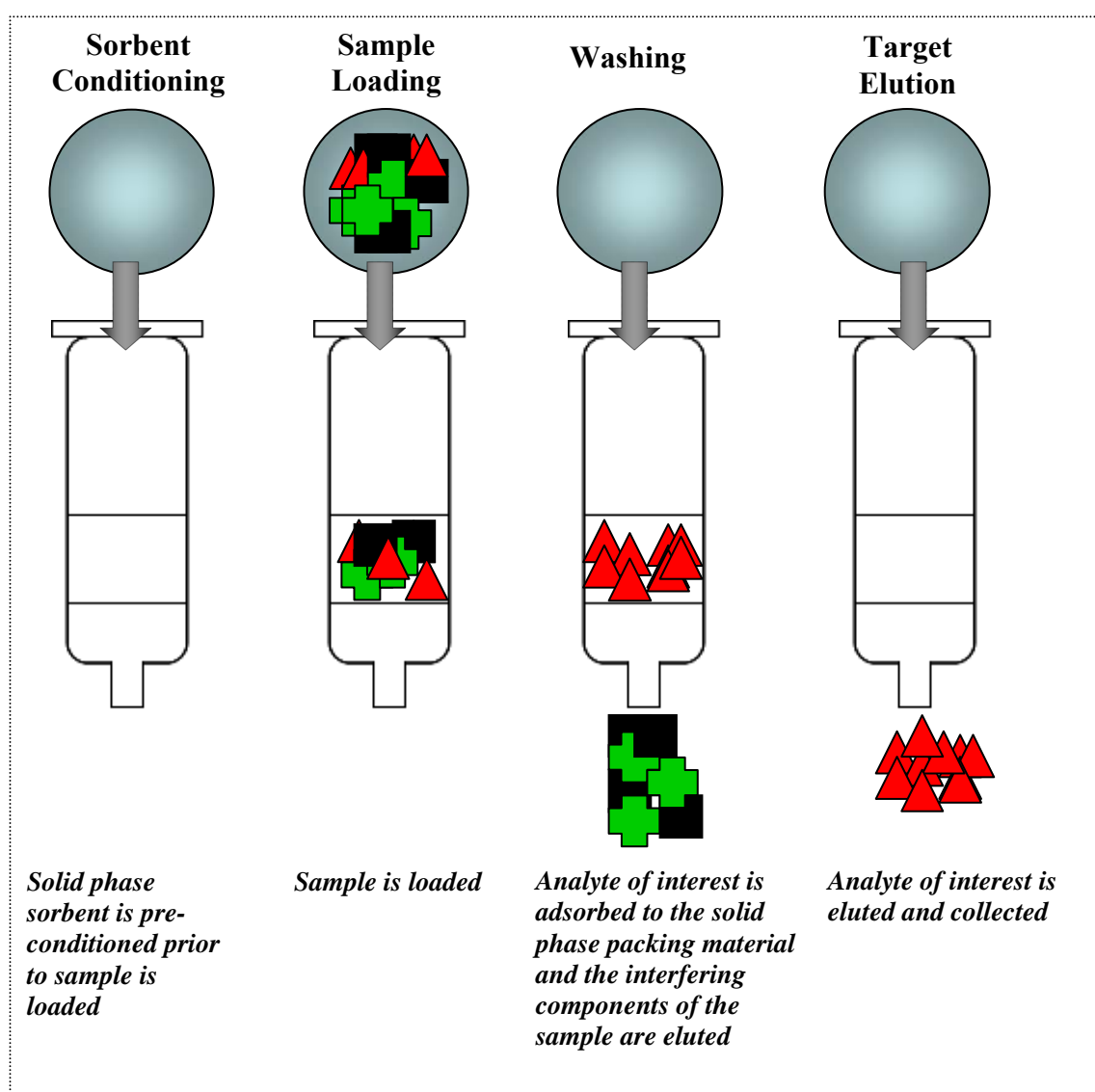
Schematic diagram of the basic experimental protocol for SPE

1.9.2. Protein precipitation

Protein precipitation is based on the interaction between the precipitation reagent and protein groups. Soluble proteins generally have a hydrophobic core surrounded by a hydrophilic surface including ionic groups that are not involved in intra-molecular binding. Organic solvents interfere with the intra-molecular hydrophobic interactions of proteins[204].

The addition of a volume of solvent (frequently acetonitrile) to the serum causes the proteins of the serum to precipitate and leaves the analyte of interest in the solvent, which can either be injected directly or dried down and reconstituted in a smaller volume to concentration before injection. While this is the fastest and simplest method for sample preparation, it is the most likely to cause ion suppression issues, especially in ESI, where the co-elution of endogenous compounds such as lipids, phospholipids and fatty acids affect the ESI droplet desolvation process[209].

1.9.3. Liquid-liquid extraction

Liquid-liquid extraction (LLE), also know as solvent extraction, is based on the partition of an uncharged analyte between an aqueous phase and a theoretically water-immiscible organic phase until equilibrium is reached[204], illustrated in Figure 1-13. LLE is a popular alternative to SPE as it is robust and sensitive, and requires no additional equipment. LLE is considered a time-consuming extraction procedure but provides extracts that are generally less prone to ion suppression[210, 211]. The most frequent criticism of liquid-liquid extraction is the lack of automation in analysis.

Figure 1-14: Schematic of liquid-liquid extraction procedure

Immiscible organic phase

Aqueous biological sample containing analyte (black dots) and biological matrix (yellow dots)

Organic phase with analyte of interest

Aqueous phase with biological matrix and confounding analytes

Shake to allow phases to mix and molecules to partition

Phase separation with gravity/ centrifugation
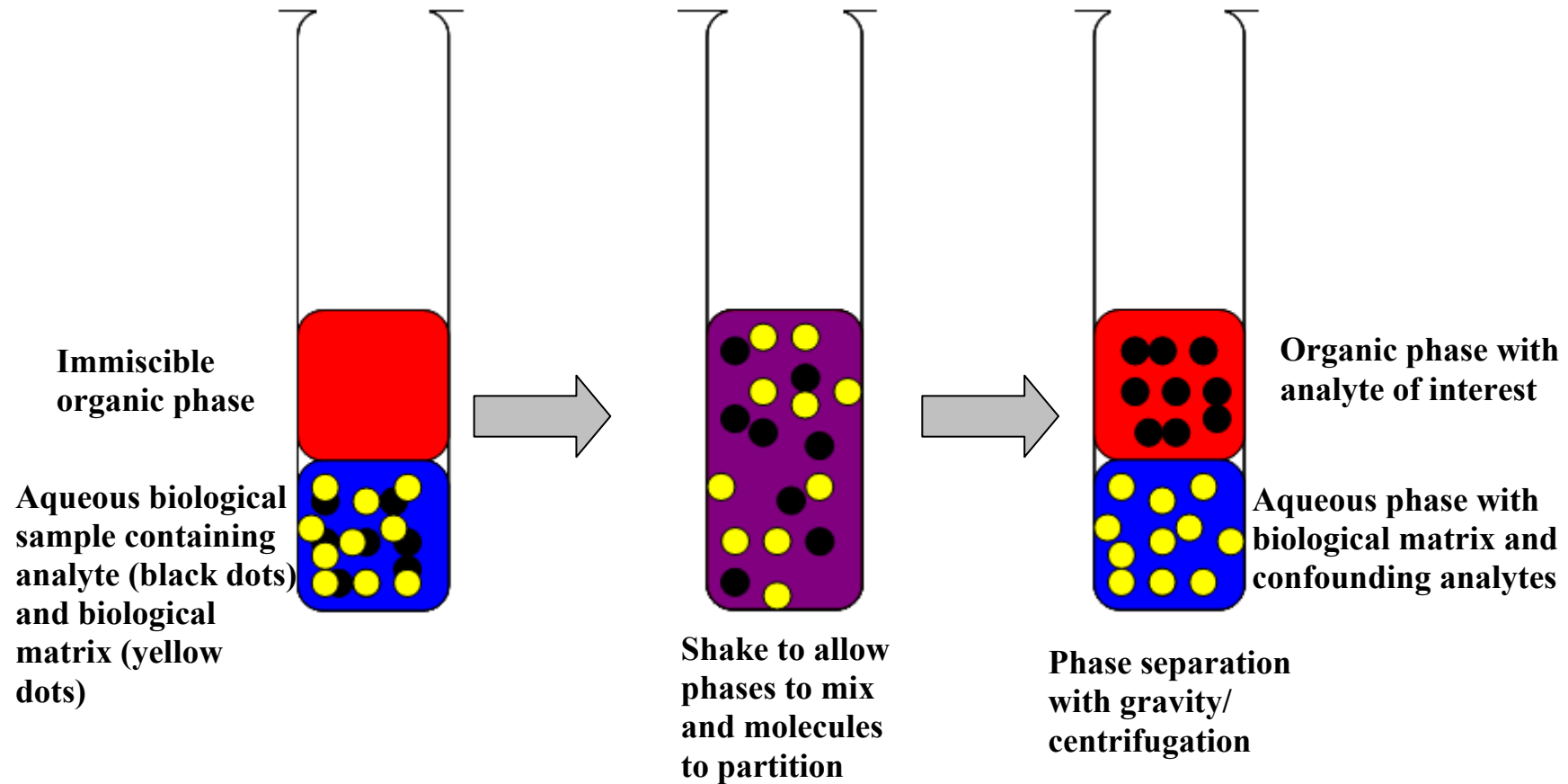
Schematic diagram of the basic experimental protocol for liquid-liquid extraction

1.10. Analytical methods for the quantification of TKIs

The development of analytical methods for the determination and quantification of tyrosine kinase inhibitors by LC-MS has predominantly been driven by pharmacokinetic studies in the drug development stage. Table 1-6 outlines recent methods published for the analysis of TKIs by HPLC-UV and LC-MS/MS.

Given the current advances in cancer research towards targeted therapies, especially TKIs, the development of analytical methods to quantify these agents is in creasing in the literature. Some methods have analysed multiple TKIs simultaneously, though, for some, this has involved complex gradient LC methods and long run times[212, 213]. TKIs are rarely administered in combination with each other and combinations of TKI and chemotherapy agents are more commonly administered. However, some clinical trials detail the use of one TKI followed by another[214], or the use of two TKIs simultaneously[215]. This would suggest that some of the methods published are unnecessarily complex, and are more focussed on analytical novelty than application practicality.

The method developed in this thesis is the only validated method for the quantification of TKIs from *in vitro* samples[216]and hence, represents a valuable laboratory research tool. Also, this method has been shown to be applicable for the analysis of multiple TKIs in a short run time, with a simple, stable isocratic elution. With minor alterations this method would also be applicable for the analysis of clinical samples (blood and tissue*)* samples.

As discussed in further detailed in Section 3.9.6 and Section 3.9.7, the method developed in this thesis has equivalent, if not greater, sensitivity than reported in comparative assays. The use of an LLE extraction method is also simply straightforward and easily transferable to any lab setting.

Table 1-6: Comparison of Analytical Methods for Tyrosine Kinase Inhibitors Biological Matrices.

Analytes Determined	Biological Matrix	Sample Clean up	Analytical Method	Run Time	Sensitivity (LOQ)	% Recovery	Author, Date	Ref
Dasatinib Lapatinib *Erlotinib Imatinib Gefitinib Sorafenib*	**Cancer cell-line models**	**LLE**	**Isocratic Elution, LC-MS/MS**	**8 mins**	**200pg/million cells** **400pg/million cells**	**86-112%**	**Roche 2009**	**[216]**
Dasatinib, Imatinib, Nilotinib	Human Plasma	Protein Precipitation	Gradient Elution, LC-MS/MS	20 mins	78.1ng/ml 62.5ng/ml 61.5ng/ml	95-114%	De Francia 2009	[212]
Dasatinib, Imatinib, Nilotinib	Mouse Plasma	Protein Precipitation	Hydrophilic Interaction LC-MS/MS	-	ng/ml range – data not shown	-	Hseih 2009	[217]
Dasatinib, Imatinib, Nilotinib Sunitinib, Sorafenib, Lapatinib	Human Plasma	Protein Precipitation	Step-wise gradient elution, LC-MS/MS	20 mins	1ng/mL 1ng/mL 1ng/mL 1ng/mL 10ng/mL 5ng/mL	93.3%	Haouala 2009	[213]

Analytes Determined	Biological Matrix	Sample Clean up	Analytical Method	Run Time	Sensitivity (LOQ)	% Recovery	Author, Date	Ref
Erlotinib					12.7nM	96-109%		
Gefitinib	Cell Culture				11.2nM	86-107%		
Sunitinib	Media	Protein			12.6nM	74-84%	Honeywell	
Sorafenib	Blood	Precipitation	LC-MS/MS	5 mins	10.8nM	90-105%	2010	[218]
Erlotinib (OSI-774)	Human plasma	LLE	LC-MS/MS	5 mins.	10ng/mL	79-87%	Masters 2007	[219]
Erlotinib (OSI-774)	Human plasma	LLE	LC-UV	3 mins.	100ng/mL	approx. 100%[7]	Lepper 2003	[220]
Gefitinib	Human plasma, mouse plasma and tissues	Protein Precipitation	LC-MS/MS	3 mins.	1ng/mL (human) 5ng/mL (mouse)	81-103%	Zhao 2005	[221]
Gefitinib	Plasma	LLE	on-column focusing gradient capillary LC-MS/MS	-	0.1ng/mL	-	Gueten 2005	[222]
Gefitinib	Human plasma	LLE	LC-MS/MS, isocratic	5 mins	0.5 ng/ml	111-124%	Jones 2002	[223]
Imatinib	Human Plasma	SPE	Gradient elution - LC-UV	45 mins	0.05μg/mL	96%	Widmer 2004	[224]

---

[7] Actually recovery not specified

Analytes Determined	Biological Matrix	Sample Clean up	Analytical Method	Run Time	Sensitivity (LOQ)	% Recovery	Author, Date	Ref
Imatinib	Human Plasma	Protein Precipitation	Flow injection analysis LC-MS/MS	3.2 mins	30ng/mL	97-99% [8]	Mičová 2010	[225]
Imatinib	Human Plasma	LLE	LC-UV/DAD	12 mins	80ng/mL	98%	Roth 2010	[226]
Imatinib	Plasma	LLE	LC-MS/MS	-	10ng/mL	90%	Titier 2005	[227]
Lapatinib	Human Plasma	Turbulent flow on-line extraction	Isocratic Elution, LC-MS/MS	<0.4 mins	-	-	Hsieh 2004	[205]
Lapatinib	Human Plasma	On-line Extraction	LC-MS/MS	3 mins	15ng/ml	75%	Bai 2006	[200]
Nilotinib Dasatinib	Human Plasma	SPE	HPLC-UV	40 mins	10ng/mL (nilotinib)	72-78%	Masatomo 2009	[228]
Nilotinib Imatinib CGP-74588[9]	Human Plasma	SPE	LC-UV	35 mins	50ng/mL	80.1% 91.8% 89.0%	Davies 2010	[229]

---

[8] Though ion suppression of 78-87% was reported
[9] Imatinib metabolite

46

Analytes Determined	Biological Matrix	Sample Clean up	Analytical Method	Run Time	Sensitivity (LOQ)	% Recovery	Author, Date	Ref
Sorafenib	Human plasma	Protein Precipitation	LC-MS/MS	6 mins	7.3ng/mL	95.8-97%	Zhao 2007	[230]
Sunitinib	Human plasma	LLE:	LC-MS/MS, isocratic	3 mins	0.2ng/mL	-	Minkin 2008	[231]
Sunitinib	Human plasma	LLE	LC-UV	10 mins	10ng/mL	20ng/mL-50%, 60ng/mL-56.4% 200ng/mL-70.5%	Blanchet 2009	[232]
Sunitinib SU1124	Monkey tissue	LLE	LC-MS/MS	5 mins	(2.10 ng/g)	-	Barattè 2004	[233]
ZD6474 (Vandetanib)	Mouse plasma and tissue	LLE	LC-MS/MS	5 mins	20ng/mL (plasma) 10 ng/mg (tissue)	88-90%	Zirrolli 2005	[234]

Table 1-6 details the validated analytical methods of the quantification of TKIs. The method highlighted in yellow has been developed within this thesis.

1.11. Multiple myeloma

Multiple myeloma (MM) is a disorder which is characterised pathologically, by malignant plasma cell accumulation, which is generally derived from one clone of the bone marrow[235, 236]. As illustrated in Figure 1-15, plasma cells are derived from the B cells (B-lymphocytes), a type of white blood cell, made in the bone marrow, whose normal function is the production of antibodies as a response to an a infection or disease[237]. The clinical manifestations of this malignancy are heterogeneous and include destructive bone lesions, anaemia hypercalcaemia and renal insufficiency. The median survival time after diagnosis is 3 years with alkylating agent therapies, with improvements in treatment increasing survival times[238].

Figure 1-15: Hematopoietic Tree Plasma Cell[239]
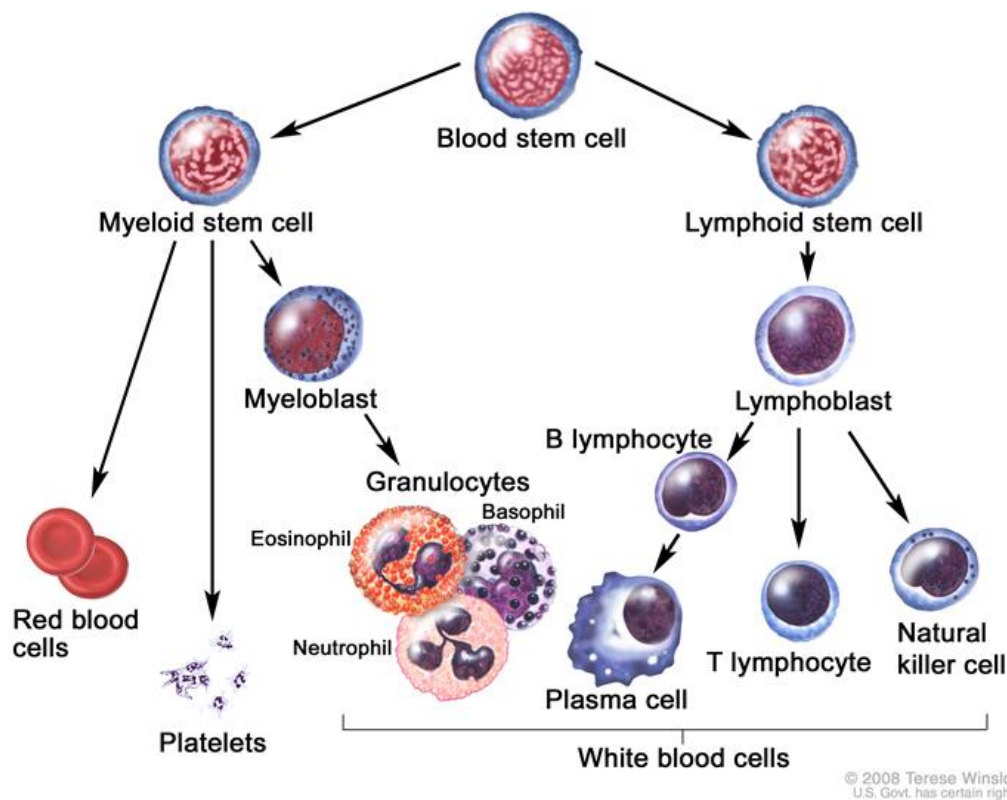
Figure 1-15 shows the generation of plasma cells. © 2008 Terese Winslow, U.S. Govt. has certain rights. Image reproduced with permission.

1.11.1.   Treatments in Multiple Myeloma

The treatment of patients with MM is generally stratified into two options, as illustrated in Figure 1-15, depending on eligibility for transplantation[240]. Transplant eligibility is based primarily on age and patient fitness. While the outcome of patients randomized on early or late stage autologous peripheral blood stem cell transplantation has been equivalent, early treatment decisions after diagnosis are required as alkylating agents may hamper subsequent stem cell collection[241].

Traditionally patients who were eligible for transplantation were given a combination of vincristine, doxorubicin and dexamethasone (VAD) to reduce tumour mass prior to transplantation. The introduction of novel agent-based therapies has replaced long established cytotoxic protocols such as VAD. The most commonly used new therapies include thalidomide, lenalidomide and bortezomib. There are three main treatment regimes - melphalan, prednisone, thalidomide (MPT), melphalan, prednisone, bortezomib (MPV) and melphalan, prednisone, lenalidomide (MPR)[238].

- Palumbo *et al.*[242], demonstrated the benefit of the addition of thalidomide to the melphalan, prednisone (MP) standard therapy. Patients showed a higher response rate and longer event-free survival with MPT when compared to MP which was confirmed in subsequent studies[243, 244].
- The combination of MPV was studied by Mateos *et al.*[245], where V indicates Velcade, the trade name for bortezomib. This study showed that in newly diagnosed elderly patients, 85% were alive after three years compared to 26 months with MP alone.
- A phase I/II study by Palumbo *et al.*[246], examined that the combination of MPR, where R indicates Revlimid (lenalidomide). The maximum tolerated dose was defined and 81% of patients achieved partial response.

Of the novel agents discussed here, thalidomide will be discussed in greater detail, as the remit of the project was to examine thalidomide in patient serum.

Figure 1-16: Treatment strategy for multiple myeloma
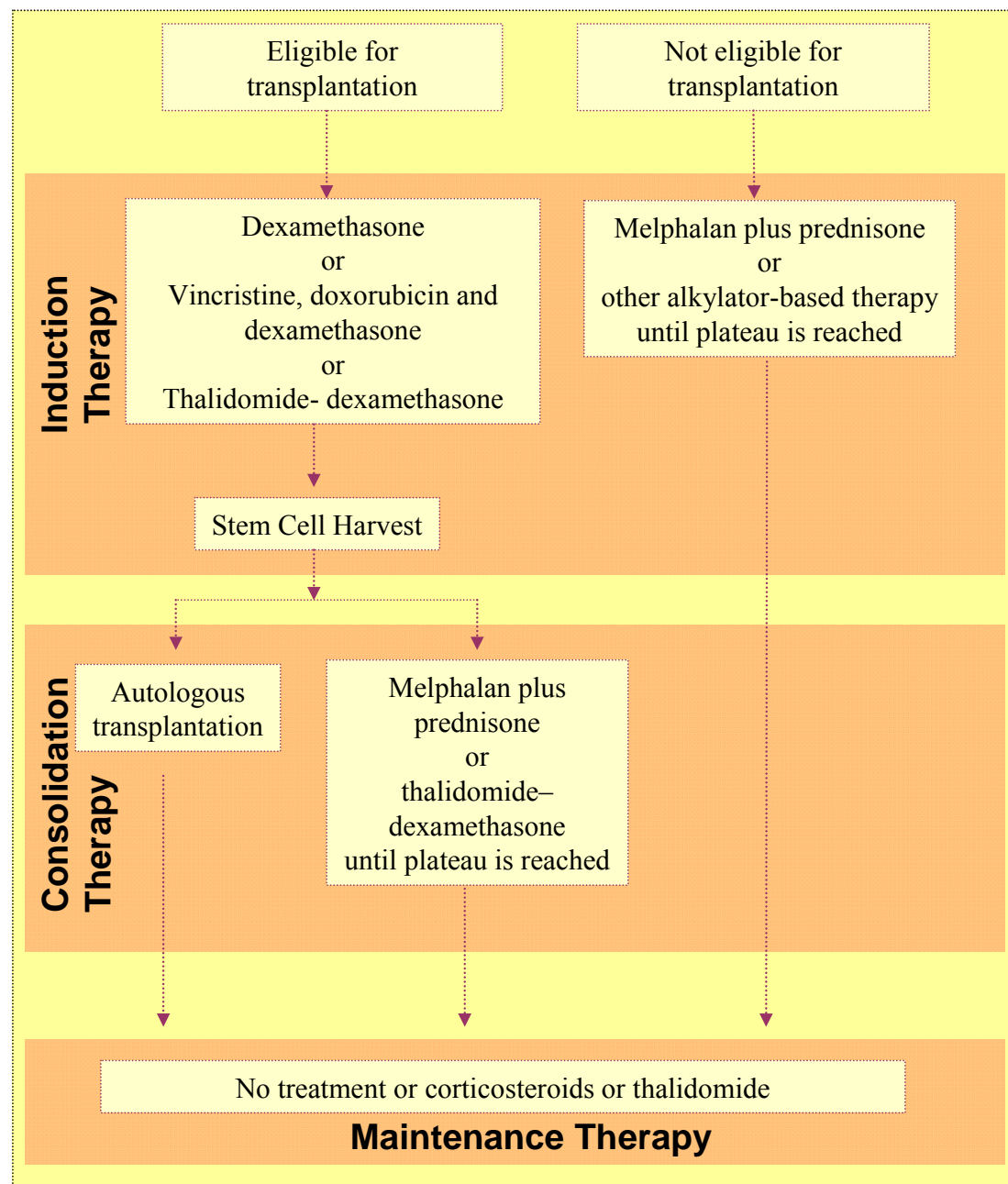
The treatment strategy of multiple myeloma, adapted from Kyle[235].

1.11.2. Thalidomide

Thalidomide (α-phthalimidoglutarime) is a synthetic glutamic acid derivative currently produced by Celgene Corp, Warren, NJ. Thalidomide is reported to have been first synthesised in 1954 by Chemie Grunenthal in West Germany[247, 248]. It was sold as an over-the-counter medication for the effects of morning sickness due to its perceived safety, though was never approved by the FDA in the US due concerns about neuropathy[249]. In the early 1960's it received notoriety and was withdrawn from the market due to two independent clinical reports detailing birth defects in babies whose mothers had taken thalidomide[250, 251]. The use of thalidomide during the first trimester of pregnancy led to phocomelia, defects of the long bones, absence of auricles, cleft lip and cardiac and gastrointestinal anomalies[252]. Thalidomide re-emerged in the clinic when Dr Sheskin discovered a benefit of thalidomide in a patient suffering erythema nodosum leprosum (ENL), a potential complication of lepromatous leprosy[253]. This led to a WHO investigation which showed complete remission of symptoms within weeks of treatment[254]. This finding led to renewed clinical interest in thalidomide in areas of rheumatoid arthritis, systemic lupus erythematosus and other autoimmune disorders.

1.11.3. Thalidomide in multiple myeloma

A study of thalidomide in a variety of cancer types was prompted by the inhibition of growth seen in foetal tissue. However, no significant results were seen in this study, possibly due to the numbers of malignancies examined and the lack of focus of the studies[240, 255, 256]. The benefit of thalidomide in multiple myeloma was first noticed following a study by Singhal *et al.*[257], on 84 patients with refractory myeloma. This result, though carried out in an uncontrolled patient group, was remarkable as most of the patient enrolled, who had already relapsed following high-dose chemotherapy, showed reduced tumour burden following thalidomide treatment. A randomized trial by the Eastern Cooperative Oncology Group (ECOG) showed that a thalidomide-dexamethasone combination was more effective than dexamethasone alone. Based on this study thalidomide was granted accelerated approval by the FDA[258].

1.11.3.1.   Mechanism of action and pharmacokinetics of thalidomide

Thalidomide has a chiral centre and as such, the two different enantiomers of thalidomide should have different pharmacokinetic properties, however, at physiological pH and temperature, thalidomide will rapidly interconvert to a racemic mixture[259]. A sedation effect appears to be primarily due to the *(R)* isomer while the teratogenic effect has been linked to the *(S)* isomer[260, 261]. The precise mechanism of action of thalidomide is unknown though there are numerous immunomodulatory and non-immunomodulatory properties.

Thalidomide's effect on TNFα

Thalidomide inhibits the synthesis of tumour necrosis factor alpha (TNF-α). TNF-α is pro-inflammatory cytokine that regulates the inflammatory cascade. The action of thalidomide on TNFα is felt to be largely responsible for the clinical benefit seen in patients with ENL[249].

Thalidomide's effect on angiogenesis

Tumour development was first associated with angiogenesis in the 1970s but it was not until 1994 that it was shown that thalidomide inhibited basic fibroblast growth factor (bFGF)-induced angiogenesis[262]. Vascular endothethial growth factor (VEGF) and bFGF are produced in excess in a variety of malignancies[263]. Thalidomide has been shown to inhibit VEGF action in co-culture models of bone of multiple myeloma cell lines and marrow stromal cells[264]. It has been proven that the anti-angiogenic properties of thalidomide are linked with its teratogenicity.

Thalidomide's effect on T Cells

Thalidomide has also been shown to co-stimulate primary human T-lymphocytes, inducing their proliferation cytokine production and cytotoxic activity[265]. Through this stimulation of the autoimmune system, thalidomide enhances an immune anticancer response.

1.11.3.2.   Adverse effects of thalidomide

The major concern in terms of adverse effects of thalidomide is teratogenicity. These concerns are addressed by a system called System for Thalidomide Education and Prescribing Safety (STEPS), whereby the physicians, nurse practitioners and pharmacists must be registered with the educational program. Furthermore education is given and sexually active patients are required to use two forms of contraception[266, 267].

The most common adverse effect associated with thalidomide are, constipation, neuropathy, somnolence, depression and venous thromboembolism. In a recent review, Mateos discusses the incidences of grade 3 and grade 4 adverse effects in multiple myeloma trials[268]. The addition of other agents to thalidomide generally increases the incidence of adverse effects.

1.11.4.   Thalidomide metabolism
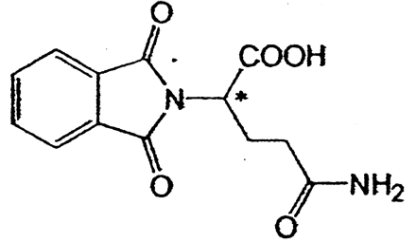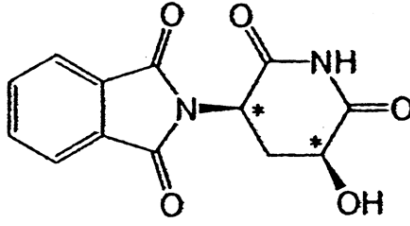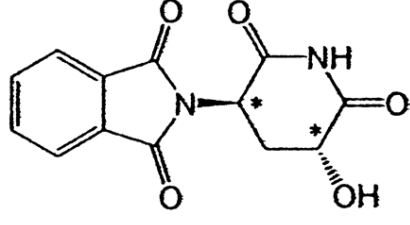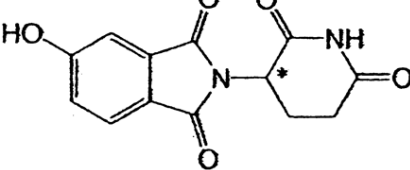
In 2000, Teo *et al*.[269], completed the first comprehensive study on the role of various human cytochrome P450 (CYP) isozymes on thalidomide metabolism. A previous study showed that metabolite formation was reduced with CYP inhibition but failed to identify the metabolite or the CYPs involved. This study showed that human CYP isozymes showed little or no effect on thalidomide metabolite formation. The author concluded that the interactions between thalidomide and other drugs are unlikely due to thalidomide's minimally metabolism by hepatic CYPs.

In 2003, Lu *et al*.[270], published work based on thalidomide metabolites in mice and multiple myeloma patients. Having developed methods for the analysis of the hydroxylated and hydrolysis products of thalidomide by LC-MS, they used this method to detect the metabolite products in the urine of mice and MM patients. From the analysis of patient serum, the authors determined that the "lack of detectable hydroxylated metabolites" in MM patients who were responding to treatment suggested that the metabolites are not responsible for the therapeutic effect.

Chung et al.[271], analysed the thalidomide levels in the plasma of mice, rabbits and five MM patients over 24 hours after the first dose. The authors noted that hydroxylation products were not detected in any of the 5 patient samples, though they were detected in mice plasma and moderately in rabbit samples. Table 1-7 gives the structures of the main metabolites of thalidomide mouse urine.

Table 1-7: Thalidomide metabolites found in mouse urine[271]

Mol. Weight	Metabolite	Structure
276[*]	N-(o-carboxybenzoyl) glutamic acid imide	
292[†,‡]	cis-5′-Hydroxy-N-(o-carboxybenzoyl) glutamic acid imide	
294[*]	N-(o-carboxybenzoyl) isoglutamine	
292[†,‡]	trans-5′-Hydroxy-N-(o-carboxybenzoyl) glutamic acid imide	
276[*]	Phthaloylisoglutamine	
450[†]	Thalidomide-5-O-glucuronide	

276*	Phthaloylglutamine	
274†	*cis*-5′-Hydroxythalidomide	
274†	*trans*-5′-Hydroxythalidomide	
274†	5-Hydroxythalidomide	

* Hydrolysis product.

† Hydroxylation product.

‡ Not yet confirmed by comparison with authentic standard.

55

1.11.5.   Thalidomide quantification methods

Several analytical methods have been published for the quantification of thalidomide. Given that the agent is approximately 50 years old, it is not surprising that there is a body of work on thalidomide. Table 1-8 details the validated analytical methods available in the literature for the quantification of thalidomide by HPLC-UV or LC-MS. Every effort has been made to ensure that this table is as comprehensive as possible.

Some of the original analytical methods developed for thalidomide focussed on the separation and analysis the stereoisomers of the agent[272]. Early on in the analytical history of the drug stability was also recognised as a problem but the majority of authors have addressed the issue of thalidomide hydrolysis in serum through the acidification of the sample prior to storage. A variety of sample clean-up methods have also been applied including SPE[273] and PPT[274] and LLE[275], though it should be noted that, for the three most recent published methods, the LLE method described are adaptations of each other[276-278].

The method developed in this thesis, Section 5, is highlighted in yellow in Table 1-8. This method employs a simple isocratic separation, and a straightforward LLE extraction. When compared to the other methods published, this method is more sensitive, and only a small volume of patient serum is required for the accurate quantification of thalidomide. This is also the only validated method for the quantification of thalidomide in cell-line models, though the application of this is discussed further in Section 5.5.2. Overall a sensitive straight-forward method has been developed which compares very well against published literature.

Table 1-8: Thalidomide analytical methods

Analyte, ISTD	Biological Matrix	Sample Storage & Clean up	Analytical Method	Run Time	Sensitivity	% Recovery	Author Date	Ref
Thalidomide Umbelliferone	Human serum (0.1mL) Cell-line models	-80°C, 1:1(v/v) 25mM citrate buffer pH1.5, LLE	**LC-MS/MS,** Prodigy C18 (150mm x2.0mm, 5µm) ACN/Water/FA, (30/70/0.1)	13 mins	>3ng/mL	91.8% – 115.1%	Roche, unpublished	
Thalidomide Phthalimide	Plasma of Hepatocellular carcinoma patients (1mL)	-80°C, 2/1 (v/v) in stability solution. Modified LLE[10]	**HPLC-UV** BDS Hypersil column (250 × 4.6mm, 5µm) ACN/10mM ammonium acetate buffer (pH 5.5) (25/75, v/v)	10 mins	LOQ: 100ng/mL	>90% within 0.05– 50µg/mL	Saccomanni 2008	[276]
Thalidomide Phenacetin	Human serum from mesothelioma patients. Rat serum and tissue (0.2mL)	Serum 1/1 (v/v) tissue 1/4 w/v) citrate-phosphate buffer (pH 2, 0.2M), stored at −80°C. LLE	**HPLC-UV** vancomycin column (Chirobiotic V™, 250×4mm) 14% acetonitrile in 20mM ammonium formate, pH 5.4	>18 mins	LOQ ~25ng/mL in serum	54%-100% for enantiomers in different matrices	Murphy-Poulton 2006	[275]

---

[10] Adpated from Yang *et al.,* 2005

Analyte, ISTD	Biological Matrix	Sample Storage & Clean up	Analytical Method	Run Time	Sensitivity	% Recovery	Author Date	Ref
Thalidomide Phenacetin	Rat plasma (0.1mL)	-20°C 200μL ice-cold acetonitrile/methanol (1:1, v/v) containing 2% (v/v) acetic acid	**HPLC-UV** Hypersil C18, (200mm×4.6mm, 5μm) ACN/10mM ammonium acetate buffer (pH 5.50) (28:72, v/v)	11 mins	LOQ: 51.6ng/mL[11]	>90%	Yang 2005[12]	[277]
Thalidomide Phenacetin	HBSS[13] buffer for transport assays in Caco-2 cells (0.4mL)	1/2 (v/v) ice-cold acetonitrile/methanol mixture containing 2% acetic acid (v/v)	**HPLC-UV** Spherex C18 column (150×4.6 mm; 5 μm) ACN:10mM ammonium acetate (24:76, v/v, pH 5.5)	10 mins	LOQ: 6.4ng/mL[14]	90-110%	Zhou 2003	[278]
Thalidomide	Plasma and semen from HIV-seropositive patients (0.5mL)	0.025M Sörensen's citrate buffer pH 1.5, -70°C SPE	**LC-MS-MS** Summit, ODS C18 (35x3.2mm, 3μm) H2O: ACN: Acetic Acid 75/25/0.1	4 mins	5ng/mL	Plasma> 69% Semen 78%	Teo 2002	[279]

---

[11] Reported as 0.02μM
[12] Adapted from Zhou *et al.,* 2003
[13] Hanks Balanced Salt Solution
[14] Reported as 0.32ng/50μL aliquot of thalidomide in HBSS

Analyte, ISTD	Biological Matrix	Sample Storage & Clean up	Analytical Method	Run Time	Sensitivity	% Recovery	Author Date	Ref
Thalidomide Phenacetin	Human serum (0.5mL)	Protein precipitation, using trichloroacetic acid	**HPLC-UV** Discovery C18 (125 x 4.6mm, 5uM), 75% MeOH/0.1M potassium dihydrogenphate[15] pH3	> 16 mins	LOQ: 0.222 mg/L	79%-84%	Toraño 1999	[274]
Thalidomide enantiomers Labetalol	Plasma (1mL)	1:1(v/v) 0.025M phosphate buffer, pH2.5 SPE	**HPLC-UV** Bioptic[16] (150 x 4.5mm) 2-propanol: 0.1M phosphate buffer, pH4, (2:98, v/v)	13 mins	Not specified	Not specified	Haque 1998	[272]
Thalidomide Phenacetin	Human serum (0.5mL)	10% H_2SO_4 (7.4μL) in 500μL serum, -35°C	**HPLC-UV** Nova-Pak C18 (300 x 3.9, 4μm), Gradient elution consisting of water, ACN, and NaH_2PO_4 buffer, 0.5 M, pH 3.0.	20 mins	LOQ: 50ng/mL	Not specified	Simmons 1997	[280]

---

[15] pH adjusted with 43% phosphoric acid solution
[16] Racemic analysis

Analyte, ISTD	Biological Matrix	Sample Storage & Clean up	Analytical Method	Run Time	Sensitivity	% Recovery	Author Date	Ref
Thalidomide Ciprofloxin	Plasma of ENL[17] patients (1mL)	SPE[18]	**HPLC-UV** Nucleosil C8 (150x4.6mm, 5μm) 0.01M potassium dihydrogen phosphate 21% ACN (v/v) 4.5mM Heptane sulfonic acid pH2.3[19]	~20 mins	LOQ: 0.0625 mg/L	79.5%	Delon 1995	[281]
Thalidomide Phenacetin	Rat plasma and blood (0.2-2mL)	1:1 (v/v) 0.025M Sörensen's citrate buffer, pH 1.5, -25°C LLE (Diethyl –ether)	**HPLC-UV** LiChromart RP-C18 (250x4mm 7μm) ACN :water (35:65)	> 6 mins	Not specified	Plasma 93% Blood- 87%	Eriksson 1992	[282]

Table 1-8 details the validated analytical methods of the quantification of thalidomide. The method highlighted in yellow has been developed within this thesis.

---

[17] Erythema nodusum leprosum
[18] No reference is made to stabilising the samples to avoid hydrolytic degradation
[19] Adjusted with concentrated orthophosphoric acid

1.11.6.   Aims of thesis

The aims of this thesis were

- To develop an analytical method for the quantification of pharmacokinetically relevant concentrations of dasatinib and lapatinib in cells.

- To explore to the applicability of LC-MS/MS for the quantification of multiple tyrosine kinase inhibitors.

- To use this analytical method to explore the interaction of dasatinib with ABC transport proteins P-gp, BCRP and MRP-1.

- To explore the interaction of lapatinib with P-gp and to determine if lapatinib inhibition of P-gp is as a competitive substrate.

- To examine the interaction of lapatinib with BCRP and MRP-1.

- To develop an analytical method for the quantification of thalidomide levels in serum.

- To assess the thalidomide levels in a multiple myeloma patients.

SECTION 2.0 Materials and methods

2. Materials and methods

2.1. *Cell culture methodology*

The following materials and equipment were used for all cell culture based experiments in this thesis.

2.1.1. Cell culture reagents

- Cell culture media, DMEM: HamsF12 50:50 (D8437), MEM (M5656), RPMI 1640 (R8758), DMEM (D5671), EDTA (E9884), DMSO (D5879), *p*-nitrophenol phosphate, (1040), Triton-X-100 (CAS #9002-93-1), NaOH (S5881) were purchased from Sigma, Dublin, Ireland.
- L-Glutamine, 200mM 100X, (25030), Trypsin 10X, (043-05090) Na-Pyruvate, 100mM (11360) and Non Essential Amino Acids (NEAA) 100X (11140) were purchased from Gibco
- PBS, Oxoid, BR0014
- Foetal Calf Serum (FCS), (DE14-801F) was purchased from Biowhittaker, The same batch of serum was used for all cell culture experiments (Lot #7SB0015).

2.1.2. Cell culture solutions

- PBS: PBS solution was prepared as 1 tablet in 100mL of UHP water and autoclaved
- Sodium Acetate Buffer: 0.1M sodium acetate, 0.1% (v/v) triton-X-100 pH 5.5
- Phosphatase Substrate: 10mM p-nitrophenol phosphate solution in 0.1M sodium acetate
- 1N NaOH: 40g/L NaOH in UHP
- EDTA, 1%(w/v) solution in UHP, autoclaved
- 1X trypsin: 50mL of 10X trypsin and 10mL of 1% EDTA solution was added by filtration to 440mL of sterile PBS.

2.1.3. Cell culture equipment

- Cytoguard laminar airflow cabinet, Holten LaminAir Maxisafe,
- Sterile universal container, Sterilin, 128a
- 96-well plates, Costar, 3599
- Cell-culture flasks: T75cm², T25cm² vented and non vented flasks were purchased from Corning
- Cryovials, Greiner
- Disposable Haemocytometer Fast Read 102, Immune Systems Limited, BVS100

2.1.4. Cells, cell culture and aseptic technique

Cell culture procedures were strictly adhered to as outlined in NICB Cell Culture SOPs, [#001-01, #002-01 and #003-01]

All cell culture work was carried out in a class II laminar airflow cabinet. All experiments involving cytotoxic compounds were conducted in a cytoguard laminar airflow cabinet. Before and after use, the laminar airflow cabinet was cleaned with 70% industrial methylated spirits (IMS). Any items brought into the cabinet were also swabbed with IMS. Only one cell line was used in the laminar airflow cabinet at a time and upon completion of work with any given cell line, the laminar airflow cabinet was allowed to clear for at least 15 minutes before use. This was to eliminate any possibilities of cross-contamination between cell lines. The cabinets were cleaned weekly with industrial disinfectants (Virkon, Antech International, P0550). Details pertaining to the cell lines used for the experiments detailed in this thesis are provided in Table 2-2. All cells were incubated at 37°C with an atmosphere of 5% CO2. Cell lines such as DLKP and DLKP-A did not have any CO_2 requirement. Cells were fed with fresh media or sub-cultured every 2-3 days in order to maintain active cell growth.

2.1.4.1.   Cell-lines

Table 2-1 outlines the details and sources of all cell-lines used in this thesis. Table 2-2 outlines the media and growth requirements for all cell-lines

Table 2-1: Details of cell-lines used

Cell Line	Details	Source
DLKP	Non-small lung cell carcinoma[283]	NICB
DLKP-A	Lung, adriamycin resistant variant of DLKP, selected by Alice Redmond.[284]	NICB
DLKP-Sq	Poorly differentiated. squamous cell lung carcinoma, established by Shirley McBride[285]	NICB
DLKP-Sq/Mitox-BCRP	Squamous cell lung carcinoma resistant variant of DLKP-Sq, selected with mitoxantrone, selected by Helena Joyce	NICB
DLKP-Sq/Mitox-MDR	Squamous cell lung carcinoma resistant variant of DLKP-Sq, selected with mitoxantrone, selected by Helena Joyce	NICB
A549	Lung adenocarcinoma	ECACC
A549-tax	Lung, a taxol resistant variant of A549, selected by Laura Breen. [286]	NICB
HL60/S	Acute myeloid leukaemia cells[287, 288]	ECACC
HL60/Adr	Acute myeloid leukaemia cells, adriamycin selected.[288]	Melvin Centre, Kansas State University
HL60/Mdr1	Acute myeloid leukaemia cells; Mdr1 transfected	Balazs Sarkadi, Hungary
HL60/Mxr	Acute myeloid leukaemia cells; MXR transfected	Balazs Sarkadi, Hungary
RPMI-2650/Tax	nasal septum carcinoma, variant selected at NICB (Yizheng Liang) by exposure to increasing conc. of taxol (final conc. 200ng/ml) over 6 months[289]	NICB
NCI –Adr/Res	Ovarian; Adriamycin-selected	NCI
2008/MRP-1	human ovarian carcinoma transfected to over-express MRP-1 which is predominantly localized in the plasma membrane [290]	NCI
KB-3-1	Cervical; KB-3-1 is a subclone from KB cells, which is a HeLa derivative[291].	Prof Gottesman, NCI
KB-8-5-11	Resistant variant of KB-3-1 developed with Colchicine[291]	Prof Gottesman, NCI
IGROV-1CDDP[20]	Resistant variant of IGROV-1, epithelial ovarian carcinoma, cisplatin selected[292]	Dr Britta Stordal/ Prof Jan Schellens

NICB: National Institute for Cellular Biotechnology, DCU, Dublin, Ireland

NCI: National Cancer Institute, Bethesda USA

ECACC, European Collection of Animal Cell Cultures, Salisbury, Wiltshire, UK.

---

[20] IGROV-1CDDP cell-line was used in collaboration with Dr Britta Stordal

Table 2-2: Cell-lines used and their growth requirements

Cell Line	Basel media	(%) FCS	CO_2	Additives
DLKP	DMEM*: Hams F12 50:50	5	Non-CO_2	-
DLKP-A	DMEM: Hams F12 50:50	5	Non-CO_2	-
DLKP-Sq	DMEM: Hams F12 50:50	5	Non-CO_2	-
DLKP-Sq/Mitox/ MDR	DMEM: Hams F12 50:50	5	Non-CO_2	-
DLKP-Sq/Mitox/ BCRP	DMEM: Hams F12 50:50	5	Non-CO_2	-
A549	DMEM: Hams F12 50:50	5	CO_2	-
A549-tax	DMEM: Hams F12 50:50	5	CO_2	-
HL-60/S	RPMI	10	CO_2	-
HL-60/Adr	RPMI	10	CO_2	-
HL-60/Mdr1	RPMI	10	CO_2	-
HL-60/Mxr	RPMI	10	CO_2	-
RPMI-2650/Tax	MEM	10	CO_2	1% L-glutamine 1% Na Pyruvate 1% NEAA
NCI –Adr/Res	RPMI	10	CO_2	
KB-3-1	DMEM	10	CO_2	2% L-glutamine 1% Na Pyruvate
KB-8-5-11	DMEM	10	CO_2	2% L-glutamine 1% Na Pyruvate
2008/MRP-1	RPMI	10	CO_2	
IGROV-1CDDP	RPMI	10	CO_2	

DMEM: Dulbecco's Modified Eagle's Medium

NEAA: Non Essential Amino Acids

2.1.5. Basic culture techniques

2.1.5.1.   *Sub-culturing of cell lines*

The waste cell culture medium was removed from the tissue culture flask to a sterile bottle. For anchorage-dependent cell lines, the flask was rinsed with 1mL of 1X trypsin solution to ensure the removal of any residual media. A volume of 2mL of trypsin was then added to the flask and was incubated at 37°C for the required period of time until all cells were detached from the inside surface of the culture flask. The trypsin was deactivated with an equal volume of complete media. The cell suspension was removed from the flask and placed in a sterile universal container and centrifuged at 200g for 5 minutes. The supernatant was then discarded from the universal and the pellet was suspended in complete medium. A cell count was performed. An aliquot of cells was then used to re-seed a flask at the required density with fresh media.

For the sub culturing of suspension cell-lines the use of trypsin was not required.

2.1.5.2.   *Cryopreservation of cells*

Cells for cryopreservation were harvested in the log phase of growth. Cell pellets were resuspended in a suitable volume of FCS. An equal volume of a 10-20% DMSO/FCS solution was added drop-wise to the cell suspension. A total volume of 1mL of this suspension was then placed in a cryovial. These vials were then placed in the vapour phase of a liquid nitrogen container, which was equivalent to a temperature of -80°C. After a period of three hours, vials were removed from the vapour phase and transferred to the liquid phase for storage (-196°C).

2.1.5.3.   *Thawing of cryopreserved cells*

A volume of 5mL of fresh warmed growth media was added to a sterile universal. The cryopreserved cells were removed from the liquid nitrogen tank and thawed rapidly at 37°C. The cells were removed from the vials and transferred to the media aliquot. The resulting cell suspension was centrifuged at 200g for 5 minutes. The supernatant was removed and the pellet resuspended in fresh culture medium. Thawed cells were then added to an appropriately sized tissue culture flask with a suitable volume of fresh growth media.

2.1.5.4.   *Sterility monitoring of cell culture solutions*

Sterility testing was performed on all cell culture media and related culturing solutions. Samples of prepared basal media were incubated at 37°C for a period of seven days. This ensured that no bacterial or fungal contaminated media was used.

2.1.5.5.   *Mycoplasma analysis of cell lines*

Cell lines were tested for possible mycoplasma contamination in house by Mr. Michael Henry, according to the SOP 007-01.

2.1.6. Safe handling of cytotoxic drugs

Cytotoxic drugs were handled with extreme caution at all times in the laboratory, due to the potential risks in handling them. Disposable nitride gloves were worn at all times and all work was carried out in cytotoxic cabinets. All drugs were stored in a safety cabinet at room temperature or in designated areas at 4°C. All agents were disposed of by incineration.

2.1.7. In vitro proliferation assays

2.1.7.1.   *In-vitro toxicity assay for anchorage-dependant cell lines*

Cells in the exponential phase of growth were harvested by trypsinisation (Section 2.1.5.1.). Cell suspensions contain 1×10^4 cells/mL in the appropriate culture medium were aliquoted at 100μL/well in 96-well plates using a multichannel pipette. Plates were gently agitated in order to ensure an even dispersion of cells over the well surface area. Cells were incubated overnight at 37°C and 5% CO_2. Test drug dilutions were prepared a 2X their final concentration in cell culture medium. Volumes of the drug dilutions (100μL) were then added to each well using a multichannel pipette. Plates were then mixed gently as above. Cells were incubated for a further 6-7 days at 37°C and 5% CO_2 until the control wells reached approximately 80-90% confluency. Assessment of cell survival in the presence of drug was determined by the acid phosphate assay (Section 2.1.7.3.). The concentration of drug which caused 50% cell kill (IC_{50} of the drug) was determined from a plot of the % survival (relative to the control cells) versus cytotoxic drug concentration.

2.1.7.2.   Combination toxicity assays

As described in Section 2.1.7.1, plates were seeded at 1 x 10^4 cells/mL and incubated overnight at 37^0C and 5% CO_2. Cytotoxic drug dilutions, tyrosine kinase inhibitor (TKI) drug dilutions, and inhibitor drug dilutions were prepared at 4X of their final concentration in media. Volumes of 50μL of the drug dilution and 50μL of the TKI dilution were added to each relevant well. The final volume of each well was brought up to 200μL where necessary with drug-free media. Plates were then mixed gently as above. Cells were incubated for a further 6-7days at 37°C and 5%CO_2 until the control wells reached approximately 80-90% confluency. Assessment of cell survival in the presence of drug was determined by the acid phosphate assay (Section 2.1.7.3)

2.1.7.3.   Assessment of cell number – Acid Phosphatase Assay

Following the incubation period of 6-7 days, media was removed from the plates and disposed of. Each plate was washed with PBS and this was then removed. Efforts were made to ensure that no residual PBS remained in the wells as this would interfere with the final reading. To each well, 100μL of freshly prepared phosphatase substrate was added. Phosphatase substrate was prepared as described in Section 2.1.2. The plates were incubated in the dark at 37°C for up to 2 hours, monitoring colour development. The enzymatic reaction was stopped by the addition of 50μL of 1N NaOH. The plate was read in a dual beam plate reader at 405nm with a reference wavelength of 620nm (BIO-TEK®, Synergy HT).

2.1.8. Accumulation and efflux studies

2.1.8.1.   Accumulation assay in adherent cell-lines

The triplicate T25cm^2 flasks were seeded with 5 mL of 5 x 10^4 cells/mL and allowed to attach overnight. The cells were exposed to the desired concentration of agent, prepared in complete media and incubated at 37°C with 5% CO_2 for the desired time. After this period, the media was removed and the flasks were rinsed with 5mL of cold PBS and 2mL of trypsin was added. The cells were allowed to detach over a period of 5 minutes. Once the cells detached the trypsin was deactivated with 2mL of complete media and the cells suspension was placed in a non-sterile extraction tube. The samples were centrifuges at 200g for 5 minutes. The supernatant was carefully removed and the cell

pellet was resuspended in 1mL of PBS. At this stage 50μL of the cell suspension was removed for cell count analysis by Guava flow cytometry. Alternatively 9μL of cell suspension was removed and counted in a haemocytometer Fast Read 102 (Immune Systems Limited).

The samples were centrifuged again and the supernatant was carefully removed again and the cell pellets in the extraction tubes were frozen at -20°C until required.

In the case of thalidomide accumulation studies, cell pellets were stored in 50μL of 25mM citrate buffer, pH 1.5, (as detailed in Section 2.2.3.2).

2.1.8.2.   *Efflux in adherent cell-lines*

The triplicate T25cm^2 flasks were seeded with 5 mL of 5 x 10^4 cells/mL and allowed to attach overnight. Following the overnight period, the cells were exposed to a concentration of tyrosine kinase inhibitor for 2 hours. After 2 hours, the drug was removed and the cells were rinsed with 5mL PBS. The control flasks were trypsinised at this point. Dependant on experimental requirements, 5mL of warmed media or 5mL of warmed media with MDR inhibitor was then added to the remaining flasks and these were returned to the incubator for the required time periods. Cell pellets were prepared from the remaining flasks as described.

In the case of thalidomide efflux studies, cell pellets were stored in 50μL of 25mM citrate buffer, pH 1.5, (as detailed in Section 2.2.3.2).

2.1.8.3.   *Accumulation in suspension cell-lines*

As in Section 2.1.8.1, triplicate T25cm^2 flasks seeded with 5mL of 5x10^4 cells/mL. The TKI was prepared in cell culture medium to 2X the final required concentration and 5mL of the drugged media was added to each flask and incubated for 2 hours. Following incubation the cell suspension was pipetted to a non-sterile extraction tube. The samples were centrifuged at 200g for 5 minutes, the supernatant was removed and the cell pellet was washed with 5mL of cold PBS. The samples were centrifuged at 200g for 5 minutes. The supernatant was carefully removed and the cell pellet was resuspended in 1mL of PBS. At this stage, 9μL of the cell suspension was removed for cell count.

2.1.8.4.   *Efflux in suspension cell-lines*

Triplicate T25cm^2 flasks were seeded with 5mL of 5 x 10^4 cells/mL. Following the overnight period the cells were exposed to a concentration of tyrosine kinase inhibitor for 2 hours. After 2 hours samples were pipetted into extraction tubes and centrifuged at 200g for 5mins.   The supernatant media was removed; the cell pellet was reconstituted in 4mL of PBS and centrifuged again at 4000rpm for 5 minutes. At this stage, the control samples were taken and counted.   Drug-free media or media containing the appropriate MDR inhibitor was added to the cell pellets at this stage and the samples returned to the incubator for a further 30, 60, 90 or 120 minutes. After this further incubation period had elapsed, samples were centrifuged and the supernatant media removed.   The cell pellet was reconstituted in 1mL of PBS and an aliquot removed for counting.

2.2. Analytical methodology

The following materials and methods were used in relation to analytical methodologies.

2.2.1. Extraction and LC-MS reagents

- Lapatinib ditosylate (SRP01211l), dasatinib (SRP00930d), gefitinib (SRP01240g), erlotinib HCl (SRP01331e), imatinib mesylate (SRP00530i), sorafenib tosylate, (SRP01590s) lenalidomide (SRP016751l), and bortezomib (SRP02310b), were purchased from Sequoia Chemicals, Pangbourne, UK.

- Water MS grade (39253), acetonitrile MS grade (34967), propan-2-ol MS grade (34965), formic acid ammonium salt (ammonium formate) (F2004), formic acid (33015), tert-butyl methyl ether (*t*BME) (34875), 1-chlorobutane (34958), human serum (S7023), thalidomide (T144) were purchased from Sigma-Aldrich, Dublin.

- Chloroform (C05C11X), dichloromethane (C10A11X), and ethyl acetate (C13C11X) were purchased from Fischer Scientific Ireland.

Details of all the drugs used during the course of this project including storage and disposal conditions are given in Appendix I

2.2.2. Extraction and LC-MS equipment

- LC system: 1200 Series Rapid Resolution LC

- MS system: 6410 Series Triple Quadrupole LC/MS

- Genevac EZ-2 evaporator, Ipswich, UK

- Blood-tube mixer: Stuart Scientific, UK

- Glass pastuer pipette: 2mL 150mm glass pastuer pipettes (612-1701), VWR, Ireland

- Extraction tubes: 10mL PPE tubes, VWR, Ireland

- LC vials: 1.1 mL, conical bottomed, Chromacol vials purchased from Fisher Scientific, Ireland.

- pH meter: Jenway 3320, instrument was calibrated before each use.

- LC-columns were purchased from Phenomenex UK, Agilent UK and Apex Scientific, Maynooth, Ireland.

Table 2-3: Chromatography columns used is this thesis

Column Name	Dimensions	Packing Material	Particle Size	Application	Source
SynergSi Hydro	150mm x 2.0mm	C18	4μm	TKI optimisation	Phenomenex, UK
Hyperclone	150mm x 2.0mm	C18	3μm	**TKI separation - validated**	Phenomenex, UK
Hyperclone	150mm x 4.6mm	C18	3μm	TKI optimisation	Phenomenex, UK
Prodigy	150mm x 2.0mm	C18	5μm	**Anthracycline separation - validated** also Thalidomide-Umbelliferone optimisation	Phenomenex, UK
Prodigy	150mm x 4.6mm	C18	5μm	**Thalidomide-Umbelliferone - validated**	Phenomenex, UK
Agilent XBD	50mm x 4.6mm	C18	1.8μm	Thalidomide-Umbelliferone optimisation	Agilent, UK
Agilent Eclipse	150mm x 4.6mm	C18	5μm	Thalidomide-Umbelliferone optimisation	Agilent, UK
ZORBAX SB	150mm x 2.1mm	Phenyl	5μm	Thalidomide-Umbelliferone optimisation	Agilent, UK
YMC-UltraHT	50mm x 2.0mm	C18	2μm	Thalidomide/ Lenalidomide optimisation	Apex Scientific, Ireland

2.2.3. Extraction and LC-MS solutions

2.2.3.1.   *Dasatinib - lapatinib quantification*

- Stock solutions: All TKIs (lapatinib, dasatinib, erlotinib, gefitinib, imatinib, sorafenib) were prepared at 50μg/mL in ACN and stored at -20°C. Day stocks were prepared at 10μg/mL in ACN.

- 10mM Ammonium formate, pH 4: Ammonium formate was accurately weighed (630.6mg) and added to 800mL of LC-MS grade water. Formic acid was added drop-wise to adjust the pH4. The volume was then adjusted to 1L.

- Lapatinib and dasatinib mobile phase: 540mL of ACN and 460mL of 10mM ammonium formate measured separately and mixed.

- 1M ammonium formate pH 3.5 extraction buffer: 31.5g of ammonium formate was dissolved in 400mL water. The pH was adjusted to pH3.5 using formic acid. The volume was then adjusted to 500mL.

- Lapatinib/dasatinib extraction solvent: *t*BME/ACN, 3/1 v/v

- Lapatinib internal standard: 500ng/mL lapatinib in ACN, prepared fresh from the day stock

- Dasatinib internal standard: 500ng/mL dasatinib in ACN, prepared fresh from the day stock

2.2.3.2.   *Thalidomide quantification*

- Primary stock solutions of thalidomide, lenalidomide and umbelliferone were prepared at 1mg/mL in ACN and stored at -20°C

- Working stock solutions were prepared fresh daily to a concentration of 100μg/mL in acetonitrile of thalidomide and 10μg/mL of umbelliferone

- Umbelliferone internal standard: 600ng/mL prepared fresh from 10μg/mL working stock in ACN

- Citrate buffer, pH1.5: 25mM (7.35g/L) sodium citrate in water (MS grade), pH adjusted with HCl to 1.5

2.2.3.3.   Anthracycline quantification

- Mobile Phase: To 720 ml of MS grade water, 720μL of formic acid was added. The pH was very carefully adjusted to pH 3.2 using concentrated ammonium formate (300 mg/ml, in MS grade water). Finally, 280 mL of MS grade acetonitrile was added and the bottle was gently shaken to mix.

- Extraction buffer: 1MAmmonium formate, pH8.5, aliquoted and stored at -20°C

- Internal standard: Daunorubicin 200ng/mL in water

- Silver nitrate: Prepared as 33% (w/v) in water and stored at -20°C, wrapped in tinfoil.

2.2.4. Flow injection analysis

Flow injection analysis was used to identify the precursor ion and products ions as well to optimise the fragmentor voltage and collision energy for each transition. Pure drug was prepared at 250ng/mL in ACN. For the determination of the precursor ion, 10μL were injected six times using an injector program. For the determination of the optimum fragmentor voltage, product ion and optimum collision energy for each transition, the injection volume was changed to 5μL. The sample was injected twice at each condition.

2.2.5. Dasatinib and lapatinib quantification

2.2.5.1.   Liquid-liquid extraction procedure

To the cell pellet, 100μL of 500ng/ml internal standard was added. Dasatinib 500ng/mL was used as the internal standard for lapatinib and conversely, 500ng/mL lapatinib was used as the internal standard for the quantification of dasatinib. Also 200μL of 1M ammonium formate pH 3.5 buffer and 1.6mL of extraction solvent tBME/ACN (3:1) was added to the cell pellet. The extraction tubes were vortexed and mixed on a blood tube mixer for 15 minutes. The samples were centrifuged at 3200g for 5 minutes; the organic layer was removed with a glass pasteur pipette and 1.1mL of solvent was transferred to conical bottomed glass LC autosampler vials. The vials were evaporated to dryness using a Genevac EZ-2 evaporator at ambient temperature, without light. The samples were reconstituted in 40μL of acetonitrile with 20μL injected automatically by the autosampler

2.2.5.2. Preparation of standard curve

To an extraction tube, 50µL of cell suspension in water was added, as well as 100µL of 500ng/mL internal standard and 100µL of analyte varying in concentration from 1ng/mL to 2000ng/mL. Samples were extracted as outline in Section 2.2.5.1. Each concentration point was extracted in triplicate. Samples were analysed by LC-MS at intervals during the sample run time.

2.2.5.3. Preparation of recovery samples

Recovery samples were used to determine the extraction efficiency of an extraction system. Two types of recovery samples are used in this thesis.

"Calculated" recovery samples were prepared by calculating the mass of analyte injected and preparing this concentration of analyte in a 2X concentration and adding to a 2X concentration of the internal standard. As an example, 100µL of 100ng/mL of dasatinib was added to an extraction tube. This was a mass of 10ng in the tube. A volume of 1.6mL of extraction solvent and 100µL of internal standard was added to the tube. A volume of 1.1mL of solvent was removed and dried down. Assuming 100% recovery of the analyte in the solvent the mass of the analyte in the vial was 6ng (1.1/1.8*10). The sample was reconstituted in 40µL and 20µL was injected. This equated to 3ng on column. This was 3ng in 20µL equates to 150ng/mL. A 2X of this is prepared and mixed with a 2X of the internal standard. Samples are dried down and reconstituted and injected.

"No matrix" recovery samples were prepared in a manner similar to the standard curve. Extraction tubes were spiked with analyte and internal standard, however, no cell pellet was added to the extraction tube. Samples were extracted as outlined in Section 2.2.5.1.

2.2.5.4. System standard preparation

A 10mL solution of lapatinib 100ng/mL and 100ng/mL dasatinib was prepared in acetonitrile and divided into 200µL aliquots. Aliquots were stored at -20°C. A system suitability standard was analysed before each run to verify the instrument was operating as normal. During the analysis of a batch of samples, system standards and mobile phase blanks were run at intervals to identify any potential instrumentation errors.

2.2.5.5.   *Chromatographic and mass spectrometric conditions*

Chromatographic separation was achieved using a Hyperclone BDS C18 column (150mm×2.0mm i.d., 3μm particle size) with a SecurityGuard C18 guard column (4mm×3.0mm i.d.) both from Phenomenex, UK, though if available a small diameter guard column should be used. An optimised mixture of acetonitrile−10mM ammonium formate pH 4 (54:46, v/v) was used as mobile phase, at a flow rate of 0.2mL/min. The column temperature was maintained at 20°C and the temperature of the autosampler was maintained 4°C. The complete chromatographic run time of each sample was 10 minutes, which separated dasatinib and lapatinib from each other with retention times 2.3 and 5.1 minutes respectively. Peaks were quantified using Agilent Masshunter Software (Version B.01.04).

The mass spectrometer was operated using an ESI source in the positive ion detection mode. The ionisation temperature was 350°C, gas flow rate was 11L/min and nebulizer pressure was 345kPa. Nitrogen was used as the ionisation source gas and ultrapure nitrogen, the collision cell gas.

Analysis was performed using MRM mode with the following transitions: m/z 581→m/z 365 for lapatinib, and m/z 488→m/z (231 and 401) for dasatinib, with a dwell time of 200ms.

Quantification was based on the integrated peak area as determined by the Masshunter Quantification Analysis software which quantitates the peak areas of the MRM transitions of each analyte. Table 2-4 details the transitions optimised for all TKIs used in this thesis, * indicates quantifier ion.

Table 2-4: Summary of MRM transition conditions for TKIs

Name	Precursor Ion	Optimum Fragmentor Voltage	Product Ion	Optimum Collision Energy
Dasatinib	488	120	401*	30
			231	50
Lapatinib	581	200	365*	40
Gefitinib	447.2	160	128*	30
Erlotinib	393.9	160	278*	35
			336	25
Imatinib	494.2	120	394*	25
			217	25
			99	30
Sorafenib	399.1	100	252*	35
			326	20

2.2.6. Thalidomide quantification

2.2.6.1.   Sample handling

A blood sample of 10 mL of was collected in additive free blood tubes and the blood was allowed to clot for 30 minutes to 1 hour. The clinical specimens were then transported from the Mater Hospital to NICB. All blood samples were collected under the full ethical approval of the hospital Ethics committee. In the lab, the non-clotted serum was transferred into a 15mL Falcon tube and spun down @400g, 30min at 4°C. An aliquot of serum supernatant was mixed 1/1 (v/v) with 25mM citrate buffer pH1.5 in extraction tubes. Samples were frozen at -80°C until extracted.

2.2.6.2.   Liquid-liquid extraction procedure

A 200μL aliquot of sample (serum: citrate 1:1, v/v) was added to a polypropylene extraction tube. To this, 50μL of internal standard (600ng/mL umbelliferone) was added, along with 50μL of acetonitrile and 2mL of extraction solvent (ethyl acetate/ACN, 3:1, v/v). The extraction tubes were vortexed and mixed on a blood tube mixer for 5 minutes. The samples were centrifuged at 3200g for 5 minutes. The 1.1mL of the organic layer was removed with a glass pasteur pipette and transferred to a conical bottomed glass LC autosampler vial (Chromacol). The vials were evaporated to dryness using a Genevac EZ-2 (Ipswich, UK) evaporator at ambient temperature, without light. The samples were reconstituted in 50μL of mobile phase. Two injections of 20μL were injected automatically by the autosampler.

2.2.6.3.   Standard curve preparation

Human serum was mixed with citrate buffer, pH1.5, (1/1, v/v) as a biological matrix. This was to mimic the collected patient samples as thalidomide is unstable at physiological pH[282].   Thalidomide standards were prepared fresh at drug concentration of 40, 20, 10, 2, 1 0.2 and 0.1μg/mL in ACN. This equated to a serum concentration of 20, 10, 5, 1, 0.5, 0.1and 0.05μg/mL respectively.

A 200μL aliquot of serum/citrate was added to an extraction tube. To this, 50μL of internal standard, 50μL of thalidomide standard and 2mL of extraction solvent (ethyl acetate/ACN 3:1, v/v) was added. This was extracted as described in Section 2.2.6.2.

2.2.6.4.   *Chromatographic and mass spectrometric conditions*

Chromatographic separation was achieved using a Prodigy C18 column (150mm×4.0mm i.d., 5μm particle size) with a SecurityGuard C18 guard column (4mm×3.0mm i.d.) both from Phenomenex, UK. A mixture of acetonitrile: water (30:70, v/v) 0.1% formic acid was used as mobile phase, at a flow rate of 0.5mL/min. The column temperature was maintained at 20°C and the temperature of the autosampler was maintained at 4°C. The complete chromatographic run time of each sample was 13 minutes, which separated umbelliferone and thalidomide from each other with retention times of 7.9 and 9.3 minutes respectively. Peaks were quantified using Agilent Masshunter Software (Version B.01.04).

The mass spectrometer was operated using an ESI source in the positive ion detection mode. The ionisation temperature was 300°C, gas flow rate was 11L/min and nebulizer pressure was 345kPa. Nitrogen was used as the ionisation source gas and ultrapure nitrogen as the collision cell gas.

Analysis was performed in MRM mode with the following transitions: m/z 259.1→m/z (186 and 84) for thalidomide, and m/z 163.1→m/z 107 for umbelliferone, with a dwell time of 200ms. Both product ions of thalidomide were monitored, 84 m/z was the quantifier ion and 186 m/z was the qualifier ion. Table 2-5 details the transitions optimised for all multiple myeloma agents used in this thesis, * indicates quantifier ion.

Table 2-5: Summary of MRM transition conditions for multiple myeloma agents

Name	Precursor Ion	Optimum Fragmentor Voltage	Product Ion	Optimum Collision Energy
Thalidomide	259.1	120	84*	10
			186	25
Umbelliferone	163.3	130	107.1	20
Lenalidomide	260.1	90	187.2	25
			148.8*	15
			106	40
Bortezomib	367.2	130	226.3*	15
			208.1	30
			321.1	20

2.2.7. Anthracycline quantification

Epirubicin, was quantified according to the method published by Wall *et al.*[293]

2.2.7.1.   Extraction procedure

Frozen cell pellets were thawed in the dark, 200μL of water and 20 μL of 33% silver nitrate was added. The sample was vortexed. 100μL of the internal standard, daunorubicin, was added, followed by 700 μL ice cold isopropanol, 100μL ammonium formate buffer pH8.5. This mixture was mixed well before 1400μL chloroform was added using a glass pipette. The extraction tubes were mixed using a blood mixer for 5 minutes, and then they were centrifuged for 5 minutes at 3200g. A volume of 1.1mL of the organic layer was removed and placed in a glass vial. The vials were evaporated to dryness using a Genevac EZ-2 evaporator at ambient temperature, without light. The samples were reconstituted in 30μL of mobile phase with 20μL injected automatically by the autosampler.

2.2.7.2.   Standard curve preparation

A broad range of standards were prepared, ranging from 5000ng/mL to 1ng/mL. A cell pellet was spiked with 100μL of water, 100μL of epirubicin, 20μL of silver nitrate and 100μL of internal standard. Samples were extracted as described in Section 2.2.7.1.

2.2.7.3.   Chromatographic and mass spectrometric conditions

Chromatographic separation was achieved using a Prodigy C18 column (150mm×2.0mm i.d., 5μm particle size) with a SecurityGuard C18 guard column (4mm×3.0mm i.d.) both from Phenomenex, UK. Mobile phase (as described in Section 2.2.3.3) was run at a flow rate 0.25mL/min. The column temperature was maintained at 45°C and the temperature of the autosampler was maintained 4°C. The autosampler was operated with the light off. The complete chromatographic run time of each sample was 9 minutes, which separated epirubicin and daunorubicin from each other with retention times 4.2 and 7.4 minutes respectively. Peaks were quantified using Agilent Masshunter Software (Version B.01.04).

The mass spectrometer was operated using an ESI source in the positive ion detection mode. The ionisation temperature was 300°C, gas flow rate was 10L/min and nebulizer

pressure was 345kPa. Nitrogen was used as the ionisation source gas and ultrapure nitrogen as the collision cell gas.

Analysis was performed in MRM mode with the following transitions: m/z 544→m/z (397 and 86) for epirubicin, and m/z 528→m/z (321 and 363) for daunorubicin, with a dwell time of 200ms. All product ions were monitored; however, transition 544m/z →397m/z was for the quantification of epirubicin and the transition 528m/z →321m/z was used for the quantification of daunorubicin. Table 2-6 details the transitions for anthracyclines used in this thesis, * indicates quantifier ion.

Table 2-6: Summary of MRM transition conditions for anthracyclines

Name	Precursor Ion	Optimum Fragmentor Voltage	Product Ion	Optimum Collision Energy
Epirubicin	544	100	397*	10
			86	30
Daunorubicin	528	100	363	10
			321*	30

2.3. Statistical Analysis

Analysis of the difference of comparisons such as percentage survival calculated, mass of accumulated agents etc, were performed using a paired two-tailed student t-test (Excel® Microsoft).

* - p value of ≤ 0.05 was deemed significant

** - p value ≤ 0.01 was deemed more significant

*** - p value ≤ 0.005 was deemed highly significant

SECTION 3.0 Results and discussion

The development and validation of a quantification assay for dasatinib and lapatinib

3. The development and validation of a quantification assay for dasatinib and lapatinib

Introduction

Previous work carried out in our group has shown that lapatinib modulates the uptake of chemotherapeutics by inhibiting the action of the P-glycoprotein efflux protein (P-gp)[179]. To investigate if this inhibition was due to the action of lapatinib as a competitive substrate or through other mechanisms, it was necessary to develop a quantitative method. This method would be used for evaluating of the drug kinetic profiles within the cell and therefore to determine the role of MDR transport proteins on the uptake of lapatinib. To avoid the use of radio-labelled drugs our studies focus on mass spectrometry as quantification tool. Radio-labelled agents are frequently used in assays to determine the transport characteristics of the agent[58, 294]. However, the hazards associated with the use of radio-labelled material including exposure hazards, waste disposal issues and additional legislative requirements, make other methodologies preferable.

At the commencement of this body of work only one analytical LC-MS method for the quantification of lapatinib was published[200]. This method detailed a solid phase extraction (SPE) method, with a 75% recovery, to remove the analyte from the biological matrix.

Our aim was to develop a straightforward LC-MS method for the detection and quantification of lapatinib with an optimised and simplified extraction procedure, possibly using liquid-liquid extraction (LLE) as a sample clean-up step due to its compatibility with complex biological matrices.

3.1. LC separation

The optimisation of an LC separation is a process involving the adjustment of an array of parameters in a logical, sequential yet interwoven manner. The stationary phase (the column) the mobile phase and the internal standard are all under investigation.

The selection/identification of an appropriate internal standard is of crucial importance to the development of the method. The "gold standard" of internal standards is to use the deuterated form of the analyte of interest; however, this is frequently a prohibitively expensive approach. Alternative tyrosine kinase inhibitors were examined as potential internal standards.

With lapatinib as the primary focus dasatinib, gefitinib and erlotinib were evaluated as potential internal standards. Initial experiments focused on gefitinib as an internal standard, examining its separation from lapatinib on various columns.

3.1.1. Column optimisation

Preliminary investigation into the separation of lapatinib and a possible internal standard, gefitinib was performed on three columns, as outlined in Table 3-1. A buffer of 10mM ammonium formate pH4 was selected as mobile phase A (MPA) due to its compatibility with mass spectrometry, acetonitrile was used as mobile phase B (MPB). Initial separation was performed using gradient elution from 10%B to 100%B over 10 minutes. Using this as a starting point, an optimum mobile phase for isocratic separation was improved. This process was applied to all of the columns investigated.

Figure 3-1 is a representative chromatogram taken from the Beckman HPLC-UV system. These chromatograms show the effect of minor alterations of the percentage of mobile phase on the analyte retention. By increasing the ratio of organic to aqueous phase the peaks moved closer to each other and eluted faster, while the lower percentage acetonitrile causes both peaks to elute slightly later and give better baseline separation. The red trace shows elution of lapatinib and gefitinib with isocratic flow and a mobile phase composition of 78% (v/v) acetonitrile/10mM ammonium formate. The blue trace shows a lapatinib and gefitinib separation at 76% (v/v) acetonitrile/10mM ammonium formate.

Figure 3-1: Preliminary evaluation of separation of lapatinib and gefitinib
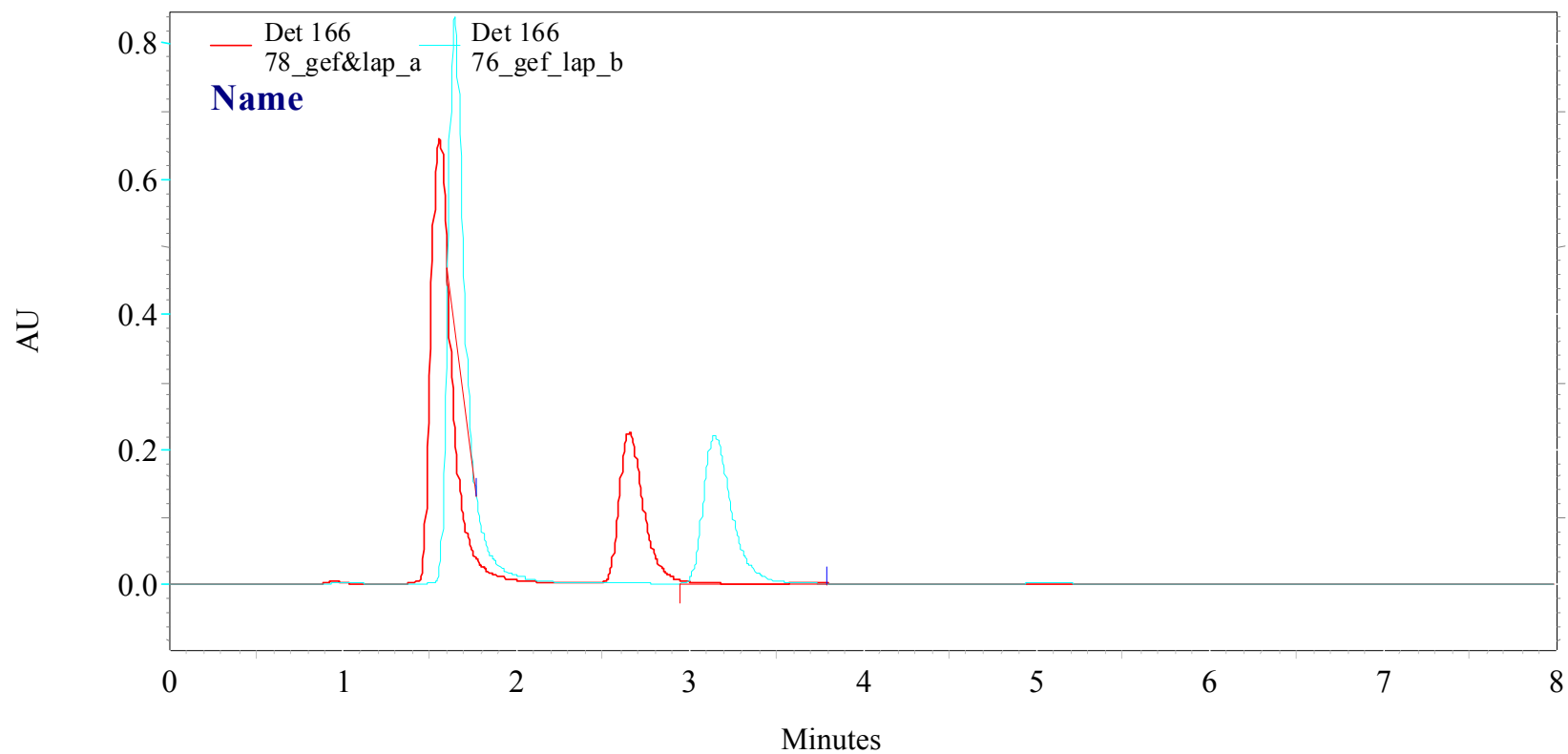
A representative chromatogram showing the separation of lapatinib and gefitinib on a SynergSi Hydro RP C18 column

At the higher ratio of acetonitrile, gefitinib eluted at 1.6mins while lapatinib had a retention time of 2.8 minutes. At the lower ratio of organic solvent in the mobile phase, 76% acetonitrile, gefitinib had a retention time of 1.8 minutes and lapatinib was eluted at 3.2 minutes.

Reverse phase chromatography is based on the partition of the analytes between a polar mobile phase and a non-polar stationary phase, normally C8 or C18. Octadecyl (C18 or ODS) columns are generally the first choice in the development of a new method and are used for the separation of moderately polar to polar solutes in the pharmaceutical industry, food analysis industry, pesticides and bio-analytics.

Table 3-1 shows the columns assessed and the separation conditions found to give the optimum separation of lapatinib and gefitinib. Each column was assessed by multiple injections of lapatinib and gefitinib in acetonitrile. Each column was equilibrated for a minimum of 10 column volumes with each alteration in mobile phase composition. Column #1 initially performed acceptably, however, on subsequent multiple injection a shift in retention times of both analytes was seen. Column #2 proved to have excellent separation of both gefitinib and lapatinib at 60% acetonitrile; however, column #3 was the most applicable column for the separation required as it gave equivalent separation to column #2 but due to a lower flow rate, lower volumes of solvents were required.

Column #1 initially performed acceptably, however, on subsequent multiple injection a shift in retention times of both analytes was seen. Column #2 proved to have excellent separation of both gefitinib and lapatinib at 60% (v/v) acetonitrile/10mM ammonium formate pH4 at 0.4mL/min. However, column #3 was the most applicable column for the separation required as it gave equivalent separation to column #2 but due to a lower flow rate, lower volumes of solvents were required

Table 3-1 Investigation of suitability of HPLC-C18 columns

#	Column Name	Stationary Phase	Particle Size	Column Size	Optimum Separation	Flow Rate	Comment
1	SynergSi Hydro RP	C18	4μm	150mm x 2.0mm	ACN:10mM Ammonium Formate pH4 (76:24)	0.4 mL/min	unsuitable
2	Hyperclone	C18	3μm	100mm x 4.6mm	ACN:10mM Ammonium Formate pH4 (60:40)	0.4 mL/min	suitable
3	Hyperclone	C18	3μm	150mm x 2.0mm	ACN:10mM Ammonium Formate pH4 (60:40)	0.2 mL/min	suitable

Table 3-1 gives the details of the of the columns used in the optimisation of the separation of gefitinib and lapatinib

3.1.2. Internal standard selection

Having determined the Hyperclone C18 150mm x 2.0mm 3μm particle size, to be the most applicable column for the separation it was then necessary to determine which tyrosine kinase inhibitor would potentially be the most applicable internal standard.

Table 3-2 compares dasatinib, erlotinib and gefitinib in terms of peak shape, separation, resolution and limit of detection by LC-MS. The asymmetry factor (AsF) of a peak is a measure of the peak shape and a means of measuring peak tailing. The perfect chromatographic peak has an asymmetry factor of 1 indicating that the peak is perfectly symmetrical; however, values up to 1.5 are generally acceptable. Peak asymmetry factor is calculated by bisecting the peak at the apex and measuring the peak width at 10% of the peak height, Figure 3-3. The peak width from the peak tail to the median is divided by the peak width from the peak front to the median. Tailing factor (TF), similar to asymmetry factor is a measure of peak shape. It is determined in a similar way but the peak width is measured at 5% of the peak height as opposed to 10% for peak asymmetry, Figure 3-2. Capacity factor (k'), also called the retention factor, is the fraction of sample compound distributed into the stationary phase divided by fraction in mobile phase. This is calculated by subtracting the column dead time (t_0) from the compound retention time (t_R), divided by the column dead time, Figure 3-4. Resolution (R_s) is a parameter which measures how well two adjacent peaks are separated, Figure 3-5.

The asymmetry of the gefitinib peak at 2.6 was greater than the maximum of 2. The resolution of all three combinations was good as there was clear baseline separation of the analytes.

Based on the AsF and TF, gefitinib was excluded from limit of detection (LOD) studies by LC-MS. Based on the separation, peak shape and LC-MS, LOD studies, dasatinib was selected as the appropriate internal standard for lapatinib. Table 3-2 details the AsF, TF k' and Rs for each separation.

Table 3-2 Assessment of internal standard

Drug	Asymmetry Factor $AsF = \dfrac{BC}{CA}$	Tailing Factor $TF = \dfrac{AB}{2AC}$	Capacity Factor $k' = \dfrac{t_R - t_0}{t_0}$	Resolution $Rs = \dfrac{(t_2 - t_1)}{\left(\dfrac{1}{2}\right)(W_1 + W_2)}$
Dasatinib	1.3	1.2	0.37	11.18
Erlotinib	1.0	1.2	0.86	7.63
Gefitinib	2.6	2.0	0.50	10.89

Asymmetry Factor, tailing factor, capacity factor and resolution were measured from HPLC-UV chromatograms.

Figure 3-2: Tailing Factor[295]

Tailing Factor

TF = AB / 2AC

A C B

5% OF PEAK HEIGHT

TIME →
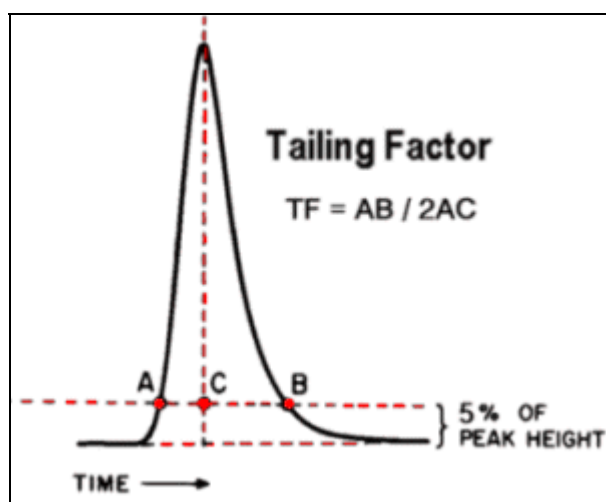
Tailing factor, a measure of peak tailing, is defined as the distance from the front slope of the peak to the back slope divided by twice the distance from the centre line of the peak to the front slope, with all measurements made at 5% of the maximum peak height.

Figure 3-3: Asymmetry Factor[295]

Asymmetry Factor:

AsF= BC/CA

A C B

10% OF PEAK HEIGHT

TIME →
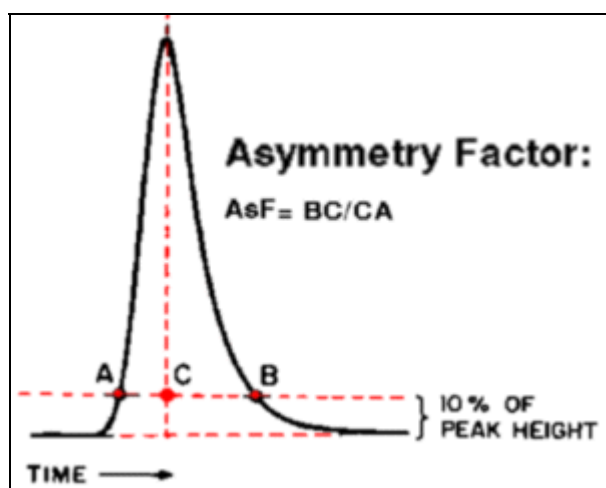
The asymmetry factor, a measure of peak tailing, is defined as the distance from the centre line of the peak to the back slope divided by the distance from the centre line of the peak to the front slope, with all measurements made at 10% of the maximum peak height.

Diagrams reproduced with the permission of the authors [295].

Figure 3-4: Capacity Factor (k')[295]

$$k' = (t_R - t_0) / t_0$$

$$k' = (t_R / t_0) - 1$$
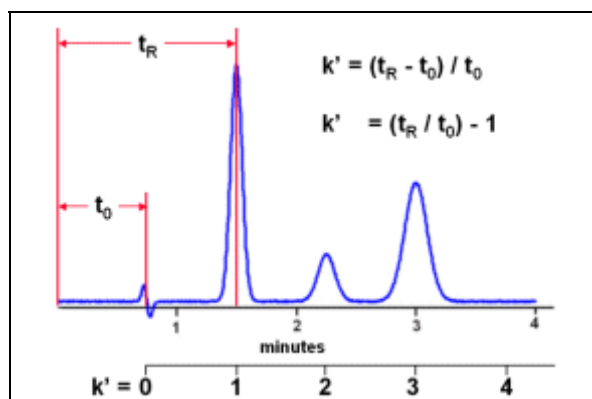
Capacity factor is a measure of the retention of a peak that is independent of column geometry or mobile phase flow rate. The capacity factor for a gradient elution cannot be calculated in this way.

Figure 3-5: Resolution (Rs)[295]

$$R_S = \frac{t_{R2} - t_{R1}}{0.5\,(w_{b1} + w_{b2})}$$
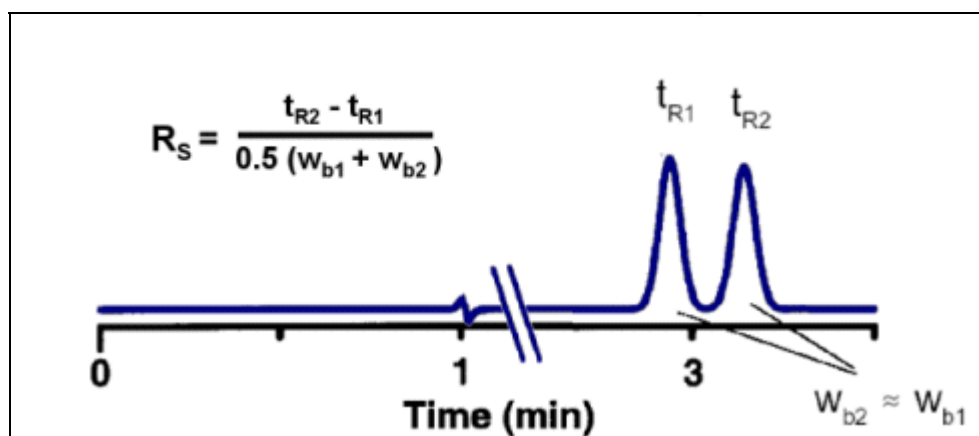
The resolution between two chromatographic peaks is a measure of how well they are separated

Diagrams reproduced with the permission of the authors [295].

3.2. Optimisation of extraction procedure

The method by Bai *et al*.[200], described a solid phase extraction step to remove lapatinib from the biological matrix. This method, however, was aimed at the extraction of lapatinib from plasma where our focus was on the extraction of lapatinib from cells. Due to the high binding affinity of TKI agents to intracellular targets, and the complex nature of cell culture samples, liquid-liquid extraction (LLE) was chosen in preference to other forms of drug extraction methods[210].

3.2.1. Solvent optimisation

A range of extraction solvents were examined. Figure 3-6 shows the recovery of 50ng of lapatinib and dasatinib using various solvents, ethyl acetate (EA), dichloromethane (DCM) and *t*-butyl methyl ether (*t*BME) alone and in combination with acetonitrile (ACN). Alone, *t*BME was the most efficient solvent for the extraction of lapatinib. DCM alone was the most efficient solvent for the extraction of dasatinib. However, the addition of ACN to the *t*BME extraction solvent improved the recovery across the solvent range, and the mixture of *t*BME: acetonitrile (3:1, v/v) gave the optimum recovery for both lapatinib and dasatinib.

Figure 3-6: Recovery of lapatinib and dasatinib with different extraction solvents
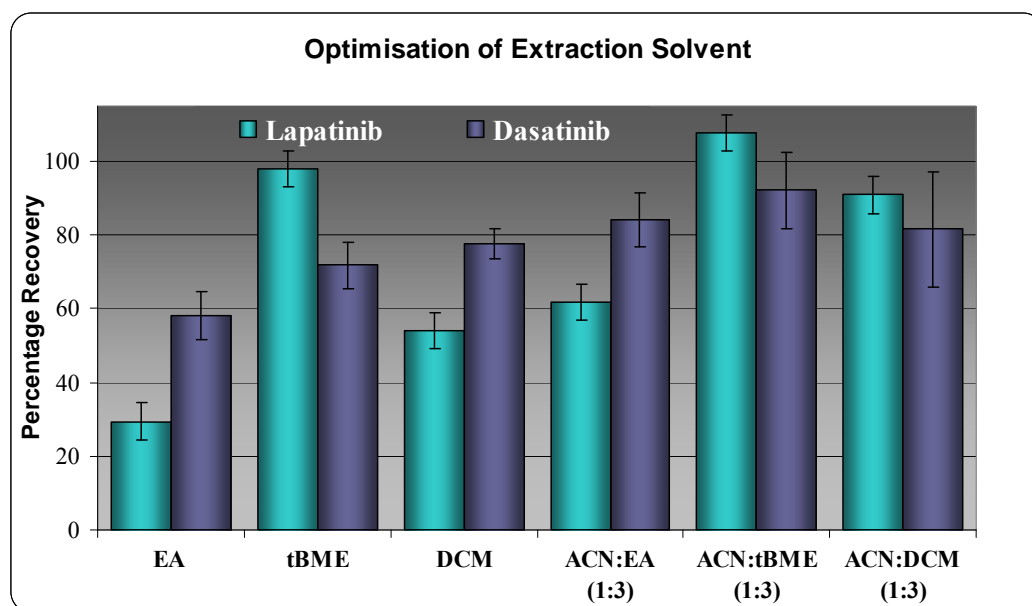
50ng of each analyte was extracted using a range of solvents and solvent mixtures. Results are presented as the average of triplicate estimates as a percentage of non-extracted samples calculated to equal 100% recovery.

3.2.2. Optimisation of extraction buffer pH

Liquid-liquid extraction is based on a partitioning of solutes between organic and aqueous solvents which are immiscible. Frequently the aqueous phase is a buffered solution. The extraction buffer controlled the pH of the extraction system and stabilised the system. The stability of a pH controlled environment allowed for reproducible extractions. Alterations in the extraction buffer pH may also increase or decrease the amount of confounding biological substances recovered[296].

Figure 3-7 shows the peak area of lapatinib and dasatinib for 50ng recovery across a range of pH buffered solutions.

Extraction buffer pH3.5 was selected as the most appropriate. While the pH3 buffer gave a better peak area, it also had greater standard deviations and thus greater inaccuracy, imprecision and irreproducibility.

At pH4 and above the recovery of lapatinib was dramatically reduced. Similarly but not to such an exaggerated extent, the recovery of dasatinib improved at lower pH buffer.

Figure 3-7: Effect of pH on lapatinib and dasatinib extraction

Effect of extraction buffer pH on lapatinib and dasatinib peak area
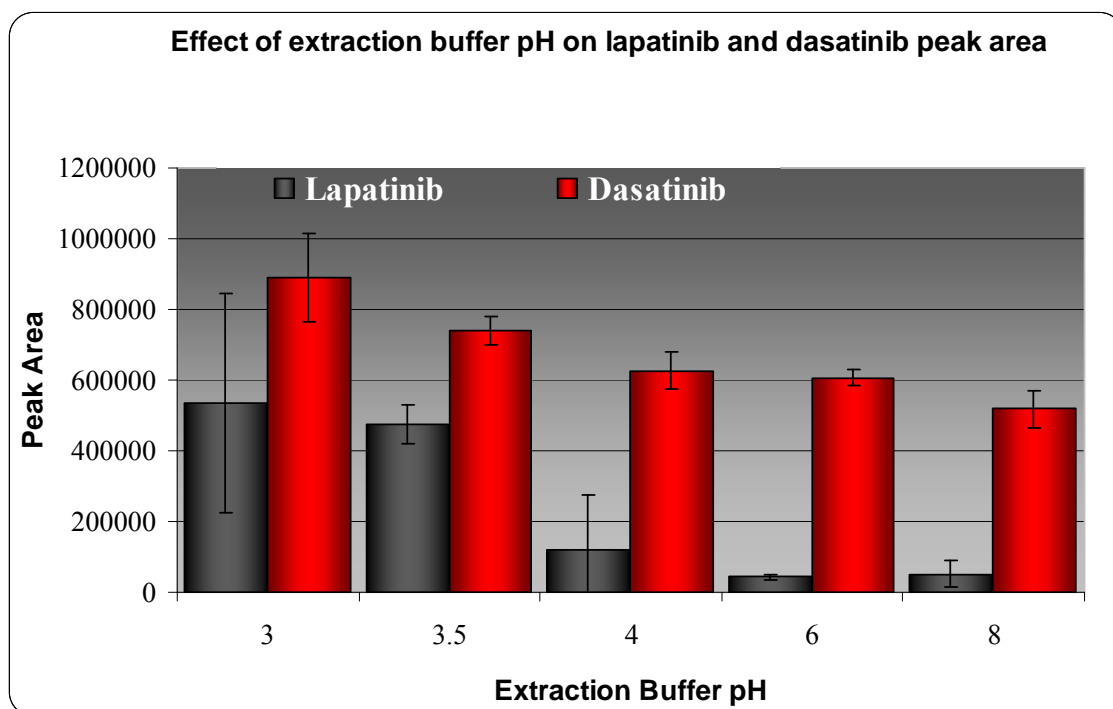
Representation of the peak areas of lapatinib and dasatinib when extracted with varying pH extraction buffer, the average and standard deviations of triplicate determinations

3.3. *Optimisation of mass spectrometry detection conditions*

Using flow injection analysis (FIA) the optimum multi-reaction monitoring (MRM) settings were determined for dasatinib and lapatinib, as well as for the additional tyrosine kinase inhibitors of interest. Table 3-4 gives the transitions from precursor to product ion as well as the optimum fragmentor voltage and optimum collision energy identified for each analyte. The quantifier ions are indicated in the table (asterisked), though all transitions were monitored with the qualifier ion which adds specificity.

Given in the sections below (3.3.1 – 3.3.4) is the development and optimisation of dasatinib for analysis by MRM. Optimisation was carried out by FIA of dasatinib at 250ng/mL, varying each condition sequentially.   The use of an injector program allowed for the multiple injection of the same compound, from the same vial, a defined number of times. This permits multiple injections to be viewed and analysed in one data file, which eliminates the majority of error associated with inter-injection variability.

The determination of the MRM transition of each TKI was carried out in a similar manner; dasatinib was selected as a representative sample.

3.3.1. Precursor ion determination

The precursor ion, also called the parent ion, is "an electrically charged molecular moiety which may dissociate to form fragments"[297]. These fragments may be charged or neutral moieties. Charged fragments can be detected, forming the basis of tandem mass spectrometry, and used to further identify the analyte. The precursor ion was determined by FIA of dasatinib, at 250ng/mL (10μL injected).

Figure 3-8: TIC of MS2Scan of dasatinib

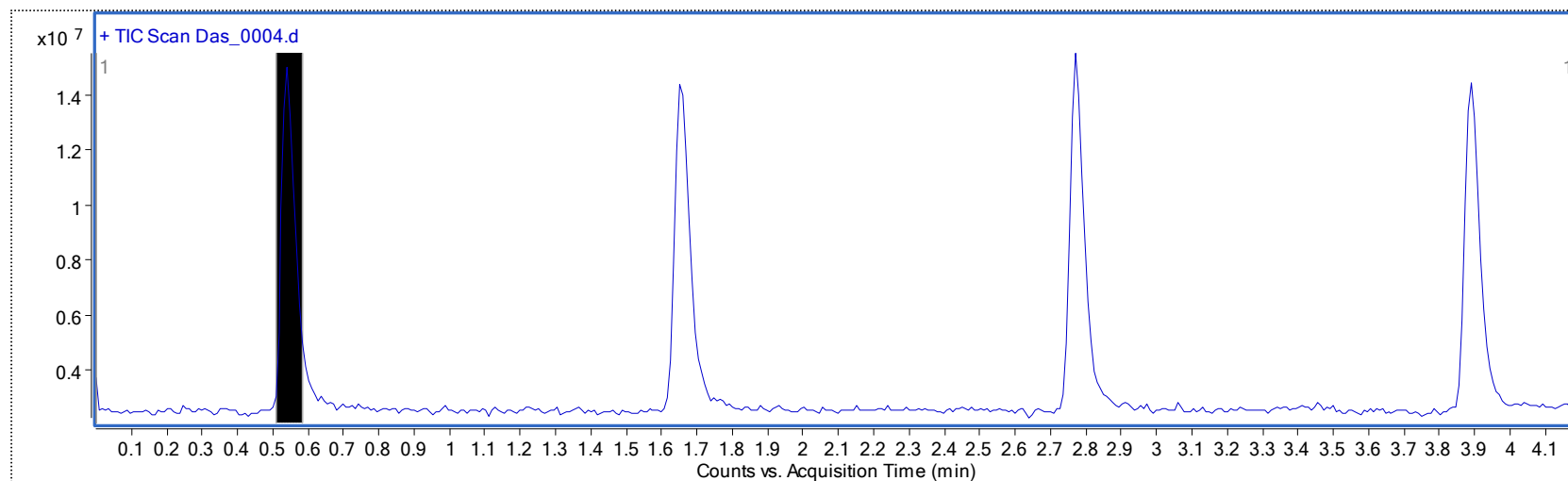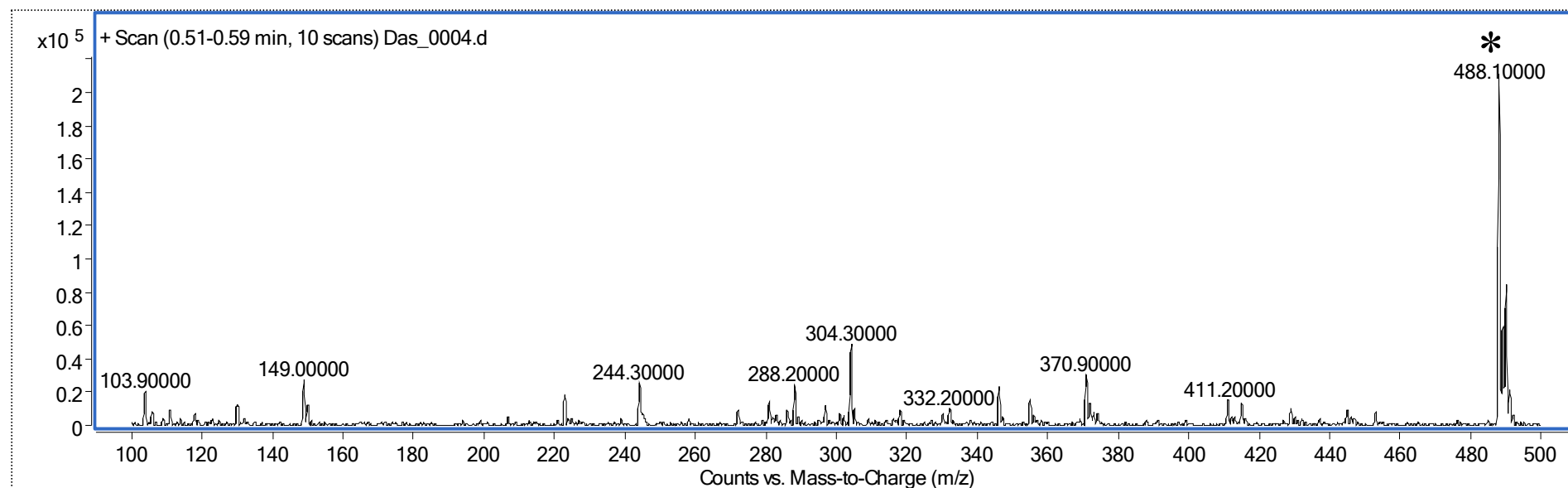**Figure 3-8 shows the total ion chromatogram (TIC) as detected in MS2Scan mode for four injections of dasatinib by Flow Injection Analysis (FIA)**

Figure 3-9: Extracted MS Spectrum

The MS spectrum of dasatinib extracted from the greyed out section of the TIC in Figure 3-8. The predominant ion, a protonated dasatinib ion, determined to be 488.1 m/z, is annotated (*). This is the precursor ion.

3.3.2. Fragmentor voltage optimisation

The ironically named fragmentor voltage (FV) is not involved in the fragmentation of the precursor ion to the product ion as one would assume, rather it acts as a filter for the MS. While it is possible to fragment the precursor ion by increasing the fragmentor voltage, this is not the purpose of the fragmentor voltage. The purpose of the fragmentor voltage is to preferentially maximise the throughput of precursor ions into the MS. As shown in Figure 3-10 optimisation of FV is achieved by monitoring the individual dasatinib precursor ion in selected ion monitor (SIM) mode, and increasing the fragmentor voltage sequentially at time segments, SIM only collects data for a preselected ion. To increase accuracy duplicate injections were performed at each condition.

By comparing the integrated peak area each set of peaks, it is possible to determine the optimum fragmentor voltage, i.e. the voltage that allowed maximum transit of dasatinib precursor ion, see Table 3-3. In the case of dasatinib, the fragmentor voltage from 120-180 gave similar peak areas. The reduction in peak area at higher fragmentor voltage is due to the precursor ion being broken down before entering the MS.

The optimum fragmentor voltage was selected to be 120.

Table 3-3: Peak Area of Integrated SIM

RT	Area	Area %	FV
0.5	935219	85.34	100
1.7	983835	89.78	100
2.8	**1088537**	**99.33**	**120**
3.9	**1051526**	**95.96**	**120**
5	1079208	98.48	140
6.1	1052601	96.05	140
7.2	1095838	100	160
8.4	1065522	97.23	160
9.5	1085210	99.03	180
10.6	1060277	96.75	180
11.7	1084343	98.95	200

RT	Area	Area %	FV
12.8	1063929	97.09	200
13.9	1047160	95.56	220
15	1035890	94.53	220
16.2	958307	87.45	240
17.3	953548	87.02	240
12.8	1063929	97.09	200
13.9	1047160	95.56	220

The correlation between peak area and fragmentor voltage as assessed by SIM ion scan

Figure 3-10: Fragmentor voltage optimisation
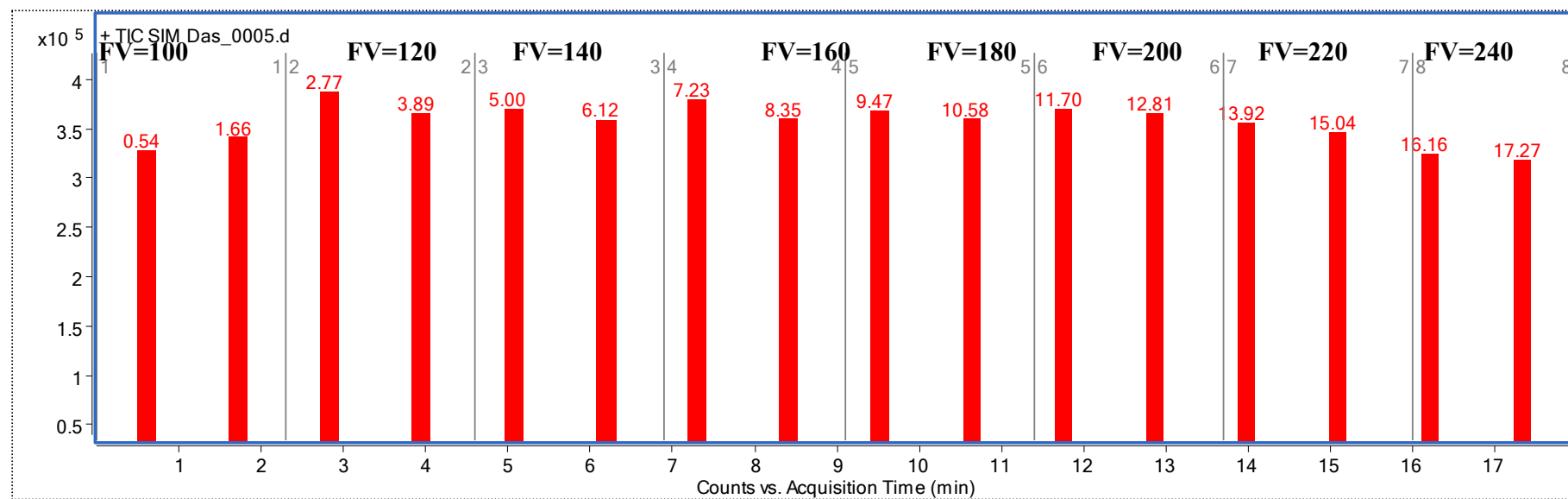
The TIC for 488.1m/z. in selected ion monitoring (SIM) mode with increasing fragmentor voltage

3.3.3. Product ion determination

The product ions are the ions detected by the detector in the third quad of the mass spec, as a result of the fragmentation of preselected precursor ions in the collision cells. By exposing the precursor ion to increasing collision energy, fragmentation occurs and the product ions can be determined as the MS2 detector scans from 100m/z to 500m/z.

By selected time segments, as highlighted in Figure 3-11 and extracting the MS spectrum we can analyse the breakdown of the precursor ion to its product ions, which gives a typical MS/MS fragmentation pattern, as shown in Figure 3-12.

Figure 3-11: TIC of Product Ion Scan
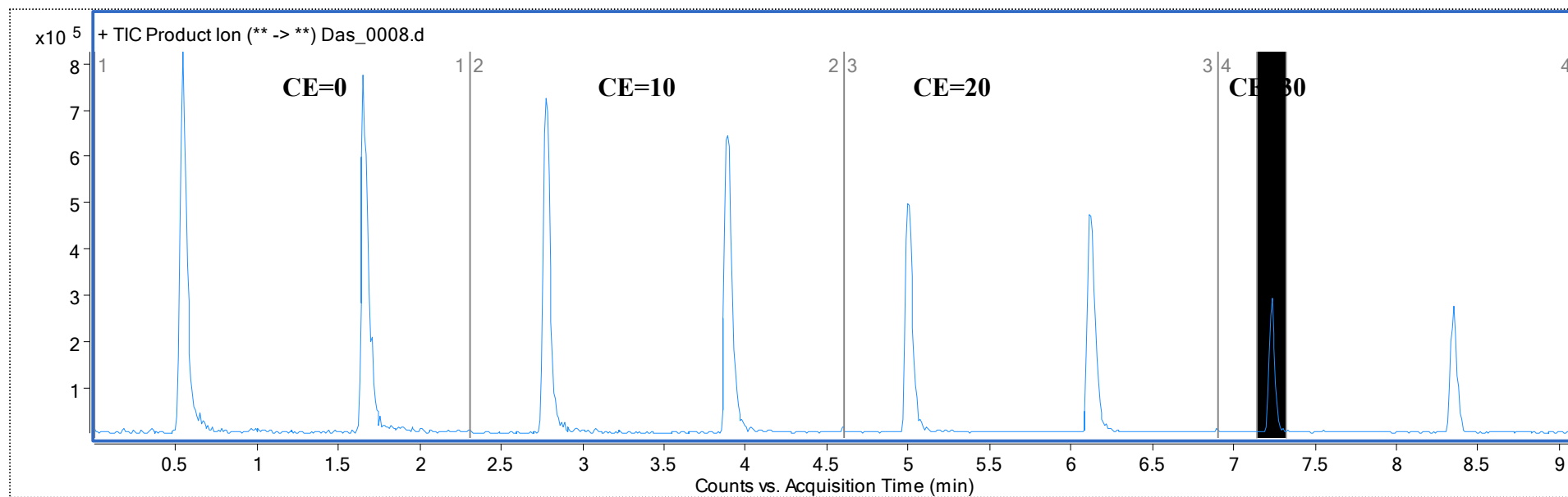
The TIC for the product ion scan with increasing collision energies. The highlighted time segment shows where the MS spectra were extracted.

Figure 3-12: Extracted MS spectra for product ion scan
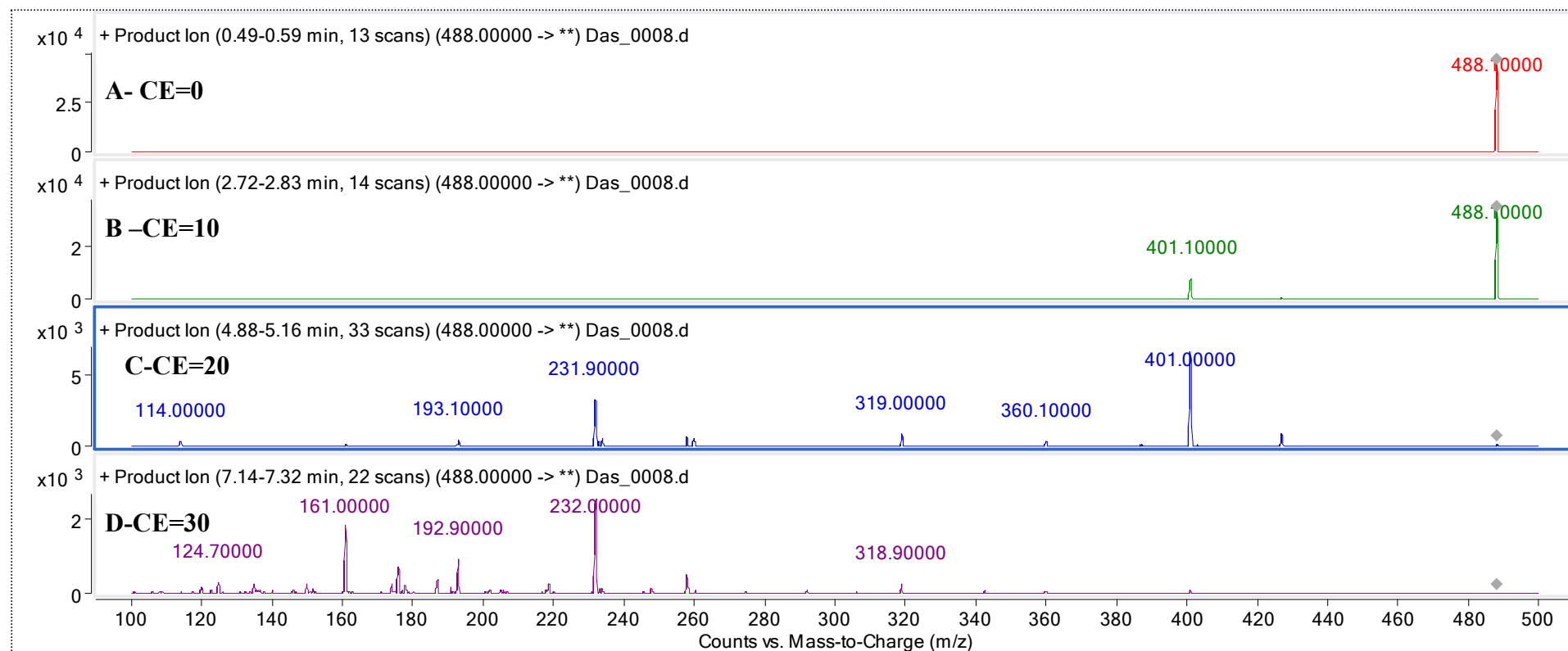
Figure 3-12 shows the extracted MS spectrum of the TIC of the product ion scan, shown in Figure 3-11. The details of spectrum A, B, C and D are detailed below.

Figure 3-12 shows the extracted MS spectrum of the TIC of the product ion scan.

- Spectrum A was extracted between 0.49 and 0.59 minutes, and shows the precursor ion with no collision energy has been applied.

- Spectrum B was extracted between 2.72 and 2.83 minutes, with a collision energy setting of 10keV. The product ion 401.1m/z was seen. A drop in the abundance of the precursor ion was also seen, indicating that 401m/z ion came from the 488m/z ion.

- Spectrum C, extracted between 4.88 and 5.16 minutes showed that a collision energy of 20keV gave a second product ion and left little precursor ion.

- Spectrum D, extracted between 7.14 and 7.32 minutes with a collision energy of 30keV showed that a high collision energy completely broke down the precursor ion so that was it no longer detectable

3.3.4. MRM transition optimisation

MRM (multi-reaction monitoring) can track many precursor ions and their multiple product ions through the MS to provide spectra that are quantifiable.

Each transition from precursor ion to product ion can have different collision energies. By optimising the MRM transition, the collision energy for each transition was optimised.

Figure 3-13: TIC and EIC for dasatinib
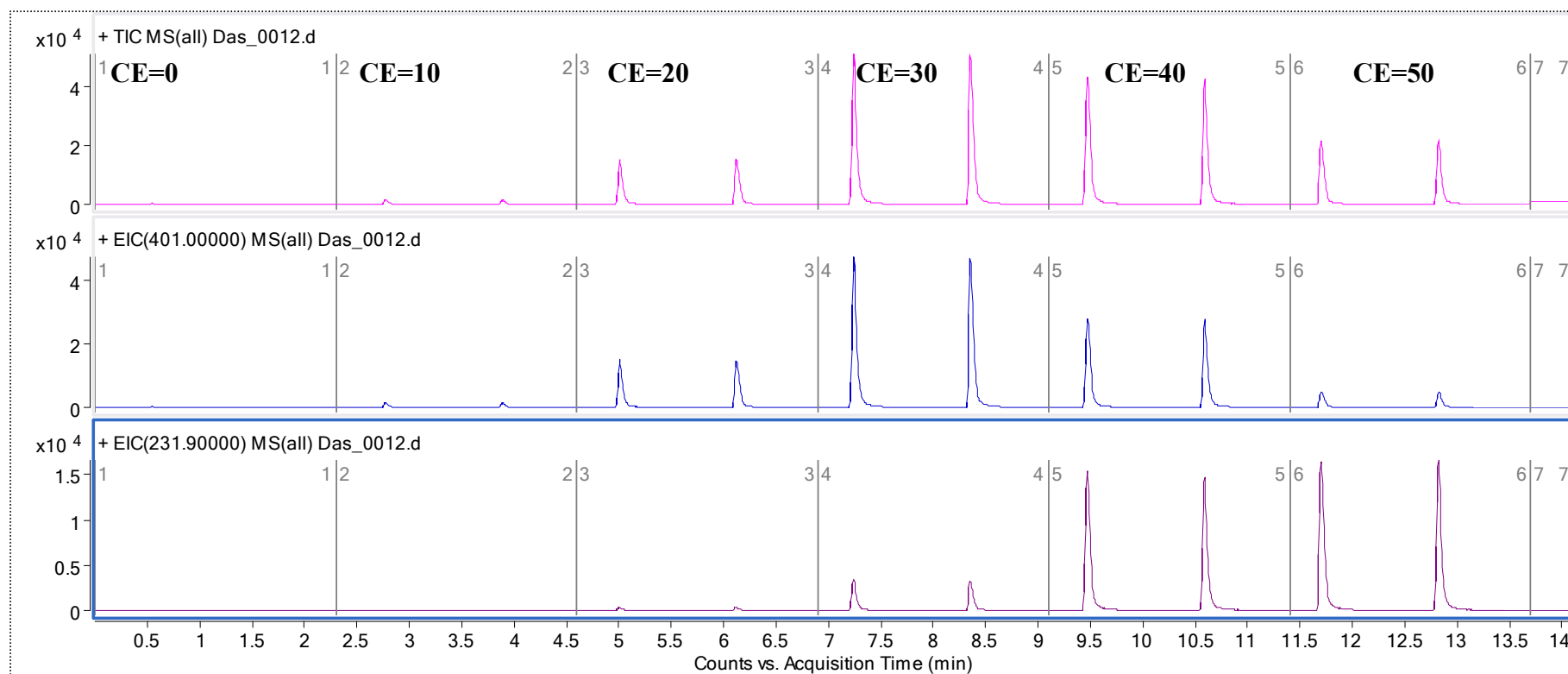
The TIC and the EIC for dasatinib with increasing collision energies.

Through flow injection analysis it was possible to determine the optimum collision energy for each transition. Figure 3-13 shows duplicate 5µL injections in each time segment. Collision energies were increased step-wise in units of 10 from a starting value of zero to 50keV. The optimum collision energy for transition 488 – 401m/z was determined to be 30keV while the optimum collision energy for transition 488-231m/z was determined to be 50keV.

While Figure 3-8 through to Figure 3-13 showed the determination of the optimum MRM transition setting for dasatinib, this is representative of the work carried out for each compound.

Table 3-4 summarises the findings of these experiments.

Table 3-4: Summary of MRM transition conditions

Name	Precursor Ion	Optimum Fragmentor Voltage	Product Ion	Optimum Collision Energy
Dasatinib	488	120	401*	30
			231	50
Lapatinib	581	200	365*	40
Gefitinib	447.2	160	128*	30
Erlotinib	393.9	160	278*	35
			336	25
Imatinib	494.2	120	394*	25
			217	25
			99	30
Sorafenib	399.1	100	252*	35
			326	20

The optimal fragmentor voltages and collision energy settings for the determination of the TKI drugs employed in this study, * indicates quantifier ion.

Quantification was based on the integrated peak area as determined by the Masshunter Quantification Analysis (Version B.01.04) software which quantifies the peak areas of the MRM transitions of each analyte.

3.4. Ion suppression

Ion suppression or ion enhancement can be one of the disadvantages of mass spectrometry analysis, particularly of bio-analytical samples. First identified by Buhrman *et al.*[298], ion suppression/enhancement effects are caused by co-eluting matrix artefacts. These co-eluting matrix components cause quantification issues; ion suppression leads to reduced detection of the signal of the desired analyte whereas ion enhancement leads to amplification of the signal of the desired analyte. Either case leads to problems in accurately quantifying the analyte of interest.

3.4.1. Ion suppression issues – extraction vessel contamination

The impact of ion suppression on the quantification of lapatinib and dasatinib was initially observed in experiments carried out to determine the optimum extraction conditions. Extracted samples run in MRM mode showed unaccountably low recovery when compared to the standard sample, which was calculated to equal 100% recovery. Ion suppression can frequently be due to biological component in the analysis, however, LLE is known to give good recovery and this level of poor recovery was dramatic. Figure 3-14 shows the effects of ion suppression on the determination of dasatinib recovery. The signal for the extracted dasatinib was suppressed by interfering background ions. The peak area the "dasatinib calculated" sample was representative of 100% and the peak area of the extracted dasatinib sampled was expressed as a percentage of the "dasatinib calculated" samples.

Similarly for lapatinib Figure 3-15, the peak area of the extracted sample is expressed as a percentage of the peak area of the "calculated" sample, which is equivalent to 100% extraction.

The contaminating ions were determined to have leached from standard laboratory polyethylene (PE) tubes. Drug standards prepared in plastic extraction tubes and extracted immediately gave good recovery while the same drug standards stored at 4°C over the weekend prior to extraction gave the appearance of low recovery since the detector was saturated with contaminating ions. When the samples were injected in duplicate, one for MRM analysis and one for MS2Scan analysis, samples with low quantifiable MRM signal had a corresponding high background in MS2Scan mode.

Figure 3-14: Example of poor dasatinib signal detection due to ion suppression
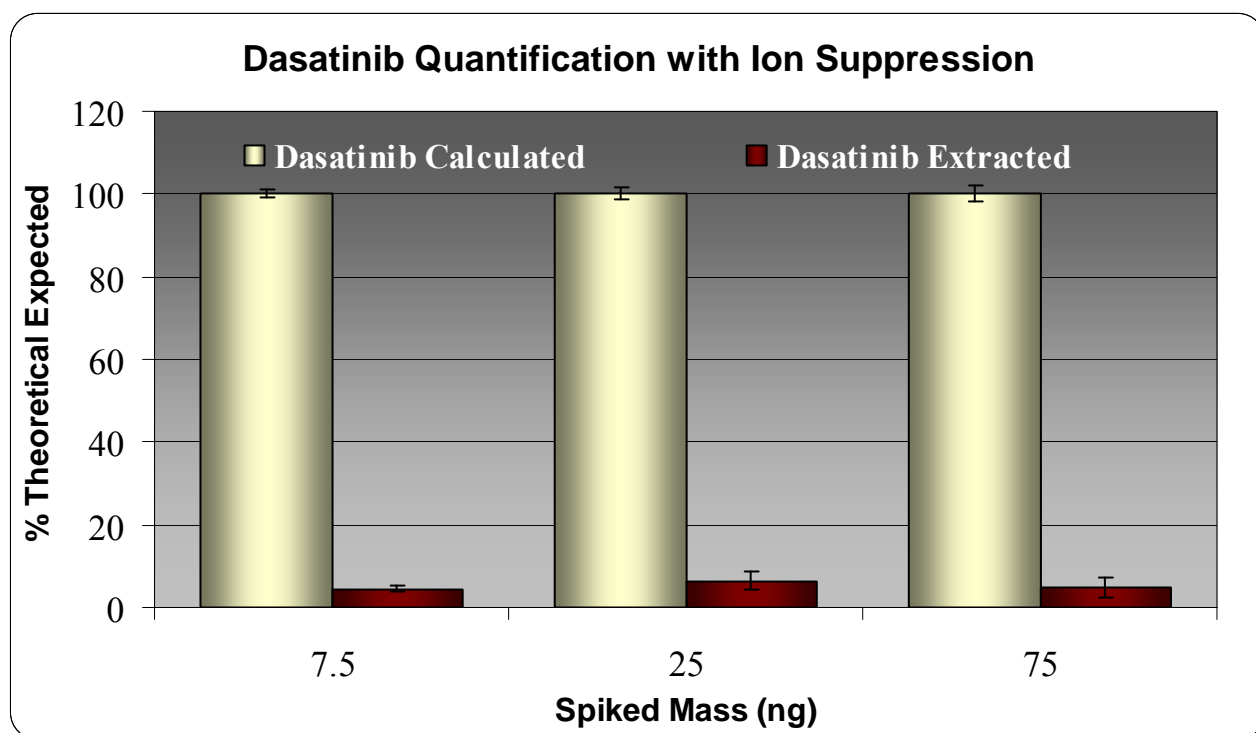
The effect of ion suppression on the detected dasatinib signal following extraction, expressed as a percentage of the expected signal. Results shown are the average of a minimum of triplicate samples.

Figure 3-15: Example of poor lapatinib signal detection due to ion suppression
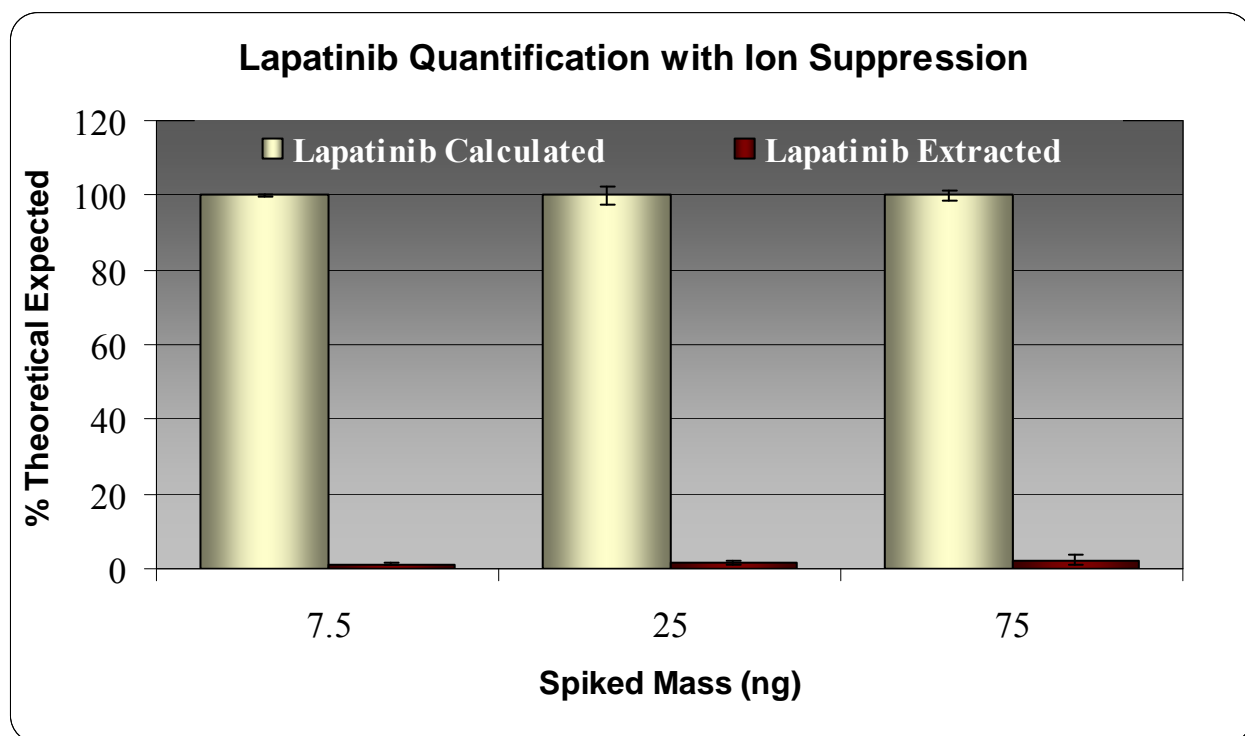
The effect of ion suppression on the detected lapatinib signal following extraction, expressed as a percentage of the expected signal. Results shown are the average of a minimum of triplicate samples.

The high level of background noise (from plasticisers leached from PE tubes) was seen to increase through the analyses of a batch of samples, increasing with the number of extracted samples injected.

Figure 3-16 shows the TIC in MS2Scan mode of three injections of a system standard (mixture of lapatinib and dasatinib in pure acetonitrile) injected at different points during running of a worklist of extracted samples. System standards are routinely injected throughout the worklist run, frequently bracketing batches of samples.

Here we see that the level of background acquired in the sample increased. This is attributed to carryover of plasticiser in the system from the extracted samples.

Following the isolation of the ion suppression issue, all drug standards were prepared in 10mL glass tubes.

Figure 3-16: Example of ion suppression from plasticiser leaching
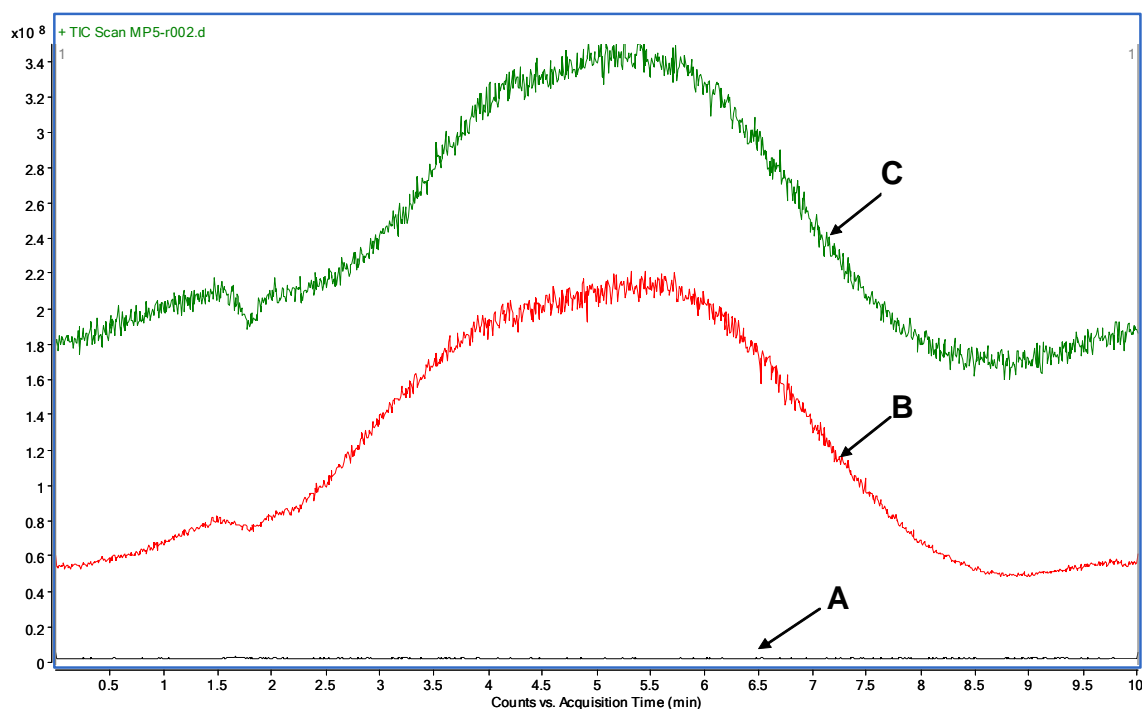
Shown here is the TIC in MS2Scan trace of three injections from the same vial (mobile phase blank). The black trace (A) shows all ions detected the start of the run, the red trace (B) shows the MS2Scan after the injection of 10 extracted samples and the green trace (C) shows the MS2Scan after the injection of an additional 10 samples.

3.4.2. Ion suppression assessment of lapatinib and dasatinib extraction

Having elucidated the problem of ion suppression it was then necessary to examine the impact of extraction and LC conditions on ion suppression

Ion suppression can be analysed by either post-column infusion method or by reconstituting standard dilutions of each agent in extracted samples, as detailed by Zirolli *et al*[234].

The level of ion suppression on lapatinib and dasatinib was initially examined by post column infusion with isocratic elution at 60% (v/v) acetonitrile: 10mM ammonium formate pH4. The analyte (2μg/mL) was introduced through a T-piece, by an infusion pump at a flow of 50μL/min, after the analytical column into the flow path, as illustrated in Figure 3-17.

Samples of mobile phase and extracted blank samples were injected from the autosampler through the analytical column into the MS, while the MS monitored, in MRM mode, the constant signal of the analyte from the infusion pump. Any ion suppression or enhancement effects would be seen as a drop or rise, respectively, in the constant signal for the analyte of interest.

Figure 3-17: Schematic of post-column infusion
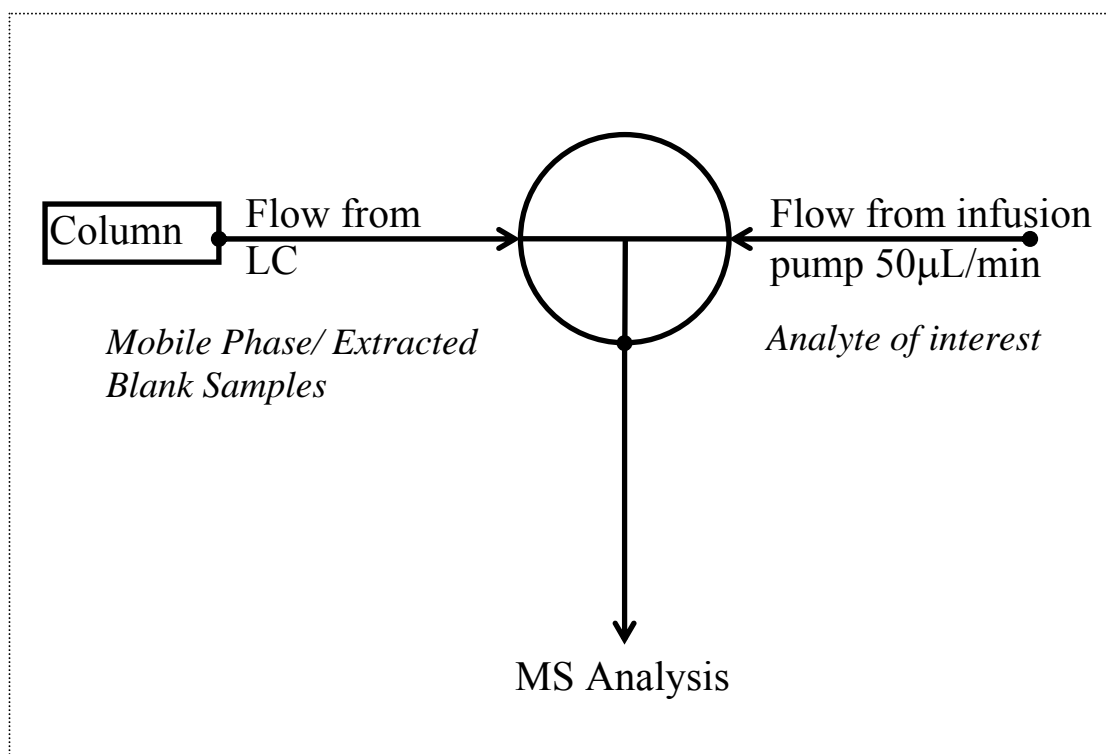
Figure 3-17 demonstrates the instrument configuration for the determination of ion suppression by post column infusion.

Figure 3-18 shows the investigation by direct post-column infusion of the effect of ion suppression on dasatinib.

- Spectrum A showed the retention time for dasatinib on column. This illustrated the time range of importance for signs of ion suppression/enhancement effects.
- Spectrum B is the MRM of dasatinib with 20μL injection of extraction blank cell sample and where ion suppression effects might be anticipated.
- Spectrum C is the MRM of dasatinib infusion with a 20μL injection of mobile phase.

The ion suppression effect of the extracted cell blank sample on dasatinib was determined to be approximately 40%. This was determined by assessing the difference between response for dasatinib pre-injection and at the expected retention time, as indicated by the dashed lines in spectrum B, Figure3-18. The injection of mobile phase, spectrum C, shows that the drop in the detection level of the infused dasatinib is from the injection of the extracted blank sample alone.

Figure 3-18 Dasatinib 2µg/mL infusion at 50µL/min
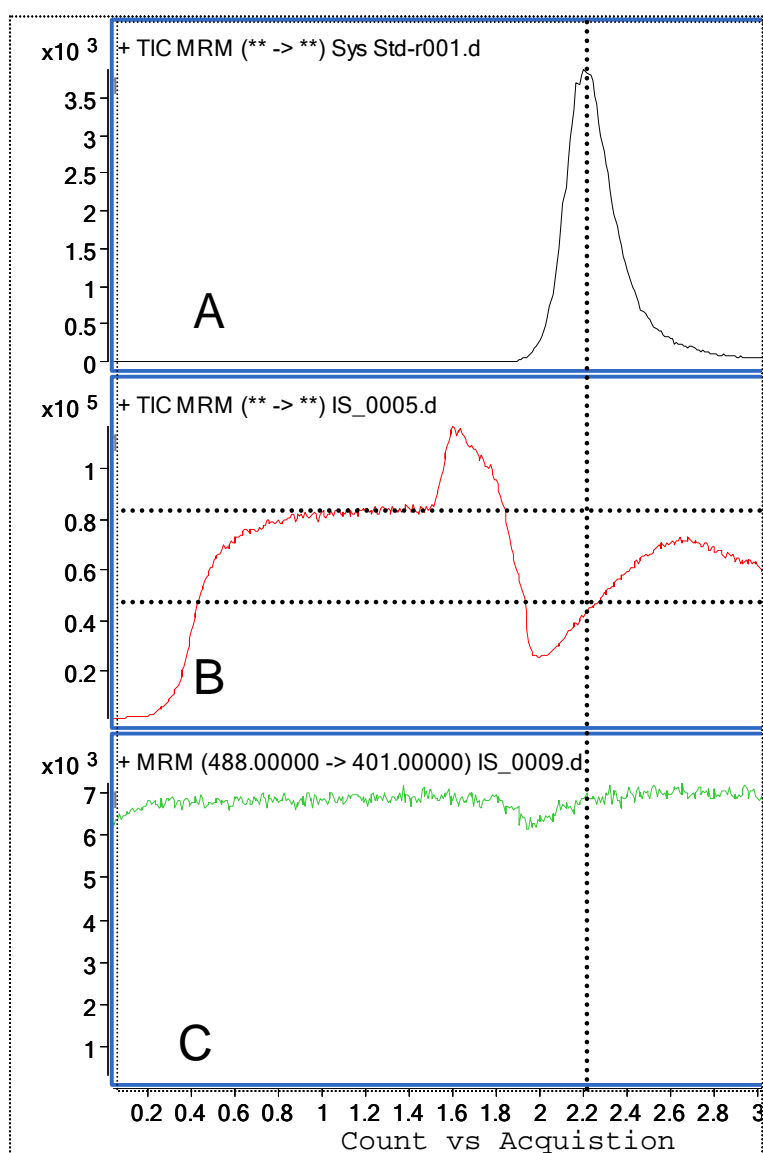
Dasatinib ion suppression investigation by direct infusion of 2µg/mL

Figure 3-19 shows the investigation by direct infusion of the effect of ion suppression on lapatinib.

- Spectrum A is the analysis of lapatinib in MRM with on-column separation which identifies the retention time of lapatinib and illustrates the time range of importance.
- Spectrum B shows the injection of an extracted cell/matrix blank sample by the autosampler. The red trace shows the detected levels of lapatinib as introduced through the T-piece, post-column, into the detector.
- Spectrum C is the injection of 20µL injection mobile phase A (60%ACN/40%10mM ammonium formate pH4), again the detected trace is of lapatinib introduced through constant infusions.

Injecting mobile phase identifies that any interfering artefacts seen in spectrum B are the result of the cell blank.

The ion suppression effect of the extracted cell blank sample on lapatinib was determined to be approximately 10%. This was assessed by determining the difference between the responses for lapatinib prior to injection (e.g. time point 0.5-1min) and the response for lapatinib at the retention time (4.4mins).

Figure 3-19: Infusion of 2µg/mL lapatinib at a constant rate of 50µL/min
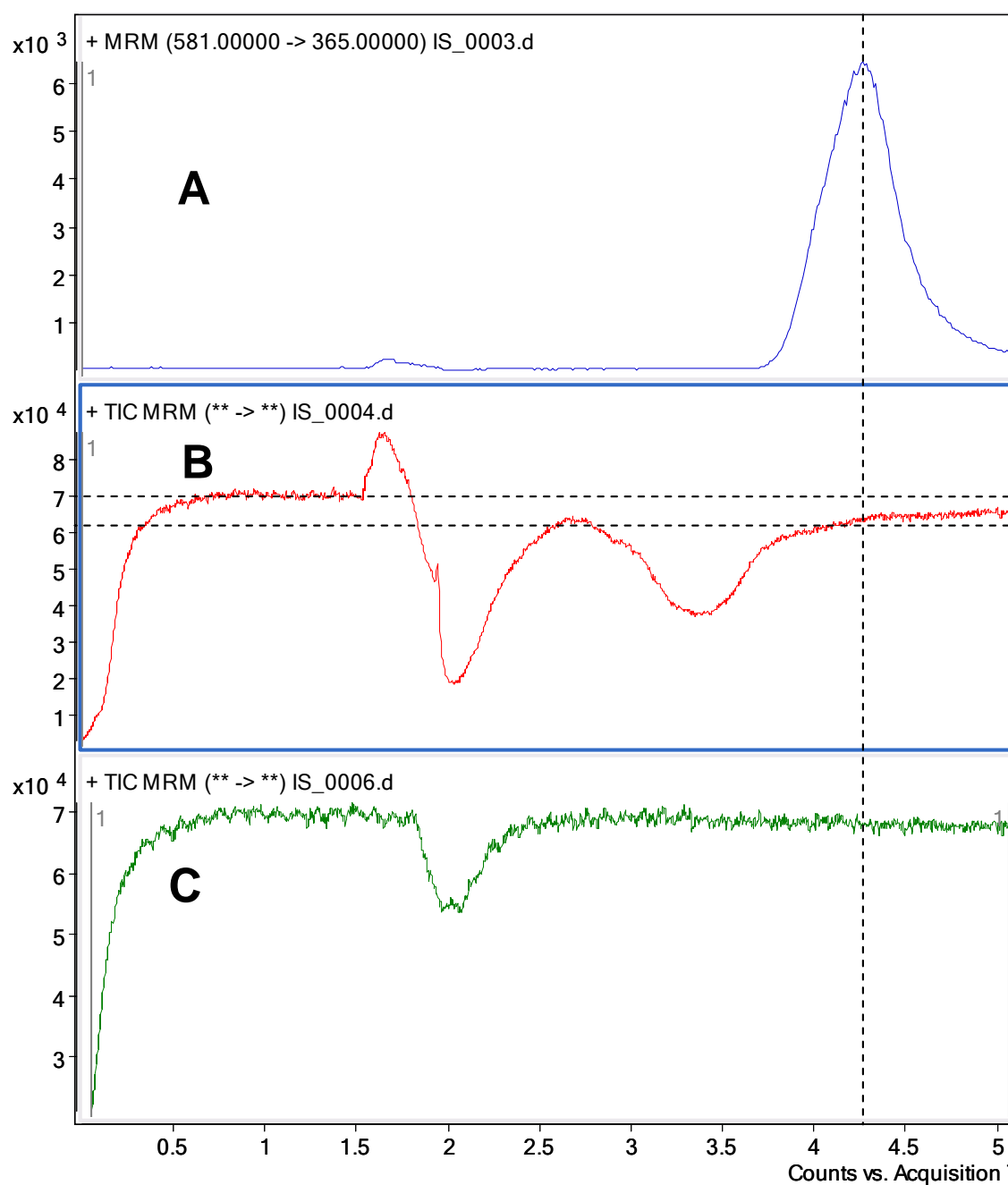
Lapatinib ion suppression investigation by direct infusion of 2µg/mL

We can see from the infusion profile of dasatinib that a small shift in retention time of dasatinib would move it out of a region where ion suppression might be anticipated. The effect of altering the ratio of the mobile phase components on the retention time of lapatinib and dasatinib was assessed.

The optimum isocratic mobile phase was found to be 54% acetonitrile: 10mM ammonium formate pH4. By accurately measuring the 460mL of mobile phase A (10mM ammonium formate pH4) and 540mL of mobile phase B (acetonitrile) and injecting both analytes, retention times of 2.39mins (dasatinib) and 5.39mins (lapatinib) were seen. This gives enough of a shift in retention time to avoid the worst area of ion suppression while still giving rapid and high efficiency separation and reasonably narrow peaks. Figure 3-20 shows a representative chromatogram of lapatinib and dasatinib separation at 54% acetonitrile.

Figure 3-20: Representative spectrum of dasatinib and lapatinib
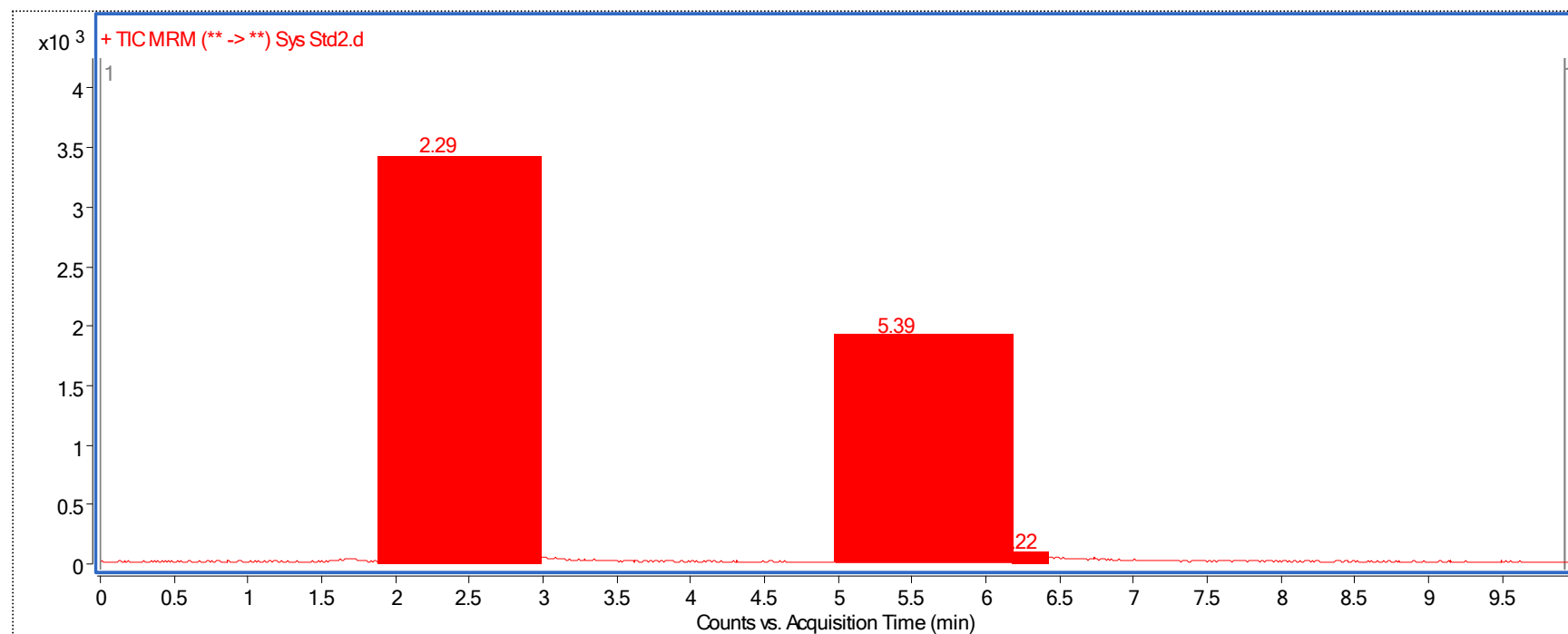
Representative spectrum of dasatinib and lapatinib separation following mobile phase optimisation

To accurately assess the level of ion suppression from the cell pellet due to the extraction process, the method outlined by Zirrolli *et al.,* was used[234].

Standard dilutions of each drug in acetonitrile were prepared. These solvent standards were added (40μL) to dry extracted cell blanks samples (post extraction samples) to clean LC vials (40μL). A volume of 20μL of each concentration was injected from each vial. The post extraction standard was normalised to the solvent standard and expressed as a percentage.

Figure 3-21 and Figure 3-22 show that under the tested conditions the ion suppression effects on the detection and quantification of lapatinib and dasatinib were found to be minimal.

Figure 3-21: Effect of Ion Suppression of Lapatinib

Figure 3-22: Effect of Ion Suppression on Dasatinib

Ion suppression was calculated as peak area of the analyte of interest in the post-extraction standard compared to the solvent standard. Data is expressed as a function of the initial mass of drug in the tube, n=3.
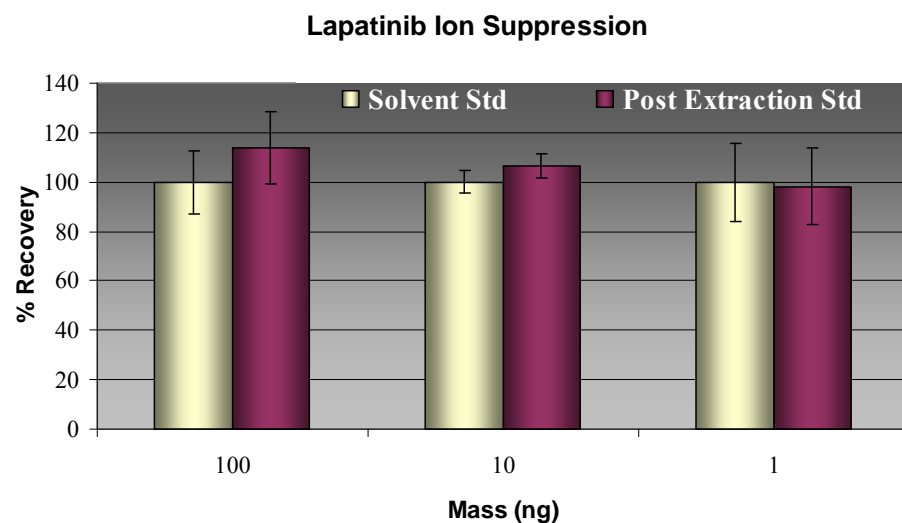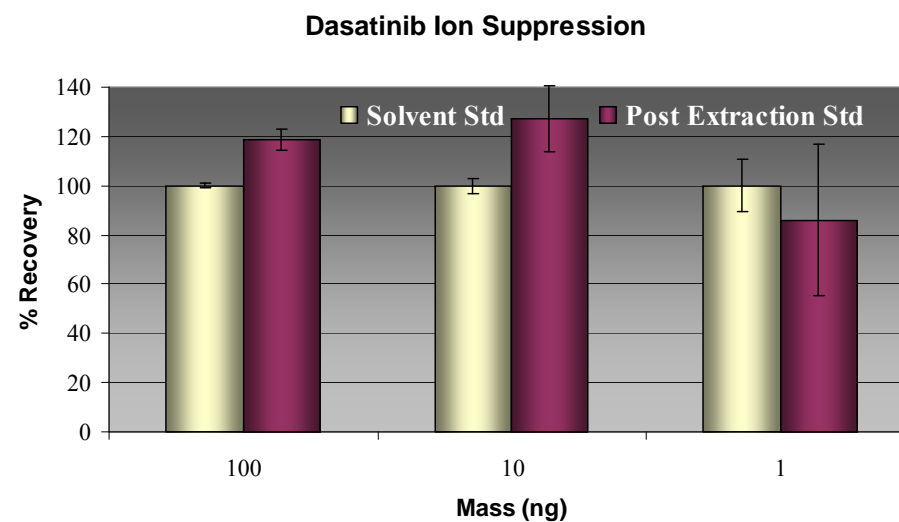
3.5. Assay validation

The overall LC-MS method was validated for the following performance parameters- linearity and range, intra-day precision (repeatability) and inter-day precision (intermediate precision), accuracy, sensitivity (LOD and LOQ), recovery and sample stability according to the guidelines described by Ermer[299]. MRM allowed individual determination of each drug necessary with the use of internal standard-based quantification.

3.5.1. Linearity and range

Regression analysis was used to assess the linearity between the peak area ratios (analyte/internal standard) and the analyte concentration.

The calibration curves for dasatinib and lapatinib were linear over the range of 0.1ng to 200ng in tube and recovery was linear. Since the TKIs resolved well from each other and were extracted with high efficiency one TKI was used as the internal analytical standard for the other agent to reduce error. Internal standard (IS) of 50ng (100μL of a 500ng/mL stock) was added to each tube. Whilst the calibration curves were linear, over such a broad range, the bias of the regression line tends to make the determination of lower drug concentration values much less accurate; hence it was decided to use a LOG_{10}-LOG_{10} plot of the peak area ratio versus the mass of drug in all calculations. The LOG_{10}-LOG_{10} plot gave typical correlation coefficients (R^2) values of 0.99, see Figure 3-23 and Figure 3-24 for dasatinib and lapatinib.

3.5.2. Precision and accuracy

Intra-day precision and accuracy was assessed over the mass range (0.1ng - 200ng) by extraction and analysis of triplicate spiked samples on the same day. (Table 3-5)

Inter-day precision and accuracy was assessed over the mass range (0.1ng - 200ng) by extraction and analysis of triplicate spiked samples over four days. (Table 3-6)

The percentage relative standard deviation (%R.S.D.) was employed as a measure of precision. The percentage accuracy was determined by dividing the average calculated drug concentration by that of the spiked known concentration. In all cases, the R.S.D. values were less than 13%, the majority were less than 10% and the average percentage accuracy was 102%.

Figure 3-23: Representative example of calibration curve for dasatinib

$$y = 1.0364x + 1.8707$$
$$R^2 = 0.9986$$

Dasatinib Standard Curve

LOG$_{10}$ Mass (ng)

LOG$_{10}$ Peak Area Ratio
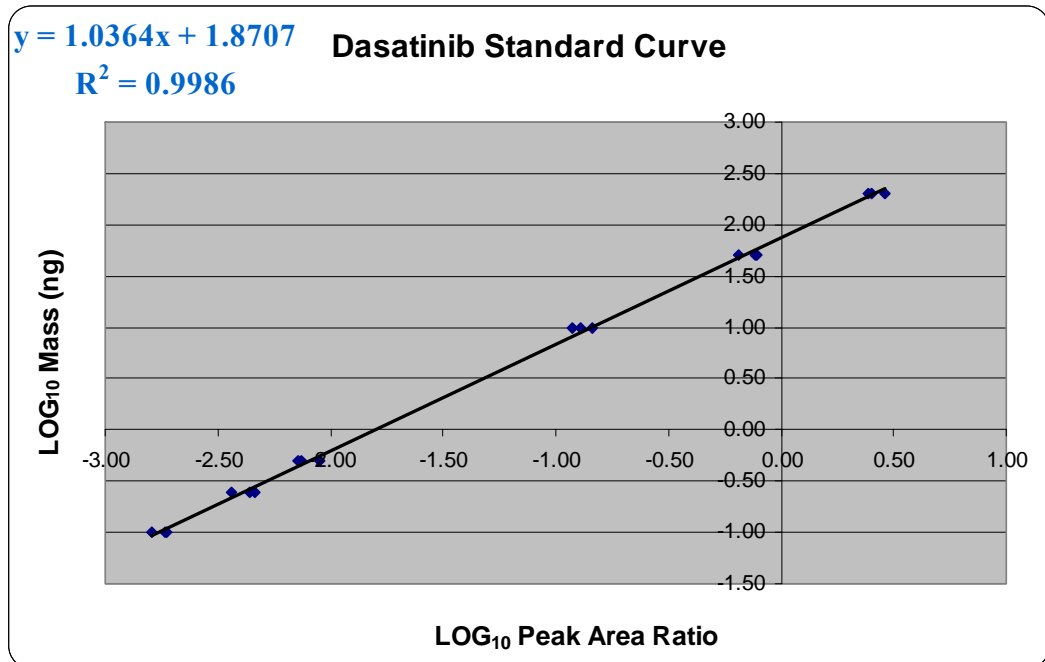
Representative standard curve for dasatinib extracted from spiked cell pellet matrix

Figure 3-24: Representative example of calibration curve for lapatinib

$$y = 1.0105x + 1.6564$$
$$R^2 = 0.9977$$

Lapatinib Standard Curve

LOG$_{10}$ Mass (ng)

LOG$_{10}$ Peak Area Ratio
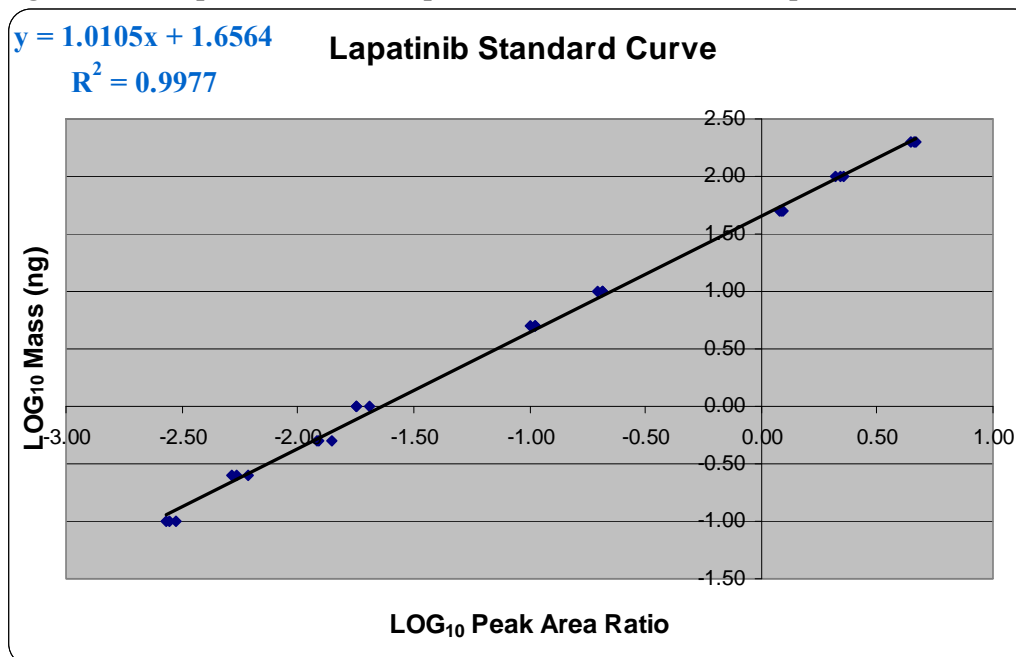
Representative standard curve for lapatinib extracted from spiked cell pellet matrix

Both Figure 3-23 and Figure 3-24 are LOG$_{10}$ /LOG$_{10}$ plots of the spiked mass versus the peak area ratio of the analyte to the internal standard. In line with ICH guidelines, more than five concentrations were used, and each concentration was examined in triplicate.

Table 3-5: Intra-day analysis for precision and accuracy (n=3) for lapatinib and dasatinib.

Spiked Mass (ng)	Lapatinib			Dasatinib		
	Mean Mass Observed (ng)	% Accuracy	% R.S.D.	Mean Mass Observed (ng)	% Accuracy	% R.S.D.
0.10	0.12	120.5	5.4	0.10	104.6	9.1
0.25	0.24	95.5	8.1	0.26	102.3	12.6
0.50	0.55	110.8	7.9	0.49	97.9	12.9
10.0	9.1	91.0	2.7	9.1	90.7	11.4
50.0	55.4	110.8	1.9	53.7	107.4	10.3
200.0	209.7	104.8	2.8	200.9	100.4	9.2

The accuracy and precision of lapatinib and dasatinib from triplicate intra-day analysis

Table 3-6: Inter-Day analysis for accuracy and precision for lapatinib and dasatinib.

Spiked Mass (ng)	Lapatinib			Dasatinib		
	Mean Mass Observed (ng)	% Accuracy	% R.S.D.	Mean Mass Observed (ng)	% Accuracy	% R.S.D.
0.10	0.11*	110.9	7.5	0.10*	97.9	9.6
0.25	0.25	99.0	6.1	0.25	100.9	2.5
0.50	0.56	111.6	7.6	0.49	98.3	2.8
10.0	8.7	87.0	8.9	10.3	102.8	6.8
50.0	53.0	105.9	8.0	54.8	109.7	6.0
200.0	199.8*	99.9	7.6	181.2	90.6	10.7

The accuracy and precision of lapatinib and dasatinib from analysis on four* independent day (*indicated 3 days)

3.5.3. Selectivity and sensitivity

The limit of detection (LOD) was defined as the mass of drug which gave a signal to noise ratio of 3:1. The signal-to-noise ratio was calculated by the Masshunter Quantification Analysis Software (Version B.01.04). Calculations were based on the peak area of each drug individually not on the peak area ratio. The limit of quantification (LOQ) was defined as the mass of drug which gave a signal to noise ratio of 5:1[300]. The limit of detection and limit of quantification are assessed on the peak area generated by the absolute mass of dasatinib or lapatinib spiked into the extraction tube and by the signal to noise ratio of the peak.

During validation spiked samples were prepared (as outlined in Section 2.2.5.2) by spiking 50μL cell suspension with the analytes of interest. This approximately equated to 2.5×10^5 cells, approximately the number of cells used for cell accumulation and efflux assays.

Given these criteria, the LOD for dasatinib detection was determined to be 10pg, which equated to 3pg on column with an R.S.D. of 15%. The LOQ for dasatinib was determined to be 50pg which equates to 15pg on column with an R.S.D. of 8%. These values for LOD and LOQ enable pharmacokinetic monitoring of both drugs in cell samples.

The LOD for lapatinib was determined to be 50pg of lapatinib in the extraction tube which equated to 15pg on column with a R.S.D. of 19%. The LOQ for lapatinib was 100pg which equates to 31pg on column with an R.S.D. of 13%.

However, Table 3-7 gives the absolute mass spiked into the extraction tube which was determined to be the LOD and LOQ as well as normalising the absolute mass to a cell number and an approximate volume.

The selectivity of the assay is increased through the use of MRM transitions for quantification. Assessed through in monitoring of the MRM transition in extracted cell samples there was no detected endogenous interaction for either dasatinib or lapatinib, see Section 9 Appendices II and III.

Table 3-7: Dasatinib and lapatinib limit of detection

	Dasatinib		Lapatinib	
	LOD	LOQ	LOD	LOQ
Absolute Mass	10pg	50pg	50pg	100pg
Normalised to cell number	40pg/million cells	200pg/million cells	200pg/million cells	400pg/million cells

The LC-MS method easily resolved both TKIs from each other. Excellent selectivity and the very low LOD and Loss were achieved due the low background when quantifying based on the molecular transitions of the ions in the collision cell (MRM).

3.5.4. Recovery/extraction efficiency

The extraction efficiency of the procedure was determined by comparing the peak areas of the extracted analytes with those from non-extracted samples. Non-extracted samples were prepared by calculating the mass of drug on column at 100% extraction. Recoveries at low, medium and high concentrations were evaluated. Recoveries for both drugs at the concentrations used were good and ranged from 86%-112%. Results are shown in Table 3-8.

Table 3-8: Lapatinib and dasatinib intra assay recovery

| Mass (ng) | Lapatinib | | Dasatinib | |
	Mean % Recovery	%R.S.D.	Mean % Recovery	%R.S.D.
0.1	112.4	21.8	99.2	16.1
10	98.6	15.6	90.7	5.4
100	85.8*	14.2	104.4	14.6

The recovery of lapatinib and dasatinib from triplicate* intra-day (*indicated n=2)

3.5.5. Stability-through freeze/thaw

The stability of lapatinib and dasatinib in the presence of cells was determined over four freeze-thaw cycle at in tube mass of 0.1, 0.5, 50 and 200ng, as shown in Table 3-9 and Table 3-10. On day one, triplicate standards were extracted and the remaining samples were frozen at -20°C. The samples were then thawed and extracted and refrozen each day for a further three days.

The data generally indicate that both agents were stable over the course of the experiment. However, it was noted that the amount of lapatinib recovered on Day 4 of the freeze-thaw assay was decreased, suggesting that this agent is slightly less stable under these conditions.

Table 3-9: Dasatinib Freeze/Thaw

Mass (ng)	First Freeze Thaw Cycle % Recovery	Second Freeze Thaw Cycle % Recovery	Third Freeze Thaw Cycle % Recovery	Fourth Freeze Thaw Cycle % Recovery
0.1	100	98.3	105.7	101.7
0.5	100	104.1	91.1	100.5
50	100	120.4	107.7	111.2
200	100	84.9	94.8	90.3

The recovery of dasatinib from four freeze/thaw cycles from triplicate intra-day analysis

Table 3-10: Lapatinib Freeze/Thaw

Mass (ng)	First Freeze Thaw Cycle % Recovery	Second Freeze Thaw Cycle % Recovery	Third Freeze Thaw Cycle % Recovery	Fourth Freeze Thaw Cycle % Recovery
0.1	100	98.2	97.8	84.8
0.5	100	102.1	101.3	89.8
50	100	109.2	102.1	81.4
200	100	92.5	98.1	88.5

The recovery of lapatinib from four freeze/thaw cycles from triplicate intra-day analysis

3.6. Multiple tyrosine kinase inhibitor analysis

The similarities in the physicochemical properties (such as lipophilicity) of many TKI inhibitors indicated that this newly developed LC-MS method might have a broader analytical applicability for this class of agents. This method was therefore applied to the detection of four other TKIs (gefitinib, erlotinib, imatinib and sorafenib) in addition to lapatinib and dasatinib. Sunitinib was also included in initial experiments but was excluded from multiple TKI extraction as sunitinib separation at these LC conditions was less than optimal.

Shown in Figure 3-25 is the TIC and one extracted MRM for each of the six TKIs investigated. The figure illustrates that although the chromatographic separation did not resolve all the TKIs from each other, MRM determination enabled individual detection and resolution of each agent.

Figure 3-25: The analysis of multiple TKIs
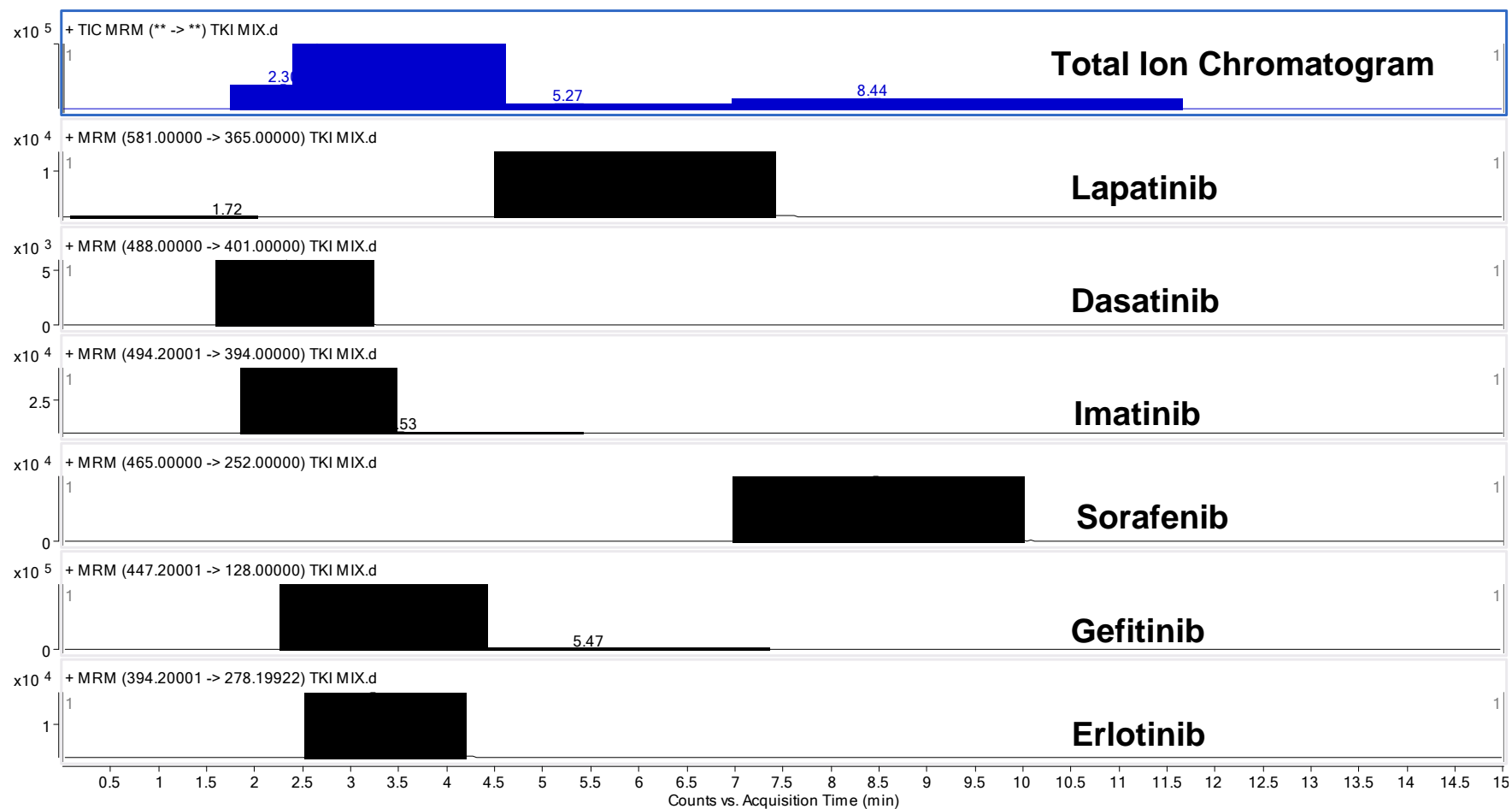
Total ion chromatogram and extracted MRM transitions of 6 tyrosine kinases inhibitors (lapatinib, dasatinib, erlotinib, gefitinib, imatinib and sorafenib), and one extracted transition for each analyte.

Preliminary examination of the other tyrosine kinase inhibitors investigated comprised of assessment of validation parameters, linearity and range, intra-day precision (repeatability) and inter-day precision (intermediate precision), accuracy, sensitivity (LOD and LOQ) and recovery at the extraction conditions already optimised for dasatinib and lapatinib. The results for the partial validation of erlotinib, imatinib and gefitinib are outlined here.

3.6.1. Linearity and range

Regression analysis was used to assess the linearity between the peak area ratios (analyte/IS) and the analyte concentration. Given the retention characteristics of erlotinib, imatinib and gefitinib the TKI lapatinib was used as the internal standard for all three TKI validations, findings summarised in Table 3-11.

3.6.1.1. *Erlotinib*

The calibration curves for erlotinib, using lapatinib as an internal standard were linear over the range of 0.05ng to 200ng in tube. The LOG_{10}-LOG_{10} plot gave typical correlation coefficients (R^2) values of 0.99, see Figure 3-26.

3.6.1.2. *Imatinib*

The calibration curves for imatinib, using lapatinib as an internal standard were linear over the range of 0.1ng to 200ng in tube. The LOG_{10}-LOG_{10} plot gave typical correlation coefficients (R^2) values of 0.99, see Figure 3-27.

3.6.1.3. *Gefitinib*

The calibration curves for gefitinib, using lapatinib as an internal standard, were linear over the range of 0.1ng to 200ng in tube. The LOG_{10}-LOG_{10} plot gave typical correlation coefficients (R^2) values of 0.99, see Figure 3-28.

Figure 3-26: Representative example of calibration curve for erlotinib

Erlotinib Standard Curve

$y = 1.0463x + 1.1477$
$R^2 = 0.9988$

X-axis: LOG_{10} Peak Area Ratio
Y-axis: LOG_{10} Mass (ng)
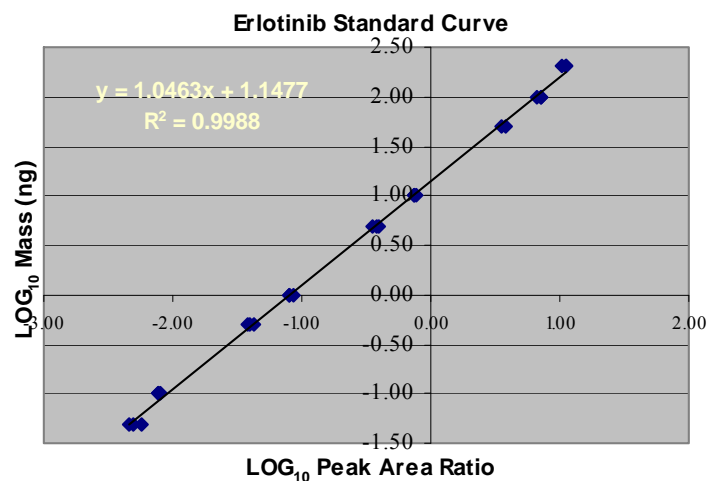
Figure 3-27: Representative example of calibration curve for imatinib

Imatinib Standard Curve

$y = 1.0255x + 1.6228$
$R^2 = 0.9992$

X-axis: LOG_{10} Peak Area Ratio
Y-axis: LOG_{10} Mass(ng)
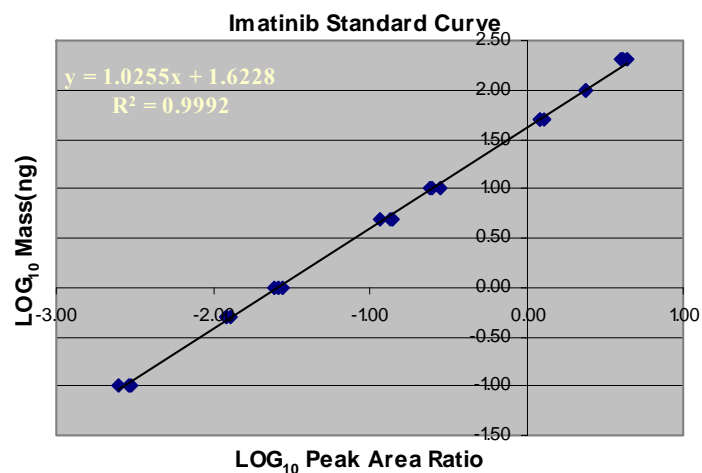
Figure 3-28: Representative example of calibration curve for gefitinib

Gefitinib Standard Curve

$y = 1.0261x - 0.4634$
$R^2 = 0.9987$

X-axis: LOG_{10} Peak Area Ratio
Y-axis: LOG_{10} Mass (ng)
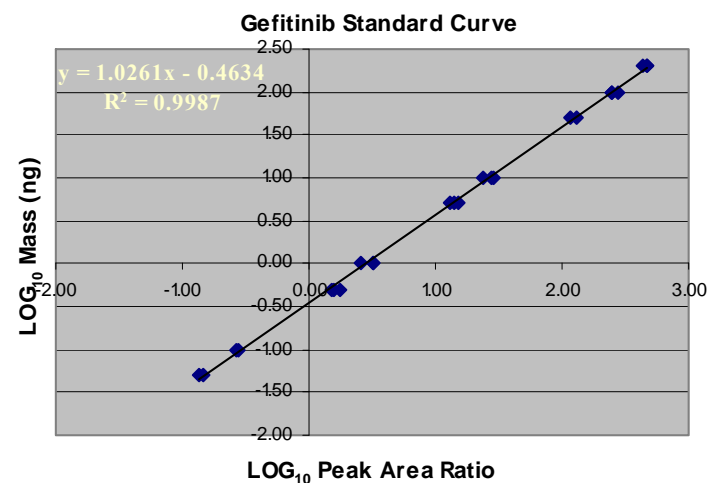
Representative standard curves for erlotinib, imatinib and gefitinib extracted from spiked cell pellet matrix

Table 3-11: Summary of linearity and range

Agent	Range	R^2	Figure
Erlotinib	0.05ng-200ng	0.99	Figure 3-26
Imatinib	0.1ng -200ng	0.99	Figure 3-27
Gefitinib	0.05ng-200ng	0.99	Figure 3-28

3.6.2. Precision and accuracy

Intra-day precision and accuracy was assessed over the mass range by extraction and analysis of triplicate spiked samples on the same day. Inter-day precision and accuracy was assessed over the mass range by extraction and analysis of triplicate spiked samples over independent days, indicated in the table for each TKI. The percentage relative standard deviation (%R.S.D.) was employed as a measure of precision. The % accuracy was determined by dividing the average calculated drug concentration by that of the spiked known concentration.

The mass range employed for erlotinib was 0.05ng -200ng in tube. The mass range employed for imatinib and gefitinib was 0.1ng - 200ng.

The precision and accuracy of the three TKIs examined here are generally good, though erlotinib does show a higher level of imprecision at the lower mass range. This is due to the slight peak broadening at these conditions. However, inter-day assay precision and accuracy is good and within range.

Table 3-12: Intra-day analysis for precision and accuracy for erlotinib.

Spiked Mass (ng)	Erlotinib		
	Mean Mass Observed (ng)	% Accuracy	% R.S.D.
0.05	0.06	118.1	12.1
0.10	0.10	103.1	16.7
0.50	0.42	83.8	13.8
1.0	0.95	94.8	1.7
5	4.7	93.6	9.7
10	10.5	105.4	4.0
50	53.4	106.9	0.5
100	104.7	104.7	8.3
200	192.6	96.3	1.5

The accuracy and precision of erlotinib from triplicate intra-day analysis.

Table 3-13: Inter-day analysis for accuracy and precision for erlotinib.

Spiked Mass (ng)	Erlotinib		
	Mean Mass Observed (ng)	% Accuracy	% R.S.D.
0.05	0.06	110.6	4.1
0.10	0.10	95.2	6.1
0.50	0.48	96.2	7.9
1.0	1.0	98.7	7.7
5	5.0	100.5	4.9
10	10.1*	100.9	4.7
50	51.9	103.8	5.1
100	102.4	102.4	5.9
200	194.1*	92.7	8.8

The accuracy and precision of erlotinib from analysis on five Independent days (* indicated n=4)

Table 3-14: Intra-day analysis for precision and accuracy for imatinib.

Spiked Mass (ng)	Imatinib		
	Mean Mass Observed (ng)	% Accuracy	% R.S.D.
0.10	0.10	98.0	9.3
0.50	0.47	93.8	2.8
1.0	1.0	100.7	5.3
5.0	5.2	103.7	9.1
10.0	10.5	104.9	9.3
50.0	52.3	104.5	3.3
100.0	102.6	102.6	1.3
200.0	181.6	90.8	4.0

The accuracy and precision of imatinib from triplicate intra-day analysis

Table 3-15: Inter-Day analysis for accuracy and precision for imatinib.

Spiked Mass (ng)	Imatinib		
	Mean Mass Observed (ng)	% Accuracy	% R.S.D.
0.10	0.10	100.7	14.0
0.50	0.46	92.4	8.2
1.0	1.0	102.7	4.8
5.0	5.5	110.7	10.0
10.0	10.6	106.5	4.7
50.0	50.1	100.2	3.2
100.0	95.3	95.3	5.6
200.0	193.5	96.8	9.5

The accuracy and precision of imatinib from analysis on five independent days

Table 3-16: Intra-day analysis for precision and accuracy for gefitinib.

Spiked Mass (ng)	Gefitinib		
	Mean Mass Observed (ng)	% Accuracy	% R.S.D.
0.10	0.09	89.4	2.6
0.50	0.57	113.6	7.1
1.0	1.1	105.6	13.3
5.0	5.2	104.6	9.1
10.0	10.0	99.8	8.2
50.0	48.6	97.2	9.5
100.0	102.1	102.1	8.1
200.0	185.5	92.7	6.1

The accuracy and precision of gefitinib from triplicate intra-day analysis

Table 3-17: Inter-Day analysis for accuracy and precision for gefitinib.

Spiked Mass (ng)	Gefitinib		
	Mean Mass Observed (ng)	% Accuracy	% R.S.D.
0.1	0.08	84.9	23.6
0.5	0.45	90.6	20.0
1.0	0.9	93.3	12.6
5.0	4.9	97.8	10.0
10.0	10.4	103.7	2.8
50.0	56.2	112.3	9.9
100.0	111.6	111.6	9.8
200.0	195.0	97.5	15.8

The accuracy and precision of gefitinib from analysis on four independent days

3.6.3. Selectivity and sensitivity

The limit of detection (LOD) was defined as the mass of drug which gave a signal to noise ratio of 3:1. The limit of quantification (LOQ) was defined as the mass of drug which gave a signal to noise ratio of 5:1[300]. The signal-to-noise ratio was calculated by the Masshunter Quantification Analysis Software (Version B.01.04). Calculations were based on the peak area of each drug individually not on the peak area ratio.

During validation spiked samples were prepared (as outlined in Section 2.2.5.2) by spiking 50μL cell suspension with the analyte of interest. This approximately equated to 2.5×10^5 cells in the tube. This is approximately the cell number used for cell accumulation and efflux assays.

3.6.3.1.   *Erlotinib*

Given these criteria, the LOD for erlotinib detection was determined to be 10pg, which equated to 3pg on column with an R.S.D. of 12% on the quantified mass. The LOQ for erlotinib was determined to be 50pg which equates to 15pg on column with an R.S.D. of 8%. These values for LOD and LOQ enable pharmacokinetic monitoring of erlotinib in cell samples.

3.6.3.2.   *Imatinib*

Given these criteria, the LOD for imatinib detection was determined to be between 50pg spiked mass which equated to 15pg on column with an R.S.D. of 13% on the quantified mass. The LOQ for imatinib was determined to be 10pg which equates to 3pg on column with an R.S.D. of 7%. These values for LOD and LOQ enable pharmacokinetic monitoring of both drugs in cell samples.

3.6.3.3.   *Gefitinib*

Given the criteria previously outlined, the LOD for gefitinib detection was determined to be 10pg spiked mass which equated to 3pg on column with an R.S.D. of 3% on the quantified mass (n=2). The LOQ for gefitinib was determined to be 100pg which equates to 30pg on column with an R.S.D. of 2%.

3.6.4. Recovery/extraction efficiency

The extraction efficiency of the procedure was determined by comparing the peak areas of the extracted analytes with those from non-extracted samples. Differing from the validation for dasatinib and lapatinib the recovery for erlotinib was assessed on two types of recovery samples. Non-extracted samples were prepared by calculating the mass of drug on column at 100% extraction. The recovery was also assessed on the extraction of the analytes without a biological matrix. The extraction efficiency of gefitinib was assessed by comparing the extracted samples with the samples with no matrix. The extraction efficiency of imatinib remains to be assessed.

3.6.4.1.   Erlotinib

Recovery across the concentration range was assessed. Recoveries for erlotinib at the concentrations used were good, with an average recovery of 97% when assessed compared to the no matrix standard and 108% when compared to the calculated standard, results are shown in Table 3-18.

Table 3-18: Erlotinib intra assay recovery

	Erlotinib No Matrix		Erlotinib Calculated	
Mass (ng)	Mean % Recovery	%R.S.D.	Mean % Recovery	%R.S.D.
0.05	97.4	12.5	110.4	6.6
0.10	97.9	2.4	86.2	22.5
0.50	97.8	3.5	94.9	4.7
1	103.1	2.8	89.5	16.4
5.	99.5	10.9	111.3	4.2
10.	93.3	17.8	138.5	12.7
50	99.3	1.2	107.8	10.5
100	88.2	1.0	114.8	2.4
200	100.2	2.1	122.0	6.9

The recovery of erlotinib was from triplicate intra-day assays.

Extraction recovery by calculation and extraction recovery compared to the no matrix samples were carried out on separate days.

3.6.4.2.   Gefitinib recovery/extraction efficiency

The extraction efficiency of the procedure was determined by comparing the peak areas of the extracted analytes with those from non-extracted samples. The recovery was assessed on the extraction of the analytes without a biological matrix (no matrix) compared to the extraction of the standard curve, with cell pellet. Recovery across the concentration range was assessed. Recoveries for both drugs at the concentrations used were good with and average recovery of 102% across the concentration range, results are shown in Table 3-19.

Table 3-19: Gefitinib intra-assay recovery

Mass (ng)	Gefitinib No Matrix	
	Mean % Recovery	%R.S.D.
0.05	98.4	3.1
0.1	97.8	0.8
0.5	103.4	0.4
1.0	104.6	3.2
5.0	108.8	8.2
10	115.0	9.9
50	111.3	13.1
100	88.4	19.0
200.	90.0	6.9

The recovery of gefitinib was from triplicate intra-day assays

3.7.   Method application

The analytical method developed and validated for the quantification for lapatinib and dasatinib was applied to

1) The quantification of intra-cellular levels of lapatinib and dasatinib to investigate the relationship between multi-drug resistance protein and tyrosine kinase inhibitors, as detailed in Section 4.

2) The quantification of dasatinib in parental and resistant cell-lines models, Section 3.7.1

3) The quantification of low level dasatinib in cardiac cells, Section 3.7.2

4) The analysis of additional TKIs (erlotinib, imatinib and gefitinib) as detailed in Section 3.6

5) The quantification of erlotinib imatinib and gefitinib in primary glioma cell cultures Section 3.8

3.7.1. Dasatinib quantification in resistant cell-line models

MDA-MB-231 is a triple negative breast cancer cell-line model. Triple negative breast cancer is a particularly difficult cancer to treat as the cells lack the oestrogen receptor, progesterone receptor and HER2 receptor, which are used as targets for treatment in other breast cancer types. A dasatinib-resistant variant of the dasatinib sensitive triple negative breast cancer cell-line MDA-MB-231 was developed by Dr Brendan Corkery[301, 302]. To determine if the mechanism of acquired resistance to dasatinib was due to alterations in the uptake and accumulation of the agent in the cells, an accumulation assay was performed to measure the difference in drug levels in the resistant and parental cell-lines.

The data indicated that transmembrane proteins were not responsible for the level of resistance seen in the MDA-MB231-Das cell-line. As there is no significant difference in the mass of dasatinib accumulated in the resistant cell-line when compared to the parental cell-line we can conclude that active transport of dasatinib out of the cell is not the mechanism of resistance, Figure 3-29.

Figure 3-29: Accumulation of 2μM dasatinib in triple negative breast cancer cell-lines

Dasatinib accumulation in MDA-MB-231 (parent) & MDA-MB-231·Das (resistant)
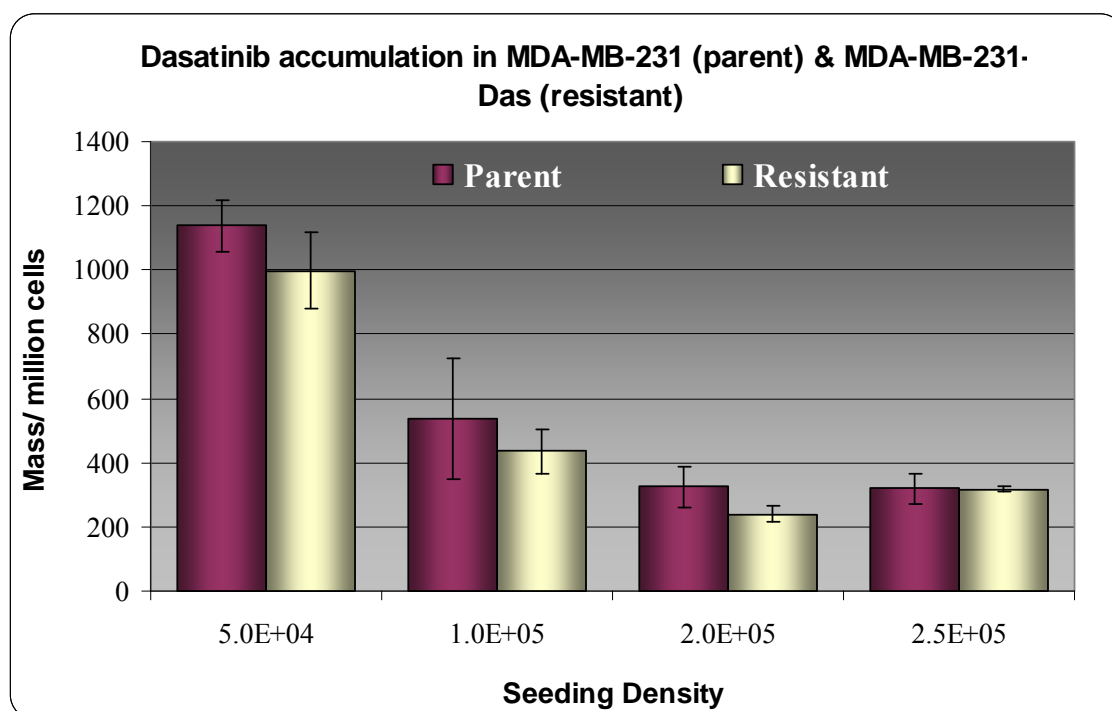
Figure 3-29 shows the effect on seeding density on the quantification of dasatinib in triple negative MDA-MB-231 cell-line model. Data indicates the average and standard deviation of triplicate estimates. The mass of drug accumulated is expressed as mass in nanograms per million cells.

3.7.2. Dasatinib accumulation in cardiac cells

In collaboration with the Dr Sundaravadivel Balasubramanian[303] of the Gazes Cardiac Research Institute at the Medical University of South Carolina we have undertaken to study the accumulation of dasatinib in two different cardiac cell types.

The major cellular components of the heart are cardiomyocytes, cardiac fibroblasts and vascular cells (smooth muscle, endothelium). Cardiomyocytes and cardiac fibroblasts together account for 90% of the cells in the myocardium. The myocardium is the muscular middle layer of the wall of the heart. Together these cells regulate the normal cardiac function[304].

Given the difference of size between the cardiomyocytes and the cardiac fibroblasts the mass of dasatinib accumulated in the cells was normalised to mass of protein, as quantified by the collaborating laboratory, Figure 3-30.

These results show that at low exposure concentrations, 100nM, and low exposure time, 30 minutes, is easily detectable using the developed method. At the earliest time point, 30 minutes, there is a difference in the accumulated levels of dasatinib. This many be due to differences in uptake and efflux of the agent from the cells.

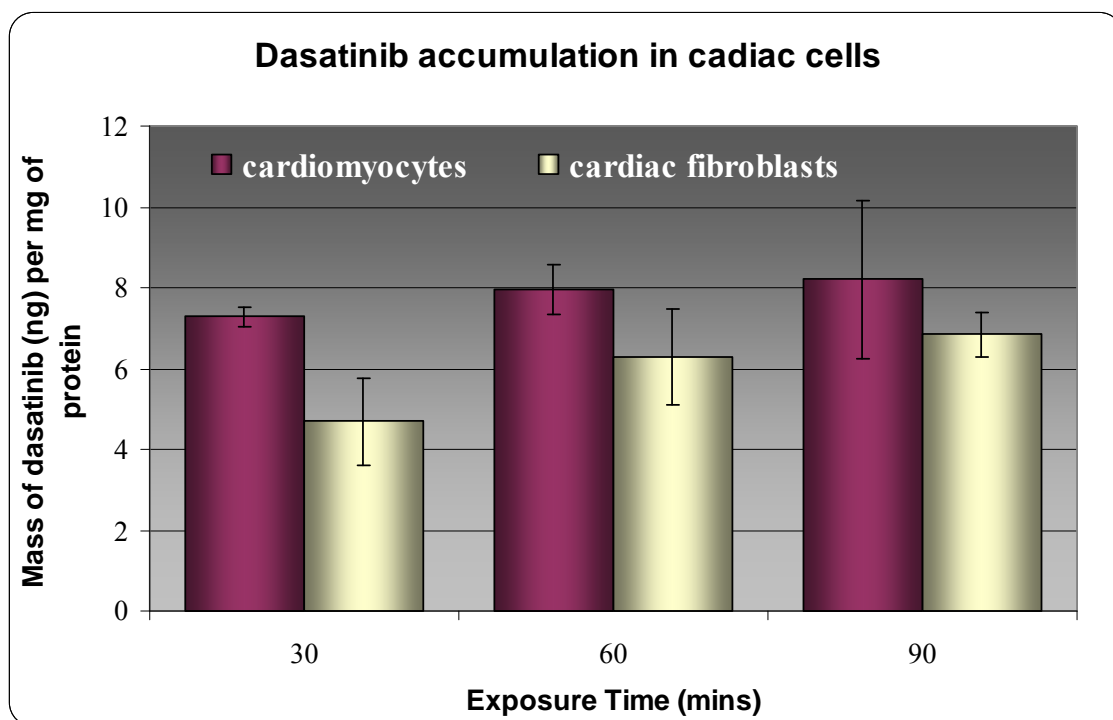**Figure 3-30: Accumulation of dasatinib in cardiac cells**

Figure 3-30 shows the accumulation of 100nM dasatinib in cardiomyocytes and cardiac fibroblasts.

3.8. Application of quantification methods to primary glioma cell cultures

In collaboration with Dr Paula Kinsella & Dr Verena Amberger-Murphy, NICB, investigations were undertaken to examine the accumulation of tyrosine kinase inhibitors in glioma primary cultures. Glioma are the most aggressive form of brain tumours, they arise from glial cells. Gliomas are categorised by histopathology, grade[21] and location into glioblastomas (GBM), astrocytomas, oligodendrogliomas, oligoastrocytomas, and ependymomas [305]. Malignant gliomas comprise WHO grade IV glioblastomas and WHO grade III astrocytoma, oligodendroglioma, and oligoastrocytoma. The prognosis for patients diagnosed with GBMs is grave with only 17-30% survival at year 1 and 3-5% survival at year 2[306].

The treatment of gliomas is hampered by the blood-brain barrier (BBB) which prevents the transport of chemotherapeutics from the blood stream to the required site of action in the brain. The invasiveness of these tumours within the brain makes curative surgical resection impossible as infiltration of the tumour cells may extend up to 2cm away from the radiographically visible contrast mass[307]. Additionally, molecularly malignant gliomas are heterogeneous with several different signalling pathways activated[308].

There is an interest in the use of tyrosine kinase inhibitors in gliomas because expression of epidermal growth factor receptor (EGFR), vascular endothelial growth factor receptor (VEGFR) and platelet derived growth factor receptor (PDGFR) are know to be up-regulated in malignant gliomas and contribute to their malignancy [309]. Erlotinib and gefitinib are TKIs which specifically target EGFR, and the TKI imatinib targets PDGFR.

Through collaboration with Beaumont Hospital, a bio-bank of glioma cell cultures were established and characterised[310]. Using the newly developed methods for the quantification of erlotinib, imatinib and gefitinib in cells, the accumulation of these agents in primary cell cultures was investigated.

---

[21] World Health Organisation classification

Figure 3-31, Figure 3-32 and Figure 3-33 all detail the accumulation of TKIs in primary glioma cell cultures. The primary cell cultures along the x-axis of the graphs are aligned the same order.

Table 3-19 is a summary of the findings of the characteristics of the primary glioma cell culture as detailed in the PhD thesis of Dr Paula Kinsella[310]. Three of the primary cell cultures used in this study were grade IV GBM and one was a grade III oligoastrocytoma.

The level of MDR transporter expression as determined by Western blot analysis is indicated in Table 3-20, represented by symbols "-" to "+++", where – indicates no detectable level of protein found, + indicates low level of protein expression, ++ indicates moderate level of protein expression and +++ indicates high level of protein expression.

**Table 3-20: Summary of characteristics of primary cell cultures and quantified TKI intra-cellular mass**

Primary Culture	Tumour Grade	Transporter Expression		Quantified TKI Mass (ng/million cells)		
		P-gp	BCRP	Gefitinib	Erlotinib	Imatinib
N070055	Oligoastrocytoma Grade III	+	+++	1125.1 +/- 230	22.1 +/- 9.7	351.52 +/- 94
N070152	GBM Grade IV	-	+++	291.5 +/- 57.6	7.6 +/- 1	86.7 +/-5.3
N08923	GBM Grade IV	+++	+++	257.5 +/- 52.4	5.5 +/- 1.1	35.8 +/-3.3
N08943	GBM Grade IV	-	+	136.2 +/- 14.7	4.4 +/- 0.3	136.9 +/-14.4

Summary findings of the characteristics of the cells investigated. Transporter status was determined by Western blot analysis and response status was determined by monolayer *in vitro* proliferation assay[310]. TKI was quantified by LC-MS.

Figure 3-31 shows the accumulation of 2μM gefitinib in four primary cultures after two hour incubation.

The greatest mass of gefitinib per cell number was accumulated in the Grade III Oligoastrocytoma, N070055, and the least was accumulated in the Grade IV GBM, N08943.
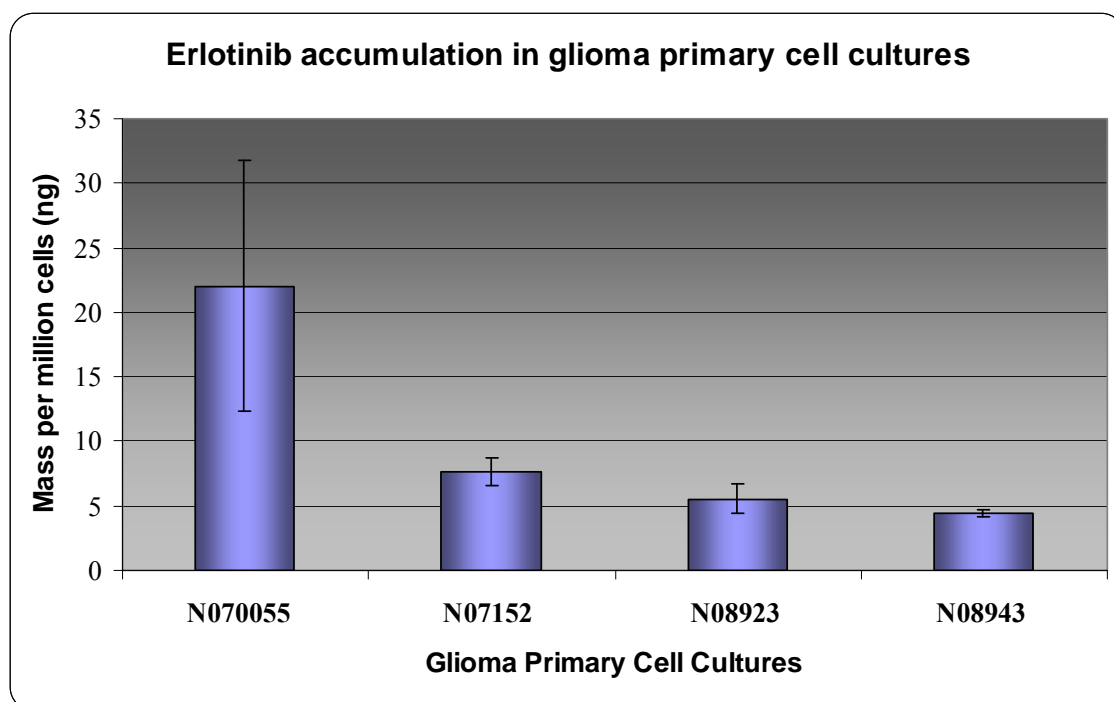
Figure 3-31: Gefitinib accumulation (2μM) in glioma primary cell cultures
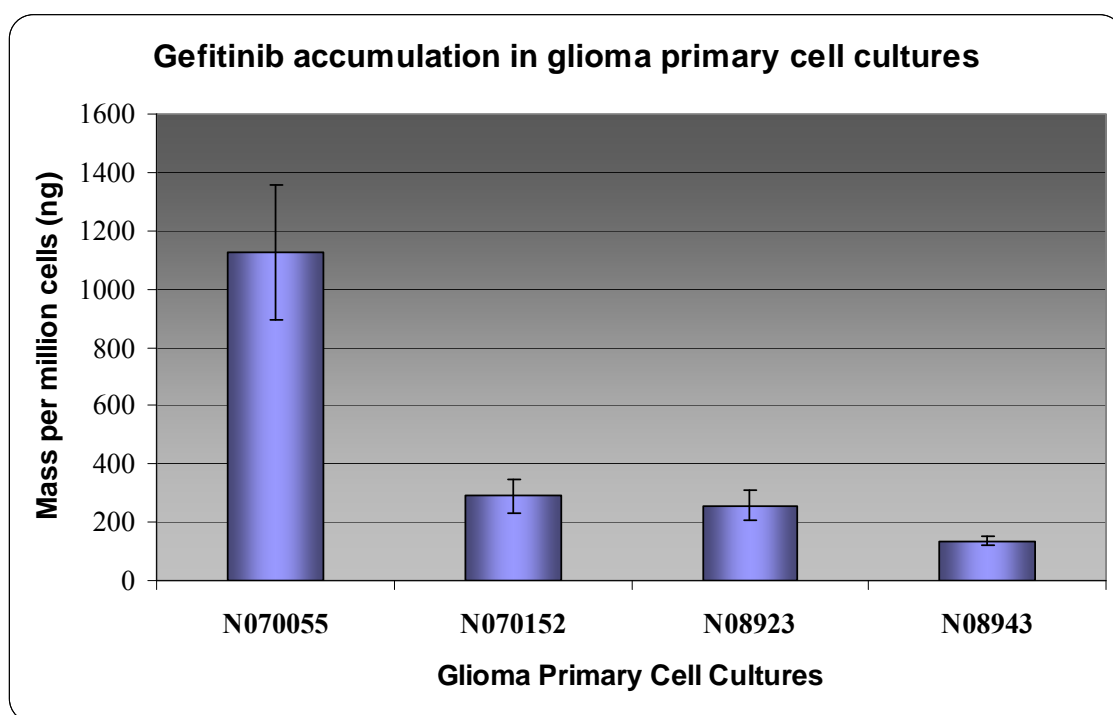
Shown is the quantified mass of gefitinib in four glioma primary cell cultures following two hours exposure to 2μM gefitinib. Data is shown as the average and SD of triplicate determinations.

Figure 3-32 shows the accumulation of 2μM erlotinib in four primary cultures following a two hour incubation. The greatest mass of erlotinib per cell number was accumulated in the Grade III Oligoastrocytoma, N070055, and the least was accumulated in the Grade IV GBM, N08943.

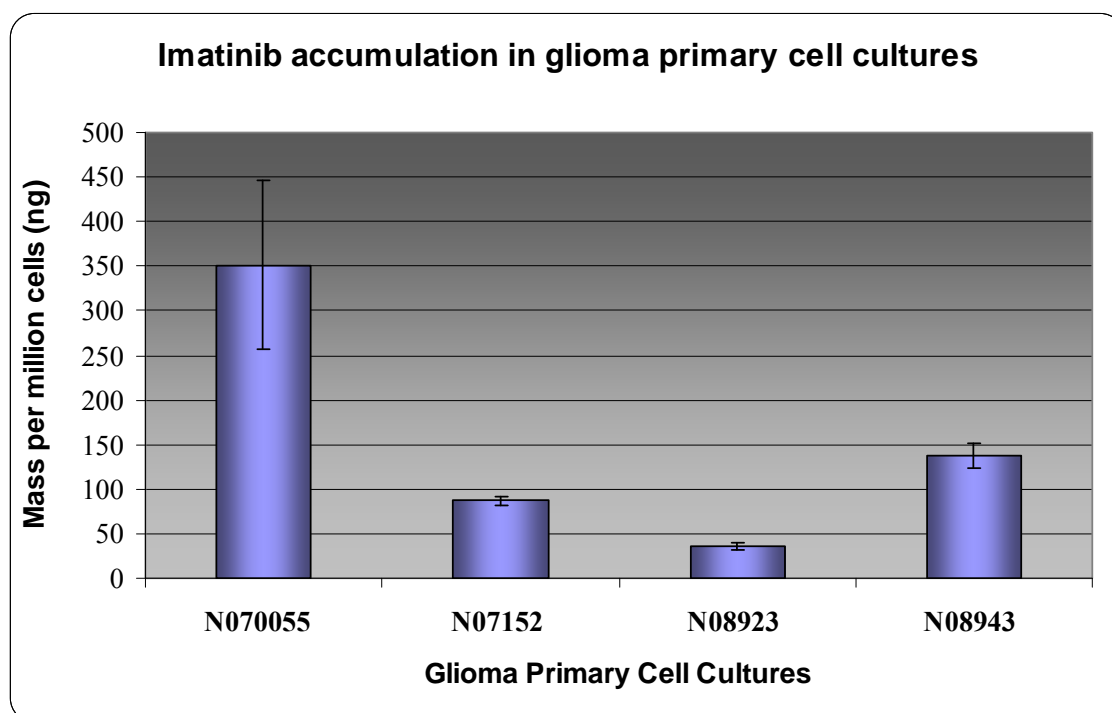**Figure 3-32: Erlotinib accumulation (2μM) in glioma primary cell cultures**

Shown is the quantified mass of erlotinib in four glioma primary cell cultures following two hours exposure to 2μM erlotinib. Data is shown as the average and standard deviation of triplicate determinations.

Figure 3-33 shows the accumulation of 2μM imatinib in four primary cultures after two hour incubation.

The greatest mass of imatinib per cell number was accumulated in the Grade III Oligoastrocytoma, N070055, and the least was accumulated in the Grade IV GBM, N08923.

Figure 3-33: Imatinib accumulation (2μM) in glioma primary cell cultures

Shown is the quantified mass of imatinib in four glioma primary cell cultures following two hours exposure to 2μM imatinib. Data is shown as the average and standard deviation of triplicate determinations.

Overall, more gefitinib accumulated in the cells than imatinib or erlotinib, with erlotinib having the least overall mass accumulated. In all three TKIs examined the grade III oligoastrocytoma, N07005, had the greatest level of accumulation, while grade IV GBM, N08943, had the lowest level for gefitinib and erlotinib and grade IV GBM, N08923, had the lowest level for imatinib. As these primary cell cultures are heterogeneous it is unlikely that the differences in the levels of TKI accumulated are due to cell size as the none of the cultures were uniform in size, differences in cell size should average out between the four cell cultures.

The lower grade N07005 significantly over-expresses BCRP and expresses low levels of P-gp and showed the greatest level of accumulation of all TKIs

In the Grade IV GBM, N070152, high levels of BCRP expression was detected and no P-gp was detected by Western blot, N08923 had high levels of BCRP and P-gp and N08943 showed high levels of BCRP and no detectable P-gp.

N08943 had the lowest accumulated mass of gefitinib and erlotinib though N08923 had the lowest level of imatinib detected.

For the three grade IV GBMs tested N070152 had a higher level of intracellular gefitinib accumulated when compared to the other two glioma cultures of the same grade.

3.9. *Discussion*

3.9.1. Separation conditions and internal standard identification

The development of an LC-MS method for the quantification of TKIs was dependent on the optimisation of separation conditions including column selection, mobile phase optimisation, and selection of an appropriate internal standard.

The optimisation of the mobile phase and stationary phase (column selection) is an intrinsically intertwined process. However, certain considerations are made at the outset of the optimisation process. For the aqueous component of the mobile phase 10mM ammonium formate was selected due to its compatibility with LC-MS. Phosphate buffers were the aqueous phase of choice for traditional HPLC; however, for hyphenated techniques such as LC-MS simple acids such as formic acids are frequently used. For our application, where the pH control of the mobile phase gives optimal separation, the ammonium salt of formic acid, ammonium formate, was used as the aqueous phase, as formate and acetate are volatile and therefore MS compatible[311]. Acetonitrile was selected as the organic modifier of the mobile phase as it is a stronger solvent than methanol, with more resolving power to separate analytes with similar retention chemistry. Reverse phase (RP) chromatography was selected due to its breadth of applications including pesticide analysis[312], forensic analysis[313], and the analysis of food-stuffs[314].

A selection of reverse phase (RP) columns were evaluated as outlined in Table 3-1. Column #1 the SynergSi-Hydro column was determined to be unsuitable for the application due to shifting retention times and instability of the retention profile. Column #2, Hyperclone C18 (100mm x 4.6mm 3µm particle size) gave perfectly acceptable separation of lapatinib and gefitinib (the internal standard used for column assessment). However, by using the narrower column (column #3), Hyperclone C18 (150mm x 2.0mm 3µm particle size), it was possible to scale down the mobile phase flow rate from 0.4mL/min to 0.2mL/min and still maintain adequate separation.

This was chosen as the most suitable column for the application as it gave suitable separation and the reduced mobile phase flow rate results in lower usage of solvent and lower volumes of waste for disposal and thereby reducing costs.

Previous methods for the analysis of lapatinib have used its deuterated analogue as an internal standard[200]. This is often, though not always, considered the best option in terms of internal standards [315, 316]. However, deuterated analogues were not available to us and as the agents are recently released, routinely available structural analogues could not be identified for use as internal standards. Also several articles reported that isotopically labelled internal standards failed to compensate for ion suppression effects[317, 318]. Several of the TKIs have broadly similar physiochemical properties and are more widely available to researchers hence we chose to investigate alternative TKIs as a potential internal standard for lapatinib.

Gefitinib, dasatinib and erlotinib were assessed as potential internal standards for lapatinib with the view to developing a method for the simultaneous analysis and quantification of two tyrosine kinase inhibitors. Table 3-2 outlines the results of the comparisons of the three potential internal standards with respect to peak shape, resolution with lapatinib and limit of detection on the LC-MS.

Generally, quantification is based on the peak area, peak height, or the ratio of the peak areas of the analyte of interest against the internal standard. Measuring the area included under the chromatographic peak, or the area under the curve, is called integration. Chromatographic peaks are integrated by adding the voltage measurements made at equal time intervals from the beginning to the end of the peak, then subtracting a "correction trapezoid" to correct for the offset of the chromatographic baseline from true zero as well as baseline drift[319]. The key to accurately determining the peak area is the ability to:

- ignore random fluctuations in baseline noise
- identify the beginning and end of the peak
- to identify the retention time (peak maximum)

Figure 3-3 illustrates the asymmetry factor. The asymmetry factor of a peak is in simple terms, a factor given to describe the peak shape. During a chromatographic

separation individual solutes develop a symmetrical or Gaussian concentration profile in the direction of the mobile phase[195]. The perfect peak should be symmetrical/ Gaussian. With continued migration through the stationary phase peaks gradually broaden and often become asymmetrical. A peak may be asymmetrical due to peak tailing or peak fronting. Peak fronting is usually a result of over-loading the column, such that some of the solute elutes early as it has been unable to interact with the column[320]. Peak tailing is caused by too much interaction between the column and solute. In a gradient elution this can be rectified by increasing the organic component in the mobile phase composition. However, in isocratic elution this is not straight-forward as increasing the organic composition will affect the resolution between the analytes of interest.

Peak asymmetry affects the ability to accurately identify the beginning and end of a peak, and therefore affects the peak area calculation, which in turn affects the analyst's ability to accurately quantify the analyte. Figure 3-34 illustrates peak fronting and peak tailing.

Figure 3-34: Illustration of peak fronting and tailing[295].
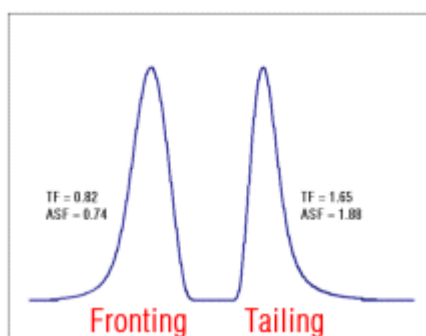
As identified by LC-UV, dasatinib and erlotinib had better peak shape with less tailing and a lower asymmetry factor than gefitinib, making them both applicable as internal standards for lapatinib. However, analysis of the LC-MS findings with dasatinib and erlotinib showed that dasatinib has a lower limit of detection than erlotinib, thus making dasatinib more suitable to our application.

LC-MS compatible 10mM ammonium formate buffer was chosen as the aqueous mobile phase. Even though the pKa of dasatinib is 5.8 and the pKa of lapatinib is

6.61[321], the pH 4 was chosen as the optimum mobile phase pH as pH 3 gave poorer lapatinib peak shape with a greater asymmetry factor than evident with a pH4 aqueous mobile phase.

Optimal resolution of dasatinib and lapatinib peaks from each other and from the void volume was achieved with 54% ACN in the mobile phase when run isocratically at 0.2mL/minute.

3.9.2. Optimisation of MRM transitions

The MRM transition was optimised for each agent in the same manner as detailed for dasatinib in Section 3.3. Detection and quantification by multi reaction mode is undoubtedly the optimum in bio-analytical methods, as the incoming ion stream is filtered for the specific ion of interest. The specific ion undergoes fragmentation in the collision cell, in the presence of an inert gas, in this case pure nitrogen, to yield product ions. The most abundant product ion is used for quantification, while any additional product ions detected are used as qualifier ions. Qualifier ions increase the specificity of the analysis. Frequently in small molecule analysis e.g. pesticide analysis, compounds which differ in structure may have indistinguishable molecular weights, however, product ion(s) increase the selectivity of the analysis. A schematic diagram for MRM mode has been included in Section 1.8.3.4.

3.9.3. Optimisation of extraction

Extraction, in terms of bio-analytical chemistry, is the process of removing the analytes of interest from other potentially confounding substances. Bio-analytical quantification methods are generally desired for the quantification of analytes in patient samples or cell-lines models. From an analytical point of view biological matrices are an additional complication. Biological matrices such as serum, blood, saliva or cells contain lipids, proteins, salts and sugars which would, if not removed, interfere with detection and damage the analytical equipment. The extraction process is based on exploiting the chemical differences between the analyte and the predominantly protein biological sample.

In terms of general bio-analytical extraction procedures, e.g. from serum, it is possible to extract using either on-line or off-line methods. On-line methods are increasingly

advantageous in terms of speed and throughput but do require additional investment in terms of equipment such as robotic liquid handling systems. Off-line extraction methods such as solid phase extraction (SPE), liquid-liquid extraction (LLE) and protein precipitation (PPT) are widely used in quantification of analytes in complex mixtures.

Solid phase extraction is probably the most prolific extraction method used in bioanalysis, with a cursory search yielding 1000s of articles directly related to SPE and LC-MS, ranging from the determination of brostallicin levels in human plasma[322] to pesticides in waste water[323]. Liquid-liquid extraction is similarly prolific and has been used to extract analytes from plant material[324], from plasma[325] and from tissue[326] for quantitative analysis. Protein precipitation (PPT), is preferred for its simplicity, however the extracts obtained are not as clean as those from SPE or LLE and may give rise to matrix effects[327]. PPT is predominantly used for the extraction of agents from plasma[213, 328], though can also be used for blood samples[329].

Due to the high binding affinity of TKI agents to intracellular targets, and the complex nature of cell culture samples, liquid-liquid extraction (LLE) was chosen in preference to other forms of drug extraction as it yields cleaner samples with less matrix effects[327]. LLE physically takes the drug from the high affinity compartment of the cells into the extraction solvent for easier separation.

Based on work by Oostendorp *et al.*[330], for the liquid-liquid extraction of gefitinib, the extraction efficiencies for dasatinib and lapatinib in various solvents alone and in combination with ACN were tested, with the summary findings presented in Figure 3-6. A combination of acetonitrile and *tert*-butyl methyl ether (*t*BME) was determined to be the optimum solvent system for both dasatinib and lapatinib in combination with extraction buffer pH 3.5. The combination of *t*BME with acetonitrile gave the optimal compromise of separating the drugs of interest from their intracellular binding sites while keeping extraction of potential interfering substances from cells to a minimum; use of the *t*BME solvent with ACN also gave the best drug recovery across a number of different pH values, Figure 3-7.

3.9.4. Optimisation of extraction buffer pH

To determine the optimum extraction system for the extraction of lapatinib and dasatinib it was also necessary to examine the effect of varying the pH of the aqueous extraction buffer. Due to its compatibility with mass spectrometry, 1M ammonium formate was selected as the aqueous buffer. The aqueous phase was tested across a pH range to determine an optimum in combination with tBME/ACN (3:1v/v) extraction solvent.

As shown in Figure 3-7 the optimum extraction buffer pH was determined to be pH 3.5 as this gave greater recovery than pH 4 but also gave lower standard deviations and noise in the recovery estimates than were evident at pH 3.

3.9.5. Ion suppression study and effects

3.9.5.1.   Ion Suppression

Ion suppression occurs in situations such as illustrated in Figure 3-35. The red crosses indicate the analytes of interest and the black triangles indicate background ions. Only a finite number of ions can be processed by the MS. In cases of high level of background ions, greater numbers of background ions than analyte ions enter the MS system leading to lower detection, whereas, as illustrated in the second scenario, with lower levels of background "noise" greater numbers of analyte ions can enter the system resulting in an improved signal and better detection.

Figure 3-35 Schematic representation of ion suppression
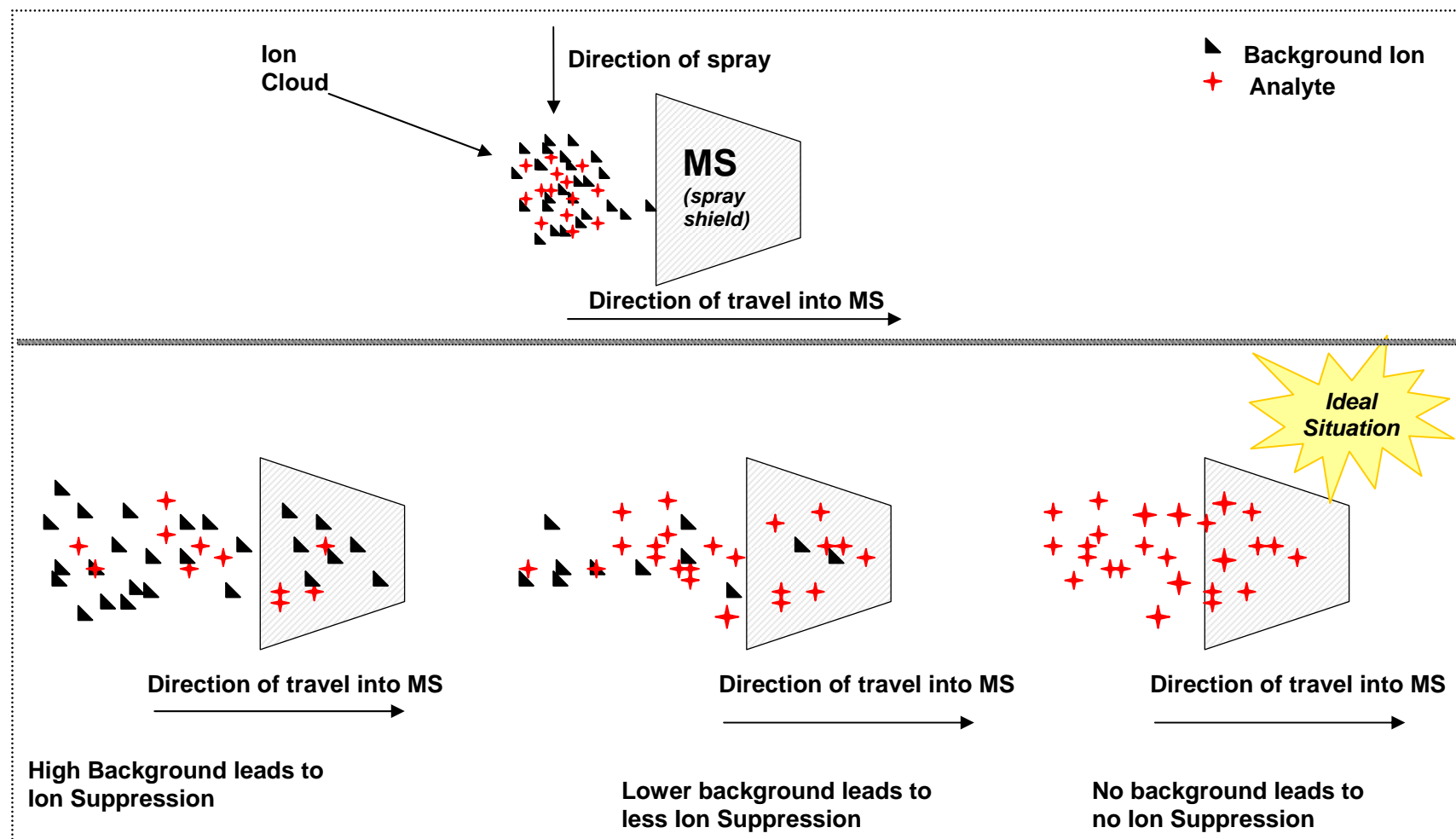
Representation of ion suppression from confounding matrix and background ions, which can saturate the detector preventing maximum ions of interest into the MS

Initially ion suppression was shown to have a dramatic effect on the results. A limitation of the QQQ system is that the MS only searches for the ions and transitions programmed for in MRM mode. While this improves specificity for quantification of known analytes, in the development stage this led to unforeseen issues.

Dramatically lower signals were detected with both analytes persistently in the initial stages of development than would have been expected with liquid-liquid extraction. As shown in Figure 3-14 and Figure 3-15, the quantified mass of the detected analyte for both lapatinib and dasatinib was initially seen to be less than 10% of the expected signal intensity. Good levels of recovery are generally seen from liquid-liquid extractions, therefore these unusual findings indicated an additional problem in the method.

The MRM mode function, (multi-reaction monitoring), illustrated in Figure 1-10, is a setting that employs the three quadrupoles to function precisely at optimised conditions, to quantify a known transition of precursor and product ion. The fragmentor voltage setting acts as a filter allowing the maximum number of precursor ions to enter the system in quadrupole one. The collision cell, considered the second quadrupole, contains pure nitrogen gas. In the collision cell a voltage is applied and the precursor ions are split into their products ions. This explosion occurs as the products ions smash in to the nitrogen ions with the energy from the voltage applied. These product ions continue to travel onwards (in the x direction) to the final quadrant, the third quadrupole. In the third quadrupole the accurate masses of the product ions are detected.

MS2Scan mode is where the first quadrupole allows all ions unfiltered into the collision cell. The collision cell directs the ions to pass unchanged through the octopole and enter into the third sector where all ions are detected.

By monitoring duplicate sample injections in MS2Scan mode, as well as in MRM mode, substantial levels of background ions were detected.

Figure 3-16 shows that the high level of background ions seen in the extracted samples was not from biological matrix. In Figure 3-16 we see three TIC spectrums, injected from the same vial and difference points during the worklist run. This sample was a

mobile phase blank. The black trace, barely visible at the bottom of the image, was injected at the start of the run, the red trace, with high abundance, was injected after 10 extracted samples and the green trace was injected after an additional 10 samples. This indicated that something in the extracted samples was carrying over and sticking to the analytical column and causing high level of ion suppression, as seen with the extremely low analyte signal, Figure 3-14 and Figure 3-15.

The high level of background detected in MS2Scan mode was attributed to the preparation and storage of stock standards in polypropylene (PE) tubes. These tubes showed no detectable level of contamination in extractions over a short storage period (1 day) but over longer periods (2-3 days) significant contamination was detected which caused the suppression of the ion signal. The contaminating ions were possibly plasticiser which leached from the plastics over a prolonged period of time in the presence of a strong solvent, acetonitrile. While it is also possible that artefacts from the biological matrix caused the background, this was eliminated as samples prepared from freshly prepared stock standards showed good recovery and low background, while samples prepared from stock standards that were stored for 3 days showed poor recovery and high background. As the biological matrix was the same in each sample set analysed the only difference was the length of time the stock standards were stored. As a result of this, stock standards were prepared fresh in glass 10mL tubes, with working calibration curves being used within an hour of being prepared.

Having identified the issue leading to poor extraction, it was then necessary to quantify the normal level of ion suppression from the biological matrix in the assay. Two methods were used to identify the level of ion suppression from the biological matrix.

Post-column infusion is frequently used for the determination of ion suppression. Post column infusion, as illustrated in Figure 3-17, involves the infusion of a concentration of the analyte, in this case 2μg/mL, using an infusion pump to provide a constant steady flow, in this case 50μL/min. This was "T"-pieced into the flow-path before the ion source but after the analytical column. Using the LC method, extracted blank samples were injected from the autosampler. The flow of analyte into the MS gives a constant signal, and as the flow was steady and controlled the signal was level. This made it

possible to determine any disturbances in the signal that may have been ion suppression or ion enhancement. By injecting the extracted cell blank sample through the analytical column it was possible to determine when any potentially confounding substances may elute and to what level these substances had an effect. The main source of commonly observed matrix effects in bio-analytical LC-MS is thought to be endogenous phospholipids and proteins[327]. Post-column infusion was initially used to determine the ion suppression of lapatinib and dasatinib as shown in Figure 3-18 and Figure 3-19.

In Figure 3-18, the ion suppression of dasatinib was assessed. The injection of an extracted blank cell sample showed dasatinib to suffer approximately 40% loss in signal due to ion suppression (spectrum B). This was identified to have been due to the extracted cell blank as an injection of mobile phase through the system showed no effect on the dasatinib signal.

Similarly in Figure 3-19 we see that the ion suppression of lapatinib at the retention time for lapatinib is approximately 10% when extracted cell blanks were injected (spectrum B). The drop in signal was due to the extraneous elements of the cells which were extracted in the LLE process. The stability of the signal when mobile phase is injected indicates that the suppressing ions were coming from the extracted cell sample.

Dasatinib suffered a much greater level of ion suppression as it elutes earlier than lapatinib and elutes closer to the column dead time. Column dead time is the time for elution of the earliest possible band, or mobile phase molecules[295].

Small changes in the ratio of organic to aqueous in the mobile phase composition have a substantial effect on the retention time of the analytes. Increasing the ratio of organic decreases the solute's interaction with the column and decreases the retention time. The optimum mobile phase for isocratic elution was found to be ACN: 10mM ammonium formate pH4, 54/46, (v/v). This was verified by premixing the solutions for mobile phase and injecting the sample. The retention time of dasatinib has shifted to 2.39 minutes and lapatinib has shifted to 5.39 minutes.

Using these conditions the new level of ion suppression was assessed using a post extraction spike method detailed in Zirrolli *et al*.[234],but developed by Matuszewski *et*

al., in 2003 [331]. Over the mass range of 1 to 100ng the percentage of signal intensity affected by the ion suppression/enhancement was minimal, Figure 3-21and Figure 3-22. This would indicate that a small shift in retention time was sufficient to alleviate the issue.

3.9.6. Assay validation

The validation of an analytical method should be designed to test the suitability of the method for its intended purpose[332]. The overall LC-MS method was validated for the following performance parameters- linearity and range, intra-day precision (repeatability) and inter-day precision (intermediate precision), accuracy, sensitivity, (LOD and LOQ), recovery and sample stability according to the guidelines described by Ermer[299]. MRM allows for the individual determination of each drug, with the use of internal standard-based quantification.

Figure 3-25 shows the extraction and detection of multiple TKIs using the method validated for lapatinib and dasatinib, without any changes. While the method is currently not completely validated for the analysis of additional TKIs, this demonstrates the broader applicability of this method to extract other TKIs and quantify by LC-MS/MS. The TKIs used in this study, erlotinib, imatinib, gefitinib and sorafenib are all clinically relevant agents.

Preliminary partial validation of erlotinib, imatinib and gefitinib has been carried out using the same exact conditions as optimised for dasatinib and lapatinib.

3.9.6.1. Linearity and Range
Dasatinib and lapatinib

For dasatinib and lapatinib analysis the standard curves were linear across the concentration range investigated. In a phase II study of dasatinib treatment in head and neck squamous cell carcinoma the maximum plasma concentration was 168.2 ng/mL[333]. In 50μL, the estimated volume of the cell pellet, this would equate to 8ng. This is comfortably within the assayed range. The mean peak plasma concentration of lapatinib in a Phase I study of lapatinib in combination with Herceptin was 1.5μg/mL, which equates approximately to 75ng in a 50μL sample[334]. These levels are within the range examined.

Erlotinib, Imatinib, Gefitinib

All three agents, erlotinib imatinib and gefitinib were linear across the concentration range employed. The upper level spiked mass was 200ng/tube. Masses greater than this were not investigated as our experience with lapatinib and dasatinib as well as with erlotinib, imatinib and gefitinib in glioma cells showed that higher mass ranges are not necessary to encompass the samples. An in tube mass of 200ng equates approximately to 4μg/mL when the volume of the cell pellet is approximated to 50μL. The maximum plasma concentration of erlotinib was found to be 2.6μg/mL for a patient receiving 150mg [220]. The maximum plasma concentration of imatinib was found to be 1.5μg/mL for a patient receiving 600mg/day[335]. The maximum plasma concentration of gefitinib was found to be 212ng/mL following a single dose of 250mg[221]. These levels are well within the range examined.

3.9.6.2. *Precision and accuracy*

Precision is a measure of how close to each other a group of results are. Accuracy is a measure of how close to the expected values a group of results are. It is possible for analysis to be precise but not accurate and for an assay to be accurate but not precise. Both precision and accuracy are important in quantitative analysis for an assay to be reliable. The precision and accuracy was assessed both inter-day and intra-day. The intra-day precision and accuracy is the evaluation of triplicate samples analysed on the same day, whereas inter-day precision and accuracy is the evaluation of triplicate samples on independent days.

Dasatinib and lapatinib

The average inter-day accuracy across the concentration ranged examined was 100% and 102% for dasatinib and lapatinib respectively. The average precision (%R.S.D.) across the concentration range was 6.4% and 7.6% for dasatinib and lapatinib respectively. With an average inter-day precision of less than 10% the reproducibility of the method was deemed acceptable.

Erlotinib, Imatinib, Gefitinib

The precision and accuracy for erlotinib, imatinib and gefitinib was assessed both intra-day (repeatability) and inter-day (reproducibility). The average inter-day accuracy across the concentration range was 100.1%, 100.7% and 99% respectively for erlotinib, imatinib and gefitinib. The average inter-day precision was 6.1% 7.5% and 13.1% respectively.

The developed extraction and separation procedure was deemed acceptable for the extraction and separation of each agent individually from the internal standard. The method had good repeatability and good reproducibility as well as a high level of accuracy.

3.9.6.3.   *Selectivity*

Selectivity and specificity are terms that are often used interchangeably. Vessman *et al.*[336], discusses, in detail the definitions of these terms as defined by various interested organisations. The Western European Laboratory Accreditation Cooperation (WELAC) definitions of selectivity and specificity are:

- *Selectivity* of a method refers to the extent to which it can determine particular analyte(s) in a complex mixture without interference from other components in the mixture

- A method which is perfectly selective for an analyte or group of analytes is said to be *specific*

The International Conference on Harmonisation (ICH) defines specificity as

- *Specificity* is the ability to assess unequivocally the analyte in the presence of the components which may be expected to be present. Typically these might include impurities, degradants, matrix etc.

However, in its most basic format, according to G.D Christian [337] a method is specific when the analyte alone is responsible for the signal that is measured.

The necessity for method selectivity and specificity and the intense focus that has come to bear on this requirement is a remnant of validation guidelines developed for the application of HPLC-UV methods. In terms of MS and in particular tandem MS, selectivity and specificity are more clear-cut and apparent. Both the selectivity and specificity are inherently linked to the mode of action of the triple quadrupole mass spectrometry. As shown in Figure 1-12, a triple quadrupole consists of three chambers, MS1, the collision cell and MS2. The triple quadrupole system allows for multiple reaction monitoring (MRM), and the ability to track ions of specific mass to charge ratio (m/z) though the system and monitor the break down from precursor to product ions. This is the specificity of tandem mass spectrometry (MS/MS). The ability to monitor more than one product ion gives increased selectivity.

Of the six TKIs investigated four, imatinib, dasatinib, erlotinib and sorafenib had multiple transitions from precursor to product ions. The ability to monitor additional

product ions increases the specificity of the analysis. While lapatinib and gefitinib had only one product ion the incorporation of both the retention characteristics and mass transitions make this assay specific for all analytes selected.

3.9.6.4. *Sensitivity*

LC-MS is inherently more sensitive than LC-UV detection because LC-MS can monitor individual ions whereas; LC-UV is reliant on an entirely different detection system. There are three types of UV detectors, which are single wavelength detectors, variable wavelength detectors and fast scan or diode-array detectors[338]. However, MS detectors combine specificity, selectivity and sensitivity[339].

The increased sensitivity of the LC-MS gave the ability to quantify in the picogram range. Quantification was based on the mass transitions from precursor to product ion. The increased sensitivity of the Agilent Triple Quadrupole MS is in part due to the orientation of the ionisation. The orthogonal orientation of the nebuliser spray to the sample capillary reduces the background noise from the samples allowing lower LOD and LOQ. This is because any ions that are uncharged in the source do not make it into the MS system. The MS is capable of being saturated i.e. it can only "count" a finite number of ions, it is imperative for high sensitivity to increase the number of analyte ions entering the system at a cost to the number of eluent ions and potentially confounding ions that would otherwise "dilute" the signal and result in reduced sensitivity.

For the determination of the limit of quantification (LOQ) and limit of detection (LOD), guidelines by Shah *et al.*[300], were followed, whereby the LOQ was defined as the mass of drug which gave a signal to noise ratio of 5:1 and the LOD was defined as the mass of drug which gave a signal to noise ratio of 3:1. Noise is the width of the baseline created by background fluctuations such as the detector electronics, pump oscillations and/or a dirty column or the baseline signal in the absence of the analyte[340]. Practically speaking the LOD is the minimum level at which we can identify the presence of the analyte of interest in the spectrum, whereas the LOQ is the level whereby we can, with confidence, quantify the mass of analyte present against the background of matrix ions.

Dasatinib and lapatinib

The method developed here showed sensitivity comparable to if not better than recently published methods, with an LOQ of 200pg/million cells and 400pg/million cells for dasatinib and lapatinib respectively. If the cell pellet volume is estimated to be approximately 50μL, this gives an LOQ of 1ng/mL and 2ng/mL for dasatinib and lapatinib respectively. Other published methods for the quantification of dasatinib and LOQ of 78.1ng/mL[212]. The method by Haouala *et al.*[213], reported a similar LOQ for dasatinib, 1ng/mL but is a longer more complex method.

Previously reported LOQs for lapatinib were 5ng/mL[213] and 15ng/mL[200], indicating that the method developed here is more sensitive than those currently in the literature.

Erlotinib, Imatinib, Gefitinib

The developed method has shown good sensitivity for the three additional TKIs assessed. The LOQ was found to be 50pg, 50pg and 100pg spiked mass for erlotinib imatinib and gefitinib respectively. If the approximate volume of the cell pellet is estimated to be 50μL then the LOQ is determined to be 1ng/mL for erlotinib and imatinib and 2ng/mL for gefitinib. This compares favourable with recently published LC-MS methods.

An LOQ of 10ng/mL[219] and 6.2ng/mL (reported as 12.7nM)[218] for erlotinib has been reported previously. The method developed here is more sensitive for erlotinib than these LC-MS methods. An LOQ of 1ng/mL[213] as been previously reported for imatinib, though, as already described this gradient method is more complex and has a longer retention time than the method developed here. An LOQ of 1ng/mL[221] 0.5ng/mL[223] and 0.1ng/mL[222] have been reported for the analysis of gefitinib. The most recent publication also reported an LOQ of 4.9ng/mL (reported as11.2nM)[218]. Quantified in this method is an LOQ of 2ng/mL. The method validated here is more sensitive for erlotinib than previously reported methods, similar sensitivity for imatinib as previously reported and not quite as sensitive as the current published methods for gefitinib. However, the sensitivity of this method for gefitinib is suitable for the requirement of the quantification of gefitinib in cells.

3.9.6.5. Recovery/extraction efficiency

The percentage recovery and the extraction efficiency of the method were established by direct comparison of the peak areas of the extracted sample compared to that of a pure solvent standard. The peak area of the pure solvent standard was normalised to 100% extraction.

We have seen that both ion suppression and the extraction system employed play equally important roles in the measurement, the detection and hence the extraction recovery. Figure 3-14 and Figure 3-15 show the detected analyte signal in a suppressed detection system. Through the identification of the source of the contaminant and sensitivity dramatically improved, allowing for a calculation of extraction efficiency using LC-MS, Table 3-9.

Dasatinib and lapatinib

For validation studies the recovery was assessed at three concentrations 100, 10, 0.1ng for both lapatinib and dasatinib. We determined the recoveries for both drugs ranged from 86-112%. The recovery associated with the liquid-liquid extraction method developed here is compared, in Table 1-6 with validated published methods available to date in the literature. It is clear that our method compares favourably to those outlined here, with some methods showing no evidence of recovery determination in the validation [205, 217], existing lapatinib methodology showing significantly lower recovery (75%)[200] and recently published dasatinib methodologies showed similar recovery ranges[212, 213].

Erlotinib, Gefitinib

The recovery for erlotinib was determined to be 97% when compared to the "no matrix" recovery sample and 108% when compared to the calculated recovery sample. This is inline with published methods such as Honeywell *et al.*[218], 96-109%, and Leper *et al.*[220], (~100%) and superior to the method published by Masters *et al.*, 79-87%[219]. For gefitinib the average recovery was determined to 101.9%, ranging from 88%-114% across the concentration range when compared to the "no matrix" recovery sample. This is similar to previously published methods detailing recoveries of 81-103 %[221] and more accurate than 111-124% as published by Jones *et al.*[223].

3.9.6.6.   *Stability through freeze/thaw*

Sample stability is important in the development of bio-analytical methods though most validation advice and literature is geared towards the validation of serum as the biological matrix. However, our study is based on the quantification of TKIs in cells with the cell pellet as our biological matrix. For our study we chose freeze/thaw cycles of these cell samples as an indication of sample stability. As described by Dadgar *et al.*[341], there are many types of stability validation for biological matrices and sample stability there within, including (i) long term stability of analytes (ii) stability of the reference standard (iii) short term stability of analytes (iv) in-process stability (v) processed sample stability (vi) freeze-thaw stability.

Long term stability is more relevant for the validation of an analytical method for the analysis of serum as samples from a clinical study are potentially stored for long periods of time until the clinical study is complete and all samples can be analysed together. Concurrently with the validation for long term stability is the stability of the matrix itself and whether matrix degradation can lead to interferences. Also of interest is that Dadgar states that the long term stability of a matrix should be evaluated for each applicable matrix and that inter-species extrapolation is invalid. This is predominantly relevant to the validation of serum as the biological matrix.

More relevant for the intended purpose of this method is a freeze thaw stability analysis, predominantly as the cell samples are stored for short periods before extraction and post extraction samples are directly injected with minimal lag time. Potential instability would most likely come from samples being moved thus inducing a freeze thaw cycle.

As pointed out by Karnes[342] there is very little FDA guidance on the issue of stability testing, though generally accepted principles were set down by Trissel [343] in 1983.

Table 3-9 and Table 3-10 show stability of dasatinib and lapatinib, respectively. As can been seen from the results, dasatinib is very stable over the tested conditions. Lapatinib is acceptably stable though some deterioration in stability is seen on the fourth freeze/thaw cycle. This would indicate that either the analyte is breaking down under the test conditions or that additional components are interfering with the detection of the analyte. Additional analysis to determine the cause of the instability is unnecessary as

this level of instability is acceptable and indicates that no more than three freezer/thaw cycles should be allowed prior to extraction and analysis. Realistically samples rarely, if ever, undergo freeze/thaw cycles.

The stability of erlotinib, gefitinib and imatinib remains to be tested.

3.9.7. Summary of method validation

Overall the use of a liquid–liquid extraction clean-up stage gives the simplicity of application making the method accessible to other researchers undertaking large numbers of analyses without the need for extra equipment or expensive clean-up columns, while an isocratic elution scheme gives a simple, robust and reproducible chromatographic method.

In summary the method outlined and validated here compares excellently with other methods published in the literature, detailed in Table 1-6.

- The method developed here for dasatinib is more sensitive than De Francia *et al.*[212], 1ng/mL compared to 78ng/mL. The sensitivity for our method is equivalent to Haouala *et al.*[213], however, our method is more straight-forward, with a isocratic separation compared to a step-wise gradient elution and faster with a 8 minute run time in comparison to a 20 minute run time.

- This method is more sensitive for lapatinib than the method of Bai *et al.*[200], for the quantification of lapatinib - 2ng/mL compared to 15ng/mL.

- Our experimental approach has yielded superior levels of sensitivity and the specificity of the analytical method may also allow for broader applicability to the determination of a number of other TKI agents and from other biological matrices, e.g. patient serum.

- The partial validation of this method for erlotinib indicated that the range is suitable for the investigation of cell and patient samples. The sensitivity is superior to previously published method and the recovery is excellent.

- The partial validation of this method for imatinib indicated it is suitable for the analysis of imatinib across a broad concentration range, with sensitivity in line with work already published.

- Likewise this method is suitable for the analysis of gefitinib in cell and possibly patient samples with a good range a linear response range. The sensitivity of the assay is acceptable for the application and could possibly be improved with alternations to the analytical separations. The recovery for gefitinib is also excellent.

3.9.8. Method applicability

3.9.8.1.　　Analysis of dasatinib in resistant cell-line models

The clear strength of this method is its applicability to determine useful information about the resistance of lapatinib and dasatinib in cell-line models.　The cellular mechanism of resistance can be attributed to many factors including a) the inducement of the over-expression of ABC multi drug transporters as a response to drug exposure b) modulations of the cell death pathways, where by the cell avoids apoptosis by switching on other cellular pathways.

MDA-MD-231 is a triple negative breast cancer cell-line which is sensitive to dasatinib. Through continuous selection with dasatinib, a resistant variant was developed, by Dr Brendan Corkery[302].　To determine if resistance was due to changes in the membrane transport proteins, we investigated the level of dasatinib accumulation in the parental and resistant models.　The data indicated no significant difference between the mass of drug accumulated between the resistant and parental cell-lines.

Figure 3-29 shows the mass of dasatinib accumulated in the resistant and parental cell-lines and examines the effect of varying cell seeding density.　To eliminate and account of possible inaccuracies or errors/variations in the trypsinisation of one group of flasks compared to another, the mass of drug quantified in each flask is ultimately normalised to the number of cells in the flask, as determined through manual counting or counting by flow-cytometric methods e.g. Guava.

The lowest seeding density examined gave results in a non-linear agreement to other investigations.　This low cell number may be more vulnerable to errors in counting and this more unreliable.　Also, in Figure 3-29 we can see that there is no significant difference across the range of seeding densities investigated in the mass of dasatinib accumulated in the parental compared to the resistant.　This would indicate that the mechanism of resistance of dasatinib in MDA-MB-231 cell-line is not through the over-expression or ABC transporters.

We can see from Figure 3-29 that the LLE-LC-MS/MS method developed for the quantification of lapatinib and dasatinib not only validated but is also "fit for purpose"

i.e. the quantification of the intracellular levels of dasatinib in cancer cell-line models and the utilisation of this information to determine the resistance status of a cancer cell-line model.

3.9.8.2.   *Dasatinib analysis in cardiac cells*

The technical challenges faced in the analysis of dasatinib in two types of cardiac cells involved both the low level of dasatinib exposed to the cells (100nM), the short time frame for exposure (30 minutes) and unknown uptake properties of dasatinib in cardiac cells.

The high level of sensitivity of the method allowed for easy quantification of dasatinib in both cell types. The difference in cell size, with the cardiomyocytes being noticeably larger than the cardiac fibroblast, does lead to a bias in the evaluation of the data as the quantified mass is generally normalised to cell number. However, the normalisation of the quantified mass to the mass of total protein in the pellet reduced the effect of cell volume on the analysis.

It is clear that the method developed here is very sensitive and highly applicable to alternative cell types in addition to cancer cell-line models. The ability to accurately quantify the mass within these cells enables the researcher determine if differences in response are due to differences in accumulated mass of the agent.

3.9.9. Analysis of TKIs in glioma

Malignant gliomas are inherently difficult to treat with chemotherapeutics due to their location (inside the blood brain barrier) and their heterogeneous nature. The use of TKIs in the treatment of malignant glioma are currently being investigated[309]. Detailed in Section 3.8 is the accumulation of TKIs erlotinib, imatinib and gefitinib in primary glioma cell cultures, which were established in-house[310].

Erlotinib, a targeted therapy approved for the treatment of non small cell lung cancer (NSCLC), targets the EGFR receptor. It has been shown *in vitro* that erlotinib is a substrate of P-gp and BCRP[344]. Animal studies with knock-out mice showed that P-gp appeared to be the most effective factor in limiting brain penetration of erlotinib, though BCRP also reduced brain penetration[185].

Our results indicate that the lower grade III primary cell culture, N070055, accumulated more erlotinib than the other higher grade IV primary cell cultures. While N070055 does express low levels of P-gp and high levels of BCRP it also showed a response to erlotinib.

Imatinib, an approved therapy for the treatment of CML, is a multi-kinase inhibitor targeting PDGFR, Abl kinase, cKit. Imatinib has been shown to inhibit glioma invasion in combination with docetaxel *in vitro*[345]. In a Phase II study imatinib was detected in glioblastoma tissue however, it was suggested that imatinib does not substantially reduce proliferation and survival mechanisms[346]. In our study imatinib only showed a response in the lower grade III N070055, which also showed the greater level of accumulation than the other cell cultures. N08923 which strongly over-expresses both P-gp and BCRP had the lowest level of accumulation of imatinib, indicating that the level of imatinib is affected by ABC transporter expression.

Levels of TKI accumulated in glioma cells analysed showed that quantified mass of in the order of gefitinib> imatinib>erlotinib, however three out of four cell-lines showed response to erlotinib, two out of four were classed as responders to gefitinib and only one of the four cell-cultures responded to imatinib.

Gefitinib is an EGFR inhibitor, approved for treatment in NSCLC. It is thought that gefitinib may be of particular benefit to patients who express particular mutations of EGFR[156]. Gefitinib increases brain accumulation of topotecan [347]. However, the expression of P-gp and BCRP has been shown to limit the accumulation of gefitinib in the brain of knock-out mice.[348]

Our studies have shown that a greater mass of gefitinib accumulated in the primary cell cultures than either of the other two TKIs. Also the lower grade III, N070055, showed the greatest accumulation of gefitinib of the four cell cultures examined. However, gefitinib showed no toxic response in this cell culture.

Interestingly, considering the weight given to the expression of efflux pumps in the BBB and gliomas, this non-responsive grade IV did not have any detectable expression of P-gp and only low level expression for BCRP. N08943 also had the lowest level of accumulation of erlotinib and gefitinib, though not imatinib. This indicates that while the role of ABC transporters is important in elucidating functional logical for the response or lack of response of an agent it is not the complete picture.

3.9.10. Summary of method application discussion

Here we have shown the multiple applications of our novel method for the quantification of TKIs.

- Our developed method has been shown to be straight-forward, sensitive and suitable for the quantification of intra-cellular levels of dasatinib.

- Using the dasatinib quantification method developed, we determined that resistance in a newly developed dasatinib-resistant cell-line model, MDA-MD-231-Das, was not due to the efflux of dasatinib.

- The superior level of sensitivity in our developed method was capable of quantifying low level dasatinib accumulation in cardiac cells.

- The extraction and separation criteria have been shown to be applicable for the analysis of multiple TKIs.

- The multiple applicability of the TKI method developed has been partially validated for erlotinib, gefitinib and imatinib in cells.

- This quantification technique has been applied to the novel quantification of erlotinib, imatinib and gefitinib in primary glioma cell-cultures, and shown the differences in the uptake of TKIs in glioma cell-cultures.

SECTION 4.0 Results and discussion

Investigation of dasatinib and lapatinib interaction with MDR over-expressing cell-lines

4. Investigation of dasatinib and lapatinib interaction with MDR over-expressing cell-lines

Introduction

Having developed a method for the quantification of lapatinib and dasatinib in the biological matrix of cells, this was brought forward and applied to the investigation of the kinetics of uptake and efflux of lapatinib and dasatinib in cancer cell-line models.

This section examined the uptake and efflux of dasatinib and lapatinib in ABC transport protein over-expressing cell-line models.

For clarity, through the course of the results and discussion ABCB1, also called MDR-1 and P-glycoprotein will be referred to as P-gp, ABCC1 also called MRP or MRP-1 will be referred to as MRP-1 and ABCG2 also called MXR, ABCP and BCRP will be referred to as BCRP.

4.1. Cell-line models

The cell line models used have been extensively characterised both in-house and in the literature. Each model selected was chosen on the basis of its MDR status. Table 4-1 gives the MDR status of each cell-line in addition to the level of protein expression.

Table 4-1: Cell-line models used and the MDR expressed

Cell-line	MDR protein expressed	Level of expression	Western	Figure #	Ref.
DLKP	-	-	Y	Figure 4-1 to Figure 4-6	[283, 349]
DLKP-A	P-gp	high	Y	Figure 4-1 & Figure 4-4	[284]
DLKP-Sq	-	-	Y	Figure 4-8 & Figure 4-9	Helena Joyce
DLKP-Sq/Mitox-BCRP	BCRP	high	Y	Figure 4-8 & Figure 4-9	Helena Joyce
DLKP-Sq/Mitox-MDR	P-gp	high	Y	Figure 4-8 & Figure 4-9	Helena Joyce
A549	MRP-1	moderate	Y	Figure 4-4 to Figure 4-6	
A549-tax	P-gp	low	Y	Figure 4-4 to Figure 4-6	[5, 286]
2008/MRP-1	MRP-1	moderate	Y	Figure 4-2	
HL60/S	-	-	Y	Figure 4-1 to Figure 4-3	[287, 288]
HL60/Adr	MRP-1	moderate	Y	Figure 4-2	[288]
HL60/Mdr1	P-gp	high	Y	Figure 4-1	[123]
HL60/Mxr	BCRP	high	Y	Figure 4-3	[123]
RPMI-2650/Tax	P-gp	High	Y (from lit)	Figure 4-10 & Figure 4-11	[289]
KB-3-1	-	-	Y (from lit)	Figure 4-12	[350]
KB-8-5-11	P-gp	High	Y (from lit)	Figure 4-12	[350]
IGROV-1CDDP	P-gp	High	Y	Figure 4-7	[351]

Table 4-1 details the cell-line models used through-out this section of the thesis and the status of the MDR protein, as determined by Western blot analysis.

The DLKP cell-line was established in the NICB from the biopsy of lung carcinoma[285, 352]. DLKP-A is a resistant variant, which was selected by exposure to adriamycin, over-expresses P-gp[109]. Figure 4-1 and Figure 4-4 shows the P-gp overexpression in DLKP-A

HL-60/S, HL-60/Adr, HL-60/Mdr1 and HL-6-/Mxr are a panel of leukemic cell-lines. In this panel of cell-lines, the parental cell-line HL-60/S does not over-express any of the three main ABC transporters, P-gp, BCRP or MRP-1. HL-60/Mdr1 is a P-gp over-expressing cell-model. The P-gp over-expression was developed by transfection with the *MDR1* gene. HL-60/Adr is an MRP-1 over-expressing variant, selected by exposure to adriamycin. HL-60/Mxr is a BCRP over-expressing variant which has retrovirally transduced to over-express BCRP[123]. Figures 4-1, Figure 4-2 and Figure 4-3 show the ABC transporter expression for these cell-lines.

2008/MRP-1 is a human ovarian carcinoma transfected to over-express MRP-1 which is predominantly localized in the plasma membrane[290]. The MRP-1 expression is shown is Figure 4-2.

Table 4-2: Lane designations for Western blot analysis [6]

|	P-gp	MRP-1	BCRP
1	HL60/S (40μg)	HL60/S (40μg)	HL60/S (40μg)
2	DLKP (40μg)	DLKP (40μg)	DLKP (40μg)
3	2008/MRP-1 (10μg)	2008/MRP-1 (10μg)	2008/MRP-1 (40μg)
4	HL-60/Adr (40μg)	HL-60/Adr (40μg)	HL-60/Adr (40μg)
5	DLKP-A (10μg)	DLKP-A (10μg)	DLKP-A (40μg)
6	H1299-Taxol (40μg)	H1299-Taxol (40μg)	H1299-Taxol (40μg)
7	HL-60/Mdr (20μg)	HL-60/Mdr1 (20μg)	HL-60/Mdr1 (40μg)
8	M14 (40μg)	M14 (40μg)	DLKP-Sq/Mitox-BCRP (10μg)
9	DLKP-Sq/Mitox-BCRP (40μg)	DLKP-Sq/Mitox-BCRP (40μg)	M14 (50μg)
10	HL-60/Mxr (40μg)	HL-60/Mxr (40μg)	HL-60/Mmxr (10μg)
11	Positive control: DLKP-A (10μg)	Positive control: 2008/MRP-1 (10μg)	Positive control: DLKP-SQ/Mitox-BCRP (5μg)

Table 4-2 shows the lane designations for Western blotting for P-gp, MRP-1 and BCRP blots in figures 4-1, figures 4-2 and figure 4-3. Cell-lines which have been greyed out were not used in this thesis.

**Figure 4-1: Western blot analysis of P-gp[6]**
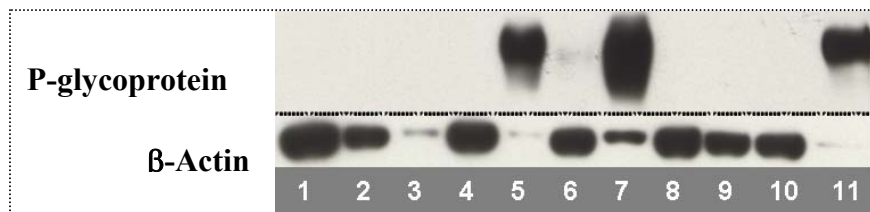
Lane 2 shows P-gp expression for DLKP, lane 5 for DLKP-A, lane 7 for HL-60/Mdr1. Lane 11 is DLKP-A, which was used as a positive control.

Figure 4-2: Western blot analysis of MRP-1[6]
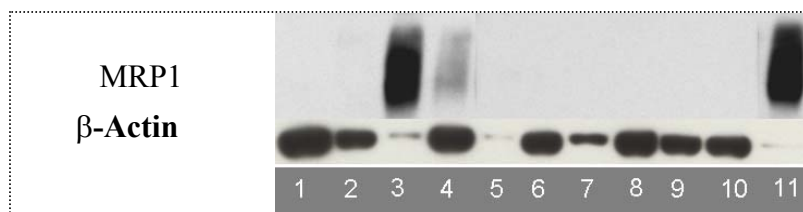
Lane 3 shows MRP-1 expression for 2008/MRP-1 and lane 4 for HL-60/Adr. Lane 11 shows the expression of MRP-1 in 2008/MRP-1 cell-line which was used as a positive control.

Figure 4-3: Western blot analysis of BCRP[6]
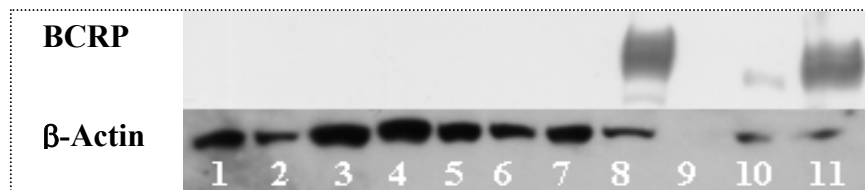
Lane 8 shows the expression of BCRP in DLKP-Sq /Mitox-BCRP and of HL-60/Mxr in lane 10.

185

Likewise, the MDR status of A549 and A549-tax has been established previously. A549, a lung adenocarcinoma cell-line model and A549-tax, the resistant variant, which was selected in-house by Dr Laura Breen, [286] were used as one P-gp model for transport assay. A549-tax has been shown to express P-gp[179], while the parental cell-line does not show any P-gp expression

Figure 4-4, Figure 4-5 and Figure 4-6 were taken from the work of Gráinne Dunne, 2009 (MSc Thesis, 2009)[7]

Figure 4-4: P-gp Western blot for A549 and A549-tax[7]

A549   A549-T   DLKP   DLKP-A

P-gp ⟶

β-Actin ⟶
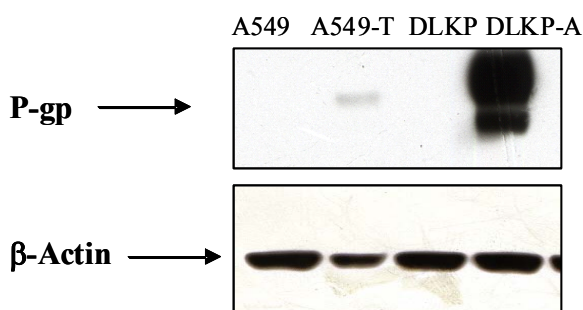
Figure 4-4 shows the P-gp expression A549, A549-tax, DLKP and DLKP-A.

Figure 4-6: BCRP Western blot for A549 and A549-tax[7]

A549   A549-T   DLKP   DLKP-A

BCRP ⟶

β-Actin ⟶
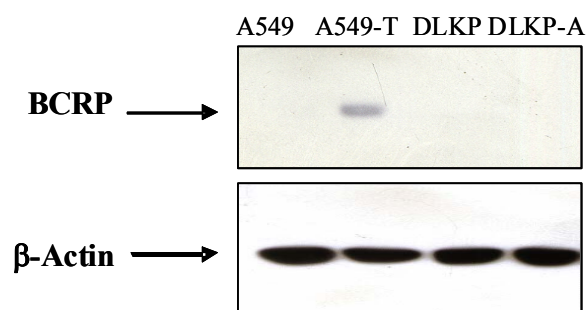
Figure 4-6 shows the BCRP expression A549, A549-tax, DLKP and DLKP-A.

Figure 4-5: MRP-1 Western blot for A549 and A549-tax[7]

A549   A549-T   DLKP   DLKP-A

MRP1 ⟶

β-Actin ⟶
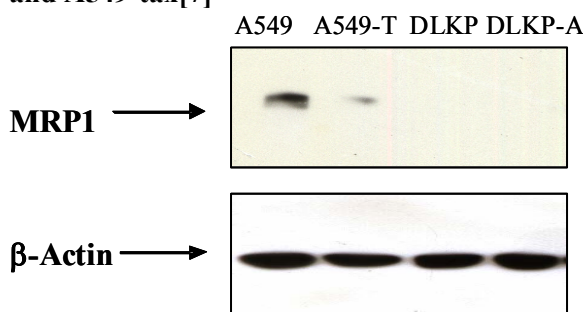
Figure 4-5 shows the MRP-1 expression A549, A549-tax, DLKP and DLKP-A.

No P-gp was detected in the parental cell-lines, while DLKP-A significantly over-expressed P-gp while A549-tax show minor expression of P-gp. MRP-1 was detected in the parental cell-line, A549, while lower expression was seen in the resistant A549-tax, neither DLKP nor the resistant DLKP-A showed any expression of MRP-1. Low levels of BCRP were detected in the resistant A549-tax cell-line

The cell-line IGROV-1 is an ovarian cell-line and IGROV-1CDDP is a resistant variant selected with cisplatin. The cell-line was originally developed in the Netherlands Cancer Institute [292]. This cell-line is used in collaboration with Dr Britta Stordal, NICB[351].

Figure 4-7: Western blot analysis of P-gp in IGROV-1CDDP cell-line[351]

Lane	Cell-line
1	IGROV-1
2	IGROV-1CDDP
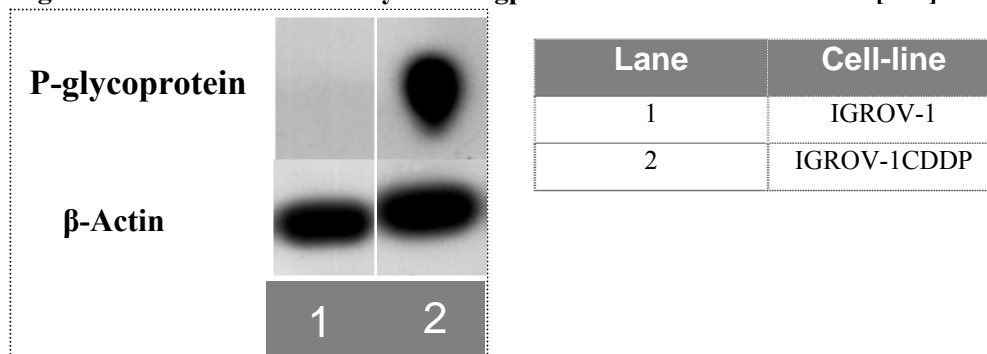
The DLKP cell-line has been characterised to contain three morphologically distinct populations. The three clones corresponding to these populations were established from the parental DLKP cells. The clones were designated M (mesenchymal-like), I (intermediate) and SQ (squamous)[285].

Within the NICB, a drug resistant variety of DLKP-Sq was established by pulsed exposure to mitoxantrone, by Helena Joyce. Uniquely, two separate mechanisms of resistance were established, resulting in "sister" resistant models, one which over-expressed BCRP (DLKP-Sq/Mitox-BCRP) and one which over-expressed P-gp (DLKP-Sq/Mitox-MDR). This work was carried out by Helena Joyce, and these images were kindly reproduced with her permission. This work is currently unpublished.

Figure 4-8: BCRP expression in DLKP-Sq/Mitox-BCRP

DLKP-Sq   DLKP-Sq/Mitox-BCRP
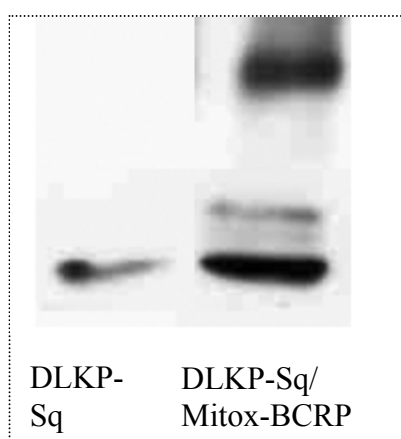
Figure 4-8 shows the BCRP expression of DLKP-Sq/Mitox-BCRP

Figure 4-9: P-gp expression in DLKP-Sq/Mitox-MDR

DLKP-SQ   SQ-Mitox-MDR   DLKP-A
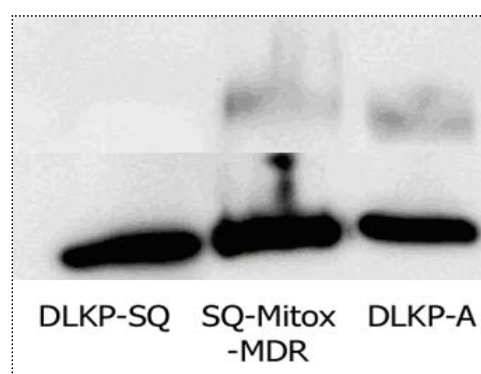
Figure 4-9 shows the P-gp expression for DLKP-Sq/Mitox-MDR. DLKP-A was included as a positive control.

The cell-line RPMI-2650Tx is a drug resistant variant of RPMI-2650 which was selected by continuous exposure to paclitaxel[289]. RPMI-2650 was originally derived from a malignant tumour of the nasal septum. Figure 4-10 and Figure 4-11 show the P-gp over-expression in RPMI-2650Tx compared to the parent, RPMI-2650, both at the protein and RNA level, by Western blot analysis and RT-PCR. Reproduced from Liang *et al*[289].

Figure 4-10: P-gp Western for RPMI-2650Tx[289]
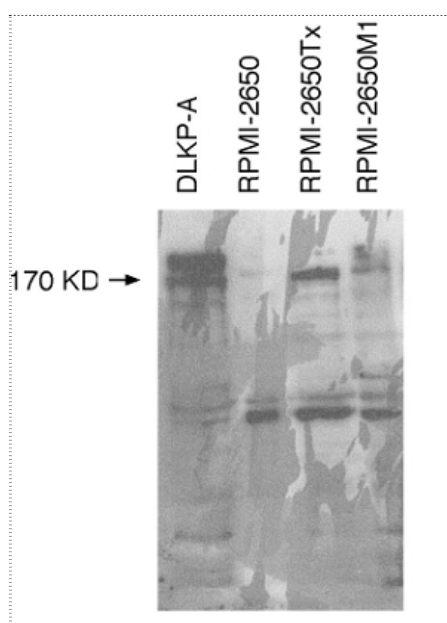
The expression of P-gp in RPMI-2650Tx by Western blot analysis, DLKP-A was included as a positive P-gp control, reproduced from Liang *et al.*[289]

Figure 4-11: RT-PCR for RPMI-2650Tx[289]
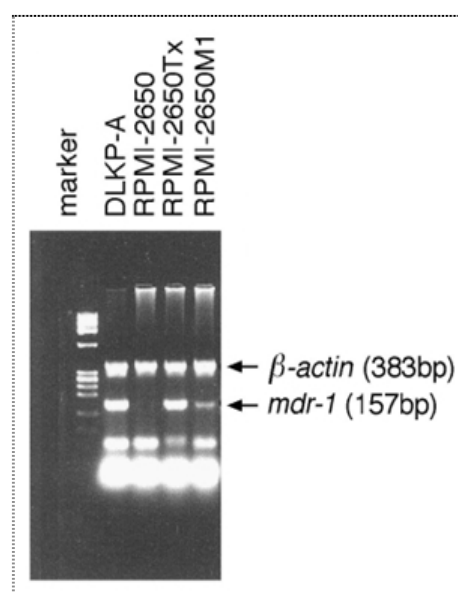
The RT-PCR analysis confirmed up-regulation of the mdr-1 gene expression, which encoded for P-gp expression, reproduced from Liang *et al.*[289]

The cell-line KB -3-1 is a subclone of KB cells, which is a HeLa derivative[291] KB-8-5-11 is a resistant variant of KB-3-1 developed by selection with colchicine[291]. The P-gp overexpression of KB-8-5-11 has previously been reported [350, 353-355] as well as having been confirmed in-house, data not shown.

Figure 4-12: Western blot analysis of KB-3-1 and KB-8-5-11 cell-lines[350]

Lane	Cell-line
1	KB 3–1
2	KB 8–5
3	KB 8–5-11
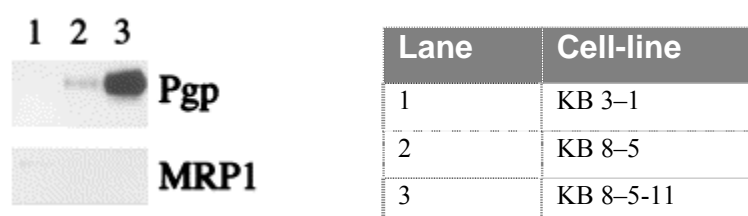
4.2. Dasatinib

At the commencement of this body of work there had been little reported on the relationship between dasatinib and the ABC protein pumps. An article published by Kamath *et al.*[173], stated that dasatinib was not a P-gp substrate. However, work published in 2008 [174] and 2009 [175] identified that dasatinib was a substrate for P-gp and BCRP.

In this section the role of P-gp, MRP-1 and BRCP in the transport of dasatinib is examined.

Note: Throughout this section, accumulation/efflux graphs in two different colours represent two different cell-lines, whereas two shades of the same colour represent the same cell-line treated with and without an inhibitor.

4.2.1. The interaction of dasatinib with P-glycoprotein

P-glycoprotein is responsible for the resistance of many forms of cancer to a multitude of chemotherapeutics, including the TKI imatinib. Here, using a range of P-gp over-expressing cell-line models, the transport of dasatinib by P-gp was examined.

4.2.1.1.   DLKP and DLKP-A cell-line models

Figure 4-13 shows the accumulation of increasing concentrations of dasatinib in DLKP and DLKP-A cell-lines over two hours. Even though the overall level of drug accumulation was low, the difference between the level of dasatinib accumulated in DLKP and the P-gp over-expressing-DLKP-A was significant. Significantly more dasatinib was accumulated in the parental cell-line compared to the P-gp over-expressing cell-line. Evaluation of significance at the lowest concentration (0.1μM) resulted in a p value of 0.000072.

Elacridar is a P-gp inhibitor which completely inhibits the action of P-gp at 0.25μM[7, 356]. Elacridar was added to the cell culture media to investigate the effect of preventing P-gp action from the point exposure to dasatinib. Figure 4-14 and Figure 4-15 shows this accumulation profile over time in DLKP-A. The difference between the level of dasatinib accumulated in the experimental arm with the inhibitor and the arm without inhibitor was significant, with an average of 90% less accumulated in the inhibitor free experiment.

Interestingly the inhibition of P-gp from the point of exposure shows that the level of dasatinib accumulation in the resistant DLKP-A is almost equivalent to the parental levels of accumulation, Figure 4-19.

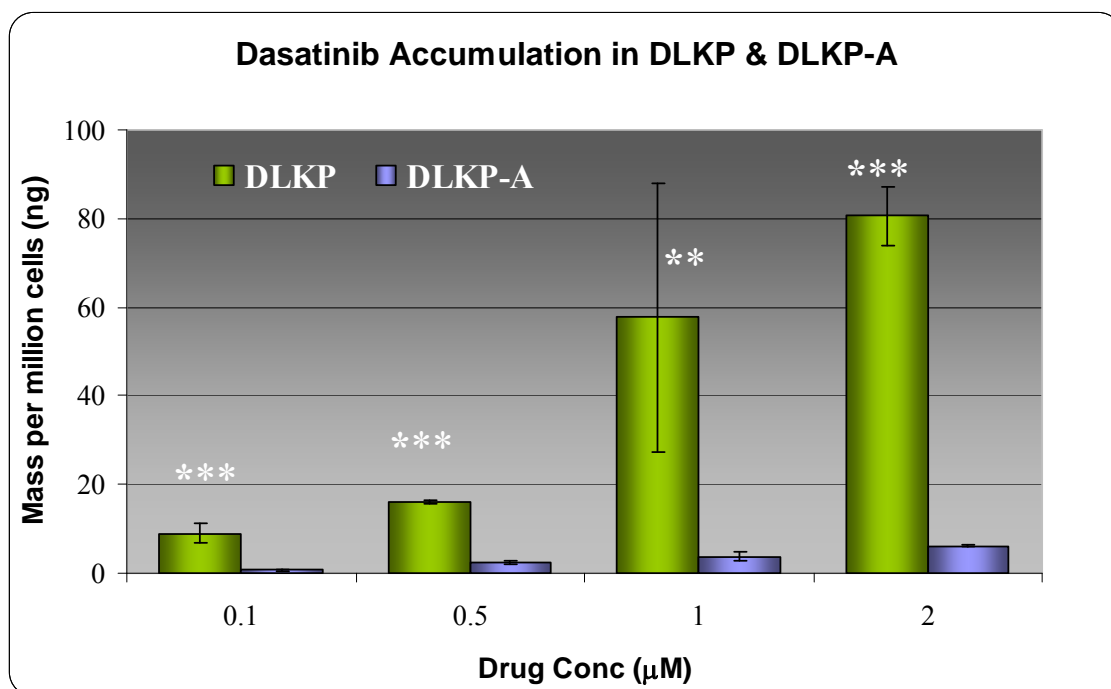**Figure 4-13: Dasatinib Accumulation in DLKP and DLKP-A**

Figure 4-13 shows the accumulation of dasatinib across an increasing concentration range after two hours of drug exposure, in DLKP and DLKP-A. Analysis was carried out in technical triplicates on biological duplicates. The quantified mass was normalised to mass per million cells. Statistical significance was calculated used the paired student t-test of unequal variance, (see Section 2.3). Statistical significance was calculated between the parental (DLKP) and resistant (DLKP-A) model at each concentration.

Figure 4-14: Accumulation of 1μM dasatinib in DLKP-A

1μM Dasatinib Accumulation in DLKP-A

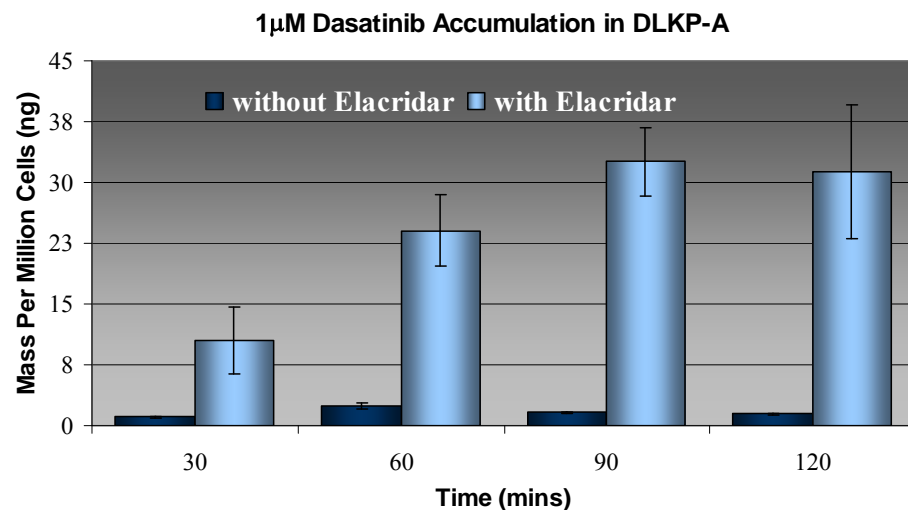Figure 4-14 shows the accumulation of 1μM dasatinib in DLKP-A cell-line model. Accumulation levels are illustrated in the presence and absence of P-gp inhibitor, elacridar. The quantified mass was normalised to mass per million cells.

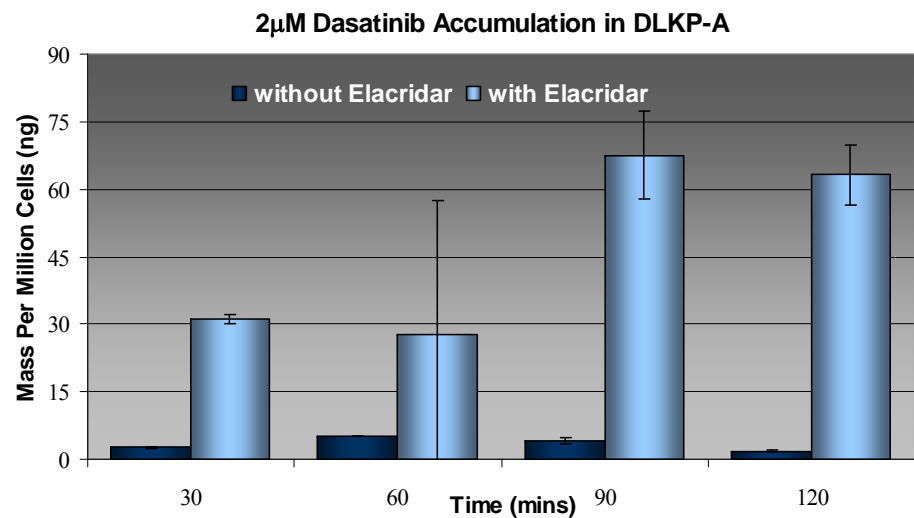**Figure 4-15: Accumulation of 2μM dasatinib in DLKP-A**

2μM Dasatinib Accumulation in DLKP-A

Figure 4-15 shows the accumulation of 2μM dasatinib in DLKP-A cell model. Accumulation levels are illustrated in the presence and absence of P-gp inhibitor, elacridar. The quantified mass was normalised to mass per million cells.

To further investigate the transport of dasatinib in P-gp expressing cell-lines a series of efflux assays were performed. Figure 4-16, Figure 4-17 and Figure 4-18 show the efflux of dasatinib in DLKP and DLKP-A with and without elacridar.

In DLKP, the parental cell-line, there was no difference in the intracellular level of dasatinib at the efflux time points with and without the inhibitor. However, in DLKP-A, the P-gp over-expressing cell-line, dasatinib was retained inside the cell in the presence of the inhibitor.

The difference in the quantified intracellular mass of dasatinib in the presence and absence of elacridar was significant in DLKP-A at all time points and at both 1μM and 2μM concentrations of dasatinib. However, when the accumulated mass of dasatinib in DLKP with and without elacridar was compared there was no significant difference in intracellular dasatinib.

Figure 4-19 shows an interesting trend where there appears to be an increased intracellular concentration at 90 minutes compared to 60 minutes. This is possibly due to an experimentally error in the assay timing, that possible the flasks at 60 minutes were exposed to dasatinib for a shorter time period than the other time points. As the same trend is not seen in the assay at 2μM, which was carried out on biological duplicates this is not believe to be a true biological trend. However the effect of comparing the samples treated with elacridar to the samples without is significant.

Given the complexity of efflux assays and higher level of error associated them efflux assays, further analysis to test the effect of P-gp on an agent were carried out as accumulation assays in the presence of an inhibitor.
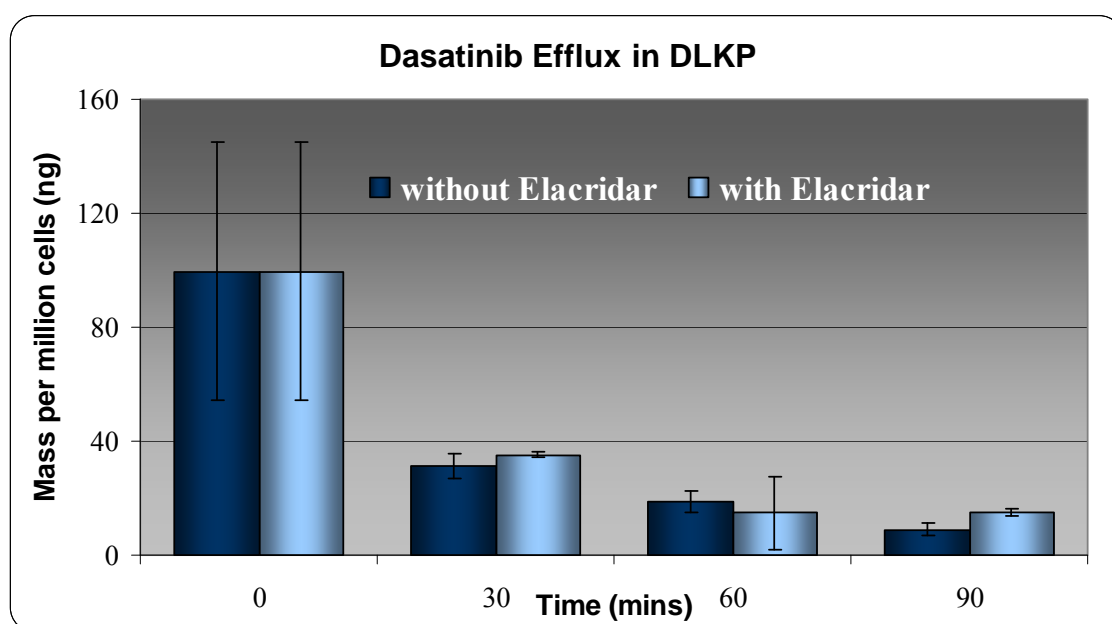
Figure 4-16: Efflux of 2µM dasatinib in DLKP

Figure 4-16 shows the efflux of 2µM dasatinib in parental cell-line DLKP over 90 minutes. Results shown are the average of technical triplicates. The quantified mass was normalised to mass per million cells

Table 4-3: Statistical significance

Time (mins)	p-value
30	0.289191
60	0.63928
90	0.011066

p-values determined by paired student's t-test of unequal variance. Comparison was made between samples with and without elacridar samples at each time point.

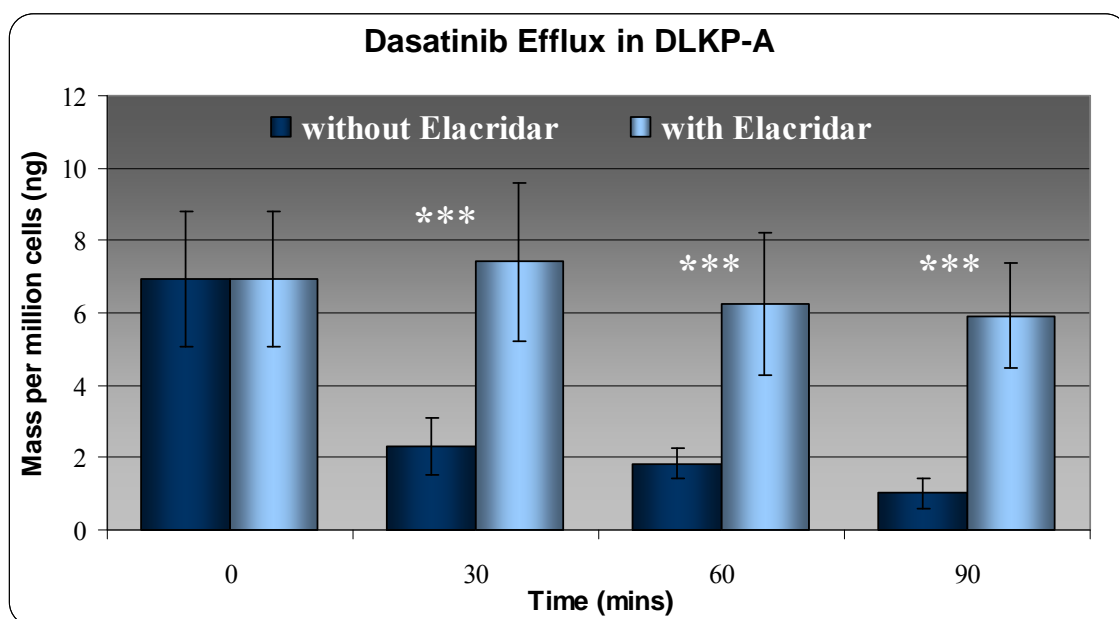**Figure 4-17: Efflux of 2µM dasatinib in DLKP-A**

Dasatinib Efflux in DLKP-A

Figure 4-17 shows the efflux of 2µM dasatinib in resistance cell-line DLKP-A over 90 minutes. Results shown are the average of technical triplicates, on biological duplicates. The quantified mass was normalised to mass per million cells. Statistical significance was calculated used the paired student t-test of unequal variance, (see Section 2.3).

Table 4-4: Statistical significance

Time (mins)	p-value
30	0.001457
60	0.002337
90	0.000249

p-values determined by paired student's t-test of unequal variance. Comparison was made between samples with and without elacridar at each time point.

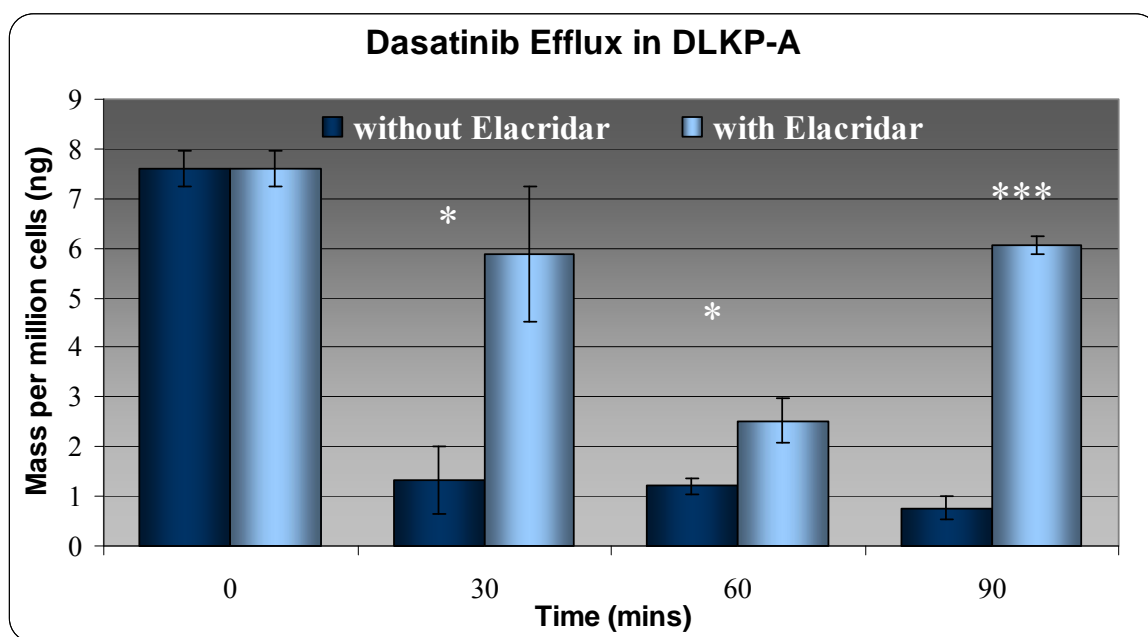**Figure 4-18: Efflux of dasatinib 1µM in DLKP-A**

Dasatinib Efflux in DLKP-A

Figure 4-18 shows the efflux of 1µM dasatinib in the P-gp over-expressing cell-line DLKP-A over 90 minutes. Results shown are the average of technical triplicates (technical repeats). The quantified mass was normalised to mass per million cells. Statistical significance was calculated used the paired student t-test of unequal variance, (see Section 2.3).

Table 4-5: Statistical significance

Time (mins)	p-value
30	0.0145447
60	0.0259020
90	0.0000156

p-values determined by paired student's t-test of unequal variance. Comparison was made between samples with and without elacridar at each time point.

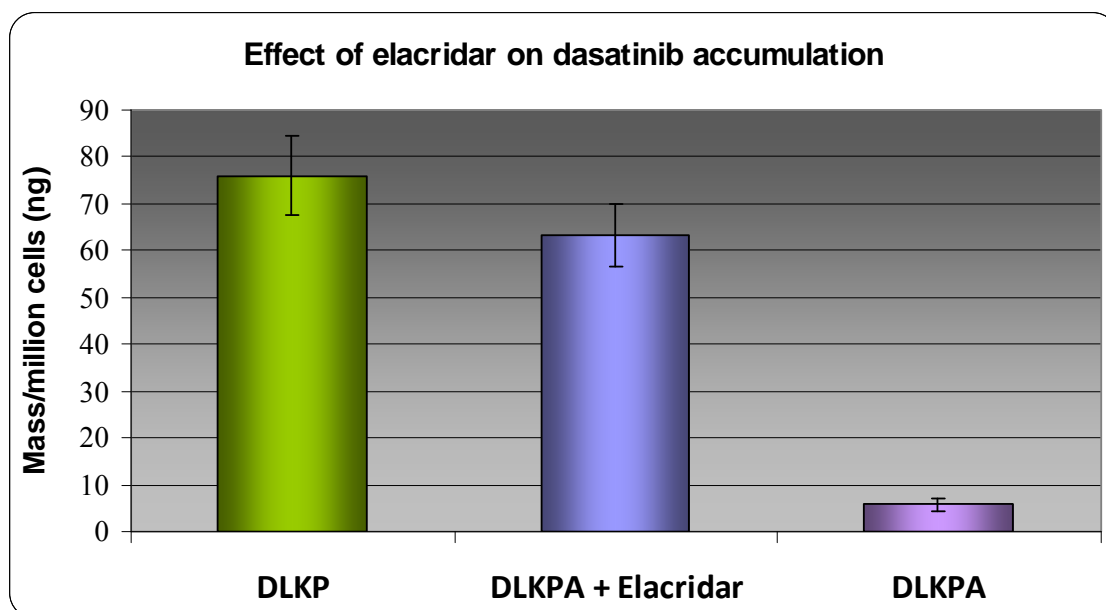**Figure 4-19: Overall effect of elacridar on dasatinib accumulation**

Figure 4-20 shows the effect of elacridar on dasatinib accumulation. The green bar represents 2μM accumulation in DLKP after 2 hours, the blue bar represents the accumulation of 2μM dasatinib in DLKP-A after 2 hours with elacridar present. The purple bar shows the mass of dasatinib accumulated in DLKP-A after two hours with no elacridar present. The green and the purple bars are the average and SD of biological duplicates. The blue bar is the average and SD of technical triplicates.

To examine the effect of dasatinib transport by P-gp, on resistance in the cell lines the cytotoxicity of dasatinib was analysed using an *in vitro* proliferation assay in combination with P-gp inhibitor elacridar. The setup of the assay was such that the plate was split horizontally so that the exact same concentration of dasatinib was applied to the cells with and without elacridar. Dasatinib was assessed across a concentration range while a fixed concentration of elacridar was added, 0.25μM.

The inclusion of elacridar had no impact on the sensitivity of DLKP to dasatinib, Figure 4-20. However, the inclusion of elacridar in the proliferation assay for DLKP-A had a significant impact on dasatinib toxicity, Figure 4-21. A p-value of 0.000158 was determined for the lowest concentration (0.1μM) of dasatinib examined. The IC_{50}, toxicity at which 50% cell kill is achieved, was determined to be 0.47μM dasatinib in combination with elacridar while the IC_{50} of dasatinib alone was 3.65μM. This represents a 7-fold resistance to dasatinib associated solely with P-gp expression.

It should also be noted that the parental cell-line, DLKP, is still more sensitive to dasatinib than the resistant DLKP-A after the protecting effect of P-gp has been neutralised. At 100nM dasatinib, the parental cell-line experienced 75% cell kill, while in the resistant cell-line, DLKP-A, experienced only a 25% cell kill in combination with elacridar. This would indicate that other mechanisms of resistance are present in DLKP-A, though P-gp over-expression does play a significant role in cell protection.

Figure 4-20: *In vitro* proliferation assay of dasatinib plus elacridar in DLKP

Dasatinib in combination with elacridar in DLKP
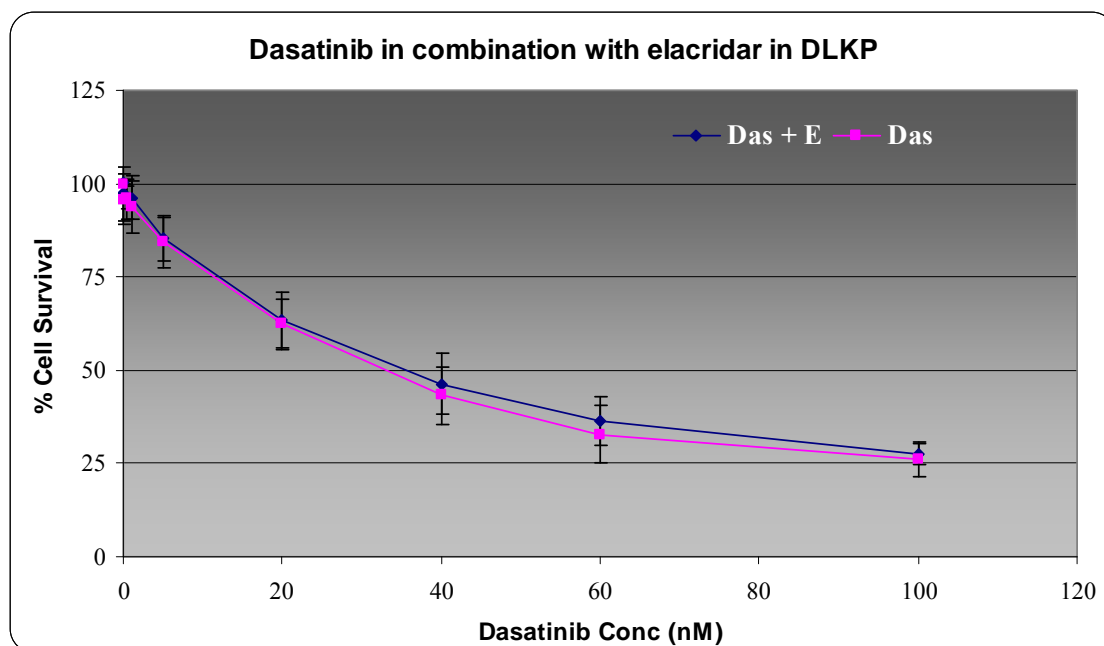
The % cell survival DLKP was determined by acid phosphatase assay in response to a six day treatment of dasatinib in combination with elacridar. Data are mean and standard deviation of biological triplicates.

Figure 4-21: *In vitro* proliferation assay of dasatinib plus elacridar in DLKP -A

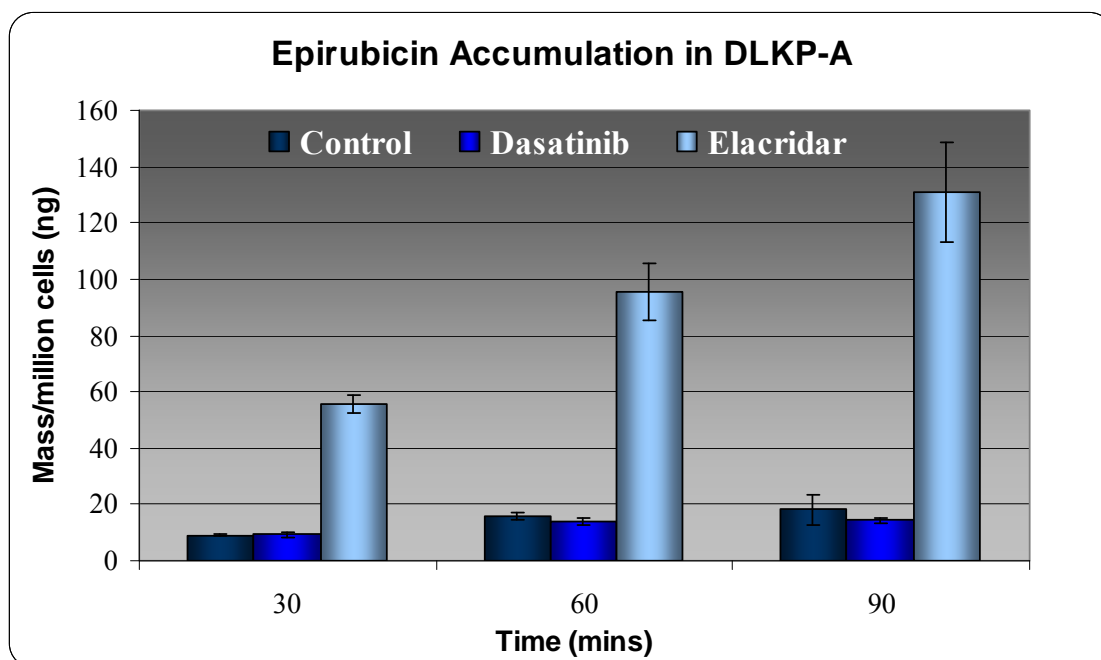**Dasatinib in combination with elacridar in DLKP-A**
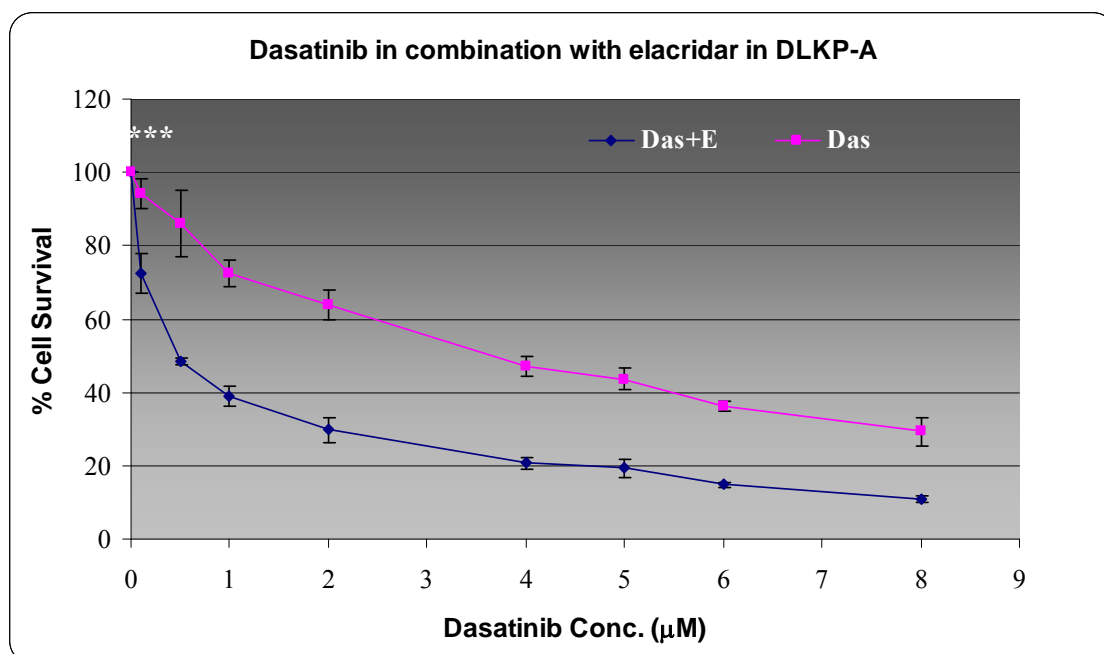
The % cell survival was determined by acid phosphatase assay in response to a six day treatment of dasatinib in combination with elacridar. Data are mean and standard deviation of biological triplicates.

To examine the effect of dasatinib on P-gp function, rather than the effect of P-gp function on dasatinib, the accumulation of a known P-gp substrate was assessed. Epirubicin is a known P-gp substrate[10]. By comparing the accumulation profile of epirubicin in P-gp over-expressing DLKP-A to epirubicin accumulation inhibited by elacridar and epirubicin accumulation in the presence of dasatinib it is possible to determine the effect of dasatinib on the function of P-gp. Epirubicin was quantified by LC-MS/MS[293] (Section 2.2.7).

This effect was also examined toxicologically in DLKP and DLKP-A. The effect of dasatinib in combination with epirubicin or taxol was assessed by *in vitro* proliferation assays, Figure 4-23 to Figure 4-26. The addition of dasatinib to either epirubicin or taxol in either DLKP or DLKP-A cell line model did not increase the effect of either chemotherapeutic agent.

Figure 4-22: Epirubicin accumulation in DLKP-A

The accumulated mass of epirubicin in DLKP-A alone and in the presence of dasatinib or elacridar. Results shown are the average of technical triplicates and standard deviations. The quantified mass was normalised to mass per million cells

Figure 4-23: Combination of epirubicin and dasatinib in DLKP-A cell-line

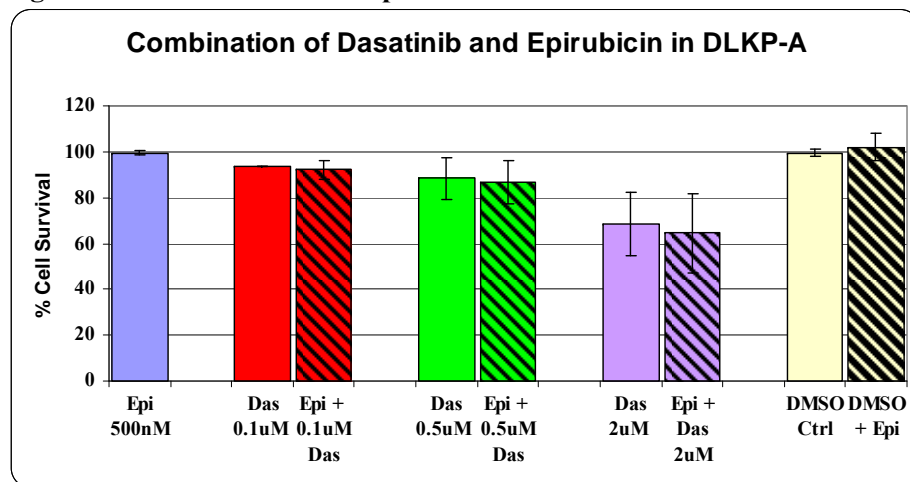**Combination of Dasatinib and Epirubicin in DLKP-A**

Figure 4-31 shows the % cell survival in DLKP-A as determined by acid phosphatase assay in response to a seven day treatment of fixed concentration epirubicin (500nM) in combination with increasing concentrations of dasatinib. Data shown are mean +/- SD of triplicate determination.

Figure 4-24: Combination of taxol and dasatinib in DLKP-A cell-line

Combination of Dasatinib and Taxol in DLKP-A

Figure 4-32 shows the % cell survival in DLKP-A as determined by acid phosphatase assay in response to a seven day treatment of fixed concentration taxol (100nM) in combination with increasing concentrations of dasatinib. Data shown are mean +/- SD of triplicate determination.

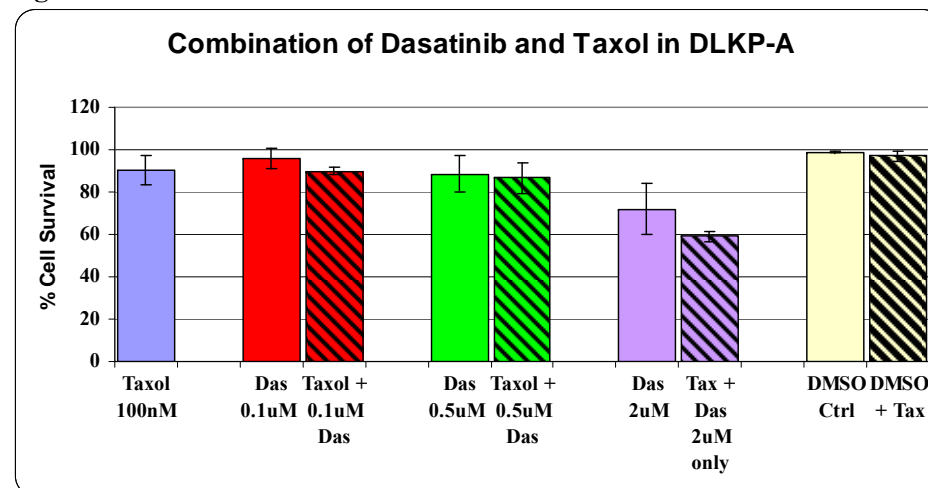**Figure 4-25: Combination of epirubicin and dasatinib in DLKP**

Figure 4-33 shows the % cell survival in DLKP as determined by acid phosphatase assay in response to a seven day treatment of fixed concentration epirubicin (3nM) in combination with increasing concentrations of dasatinib. Data shown are mean +/- SD of triplicate determination.

Figure 4-26: Combination of taxol and dasatinib in DLKP

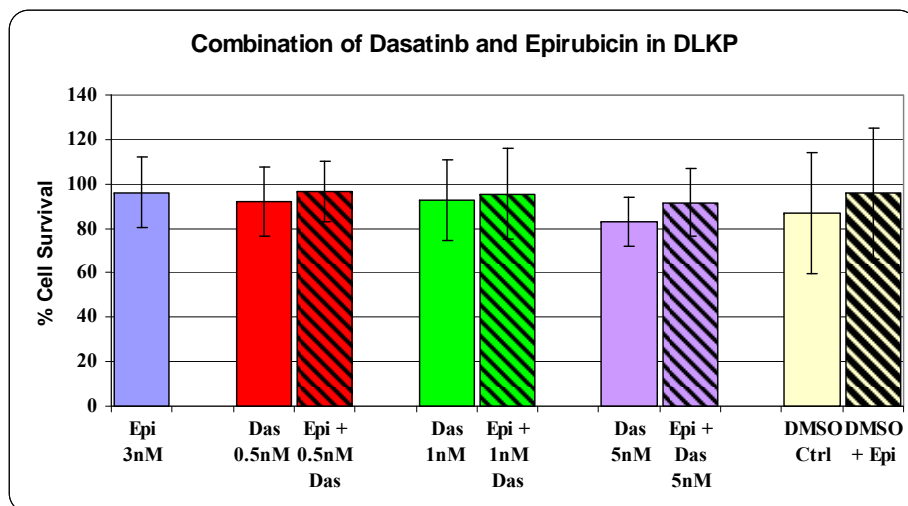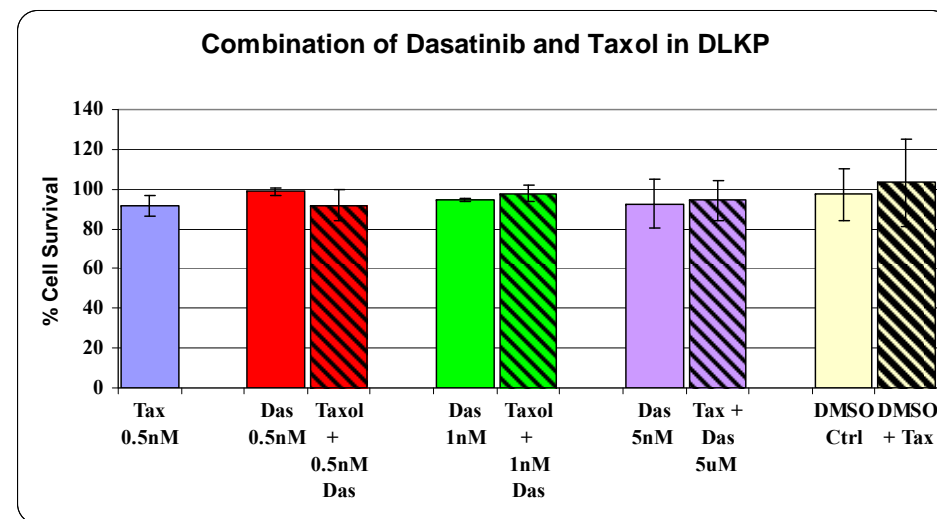Figure 4-34 shows the % cell survival in DLKP as determined by acid phosphatase assay in response to a seven day treatment of fixed concentration taxol (0.5nM) in combination with increasing concentrations of dasatinib. Data shown are mean +/- SD of triplicate determination.

4.2.1.2.   DLKP-SQ and DLKP-Sq/Mitox-MDR cell-line models

The DLKP-Sq/Mitox-MDR cell-line model, which was recently developed by Helena Joyce in our laboratory, highly over-expresses P-gp, as described in Section 4.1. The resistant model was developed by pulsed selection with mitoxantrone.

Figure 4-27 shows the accumulation of dasatinib in the P-gp over-expression model compared to the parental cell-line. Significantly less intracellular dasatinib was quantified in the resistant cell-model compared to the parental model.

When the effect of elacridar on the accumulation was examined, Figure 4-28, we can see that there was significantly more intracellular dasatinib present when the P-gp inhibitor elacridar was added to the cell culture media. When Figure 4-28 and Figure 4-29 are compared we see that the level of dasatinib accumulated after two hours in DLKP-Sq/Mitox-MDR with elacridar present was similar to levels accumulated in DLKP-Sq after two hours.

The cytotoxic effect of dasatinib and the effect of P-gp on the resistance of dasatinib were examined using *in vitro* proliferation assays. Figure 4-30 and Figure 4-30 shows the effect of P-gp inhibition on the cytotoxic resistance of known P-gp substrates, taxol and epirubicin. This demonstrated the dramatic effect of functional P-gp in protecting the cell and the effect on toxicity of P-gp inhibition. Figure 4-32 shows that effect of elacridar on dasatinib cytotoxicity. While there was a clear significant difference in the accumulation of dasatinib in DLKP-Sq/Mitox-MDR with and without elacridar, the difference in the cytotoxic effect of dasatinib on DLKP-Sq/Mitox-MDR with and without elacridar was not significant. There was a visible trend that the inhibition of P-gp by elacridar increased the cytotoxicity of dasatinib but standard deviations in the assay meant that the difference was not clearly significant.

Figure 4-32 and Figure 4-33 show the effect of dasatinib in combination with P-gp substrates epirubicin and taxol. The addition of dasatinib did not increase the cytotoxic effect of either chemotherapeutic.

Figure 4-27: Accumulation of dasatinib in DLKP-Sq and DLKP-Sq/Mitox-MDR
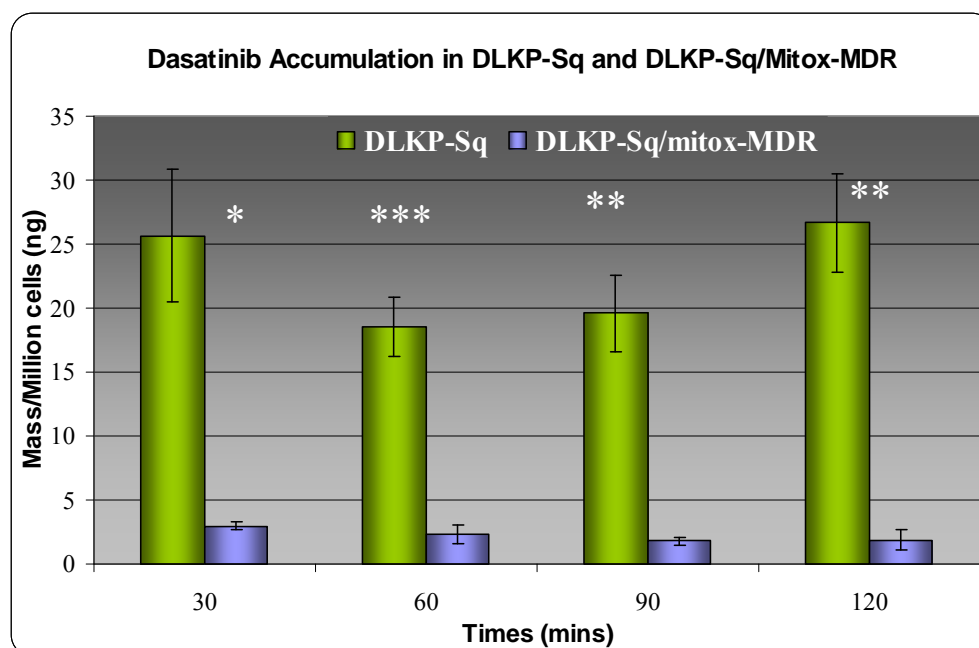
The comparison between the accumulation of 1μM dasatinib at 30 minute intervals over a two hour period, in DLKP-Sq and DLKP-Sq/Mitox-MDR. Analysis was carried out in technical triplicates. The quantified mass was normalised to mass per million cells.

Table 4-6: Statistical significance

Time (mins)	p-value
30	0.017
60	0.004
90	0.009
120	0.006

p-values were determined by paired student's t-test of unequal variance. Comparison was made between samples with and without elacridar at each time point.

Figure 4-28: Dasatinib accumulation in DLKP-Sq/Mitox-MDR with and without elacridar
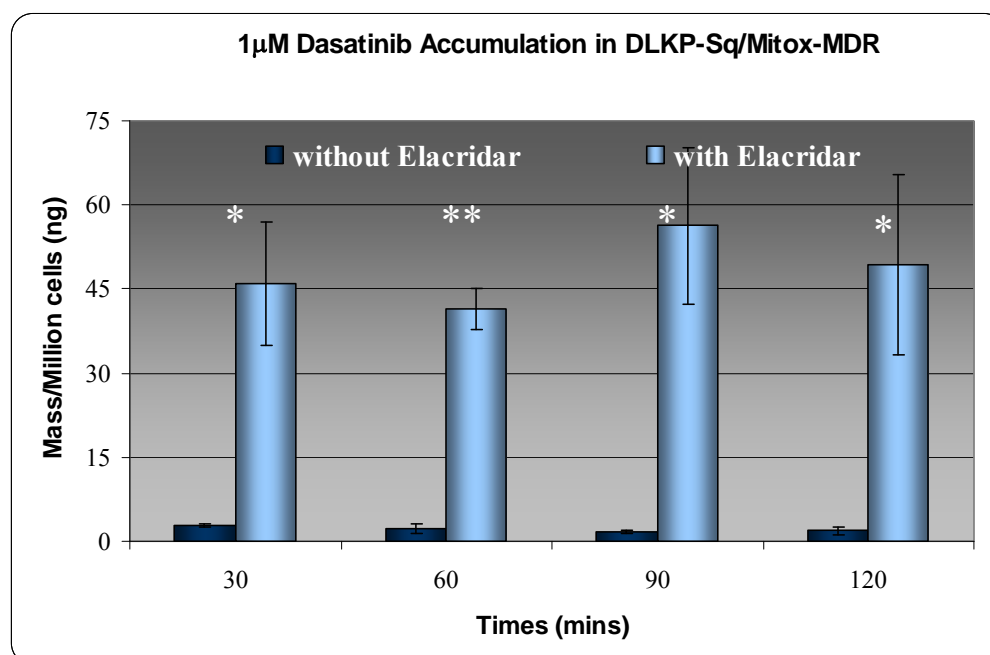
Figure 4-28 shows the accumulation of 1μM dasatinib at 30 minute intervals over a two hour period, DLKP-Sq/Mitox-MDR with and without elacridar. Analysis was carried out in technical triplicates. The quantified mass was normalised to mass per million cells.

Table 4-7: Statistical significance

Time (mins)	p-value
30	0.021
60	0.002
90	0.021
120	0.036

p-values were determined by paired student's t-test of unequal variance. Comparison was made between samples with and without elacridar at each time point.

Figure 4-29: *In vitro* proliferation assay of taxol plus elacridar in DLKP-Sq/Mitox-MDR

Taxol in Combination with Elacridar in DLKP-Sq/Mitox-MDR

Figure 4-30 shows the % cell survival in DLKP-Sq/Mitox-MDR which was determined by acid phosphatase assay in response to a six day treatment of taxol in combination with elacridar. Data are mean and standard deviation of biological triplicates.

Figure 4-30: *In vitro* proliferation assay of epirubicin + elacridar in DLKP-Sq/Mitox-MDR

Epirubicin in Combination with Elacridar in DLKP-Sq/Mitox-MDR

Figure 4-30 shows the % cell survival in DLKP-Sq/Mitox-MDR which was determined by acid phosphatase assay in response to a six day treatment of taxol in combination with elacridar. Data are mean and standard deviation of biological triplicates.

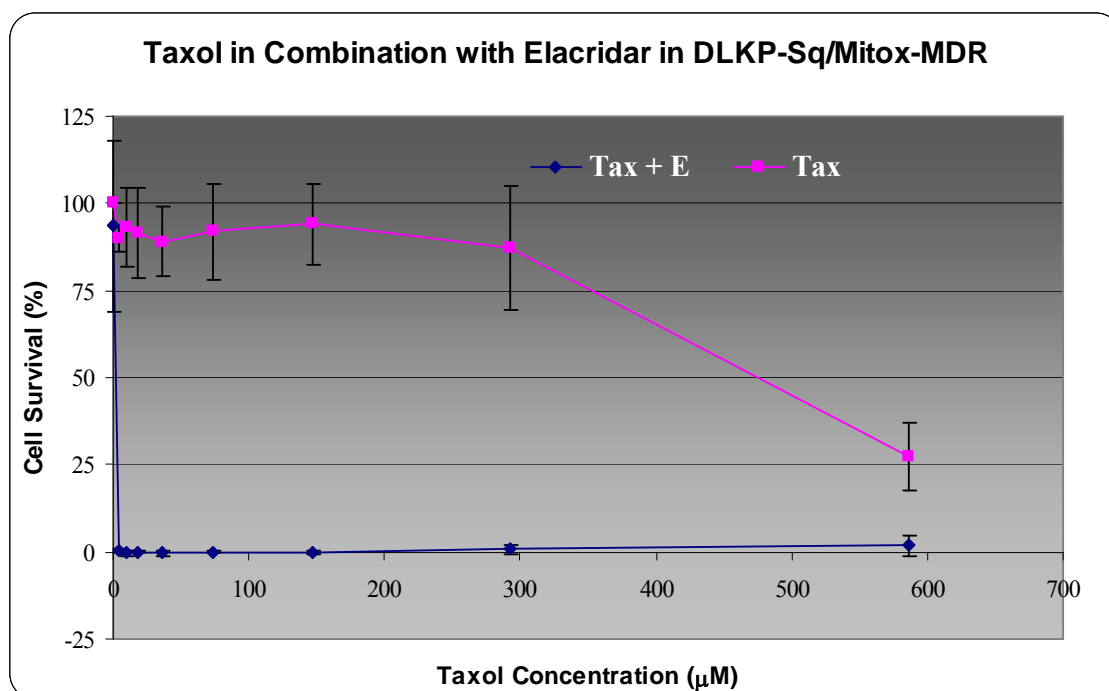**Figure 4-31:** *In vitro* proliferation assay of dasatinib + elacridar in DLKP-Sq/Mitox-MDR
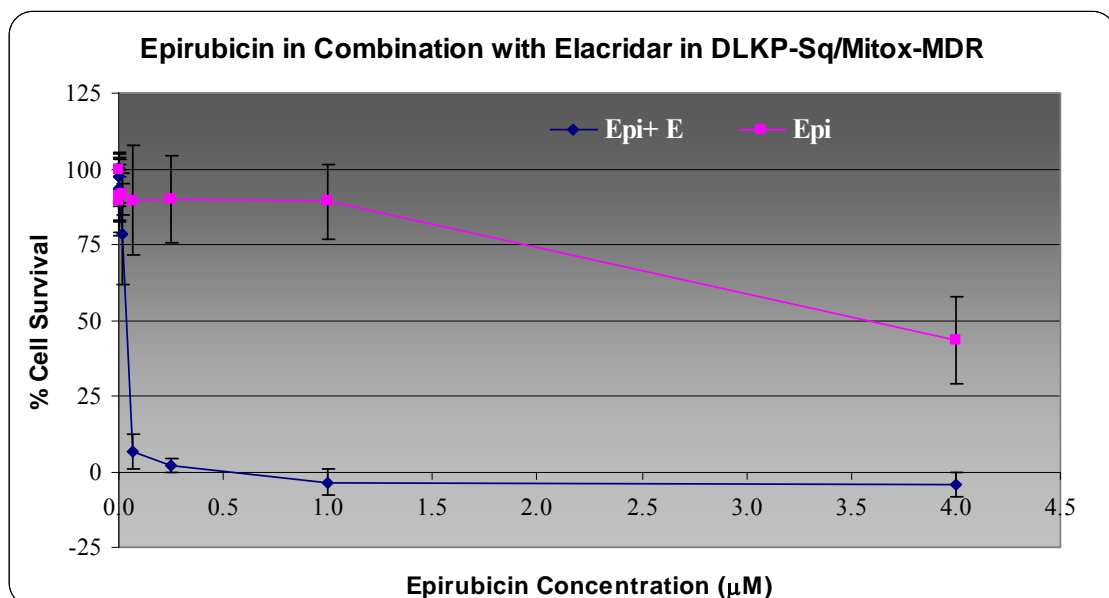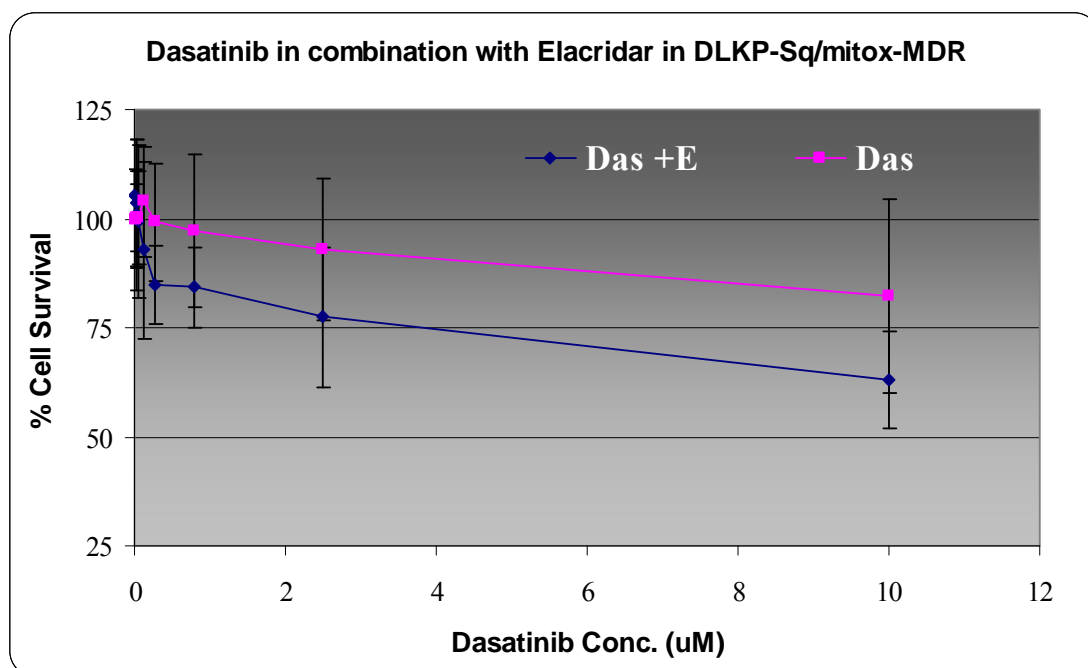

Figure 4-32 shows the % cell survival in DLKP-Sq/Mitox-MDR which was determined by acid phosphatase assay in response to a six day treatment of taxol in combination with elacridar. Data are mean and standard deviation of biological triplicates.

Figure 4-32: Combination of epirubicin and dasatinib in DLKP-Sq/Mitox-MDR

The % cell survival in DLKP-Sq/Mitox-MDR as determined by acid phosphatase assay in response to a seven day treatment of fixed concentration epirubicin (1.5μM) in combination with increasing concentrations of dasatinib. Data shown are mean +/- SD of triplicate days.
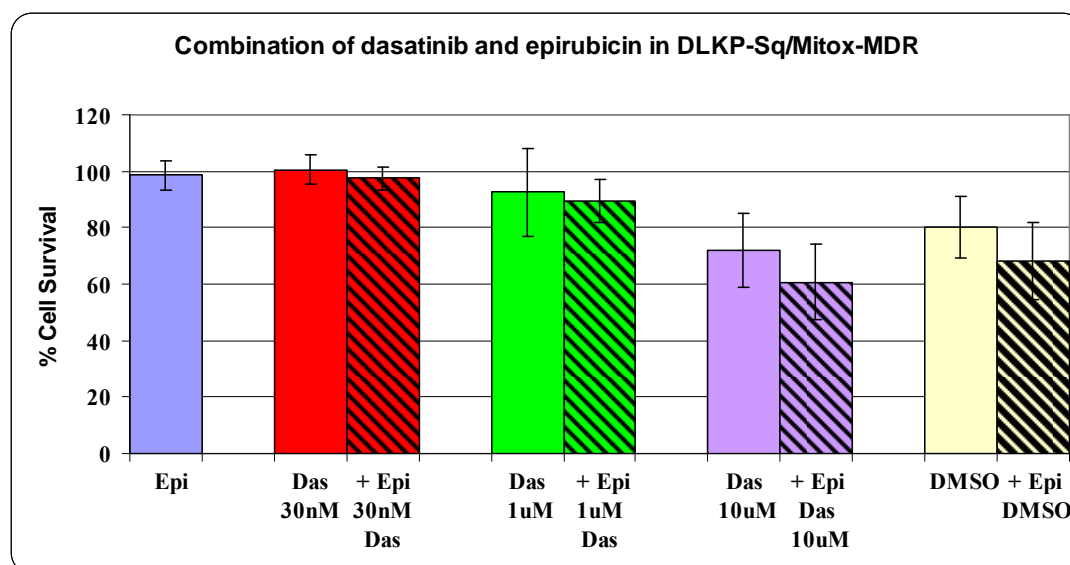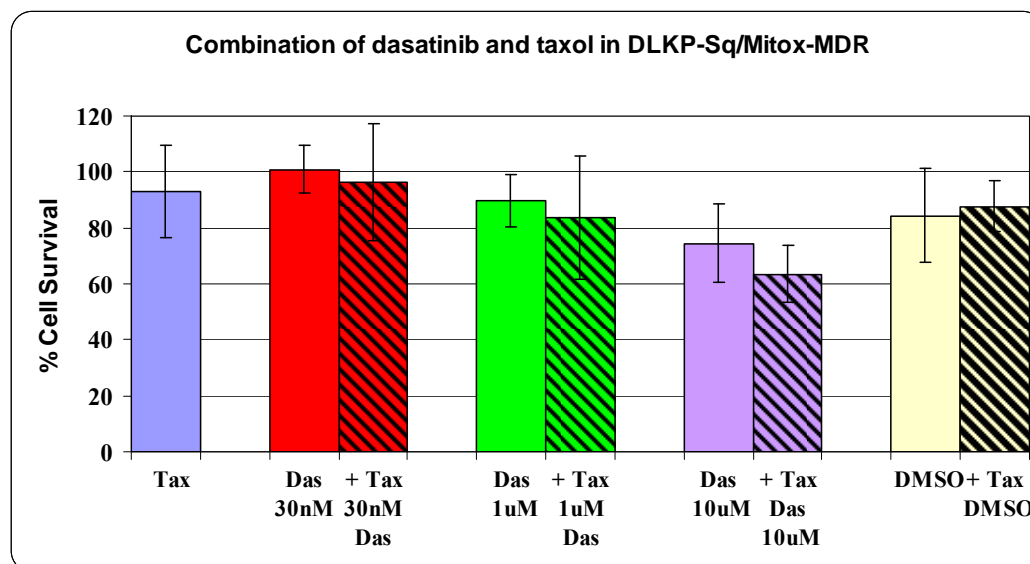
Figure 4-33: Combination of taxol and dasatinib in DLKP-Sq/Mitox-MDR

The % cell survival in DLKP-Sq/Mitox-MDR as determined by acid phosphatase assay in response to a seven day treatment of fixed concentration taxol (234μM) in combination with increasing concentrations of dasatinib. Data shown are mean +/- SD of triplicate days.

4.2.1.3. *IGROV-1 and IGROV-1CDDP cell-line model*

The cell-line models IGROV-1CDDP is a resistant variant for the ovarian model IGROV-1. The mechanism of resistance is mediated through P-gp over-expression as a result of pulse selection with cisplatin, an agent commonly used in the treatment of ovarian cancer. TLDA data showed the up-regulation of P-gp at RNA level and the lack of over-expression of other ABC transporters. The lack of BCRP and MRP-1 expression has been confirmed by Western blot[357]. Work carried out by Stordal *et al.,* showed P-gp mediated resistance in IGROV-1CDDP[357].

The accumulation of dasatinib, 1μM, was examined in the IGROV-1CDDP cell-line model. The addition of elacridar increased the intracellular concentration of dasatinib across the time course examined. The average fold increase of intracellular dasatinib was 16.8 (+/-1.4) across all time points, ranging from 15 to 18. The difference in accumulated mass was in all cases significant.

Inhibition of P-gp by elacridar was shown to have an effect on the cytotoxicity of dasatinib in IGROV-1CDDP, Figure 4-35, through the incorporation of elacridar had no effect on dasatinib in the parental cell-line IGROV-1, Figure 4-36.

The functionality of P-gp resistance mechanism in IGROV-1CDDP was demonstrated by the *in vitro* cytotoxicity assays carried out in IGROV-1CCDP and the parental IGROV-1 cell-line with and without elacridar, Table 4-9. This analytical technique can therefore also be used to investigate further mechanisms for cross-resistance.

Figure 4-34: Dasatinib accumulation in IGROV-1CDDP

Dasatinib Accumulation in IGROV-1CDDP
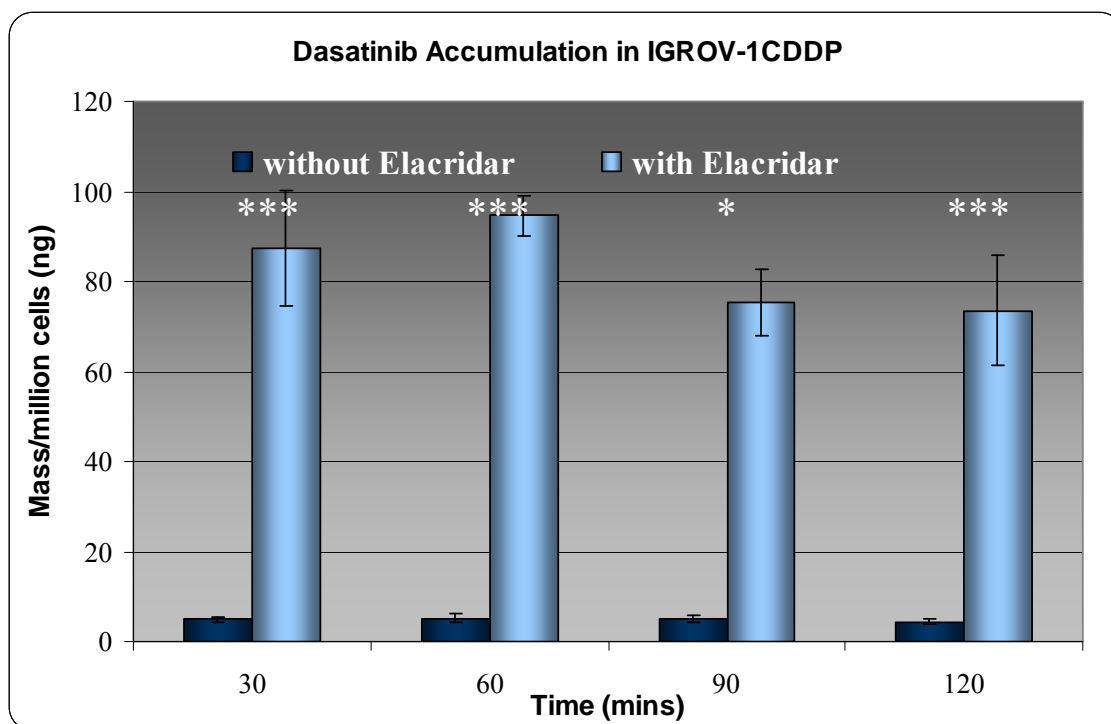
Figure 4-34 shows the accumulation of 1μM dasatinib in resistance cell-line IGROV-1CDDP over 120 minutes. Results shown are the average of technical triplicates. The quantified mass was normalised to mass per million cells. Statistical significance was calculated used the paired student t-test of unequal variance, (see Section 2.3).

Table 4-8: Statistical significance

Time (mins)	p-value
30	0.00002
60	0.00113
90	0.02060
120	0.00035

p-values were determined by paired student's t-test of unequal variance. Comparison was made between samples with and without elacridar at each time point.

213

Figure 4-35 *In vitro* proliferation assay of dasatinib plus elacridar in IGROV-1CDDP[357]

Figure 4-35 shows the % cell survival of IGROV-1CDDP determined by acid phosphatase assay in response to a six day treatment of taxol in combination with elacridar. Data are mean and standard deviation of biological triplicates.

Figure 4-36: *In vitro* proliferation assay of dasatinib plus elacridar in IGROV-1[357]

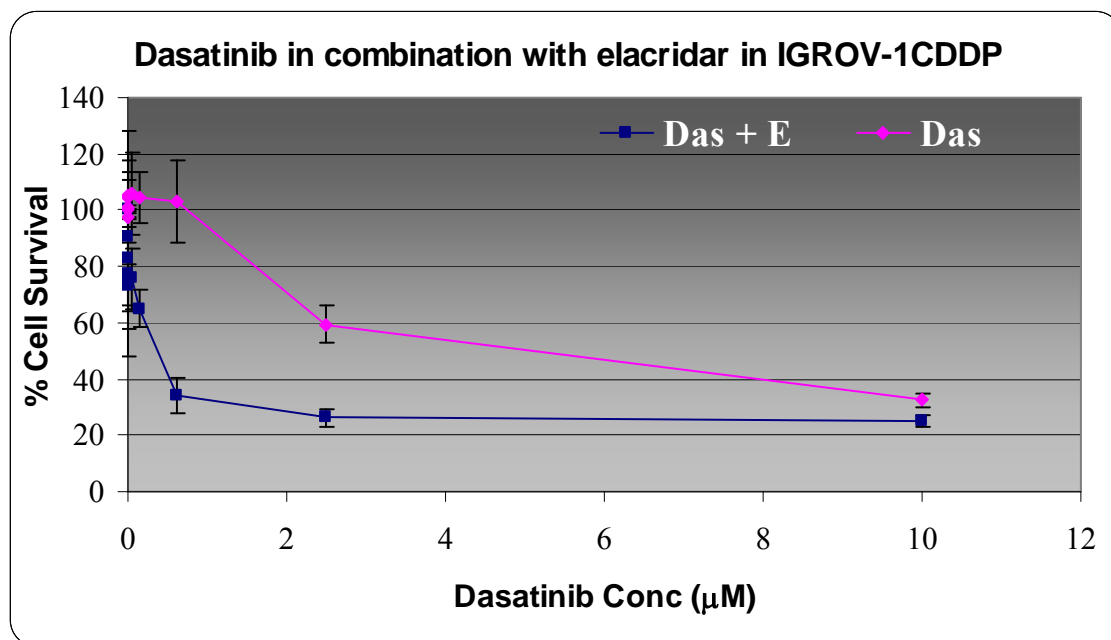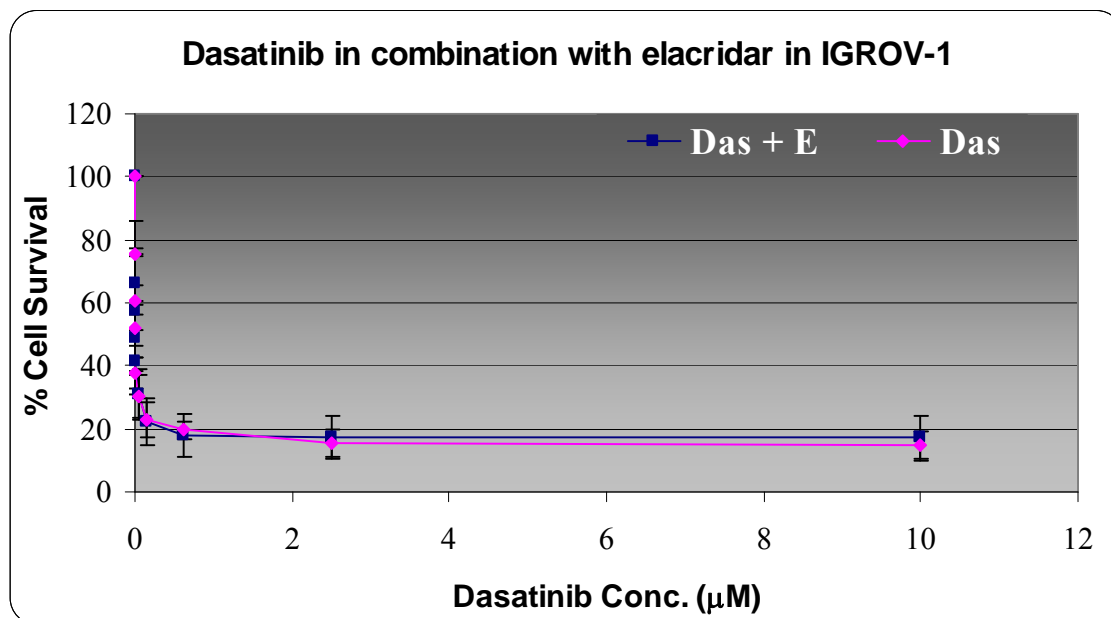**Figure 4-36 shows the % cell survival of IGROV-1 determined by acid phosphatase assay in response to a six day treatment of taxol in combination with elacridar. Data are mean and standard deviation of biological triplicates.**

Table 4-9: IC$_{50}$ results for selected P-gp substrates in IGROV-1 and IGROV-1CDDP[357]

Drug (Units)	IGROV-1 Mean ± SD	IGROV-1CDDP Mean ± SD	Resistant vs Sensitive Fold	Resistant vs Sensitive p-value	IGROV-1 +/- Elacridar p-value	IGROV-1CDDP +/- Elacridar p-value
Cisplatin (ng/ml)	43.2 ± 16.8	809.3 ± 344.8	18.7	0.000003		
+Elacridar 0.25μM	41.3 ± 28.6	575.1 ± 366.1	13.9	0.0271	0.8792	0.3020
Taxol (ng/ml)	0.99 ± 1.1	127.9 ± 64.8	128.9	0.007807		
+ Elacridar 0.25μM	0.6 ± 0.4	0.3 ± 0.6	0.5	0.8692	0.0318	0.0021
Epirubicin (ng/ml)	6.8 ± 4.3	363.4 ± 218.5	53.2	0.047517		
+ Elacridar 0.25μM	2.6 ± 2.8	1.9 ± 2.3	0.7	0.9201	0.1967	0.0460

IC$_{50}$ values determined from proliferation assays. Results are expressed as IC$_{50}$ +/- SD. Fold difference in resistance was calculated between the parental and resistant cell-line.

4.2.1.4.   KB-8-5-11 cell-line model

The KB-8-5-11 cell-line was established in 1985 from the parental cell-line KB-3-1 which was cloned from the KB human cell-line. The KB human cell-line is a HeLa-derived cell-line[291]. KB-8-5-11 was selected by exposure to colchicine[291]. This model was selected for examination as it highly over-expressed P-gp and was well reported in the literature.

A brief examination of the accumulation of dasatinib in the resistant model was investigated at two separate drug concentration, 1µM and 0.1µM dasatinib, Figure 4-37 and Figure 4-38. The peak plasma concentration of dasatinib has been found to be approximately 1µM[358]. At both concentrations examined the addition of elacridar increased the intracellular mass of dasatinib. The method can clearly distinguish a significant difference in accumulation, even at a low exposure concentration.

Figure 4-37: Accumulation of 1µM dasatinib in KB-8-5-11

Figure 4-37: shows the accumulation of 1µM dasatinib in KB-8-5-11 over 120 minutes. Results shown are the average of technical triplicates. The quantified mass was normalised to mass per million cells. Statistical significance was calculated used the paired student t-test of unequal variance, (see Section 2.3).

Table 4-10: Statistical significance

Time (mins)	p-value
30	0.0002
60	0.0185
90	0.0226
120	0.0067

p-values were determined by paired student's t-test of unequal variance. Comparison was made between with and without elacridar samples at each time point.

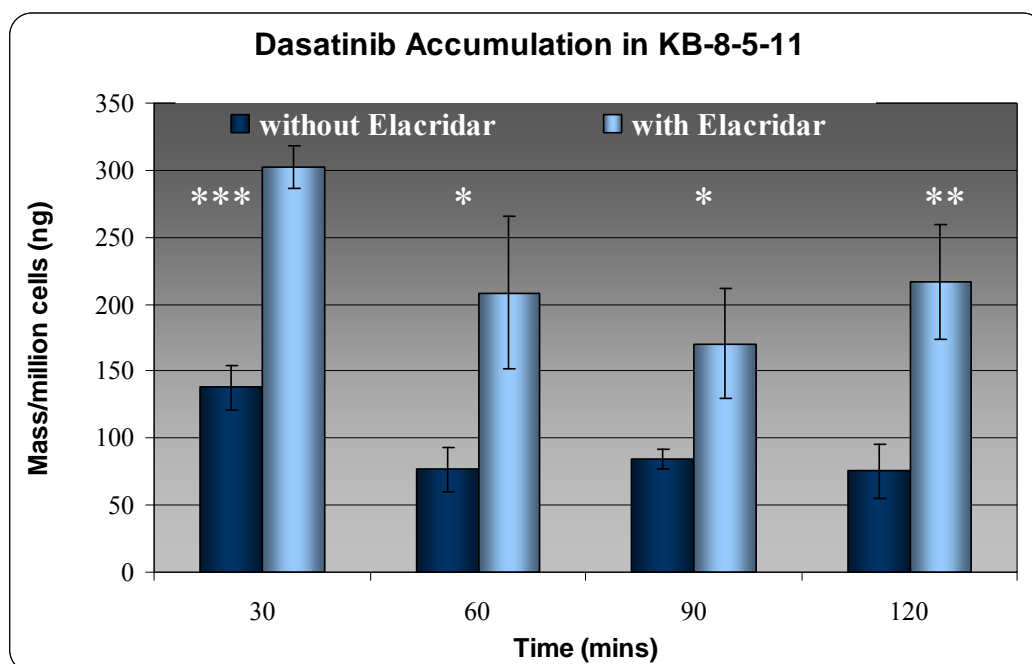**Figure 4-38: Accumulation of 0.1µM dasatinib in KB-8-5-11**
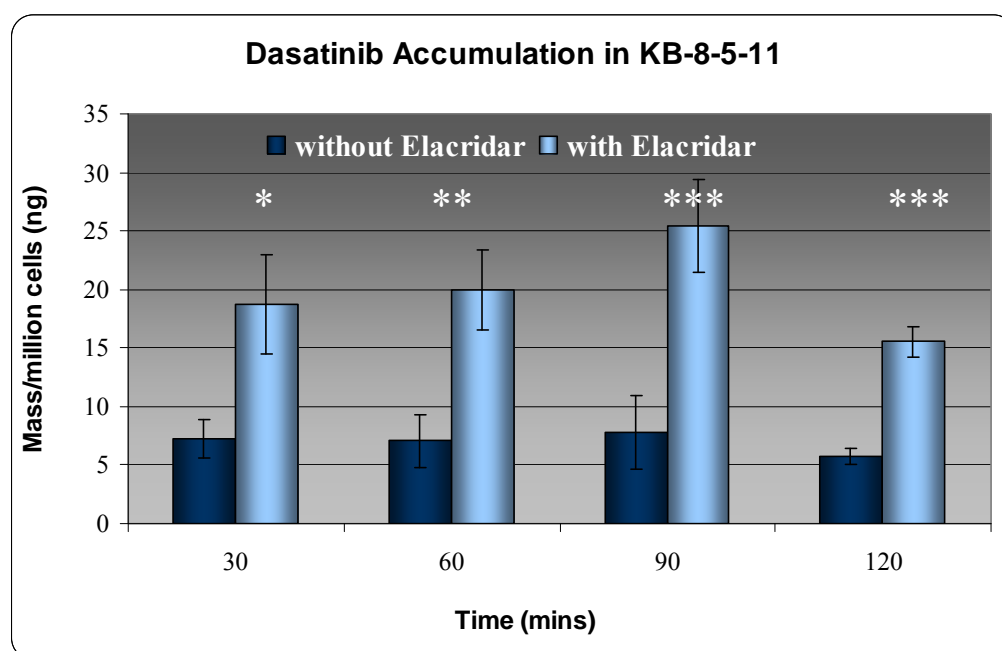
Figure 4-38 shows the accumulation of 0.1µM dasatinib KB-8-5-11 over 120 minutes. Results shown are the average of technical triplicates. The quantified mass was normalised to mass per million cells. Statistical significance was calculated used the paired student t-test of unequal variance, (see Section 2.3).

Table 4-11: Statistical significance

Time (mins)	p-value
30	0.0115
60	0.0054
90	0.0037
120	0.0004

p-values were determined by paired student's t-test of unequal variance. Comparison was made between samples with and without elacridar at each time point.

4.2.1.5.   A549 and A549-tax cell-line models

A549 is a lung adenocarcinoma cell-line. A549-tax is a P-gp expressing resistant variant developed through exposure to taxol[286]. The A549 and A549-tax cell-line model was also investigated as the A549-tax cell-line model expresses a low level of P-gp and is mildly resistant (5-fold) to taxol[286].

There was little or no difference in the level of dasatinib accumulated in the P-gp expressing cell line (A549-tax) compared to the P-gp non expressing cell-line (A549), Figure 4-39. Also, more dasatinib was accumulated in the A549 and A549-tax cell models, Figure 4-39 compared to the DLKP and DLKP-A cell models, Figure 4-13.

Figure 4-40 and Figure 4-41 shows the efflux of dasatinib in A549 cell-line and A549-tax over time in the presence and absence of P-gp inhibitor, elacridar. However, in the A549 and A549-tax model there was no significant difference in the intracellular level of dasatinib in the P-gp expressing cell-line between the experiment with and without inhibitor.

The efflux of 1µM dasatinib was assessed over 120 minutes in A549 and A549-tax, Figure 4-40 and Figure 4-41. While there was a difference in the quantified intracellular mass of dasatinib in A549-tax with and without the inhibitor, there was also a difference in the intracellular mass of A549 with and without elacridar. The data suggests that while there is a mechanism for dasatinib exclusion from A549-tax, it is not P-gp mediated. Also there appears to be no active efflux of dasatinib from A549, as the intracellular mass was sustain over the 120 minute assay.

The effect of elacridar on dasatinib toxicity was assessed by *in vitro* proliferation assays, Figure 4-42 and Figure 4-43. The addition of elacridar had no effect on dasatinib potency in A549 and had a small but insignificant effect in A549-tax.

Figure 4-39: Dasatinib Accumulation in A549 and A549-tax
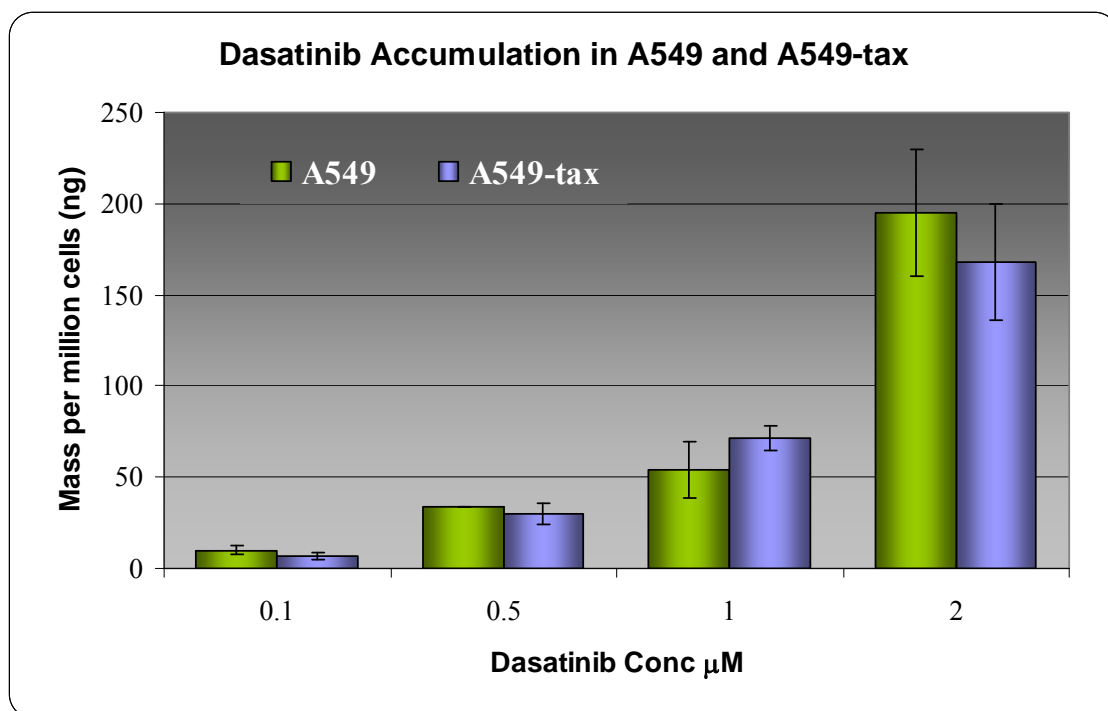
Figure 4-39 shows the accumulation of dasatinib in A549 and P-gp expressing A549-tax cell-lines after 2 hours with varying concentrations. Analysis was performed on technical triplicates. The quantified mass was normalised to mass per million cells.

Figure 4-40: Efflux of 1μM dasatinib in A549-tax
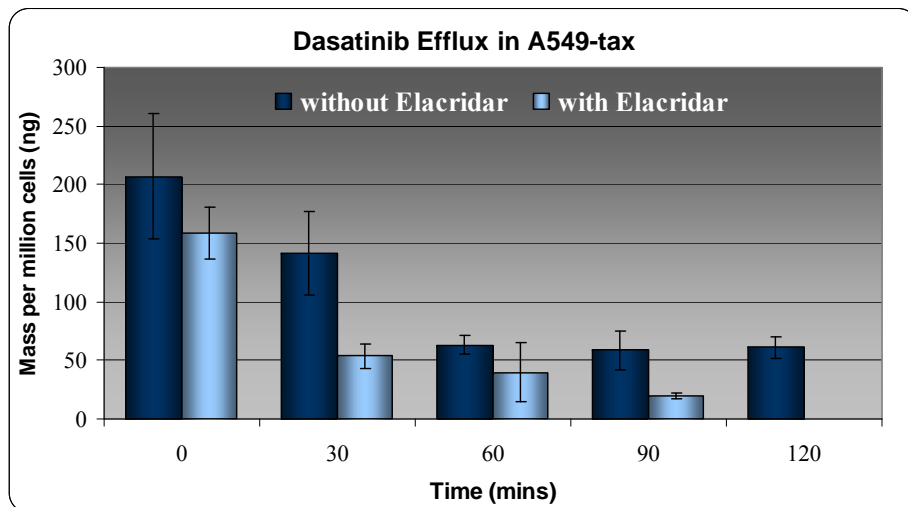
Analysis was performed on technical triplicates. The quantified mass was normalised to mass per million cells.

Figure 4-41: Efflux of 1μM dasatinib in A549
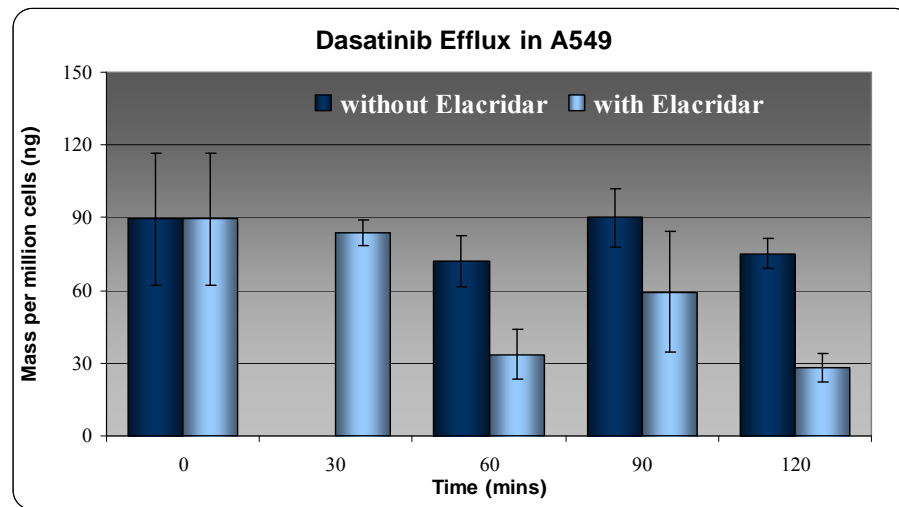
Analysis was performed on technical triplicates. The quantified mass was normalised to mass per million cells.

Figure 4-42: *In vitro* proliferation assay of dasatinib plus elacridar in A549-tax

Figure 4-43 shows the % cell survival in A549-tax as determined by acid phosphatase assay in response to a six day treatment of increasing concentrations of dasatinib in combination with a fixed concentration of elacridar (0.25μM). Data shown are mean and standard deviation of triplicate determinations.

Figure 4-43: *In vitro* proliferation assay of dasatinib plus elacridar in A549

Figure 4-44 shows the % cell survival in A549 as determined by acid phosphatase assay in response to a six day treatment of increasing concentrations of dasatinib in combination with a fixed concentration of elacridar (0.25μM). Data shown are mean +/- SD of triplicate days.

4.2.1.6.   RPMI-2650/Tx cell-line model

RPMI-2650/Tx is the taxol derived, P-gp expressing resistant variant of RPMI-2650. Given that the taxol resistant variant of A549, A549-tax, showed no difference in the levels of dasatinib accumulation, an additional model was selected. This model had also been induced by taxol selection.

The mass of dasatinib accumulated in the presence of the P-gp inhibitor was significantly greater than without an inhibitor present, Figure 4-44.

The presence of an inhibitor also had a significant impact on the cytotoxicity of dasatinib in RPMI-2650/Tx at concentrations below 2.5µM, Figure 4-45.

Figure 4-44: Dasatinib accumulation in RPMI-2650/Tx
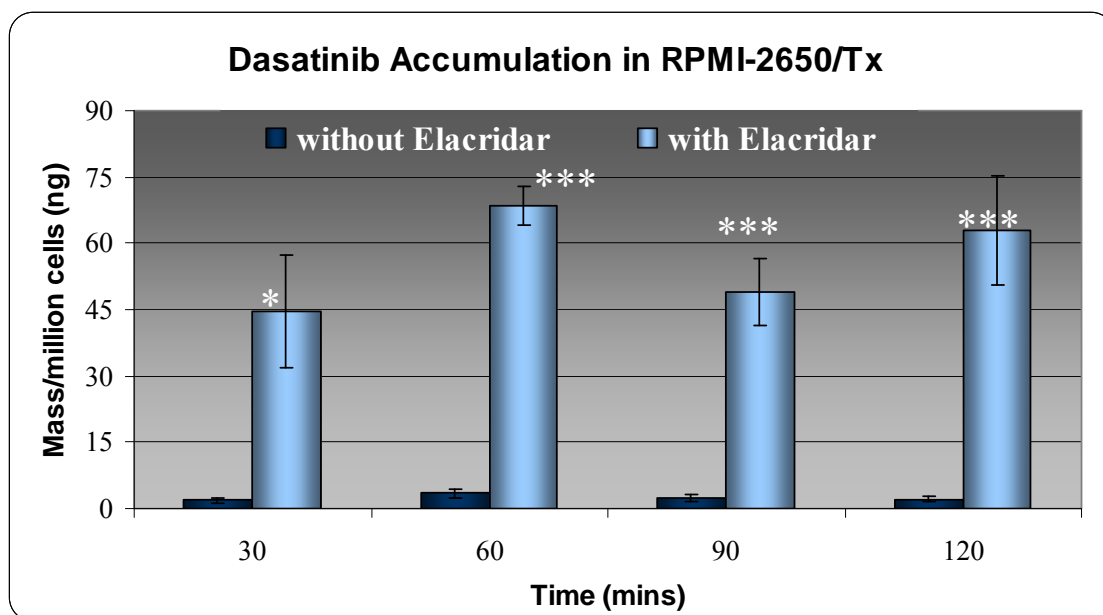
Figure 4-44 shows the accumulation of 1µM dasatinib in RPMI-2650/Tx over 120 minutes. Results shown are the average of technical triplicates. The quantified mass was normalised to mass per million cells. Statistical significance was calculated used the paired student t-test of unequal variance, (see Section 2.3)

Table 4-12: Statistical significance

Time (mins)	p-value
30	0.0286
60	0.0010
90	0.0080
120	0.0134

p-values were determined by paired student's t-test of unequal variance. Comparison was made between samples with and without elacridar at each time point.

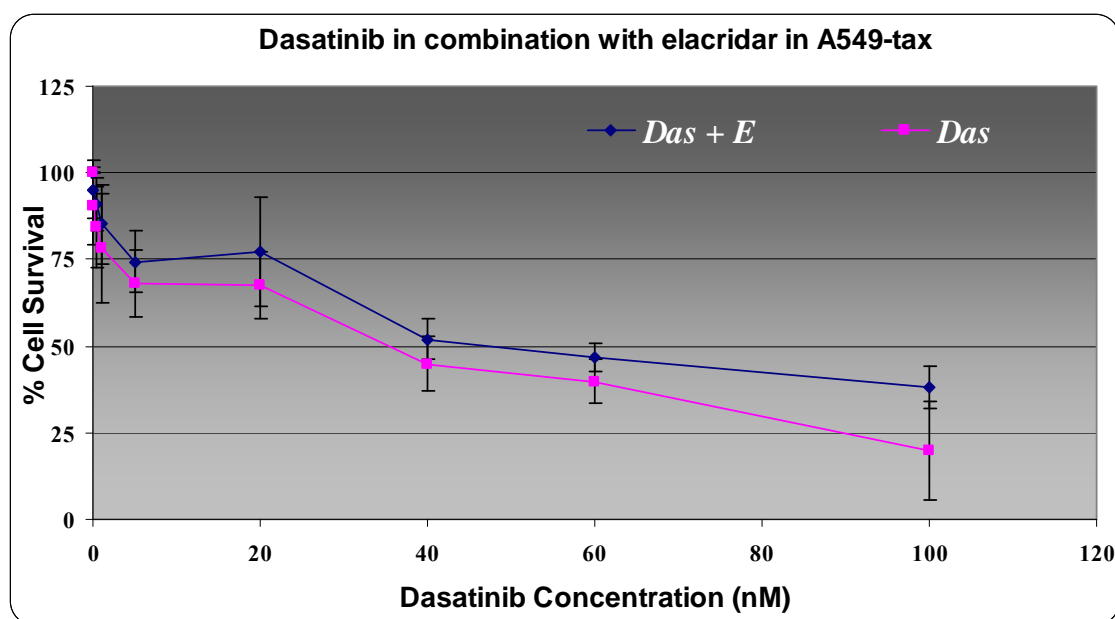**Figure 4-45:** *In vitro* proliferation assay of dasatinib plus elacridar in RPMI-2650Tx
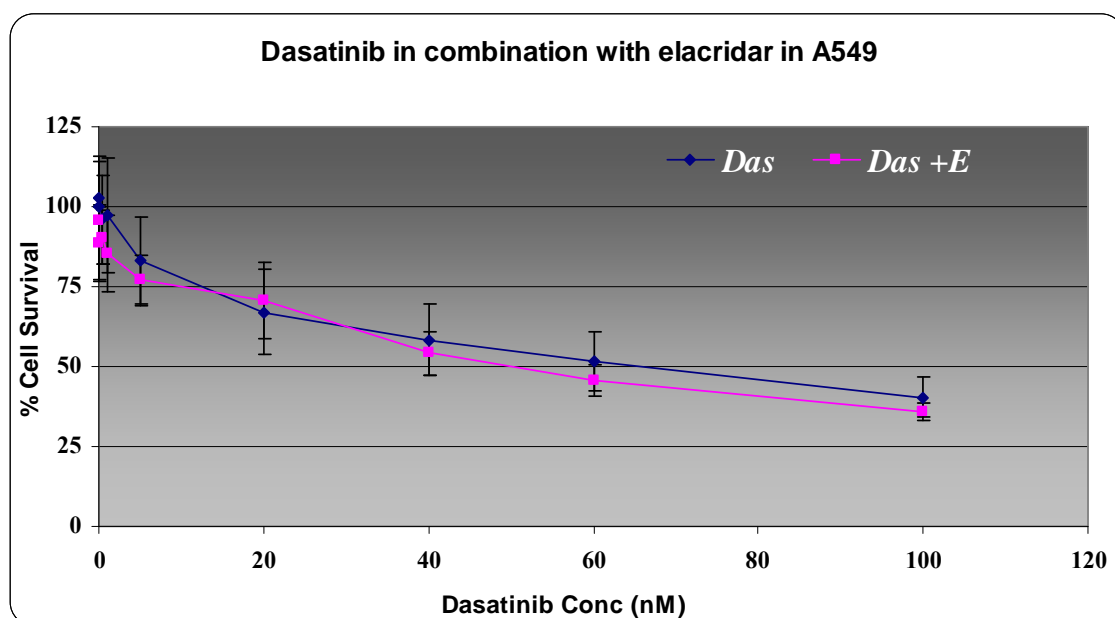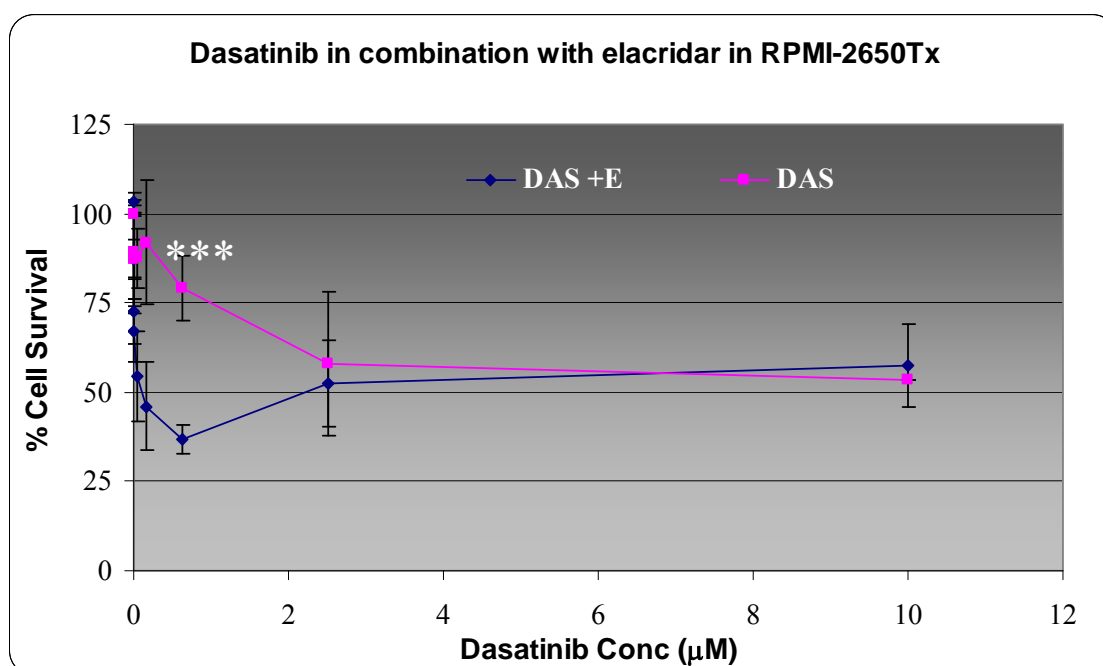

Figure 4-45 shows the % cell survival in RPMI-2650/Tx as determined by acid phosphatase assay in response to a six day treatment of increasing concentrations of dasatinib in combination with a fixed concentration of elacridar (0.25µM). Data shown are mean +/- SD of triplicate determinations. The impact of elacridar was significant at concentrations below 2.5µM

4.2.1.7.   Summary of results for the effect of P-gp on dasatinib

A range of P-gp over-expressing cell-line models were used for this investigation.

A significant difference was seen in the accumulation of dasatinib in DLKP and P-gp over-expressing DLKP-A. That P-gp was significantly involved in the causation of this difference was verified by both accumulation and efflux assay which incorporated P-gp inhibitor elacridar in the assay.

As the observation of dasatinib being as a substrate of P-gp was further validated in subsequent cell-line models including DLKP-Sq and DLKP-Sq/Mitox-MDR. Again a significant difference was quantified in the intracellular mass of dasatinib accumulated in the parental and the P-gp over-expressing resistant model was quantified. While the resistance phenotype is predominantly P-gp driven, the analysis of the cytotoxicity assays showed that epirubicin and taxol resistance was solely P-gp related while dasatinib resistance was partially P-gp mediated. This is shown by the incomplete reversal of resistance to dasatinib in the P-gp over-expressing model.

The accumulation of dasatinib in the resistant ovarian cell model IGROV-1CDDP was examined in combination with elacridar. A significant difference was seen between the levels of dasatinib accumulated in the cell-line with and without elacridar. The inhibition of P-gp by elacridar substantially increased the mass of dasatinib in the cell. Cytotoxically the addition of elacridar to the dasatinib toxicity assay for the parental cell line had no effect however the addition of elacridar in IGROV-1CDDP increased the effectiveness of dasatinib.

The effect of P-gp on dasatinib was further validated in the cell-lines KB-8-5-11 and RPMI-2650/Tx in combination with elacridar.

Of the P-gp cell-line models studied only A549-tax did not show the same trend as the other cell-lines. This is possible a function of the low level of P-gp over-expression in this cell-line.

4.2.2. The interaction of dasatinib with BCRP

Breast Cancer Resistant Protein, BCRP, is a half-transporter involved in the transport of mitoxantrone, while the mutant variant R482G is involved in the transport of anthracyclines and Rhodamine 123, (Section 1.3.4). A study published at the end of 2009 by Lagas *et al.,* demonstrated that dasatinib is a substrate of BCRP[175]. This study by Lagas *et al.,* focussed on the limited concentration of dasatinib in the central nervous system (CNS) and the implications in primary and metastatic brain tumours[175].

Using DLKP-Sq/Mitox-BCRP, the BCRP over-expressing "sister" cell-line of DLKP-Sq/Mitox-MDR, the accumulation of 1μM dasatinib was assessed in comparison to the parental cell-line, DLKP-Sq. At all time points examined, significantly more dasatinib was accumulated in the parental cell-line, Figure 4-46.

As well as being a P-gp inhibitor, elacridar also inhibits the action of BCRP[359]. When the accumulation of dasatinib in the presence and absence of elacridar was examined (in the BCRP-overexpressing cell line model), significantly more intracellular dasatinib was detected in the flasks with elacridar present, Figure 4-47. Also it was seen that the mass of dasatinib did not change significantly between the first and last time points.

Figure 4-46: Dasatinib accumulation in DLKP-Sq and DLKP-Sq/Mitox-BCRP

Dasatinib Accumulation in DLKP-Sq and DLKP-Sq/Mitox-BCRP
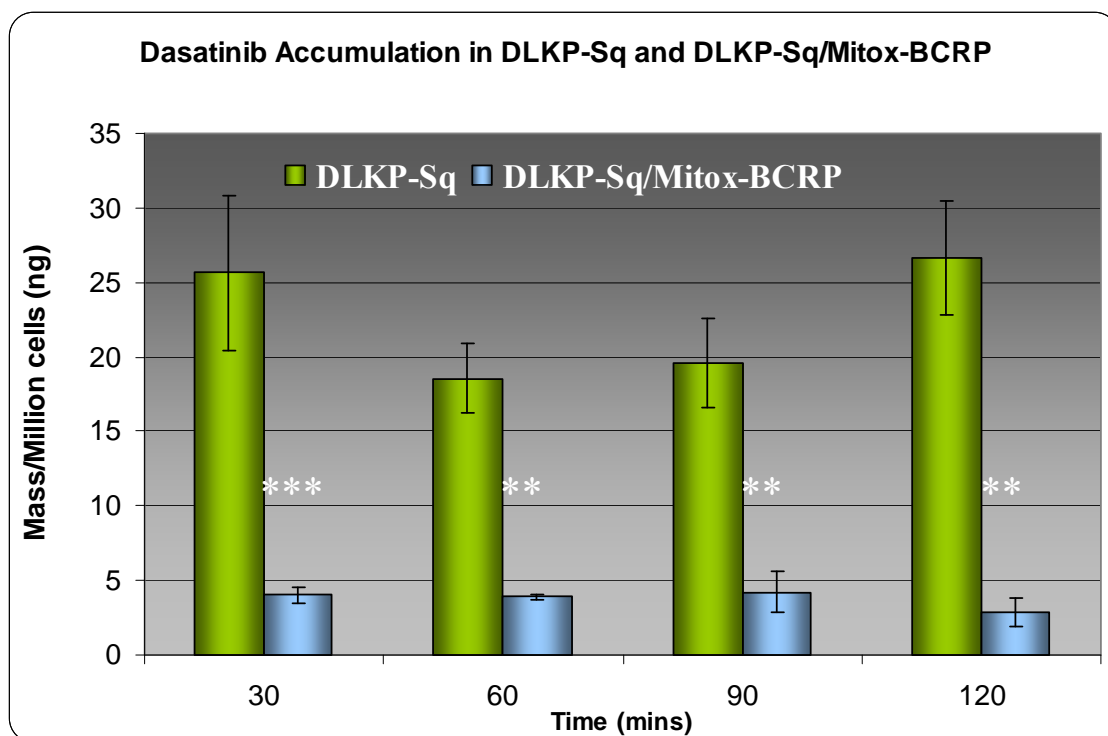
Figure 4-46 shows the accumulation of 1μM dasatinib in DLKP-Sq and BCRP over-expressing DLKP-Sq/Mitox-BCRP cell-lines over two hours with samples taken every 30 minutes. Analysis was performed on technical triplicates. The quantified mass was normalised to mass per million cells. Statistical significance was calculated used the paired student t-test of unequal variance, (see Section 2.3).

Table 4-13: Statistical significance

Time (mins)	p-value
30	0.0176
60	0.0082
90	0.0052
120	0.0059

p-values were determined by paired student's t-test of unequal variance. Comparison was made between the dasatinib accumulated in the parental and BCRP resistant model at each time point.

Figure 4-47: Dasatinib accumulation in DLKP-Sq/Mitox-BCRP
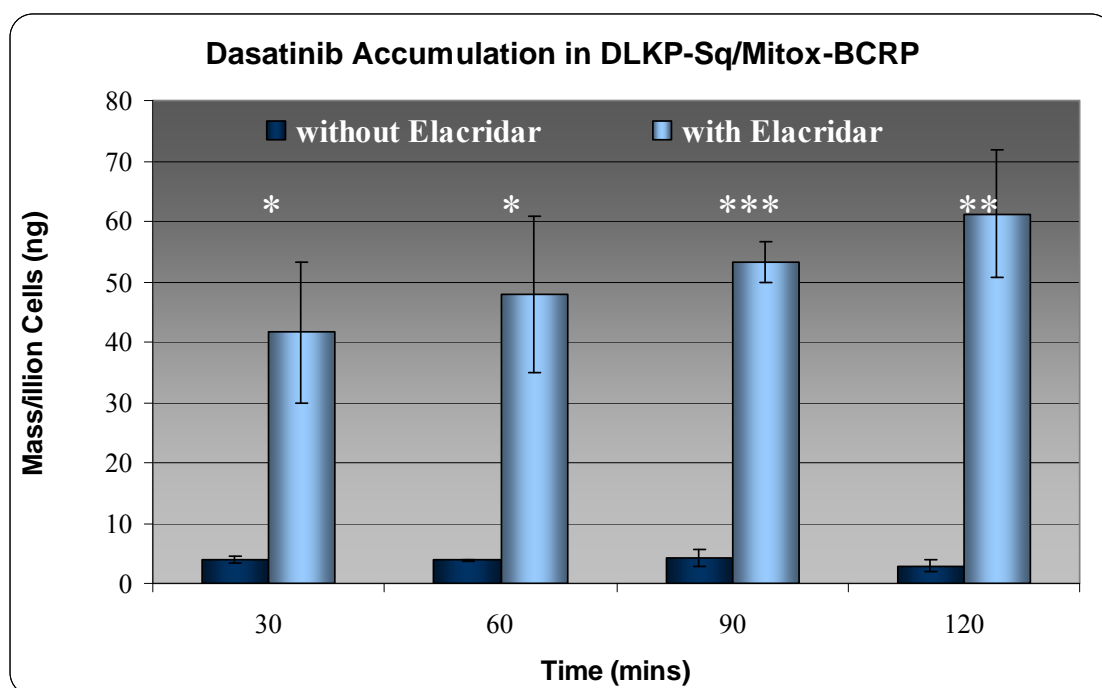
Figure 4-48 shows the accumulation of 1μM dasatinib, with and without elacridar, in BCRP over-expressing DLKP-Sq/Mitox-BCRP cell-lines over two hours with samples taken every 30 minutes. Analysis was performed on technical triplicates. The quantified mass was normalised to mass per million cells. Statistical significance was calculated used the paired student t-test of unequal variance, (see Section 2.3).

Table 4-14: Statistical significance

Time (mins)	p-value
30	0.0300
60	0.0278
90	0.0005
120	0.0100

p-values were determined by paired student's t-test of unequal variance. Comparison was made between samples with and without elacridar at each time point.

The cytotoxic effect of dasatinib on BCRP over-expressing cell-line DLKP-Sq/Mitox-BCRP was examined in a 7 day *in vitro* proliferation assay, Figure 4-48. The inhibition of BCRP by elacridar increased the potency of dasatinib, resulting in increased cell kill. The IC_{50} for dasatinib in DLKP-Sq/Mitox-BCRP was 174nM, the IC_{50} for dasatinib with a fixed dose of elacridar (0.25μM) was 60nM, representing a fold change of 2.9 due to the addition of elacridar, Figure 4-48.

As expected, due to the lack of detectable levels of P-gp and BCRP, in the parental cell-line the addition of elacridar had no effect on dasatinib potency, Figure 4-49. Interestingly though the potency of dasatinib in the parental and resistant (without elacridar) were similar, Figure 4-50. The increase in BCRP expression did not itself lead to increased resistance to dasatinib, however in the BCRP resistant cell-line model the potency of dasatinib was increased with the addition of a BCRP inhibitor, elacridar.

Figure 4-48: In vitro proliferation assay of dasatinib plus elacridar in DLKP-Sq/Mitox-BCRP

Figure 4-49 shows the % cell survival in DLKP-Sq/Mitox-BCRP, determined by acid phosphatase assay in response to a six day treatment of increasing concentrations of dasatinib in combination with a fixed concentration of elacridar (0.25µM). Data shown are mean and standard deviations of triplicate determinations. The asterisk indicates significance as determined by paired student's t-test of unequal variance between the cell survival determined with and without elacridar at 100nM.

Figure 4-49: *In vitro* proliferation assay of dasatinib plus elacridar in DLKP-Sq

Figure 4-50: Comparison of dasatinib in DLKP-Sq and DLKP-Sq/Mitox-BCRP

Dasatinib in combination with elacridar in DLKP - Sq

Dasatinib in DLKP-Sq and DLKP-Sq/Mitox-BCRP

Figure 4-49 shows the % cell survival in DLKP-Sq, determined by acid phosphatase assay in response to a six day treatment of increasing concentrations of dasatinib in combination with a fixed concentration of elacridar (0.25μM). Data shown are mean and standard deviations of triplicate determinations.

Figure 4-50 shows the comparison of DLKP-Sq and DLKP-Sq/Mitox cell survival after exposure to dasatinib. Data shown are mean and standard deviations of triplicate determinations.

The efflux protein BCRP has a more selective transport profile than P-gp. BCRP does not transport taxol, vincristine or verapamil. However, irinotecan and its active metabolite SN-38 are substrates of BCRP[90]. BCRP can have functional variants, where by a mutation in the sequence leads to an amino acid substitution. The wild-type BCRP has an arginine (R) at position 482. Two know variants exist; variant R482T which has threonine (T) at position 482 and variant R482G where position 482 is the amino acid glycine (G). These variations can lead to functional changes. The wild type BCRP does not transport the anthracycline, epirubicin, where as the R482G variant does transport anthracyclines, (Section 1.3.4)[93].

The effect of epirubicin on DLKP-Sq/Mitox-BCRP was examined by *in vitro* proliferation assays in combination with elacridar to test if the BCRP over-expressed was variant or wild-type. The addition of elacridar increased the toxicity of epirubicin, Figure 4-51. The IC_{50} of epirubicin alone was 40nM and in combination with elacridar, 28nM. This suggests that DLKP-Sq/Mitox-BCRP expresses a variant of BCRP rather than the wild type of the transporter (which does not pump epirubicin).

To show conclusively that the resistance mechanism in this cell-line was mediated through the over-expression of ABC transporter BCRP not P-gp, an *in vitro* proliferation assay of taxol in combination with elacridar was performed. As expected, as taxol is not a substrate of BCRP, no alteration in toxicity was seen with the addition of elacridar, Figure 4-52. The irinotecan metabolite SN-38 is a known substrate of BCRP. Elacridar potentiates the toxicity of SN-38 in DLKP-Sq/Mitox-BCRP, Figure 4-53.

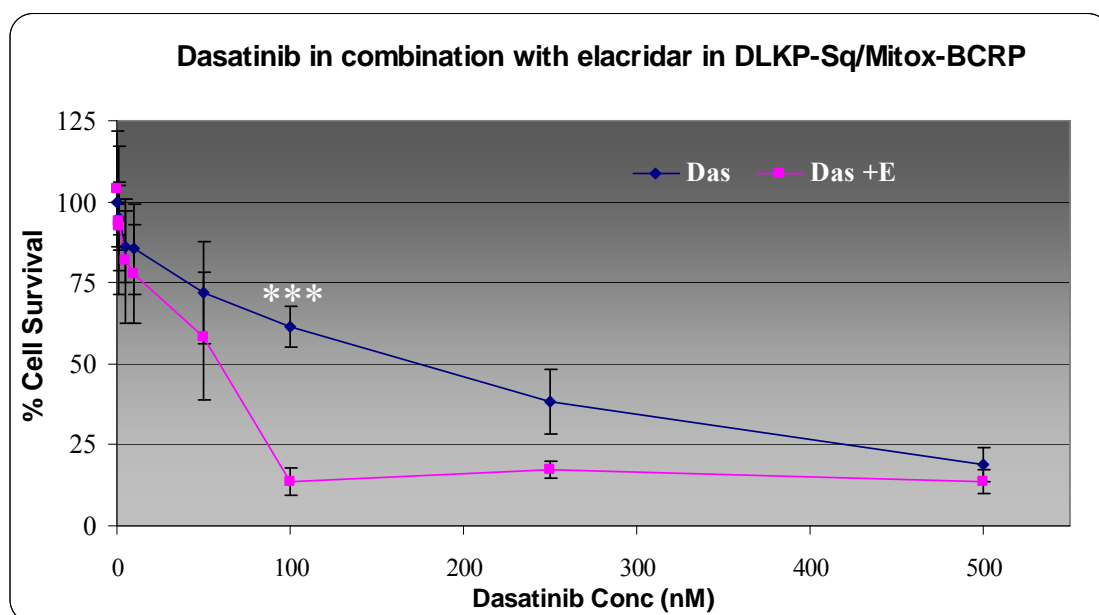**Figure 4-51:** *In vitro* proliferation assay of epirubicin/elacridar in DLKP-Sq/Mitox-BCRP
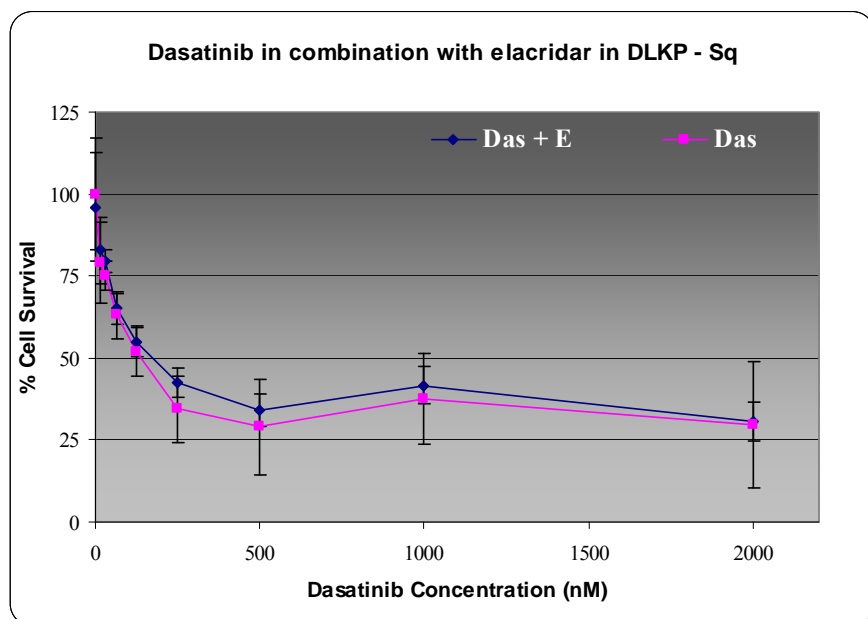

Figure 4-51 shows the % cell survival in DLKP-Sq/Mitox-BCRP, determined by acid phosphatase assay in response to a six day treatment of increasing concentrations of epirubicin in combination with a fixed concentration of elacridar (0.25μM). Data shown are mean and standard deviations on triplicate determinations.

Figure 4-52: In vitro proliferation assay of taxol plus elacridar in DLKP-Sq/Mitox-BCRP
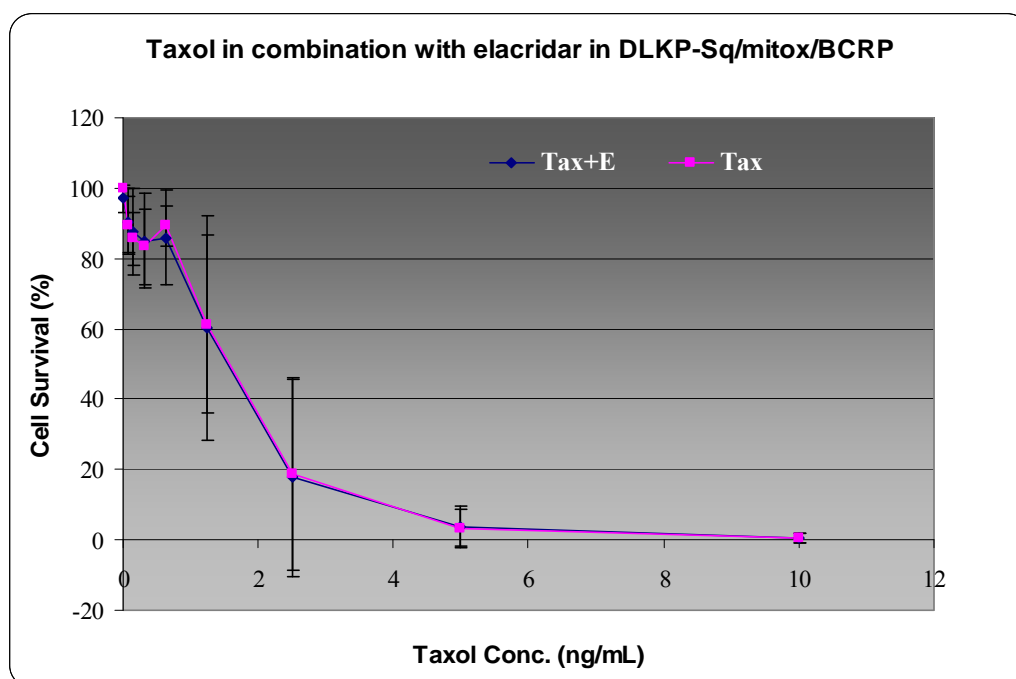
Taxol in combination with elacridar in DLKP-Sq/mitox/BCRP

Shown is the % cell survival following exposure to a concentration range to taxol alone and in combination with a fixed concentration of elacridar (0.25μM). Data shown is the average and standard deviations of biological triplicates.

Figure 4-53: *In vitro* proliferation assay of SN-38 plus elacridar in DLKP-Sq/Mitox-BCRP
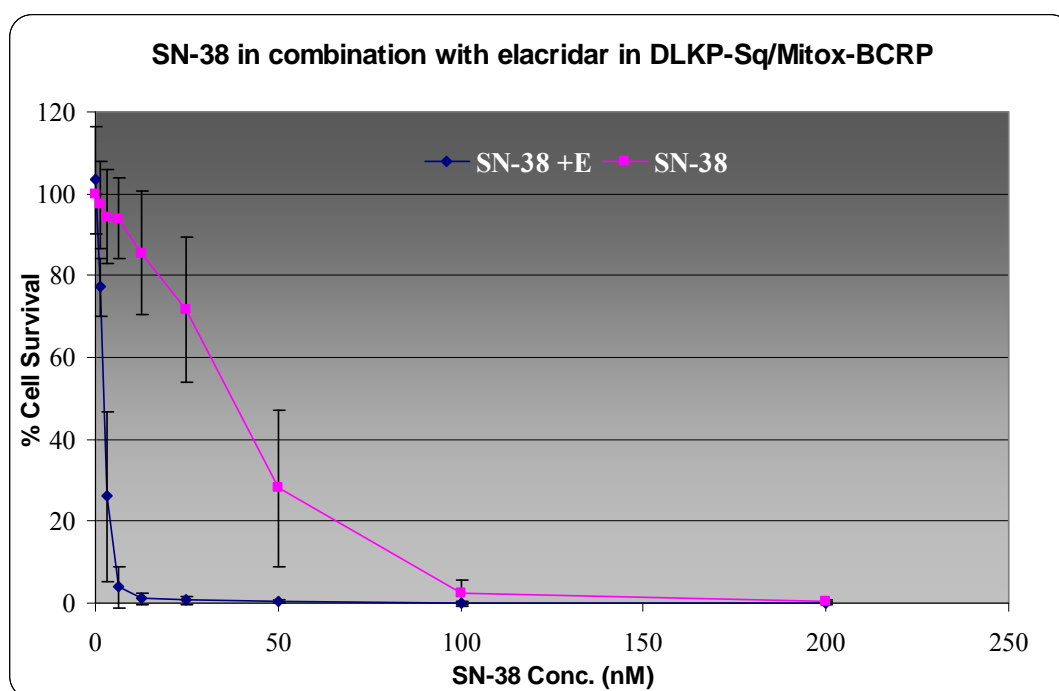
SN-38 in combination with elacridar in DLKP-Sq/Mitox-BCRP

Shown is the % cell survival following exposure to a concentration range to taxol alone and in combination with a fixed concentration of elacridar (0.25μM). Data shown is the average and standard deviations of biological triplicates.

235

To examine if dasatinib potentiates or inhibits the activity of BCRP, the effect of dasatinib in combination with epirubicin and SN-38 was examined by *in vitro* proliferation assays. No effect was seen with the addition of dasatinib to epirubicin or to SN-38, Figure 4-54 and Figure 4-55.

To examine if the dynamic accumulation of epirubicin was affected by dasatinib, the accumulated mass epirubicin was quantified over 90 minutes at 30 minute intervals, Figure 4-56. Technical triplicates were quantified at each condition and each time point. One batch of flasks contained epirubicin only, to monitor the natural accumulation pattern. One batch of flasks contained epirubicin and elacridar, as a positive control for the inhibition of BCRP and one batch contained epirubicin and dasatinib.

The addition of elacridar had a small but significant effect on the accumulation of epirubicin. The mass of intracellular epirubicin was increased at each time-point. The addition of dasatinib to the accumulation of epirubicin had no discernible effect at 30 and 60 minutes, however, at 90 minutes a small but significant decrease in the intracellular mass of dasatinib was calculated, Figure 4-56.

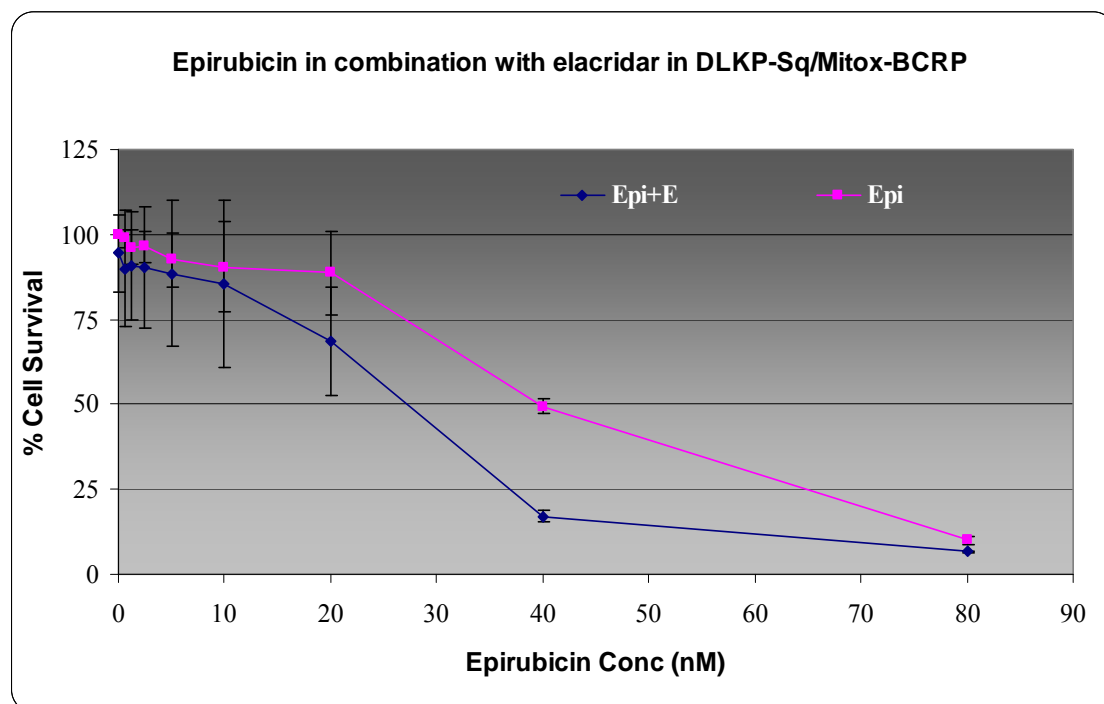**Figure 4-54: Epirubicin in combination with dasatinib in DLKP-Sq/Mitox-BCRP**
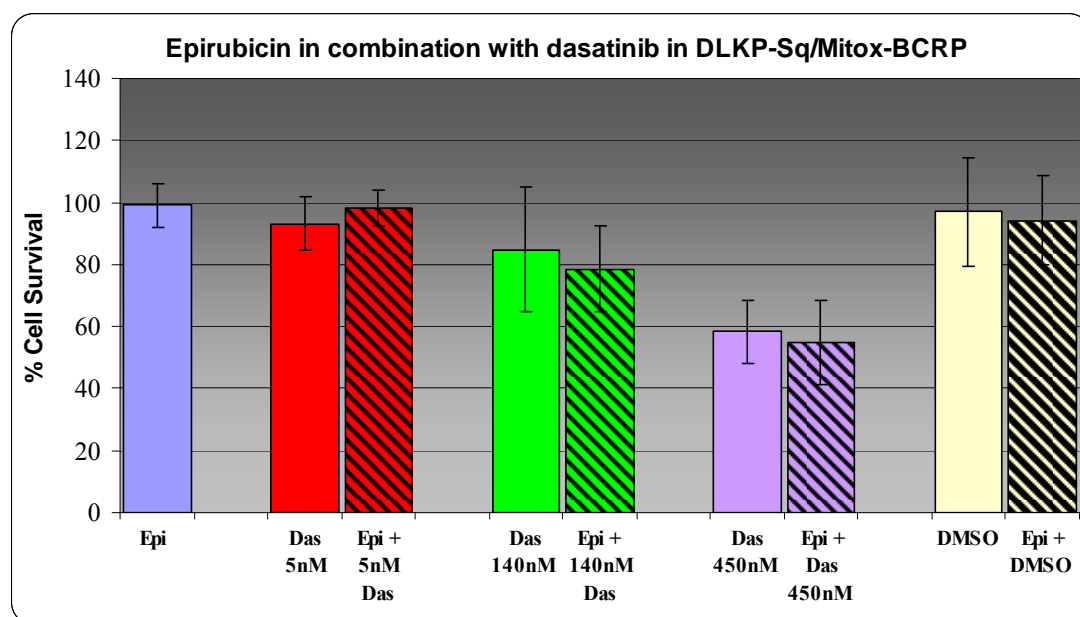
Figure 4-54 shows the % cell survival in DLKP-Sq/Mitox-BCRP as determined by acid phosphatase assay in response to a six day treatment of fixed concentration epirubicin (12.5nM) in combination with increasing concentrations of dasatinib. Data shown are mean +/- SD of triplicate determinations.

**Figure 4-55: SN-38 in combination with dasatinib in DLKP-Sq/Mitox-BCRP**
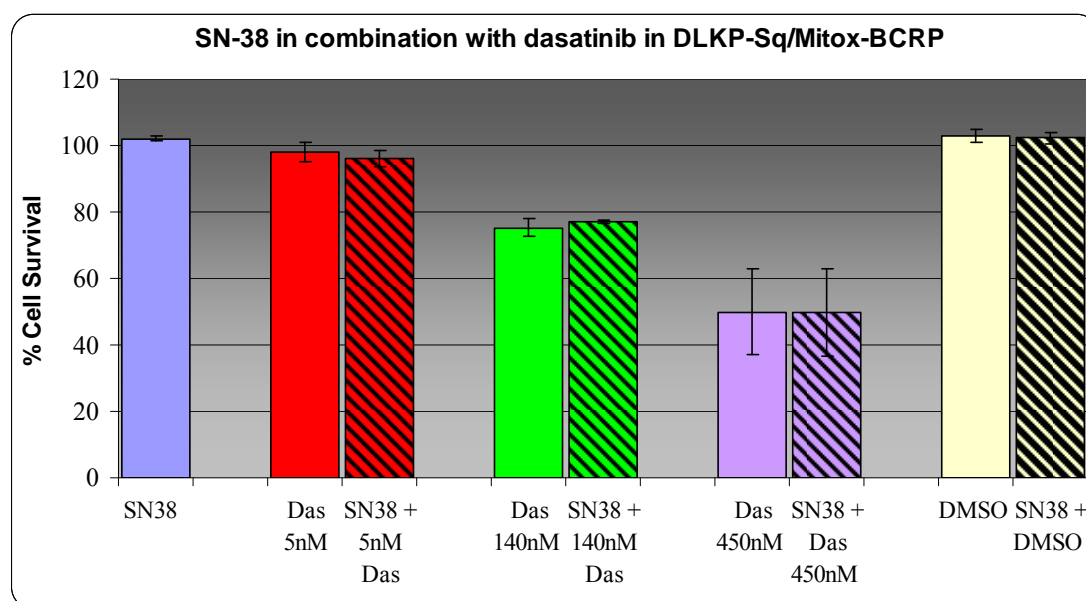
Figure 4-55 shows the % cell survival in DLKP-Sq/Mitox-BCRP as determined by acid phosphatase assay in response to a six day treatment of fixed concentration SN-38 (3.1nM) in combination with increasing concentrations of dasatinib. Data shown are mean +/- SD of triplicate determinations.

Figure 4-56: Epirubicin accumulation in DLKP-Sq/Mitox-BCRP

Figure 4-56: Epirubicin accumulation in DLKP-Sq/Mitox-BCRP
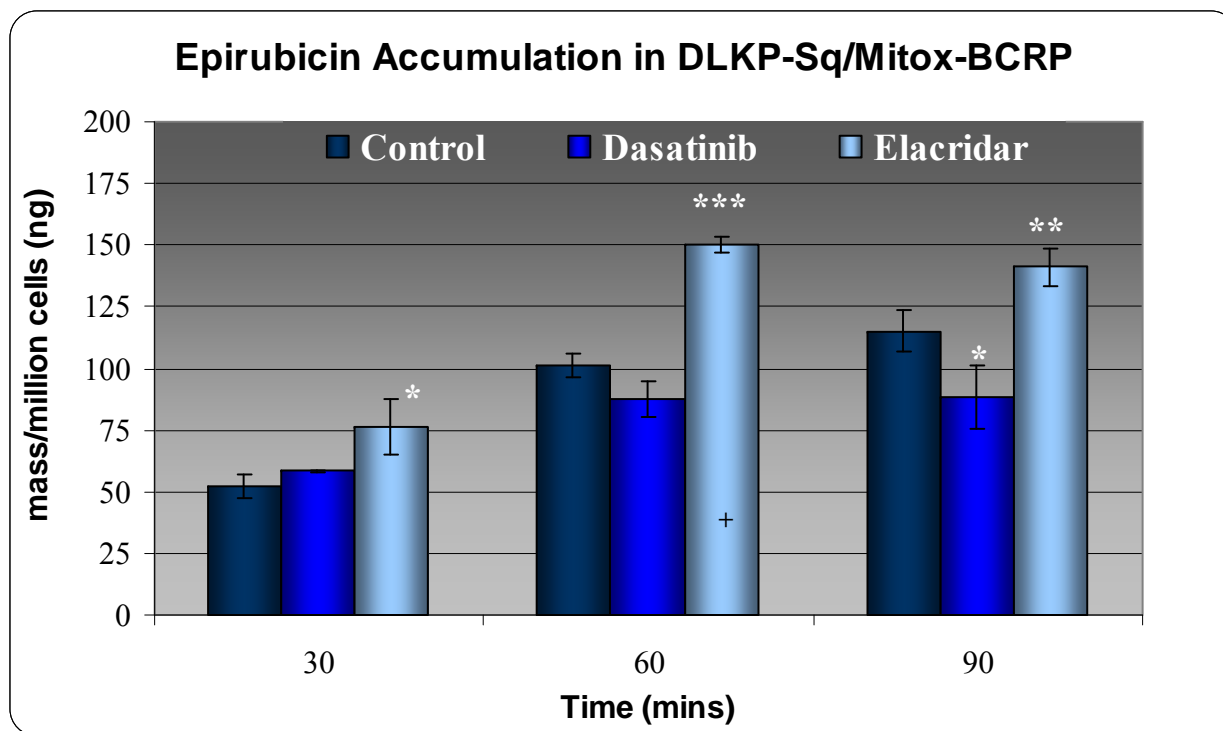
Figure 4-56 shows the accumulated intracellular mass of epirubicin over 90 minutes, alone and in combination with dasatinib or in combination with elacridar. Data represents the average and standard deviation of technical triplicates, (+ indicates n=2). Statistical significance was calculated using the paired two-tailed student t-test with unequal variance. Statistical significance was tested by comparing the epirubicin samples with dasatinib to the control samples at individual time points and the epirubicin samples with elacridar to the control samples at each individual time point.

4.2.3. The interaction of dasatinib with MRP-1

To further study the profile of dasatinib with the three main ABC transport proteins the kinetics of dasatinib uptake and efflux was examined in the MRP-1 over-expressing cell-lines, HL-60/Adr and 2008/MRP-1. The relationship between dasatinib and MRP-1 is so far unreported.

HL-60/Adr is a drug-resistant leukemic cell-line which was selected with adriamycin to over-express MRP-1[360]. The parental HL-60/S cell-line does not express any of the ABC transporters. Figure 4-57 shows the accumulation of dasatinib in HL-60/Adr in comparison to the parental cell-line HL-60/S. There was no predominant trend or difference between the MRP-1 expressing cell-line and the parental cell-line when assessed over biological duplicates.

Sulindac sulphide is the active form of sulindac. At non toxic levels, this non-steroidal anti-inflammatory drug (NSAID) has been shown to significantly increase the cytotoxicity of anthracyclines in MRP-1 expressing cell models as sulindac sulphide inhibits the action of MRP-1[109].

Figure 4-58 shows the efflux of 1μM dasatinib in HL-60/Adr in the presence and absence of sulindac sulphide (5μM). The addition of the inhibitor did not reduce the rate of efflux of dasatinib from the cells.

In a second MRP-1 over-expressing cell-line, 2008/MRP-1, the accumulation of dasatinib in the presence and absence of an inhibitory concentration of sulindac sulphide was quantified. Though a slight increase in the dasatinib intracellular concentration was seen in the inhibited flasks, this was not significant, Figure 4-60.

These results suggest that dasatinib is not a substrate of MRP-1.

Figure 4-57: Dasatinib accumulation in HL-60/Adr
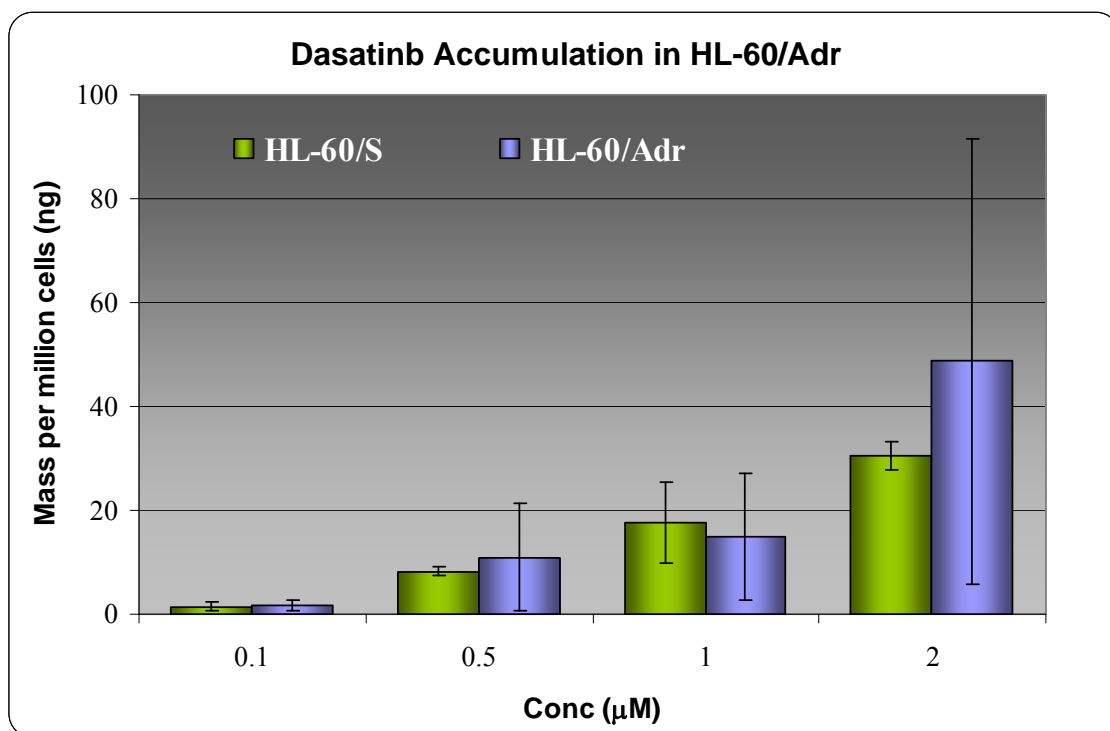
Figure 4-58 shows the accumulation of dasatinib in HL-60/Adr in comparison to the parental cell-line HL-60/S, across a concentration range. Data represents the average and standard deviation, n=6. The quantified mass was normalised to mass per million cells.

Figure 4-58: Efflux of 1μM dasatinib in HL-60/Adr
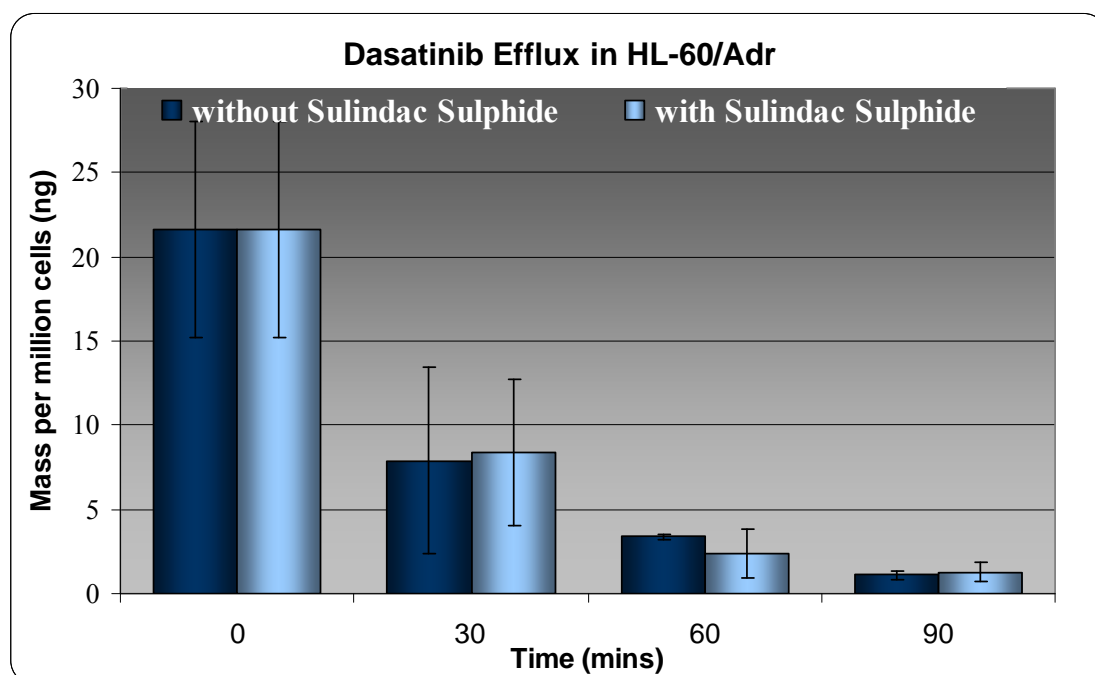
Figure 4-59 shows the efflux of dasatinib in HL-60/Adr cell line with and without the MRP-1 inhibitor sulindac sulphide. The quantified mass was normalised to mass per million cells. Data represents the average and standard deviation of technical triplicates

Figure 4-59: Dasatinib accumulation in 2008/MRP-1 with and without sulindac sulphide
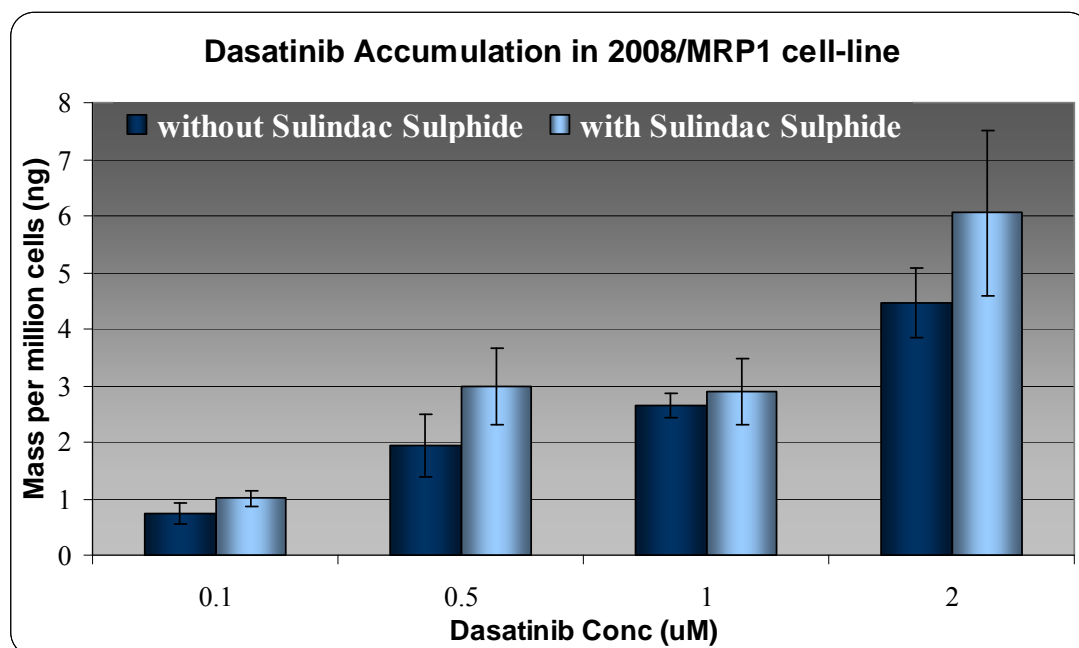
Figure 4-60 shows the efflux of dasatinib in 2008/MRP1 cell line with and without the MRP-1 inhibitor sulindac sulphide. Analysis was preformed in triplicate. The quantified mass was normalised to mass per million cells

4.3. *Lapatinib*

4.3.1. The interaction of lapatinib with P-glycoprotein

To investigate lapatinib as a substrate for transport proteins, P-gp, MRP-1 and BCRP, accumulation assays were carried out in various cell-lines. Through work carried out by Collins *et al.*[179], it was previously demonstrated that lapatinib inhibits the action of P-gp. Lapatinib has also been shown to alter the expression level of P-gp[7, 180]. To identify if competitive inhibition plays a role in this inhibition of lapatinib, lapatinib transport was examined in cell-line models which over-express P-glycoprotein.

4.3.1.1. *A549 and A549-Tax*

A549, a lung adenocarcinoma cell-line model and A549-tax, the resistant variant, which was selected in-house by Dr Laura Breen, [286] were used as one P-glycoprotein model for transport assay. A549-tax has been shown to express low but measurable levels of P-gp[179], while the parental cell-line does not show any P-gp expression.

To determine if P-gp plays a role in the level of cellular accumulation of lapatinib, A549 and A549-tax were exposed to increasing concentrations of lapatinib in media. The cells were exposed to the drug for 2 hours. Assays were carried out in technical triplicates. At the lower concentrations (0.1μM and 0.5μM) there was slightly but not significantly less intracellular lapatinib quantified. At 1μM and 2μM there was equal and slightly more lapatinib accumulated in the P-gp resistant cell-line than the parent. Overall, across the concentration range there was no difference between the parent and resistant models, Figure 4-61.

The *in vitro* toxicity of lapatinib in combination with elacridar in A549 and A549-tax showed that elacridar did not increase the toxicity of lapatinib in either the parental of the resistant cell-line, Figure 4-61 and Figure 4-62.

Figure 4-60: Lapatinib accumulation in A549 and A549-tax after 2 hours.
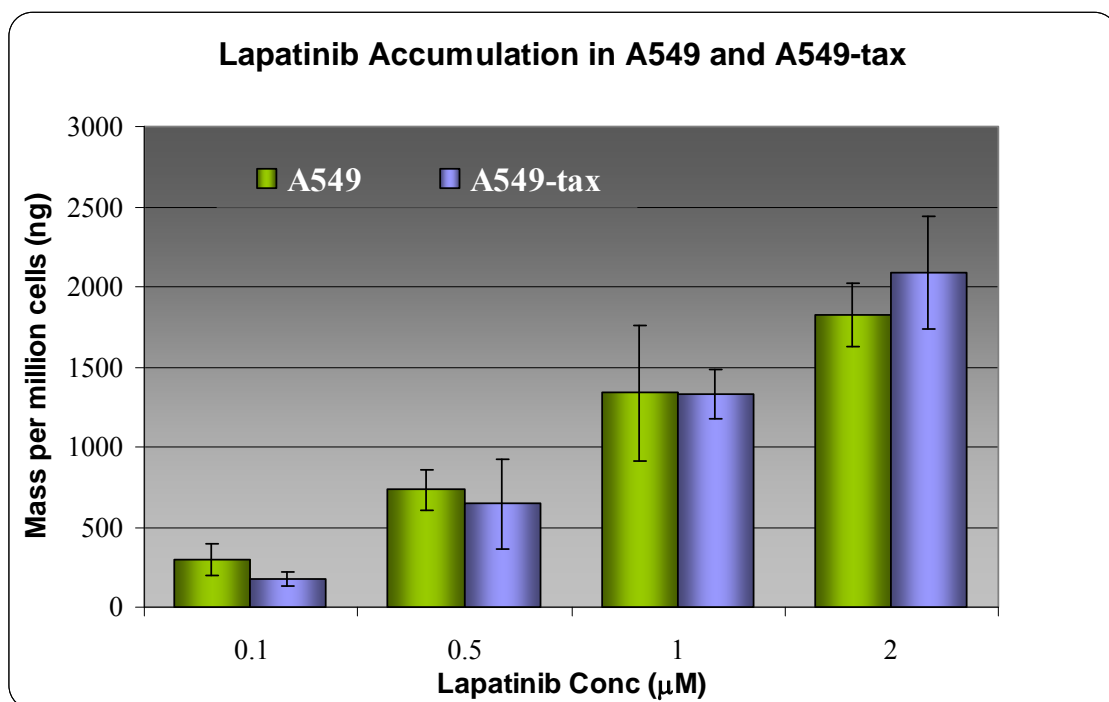
Figure 4-61 shows the mass of lapatinib accumulated after exposed of A549 and A549-tax to increasing concentrations of drug. Mass of drug detected has been normalised to cell number and the results expressed the average and standard deviation as mass per million cells in nanograms. Analysis was preformed in technical triplicates.

Figure 4-61: *In vitro* **toxicity assay of lapatinib plus elacridar in A549-tax**
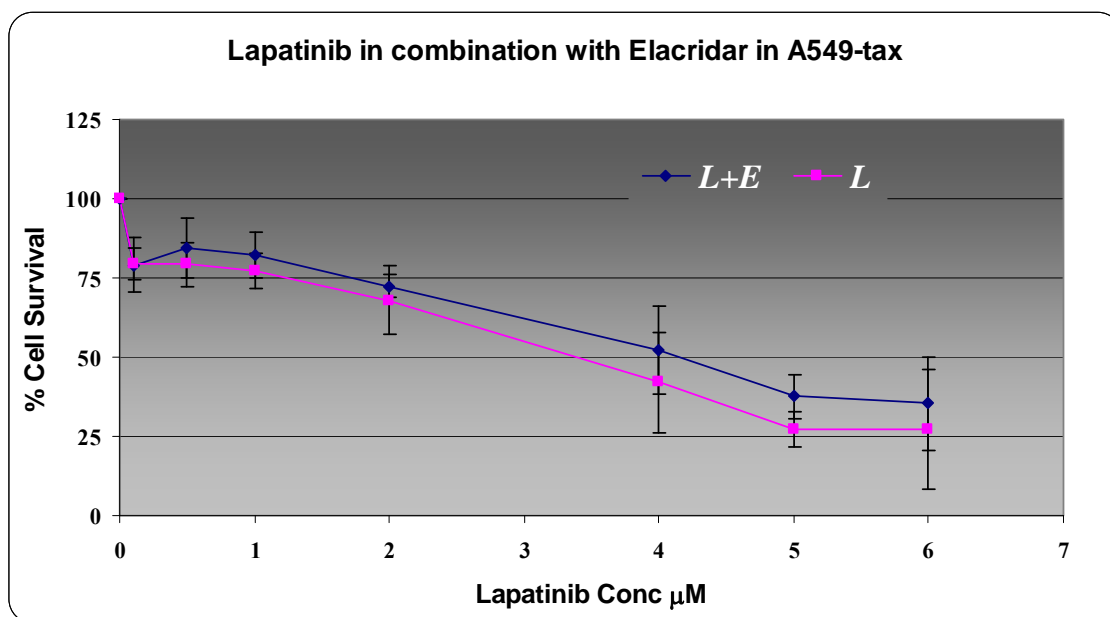
Figure 4-62 shows the % cell survival in A549-tax as determined by acid phosphatase assay in response to a six day treatment of increasing concentrations of lapatinib in combination with a fixed concentration of elacridar (0.25μM). Data shown are mean +/- SD of triplicate determinations.

Figure 4-62: *In vitro* **toxicity assay of lapatinib plus elacridar in A549**
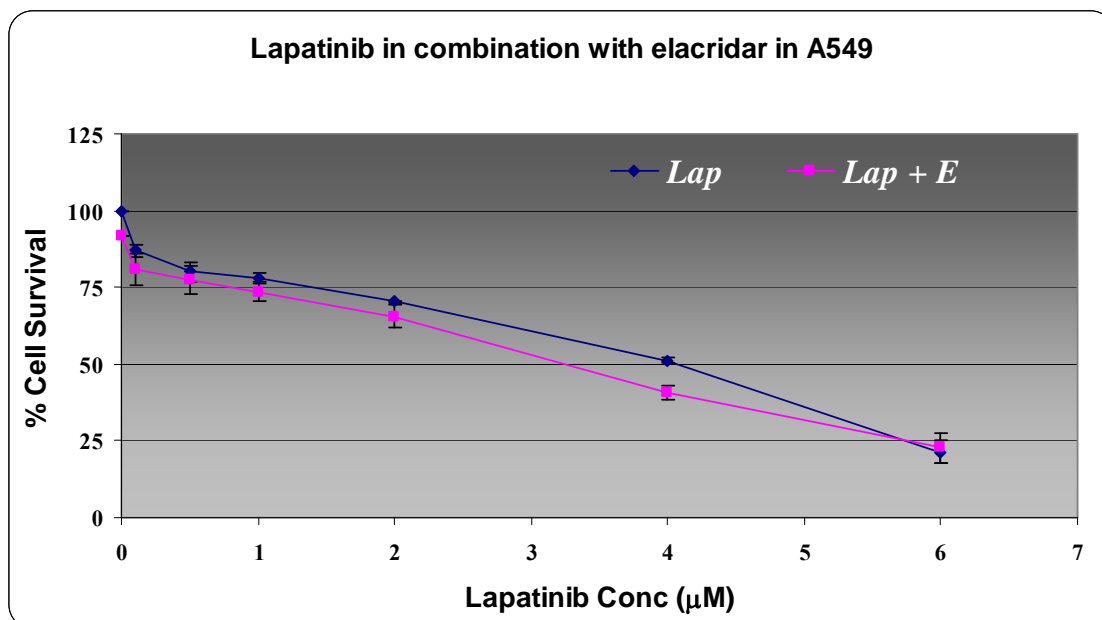
Figure 4-63 shows the % cell survival in A549 as determined by acid phosphatase assay in response to a six day treatment of increasing concentrations of lapatinib in combination with a fixed concentration of elacridar (0.25μM). Data shown are mean +/- SD of triplicate determinations.

4.3.1.2. HL-60/Mdr-1

The leukemic cell-line model HL-60/Mdr-1 has been transduced to over-express P-gp. HL-60/S, the parental cell-line does not over-express any multi-drug resistant proteins and therefore was used as a control. By exposing HL-60/s and HL-60/Mdr-1 to increasing concentrations of lapatinib in media we can examine the role of P-gp in the transport of lapatinib.

The level of intracellular accumulation of lapatinib was comparable between the cell-lines across a concentration range (0.1μM-2μM). No significant difference in lapatinib accumulation was detected between the resistant and the parental cell-line, Figure 4-63.

Figure 4-63: Lapatinib accumulation in HL-60/S and HL-60/Mdr-1
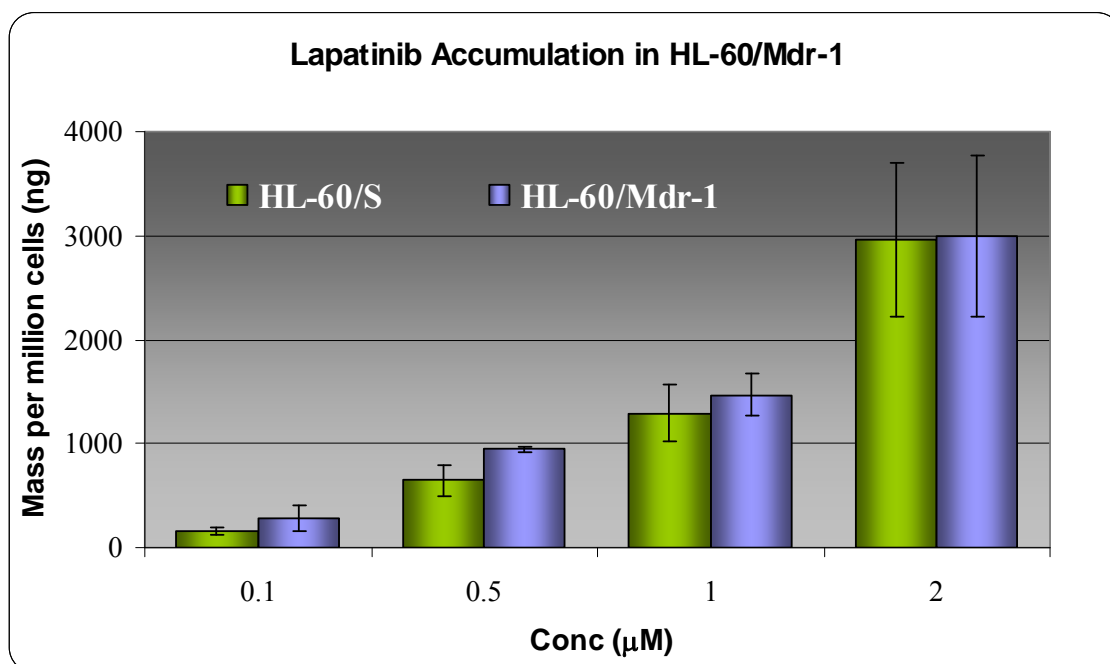
Figure 4-64 shows the accumulation in mass per million cells of lapatinib across a concentration range in the leukemic suspension cell-line HL-60/Mdr-1 and HL-60/S cell-line. Data represents the average and standard deviation of technical triplicates. The quantified mass was normalised to mass per million cells

4.3.1.3.   DLKP and DLKP-A

DLKP[285], a lung cell-line, and the drug resistant variant DLKP-A[109], were selected as a model for drug transport assay as DLKP-A has be shown to significantly over-express P-gp, while the parental cell-line does not express P-gp.

The level of lapatinib accumulated in DLKP-A in comparison to the parental cell-line was examined across a concentration range for two hours to determine if P-gp is exerting an effect on the kinetics of lapatinib uptake and accumulation in the cell-line model.

Across the concentration range there was no significant difference between the levels of lapatinib accumulated in the P-gp over-expressing DLKP-A, and the parental DLKP, Figure 4-64.

To examine the efflux profile of lapatinib in DLKP and DLKP-A the intercellular level of lapatinib was quantified after the cells were allowed to efflux in media with and without inhibitor present. Examination of the efflux profile of lapatinib in DLKP-A and DLKP showed that the addition of P-gp inhibitor elacridar had no effect on the efflux profile of lapatinib.

Figure 4-65 gives the timed efflux profile of lapatinib in the presence and absence of P-gp inhibitor, elacridar, in DLKP-A cell-line model after a two hours exposure to 2μM lapatinib. The rate of efflux for both arms of the study shows an equivalent trend and similar quantitative levels of lapatinib present.

Similar to Figure 4-65, Figure 4-66 showed the efflux profile of lapatinib in DLKP in the presence and absence of elacridar in the cell culture media following accumulation for two hours.

Figure 4-64: Lapatinib accumulation in DLKP and DLKP-A
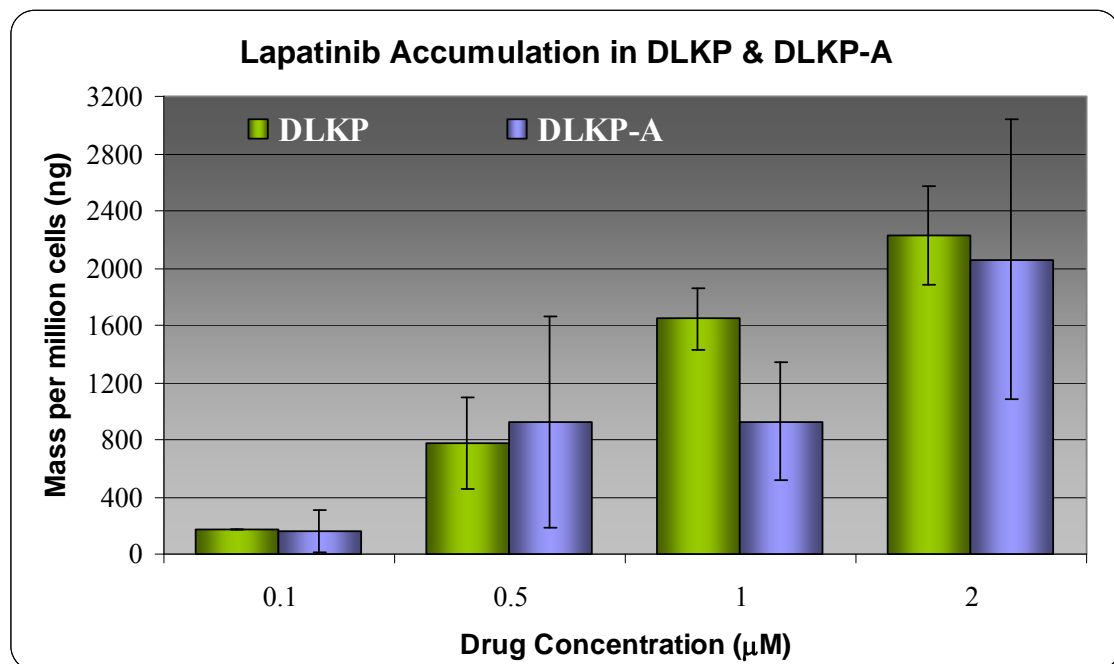
Figure 4-64 shows the accumulation in mass per million cells of lapatinib in DLKP and in the resistant variant DLKP-A across increasing concentrations range, after two hours exposure. Data represents the average and standard deviation, n=6. The quantified mass was normalised to mass per million cells

Figure 4-65: Efflux profile of lapatinib in DLKP-A with and without elacridar

Lapatinib Efflux in DLKP-A
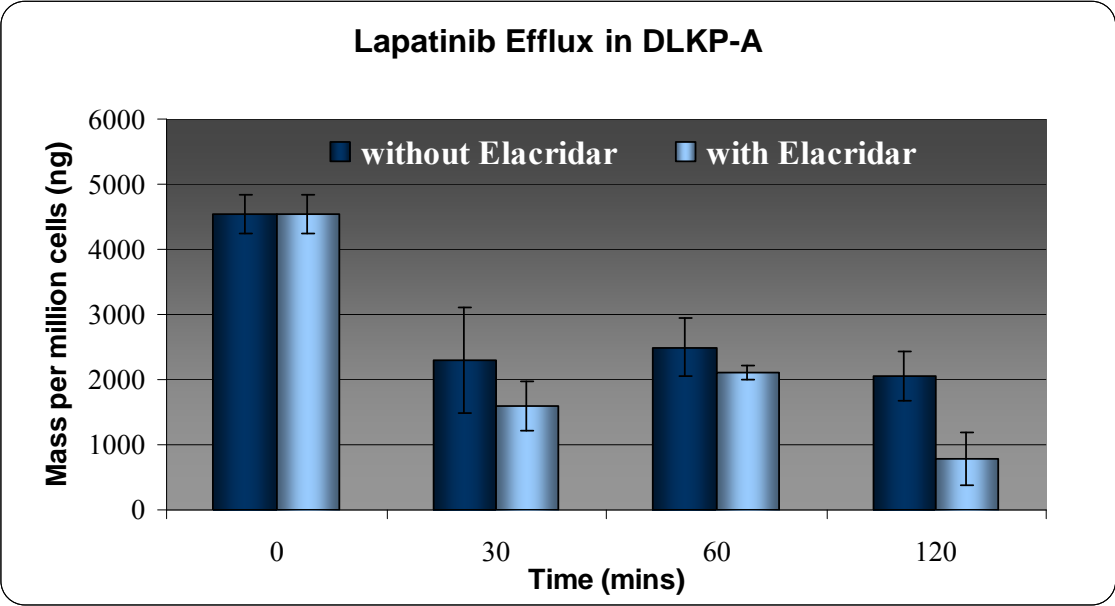
Efflux profile of 2μM lapatinib in DLKP-A, with 0.25μM elacridar. Data represents the average and standard deviation of technical triplicates. The quantified mass was normalised to mass per million cells.

Figure 4-66: Efflux profile of lapatinib in DLKP with and without elacridar

Lapatinib - Efflux Assay DLKP
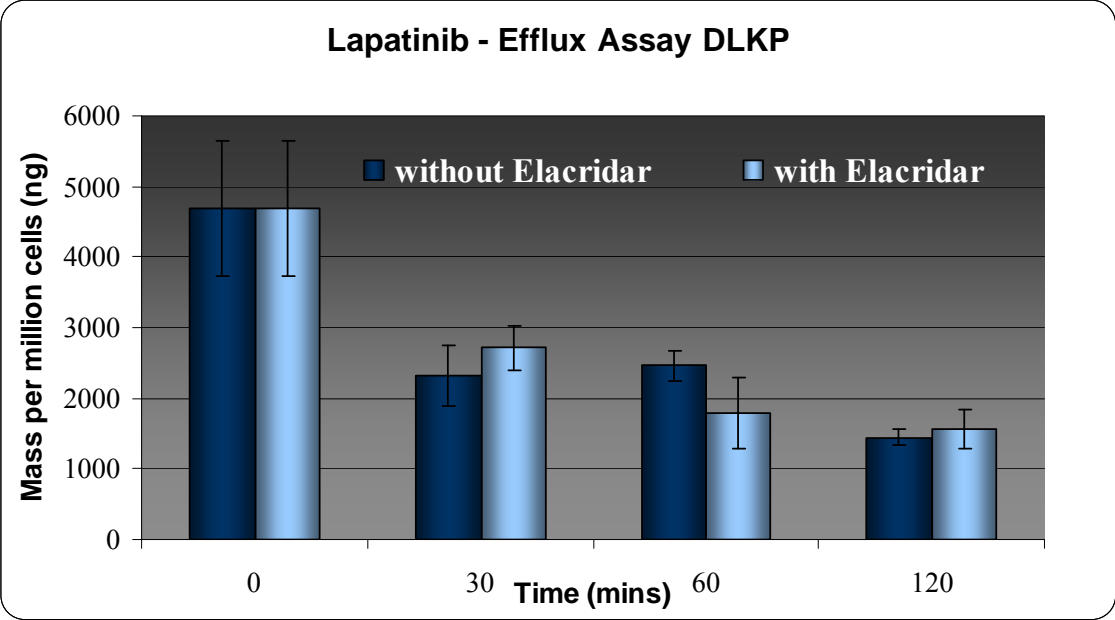
Efflux profile of 2μM lapatinib in DLKP, with 0.25μM elacridar Data represents the average and standard deviation of technical triplicates. The quantified mass was normalised to mass per million cells.

The effect of inhibition of P-gp on the cytotoxicity of lapatinib was investigated. In both the P-gp over-expressing model (DLKP-A) and the parental model (DLKP) no significant effect was seen from the addition of elacridar to a range of lapatinib concentrations, Figure 4-67 and Figure 4-68.

The effect of lapatinib in combination with other chemotherapeutics, epirubicin, paclitaxel, 5- fluorouracil, vinblastine, docetaxel, has been extensively researched. Synergistic toxicity was observed with lapatinib when combined with P-gp substrates epirubicin, paclitaxel, docetaxel and vinblastine in DLKP-A and A549-T. However, no synergy was observed in when lapatinib was combined with 5- fluorouracil[7].

To demonstrate kinetically the effect of lapatinib on a P-gp substrate, the accumulated mass of epirubicin was monitored. Elacridar was included as a positive control to demonstrate the effect complete inhibition of P-gp would have on the quantified mass.

Lapatinib inhibits the accumulation of epirubicin to an equal if not greater extent than elacridar, Figure 4-69.

Overall this data indicates that lapatinib is not a substrate of P-gp but does inhibit the transporter.

Figure 4-67: *In vitro* toxicity assay of lapatinib plus elacridar in DLKP

Lapatinib in combination with elacridar in DLKP
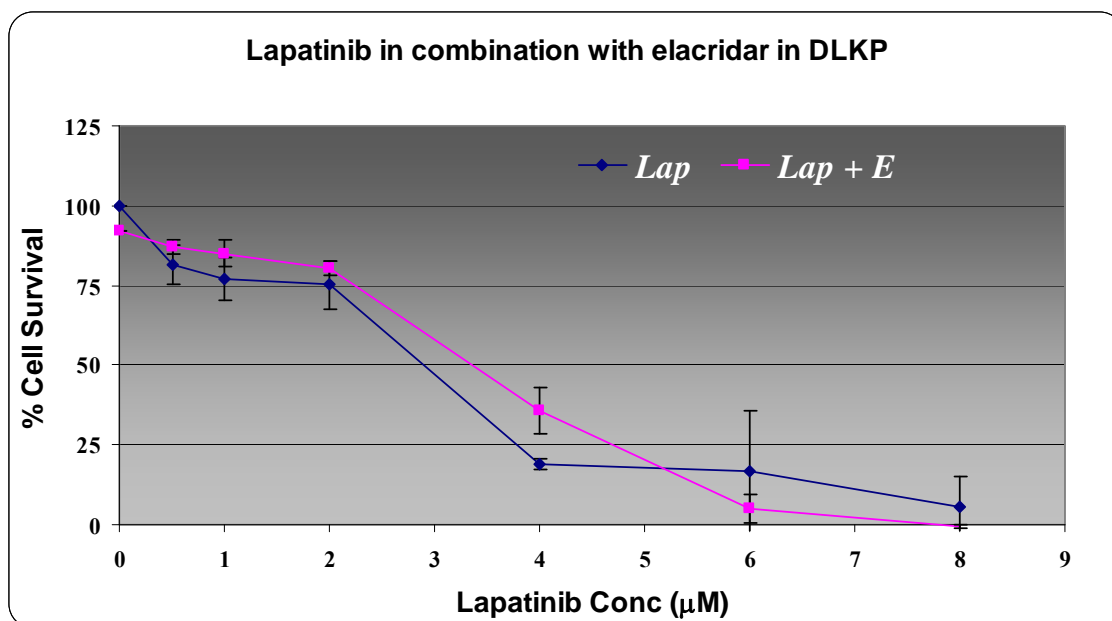
Figure 4-67 shows the % cell survival in DLKP as determined by acid phosphatase assay in response to a seven day treatment of increasing concentrations of lapatinib in combination with a fixed concentration of elacridar (0.25μM). Data shown are mean +/- SD of triplicate determinations.

Figure 4-68: *In vitro* toxicity assay of lapatinib plus elacridar in DLKP-A

Lapatinib in combination with elacridar in DLKP-A
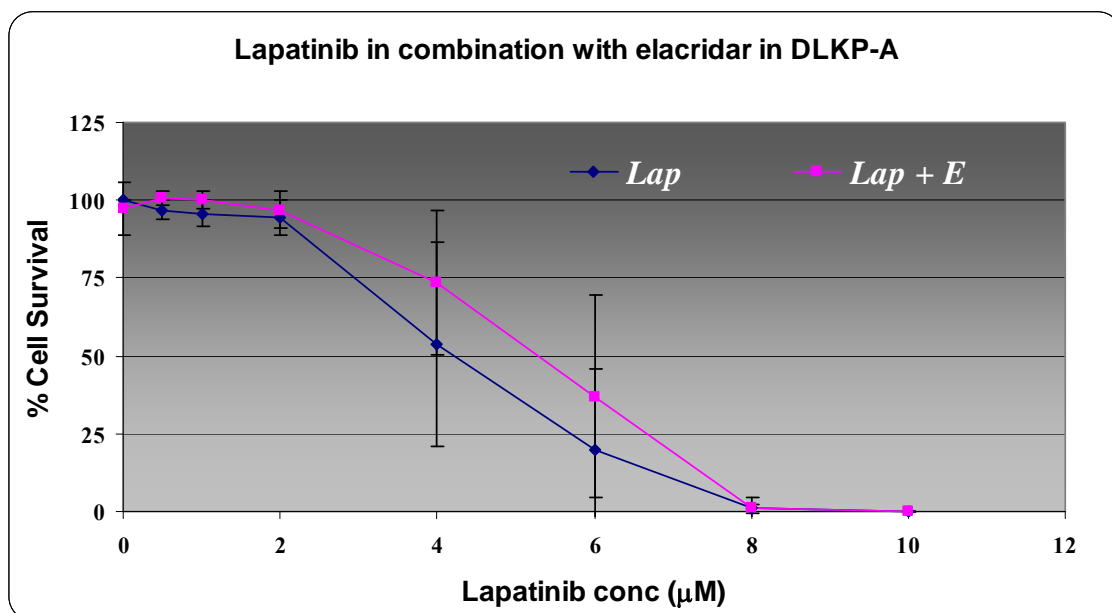
Figure 4-68 shows the % cell survival in DLKP as determined by acid phosphatase assay in response to a seven day treatment of increasing concentrations of lapatinib in combination with a fixed concentration of elacridar (0.25μM). Data shown are mean +/- SD of triplicate determinations.

Figure 4-69: Epirubicin accumulation in DLKP-A
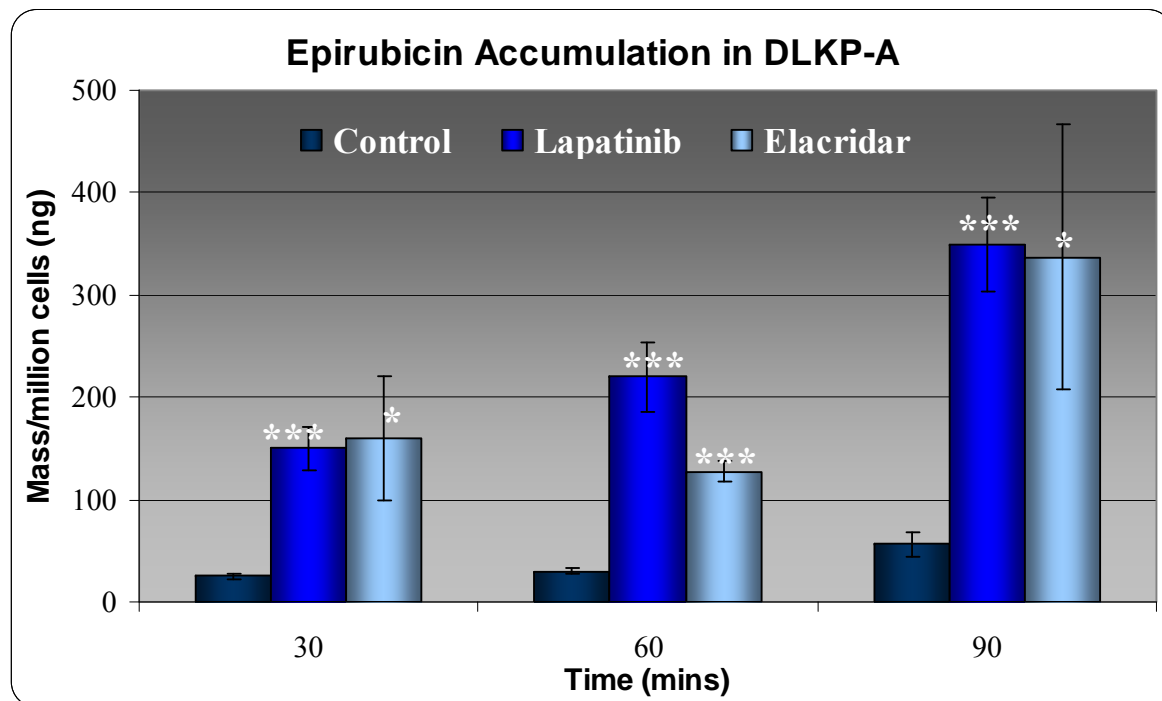
Epirubicin Accumulation in DLKP-A

Table 4-15: Statistical Significance

Time (mins)	Lapatinib *vs* Control	Elacridar *vs* Control
30	0.00051	0.01812
60	0.00064	0.00008
90	0.00043	0.02026

p-values determined by paired student's t-test of equal variance. Comparisons were made between epirubicin accumulation and epirubicin accumulation with lapatinib or epirubicin accumulation and epirubicin accumulation with elacridar.

Shown is the accumulated intracellular mass of epirubicin over 90 minutes, alone and in combination with 2μM lapatinib or 0.25μM elacridar. Data represents the average and standard deviation of technical triplicates. Statistical significance was calculated used the paired student t-test with equal variance. Statistical significance was tested by comparing the epirubicin samples with lapatinib to the control samples at individual time points and epirubicin samples with elacridar to the control samples at each individual time point.

4.3.2. The interaction of lapatinib with BCRP

Breast Cancer Resistant Protein, BCRP, is a half-transporter involved in the transport of mitoxantrone. HL-60/Mxr is a leukemic cell-line, transfected with the *MXR* gene to over-express the BCRP transporter protein. In this assay HL-60/S was used as the control as it does not over-express any ABC transporter.

The accumulated mass of lapatinib in the cell-line models examined in Figure 4-70 showed that the transporter BCRP had little of no effect on the intracellular mass of lapatinib.

Figure 4-71 further expands on the relationship between lapatinib and BCRP efflux protein. An inhibitory concentration of $0.25\mu M$ elacridar was added and the efflux pattern was observed.

There was no significant difference between the mass of drug in the cell in the flasks treated with the inhibitor when compared to the flasks efflux in cell culture media alone. The addition of elacridar did not appear to maintain the intracellular concentration of lapatinib.

A brief examination on the influence of lapatinib on BCRP modulation was examined in the DLKP-Sq/Mitox-BCRP cell-line. Accumulation in the presence of lapatinib and elacridar showed that, over prolonged exposure, lapatinib may have an effect on the accumulation of epirubicin. However, at the lower time-points the addition of lapatinib to the cell-culture media appeared ineffectual.

Overall, lapatinib is not a substrate of BCRP but does have a modulatory effect on the action of BCRP.

Figure 4-70: Lapatinib accumulation in HL-60/Mxr

Lapatinib Accumulation in HL-60/Mxr
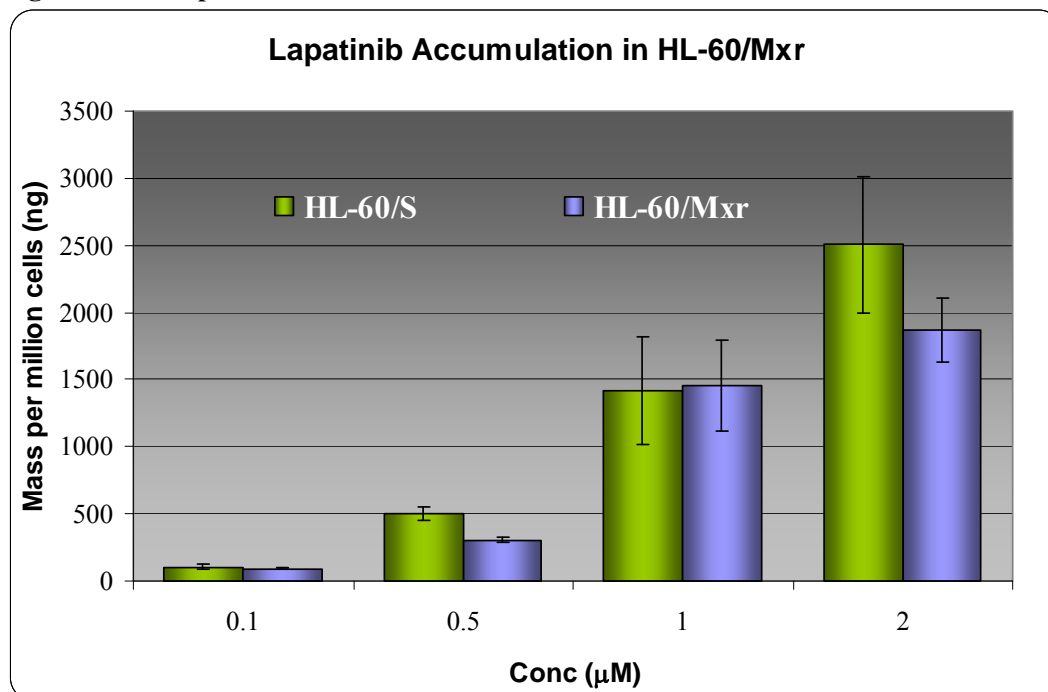
Figure 4-71 quantifies the mass of lapatinib accumulated in HL-60/Mxr and HL-60/S cell-lines after two hours exposure over increasing lapatinib concentration. Analysis was performed on technical triplicates. The quantified mass was normalised to mass per million cells.

Figure 4-71: Lapatinib efflux in HL-60/Mxr

Lapatinib Efflux in HL-60/Mxr
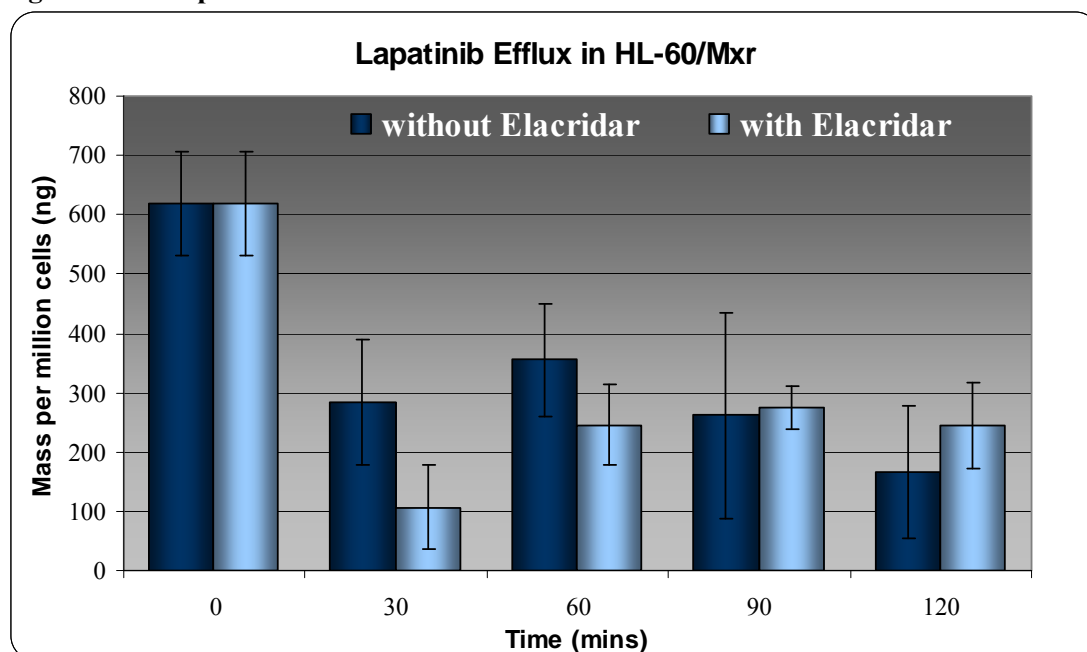
Figure 4-72 shows the efflux profile of 1µM lapatinib in HL-60/Mxr in the presence and absence of 0.25µM elacridar. Analysis was performed on technical triplicates. The quantified mass was normalised to mass per million cells.

255

Figure 4-72: Epirubicin accumulation in DLKP-Sq/Mitox-BCRP
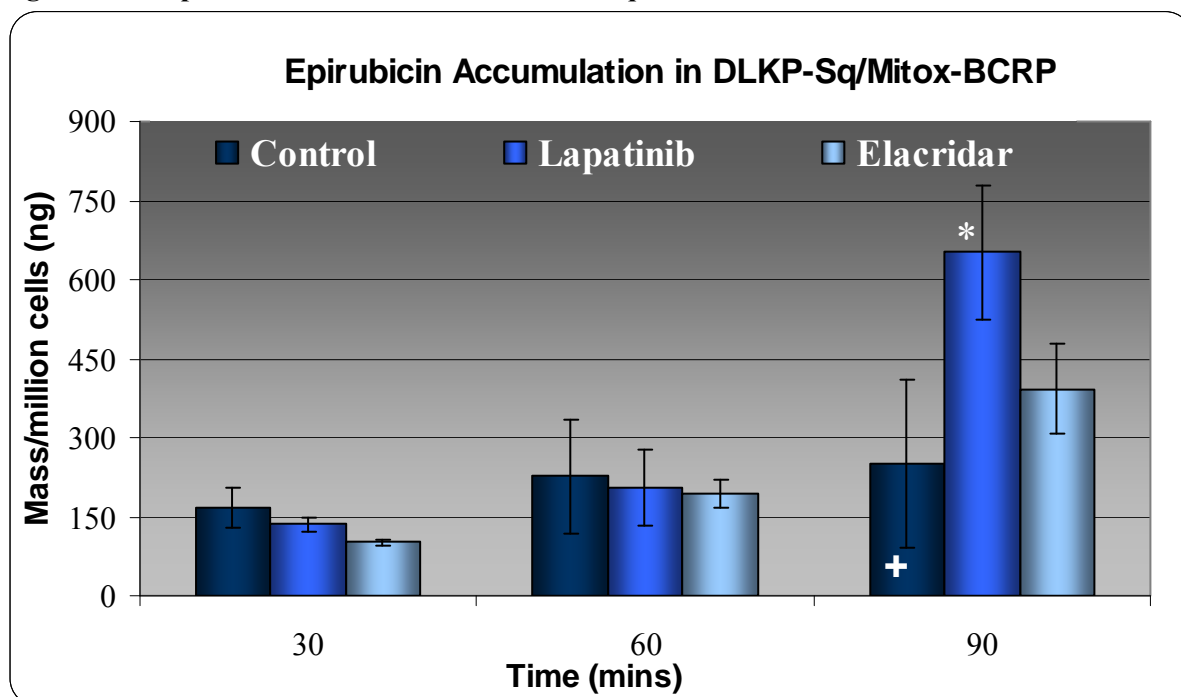
Epirubicin Accumulation in DLKP-Sq/Mitox-BCRP

Shown is the accumulated intracellular mass of epirubicin over 90 minutes, alone and in combination with lapatinib or elacridar. Data represents the average and standard deviation of technical triplicates, (+ indicates n=2). Statistical significance was calculated used the student t-test with equal variance. Statistical significance was tested by comparing the epirubicin samples with lapatinib to the control samples at individual time points and epirubicin samples with elacridar to the control samples at each individual time point.

4.3.3. The interaction of lapatinib with MRP-1

MRP-1, an ABC transport protein, is responsible for the transport of anthracyclines, vinca alkaloids, epipodophyllotoxins and methotrexates. To date the relationship between lapatinib and MRP-1 is unreported. Using the MRP-1 over-expressing cell-line model, HL-60/Adr as an *in vitro* model, the connection between lapatinib transport and MRP-1 was investigated.

Figure 4-73 shows the accumulation of lapatinib over a two hour period across an increasing lapatinib concentration range in the HL-60/Adr cell-line with HL-60/S used as a control. There was no significant difference in the levels of lapatinib accumulated in the MDR negative cell-line HL-60/S and the MRP-1 over-expressing cell-line HL-60/Adr.

Sulindac sulphide, the active form of sulindac is an MRP-1 inhibitor was used to inhibit the action of MRP-1. In the analysis, the intracellular level of lapatinib in HL-60/Adr was quantified following the efflux in the presence and absence of sulindac sulphide. The intracellular mass of lapatinib present was equivalent in both the inhibitor positive and control samples, Figure 4-74.

Figure 4-73: Lapatinib accumulation in HL-60/Adr
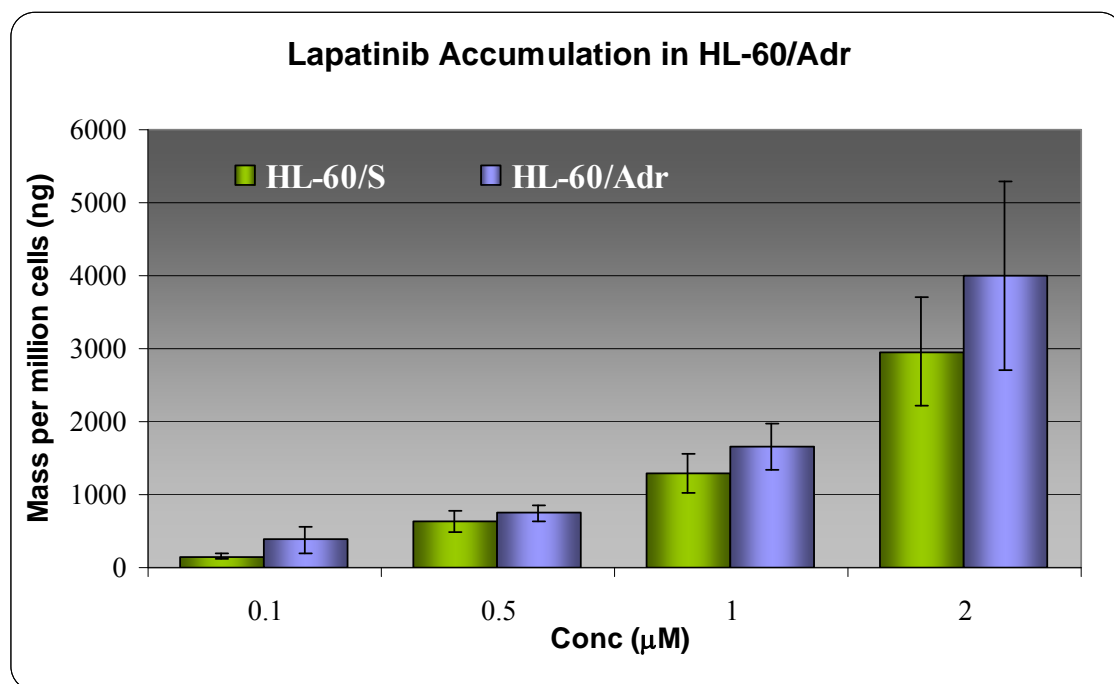
Figure 4-74 shows an accumulation across a concentration range of lapatinib in HL-60-Adr cell-line, and HL-60/S cell-line. Data represents the average and standard deviation, n=3. The quantified mass was normalised to mass per million cells.

Figure 4-74: Lapatinib Efflux in HL-60/Adr
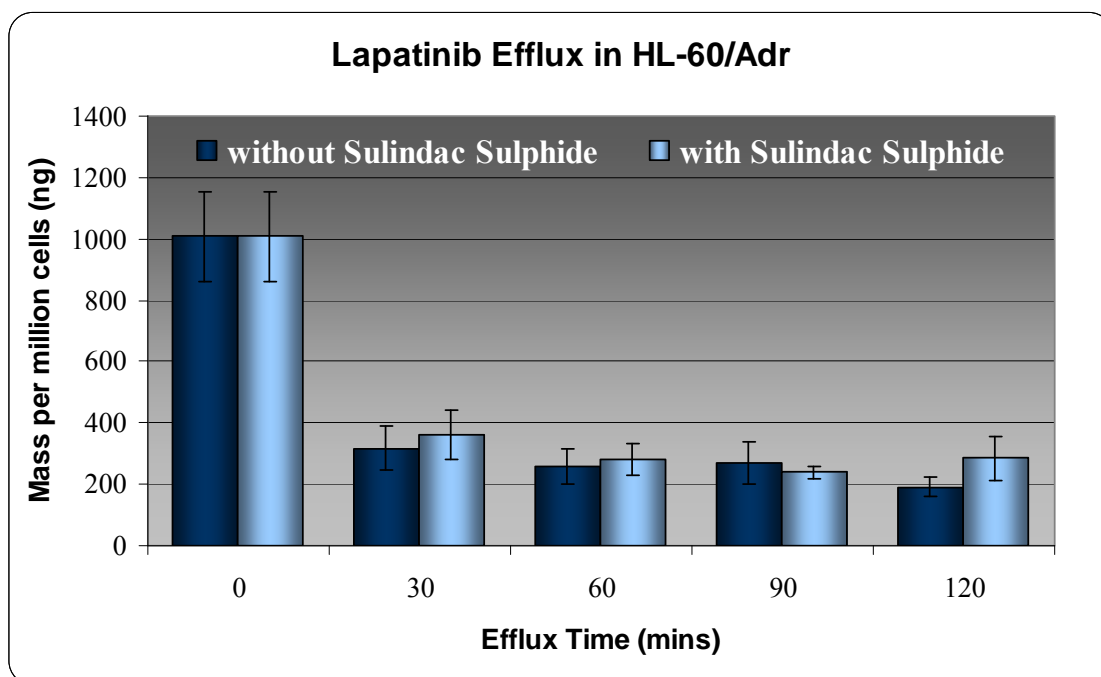
Figure 4-75 shows the efflux profile of 1μM Lapatinib in HL-60/Adr in the presence and absence of 5μM sulindac sulphide over a two hour time frame. Data represents the average and standard deviation, n=3. The quantified mass was normalised to mass per million cells.

4.4. Discussion

The conventional chemotherapy drugs, used in the treatment of many forms of advanced cancer, attack proliferating healthy and cancerous cells leading to potentially serious side effects including myelosuppression, hair loss and gastrointestinal problems. The emerging goal of cancer pharmacology research is the development and optimal application of targeted therapies. Targeted therapies include drugs which are specifically active in cancer cells thereby giving increased activity while having reduced toxicity and side effects.

Resistance to the therapeutic actions of cancer drugs is a significant clinical challenge [3]. In particular, the over expression of cellular drug efflux pumps, such as P-gp, in tumour cells is thought to play a significant role in the resistance phenotype[361]. Research now indicates that many TKIs may interact with drug efflux pumps and in some cases these pumps may play a role in resistance to these newer anti-cancer agents[362].

Using a panel of MDR over-expressing cell-lines, which were chosen based on their MDR status, the role of MDR proteins in the transport of lapatinib and dasatinib was examined.

LC-MS/MS was chosen as the analytical methodological approach most applicable to this study for a variety of reasons. Accumulation and efflux studies can be preformed using radio-labelled agents and detection by scintillation counter giving a reading of counts per million. Drug accumulation and transport in animal models can also be detected PET imaging and radiotracers. However, LC-MS is fast becoming a standard tool in any bio-analytical laboratory. The technique is sensitive, accurate and generally straight-forward. Techniques can also be transferred with relative ease from laboratory to laboratory, assisting inter-agency collaboration. LC-MS also avoids the use of radio-labelled agents and radiotracers and avoids the requirement of specialist licences required to work with radio-active material. Also analytical methodologies developed for the quantification of intracellular levels of TKIs could be translated into the analysis of pharmacokinetics of TKIs in patient serum, which is not possible with other techniques.

The cell-lines selected in this study, both new and established, have been previously well characterised both in the literature [179, 283, 284, 286-289, 350, 351, 363] and internally[6, 7], to express the multi-drug resistant proteins of interest.

4.4.1. Dasatinib

Dasatinib is approved for use clinically in imatinib-resistant and imatinib tolerant CML (chronic myelogenous leukaemia). Imatinib resistance is typically due to mutation is the kinase domain, in the drug-kinase interaction region[162, 364]. However, additional mechanisms for acquired resistance have been proposed which links of the over-expression of ABC transporters with imatinib resistance[123, 169, 170].

Therefore, determination of the relationship between dasatinib and the ABC multi-drug resistance proteins is of critically clinical important. If dasatinib resistance is as a result of ABC transporter over-expression, then its position as a treatment for imatinib-resistant CML could be compromised.

4.4.1.1.   Interaction of dasatinib with P-glycoprotein
Dasatinib as a P-glycoprotein substrate

In 2008, Kamath *et al.*[173], showed in a Caco-2 cells permeability assay a BA/AB efflux ratio of 2.2, suggesting that dasatinib may be a substrate of an intestinal efflux transporter such as P-gp. However, to confirm these findings the authors tested the levels of unabsorbed dasatinib in the gastrointestinal tract of wild type and P-gp knock-out mice. From this, the authors concluded that as there was no differences the levels of unabsorbed dasatinib in the wild type and P-gp knock-out mice that dasatinib was not a P-gp substrate and P-gp did not limit the oral absorption of dasatinib

Using the lung squamous carcinoma, DLKP and its P-gp over-expressing variant DLKP-A, a preliminary examination of the effect of P-gp on dasatinib was performed by carrying out a two-hour accumulation assay, with increasing the concentrations of dasatinib. Figure 4-13 shows the comparison between the parental cell-line and the P-gp over-expressing cell-line. Significantly more dasatinib was accumulated in the experimental time frame in DLKP compared to DLKP-A. This suggests that P-gp plays a role in decreasing the accumulated mass of dasatinib.

To identify the specific effect of P-gp on the intracellular mass of dasatinib in DLKP-A, two specific concentrations ($2\mu M$ and $1\mu M$) were selected and examined in accumulation assays over 120 minutes, at 30 minutes intervals. Experimentally,

dasatinib and elacridar, a P-gp inhibitor were added to flasks while other flasks (dasatinib only) were allowed accumulate over time without any inhibitor present.

Figure 4-14 and Figure 4-15 showed that there was a significant difference in the mass of dasatinib accumulated in the uninhibited arm of the experiment when compared to the experimental arm, where P-gp was inhibited. The inhibition of P-gp led to a substantial increase in the mass of dasatinib accumulated. The inhibition of P-gp in the accumulation of 2μM and 1μM dasatinib in DLKP-A yielded intracellular masses of dasatinib similar (though not equal) to the mass of dasatinib accumulated in DLKP, Figure 4-19.

Figure 4-16, Figure 4-17 and Figure 4-18 showed the efflux profile of dasatinib in DLKP and DLKP-A in the presence and absence of elacridar. The parental cell-line, DLKP, showed no difference in the efflux profile when the inhibitor was added. However, in DLKP-A, the P-gp over-expressing model, the inhibition of P-gp sustained the intracellular mass of dasatinib, as quantified by LC-MS/MS, whereas the inhibitor-free arm showed approximately a 75% reduction in the intracellular mass of dasatinib after 30 minutes. This was confirmed by the subsequent analysis of the efflux of 1μM dasatinib, Figure 4-18. Again the inhibition of P-gp by elacridar sustains the intracellular mass of dasatinib. This showed that inhibiting P-gp prevented dasatinib from being pumped from the cell, which sustained the intracellular mass of dasatinib. This would support the evidence that dasatinib is a substrate of P-gp.

The DLKP-Sq/Mitox-MDR cell-line model was generated by pulsed exposure to mitoxantrone (Helena Joyce, data unpublished). Western blot analysis and cytotoxicity analysis from characterisation experiments showed that P-gp was highly over-expressed in this model. The accumulation of 1μM dasatinib, over two hours, showed very low levels of dasatinib accumulated when compared to the parental DLKP-Sq cell-line, Figure 4-27. Examination of the accumulation profile in the presence or absence of elacridar shows that the inhibition of P-gp from the moment of exposure to dasatinib significantly increases the intracellular mass of dasatinib by an average of 20 fold.

The IGROV-1CDDP has been characterised as an P-gp over-expressing model of ovarian cancer[357]. Accumulation of 1μM dasatinib over 120 minutes in the presence and absence of elacridar showed remarkable differences in the accumulated mass of dasatinib. The inhibition of P-gp increased the intracellular mass of dasatinib on average 16 fold, Figure 4-35.

The cell-line model KB-8-5-11 again confirmed these findings, Figure 4-38 and Figure 4-39. The inhibition of elacridar increased the intracellular mass of dasatinib. The inhibition was also insignificant at very low concentrations of dasatinib, 0.1μM, Figure 4-39. In the KB-8-5-11 P-gp model the fold change in dasatinib accumulated was not as vast, with a more moderate average fold change of 2.5 for both concentrations examined.

The lung adenocarcinoma cell-line A549-tax had previously been used as a P-gp model[179]. Across a concentration range (0.1 -2μM) after two hour exposure no difference was seen in the accumulated mass of dasatinib between the parental and the resistant model, Figure 4-40. Likewise the inhibition of P-gp and the examination of intracellular dasatinib by efflux assay led to no increased intracellular dasatinib in the inhibited P-gp, Figure 4-41.

As the body of evidence so far determined that dasatinib was in fact a P-gp substrate, the lack of effect in A549-tax was unusual. To determine if P-gp derived from exposure to taxol selection showed a difference in selectivity for dasatinib another taxol derived resistant model was examined. RPMI-2650Tx cell-line which over-expresses P-gp was selected with taxol. This over-expression of P-gp reduced the accumulation of dasatinib at 1μM by approximately 20 fold.

The difference in the accumulation profile of dasatinib in A549-tax and other P-gp over-expressing models may be attributed to the difference in levels of P-gp over-expression. Given the low levels of P-gp expression in A549-tax, this may not be the best cell-line model for the examination of transport function due to P-gp expression. When examining the accumulation profile of radiolabelled docetaxel (^{14}C) in A549 and A549-tax cell-line models, Dr Denis Collins noted that the accumulation of

docetaxel was very similar for both the parental (A549)and resistant cell-lines (A549-tax)[5]. Also the cross-resistance of A549-tax to epirubicin was negligible when compared to parental A549[7].

These results showed that dasatinib is a substrate of P-gp and that P-gp modulates the uptake and efflux of dasatinib. This is consistent with recently published literature evidence that identifies dasatinib as a P-gp substrate[174, 175]. Hiwase *et al.*[174], demonstrated using two over-expressing cell-line models in which the addition of the P-gp inhibitor PSC833 increased the intracellular uptake and retention of dasatinib. Using *in vivo* transport assays in polarised canine kidney cell-line MDCK-II, Lagas *et al.*[175], suggested that endogenous P-gp was responsible for the transport of dasatinib. Hegedus *et al.*[365], recently demonstrated that dasatinib was a high affinity substrate for P-gp and BCRP in cell-lines models. Cell-lines K562/ACBB1 and K562/ABCG2 had been selected and stably transduced from the parental K562 to over express the MDR protein of interest. This is not only seen in stably transduced cell-lines, Chen *et al.*[366], showed *in vitro* and *in vivo* that P-gp limited the brain concentration of dasatinib. As this study (Chen *et al,*[366]) was conducted in wild type and P-gp knock-down mice it is unclear why initial reports by Kamath *et al.*[173], did not find dasatinib to be a P-gp substrate.

The effect of P-glycoprotein on dasatinib resistance

The effect of P-gp over-expression on dasatinib resistance was examined by *in vitro* toxicity assays. In P-gp models DLKP-A (Figure 4-22), DLKP-Sq/Mitox-MDR (Figure 4-32) and IGROV-1CCDP (Figure 4-36) resistance to dasatinib was reversed by the addition of P-gp inhibitor, elacridar. In the parental cell-line models, DLKP (Figure 4-21), DLKP-Sq (Figure 4-54) and IGROV-1(Figure 4-37) the addition of elacridar had no effect on the chemo-toxicity of dasatinib, as expected.

The effect of elacridar on known P-gp substrate chemotherapy agents, epirubicin and taxol, was examined in DLKP-Sq/Mitox-MDR and IGROV-1CDDP. Similar to the profile for dasatinib, the addition of elacridar increased the toxicity of the chemotherapy agents.

This indicated that a) the predominant mechanism of resistant in these cell-lines is through the over-expression of ABC transport P-gp, b) cross-resistance to dasatinib is modulated through the over-expression of P-gp and c) the addition of a P-gp inhibitor such as elacridar increases the toxicity of dasatinib.

However, dasatinib-induced resistance is not necessarily P-gp-mediated, as shown in Section 3.7.1, where a dasatinib resistant cell-line model was generated by continuous exposure of dasatinib to a dasatinib-sensitive triple-negative breast cancer cell-line, MDA-MB-231.

Our findings are in accordance with current finding where the expression of P-gp increased a dasatinib resistant phenotype [174, 365]. Both groups demonstrated in cell-line models (K562 and variants) that IC_{50} of dasatinib was increased in resistant models compared to the parent models and could be reversed with a specific P-gp inhibitor (PSC833).

Dasatinib as a P-glycoprotein inhibitor

To examine if dasatinib modulated the function and activity of P-gp the accumulation of a highly efficient P-gp substrate (epirubicin) was examined by LC-MS/MS. Elacridar was included as a positive control for P-gp inhibition. Dasatinib did not alter the accumulation profile of epirubicin in DLKP-A, (Figure 4-22). *In vitro* toxicity assays on the combination of P-gp substrates epirubicin and taxol also showed no effect on the addition of dasatinib in with either DLKP-A and DLKP-Sq/Mitox-MDR, (Figure 4-23, Figure 4-24, Figure 4-33, Figure 4-33). In our studies, dasatinib did not inhibit the action of P-gp.

Hegedus *et al.*[365], suggested that at high micromolar (>2μM) concentrations dasatinib may have an inhibitory effect on P-gp. This was shown by fluorescent dye extrusion studies monitoring the dye calcein-AM in P-gp over-expressing cell-line. Verapamil was used a P-gp inhibitor. A more recent publication by Dohse *et al.*[367], showed that dasatinib inhibited rhodamine 123 efflux but to a lesser extent than nilotinib and imatinib and at higher concentrations. Interestingly, this group also examined also the capability of dasatinib (and nilotinib and imatinib) to compete for P-gp binding sites. Dasatinib was shown to interact at the prazosin binding site of P-gp, though very weakly, even at high concentrations (20μM).

Drug binding sites in P-gp which are involved in transport are the H site and the R site. The H site is selective for Hoeschst 33342 and colchicine[368] and the R site is selective for rhodamine 123 and anthracycline[369]. Substrate binding at one site stimulates transport at the other site. Binding at prazosin site is suggested to stimulate transport at both the H and R site though is not directly implicated in transport itself[370].

Summary

- In summary dasatinib is a substrate of P-gp and increased cellular expression of P-gp increased resistance to dasatinib.

- The addition of elacridar, a P-gp inhibitor, increased the intracellular mass of dasatinib accumulated and prevented the active efflux of dasatinib (in efflux assays).

- The addition of elacridar was also shown to increase the sensitivity of resistant cell-line models to dasatinib, indicating that P-gp and decreased intracellular mass has a direct link in resistance to dasatinib.

- Dasatinib does not appear to be a P-gp inhibitor at clinically relevant concentrations. An inhibition of the action of P-gp by dasatinib in the literature has only been seen at high dasatinib concentrations.

- Also, the cell-line models used here, with the exception of A549-tax were excellent P-gp cell-line models, for the examination of (dasatinib) substrate specificity and transport.

4.4.1.2. *Interaction of dasatinib with BCRP*

As dasatinib is typically employed once there is evidence of imatinib resistance in a patient and given that it is known that imatinib resistance can occur through BCRP over-expression[170], the determination of the relationship between dasatinib and BCRP is of interest and clinically relevant.

Using the resistant BCRP cell-line model DLKP-Sq/Mitox-BCRP, developed through exposure of DLKP-Sq cells with mitoxantrone, the effect of BCRP on dasatinib transport was examined. The mass of dasatinib accumulated in the transporter naïve DLKP-Sq parental model was substantially more than in the resistant model, Figure 4-46. Examination of the mass of dasatinib accumulated over two hours showed a fold increase of 10-20 times dasatinib accumulated in the presence of elacridar compared to dasatinib alone across the experimental time frame. The difference in accumulated mass in the resistant and parental model (Figure 4-46), as well as between the inhibited and non-inhibited resistant cell-line (Figure 4-47) suggest that dasatinib is a substrate of BCRP. From the literature it has been recently shown that dasatinib is transported by BCRP[174, 175, 366]. These studies have included *in vivo* studies, as well directional flux assays and over-expressing cell-line models with inhibitor.

Also of note is that the increase in accumulated mass from 30 minutes to 120 minutes was not significantly different from the first to the last time-point. While the accumulated mass was different in both the inhibited and uninhibited samples this trend was the same. One group has reported that maximum dasatinib uptake occurs within 5 minutes[174], whereas other TKIs like imatinib accumulate over two hours. Our experiments with dasatinib accumulation would agree with these earlier findings.

In vitro proliferation toxicity assays of DLKP-Sq and DLKP-Sq/Mitox-BCRP for dasatinib show similar sensitivities for both cell-lines to the agent, Figure 4-50. However, the addition of elacridar (BCRP inhibitor) decreased the IC_{50} of dasatinib in DLKP-Sq/Mitox-BCRP, Figure 4-48. This indicated that BCRP mediated decrease of the intracellular concentration of dasatinib, decreased the effectiveness of the dasatinib. This would indicate that even though the resistant cell-line DLKP-

Sq/Mitox-BCRP has increased ABC transport protein expression this is not seen in the resistance profile. However, the inhibition of BCRP increased the sensitivity to the resistant cell-line to beyond the sensitivity of the parental cell-line. The DLKP-Sq/Mitox-BCRP was ultimately more modulatable, as inhibition of the BCRP increased the toxicity of dasatinib in DLKP-Sq/Mitox-BCRP, Figure 4-48, beyond that of the parental cell-line. As expected, the addition of a fixed inhibitory concentration of elacridar had no effect on the parental cell-line Figure 4-49. This would suggest that up-regulation of ABC transport BCRP is not the only molecular change in this cell-line DLKP-Sq/Mitox-BCRP compared to the parental cell-line.

One hypothesis to explain this modulation comes for the agent used to develop resistance. Mitoxantrone is a DNA damaging agent. Previously treatment with DNA damaging agents such as cisplatin and temozolomide has been shown to increase the levels of phospho-src (*p*-src)[371, 372]. Src kinase, one of the targets for dasatinib, is upstream of the Raf-MEK pathway. Also, the differential regulation of BCRP by way of the MEK-ERK pathway as reported Imai *et al.*[373]. This group purposed that BCRP is transcriptionally up-regulated by inhibition of MEK-ERK-RSK pathway and post-transcriptionally down-regulated through an undetermined MEK-ERK-non-RSK pathway[373], see Figure 1-5. It is therefore possible, through our results are preliminary, to suggest that up-regulation of BCRP as a response to mitoxantrone also up- regulated *p*-src, a target of dasatinib, thus making the resistant BCRP expressing DLKP-Sq/Mitox more sensitive to dasatinib when the protecting effect of BCRP was negated.

BCRP does not transport taxol, vincristine or verapamil. However, irinotecan and its active metabolite SN-38 are substrates of BCRP[90]. BCRP can have functional variants, where by a mutation in the sequence leads to an amino acid substitution. The wild-type BCRP has an arginine (R) at position 482. Two known variants exist; variant R482T which has threonine (T) at position 482 and variant R482G where position 482 is the amino acid glycine (G). These variations can lead to functional changes. The wild type BCRP does not transport the anthracycline, epirubicin, where as the R482G variant does transport anthracyclines, (Section 1.3.4)[93].

Figure 4-51 shows the increase in toxicity of epirubicin in DLKP-Sq/Mitox-BCRP, when modulated by the addition of elacridar. Taxol toxicity was not modulated by the inhibition of BCRP (Figure 4-52), while SN-38 toxicity was modulated by elacridar addition (Figure 4-53). This suggests that the BCRP over-expressed in this cell-line is R482G variant (or other epirubicin transporting variant) not wild type BCRP.

The accumulation of epirubicin in the DLKP-Sq/Mitox-BCRP alone or in the presence of dasatinib or elacridar showed that elacridar increases the intracellular mass of epirubicin, again suggesting that a variant form of BCRP rather than wild type. Dasatinib modulated a small, but significant, decrease in intracellular epirubicin at 90 minutes. The results of *in vitro* toxicity assays of combinations of epirubicin plus dasatinib and SN-38 plus dasatinib showed no additive effective from dasatinib in combination with these agents, Figure 4-54 and Figure 4-55. Hegedus *et al*., showed that dasatinib inhibited BCRP[365]. However, results from that study showed that BCRP inhibition by dasatinib occurred at $10\mu M$ dasatinib. This was above our test range. Dohse *et al*.[367], showed that dasatinib exposure (12 hours) decreased BCRP surface expression. The authors affirm that 12 hours was selected for optimised results but do not state how soon after exposure to dasatinib does expression being to decrease, though 1nM dasatinib was potent enough to decrease BCRP. The effect of dasatinib in BCRP may be linked to the decrease in epirubicin accumulated after 90 minutes in the presence of $2\mu M$.

Summary

- In summary, dasatinib is a substrate of the ABC transport protein BCRP.

- The inhibition of BCRP by elacridar increased the accumulated intracellular mass of dasatinib in BCRP over-expressing cell-line model. Inhibition of BCRP over-expression also modulated the potency of dasatinib, indicating that decreased intracellular accumulation results in decreased efficacy of dasatinib.

- In the cell model DLKP-Sq/Mitox-BCRP there does appear to be a change, additional to the over-expression of BCRP, through the MEK pathway, though this is undefined.

4.4.1.3.   *Interaction of dasatinib with MRP-1*

To date there has been no connection made in the literature between MRP-1 and dasatinib. Here we examined whether dasatinib is a substrate of MRP-1. Through the accumulation of dasatinib in the leukemic cell-line HL-60/S, the parental cell-line, and the MRP-1 over-expressing cell-line Hl-60/Adr we looked for any potential relationship between dasatinib and MRP-1.

The accumulation assay, Figure 4-57 and the efflux assay, Figure 4-58 showed no change in the intracellular mass of dasatinib either as a result of MRP-1 over expression or the presence of an inhibitor. This would indicate that dasatinib is not a substrate for MRP-1.

Additionally the accumulation of dasatinib in the presence and absence of the sulindac sulphide in the MRP-1 expressing cell-line 2008/MRP-1 was analysed. This cell-line model highly over-expresses MRP-1. At all concentrations examined (0.1-2μM) the accumulation of dasatinib does not appear to be modulated by the expression of MRP-1 as the inhibition of MRP-1 did not increase the intracellular mass.

This would indicate that dasatinib is not an MRP-1 substrate.

Imatinib was the first generation TKI used in the treatment of CML. Imatinib has been showed to be a substrate on MRP-1[167]. Dasatinib is used a second-line therapy for treatment of imatinib resistant and imatinib intolerant patients. In addition to its primary use in Acute Myeloid Leukaemia, imatinib is used as a treatment for gastrointestinal stromal tumours (GIST). A study by Théou *et al*.[374], assessed the MDR protein expression in GIST. This study showed that 62% of GIST were positive for MRP-1, making the interaction of between dasatinib and MRP-1 incredibly relevant to treatment options.

Since dasatinib is not an MRP-1 substrate, dasatinib as a therapy is not likely to be affected by the expression of MRP-1 meaning no reduction in therapeutic efficacy would be anticipated as a result of active MRP-1 efflux, a common resistance protein in GIST. Dasatinib is also not a substrate for OCT1 (organic cation transporter-1) which has been shown to lower the intracellular level of imatinib[176].

Summary

- In summary dasatinib is not a substrate of MRP-1 ABC transporter.

4.4.2. Lapatinib

4.4.2.1.   Interaction of lapatinib with P-glycoprotein

A549-tax is known to express low levels of P-gp, HL-60/Mdr expresses moderate levels of P-gp and DLKP-A highly over expresses this transporter. Previously work by Collins *et al.*[179], has shown that lapatinib inhibits the action of P-glycoprotein and suggests that lapatinib has a high affinity for a binding site affecting transport in the protein. Molina *et al.*[178], have also shown that lapatinib increases the accumulation of topotecan, a P-gp and BCRP substrate, in P-gp and BCRP-expressing cells.

The levels of lapatinib accumulated can be examined in a multi-dimensional approach. That is, the level of accumulation can be examined with respect to exposure time or with respect to drug concentration. Here we have chosen a preliminary examination of the effect across a concentration range over a period of two hours. This fixed time point was chosen to allow sufficient time for any efflux action to be seen. Varying the concentration range to the nanomolar exposure range allowed the determination of the effect of clinically and sub-clinically relevant concentrations on the cell-line models.

The levels of lapatinib accumulated in each P-gp-expressing model were examined with reference to its parental, non P-gp expressing, cell-line. The LC-MS/MS method developed in Section 3 was used to quantify the intracellular mass of lapatinib.

In a study carried out by Polli *et al.*[177], the authors state that lapatinib is substrate for the efflux protein P-gp and BCRP, however, the study did not identify the concentration of lapatinib used in the substrate assay. Figure 4-60, Figure 4-63 and Figure 4-64 show the level of lapatinib accumulation in A549 compared to A549-tax, DLKP compared to DLKP-A and HL-60/S compared to HL-60/Mdr, respectively. When examining Figure 4-60, the accumulation profile of lapatinib in A549 vs A549-tax (non-expressing vs lowly expressing) no significant difference was seen in the level of drug accumulated indicating that low levels of P-gp do not affect the disposition of lapatinib *in vitro.*

When comparing DLKP and DLKP-A cell-lines in, Figure 4-63, there was also no significant difference in the level of lapatinib accumulated between the parental, non-P-gp-expressing cell-line and the highly over-expressing DLKP-A variant. Figure 4-65 showed the efflux profile of lapatinib in P-gp over-expressing DLKP-A. With the addition of $0.25\mu M$ elacridar, a P-gp inhibitor, it was possible to clearly define if lapatinib is a P-gp substrate. Over a two hour incubation period all samples where exposed to $2\mu M$ lapatinib. Following this exposure step, the lapatinib-containing media was removed. The control samples were given fresh media and efflux profile was examined over time while the test samples were given media contained the P-gp inhibitor (elacridar). The rational behind the experimental design was that by inhibiting the pump at a point where the agent was inside the cell one could determine the rate and the level of effect the pump has on the transport of the agent out of the cell. By examining the efflux profile of lapatinib in the DLKP-A cell model we can see that the inclusion of an inhibitory concentration of elacridar, a specific P-gp inhibitor, did not change the efflux profile, Figure 4-65. This would indicate that lapatinib is not a substrate of P-gp. As the efflux profile was examined in the presence and absence of elacridar it is possible to say with some level of certainty that the presence of a P-gp inhibitor does not prevent the efflux of lapatinib from the cell model, therefore lapatinib is not being extruded from the cell by P-gp.

For completeness, the cell model DLKP was also examined using similar methodology, by taking samples at time points to quantify the drug level in the cells, Figure 4-66. Similar to the DLKP-A model, the DLKP cell line showed no difference in the level of drug maintained in the cell in the presence or absence of elacridar.

In third cell model Figure 4-63, the leukemic cell-line model HL-60/S, and HL-60/Mdr-1 no difference was seen in the accumulation of lapatinib in the P-gp over expressing HL-60/Mdr-1 model in comparison to the HL-60/S model which does not over-express any of the ABC transporters.

The accumulation profiles, the efflux profile and the toxicity assays indicate that lapatinib is not a substrate for P-gp.

The *in vitro* toxicity studies showed, in Figure 4-61 and Figure 4-62, the profile of lapatinib in combination with elacridar in A549 and A549-tax. The addition of P-gp inhibitor elacridar had no effect on the toxicity of lapatinib. This additionally indicated that P-gp is not responsible of lapatinib resistance as the inhibition of P-gp was ineffective in reducing the resistance to lapatinib.

Figure 4-67 and Figure 4-68 show the effect of the addition of P-gp inhibitor elacridar on the toxicity profile of DLKP and DLKP-A. There was no significant difference in the percentage cell survival between lapatinib alone and lapatinib in combination with elacridar in DLKP. In DLKP-A there was also no significant difference in the percentage cell survival between the lapatinib and lapatinib with elacridar. However, it still remains clear that, at clinically relevant, concentrations lapatinib is not a P-gp substrate.

Several authors have shown that lapatinib inhibits the function of P-gp [178, 179, 375, 376]. Exposure to lapatinib is also seen to potentiate the expression level of P-gp [180]. An accumulation of classic P-gp substrate epirubicin was carried out in Figure 4-69. The addition of lapatinib increased the accumulation of epirubicin in the P-gp over-expressing cell-line. The effect of level of inhibition of P-gp can be deduced to be similar to the level of inhibition of elacridar similar intracellular masses of epirubicin was quantified when either elacridar or lapatinib were used as inhibitors.

Summary

- In summary, it has been shown that lapatinib is not a substrate of the ABC transporter, P-gp.

- The cellular expression of P-gp does not increase resistance to lapatinib. We have confirmed previous finding that lapatinib inhibits the function of P-gp. Therefore, over-expression of the MDR transporter P-gp is unlikely to contribute to resistance to lapatinib, though lapatinib did modulate the activity of P-gp.

4.4.2.2. *Interaction of lapatinib with BCRP*

BCRP, breast cancer resistant protein, described in 1998 by Doyle *et al*.[60], has been found in many tissues and cells including the blood brain barrier, intestine and various tumours [377].

It addition to its interaction with P-gp, lapatinib has been shown to be a BRCP inhibitor [178]. Polli *et al*.[177], similarly indicated that lapatinib decreased the BCRP-mediated transport of cimetidine. However, there is little literature evidence clarifying the status of lapatinib as a BCRP substrate.

The leukemic cell-line HL-60-Mxr was used as a BCRP over-expressing model. Accumulation assays were carried out across a concentration range, with samples taken after a two-hour exposure period. Figure 4-70 shows the accumulation of lapatinib in HL-60/S and HL-60/Mxr. A small and insignificant reduction in intracellular lapatinib quantified was noted the BCRP over-expressing cell-line compared to the parental cell-line.

To examine further the relationship between lapatinib and BCRP, an efflux profile of HL-60/Mxr in the presence and absence of elacridar, a BCRP inhibitor, was performed,
Figure 4-71. The similarity of the profile with and without elacridar present suggests that lapatinib is not being pumped by BCRP. Also, the lack of maintenance of the level of intercellular accumulation in the presence of elacridar suggests that BCRP is not responsible for the efflux of lapatinib from the cell. These results suggest that lapatinib is not a substrate of BCRP.

The analysis of the epirubicin accumulation in DLKP-Sq/Mitox-BCRP cell-line showed an increased mass of epirubicin as a result of lapatinib inhibition of BCRP at 90 minutes, Figure 4-72. This indicates that lapatinib may inhibit the BCRP protein. A recent publication identifies lapatinib as a BCRP inhibitor, however, 10μM lapatinib was required to inhibit BCRP efflux[378].

Summary

- In summary lapatinib is not a substrate of BCRP ABC transporter.

- However, lapatinib does inhibit the action of BCRP after some exposure time.

4.4.2.3. *Interaction of lapatinib with MRP-1*

The third of the ABC transporters that we focussed on was MRP-1. Also called ABCC1, this is the most prominent member of the C branch of the ABC superfamily of drug transporters. Unlike P-gp and BRCP, little has been reported on the relationship between MRP-1 and lapatinib.

The leukemic cell-line HL-60-Adr was used as an MRP-1 over-expressing model. Accumulation assays were carried out across a concentration range, with samples taken after a two-hour exposure period. Figure 4-74 shows the accumulation of lapatinib in HL-60/S and HL-60/Adr. A slightly greater, though not significantly greater, mass of lapatinib was accumulated in the MRP-1 over-expressing cell-line model, when compared to the parental cell-line.

To examine this further, an efflux profile of HL-60-Adr in the presence and absence of sulindac sulphide, a MRP-1 inhibitor was performed. The similarity of the efflux profile with and without the inhibitor present suggests that MRP-1 does not play a role in the efflux of lapatinib. As such, lapatinib is not a substrate of MRP-1.

Summary

- In summary, lapatinib was not shown to be a substrate of MRP-1

4.5. Overall findings

- Overall, the LC-MS/MS method developed in Section 3 was used to determine the status of dasatinib and lapatinib as substrates of the main ABC transporter P-gp, BCRP and MRP-1.

- The analytical method developed was sensitive, robust and reproducible for the analysis of clinically relevant concentrations of dasatinib and lapatinib in cancer cell-line models.

- The use of a liquid-liquid extraction gave clean extracts, permitted the extraction of large batches of samples and amalgamated well with the experimental requirements of cell accumulation and efflux assays

- It was possible to use the method developed here to answer questions about the pharmacokinetics of these tyrosine kinase inhibitors *in vitro.*

- Through the quantification of intracellular dasatinib by LC-MS/MS it was deduced that dasatinib is a substrate of P-gp and BCRP but not a substrate of MRP-1.

- Through the quantification of intracellular lapatinib by LC-MS/MS it was deduced that lapatinib is not substrate of P-gp, BCRP or MRP-1, though lapatinib does inhibit P-gp and at increased exposure times does have an effect on the activity of BCRP

While the work here has been carried out *in vitro* the clinical implications of this study are

- that as dasatinib is a substrate of P-gp and BCRP its efficacy is more susceptible to expression of high levels of these ABC transport proteins. Tumoural P-gp overexpression may therefore impact on therapeutic efficacy

- Lapatinib is an inhibitor of P-gp and BCRP. The incorporation of lapatinib into a chemotherapy regime which included a P-gp substrate cytotoxic may

alter both anti-tumour efficacy and systemic toxicity (since P-gp plays a significant role in the elimination of P-gp substrate agents from the body. Careful study may therefore be required to characterise the net effect (increased efficacy or increased systemic toxicity) which may result from lapatinib-containing regimens.

SECTION 5.0 – Results and discussion

The development and validation of a method for the quantification of thalidomide

5. The development and validation of a method for the quantification of thalidomide

Introduction

Thalidomide (α-N-phthalimido –glutarimide), was originally developed and marketed as an anti-morning sickness medication in the 1960 but was withdrawn following the reported associations with birth defects[249-251]. Decades later, thalidomide approved as treatment for multiple myeloma, based on a randomized clinical trial conducted by the Eastern Oncology Group[379].

Many cancer drugs are administered in a patient-normalised manner by dosing as a mass per unit body surface (BSA), mg/m^2 or mg/kg to reduce side effects and to increase efficacy. For example carboplatin is administered based on an area under the curve (AUC) calculation[380]. Epirubicin and other chemotherapy drugs are administered as mg/m^2[70].

However, thalidomide is administered to patients as a fixed dose (mg/day) rather than as a function of the patient specific criteria.

One of the side effects reported by patients receiving thalidomide is a sensation of tingling in the fingers and toes, which, if left untreated this can deteriorate into a serious condition called peripheral neuropathy. Peripheral neuropathy is characterised by paraesthesia in the hands and feet. Treatment of peripheral neuropathy is dose reduction, with some research suggesting that thalidomide therapy should be limited to less than 6 months. This however, is likely to significantly impact response[268].

While dose reduction has been shown to improve peripheral neuropathy, no correlations have been made between patient serum levels, patient doses and neuropathy experienced.

The aim of this body of work is to develop a method for the accurate quantification of thalidomide in the serum of multiple myeloma patients as prelude to attempts to investigate potential correlations between circulating levels and toxicity.

5.1. LC separation optimisation

Designing an LC method for the chromatographic separation of thalidomide involved examining a variety of components, columns, internal standard and mobile phase considerations. The results are detailed in this section.

5.1.1. Thalidomide lenalidomide separation

5.1.1.1. Internal standard selection

Tohnya *et al*.[381], detailed an LC-MS method for the quantification of lenalidomide, (CC-5013) an analogue of thalidomide, by reverse phase separation with tandem mass spectrometry. The authors used umbelliferone as an internal standard for lenalidomide. However, within the paper the authors mention their attempts to use thalidomide as an internal standard were unsuccessful due to poor peak shape.

With lenalidomide being used in a similar manner to thalidomide, and in some cases replacing the older drug, a dual method for the quantification of both thalidomide and lenalidomide would be highly advantageous and the method development initially focussed on this goal.

5.1.1.2. Separation optimisation

Methods by both Teo *et al*.[273], and Meyring *et al*.[382], detailed LC methods for thalidomide analysis, using 0.1% (v/v) acetic acid as mobile phase A, the aqueous component of the mobile phase. During the optimisation of thalidomide ionisation by flow injection analysis (detailed in Section 5.3) it was seen that acetic acid gave a high background in the Total Ion Count.

Given the compatibility of formic acid with mass spectrometry, mobile phase A was changed to 0.1% (v/v) formic acid/water and mobile phase B to 0.1% (v/v) formic acid/ACN.

Using a small reverse phase column (YMC-UltraHT Pro C18, 50 x 2.0mm I.D. 2μm particle size), a gift from Apex Scientific Ltd, the separation of thalidomide and lenalidomide was investigated. Given the similar nature of the agents and the

properties of the column used, a gradient elution approach was explored. Gradient elution generally involves increasing of the organic modifier in the mobile phase dynamically over time. One of the disadvantages of gradient elution is the time required to re-equilibrate the column to the starting conditions after the run, necessary to ensure a reproducible quantification in subsequent runs. Both the time required to re-equilibrate the column after injection and the injection volume were found to have an important impact on the development procedure. The re-equilibration time is the time required for the column to return to the starting conditions. Incomplete re-equilibration affects the partitioning of the analyte between the stationary and mobile phase and thus affects the separation, Figure 5-2.

Peak fronting and peak tailing are the distortion of what should normally be a Gaussian peak shape of the analyte in its path through the column. Peak fronting is predominantly the result incomplete interaction of the solute with the stationary phase resulting in the solute eluting slightly before to the main peak. The column may become over-loaded by injecting sample too large to be accommodated by the column, as shown in Figure 5-1, in the peak at 5.8 minutes. The solute begins to elute from the column at approximately 4.8 minutes, in comparison to the peak at 6.8 minutes which has a baseline peak width of approximately 0.2 minutes.

Figure 5-2 and Figure 5-4 are examples of the optimisation of a gradient elution method for the separation of thalidomide and lenalidomide. Given with each chromatogram are the specific pump settings for the run.

Figure 5-1: Representation chromatogram of thalidomide and lenalidomide demonstrating of column overloading
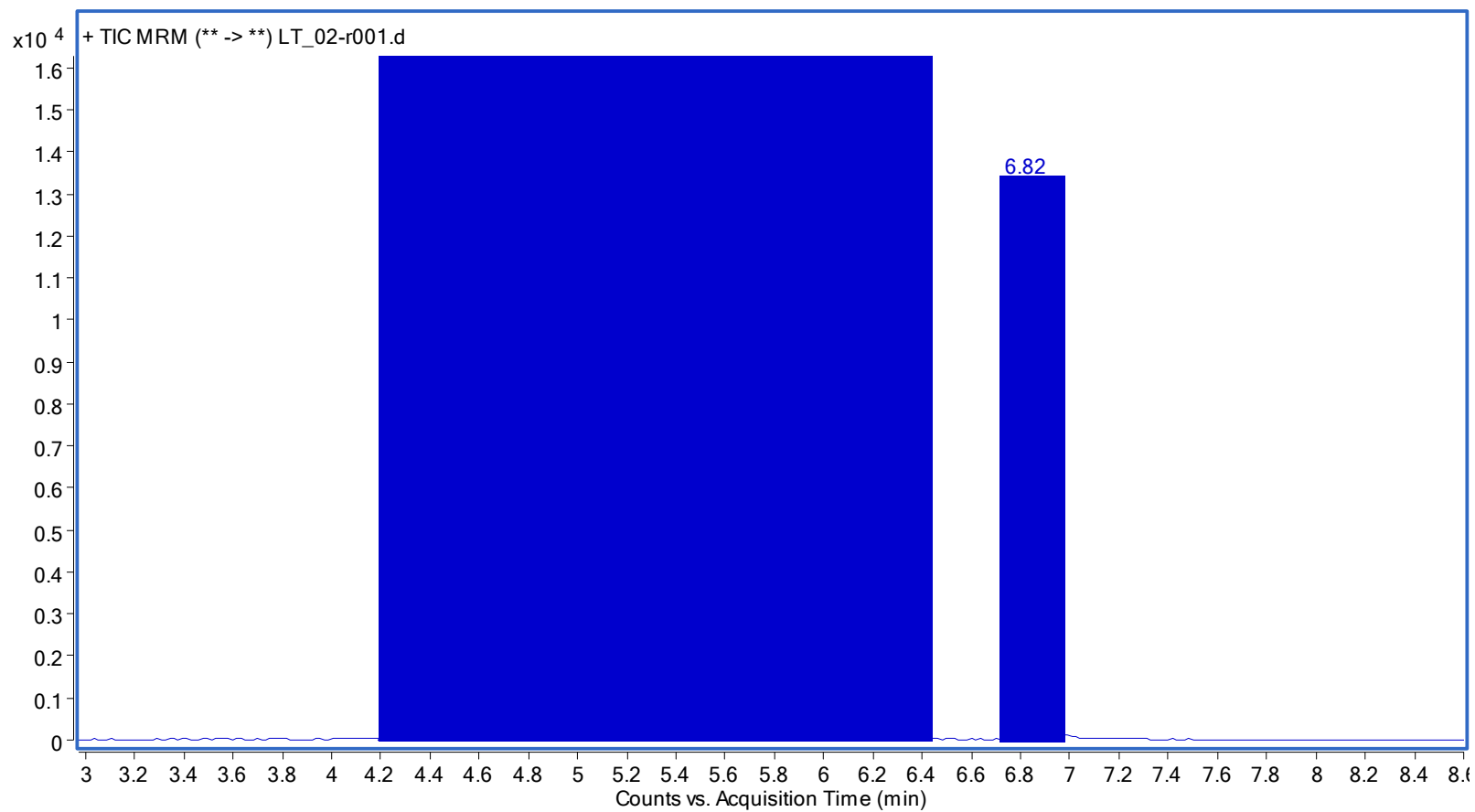
Figure 5-1 is a representative TIC trace of lenalidomide and thalidomide separation showing column overloading, peak at 5.8 minutes. A sample volume of 10μL was injected.

Figure 5-2 shows the separation of lenalidomide and thalidomide by gradient elution as described in Table 5-1. Sample A and B were exactly the same sample, run sequentially. The compound which eluted first in both chromatograms, A and B, was lenalidomide.

As seen in Figure 5-2 the column does not re-equilibrate before the beginning of the second injection (B) and the separation and peak shapes are completely distorted. The inability of the column to re-equilibrate in the time frame distorted the separation of the two analytes. Lenalidomide is more severely affected by this lack of re-equilibration.

Figure 5-2: Illustration of the effect of the failure to achieve column equilibration

Table 5-1: Pump profile for gradient elution

Time (mins)	% B
0	0
1	0
7	60
7.1	100
8.0	100
8.1	0

Table 5-1 shows gradient profile of the method. The stop time was set to 9 minutes.
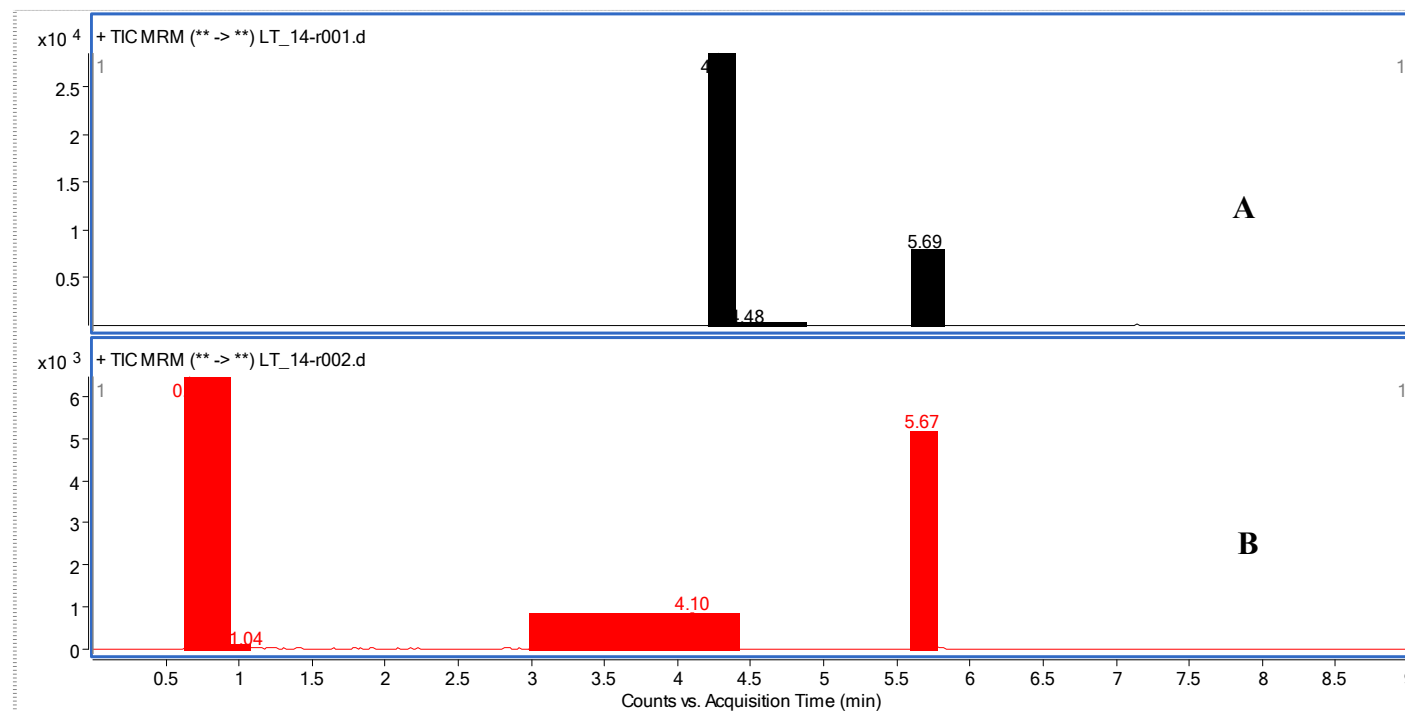
Figure 5-2 illustrates the effect of poor column equilibration on separation. These samples were run sequentially from the same vial. Trace A shows the retention time of lenalidomide to be 4.28mins and thalidomide to be 5.69 minutes. Trace B was run immediately after sample A.

By reducing the injection volume and adjusting the gradient profile a stable repeatable separation method was achieved. Figure 5-3 shows an optimised gradient elution of lenalidomide and thalidomide separation on a reverse phase column. Table 5-2 details the pump setting to control the creation of the gradient profile. The injection volume was reduced to 5µL and this was seen to have a significant effect on the peak shape.

The resolution of lenalidomide and thalidomide was calculated to be 2.2. The resolution, a unit-less factor, was calculated based on the peak width at baseline as described in the equation in Figure 5-3, where Rs is the resolution, t2 is the retention time of peak 2 (thalidomide), t1 is the retention time of peak 1 (lenalidomide), W1 and W2 it the width of lenalidomide and thalidomide respectively, measure at the baseline, as described previously Figure 3-5, Section 3.1.2.

Figure 5-3: Resolution equation

$$Rs = \frac{(t_2 - t_1)}{\left(\frac{1}{2}\right)(W_1 + W_2)}$$

The symmetry factor for lenalidomide was determined to be 1.6 while the symmetry factor for thalidomide was determined to be 1.13. The symmetry factors were determined by the Masshunter Quantification Analysis Software (Version B.01.04), whereby the symmetry of the peak was computed as the ratio between the front half-width and the back half-width.

Figure 5-4: Representation trace of the separation of thalidomide and lenalidomide

Table 5-2: Pump profile for gradient elution

Time (mins)	% B
0	0
0.5	0
4.5	60
5	100
5.5	100
6	0

Table 5-2 shows gradient profile of the method. The pump flow was 0.5mL/min. The stop time was set to 9 minutes.
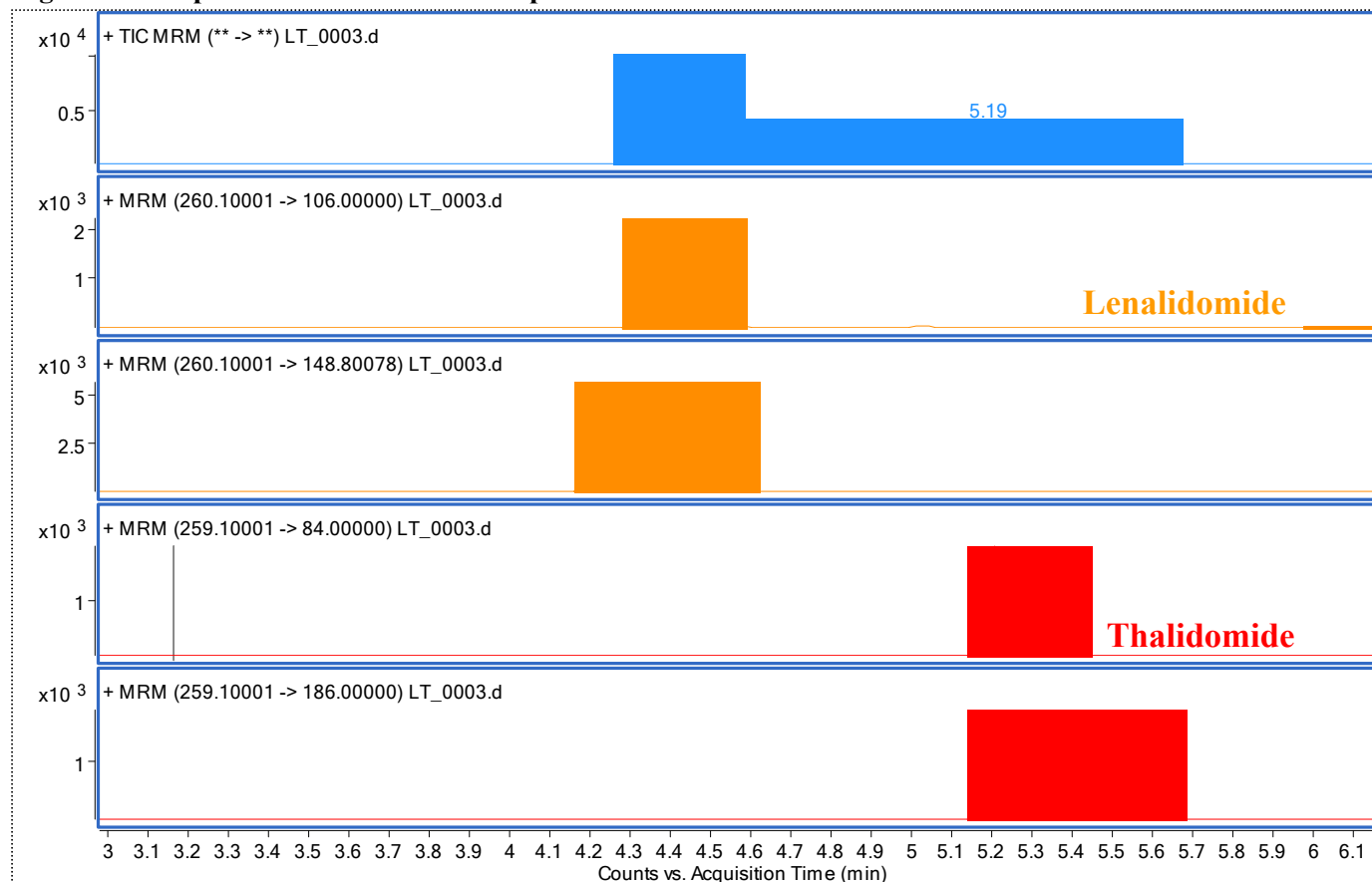
Figure 5-4 shows the separation of lenalidomide and thalidomide by gradient elution on YMC 50 x 2.0mm, 2µm particle size C18 column. Flow was 0.5mL/min and the gradient was as described in Table 5-2. Injection volume was 5µL.

However, despite good separation, good resolution, and acceptable asymmetry factors, the requirement of such a low injection volume was considered to be an unacceptable limitation of the method.

Also given the ambition to use thalidomide as an internal standard for lenalidomide, and vice versa, the use of an isocratic separation makes the validation more straightforward. In an isocratic elution scenario the column is in a state of constant equilibration and as such the ionisation of the analytes is consistent. Therefore, it is acceptable to quantify by the peak area ratio of the analyte of interest to the internal standard, providing validation was successful.

The separation of lenalidomide and thalidomide was investigated on a C18 Prodigy 4.6 x 150mm 5μm particle size column from Phenomenex (Pangbourne, UK) under isocratic flow at 0.5mL/min.

The aqueous phase, mobile phase A, was 0.1% (v/v) formic acid in water, and mobile phase B was 0.1% (v/v) formic acid in ACN. In Figure 5-5, the effect of altering the mobile phase composition was seen. Lenalidomide elutes before thalidomide in all cases. The peak shape of lenalidomide was affected by the mobile phase composition, where as the retention time of thalidomide in addition to the peak shape was significantly affected by the mobile phase composition.

All samples in Figure 5-5 were 10μL injections. Given the experience of the effect of injection volume on peak shape on the YMC 50mm x 2.0mm column it was important to explore the effect of injection volume on the peak shape on the larger Prodigy 150mm x 4.6mm column from Phenomenex.

Figure 5-5: Effect of mobile phase composition on retention time
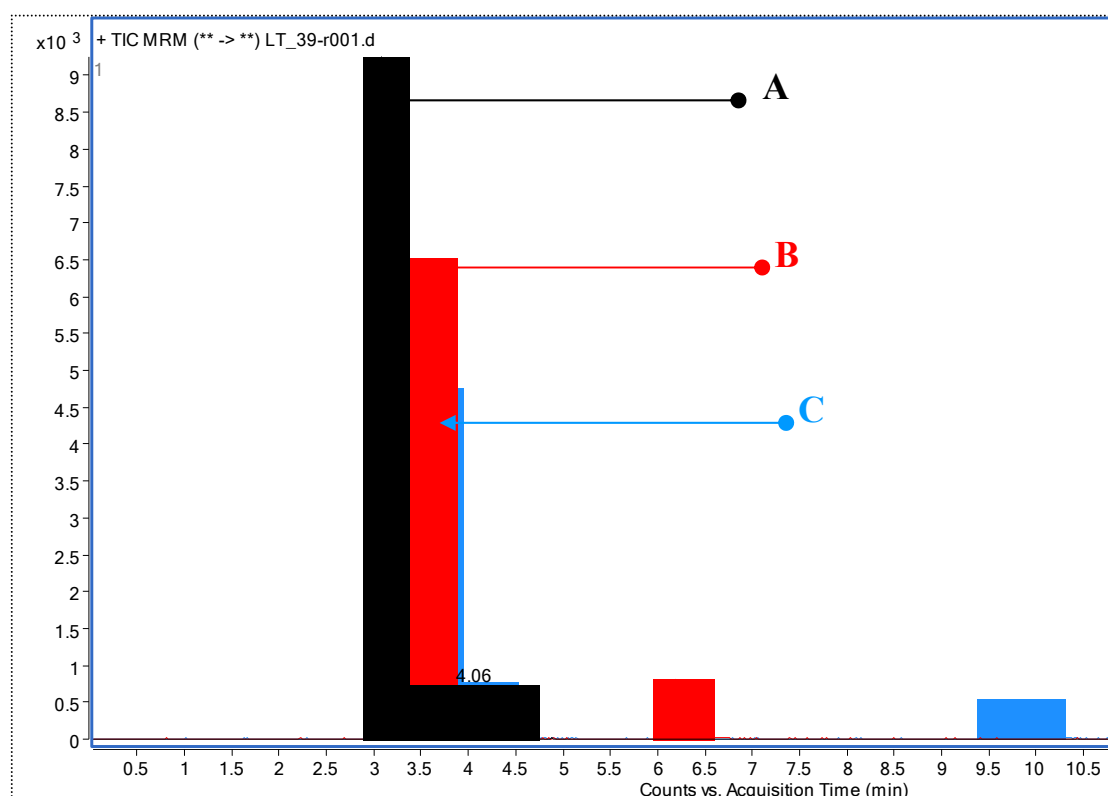
Figure 5-5 shows the overlaid chromatograms of three injections of lenalidomide thalidomide mix at different mobile phase compositions.

Table 5-3: Mobile phase composition

Label	MP composition
A	50% B
B	40% B
C	30% B

Table 5-3 shows the mobile phase composition of figure 5-5. Mobile phase A was 0.1% (v/v) formic acid/water. Mobile phase B was 0.1% (v/v) formic acid/acetonitrile.

In Figure 5-6 the effect of the injection volume on the peak shape of lenalidomide and thalidomide is examined. All injections were performed at isocratic elution at 50% (v/v) ACN/water, 0.1% formic acid.

While the 10μL injection gives the chromatographically optimum separation, this is not the most practical option. The injection volume of 20μL was selected as the peak characteristics were acceptable and the large injection volume allows for more accurate reconstitution of samples in LC vials and a reduction in sample loss.

Thalidomide and lenalidomide separation was achieved on Prodigy C18 150mm x 4.6mm 5μm particle size column with isocratic elution at 50% (v/v)ACN/water, 0.1% formic acid, with a 20μL injection volume.

Figure 5-6: Effect of injection volume on peak shape
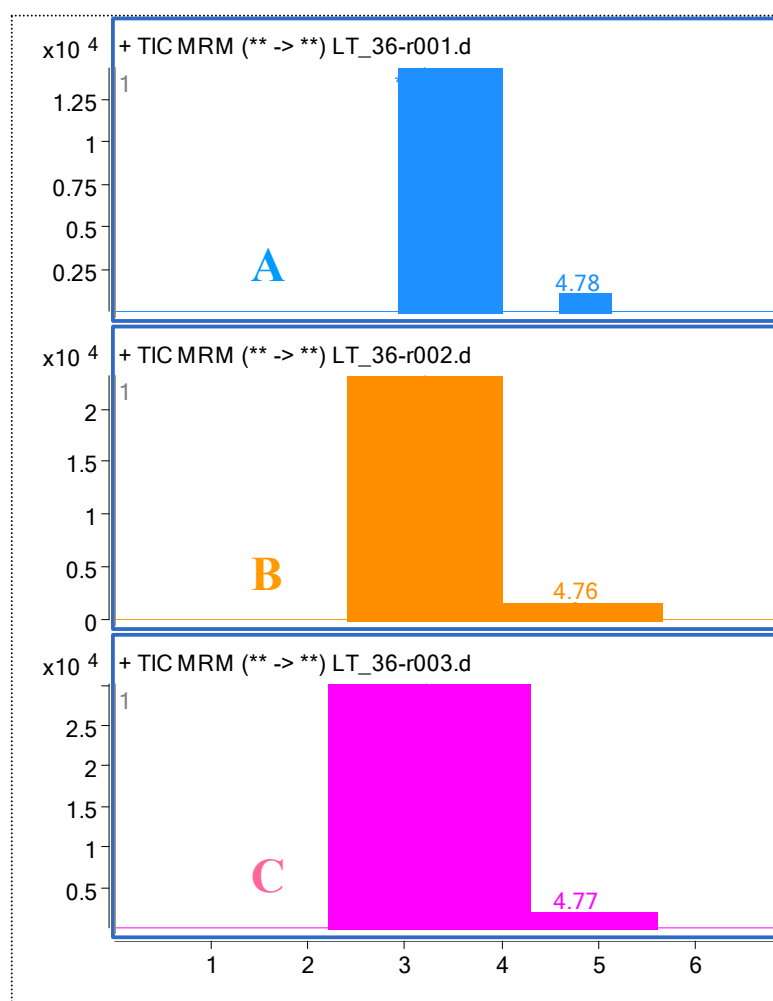
Figure 5-6 shows three TIC traces for lenalidomide and thalidomide separation on a Prodigy 4.6 x 150mm, 5μm particle size, column at 50% B. All injection conditions are identical except the injection volume.

Table 5-4: Effect of injection volume on peak symmetry

#	Inj. Vol.	Peak	RT	Area	Width	Symmetry
A	10μL	1 - Lenalidomide	3.20	120232	0.12	1.21
		2 - Thalidomide	4.78	10882	0.16	0.51
B	20μL	1 - Lenalidomide	3.21	242187	0.13	1.11
		2 - Thalidomide	4.76	21999	0.21	1.38
C	30μL	1 - Lenalidomide	3.23	361149	0.12	1.45
		2 - Thalidomide	4.77	31979	0.24	1.13

Table 5-4 gives the details of the peak characteristics as determined by the Masshunter Qualitative Analysis Software, (Version B.01.03).

5.1.2. Thalidomide umbelliferone separation optimisation

Chromatographically, lenalidomide was a good internal standard for thalidomide and vice versa, however, examinations of the extraction properties of both analytes revealed differences in chemical properties. Lenalidomide had significantly different extraction properties compared to thalidomide. This made it unusable as an internal standard for thalidomide.

5.1.2.1.   *Internal standard selection*

Umbelliferone has been used as the internal standard for lenalidomide quantification and was evaluated as an internal standard for thalidomide[381].

5.1.2.2.   *Separation optimisation*

Five columns were evaluated for the separation of umbelliferone and thalidomide.

- Agilent XBD C18, 50mm x 4.6mm, 1.8μm particle size

- Agilent C18 Eclipse, 150mm x 4.6mm, 5μm particle size

- ZORBAX SB-Phenyl, 150mm x 2.1mm, 5μm particle size

- Phenomenex Prodigy C18, 150mm x 2mm, 5μm particle size

- Phenomenex Prodigy C18, 150mm x 4.6mm, 5μm particle size

NOTE: For all separation optimisations detailed for each column, mobile phase A was 0.1% (v/v) formic acid/water and mobile phase B was 0.1% (v/v) formic acid/ACN. A mixture of thalidomide umbelliferone was prepared at 250ng/mL of each agent. The ratio of mobile phase A/B was altered in the optimisation as specified in each section. Mobile phase flow rate is also specified for each column investigated.

Column 1 - Agilent XBD C18 4.6 x 50, 1.8µm

The Agilent XBD C18 4.6 x50mm column is a small wide column with small particle size (1.8µm), capable of sustaining backpressure of up to 400bar. Figure 5-7 shows the separation of umbelliferone and thalidomide and the effect of varying mobile phase composition. The pump was run as 1mL/min with isocratic elution.

Outlined in Table 5-5 are the details of the mobile phase composition and the injection volume for each injection in Figure 5-7.

Figure 5-7: Umbelliferone thalidomide separation
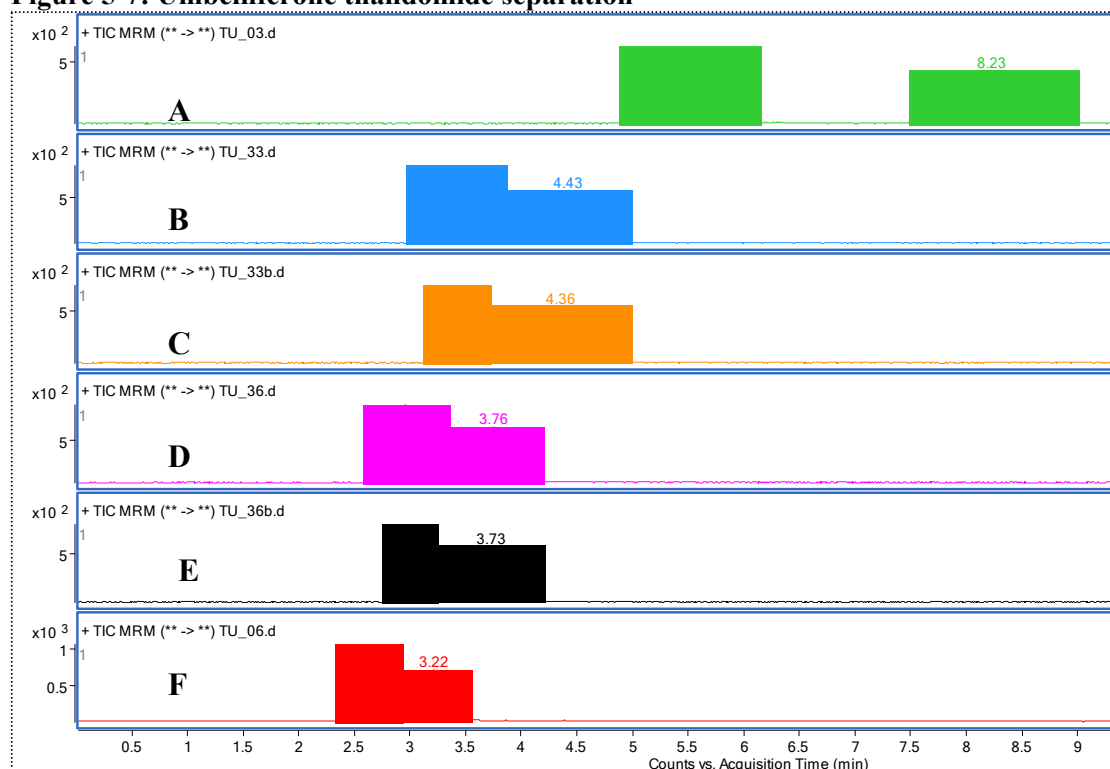
Figure 5-7 shows the separation of umbelliferone and thalidomide on the Agilent XBD 4.6 x 50mm column.

Table 5-5: Details of samples in figure 5-7

	% B	Inj. Vol. (µL)		% B	Inj. Vol. (µL)
A	20	10	D	28	10
B	26	10	E	28	5
C	26	5	F	30	10

Table 5-5 shows the conditions for each injection in Figure 5-7 where A = 0.1% (v/v) formic acid/water and B =0.1% (v/v) formic acid/ACN

Column 2 – Agilent Eclipse 4.6 x150mm, 5μm

The Eclipse 4.6mm x 150mm column is a standard length wide internal diameter C18 reverse phase column.

Figure 5-8 shows the separation of umbelliferone and thalidomide and the effect of varying mobile phase composition. The pump was run as 0.5mL/min with isocratic elution.

Figure 5-8: Umbelliferone thalidomide separation
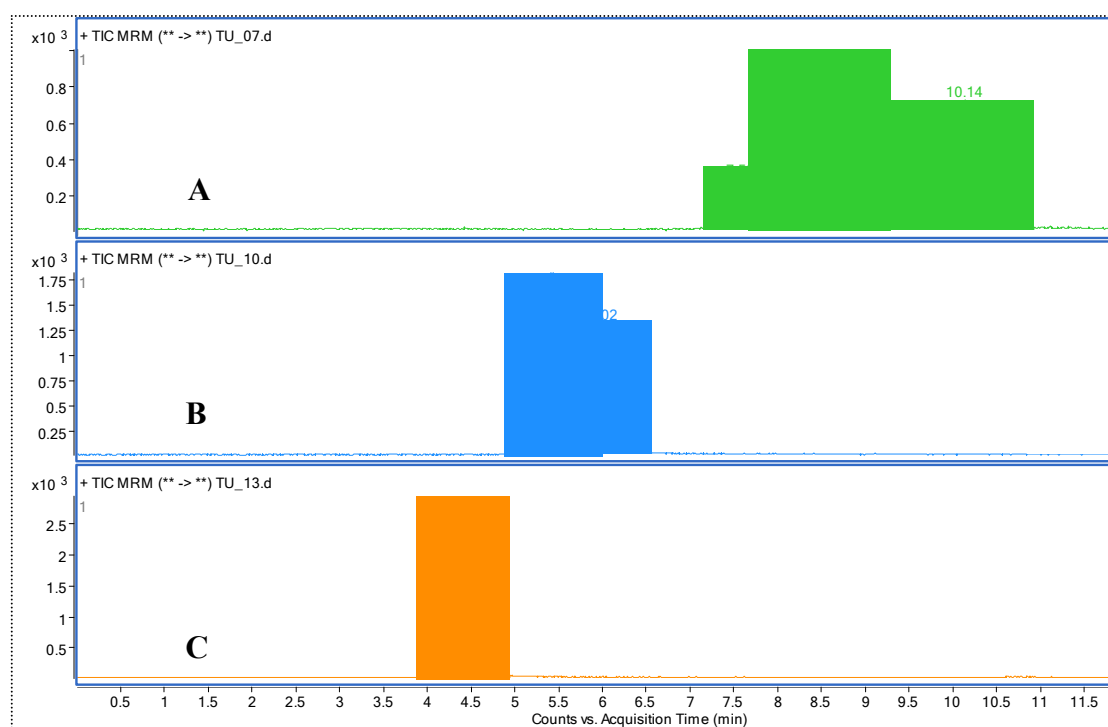
Figure 5-8 shows the difference in separation of umbelliferone and thalidomide in three injections of the same sample mix at different mobile phase mixtures.

Table 5-6: Details of samples in Figure 5-8

	% B	Inj. Vol. (μL)
A	30	20
B	40	20
C	50	20

Table 5-6 shows the conditions for each injection in Figure 5-8 where A = 0.1% (v/v) formic acid/water and B =0.1% (v/v) formic acid/ACN

Column 3 - ZORBAX SB-Phenyl 2.1 x 150mm, 5µm

Given that both thalidomide and umbelliferone have ring components in their structures (see Appendix I), a column with a phenyl functional group was explored. Figure 5-9 shows the separation of umbelliferone and thalidomide on a Zorbax phenyl column. Mobile phase composition was altered as detailed in Table 5-7.

Figure 5-9: Umbelliferone thalidomide separation
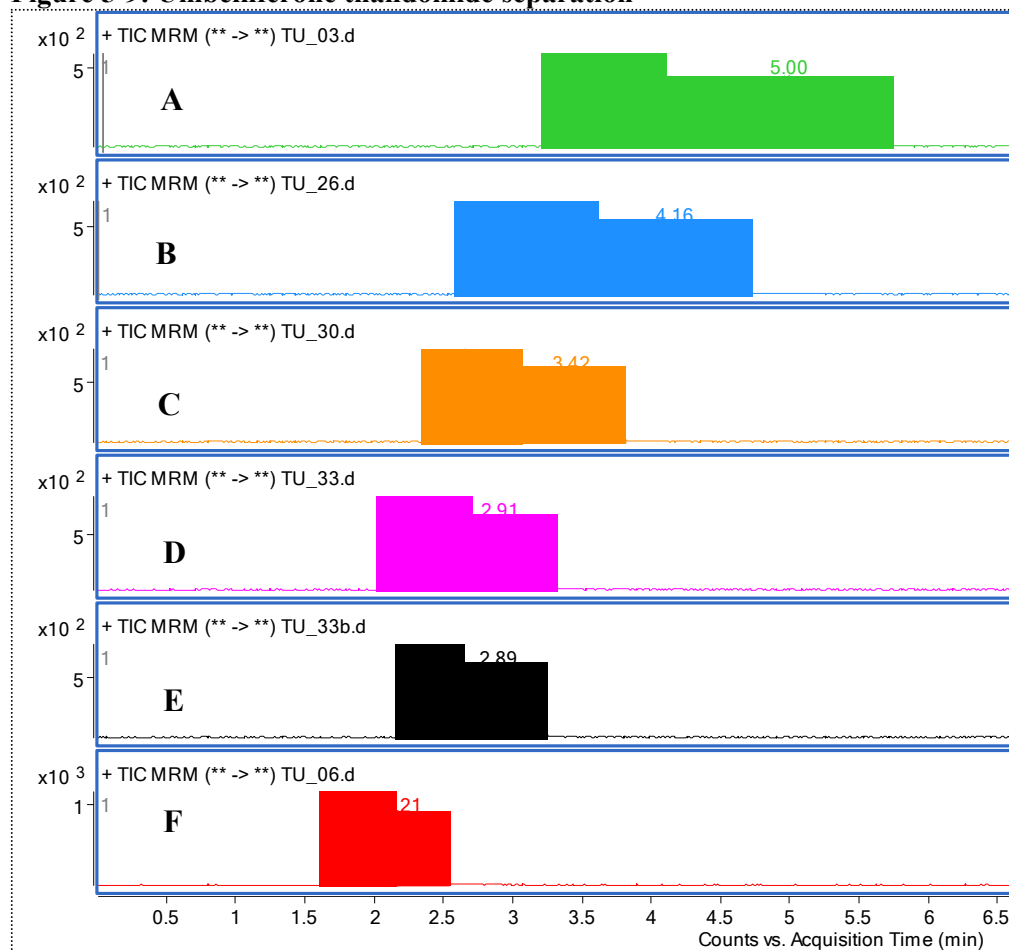
The effect of varying mobile phase composition on the retention and separation of umbelliferone and thalidomide

Table 5-7: Details of run conditions in Figure 5-9

	% B	Inj. Vol. (µL)		% B	Inj. Vol. (µL)
A	20%	10	D	26%	10
B	22%	10	E	26%	5
C	24%	10	F	30%	10

Column 4- Phenomenex Prodigy C18 150 x 2mm, 5μm

The Phenomenex Prodigy C18 is a standard length narrow reverse phase column. Shown in Figure 5-10 is the separation of umbelliferone and thalidomide on the prodigy 150 x 2.0mm column, with isocratic elution at 0.2mL/min.

Figure 5-10: Umbelliferone thalidomide separation
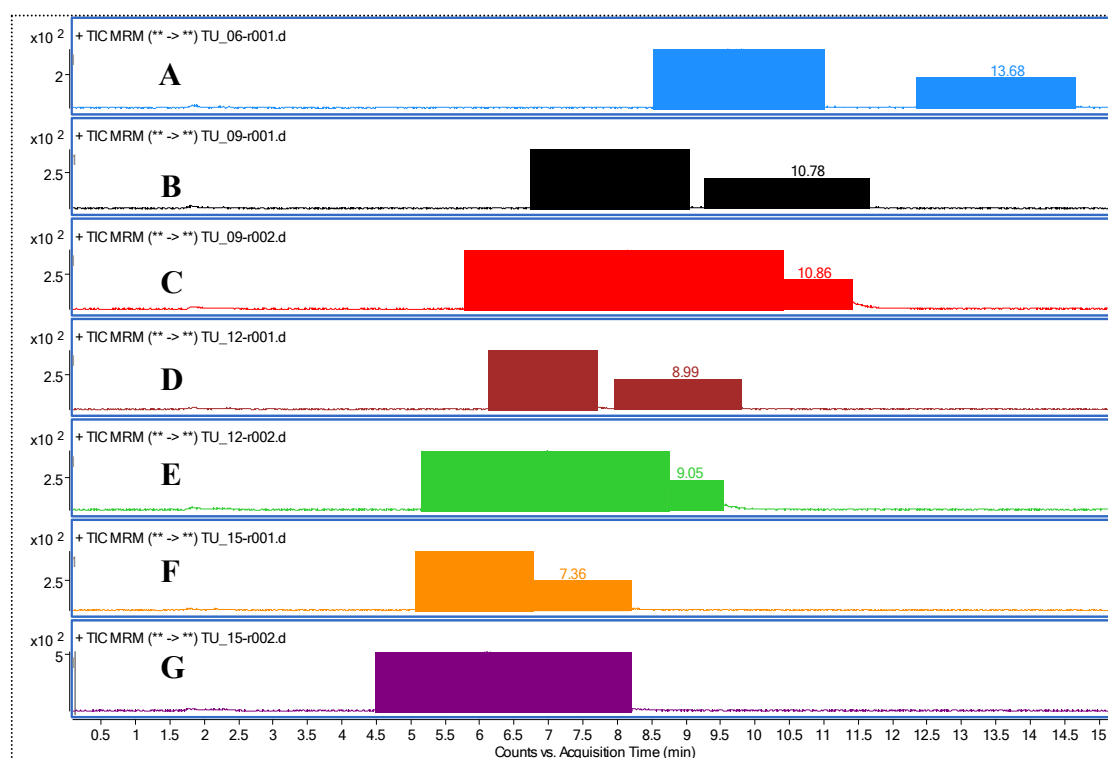
Figure 5-10 shows the separation of umbelliferone and thalidomide at mobile phase compositions ratio varying from 20% to 26%B. Alternation of injection volume was also seen to have an effect.

Table 5-8: Details of run conditions in figure 5-10

	% B	Inj. Vol. (μL)			% B	Inj. Vol. (μL)
A	20%	10		E	24	20
B	22%	10		F	26	10
C	22%	20		G	26	20
D	24	10				

Table 5-8 shows the conditions for each injection in Figure 5-10 where A = 0.1% (v/v) formic acid/water and B =0.1% (v/v) formic acid/ACN

Column 5 - Phenomenex Prodigy C18 150 x 4.6mm, 5μm

Figure 5-11 shows the separation of umbelliferone and thalidomide and the effect of varying mobile phase composition. The pump was run as 0.5mL/min with isocratic elution.

Only one peak (umbelliferone) appears in the sample A as the retention time of the second peak (thalidomide) was later than the run stop time of 20 minutes.

A mobile phase mixture of between 20% and 30% B (A =0.1% (v/v) formic acid/water and B = 0.1% (v/v) formic acid/ACN) appears to be the area of interest and the optimum separation – with good baseline resolution, acceptable peak shape and appropriate injection volume for the application.

Figure 5-11: Umbelliferone-thalidomide separation
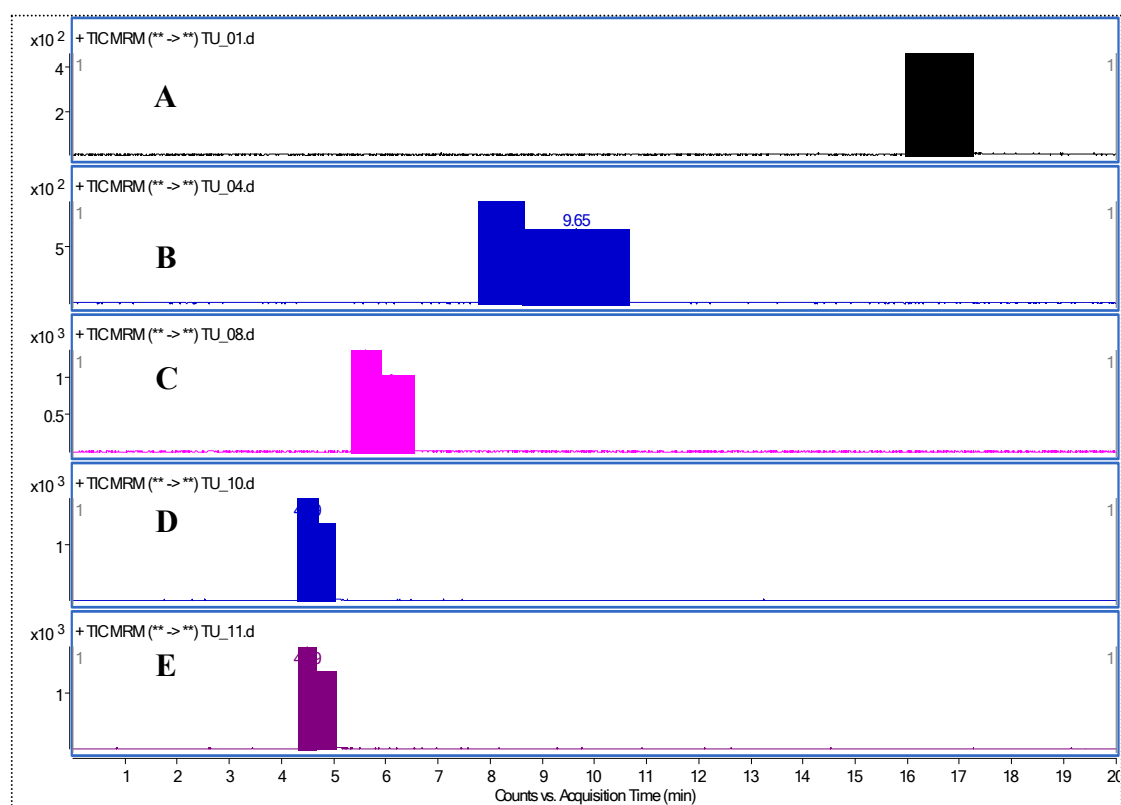
Figure 5-11 shows the separation of umbelliferone and thalidomide at mobile phase composition ranging from 20% to 60% mobile phase B.

Table 5-9: Details of run conditions in Figure 5-11

	% B	Inj. Vol. (μL)
A	20%	10
B	30%	10
C	40%	10
D	50%	10
E	60%	10

Table 5-9 shows the conditions for each injection in Figure 5-11 where A = 0.1% (v/v) formic acid/water and B =0.1% (v/v) formic acid/ACN

Figure 5-12 shows the separation at 24%/0.1% (v/v) ACN/FA/water and the effect of varying the injection volume on the peak shape. Table 5-10 details the peak characteristics of Figure 5-12.

Sample A has good baseline separation and peak shape but a long retention time. Sample B has baseline separation but a deteriorating peak shape. Sample C is assessed a single peak by the software due to the lack of baseline separation.

Figure 5-12: Umbelliferone thalidomide separation at 24% mobile phase B

Figure 5-12 shows the retention time of umbelliferone and thalidomide at 24% mobile phase B and at 10μL, 20μL and 30μL injections.

Table 5-10: Peak characteristics at 24% mobile phase B

	Inj. Vol. (μL)	Peak	RT	Area	Symmetry
		1-Umbelliferone	11.85	11780	1.23
A	10	2-Thalidomide	15.39	10406	0.67
		1-Umbelliferone	11.81	21079	1.57
B	20	2-Thalidomide	15.37	18402	1.45
C	30	-no separation-	11.81	64025	1.25

Table 5-10 gives the injection volume (μL) and the subsequent retention times, areas and peak symmetry for separation at 24% mobile phase B, was determined by the Masshunter Qualitative Analysis Software, (Version B.01.03).

Figure 5-13 shows the separation at 28%mobile phase B (A = 0.1% (v/v) formic acid/water mobile phase B = 0.1% (v/v) formic acid/ACN) and the effect of varying the injection volume on the peak shape. Table 5-11 details the peak characteristics of Figure 5-13.

Both samples A and B have good baseline separations and peak shapes. Sample C is assessed a single peak by the software due to the lack of baseline separation.

Figure 5-13: Umbelliferone thalidomide separation at 28% B
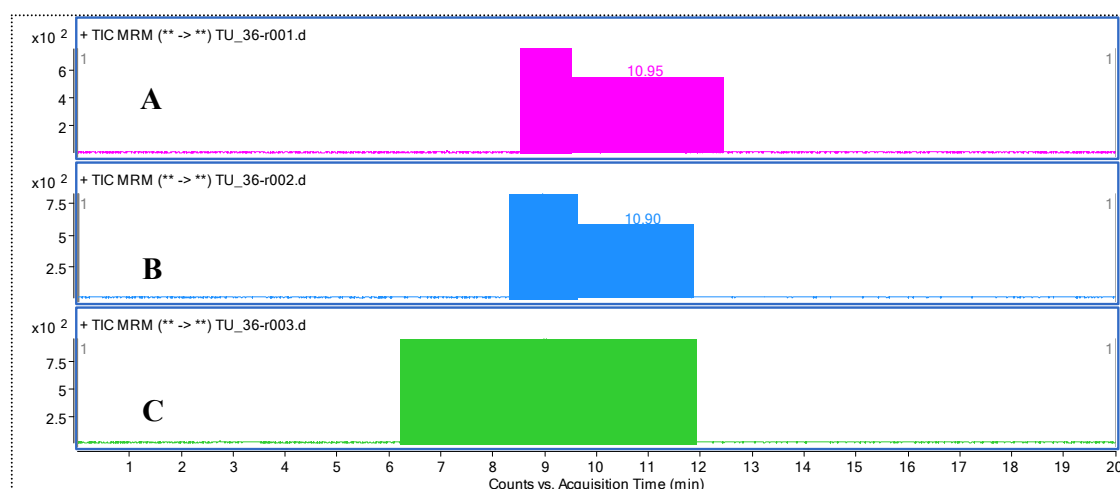
Figure 5-13 shows the retention time of umbelliferone and thalidomide at 28%B and at 10μL, 20μL and 30μL injections.

Table 5-11: Peak Characteristics at 28% B

	Inj. Vol. (μL)	Peak	RT	Area	Symmetry
A	10	1-Umbelliferone	8.98	15393	1.07
		2-Thalidomide	10.95	12772	1.64
B	20	1-Umbelliferone	8.96	22150	1.23
		2-Thalidomide	10.9	17846	1.28
C	30	-no separation-	9.03	83964	0.87

Table 5-11 gives the injection volume (μL) and the subsequent retention times, areas and peak symmetry for separation at 28%B, was determined by the Masshunter Qualitative Analysis Software, (Version B.01.03).

Figure 5-14 shows the separation at 30%B (A = 0.1% (v/v) formic acid/water mobile phase B = 0.1% (v/v) formic acid/ACN) and the effect of varying the injection volume on the peak shape. Table 5-12 details the peak characteristics of Figure 5-14.

Both samples A and B have good baseline separations and peak shapes. Sample C is assessed a single peak by the software due to the lack of baseline separation.

Figure 5-14: Umbelliferone thalidomide separation at 30% B
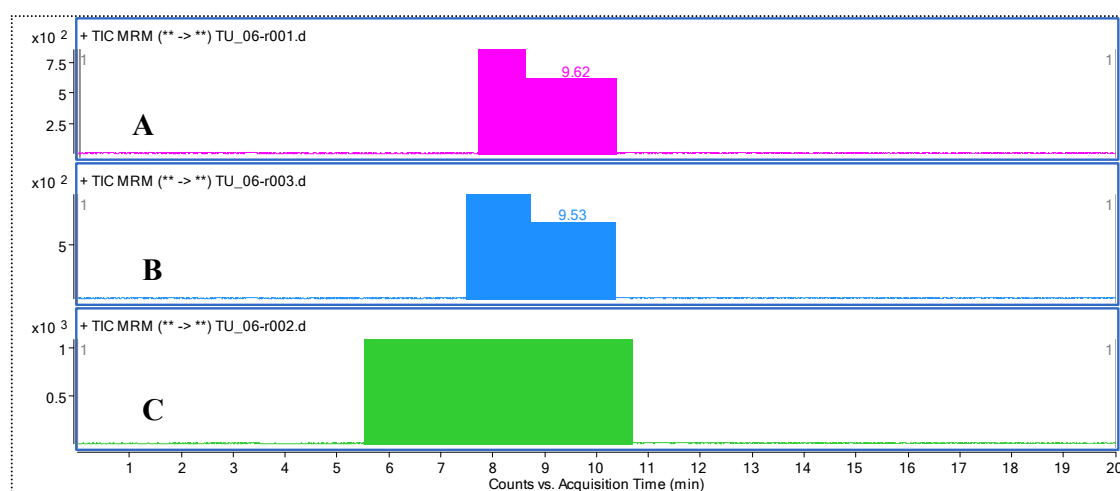
Figure 5-14 shows the retention time of umbelliferone and thalidomide at 30%B and at 10μL, 20μL and 30μL injections.

Table 5-12: Peak Characteristics at 30% B

	Inj. Vol. (μL)	Peak	RT	Area	Symmetry
A	10	1-Umbelliferone	8.11	15615	0.96
		2-Thalidomide	9.62	12483	1.02
B	20	1-Umbelliferone	8.1	22984	1.29
		2-Thalidomide	9.53	19500	0.88
C	30	-no separation-	8.1	87290	0.74

Table 5-12 gives the injection volume (μL) and the subsequent retention times, areas and peak symmetry for separation at 30%B, was determined by the Masshunter Qualitative Analysis Software, (Version B.01.03).

Figure 5-15 shows the separation at 32%B (A = 0.1% (v/v) formic acid/water mobile phase B = 0.1% (v/v) formic acid/ACN) and the effect of varying the injection volume on the peak shape. Table 5-13 details the peak characteristics of Figure 5-15.

Sample A has good symmetry but barely has baseline separation. Sample B does not achieve baseline separation and sample C is assessed a single peak by the software due to the lack of baseline separation.

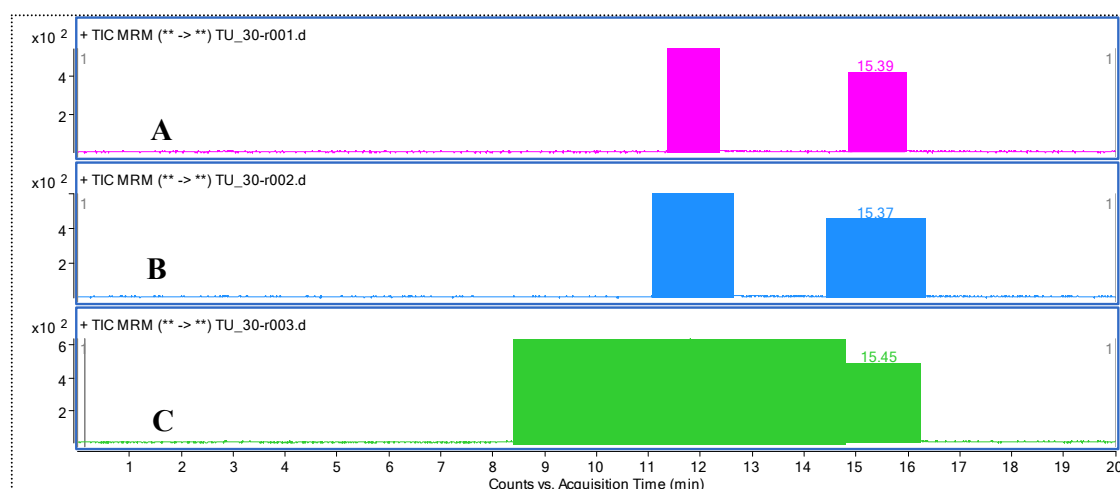**Figure 5-15: Umbelliferone thalidomide separation at 32% B**
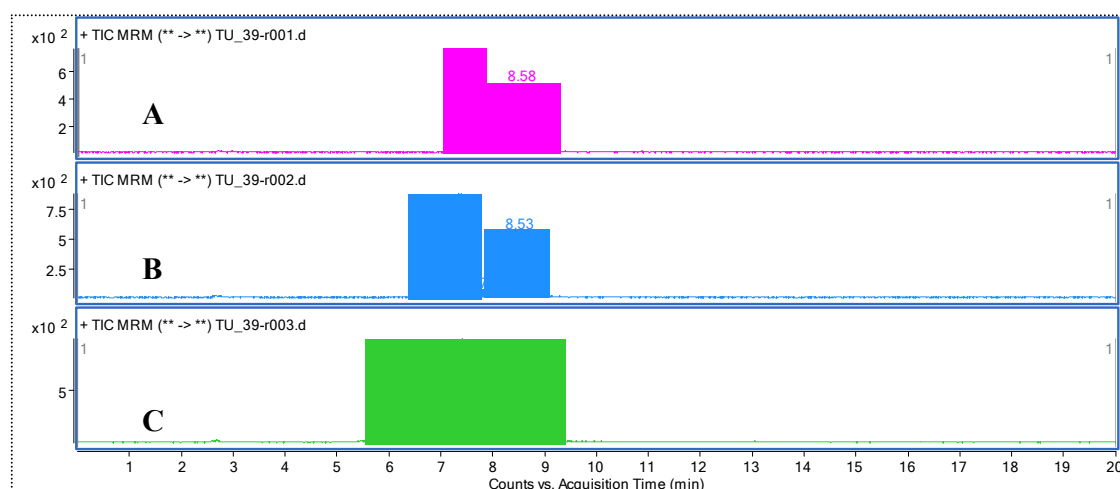
Figure 5-15 shows the retention time of umbelliferone and thalidomide at 32%B and at 10µL, 20µL and 30µL injections.

Table 5-13: Peak Characteristics at 30% B

	Inj. Vol. (µL)	Peak	RT	Area	Symmetry
A	10	1-Umbelliferone	7.4	12610	0.88
		2-Thalidomide	8.58	9291	0.81
B	20	1-Umbelliferone	7.39	24926	2.14
		2-Thalidomide	8.53	18036	1.7
C	30	-no separation-	7.43	64440	0.82

Table 5-13 gives the injection volume (µL) and the subsequent retention times, areas and peak symmetry for separation at 32%B, was determined by the Masshunter Qualitative Analysis Software, (Version B.01.03).

- Column 5 - Phenomenex Prodigy C18 150 x 4.6mm, 5µm particle size, with a mobile phase of 70% (v/v) water/ACN, 0.1%FA, with a 20µL injection volume was selected as the optimum separation criteria.(Figure 5-14, chromatogram B).

5.2. Extraction optimisation

An extraction procedure is employed to remove analyte from the matrix containing the agent of interest, e.g. serum, prior to analysis by LC-MS. Removing the target analyte from the biological matrix gives cleaner samples, improved sensitivity and prolongs the life-time of the analytical equipment.

Initial experiments varied many conditions including the samples volume, the extraction solvent, the extraction solvent volume and the aqueous component of the liquid-liquid extraction. The development process and the findings of the optimisation processes are outlined below.

The primary focus of the extraction optimisation process is to remove biological materials (serum) prior to quantification by LC-MS to yield cleaner samples. Liquid-liquid extraction was chosen to investigate due the suitability of this method for drug extraction from a wide variety of biological matrices. Preliminary experiments examined the extraction potential of each solvent on 1mL of spiked serum sample. Samples were spiked with 20ng of thalidomide and 20ng of lenalidomide (serum concentration 20ng/mL). A volume of 2.5mL of solvent was used in the extraction. The recovery was calculated based on the peak area of the extracted sample compared to the peak area of a pure drug calculated to be equal to 100% recovery.

Some of the extraction solvents examined were less suitable for the extraction process. These are marked in Table 5-14. The technical challenges generally involved the lack of formation of a distinct discrete solvent layer. In the samples marked, either no discernible layer was formed or the solvent layer volume was less than expected.

The startling poor recovery of lenalidomide highlighted the differences in the extraction profile of both analytes and the requirement of an alternative internal standard, as described in Section 5.1.2.

Table 5-14: Preliminary examination of a range of solvents

Extraction Solvent	Thalidomide % Recovery	SD	Lenalidomide % Recovery	SD	Comments
Control	100.0	2.7	2.7	100.0	
t-BME	70.9	1.9	2.6	4.4	
Chloroform*	81.2	3.3	4.0	9.9	unsuitable
Dichloromethane*	87.4	1.5	1.7	7.1	unsuitable
Ethyl Acetate	83.4	4.6	5.5	14.7	
Chloro-1-butane	-	-		-	no layer formed
t-BME/ACN (1:1)	69.4	4.7	6.8	13.8	
Chloroform/ ACN* (1:1)	97.6	7.8	7.9	17.1	unsuitable
Dichloromethane/ ACN (1:1)	-	-			no layer formed
Chloro-1-butane/ ACN (1:1)	109.7	6.4	5.9	8.0	
Chloro-1-butane/ ACN (1:4)	98.6	7.8	8.0	17.3	
Ethyl Acetate/ ACN (1:1)	76.8	2.2	2.8	27.4	

Table 5-14 shows the effect of a range of solvents on the recovery of thalidomide and lenalidomide. The recovery was calculated based on the peak area of the extracted sample compared to the peak area of a pure drug calculated to be equal to 100% recovery. Data shown is the average of triplicate intra-day samples, unless indicated, * indicates n=2.

Solvents highlighted in yellow were carried forward for further examination.

Combinations of ACN with ethyl acetate, chloro-1-butane and *t*BME were then examined further. Each solvent mixture was prepared first and mixed well before adding to the spiked sample. The sample volume was reduced to 0.5mL and 2.4mL of solvent was added to the samples. Samples were spiked with 10ng of thalidomide (20ng/mL).

Figure 5-16: The effect of solvent ratios on thalidomide recovery
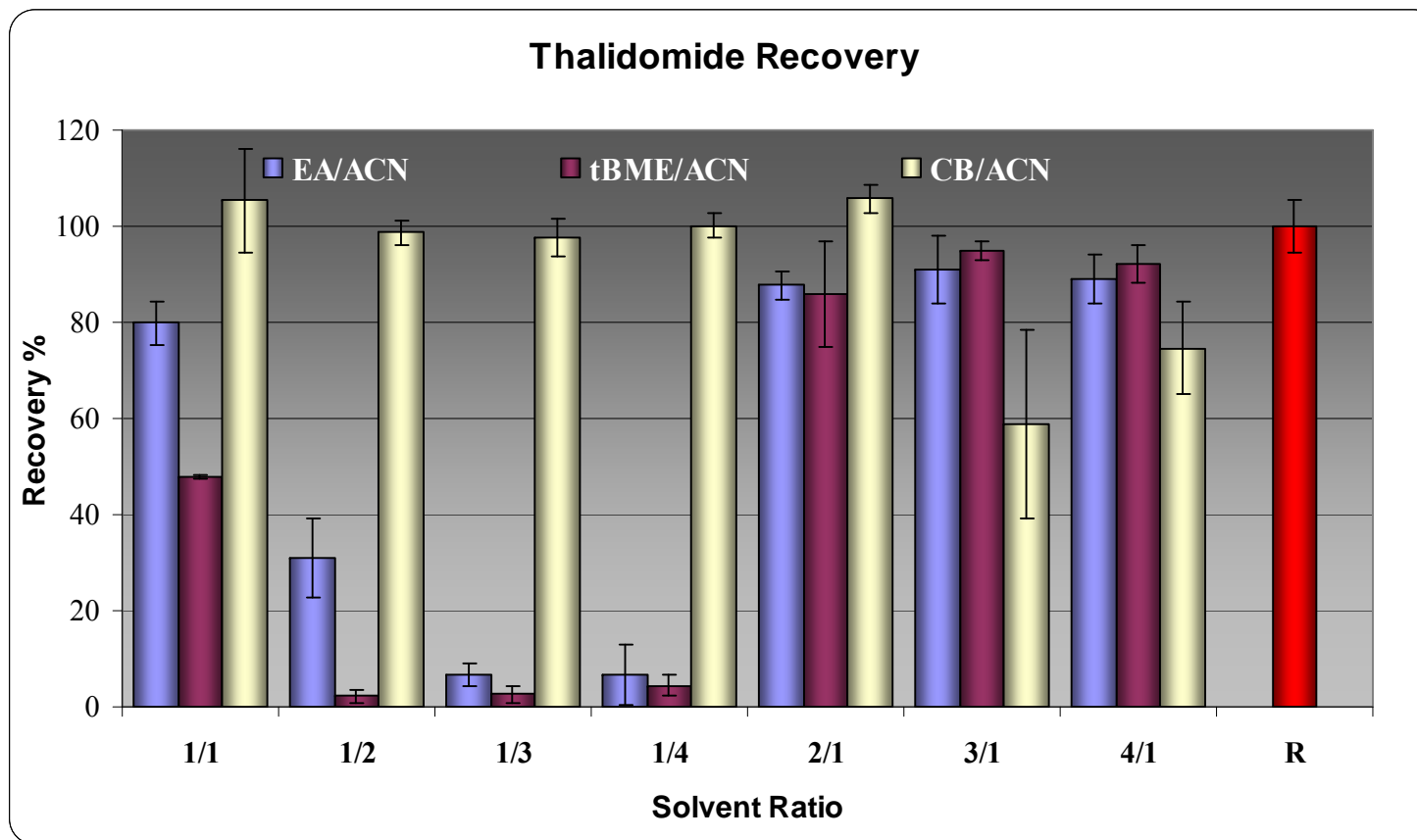
Figure 5-16 shows the effect of varying ratio of solvent with ACN. The recovery was calculated based on the peak area of the extracted sample compared to the peak area of a pure drug calculated to be equal to 100% recovery. The red bar (R) illustrates the recovery sample. Data shown is the average of triplicate intra-day samples.

Initial experiments were carried out with serum only. However, all clinical samples were stored 1:1 (v/v) with citrate buffer (25mM sodium citrate, pH1.5). Thalidomide is known to be unstable at physiological pH in aqueous conditions. The acidification of the samples through the addition of a buffer has been shown to increase sample stability [282].

Therefore, the effect of citrate buffer on the recovery potential of thalidomide was assessed. Figure 5-17 shows the effect of citrate buffer on extraction recovery. A sample volume of 500μL of serum was used in the serum-only arm of the experiment, in the serum/water arm 500μL of serum and 500μL of water was used and in the citrate arm 500μL of serum and 500μL of citrate. The serum-only arm was included to maintain continuity with previous experiments. The serum/water arm was included to account for any differences attributed to additional volume.

The extraction solvents of chloro-1-butane/ACN (4/1, v/v) and ethyl acetate/ACN (3/1, v/v) gave the best recovery of recovery when combined with the citrate buffer.

These two solvent mixture and a mixture of *t*BME/ACN (3/1, v/v) was carried forward and the recovery was assessed over a thalidomide concentration range. All samples were prepared as serum/citrate (1/1, v/v)

Figure 5-17: The effect of citrate buffer on extraction efficiency
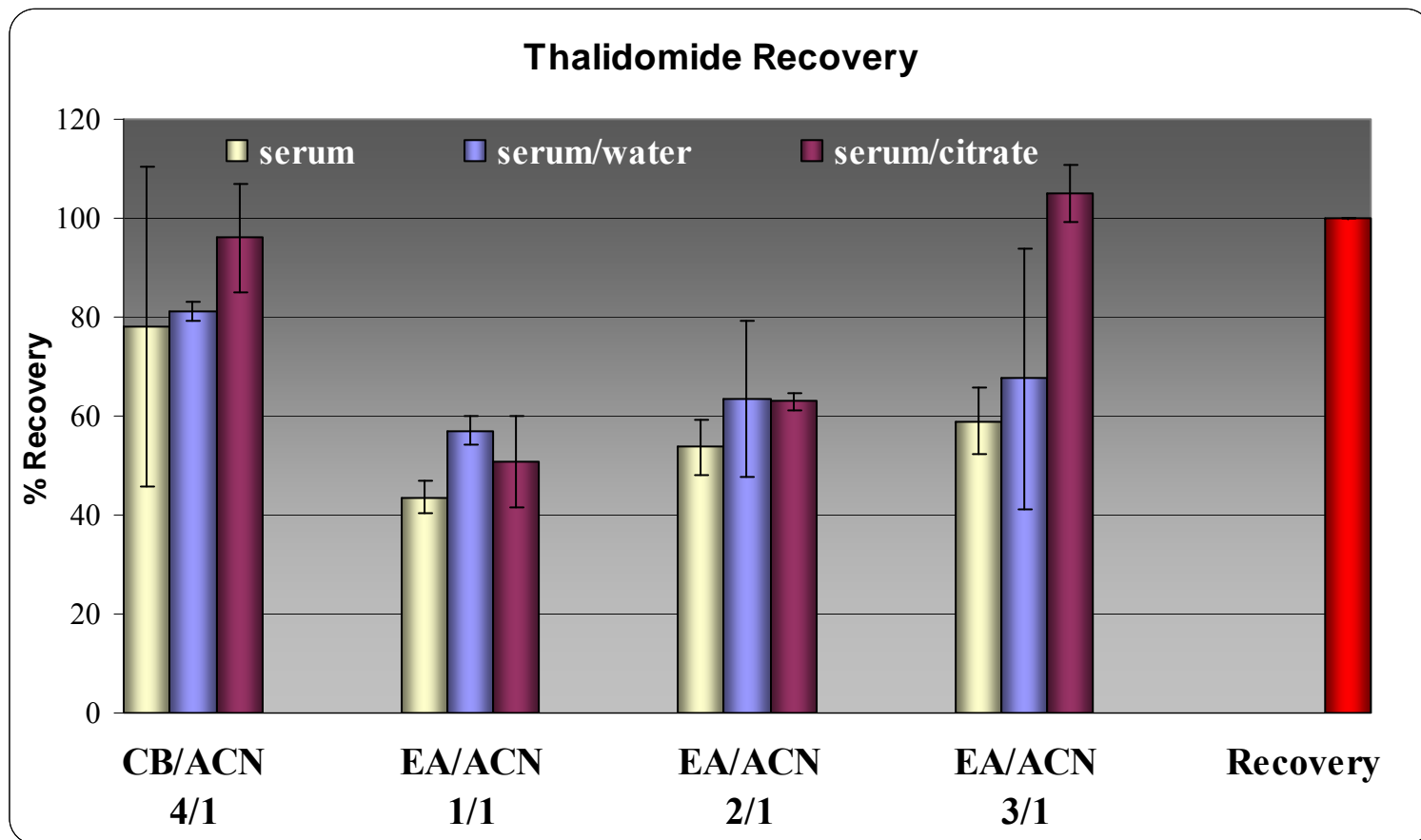
Figure 5-17 shows the effect of citrate on the extraction efficiency of each solvent. The data shown is the average and standard deviation, n=6.

The two solvent mixture, CB/ACN (4/1, v/v), EA/ACN (3/1, v/v) and the mixture of tBME/ACN (3/1, v/v) were carried forward and examined in more detail. The recovery of thalidomide was assessed over a concentration range to verify that the recovery was dynamic across the range. All samples were prepared in serum/citrate (1/1, v/v)

The extraction solvent mixture of EA/ACN (3/1, v/v) was selected as the most appropriate solvent combination. The average recovery across the concentration range was 100.2% with a percent standard deviation of 3.2%. ACN/CB gave lower recoveries, especially at the lower concentrations examined. ACN/tBME also gave good recoveries, with an average recovery of 99% with a 5% deviation.

Figure 5-18: Recovery of thalidomide across a drug concentration range
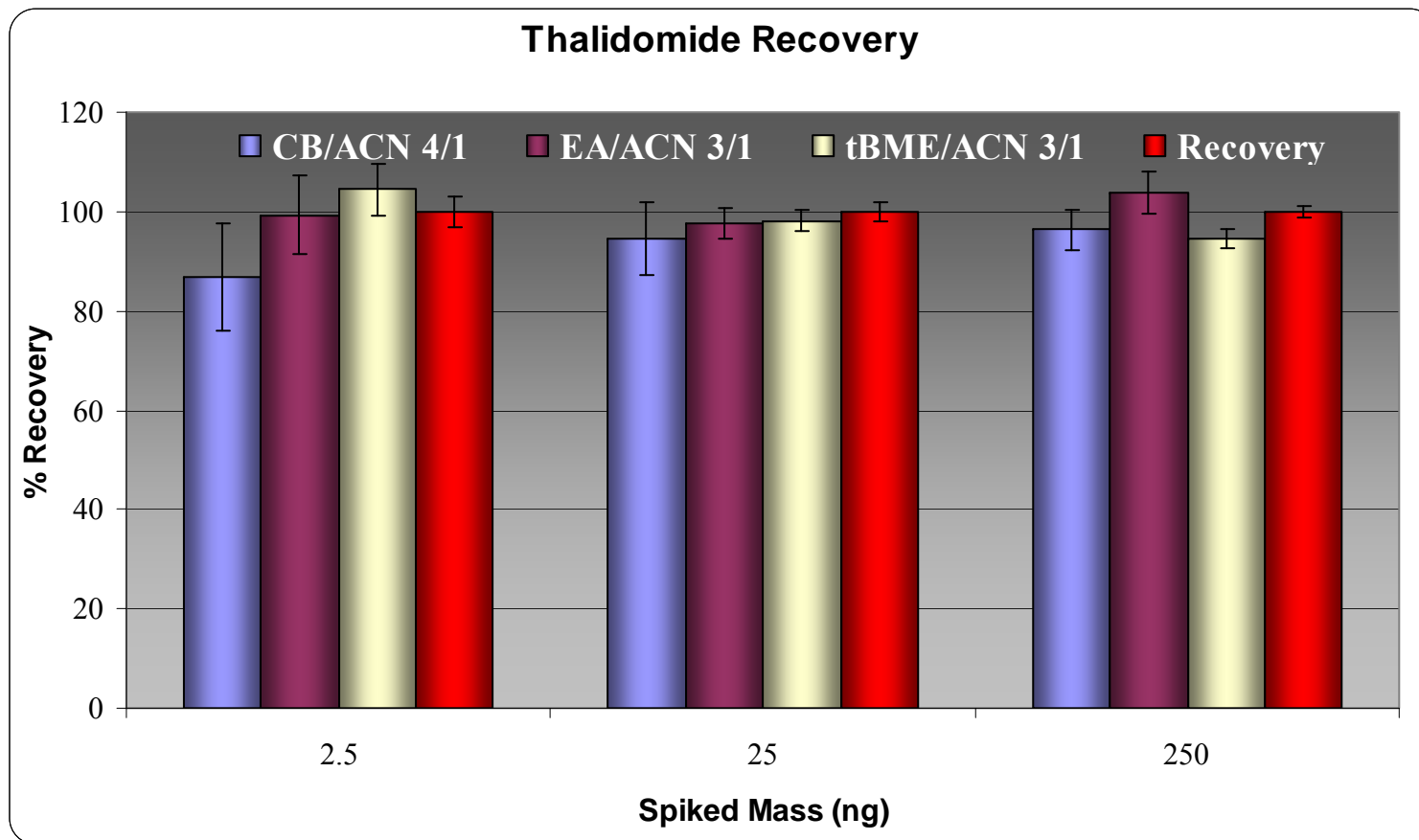
Figure 5-18 shows extraction efficiency of thalidomide in three solvent mixes. The red bar indicates the recovery samples which were calculated to be equivalent to 100% extraction. Data indicates average and standard deviation, n=3.

As discussed above (Section 5.1.2) umbelliferone was selected as an internal standard for thalidomide. The recovery of umbelliferone was assessed in the solvent mixtures above also. The samples were spiked with 10ng of umbelliferone in ACN (50µL of 200ng/mL). Table 5-15 outlines the recovery of umbelliferone with the three solvent mixes examined.

Table 5-15: The recovery of internal standard, umbelliferone

Solvent	% Recovery	% Dev
Recovery	100.0	2.3
CB/ACN 4/1	120.4	2.9
EA/ACN 3/1	114.2	5.6
tBME/ACN 3/1	119.2	8.3

Table 5-13 gives the recovery of umbelliferone Data is given as the percentage recovery assuming calculated recovery sample is 100%, n=12 for extracted samples.

EA/ACN (3/1, v/v) gave the best recovery of the three solvents for thalidomide, however, the recovery for the internal standard umbelliferone was slightly high. The recovery of umbelliferone was examined across a concentration range. A volume of 500µL of sample (serum/citrate 1/1, v/v) was spiked with 50µL of varying concentration of umbelliferone, Figure 5-19.

Figure 5-19: Umbelliferone recovery in EA/ACN (3/1, v/v) extraction
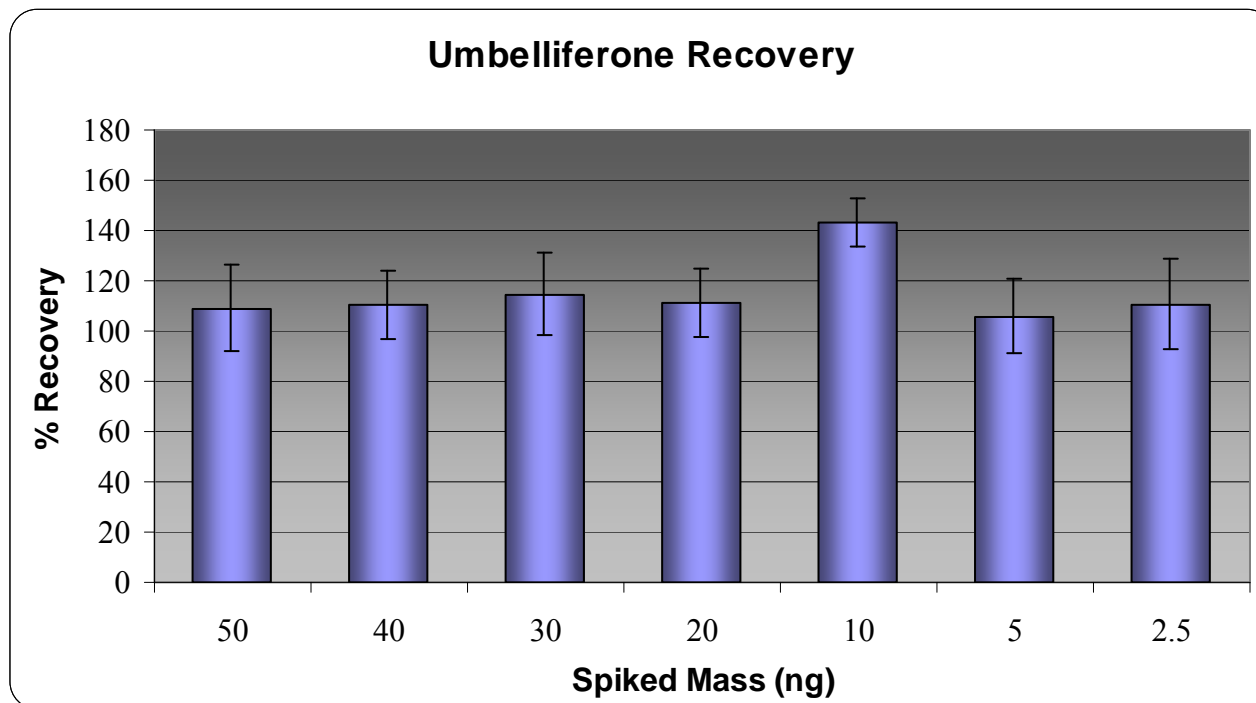
Figure 5-19 shows the extraction of umbelliferone at a range of concentrations of internal standard. Spike mass of 30ng, or 50μL of 600ng/mL was selected as the internal standard. Data indicates average and standard deviation, n=3.

The recovery of thalidomide was also assessed across a wider concentration range. A sample volume of 500μL of sample, which is 250μL of serum, was spiked with 50μL of thalidomide in acetonitrile. Figure 5-20 gives the recovery of thalidomide across a serum concentration range of 1000ng/mL to 1ng/mL. The average recovery across the concentration range was 113% +/- 7%. The extraction solvent was fixed as EA/ACN (3/1, v/v).

Figure 5-20: Thalidomide recovery
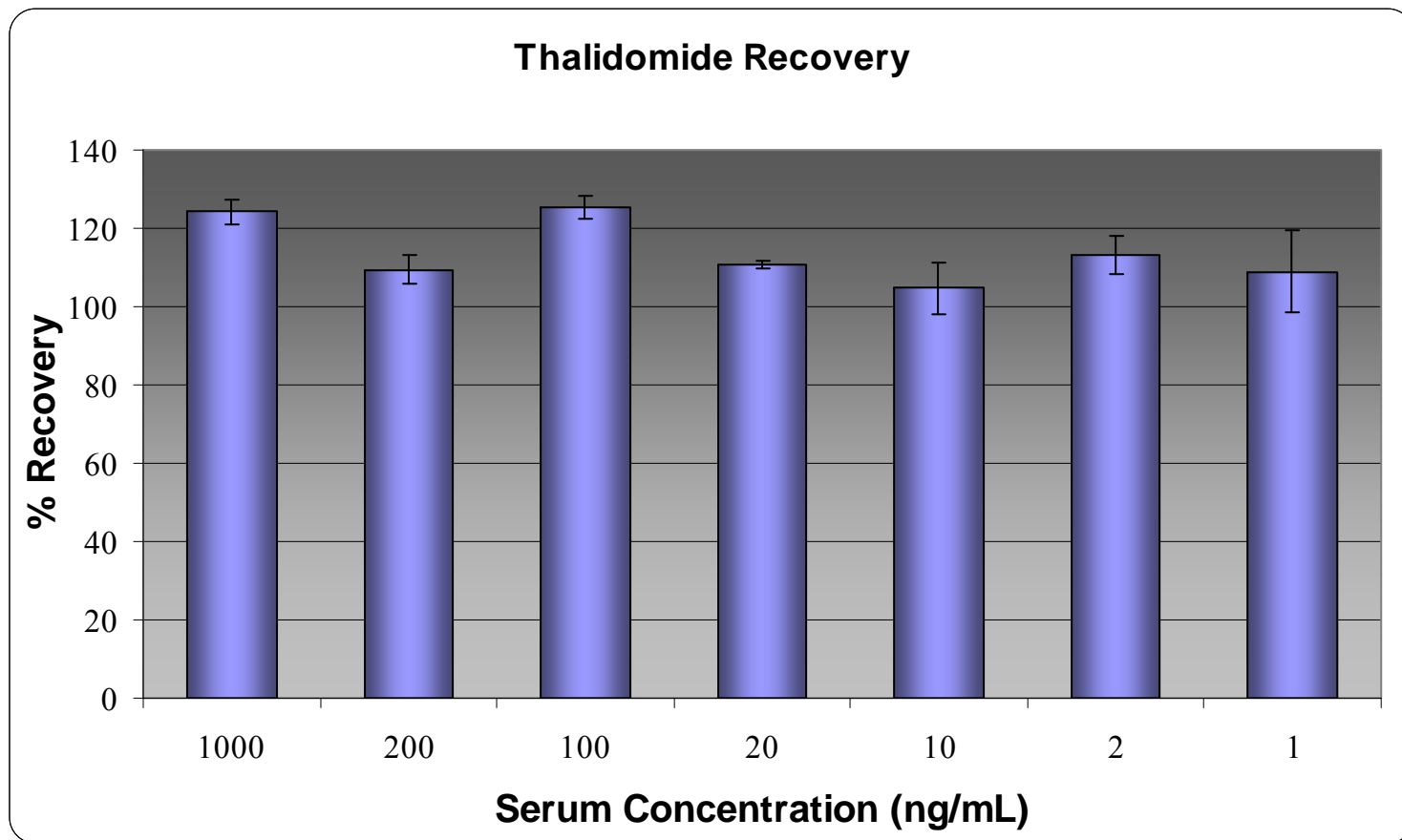
Figure 5-20 shows the recovery of thalidomide across a concentration range. Data shown is the average and standard deviations, of triplicate determinations.

5.3. *MS detection conditions*

The optimum multi-reaction monitoring (MRM) settings were determined for thalidomide and umbelliferone, as well as for the additional multiple myeloma therapies. Table 5-17 gives the transitions from precursor to product ion as well as the optimum fragmentor voltage and optimum collision energy identified for each analyte. All detected transitions were monitored for each agent as additional qualifier ions add specificity. The quantifier ions are indicated in the table with an asterisk.

5.3.1. Precursor ion determination

Initial precursor determination of thalidomide was more complicated than any of the other agents tested and as such the process for the determination of thalidomide MS detection conditions is outlined here. The other compounds mentioned were determined in a similar fashion to dasatinib, as described in Section 3.3.

Routinely the precursor ion is determined by the flow injection analysis of a 250ng/mL solution of the analyte of interest in acetonitrile. The precursor ion for thalidomide is 259m/z. This is the thalidomide ion in its protonated state [M+H$^+$]. However, the determination of the thalidomide precursor ion proved consistently difficult to isolate in the MS2Scan by flow injection analysis. Therefore, it was decided to investigate and confirm the exact mass of the precursor ion by infusion of thalidomide directly into the source using a tee-pieced infusion pump. This is set up similarly to the assembly described in figure 3-17, however, only mobile phase flowed from the LC, the analytical column was by-passed and no injections were preformed by the autosampler. Screenshots were taken of the real-time scans.

Figure 5-21 shows the real-time MS scan of thalidomide infusion.

Figure 5-21: Real-time screenshot of infusion of thalidomide
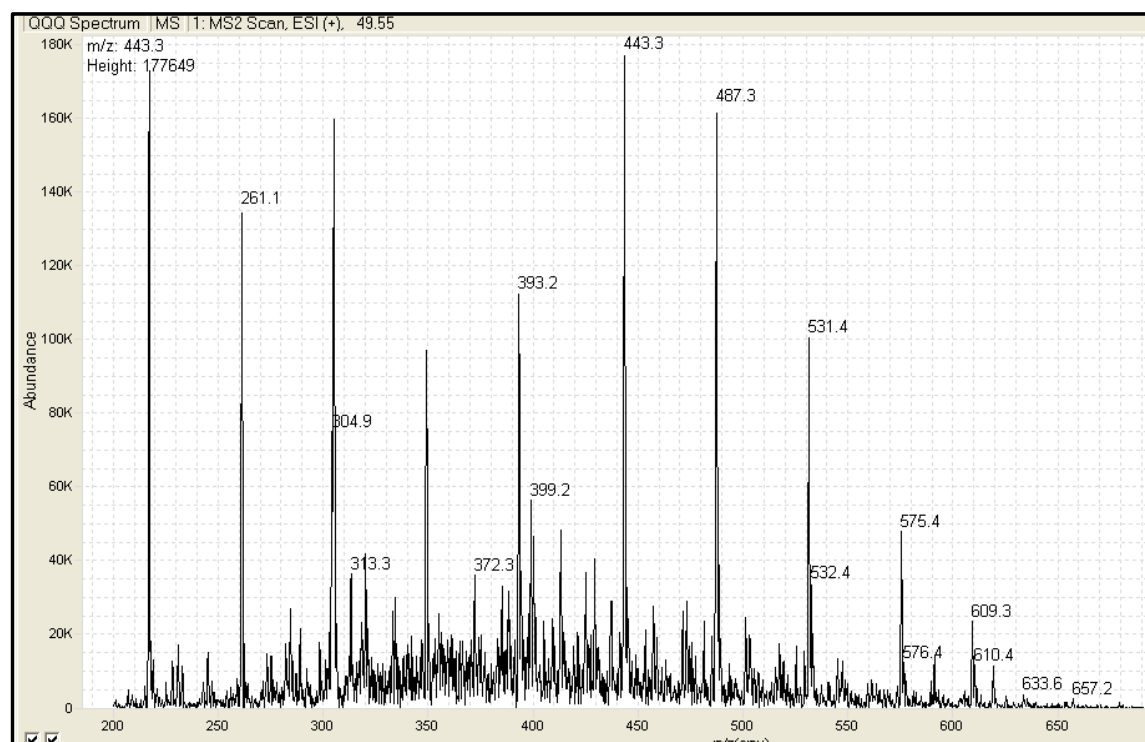
Figure 5-21 shows a real time screenshot of an infusion of thalidomide, 250ng/mL at a rate of 50μL/min.

Owning to the significant level of interfering ions present in the scan (Figure 5-21), a scan of the background was taken, where nothing was infused through the pump and only mobile phase flowed through the LC system (Figure 5-22).

Figure 5-22: Real-time screenshot of background from mobile phase
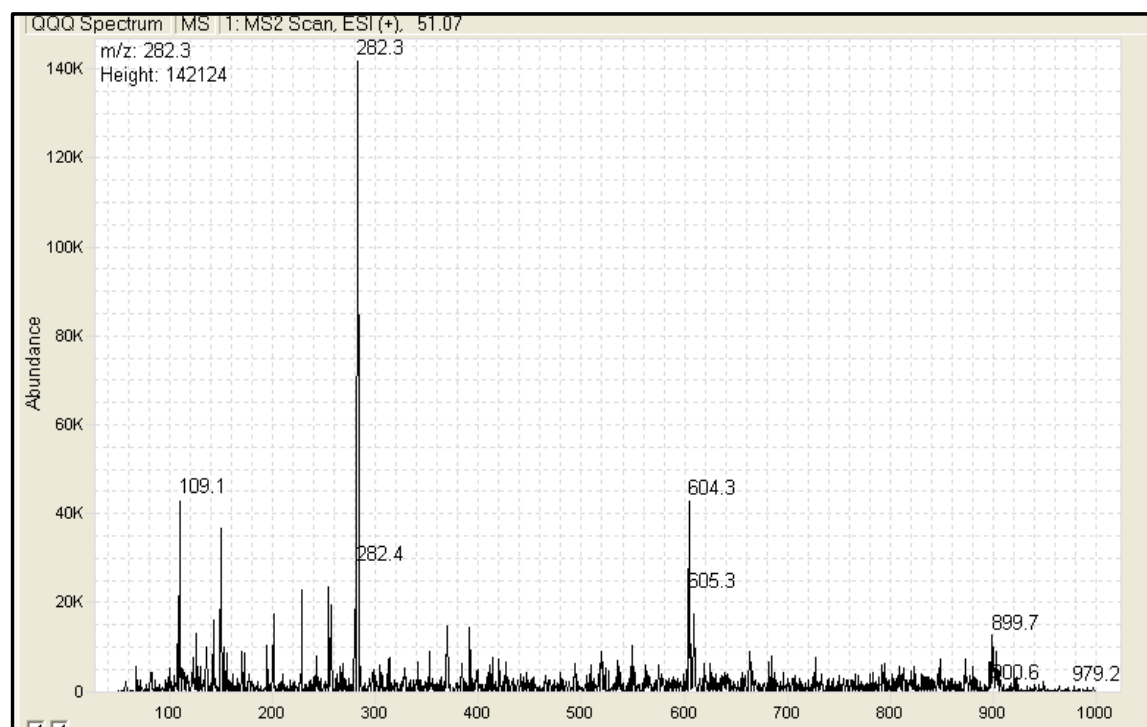
Figure 5-22 shows the background ion attributed to the mobile phase and system.

Figure 5-22 indicated that the level of interfering ions seen in Figure 5-21were due to the thalidomide solution. By preparing fresh stocks of thalidomide, in acetonitrile from a newly opened bottle, in new glassware, the precursor ion was determined to be 259.1m/z.

Figure 5-23: Real-time screenshot of fresh thalidomide infusion
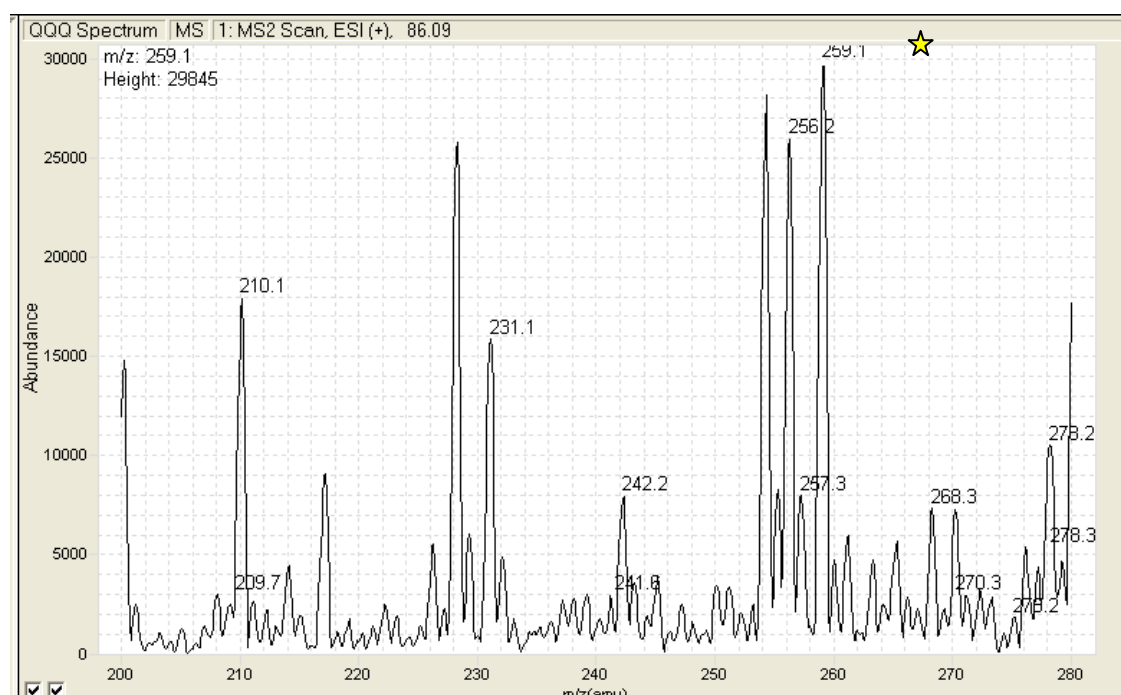
Figure 5-23 shows the MS2Scan from 200 – 280m/z. The thalidomide precursor ion was identified at 259.1m/z

Figure 5-24: Real-time screenshot of fresh thalidomide infusion
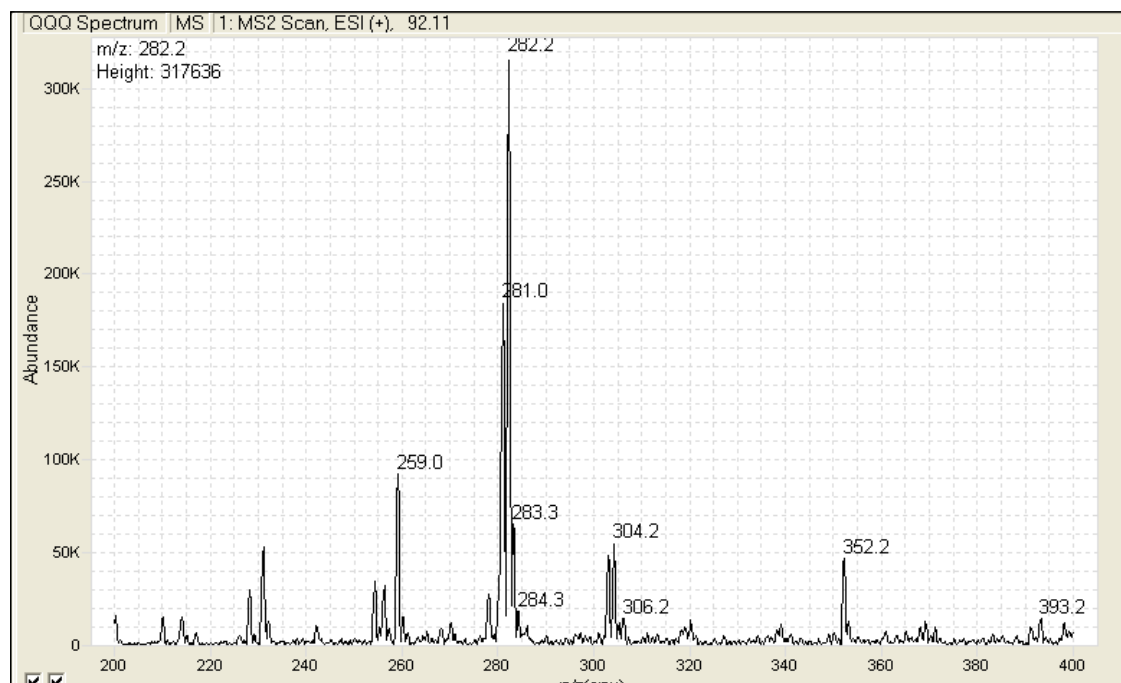
Figure 5-24 shows the MS2Scan scanning from 200-400m/z thalidomide precursor ion at 259m/z. The ion at 282m/z is present in the background scan and can be disregarded as not from the sample.

Once the precursor ion had been confirmed the experiment was repeated using flow injection analysis and freshly prepared solutions.

Figure 5-25: TIC of MS2Scan of thalidomide
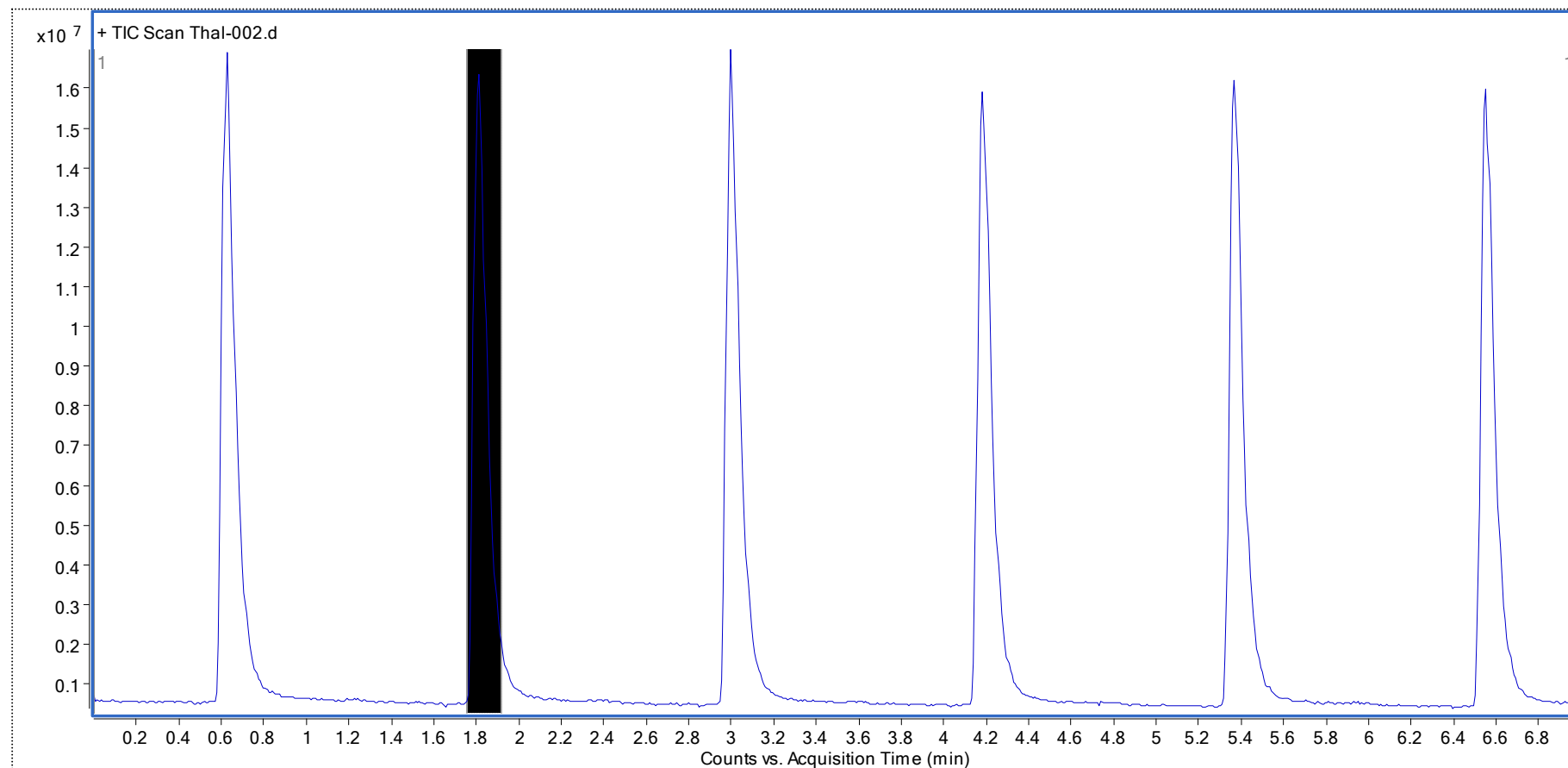
Figure 5-25 shows the TIC as detected in MS2Scan mode for six injections of thalidomide by Flow Injection Analysis (FIA)

Figure 5-26: Extracted MS Spectrum
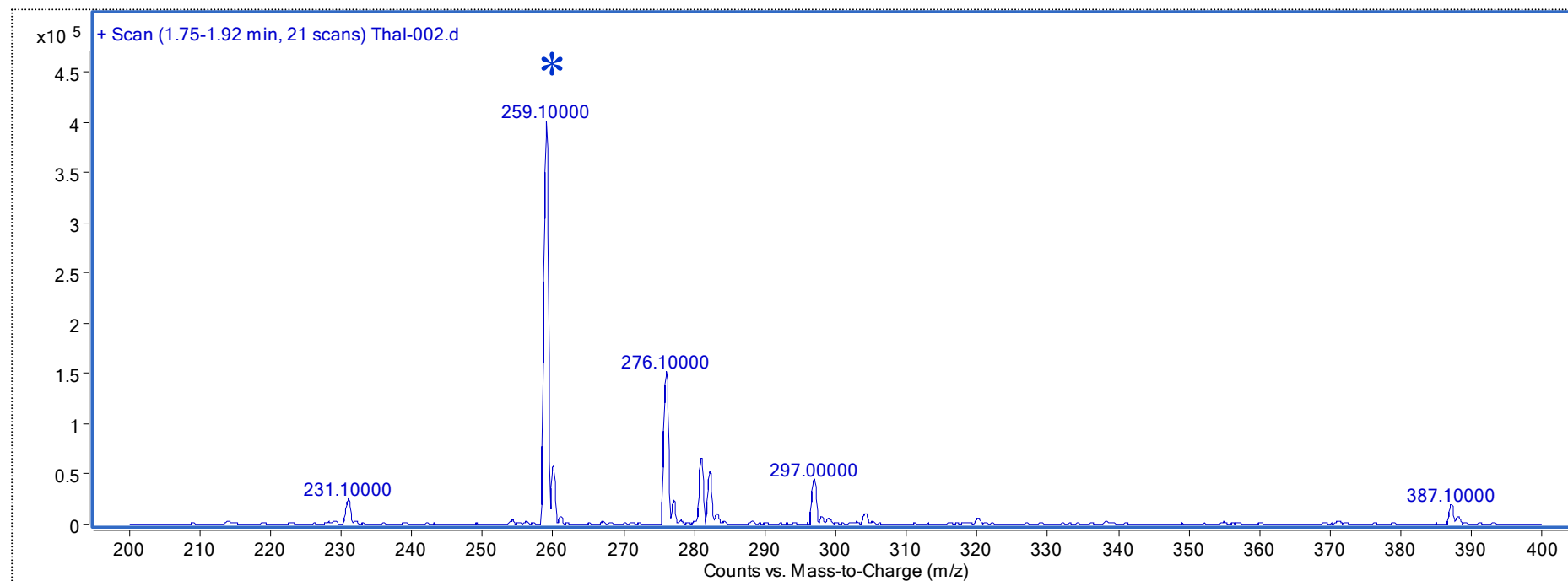
Figure 5-26 shows the MS spectrum of thalidomide extracted from the TIC (the greyed out section). The predominant ion, a protonated thalidomide ion, determined to be 259.1 m/z, is annotated (*). This is the precursor ion.

5.3.2. Fragmentor voltage optimisation

As explained in Section 3.3.2, the fragmentor voltage is a setting of the MS which acts almost like a filter, the objective being to increase the number of precursor ions entering the first quadrupole. The thalidomide ion is monitored in SIM mode. The voltage setting with the maximum peak area for the precursor ion is the optimum. Each setting was analysed in duplicate.

Figure 5-27: Fragmentor voltage optimisation
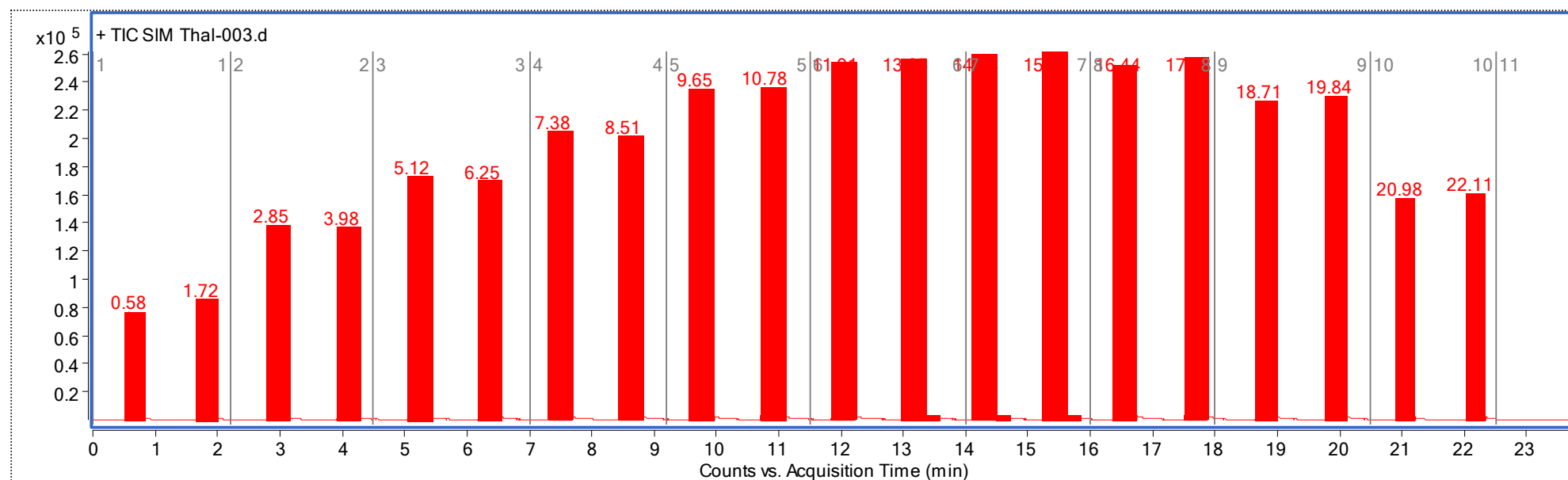
Figure 5-27 shows the TIC for 259.1m/z. in selected ion monitoring (SIM) mode with increasing fragmentor voltage

Table 5-16: Peak Area of Integrated SIM

Segment	Peak #	RT	Area	Area%	FV
1	1	0.58	402916	25.76	0
	2	1.72	484422	30.97	0
2	3	2.85	802067	51.28	20
	4	3.98	792416	50.67	20
3	5	5.12	1010100	64.58	40
	6	6.25	994100	63.56	40
4	7	7.38	1202869	76.91	60
	8	8.51	1181001	75.51	60
5	9	9.65	1382260	88.38	80
	10	10.78	1376603	88.02	80
6	11	11.91	1508782	96.47	100
	12	13.05	1512559	96.71	100
7	**13**	**14.18**	**1535811**	**98.2**	**120**
	14	**15.31**	**1563994**	**100**	**120**
8	15	16.44	1475110	94.32	140
	16	17.58	1493133	95.47	140
9	17	18.71	1279867	81.83	160
	18	19.84	1264999	80.88	160
10	19	20.98	866763	55.42	180
	20	22.11	874326	55.9	180

Table 5-16 shows peak area for the integrated area and the percentage peak area for the SIM scan of thalidomide (259.1m/z) in figure 5-28.

By comparing the integrated peak area each set of peaks it is possible to determine the optimum fragmentor voltage, i.e. the voltage that allowed maximum transit of dasatinib precursor ion. In the case of thalidomide, the fragmentor voltage from 100-140 gave similar peak areas – ranging form 96% to 100%. The drop in peak area at higher fragmentor voltage is due to the precursor ion being broken down before entering the MS.

The optimum fragmentor voltage was selected to be 120.

5.3.3. Product ion determination

Figure 5-28: TIC of Product Ion Scan
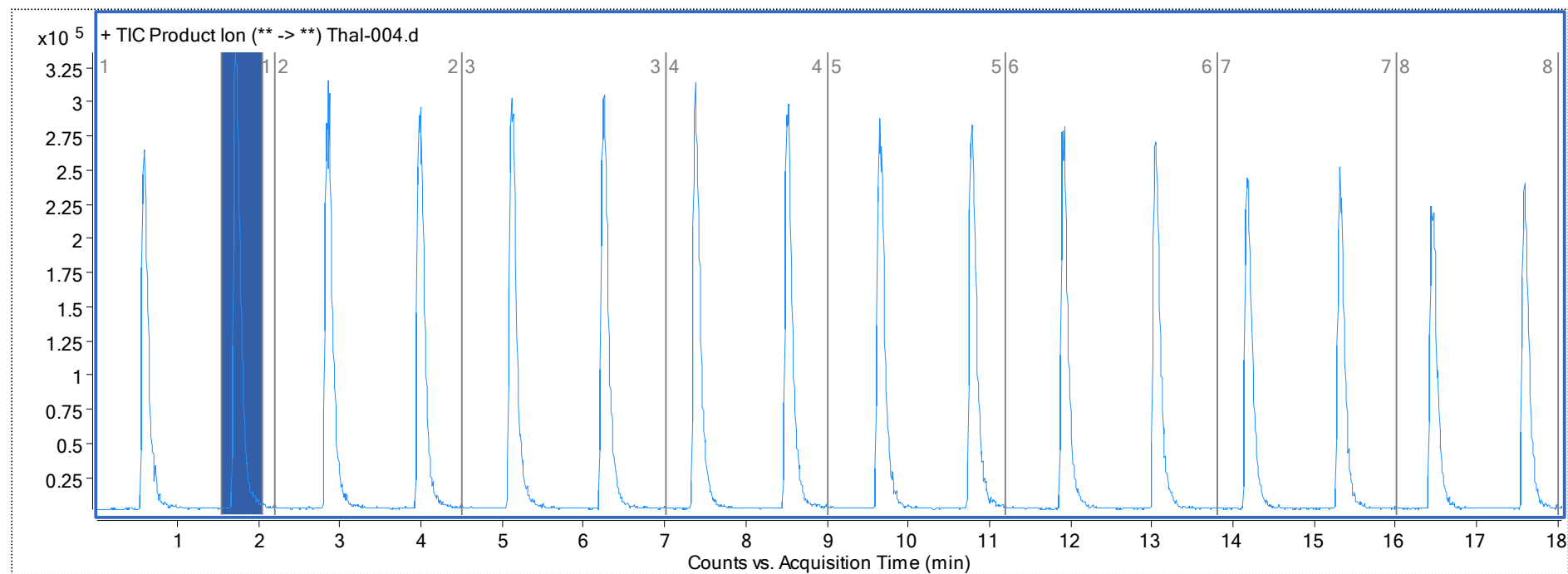
Figure 5-28 shows the TIC from the product ion scan, with increasing collision energies. The highlighted time segment shows where the MS spectra were extracted. Each segment represents an increase of 5 collision energy.

Figure 5-29: Extracted MS spectra for product ion scan
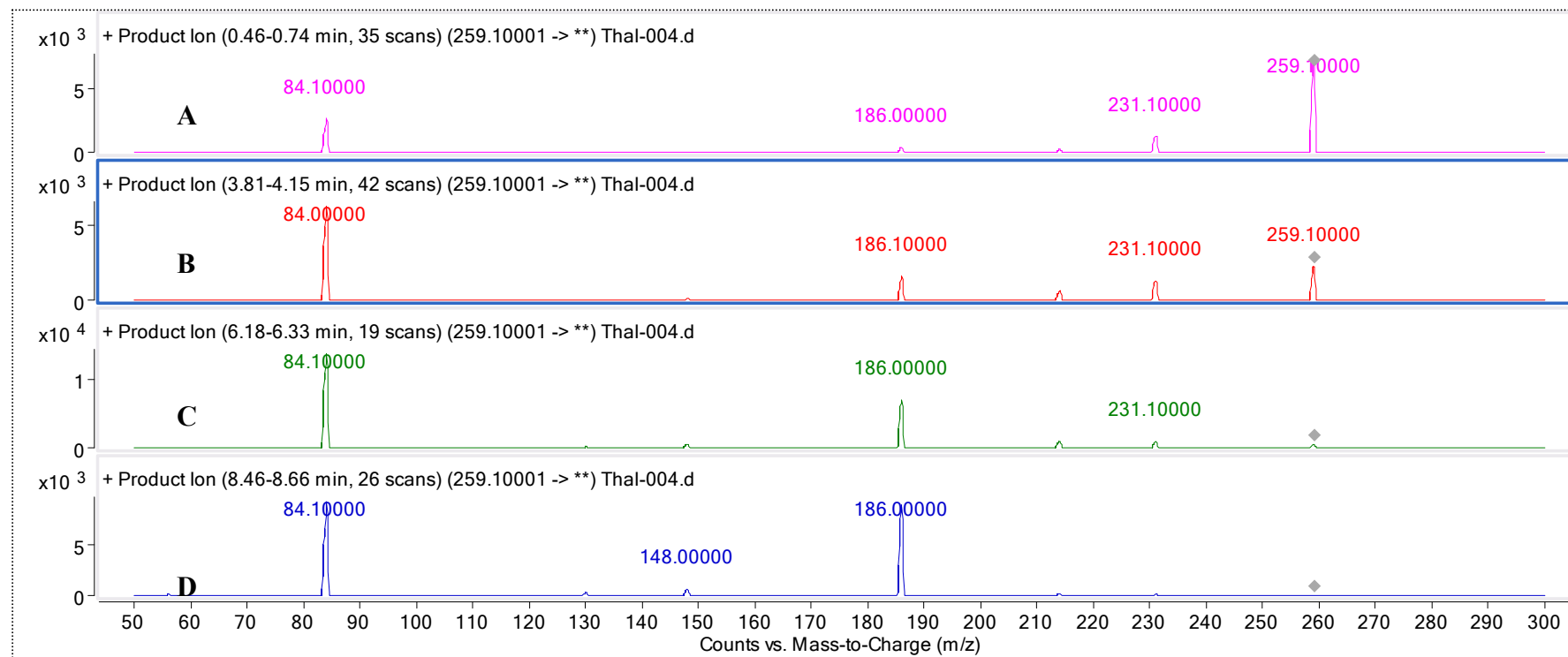
Figure 5-29 shows the extracted MS spectrum of the TIC of the product ion scan, shown in figure 5-28. Spectrum A was extracted between 0.46 - 0.74mins, CE =5, spectrum B was extracted at 3.81-4.15mins CE=10, spectrum C was extracted at 6.18-6.33minutes, CE=15 and spectrum D was extracted between 8.46 and 8.66mins, CE=20.

The correlation between the decline in abundance of 259.1m/z the increase in abundance of 84.1m/z and 186.0m/z indicating that these are the product ions for thalidomide. The ion at 231m/z does not appear to increase with the breakdown of the thalidomide precursor ion making it unacceptable as a product ion.

5.3.4. MRM optimisation

Multi-reaction monitoring is used to quantify the abundance of a species by tracking precursor ions and their product ions though the MS to provide quantifiable spectra. Each transition from precursor ion to product ion can have different collision energies. By optimising the MRM transition we optimise the collision energy for each transition.

Collision energies were increased step-wise in units of 5 from a starting value of zero to 40keV.The optimum collision energy for the transition 259.1 →84m/z was determined to be 15keV while the optimum collision energy for transition 259.1 →186m/z was determined to be 25keV, Figure 5-30.

Figure 5-30: TIC and EIC for thalidomide MRM optimisation
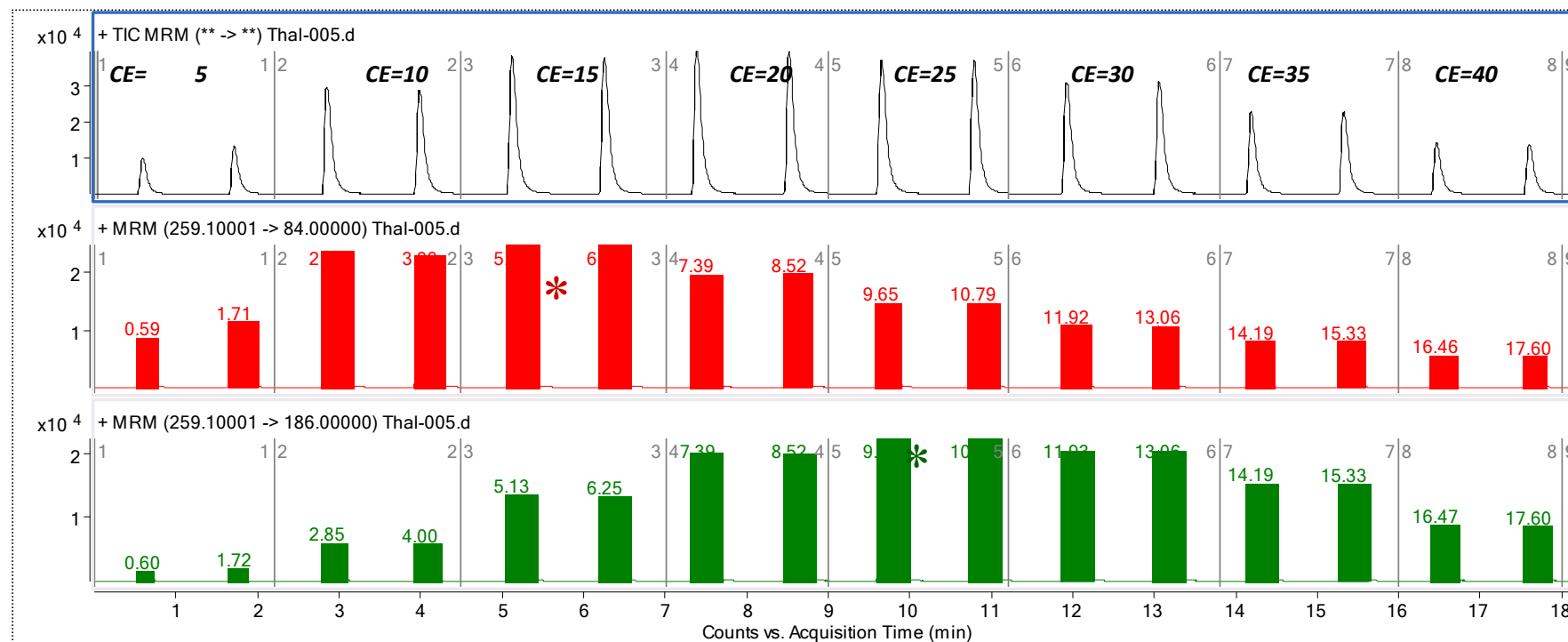
Figure 5-30 shows the TIC for the MRM for thalidomide and the extracted MRM for the transitions (259.1 →84) m/z (red trace) and the extracted MRM for (259.1 →186) m/z (green trace), * indicates optimum collision energy for each transitions.

This is representative of the work carried out for the detection condition optimisation of lenalidomide, umbelliferone and bortezomib. Bortezomib, as a multiple myeloma medication was also examined at this time. The optimised settings for each compound are detailed in Table 5-17.

Table 5-17: Summary of MRM transition conditions of multiple myeloma agents

Name	Precursor Ion	Optimum Fragmentor Voltage	Product Ion	Optimum Collision Energy
Thalidomide	259.1	120	84*	10
			186	25
Umbelliferone	163.3	130	107.1	20
Lenalidomide	260.1	90	187.2	25
			148.8*	15
			106	40
Bortezomib	367.2	130	226.3*	15
			208.1	30
			321.1	20

The optimal fragmentor voltages and collision energy settings for the determination of the multiple myeloma drugs employed in this study, * indicates quantifier ions.

5.4. Assay validation

The overall LC-MS method was validated for the following performance parameters-linearity and range, intra-day precision (repeatability) and inter-day precision (intermediate precision), accuracy, sensitivity (LOD and LOQ), recovery and sample stability according to the guidelines described by Ermer [299]. An illustrative chromatogram is provided in Figure 5-31. MRM allowed individual determination of each drug necessary with the use of internal standard-based quantification. Due to the sensitivity of the method for thalidomide, the method was validated in both a cancer cell line and serum.

Figure 5-31: Representative Chromatogram of Thalidomide and Umbelliferone
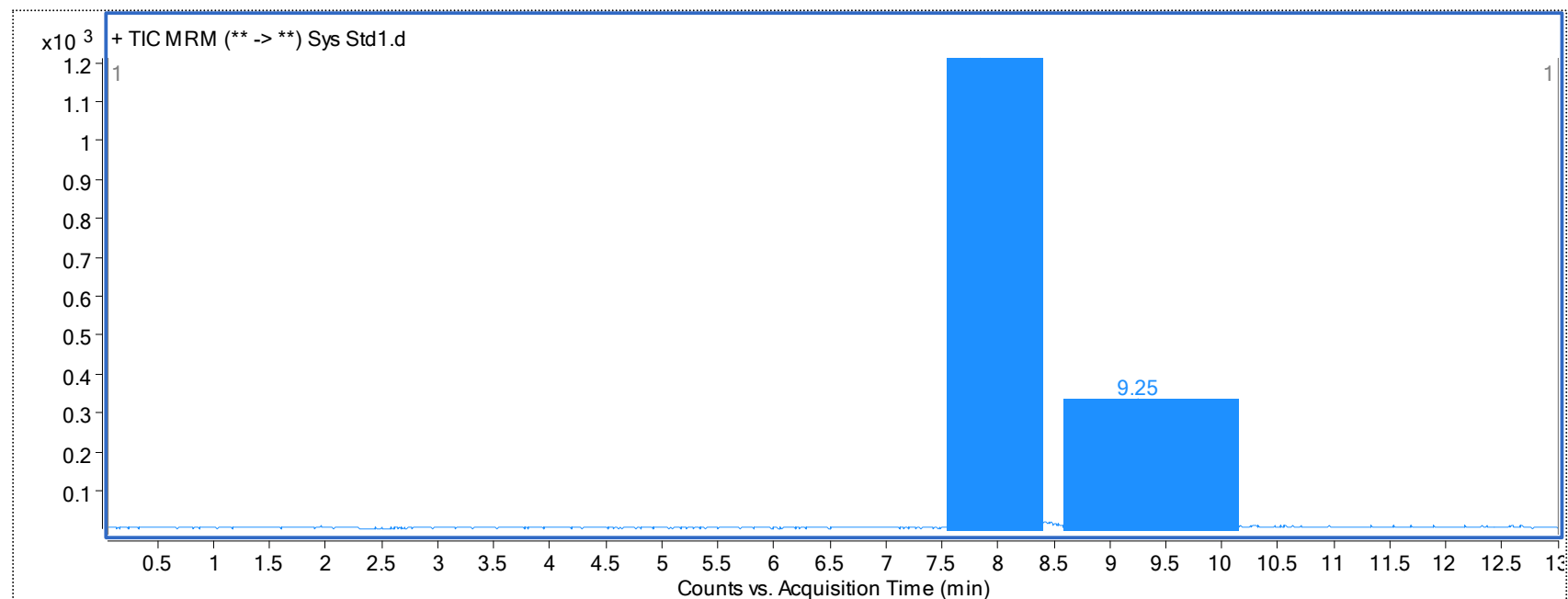
Figure 5-31 shows a representative TIC of umbelliferone and thalidomide separation

5.4.1. Assay validation in human serum

5.4.1.1.   Linearity and range

Regression analysis was used to assess the linearity between the peak area ratios (analyte/IS) and the analyte concentration.

The calibration curve for thalidomide was linear over the serum concentration range 20µg/mL to 50ng/mL. Since thalidomide and umbelliferone resolved well from each other and were extracted with high efficiency umbelliferone was used as the internal analytical standard for thalidomide to reduce error. A volume of 50µL of a 600ng/mL stock of internal standard was spiked to each tube, sample and standards. Whilst the calibration curves were linear, over such a broad range, the bias of the regression line tends to make the determination of lower drug concentration values much less accurate; hence it was decided to use a log-log plot of the peak area ratio versus the mass of drug in all calculations. A weighted linear regression plot which ensures the accuracy at lower concentrations was also examined for the analysis of the standard curve and clinical patient samples. This showed to be similarly appropriate for the lower ranges of thalidomide quantification. However, the data in this thesis is presented as a calculated by LOG_{10}-LOG_{10} plot. The LOG_{10}-LOG_{10} plot gave typical correlation coefficients (R^2) values of 0.99.

5.4.1.2.   Precision and accuracy

Intra-day precision and accuracy was assessed over the serum concentration range (20µg/mL-0.05µg/mL) by extraction and analysis of five spiked samples on the same day, Table 5-18. Inter-day precision and accuracy was assessed over the concentration range (20µg/mL-0.05µg/mL) by extraction and analysis of triplicate spiked samples over five days, Table 5-19. The percentage relative standard deviation (% R.S.D.) was employed as a measure of precision. The percentage accuracy was determined by dividing the average calculated drug concentration by that of the spiked known concentration. The precision (% R.S.D.) in all cases was less that 5%, with the average intra-day % R.S.D. 3% and the average % R.S.D. for the inter-day analysis being 1.8%. The accuracy ranges from 91% to 107%, with an average of 103% for the intra-day analysis and 100% average for the inter-day analysis.

Table 5-18: Intra-day analysis for precision and accuracy of thalidomide in serum

Spiked Serum Conc. (µg/mL)	Mean Observed Conc. (µg/mL)	Mean Accuracy Observed (%)	Precision (% R.S.D.)
20	18.2	91.2	4.1
10	10.1	100.9	2.3
5	5.3	106.8	0.7
1	1.03	103.3	4.5
0.50	0.53	106.5	3.9
0.10	0.10	98.6	4.2
0.05	0.05	98.2	1.7

The assessment of six samples over one day for intra-day precision and accuracy.

Table 5-19: Inter-day analysis for accuracy and precision of thalidomide in serum

Spiked Serum Conc. (µg/mL)	Mean Observed Conc. (µg/mL)	Mean Accuracy Observed (%)	Precision (% R.S.D.)
20	18.2	91.2	1.8
10	9.9	99.2	2.2
5	5.2	104.0	2.4
1	1.1	106.3	1.6
0.50	0.52	103.2	1.1
0.10	0.10	99.1	2.0
0.05	0.05	95.7	1.8

The assessment of triplicate samples over five independent days.

5.4.1.3. *Recovery/extraction efficiency*

The extraction efficiency of the procedure was determined by comparing the peak areas of the extracted analytes with those from non-extracted (calculated) samples and samples extracted without any matrix present.   Recoveries were evaluated across the concentration range. "Sample/Calculated" recoveries were calculated by dividing the average quantified peak area of thalidomide from duplicate injections for five extracted samples by the average quantified peak area from duplicate injections for five "calculated" samples. "Sample/No matrix" recoveries were calculated by dividing the average quantified peak area of thalidomide from duplicate injections for five extracted samples by the average quantified peak area from duplicate injections for five samples extracted without matrix (serum/citrate) in the extraction tube.

Recoveries for thalidomide drugs were generally good, with lower concentration levels showing a higher level of inaccuracy. Results are given in Table 5-20.

Table 5-20: Thalidomide intra assay recovery in serum

Serum Conc. (µg/mL)	Sample/Calculated		Sample/No Matrix	
	Mean % Recovery	% R.S.D.	Mean % Recovery	% R.S.D.
20	108.4	6.7	93.1	6.7
10	119.3	4.1	99.2	4.1
5	113.4	4.8	97.7	4.8
1	109.5	4.5	98.8	4.5
0.5	120.3	4.9	97.9	4.9
0.1	120.0	5.1	93.5	5.1
0.05	126.4	3.4	95.1	3.4

(n=5)

The average recovery across the concentration range when the extracted sample is compared to the calculated recovery sample was 117%.

The average recovery across the concentration range when the extracted sample is compared to the no matrix recovery sample was 96%.

5.4.1.4.   Stability

The stability of thalidomide in serum has been described previously [247, 273, 278, 282] highlighting the importance of prompt storage of acidified thalidomide below - 20°C. Upon arrival in the lab, all samples were processed promptly, acidified with 25mM citrate buffer, pH 1.5 and stored at -80°C, as described in Section 2.2.6.1.

The stability of thalidomide in serum was analysed over four freeze-thaw cycles at concentrations of 20, 5, 0.5, 0.05µg/mL of serum. On day 0, triplicate standards were extracted and the remaining samples were frozen at -20°C. The standards were then thawed and extracted and refrozen each day for a further four days. Samples were stored with and without citrate to examine the effect of citrate on sample stability. In samples without citrate, water was added to the serum for equate for equivalence in volumes.

Samples were assessed on the thalidomide peak area and samples extracted on Day 0 with citrate present were taken as 100%. The results are given in Table 5-21and Table 5-22. As expected, the samples without buffer degraded faster that the samples with buffer.

Table 5-21: Thalidomide stability in serum, stored with citrate

Thalidomide Serum Stability – with citrate buffer										
	Day 0		Day 1		Day 2		Day 3		Day 4	
Serum Conc. µg/mL	% Recovery	% R.S.D.	% Recovery	% R.S.D.	% Recovery	% R.S.D.	% Recovery	% R.S.D.	% Recovery	% R.S.D.
20	100	8.6	100	8.6	80	26.0	87	5.4	74[+]	11.3
5	100	5.9	102	10.1	101[+]	14.7	90	12.4	73	10.5
0.5	100	7.6	94[+]	10.8	93	7.7	92	5.1	73[+]	8.3
0.05	100	9.0	92	19.5	94	7.3	92	7.2	68[+]	15.2

Table 5-21 details the recovery of thalidomide in serum samples following four freeze/thaw cycles. All spiked serum samples were stored 1/1 (v/v) with citrate buffer. The data is the average of duplicate injections of triplicate samples (n=3, [+]n= 2)

Table 5-22: Thalidomide stability in serum, stored without citrate

Serum Conc.	Day 0		Day 1		Day 2		Day 3		Day 4	
Thalidomide Serum Stability – without citrate buffer										
μg/mL	% Recovery	% R.S.D.	% Recovery	% R.S.D.	% Recovery	% R.S.D.	% Recovery	% R.S.D.	% Recovery	% R.S.D.
20	93	9.2	90	4.7	78[+]	4.9	75[+]	9.7	74	12.6
5	93	6.7	86	10.6	74	9.8	72	5.9	91	8.8
0.5	94	8.3	90	7.4	77	7.6	72[+]	7.9	88	10.1
0.05	89	8.5	90	10.3	70[+]	9.3	73	7.2	92	11.6

Table 5-22 details the recovery of thalidomide in serum samples following four freeze/thaw cycles. All serum samples were stored spiked with thalidomide with no citrate buffer added. The data shown is the average of duplicate injections of triplicate samples (n=3, +n= 2)

The effect of the sample storage conditions was also examined on patient samples. Patient serum was processed as described in Section 2.2.6.1. In addition to storing samples with the 25mM citrate buffer at -80°C, a serum aliquot was stored with citrate at -20°C as well as without citrate buffer at -80°C and -20°C. Samples were stored for 40 days prior to analysis. Figure 5-32 graphically demonstrates the effect of storage conditions on thalidomide stability. The samples at -80°C and stored in citrate were more stable than those stored at -20°C. The citrate buffer clearly stabilises the agent.

Table 5-23 shows the p-values, as calculated using student's t-test, for the significance of loss of thalidomide between the standard storage conditions and the assayed conditions.

Figure 5-32: Effect of storage conditions on sample stability

Effect of storage conditions on sample stability
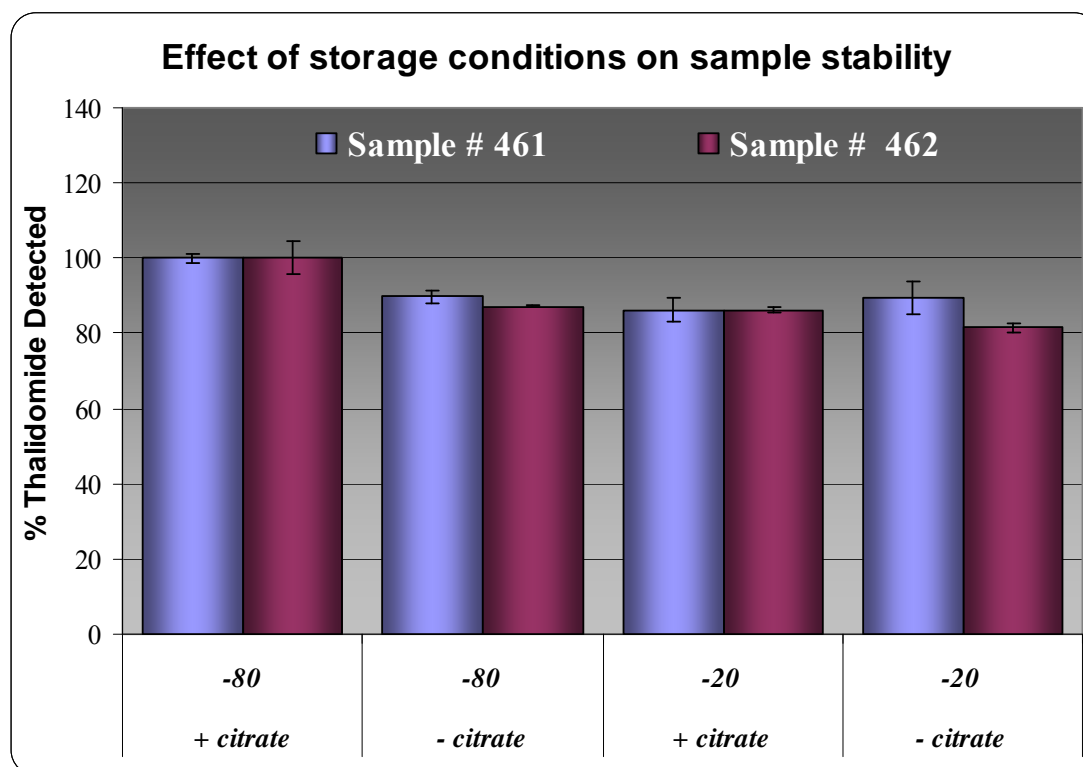
The effect of altering the storage conditions on the stability of thalidomide, in two patient samples. The standard storage condition (with citrate @ -80°C) was assessed as 100% and the other samples were assessed as a function of the standard.

Table 5-23: Effect of storage conditions on sample stability

Storage Conditions	Sample # 461			Sample # 462		
	% Thalidomide	% R.S.D.	p-value	% Thalidomide	% R.S.D.	p-value
+ citrate, -80°C	100.0	1.3		100.0	4.3	
- citrate, -80°C	89.7	1.7	0.00004	87.1	0.3	0.00515
+ citrate, -20°C	86.1	3.7	0.00054	86.1	0.9	0.00301
- citrate, -20°C	89.4	4.7	0.00649	81.6	1.6	0.00104

The standard storage condition (with citrate @ -80°C) was assessed as 100% and the other samples were assessed as a function of the standard. Significance was calculated using the paired student's t-test, of unequal variance. The p-values were calculated by comparison of each storage condition with "+ citrate -80°C".

5.4.2. Assay validation in cells

5.4.2.1.   Linearity and range

Regression analysis was used to assess the linearity between the peak area ratios (analyte/IS) and the analyte concentration.

The calibration curve for thalidomide was linear over the cell mass range of 0.39ng – 50ng in tube. Based on the validation of thalidomide with umbelliferone as an internal standard and the similarities in extraction potential, umbelliferone at the same concentration was used at as an internal standard. A volume of 50µL of a 600ng/mL stock of internal standard was spiked to each tube, sample and standards. Whilst the calibration curves were linear, over such a broad range, the bias of the regression line tends to make the determination of lower drug concentration values much less accurate; hence it was decided to use a log-log plot of the peak area ratio versus the mass of drug in all calculations.

The log-log plot gave typical correlation coefficients (R^2) values of >0.99.

5.4.2.2.   Precision and accuracy

Intra-day precision and accuracy was assessed over the mass range (0.39ng - 50ng) by extraction and analysis of six spiked samples on the same day, (Table 5-24). Inter-day precision and accuracy was assessed over the mass range (0.39ng - 50ng) by extraction and analysis of triplicate spiked samples over four days, (Table 5-25). The percentage relative standard deviation (%R.S.D.) was employed as a measure of precision. The % accuracy was determined by dividing the average calculated drug concentration by that of the spiked known concentration.

For the intra-day analysis the average accuracy was 100% with an average % R.S.D. of 2.5%.

For the inter-day analysis the average accuracy was 101% with an average % R.S.D. of 1.9%

Table 5-24: Intra-day analysis for precision and accuracy of thalidomide in cells

Spiked Mass (ng)	Mean Mass Observed (ng)	Mean Accuracy Observed (%)	Precision (% R.S.D.)
0.39	0.39	99.9	4.1
0.78	0.79	100.6	4.0
1.56	1.58	100.8	3.3
3.13	3.09	98.9	2.8
6.25	6.24	99.9	1.6
12.5	12.5	100.4	1.8
25	25	100.5	1.2

Intra-day analysis for precision and accuracy, n=6.

Table 5-25: Inter-day analysis for precision and accuracy of thalidomide in cells

Spiked Mass (ng)	Mean Mass Observed (ng)	Mean Accuracy Observed (%)	Precision (% R.S.D.)
0.39	0.40	102.94	4.19
0.78	0.79	101.45	2.35
1.56	1.57	100.61	2.46
3.13	3.11	99.61	1.09
6.25	6.28	100.47	0.69
12.5	12.5	100.30	1.93
25	25	100.76	0.86
50	50	100.76	1.51

Inter-day analysis for precision and accuracy, n=3.

5.4.2.3.   *Recovery/extraction efficiency*

The efficiency of the LLE method was assessed by comparing the peak areas of thalidomide in the extracted analytes with the peak area of thalidomide in non-extracted (calculated) samples and samples extracted without any cells present, prepared as in Section 2.2.5.3. Recoveries were evaluated across the concentration range. "Sample/Calculated" recoveries were calculated by dividing the average quantified peak area of thalidomide of duplicate injections from triplicate extracted samples, by the average quantified peak area from duplicate injections for triplicate "calculated" samples. "Sample/No matrix" recoveries were calculated by dividing the average quantified peak area of thalidomide of duplicate injections for triplicate extracted samples by the average quantified peak area from duplicate injections for triplicate samples extracted without matrix (serum/citrate) in the extraction tube.

Recoveries for thalidomide were generally good. Results are given in Table 5-26.

Table 5-26: Intra-assay recovery of thalidomide in spiked cell samples (n=3)

Spiked Mass (ng)	Sample/Calculated		Sample/No Matrix	
	Mean % Recovery	%R.S.D.	Mean % Recovery	%R.S.D.
50	92.7	5.5	111.8	5.4
5	90.7	3.6	115.1	3.6
0.5	92.1	9.7	118.4	9.7

5.4.3. Selectivity & sensitivity

The limit of detection (LOD) was defined as the mass of drug which gave a signal to noise ratio of 3:1. The limit of quantification (LOQ) was defined as the mass of drug which gave a signal to noise ratio of 5:1[300].

The sensitivity of the assay was monitored against human serum as a matrix. Given the criteria outlined, the LOD for thalidomide was determined to be approximately 0.08ng spiked mass, and the LOQ for thalidomide was determined to be approximately less than 0.3ng and greater that 0.15ng, spiked mass. With a serum volume of 100μL, therefore, the LOQ for the method described here is between 1.5ng/mL and 3ng/mL of serum.

The signal-to-noise ratio was calculated by the Masshunter Quantification Analysis Software (Version B.01.04). Calculations were based on the peak area of thalidomide, not on the peak area ratio.

Table 5-27: Thalidomide, LOD and LOQ

Spiked Mass (ng)	Mean Mass Observed (ng)	Mean Accuracy Observed (%)	Precision (% R.S.D.)	Mean Signal/ Noise
0.313	0.324	104.79	1.99	6
0.156	0.157	99.76	1.22	4
0.078	0.076	96.91	2.78	2

The limit of detection and limit of quantification of thalidomide as assessed in serum extracted samples (n=3).

The selectivity of the assay is increased through the use of MRM transitions for quantification. Assessed through in monitoring of the MRM transition in extracted cell samples there was no detected endogenous interaction for thalidomide, see Section 9 Appendices IV.

The LC-MS method easily resolved thalidomide from umbelliferone from each other and from any background from biological matrices. Due to the high sensitivity of mass spectrometric detection, low background from the liquid-liquid extraction and the specificity imparted when quantifying based on the molecular transitions of the ions in the collision cell (MRM) the method is rapid, sensitive and specific.

The ability to quantify a broad concentration range of thalidomide in two different biological matrices demonstrates the robust nature of LLE and the range of applications of the LC-MS.

5.5. *Method application*

5.5.1. Quantification of thalidomide in patient serum

This method was applied to the quantification of thalidomide levels in the serum of multiple myeloma patients

Thalidomide is administered to multiple myeloma patients at a fixed dose irrespective of age, gender or body weight. Thalidomide dosage is adjusted in response to side effects or as function of patient response. Patients showing no signs of response received increased dosage of thalidomide and patients who show unmanageable side effects have a dose reduction.

Thalidomide has been seen to cause multiple side effects including neuropathy, neutropenia, somnolence and constipation[268].

To examine the application of the developed thalidomide analysis method to the quantification of serum thalidomide levels, serum samples from multiple myeloma patients receiving thalidomide treatment were collected from patients of the Mater Misericordiae University Hospital, Eccles St, Dublin 7 under the care of Dr P O'Gorman by Dr R Rajpal under full ethical approval of the hospital Ethics committee.

The patient cohort comprised ten patients, from whom 22 samples were collected. To combat the side effect of somnolence, patients are advised to take the thalidomide medication before bed. Samples were collected in clinic the following morning and processed as detailed in Section 2.2.6.1.

Table 5-28: Characteristics of the patient cohort

Patient	# of samples	Age	Gender	Serum Conc. (ng/mL)	Dose (mg/day)	Response IMW[22]	Neuropathy NCI criteria[23]	Other side effects
				164	100		Grade 3	constipation, tiredness and low energy, pins and needle sensation
				63	50		Grade 2	low energy and tiredness marginally better
A	3	79	Female	27	50	VGPR	Grade 2	TIA[24], constipation, tiredness and low energy
				1082	200		Grade 1	Pins and needle sensation, Tiredness and low energy
				25	200		Grade 0	Pins and needle sensation improved, Tiredness and low energy
B	3	64	Male	1095	200	VGPR	Grade 0	mild Pins and needle sensation ,Tiredness and low energy
C	1	81	Male	209	100	PR	Grade 2	Neutropenic sepsis, Anaemia. Thrombocytopenia

[22] IMW – Based on International Myeloma Workshop criteria
[23] NCI – Based on National Cancer Institute
[24] TIA - transient ischemic attack

Patient	# of samples	Age	Gender	Serum Conc. (ng/mL)	Dose (mg/day)	Response IMW[22]	Neuropathy NCI criteria[23]	Other side effects
D	2	68	Male	ND	200	PR	Grade 3 (? Diabetic)	DVT, constipation, low energy , Diabetic neuropathy
				755	300			DVT, constipation, low energy , Diabetic neuropathy
E	2	59	Male	498	150[25]	PD	Grade 2	Low energy, Constipation, Ankle oedema
				1407	200			Severe low energy, constipation, Ankle oedema, skin rash
F	1	77	Male	330	150[26]	PR	Grade 2 – Grade 3	Numbness in fingers, low energy and tiredness
G	6	71	Male	454	150	VGPR	Grade 2	Skin rash, Peripheral Oedema, constipation
				781	200			Skin rash improved , Peripheral Oedema improved
				573	150			Mild skin rash , Tiredness
				479	150			Tiredness and low energy

[25] Patient switched from lenalidomide treatment to thalidomide
[26] Patient switched from thalidomide treatment to lenalidomide treatment

351

Patient	# of samples	Age	Gender	Serum Conc. (ng/mL)	Dose (mg/day)	Response IMW[22]	Neuropathy NCI criteria[23]	Other side effects
				405	150			Tiredness and low energy
				634	100			Tiredness and low energy
				550	150			Low energy constipation
H	2	58	Male	198	100	PD	Grade 1	Low energy constipation
I	1	60	Female	182	100	PR	Grade 1	Tiredness and low energy
J	1	57	Male	ND	50	VGPR	Grade 1	Nil

Table 5-28 details the patient cohort characteristics, including the detected serum concentrations, dose received, patient response and adverse effects experienced.

Abbreviations:

ND - non-detected

TIA –transient ischaemic attack

PR – partial response

VGPR - very good partial response

PD – progressive disease

DVT – deep vein thrombosis

The adverse effects reported by the patients varied from day to day. Given here is a representation of the range of side effects experienced by the patient and reported by the patient/clinician.

The International Myeloma Workshop established uniform criteria for the reporting of response in multiple myeloma[383]. CR is complete response, PR is partial response, VGPR is very good partial response, PD is progressive disease.

Thalidomide-related neuropathy was evaluated by the clinician and classified based on National Cancer Institute Common Toxicity Criteria, version 2.0[384]. Grading is as follows: Grade 0 - Normal, Grade 1 - Loss of deep tendon reflexes or paraesthesia (including tingling and numbness) but not interfering with function, Grade 2 - objective sensory loss or paraesthesia (including tingling) interfering with function but not interfering with activities of daily living and activities. Grade 3 - Sensory loss or paraesthesia interfering with activities of daily living, Grade 4 - Permanent sensory loss that interferes with function. Assessment of neuropathy was evaluated by the clinician at point of care and correlated with time of blood sampling.

The level of thalidomide quantified in all patients is shown in Figure 5-33. Two patient samples "H" and "J" are excluded from this graph due to unclear information regarding the patient starting date.

Figure 5-33: Thalidomide levels in all patients
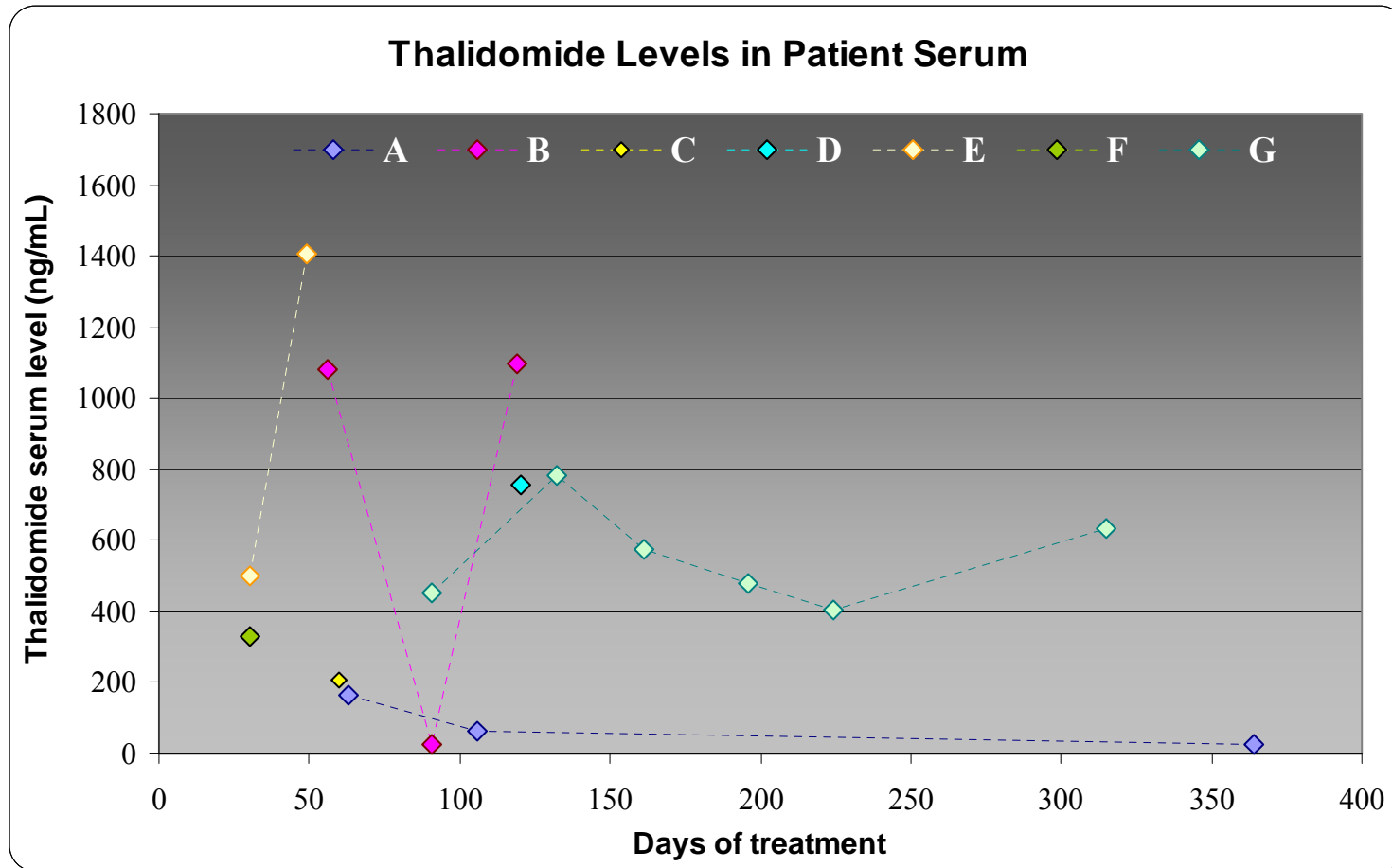
Figure 5-33 shows the thalidomide serum concentration of all patients as a function of duration of treatment

However, this does not take into account the dose of thalidomide which the patients were receiving, nor does it examine the neuropathy experienced by the patients.

There is a general correlation between patient dose and detected serum concentration is examined. Figure 5-34 shows this correlation ignoring any patient specific factors. There is a level of linearity between dose and detected serum concentration however; in general, the patients' serum level of thalidomide is not predictable from the administered dose. One sample, marked on the graph, clearly shows to be lying outside the trend. This sample, from patient B, is suspected to have been taken after a missed dose. This is discussed later.

Figure 5-34: Thalidomide levels in all patients in comparison to dosage
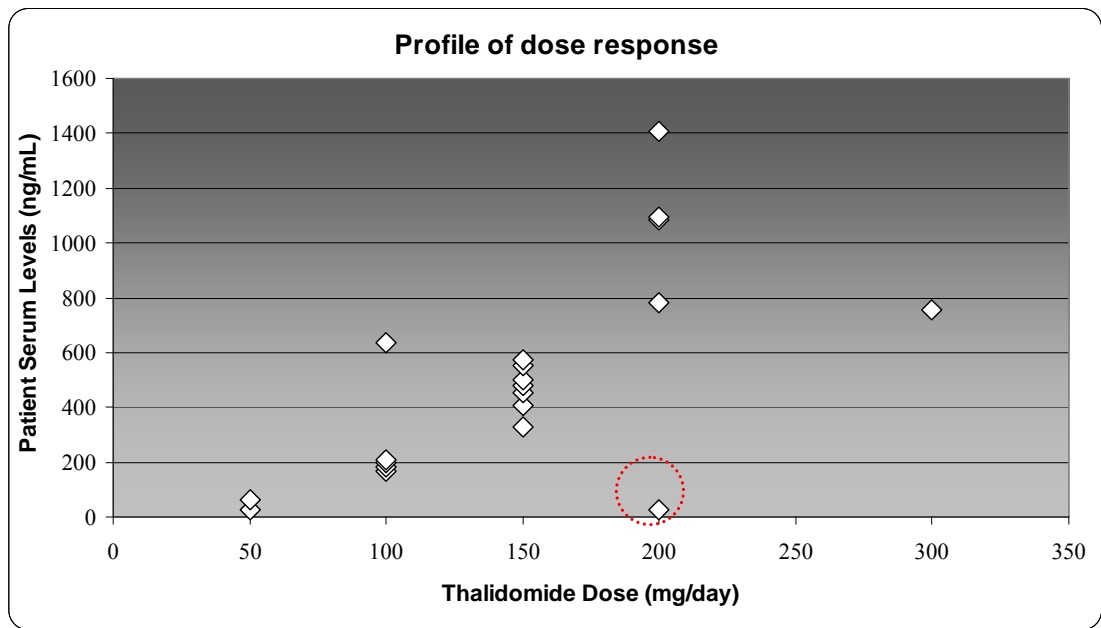
Figure 5-34 shows the thalidomide serum concentration of all patients as a function dose received.

Figure 5-35 attempts to show the correlation between the neuropathy experienced, the serum levels detected and the patient dose per sample time-point. The majority of patients cluster at Grade 2 neuropathy.

However, as neuropathy is also dependant on the duration of treatment with thalidomide the data was re-plotted to examine any correlations between the duration of treatment, neuropathy grade evaluated and dose administered, Figure 5-36.

Figure 5-35: Thalidomide levels in all patients in comparison to dose and neuropathy
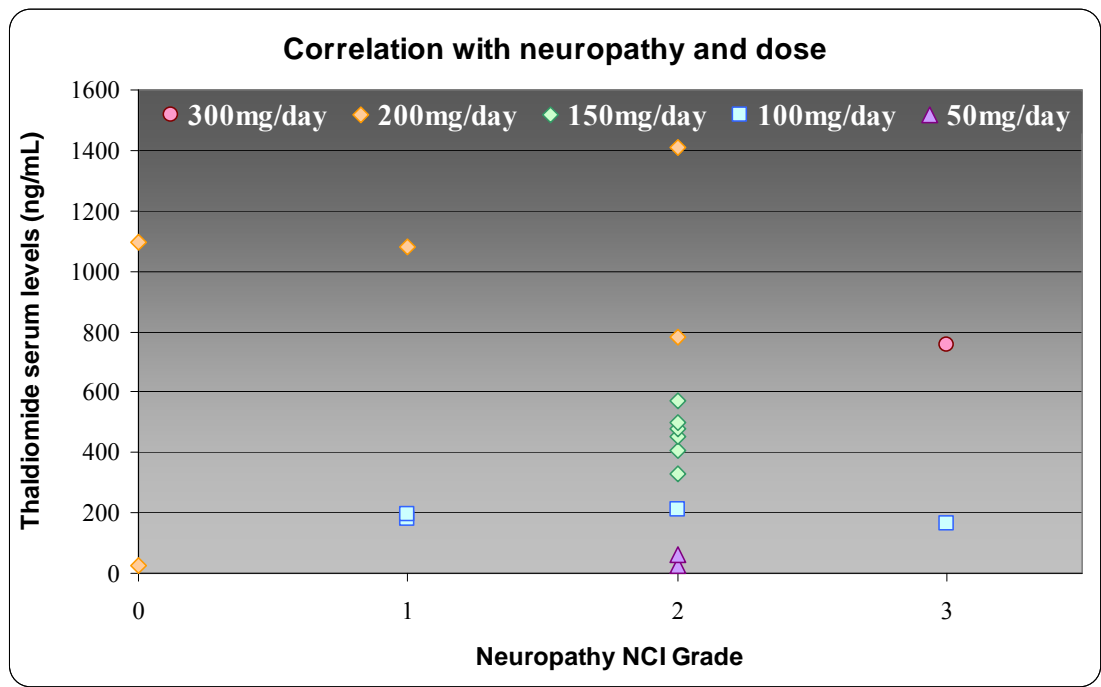
Figure 5-35 shows the relationship between neuropathy, serum levels and patient dose.

Figure 5-36: Neuropathy levels in all patients in comparison to dose and duration of treatment
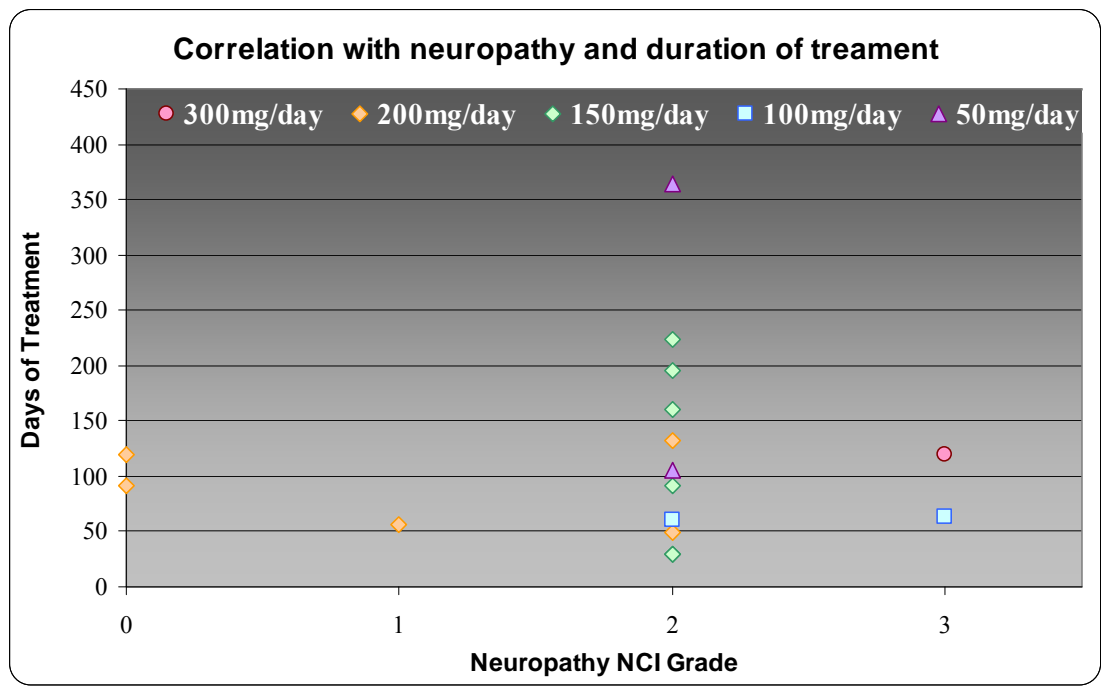
Figure 5-36 shows the relationship between neuropathy, duration of thalidomide treatment and patient dose.

Patient A is 79 year old female patient who initial dosage of 100mg/day was reduced to 50mg/day. The dose reduction showed a simultaneously serum level reduction. Figure 5-37 shows the comparison of the serum concentration in comparison to dosage level.

A reduction in the thalidomide dosage was linked to an improvement in the neuropathy level, assessed under the NCI criteria, from Grade 3 neuropathy to Grade 2 neuropathy. A marginal improvement was also noted in level of tiredness and low energy reported.

Figure 5-37: Profile of the serum levels in patient "A"
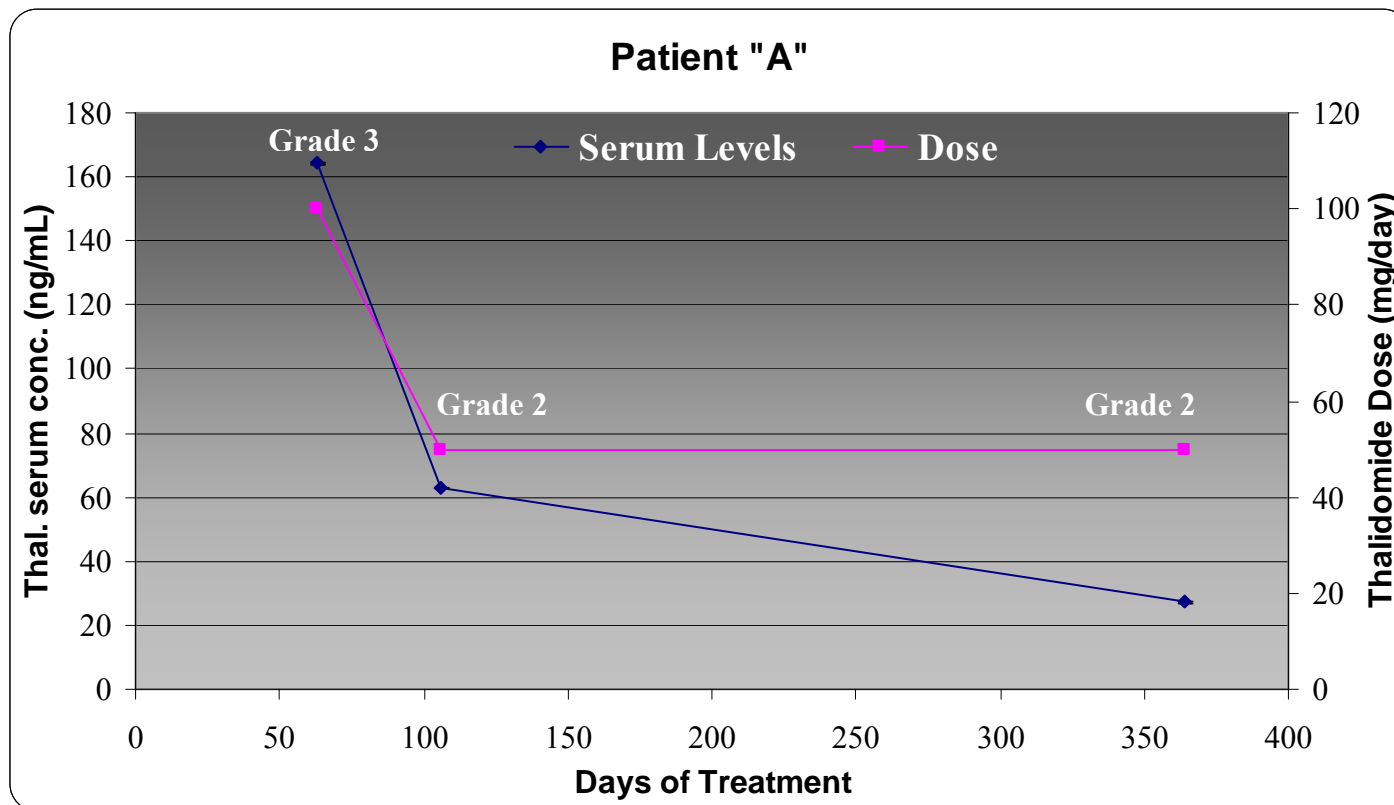
Figure 5-37 shows the comparison of serum levels over time with thalidomide prescribed dose over time. The pink line indicates the thalidomide dosage while the blue line is the quantified concentration of thalidomide in the patient serum. The neuropathy grade is indicated at each data point. Serum level quantification was the average of two aliquots of sample and the standard deviations.

Three samples were collected for Patient "B". Patient "B" is a 74 year old male, who was prescribed a consistent dosage of 200mg/day. Figure 5-38 shows the serum levels for patient "B" in comparison to the prescribed thalidomide dose.

The side effects suffered by patient "B" were tiredness and low energy and pins and needles sensation. The pins and needles sensation improved at the second time point and mild pins and needle sensation were reported at the third time point. Neuropathy levels of grade 1 to grade 0 were recorded at the time of consultation and blood sampling.

The data point at 91 days, 25ng/mL, indicates that the patient may have missed one or more doses immediately prior to the blood sample being taken.

Figure 5-38: Profile of the serum levels in patient "B"

Figure 5-38 shows the comparison of serum levels over time with thalidomide prescribed dose over time. Serum level quantification was the average of two aliquots of sample and the standard deviations. The pink line indicates the thalidomide dosage while the blue line is the quantified concentration of thalidomide in the patient serum. The neuropathy grade is indicated at each data point.

Two samples were collected from patient "E". Patient "E" is a 59 year old male, who was prescribed a 150mg/day which was increased to 200mg/day

Figure 5-39 shows the serum levels for patient "E" in comparison to the prescribed thalidomide dose.

Patient E was switched from lenalidomide to thalidomide and was reported to be a non-responder to Velcade treatment. The side effects noted in the case of patient "E" were low energy, constipation and ankle oedema. The increased dosage of thalidomide prescribed corresponded with severe low energy. Neuropathy levels of were consistently recorded as grade 2.

Figure 5-39: Profile of the serum levels in patient "E"

Figure 5-39 shows the comparison of serum levels over time with thalidomide prescribed dose over time. Serum level quantification was the average of two aliquots of sample and the standard deviations. The pink line indicates the thalidomide dosage while the blue line is the quantified concentration of thalidomide in the patient serum.

Six samples were collected from patient "G". Patient "G" is a 71 year old male, who was prescribed a dosage of 150mg/day, which was increased to 200mg/day and then reduced to 150mg/day. The final recorded dose was 100mg/day.

Figure 5-39 shows the serum levels for patient "G" in comparison to the prescribed thalidomide dose.

Patient G suffered from skin rash, peripheral oedema, and constipation. The skin rash improved to a mild rash, the peripheral oedema improved and tiredness and low energy were reported. Neuropathy levels of were consistently recorded as grade 2.

Figure 5-40: Profile of the serum levels in patient "G"

Figure 5-40 shows the comparison of serum levels over time with thalidomide prescribed dose over time. Serum level quantification was the average of two aliquots of sample and the standard deviations. The pink line indicates the thalidomide dosage while the blue line is the quantified concentration of thalidomide in the patient serum.

Two samples were collected from patient "H". Patient "H" is a 58 year old male, who was prescribed a dosage of 150mg/day, which was decreased to 100mg/day. Figure 5-41 shows the serum levels for patient "H" in comparison to the prescribed thalidomide dose.

Patient H suffered from side effects of low energy and constipation. Neuropathy levels are assessed as Grade 1. However, Patient H did not respond to thalidomide treatment with IMW criteria classified as PD, progressive disease.

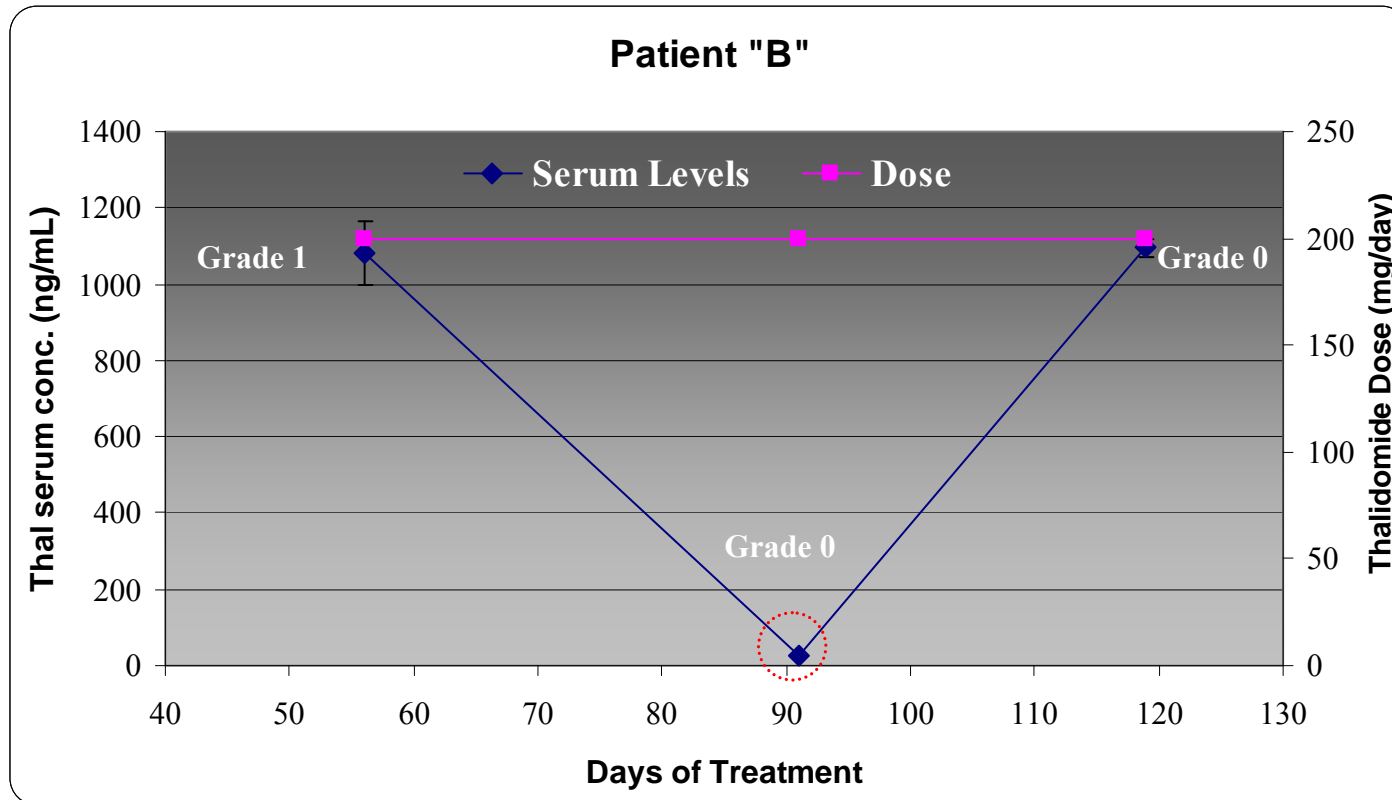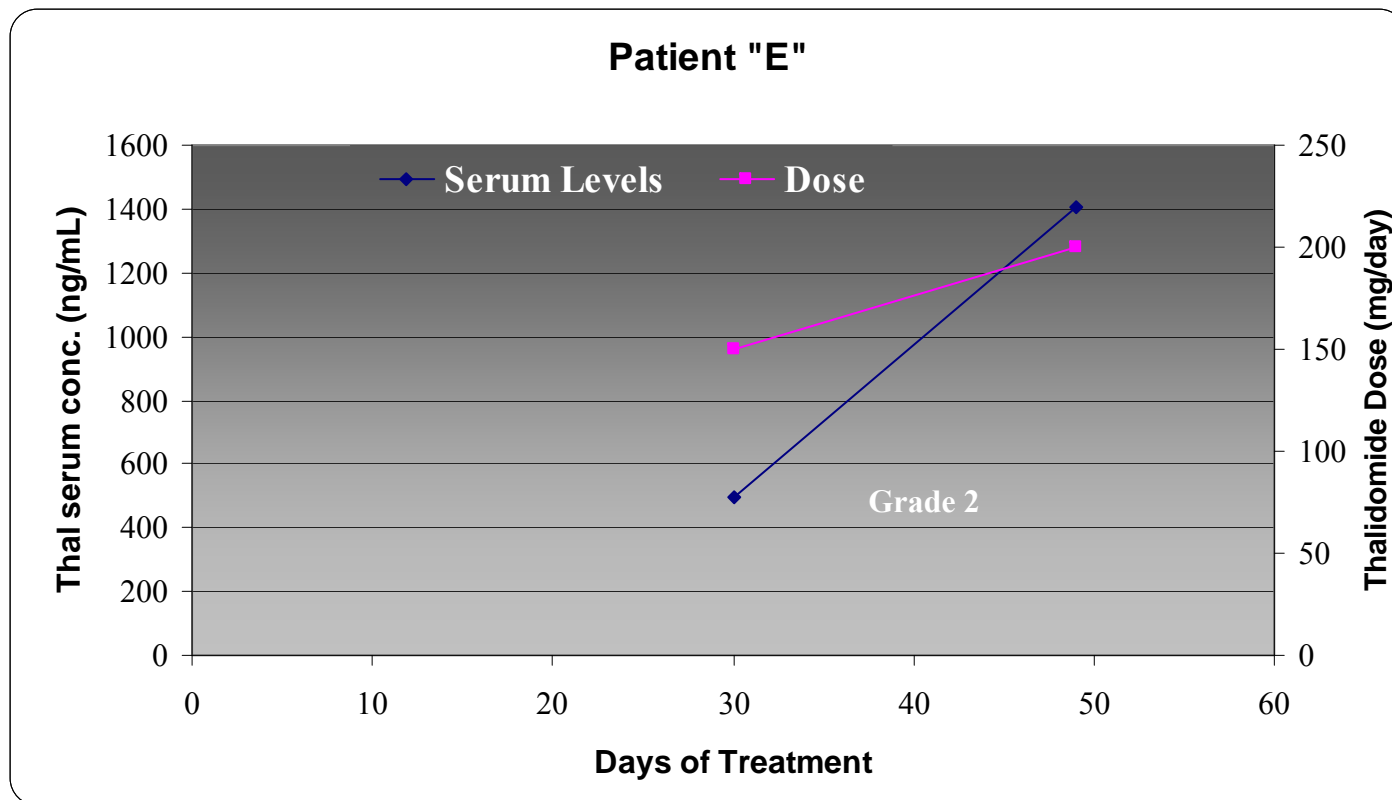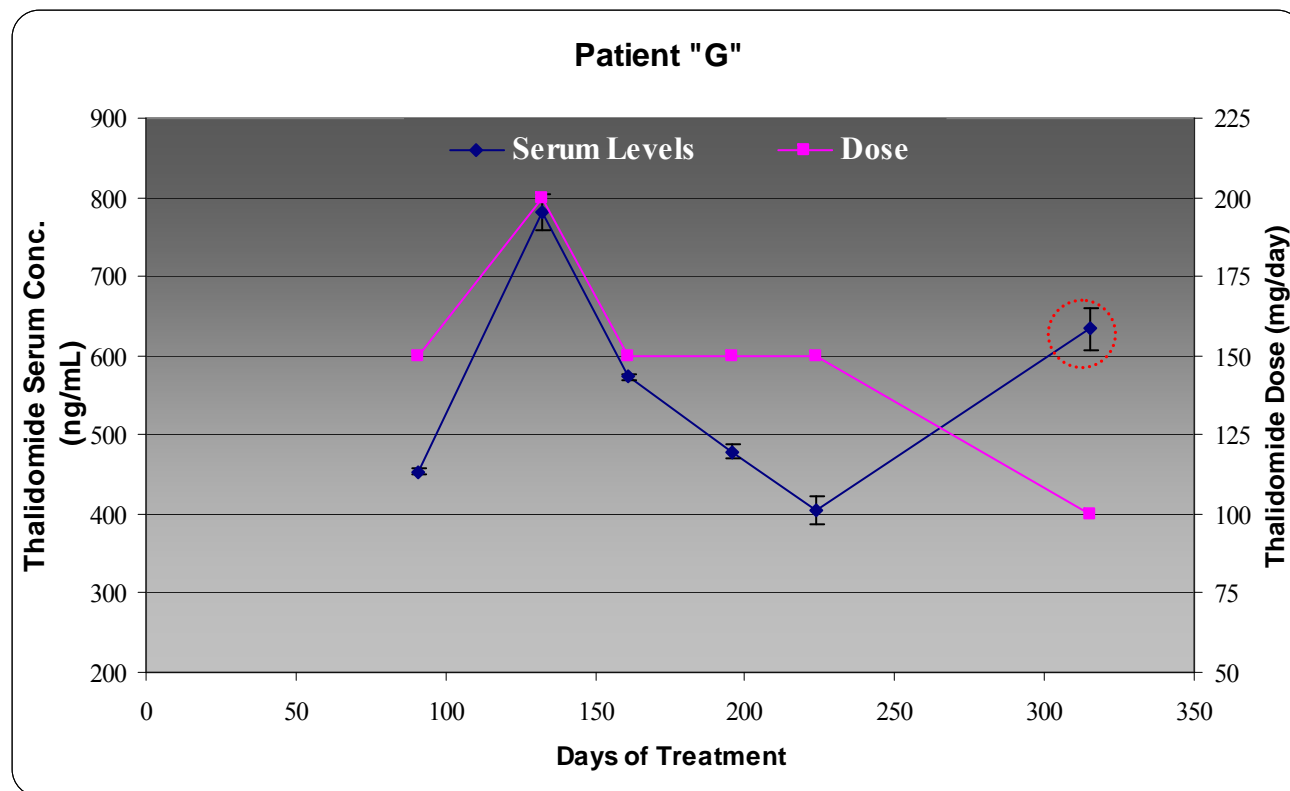**Figure 5-41: Profile of the serum levels in patient "H"**
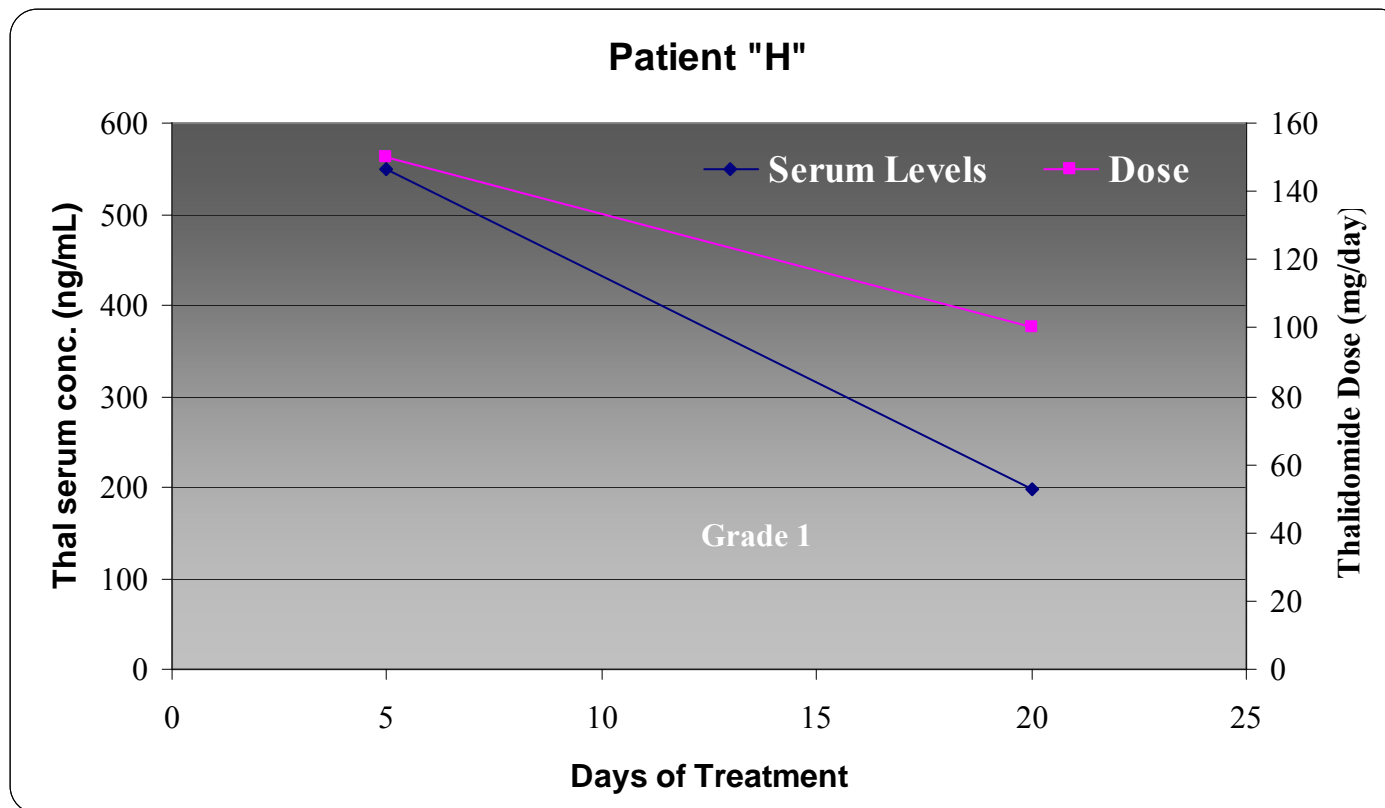
Figure 5-41 shows the comparison of serum levels over time with thalidomide prescribed dose over time. Serum level quantification was the average of two aliquots of sample and the standard deviations. The pink line indicates the thalidomide dosage while the blue line is the quantified concentration of thalidomide in the patient serum.

5.5.2. Quantification of thalidomide in cells

The pharmacokinetic evaluation of thalidomide in cell culture models has not, to our knowledge, been reported previously. Zhou *et al.*[278], describes a method of the quantification of thalidomide in Hank's balanced salt solution (HBSS), a transport buffer for the cell line, Caco-2. For this thesis, the accumulation and efflux of 2μM thalidomide in the cell-line models, DLKP and DLKP-A, was assessed over two hours, with samples taken at 15 minutes, 30 minutes, 1 hour and 2 hours. Each sample was assessed in triplicate flask.

Eight samples (flasks) out 116 samples (flasks) had detectable levels of thalidomide. Of these estimates, none were repeatable within a triplicate set.

Given the low and irreproducible levels of thalidomide found in the cell samples the stability of thalidomide in cell culture media was assessed. A solution of 2μM thalidomide was prepared in media and in HBSS and was incubated at 37°C for 24 hours. Two stocks of thalidomide were assessed one (old) was stored for 47 days at 4°C while the other (new) was prepared fresh on the day. An aliquot (100μL) was removed and immediately mixed with citrate and stored at -20°C. The results are given in Figure 5-42.

The data indicates that thalidomide is reasonably stable in DMSO at 4°C as there is minimal difference in the mass detected in the old and the new thalidomide samples. The rate of breakdown of thalidomide is faster in HBSS than in cell culture media, however, 50% of the thalidomide had degraded within 4 hours in media at 37°C. Only thalidomide in media had any quantifiable drug remaining at the 20hr and 24hr sampling time-points.

Thalidomide Stability in Media and HBSS
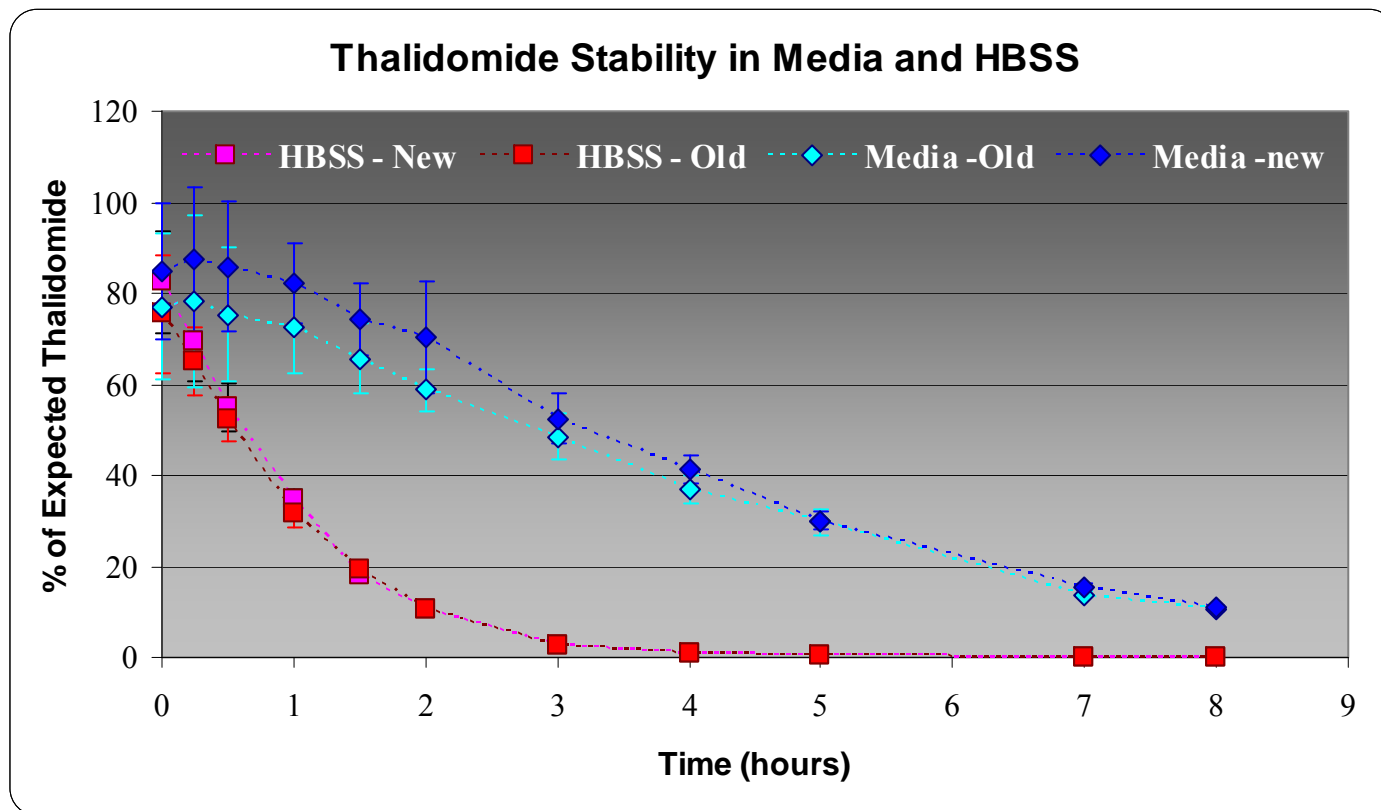
Figure 5-42 details the stability of thalidomide, fresh and 47 day old stock in HBSS and cell culture media. The data shown is the average of triplicate aliquots and their standard deviations normalised to the expected mass (50ng).

5.6. Discussion

5.6.1. Method development

The objective of this part of the research was to develop a separation and extraction method for the quantification of thalidomide in patient serum.

5.6.1.1.   Internal standard and column selection

The initial obvious choice of internal standard for thalidomide analysis was lenalidomide. Lenalidomide is a more recently developed analogue of thalidomide with similar chemistry and therefore should theoretically make a good internal standard[315]. The use of lenalidomide as an internal standard for thalidomide analysis was investigated as an efficient way of developing a method for determination of both multiple myeloma agents simultaneously. A quantification method for the analysis of lenalidomide in serum which mentions within the article that thalidomide was unsuccessful as an internal standard for lenalidomide due to poor peak shapes alone[381]. Based on this the separation of thalidomide and lenalidomide was examined. Teo *et al.*[273], used acetic acid as a mobile phase modifier, however, our initially analysis with acetic acid in the mobile phase demonstrated that this reagent was unusable due to high background in the MS detector. Using formic acid to acidify the mobile phase simplified the mobile phase preparation, reducing the possibility for mobile phase contamination and gave consistent, clean chromatograms[311].

The first column optimised for the separation of thalidomide and lenalidomide was a YMC 50mmx 2.0mm, 2µm particle size C18 column. Separation was achieved with gradient elution as outlined in Table 5-2. Baseline separation of both lenalidomide and thalidomide was achieved, with both peaks having good peak shape and the complete run-time, including re-equilibration time, was only 9 minutes. However, a maximum injection volume of 5µL was possible as peak fronting was observed with increased injection volumes. Peak fronting is usually the result of column overloading[320].

The Prodigy (150mmx4.6mm, 5µm particle size) column was also investigated. The aim was to gain baseline separation of thalidomide and lenalidomide with isocratic

flow. The use of isocratic flow is preferable when using compounds of a different chemical make-up as internal standards for each other as with isocratic flow conditions remain constant throughout the analysis. By keeping the mobile phase constant, the ionisation of each analyte remains constant and the peak area ratio of analyte to internal standard is robust. A binary mobile phase of 50% (v/v) ACN/water 0.1% formic acid gave good and repeatable separation, Figure 5-5. An injection volume of 20μL gave an acceptable peak shape, Figure5-6. An injection volume of 10μL did show excellent peak shape, however, this is too small an injection volume for our purposes. During the liquid-liquid extraction process the analyte-containing organic solvent layer is removed and transferred to a 1.1mL conical LC vial. The sample is evaporated in this vial and reconstituted for injection onto the LC in this vial. This reduces the error associated with transferring vials and increased level of sample handling. However, as the volume of the vial is 1.1mL a sufficient reconstitution volume is required to ensure complete reconstitution of the sample. To avoid loss of sensitivity it is desirable to inject a maximum possible quotient of the reconstituted sample.

Good separation of thalidomide and lenalidomide was achieved with isocratic elution and 20μL injection. This is contradictory to the finding of Tohyna et al., who reported that thalidomide was unsuitable as an internal standard for lenalidomide due to poor separation[381]. However, examination of the extraction of lenalidomide and thalidomide showed that lenalidomide was not a suitable internal standard for thalidomide. Lenalidomide showed poor recovery across all solvents ranges. Recoveries below 40% were consistently seen on inter-day analysis. Whether this low recovery for lenalidomide resulted from extraction potential or poor solubility when samples were reconstituted has thus far been unconfirmed. An alternative internal standard was sought.

Umbelliferone has previously been used as an internal standard for lenalidomide[381]. Given that in this publication the authors also tried thalidomide as an internal standard for lenalidomide and reported no issues with the extraction potential, umbelliferone was investigated as an internal standard for thalidomide. The most commonly used internal standard for the quantification of thalidomide in the literature is phenacetin.

Though deuterated standards are also commonly used in the quantification of analytes in bio-analytical chemistry, their cost frequently makes them prohibitively expensive. The use of deuterated internal standards are not always the best option for routine analysis[315].

Umbelliferone is cheap, easily available compound which is less toxic than phenacetin, the most commonly used internal standard for thalidomide.

Several separation columns were tested, four reverse-phase C18 and one phenyl column. Two of the columns investigated Agilent XBD C18 (4.6 x 50mm, 1.8μm particle size) and Phenomenex Prodigy C18 (150 x 4.6mm, 5μm particle size) gave good separation as shown in Figure 5-7 and Figure 5-11 respectively. The Prodigy (150 x 4.6mm, 5μm particle size) was selected as the most appropriate column for this method as the capability to inject the proportionally larger volume of 20μL, compared to 5μL was of particular importance. As described above an injection volume is subject to the reconstitution volume. An injection volume of 20μL was more suitable to the requirements of the method. With the exception of methods where the focus has been to separate the enantiomers of thalidomide[272, 275] all published methods shows thalidomide separation from the internal standard on a reverse phase C18 column. All reverse phase columns reported to be used in the quantification of thalidomide (except one[273]) were developed using column 125mm long or greater[276-278], details given Table 1-8. Additionally, it is interesting to note that most methods report and optimised mobile phase composition of low (<40%) organic modifier composition. This is similar to the optimised mobile phase composition described here.

The Prodigy (150 x 4.6mm, 5μm particle size) was the bests of all the columns examined for the quantification of thalidomide. It was able to separation thalidomide and umbelliferone easily from each other and from any confounding biological artefacts. Base-line separation was achieved with good resolution. A suitable injected volume for the extraction procedure was accommodated.

5.6.1.2.   *MRM conditions optimisation*

The routine method for the determination of all the MRM conditions (precursor ion, fragmentation voltage, product ion and collision energy) is through the using of flow injection analysis (FIA). However, the precursor ion for thalidomide initially proved difficult to identify. This led to the necessary utilisation of direct infusion to identify the precursor ion. The use of a direct infusion pump allows of an instantaneous response i.e. increasing the pressure of the infusion results in a chromatogram spike. The predominant molecular ions of a particular mass can then be with certainty concluded to be present in the infusion. This led the mass of precursor ion to be conclusive determination for thalidomide to be 259.1m/z which is the protonated molecular ion $[M+H]^+$. The precursor ion was reconfirmed by FIA and the remaining criteria were identified by FIA. The MRM conditions for umbelliferone, lenalidomide and bortezomib were also characterised entirely by FIA.

As previously discussed in Section 3.9.2 the use of MRM monitoring for the detection and quantification of analytes of interest gives increased specificity and selectivity compared to single reaction monitoring (SRM). The ability to simultaneously monitor multiple ions means that the most abundant product ion can be used for quantification; any additional product ions detected are monitored as qualifier ions. For thalidomide the qualifier ion, the mass transition of 259.1mz/ →186m/z. This has consistently ratio approximately 95%.

5.6.1.3.   *Extraction conditions optimisation*

The requirement of the extraction process in the bio-analytical setting is to remove the analyte of interest from extraneous substances such as proteins, lipids and salts present in the sample which could interfere with the analysis. Several sample clean-up procedures have be used previously for the extraction of thalidomide from serum including solid phase extraction[273] and protein precipitation[274]. Three recent methods report the use of a liquid-liquid extraction method for sample clean up[275-278], however both the methods by Yang *et al.*[277], and Saccomani *et al.*[276], are adaptations of the modified LLE method developed by Zhou *et al.*[278]. Zhou *et al.*[278], details a sample clean-up procedure where the matrix is removed by the addition of two volumes (compared to the matrix volume) of ice-cold

acetonitrile/methanol (1:1, v/v) containing 2% (v/v) acetic acid to the sample and the supernatant is injected after centrifugation. However, the solvents used here are not water immiscible, thus not a true liquid-liquid extraction.

The liquid-liquid extraction method for the extraction of thalidomide described here was developed from first principles by identifying the optimum solvent extraction system. The objective is to confine the sample matrix away from the immiscible analyte-containing organic solvent. A variety of immiscible solvents and mixtures with acetonitrile were examined, Table 5-14. The poor extraction recovery of lenalidomide made this agent unsuitable as an internal standard for thalidomide. Some of the solvents did not separate into discrete aqueous and organic layers. Of the eleven solvent systems tested the two which had both the best extraction recovery and the lowest level of technical difficulty were carried forward and assessed further by varying the ratio of immiscible solvent to acetonitrile and examining the effect. Frequently an aqueous buffer is added to an extraction to aid the extraction. In this case the serum is already stored on processing in an aqueous citrate buffer, pH1.5. Ultimately ethyl acetate/acetonitrile (3/1., v/v) was selected as the most appropriate solvent as it gave the best recovery of thalidomide from a mixture of serum/citrate (1/1, v/v), Figure 5-17, and across a concentration range Figure 5-18. While the mixture of choro-1-butane/ACN (4/1, v/v) gave good recovery at when extracting a spiked mass of 20ng, Figure 5-17, the recovery was variable across a concentration range, Figure 5-18. Also the additional cost involved in the disposal of chlorinated solvents makes its use less desirable when alternative options are available.

The extraction and recovery of umbelliferone was also acceptable using ethyl acetate/acetonitrile (3/1., v/v) as the extraction solvent.

5.6.2. Assay validation in serum and cells

Given the sensitivity of the assay for the detection of thalidomide, it was decided to validate the method against two different biological matrices across two different concentration ranges. The details of assay validations are outlined in Section 5.4. According to Huber *et al.,* the validation of an analytical method should be designed to test the suitability of the method for its intended purpose[332]. The intended purpose of this assay is to quantify the level of thalidomide in human serum and to quantify the mass of serum in cell pellets.

The overall LC-MS method was validated for the following performance parameters-linearity and range, intra-day precision (repeatability) and inter-day precision (intermediate precision), accuracy, sensitivity, (LOD and LOQ), recovery and sample stability according to the guidelines described by Ermer[299].

5.6.2.1.   *Selectivity*

As discussed in Section 3.9.6.2, the selectivity of the method is the ability to determine the analyte in a mixture whereas specificity is the ability to determine that the signal is solely the result of that analyte[336, 337]. Through the use of the MRM transition-based quantification it is possible to categorically identify the eluting peaks. The use of multiple transitions in MRM mode adds specificity to the method. All detected transitions for each analyte were monitored. The quantifier ion was the mass transition of 259.1m/z → 84m/z. The qualifier ion was the mass transition of 259.1m/z → 186m/z. The qualifier ratio is ratio of the peak area of the qualifier to the quantifier ion. This is set in quantification method and is one of the parameters analysed during the integration process of the software. In the case of thalidomide, the qualifier ion is approximately 95% of the quantifier ion.

5.6.2.2. *Sensitivity*

The sensitivity of the assay was monitored against human serum as a matrix. Though the method was tested against both cells and serum as a biological matrix the volume of serum present in the method is far greater than the volume of cells. Therefore, the sensitivity of the method using serum as a biological matrix should be far more challenging due to the presence of more interfering compounds.

The increased sensitivity of the LC-MS, due to orthogonal positioning of the ionisation source employed by the Agilent 6410 MS system, gave the ability to quantify in the picogram range. Quantification was based on the mass transitions from precursor to the predominant product ion. In the case of each agent the predominant product ion is marked, see Table 5-17. Teo *et al*.[273], reported the only validated LC-MS/MS method for the quantification of thalidomide in the plasma and semen of HIV patients. The LOQ reported was 5ng/mL. In our method a mass of 0.3ng was spiked into 200µL of sample matrix, which is 100µL of serum, resulted in a S/N ratio of 6, see Table 5-27. Therefore the LOQ for the method described here is between >1.5ng/mL but <3ng/mL of serum. The LOQ was defined as the mass of drug which gave a signal to noise ratio of 5:1[300]. Therefore the method developed here is more sensitive than any previously published method.

The other major advancement in terms of sensitivity of this method compared to those already published is that this method permits the accurate analysis of small sample size. Only Yang *et al*.[277], report a similar sample size but the LOQ for that method was 51.6ng/mL. The average blood sample collected for thalidomide quantification yielded approximately 2-3mL of serum. The requirement only 100µL of serum for accurate quantification of thalidomide serum levels means that either (a) less blood tubes need to be taken from the patients and (b) more information can be gathered from the sample. The ability to minimise the number of blood tubes required from the patient is important in terms of minimising patient discomfort. A blood sample is a snap-shot of a patient at a particular point in his/her treatment. The ability to maximise the information gathered from one sample is to be encouraged. Proteomic analysis of clinical serum samples can result in the determination of relevant bio-markers which may be used as predictors for response or treatment. Advances in

proteome analysis have made it possible to simultaneously identify multiple proteins and their expression changes[361].

5.6.2.3.   *Precision and accuracy*

The precision and accuracy of the method is a mark of the inherent level of error within the method. Precision is a mark of the closeness of the results to each other, while accuracy in a mark of the closeness of the result to the expected value. The precision and accuracy were assessed both on intra-day and inter-day experiments.

The average precision across the concentration range examined was 3% and 1.8% for the intra-day and inter-day analysis respectively in serum. The average precision across the concentration range examined was 2.6% and 1.8% for the intra-day and inter-day analysis respectively in cells. All samples were very close with all samples, intra and inter-day, serum and cells having a precision of <5%.

The average accuracy across the concentration range examined was 103% and 100% for the intra-day and inter-day analysis respectively in serum. The accuracy of the method was 100% and 101% for the intra and inter-day analysis respectively in cells. ICH guidelines for precision and accuracy in bioanalytical method state that the precision at each concentration should not exceed 15% with the exception of the LOQ, which should not exceed 20%[385]. The method described here is clearly significantly precise by these standards.

5.6.2.4.   *Recovery/extraction efficiency*

The extraction efficiency was established by direct comparison of the peak areas of the extracted sample compared to the peak area of a) the pure, unextracted sample calculated to be equivalent to 100% extraction or b) the sample extracted with no matrix in the tube. Overall the average percentage recovery is 106% for serum and 103% for cells. Results are given in more detail in Table 5-20 and Table 5-26. The recoveries were consistent across the concentration ranges examined. This indicates that the extraction method was repeatable and stable both for intra and inter day experiments. This is a higher recovery that obtained by Teo *et al.*[386], who detailed a 69% and 78% recovery of thalidomide in plasma and semen respectively, using SPE

as a sample preparation method for analysis by LC-MS/MS. The most recently published validated (LC-UV) method gave a recovery of >90%   within a concentration range of 0.05-50μg/mL[276]. This would indicate that the efficiency of this extraction method is superior to SPE and that while a protein precipitation method gives reasonable results the concentration range examined was somewhat limited.

5.6.2.5.   *Stability through freeze/thaw*

The stability of thalidomide in serum has been described previously [247, 273, 278, 282] highlighting the importance of prompt storage of acidified thalidomide below -20°C. All samples employed in this project were acidified with 25mM citrate buffer, pH 1.5 and stored at -80°C, as described in Section 2.2.6.1. The assay was validated using human serum as a matrix. This is compliant with the recommendations of Dadgar *et al.*[341], for the validation criteria for stability studies. This is discussed further in Section 3.9.6.5. Table 5-21and Table 5-22 detail the results of freeze thaw stability assay over four days in the presence and absence of citrate buffer. As was expected the freeze/thaw stability of thalidomide in citrate buffer is seen to be greater than in serum alone. For the stability of serum in citrate the stability is greatly reduced with increasing freeze thaw cycles. In "Day1", where the sample has been frozen once and thawed and extracted we see an average of 98% across the concentration range but by Day 4 an average of 73% of the starting agent was present.

Stability analysis was also carried out in patient samples, Figure 5-32. Two samples from different patients on subsequent days were processed and stored with and without buffer, at -80°C and -20°C. Storage of the samples at -20°C with buffer showed a loss of 14% when compared to storage at -80°C with buffer. There was a minimum of a 10% loss of thalidomide by storing the samples at -80°C without buffer. This would indicate that our procedure for storing thalidomide serum samples at -80°C with buffer is the best option. Though other authors have detailed storage at -20°C[277].

5.6.3. Thalidomide quantification in patient serum

Thalidomide, an immunomodulatory, was approved for use in patients of multiple myeloma in May 2006[387]. An initial report published in 1999 showed that thalidomide was an effective treatment in 30–40% of patients with multiple myeloma, both advanced and refractory[257]. In collaboration with Dr P O' Gorman and Dr R Rajpal of the Mater Misericordiae University Hospital, Dublin 7, samples were obtained from patients of multiple myeloma undergoing thalidomide treatment. Table 5-28 gives the details of the patient cohort. From ten patients, ranging in age from 57-81 years, two female and eight male patients, twenty one samples were collected for thalidomide quantification. Two patients were switched from thalidomide to lenalidomide during the course of their treatment. Some patients underwent dose alterations and two samples were definitely from patients who were non-compliant and one sample was from a patient who was potentially non-compliant.

5.6.3.1.   Serum level and dose correlations

The serum level was found to range from 27ng/mL to 1407ng/mL across the patient group with large variations seen between patients (Figure 5-33). The dose range of the patients ranged from 50mg/day to 300mg/day. The quantified serum level of thalidomide in patients was correlated with dose (Figure 5-34) and with dose and neuropathy (Figure 5-35).

The data shows that the dose given broadly correlates with the serum levels and that increasing or decreasing of the patient dose increased or decreased the thalidomide serum levels (Figure 5-37, Figure 5-38, Figure 5-39, Figure 5-40, Figure 5-41). This correlates with previous study which showed that patients on low dose thalidomide (200mg) had a lower C_{max} than patients on higher dose (800mg)[388]. C_{max} is the maximum concentration of the drug observed after administration, also sometimes called "peak" concentration. To the best of our knowledge this in the only study which has shown such a dynamic intra-patient variability of serum concentration at a specific time point. This could possibly be due to patient variability in dosing schedules. As the timing of medication is fully in the control of the patient it is impossible in a real clinic situation to account for this variation. The advice given to patients is to take thalidomide before bed-time, however, for some patients this may

be 7pm while for others it may be 11pm. The large inter-patient variability may in part be due to these timing variables. Another factor determining patient pharmacokinetics is diet as a high fat-containing meal cause minor changes in the C_{max} but increases the time to maximum dose from 3.5/4.3hours to 6 hours in healthy volunteers[389].

Figure 5-43, Figure 5-44 and Figure 5-45 are examples taken from the literature of thalidomide pharmacokinetics profiles. Figure 5-43 from Figg *et al.*[388], shows a study of the pharmacokinetics of thalidomide in elderly prostate cancer patients. The thalidomide level was monitored over a 30 hour period, with samples taken ever hour for the first eight hours. Figure 5-44 from Eriksson *et al.*[247], shows the pharmacokinetic profile of R and S thalidomide enantiomers in two subjects. Figure 5-45 from Saccomanni *et al.*[276], shows the plasma concentration of thalidomide in 12 male subjects affected by hepatocellular carcinoma following singular oral dose administration (200 mg/BW).

Figure 5-43: Plasma concentration versus time curve, from Figg *et al.*[388]

Plasma concentration versus time curves.
(A) Plasma concentration versus time curve (mean +/- SD) for patients in the low-dose group after a single oral dose of 200 mg of thalidomide.

(B) Plasma concentration versus time curve (mean +/- SD) for patients in the high-dose group after a single oral dose of 800 mg of thalidomide.
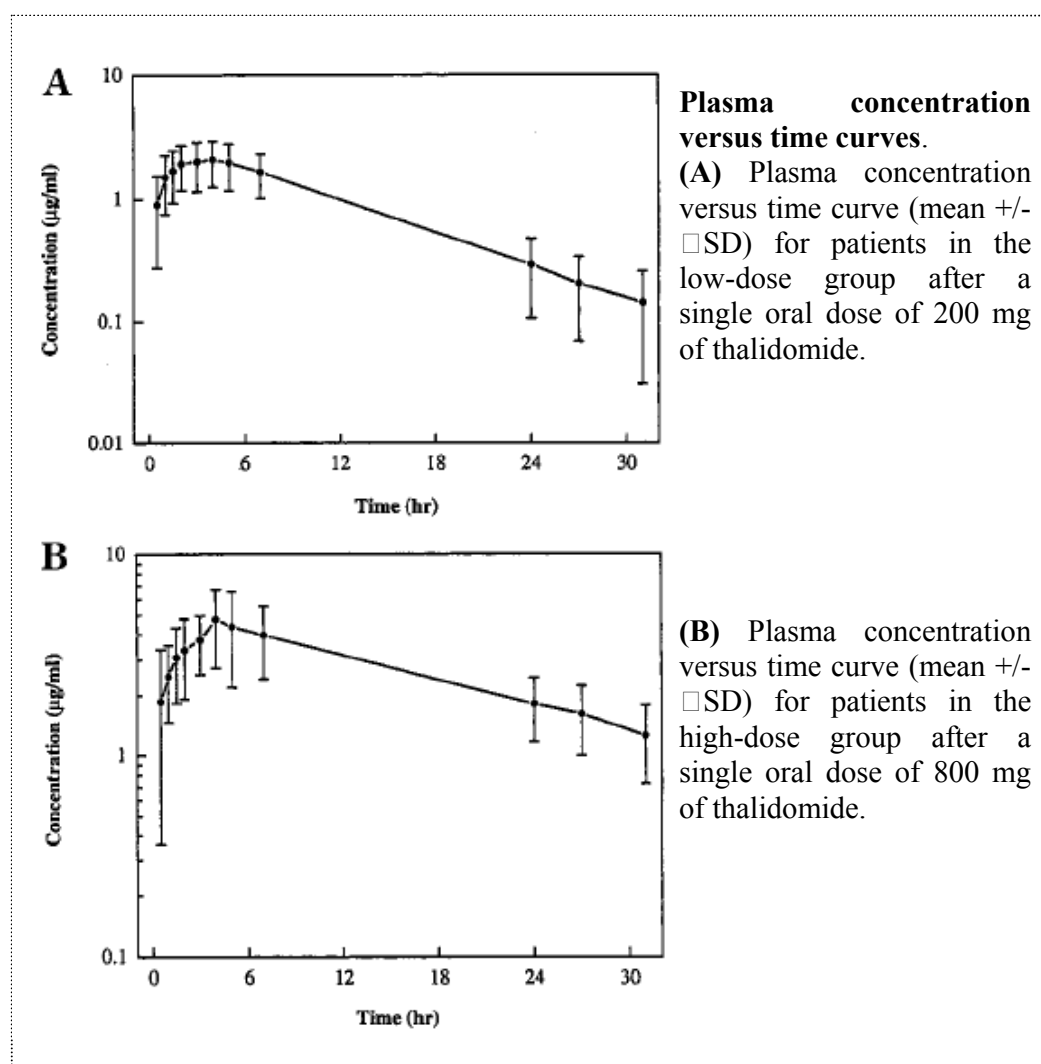
Thalidomide plasma concentration versus time in elderly prostate cancer patients who were administered low (200mg) graph A and high dose (800mg) graph B

Figure 5-44: Blood concentration curves of thalidomide, from Eriksson *et al.*[247]
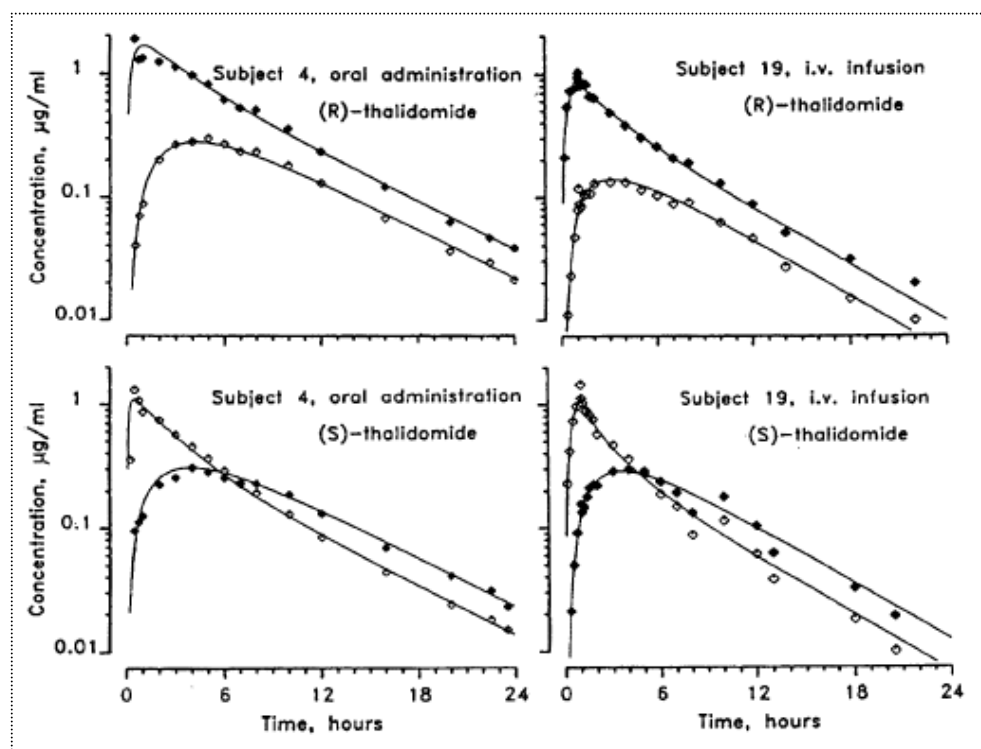
Blood concentration curves observed (R) thalidomide – filled symbols, (S) thalidomide – open symbols and fitted concentration curves after oral (1mg/kg) or intravenous (i.v.50mg of 60 min) administration of the indicated enantiomers to two subjects.

Figure 5-45: Plasma concentration profile of thalidomide, from Saccomanni *et al.*[276]
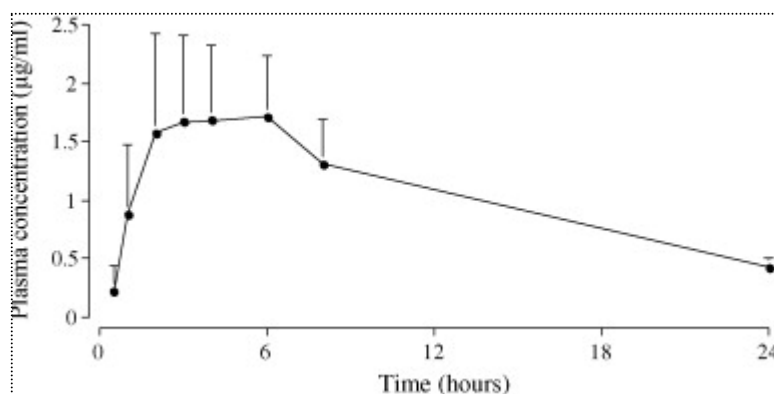
Plasma concentration versus time of thalidomide following singular oral dose administration (200 mg/BW).

5.6.3.2.   *Patient non-compliance*

Non-compliance or non-adherence is described as when a patient had missed some doses, had taken extra doses or had taken doses at the wrong time or the wrong quantity[390]. Non-compliance in oral medication is growing more important with many oral antineoplastic medications approved for use in the US such as cyclophosphamide, capecitabine, temozolomide, as well as the many of the new TKIs agents[391]. Though there is mention of patient adherence with reference to thalidomide in literature published by way of guidelines for oncology nurses, no study, to the best of our knowledge, has study the level of compliance in multiple myeloma patients received oral thalidomide.

Of ten people prescribed thalidomide, two were actually non-compliant and one patient was suspected of being temporarily non-compliant. The two patients (D and J) admitted to having been non-compliant after the results of the analytical study were analysed. One patient (B) is suspected of non compliance, this patient has not admitted or mentioned missing doses, so it quite possible that any lapse in medication was unintentional. The serum level of a fourth patient (G) also raised questions.

Patient B is suspected of being temporarily non-adherent. Of the three blood samples obtained from this patient two showed thalidomide serum levels approx 1000ng/mL (1082 and1095ng/mL) and one samples had a quantifiable thalidomide serum level of 25ng/mL. This is a factor of 40 in the difference. As is shown in Figure 5-38, the patient dose was constant. It is possible that in the case of this patient that a dose may have been missed or the timing of the medication was earlier in the day than normal. The half life of thalidomide is quite rapid. In a study of patients with prostate cancer the median T_{max} was 3.32hrs and 4.40hrs in patients receiving 200mg and 800mg of thalidomide respectively[388]. T_{max} is the time after administration when the maximum concentration of the drug is in the patient blood. This same study evaluated the elimination half-life for thalidomide to be 6.52+/-3.81 and 18.25 +/- 14.08hrs in for 200mg and 800mg thalidomide doses[388]. In our study, monitoring of the elimination rate was not possible, as to do so would have impacted on patient well-being. However, from the literature (Figure 5-43, Figure 5-44, Figure 5-45) that

approximately less than half the C_{max} is present in the patient serum at the time of blood sampling from our study.

Patient J was non-compliant, with no detected thalidomide in the serum sample. In consultation with the clinician after the analysis of the clinical samples the patient admitted non-compliance.

Patient D was initially non-compliant and the lack of disease response led the clinical team to increase the patient's dosage of thalidomide and eventual regime change. The patient dose was increased due to lack of disease response. The patient admitted non-compliance after the serum samples were analysed.

The serum levels for Patient G largely follow the trend of the prescribed dosing regime with the exception of the final sampling point. For the last sampling point assessed the prescribed dose was reduced to 100mg/day to counteract the Grade 2 neuropathy experienced. However the quantified serum concentration for thalidomide for the 6th sampling point is approximately equivalent to previous samples taken when the patient was receiving 200mg/day. It is possible that this patient either took a double dose of thalidomide prior to blood sampling or took his medication closer to the time of blood sample. This patient had not admitted non-compliance and is suspected of so called "over-adherence" to the medication rather than non-compliance.

It is startling that a minimum 3, possibly 4, out of 10 patients investigated had some level of non-compliance demonstrated. Even more so as patients involved in clinical studies are usually more adherent than the normal patient population due to patient selection and increased attention from the clinical staff[390, 392].

5.6.3.3.   *Serum level/neuropathy correlations*

When dose, quantified serum level and neuropathy (graded according to NCI criteria) was correlated we can see that regardless of dose the majority of samples had with Grade 2 neuropathy, Figure 5-35 and Figure 5-36. Neuropathy was evaluated on consultation with the clinician at the time of blood sampling. Two samples were evaluated as Grade 3, one of these patients was receiving 300mg/day and one patient was receiving 100mg/day. As the effect of thalidomide on neuropathy is cumulative over time, you would expect that the patient receiving 100mg/day with Grade 3 neuropathy have been taking thalidomide for an extended period of time. However, from the point of view of cumulative time exposure some samples with lower Grade neuropathy also align time-wise with this sample.

Two samples align with Grade 0 neuropathy; both (from the same patient) were prescribed to receive 200mg/day. However one sample, contained 1407ng/mL thalidomide and one sample had considerably less thalidomide 25ng/mL. Samples were taken approximately one month apart. It was suspected that this patient (Patient B) was partially non-adherent due to the low thalidomide serum concentration, as discussed in Section 5.5.3.2.

Peripheral neuropathy is one of the most serious adverse effects associated with thalidomide treatment. The frequency of Grade 3 and Grade 4 peripheral neuropathy in patients ranges from 3% to 15%[242, 268, 393, 394]. Peripheral neuropathy is normally managed by dose reduction or cessation, depending on the grade of neuropathy. Of the ten patients in our study three experienced Grade 3 neuropathy. However, the serum levels for these patients differed greatly (164ng/mL, 755ng/mL and 330ng/mL). This would suggest that while reduction of dose improves neuropathy, and the neuropathy is dose dependent, there does not appear to be a clear correlation between serious (Grade 3) neuropathy and thalidomide serum level. There is some indication of cumulative effect of thalidomide in that a patient receiving 50mg/mL was evaluated with Grade 2 neuropathy and had been taking thalidomide for over a year. Some authors have suggested a limit of six months should be used for treatment with thalidomide to prevent neuropathy, though this would potentially have a huge impact on treatment and response.

Overall the serum levels quantified here broadly correlate with previously reported studies determining patient serum levels, where for hepatocellular carcinoma patients receiving 200mg/BW had a serum level of approximately 1000ng/mL after 12 hours[276]. Also in a study of the pharmacokinetics of thalidomide in multiple myeloma patients who received 200mg the thalidomide serum concentration was <10μM (2500ng/mL) at 12 hours[271]. This is much higher that results seen in this study. It is possible that as this study was conducted to have minimum impact on the patient that dosing times and samples times may have varied more than anticipated.

5.6.3.4.   *Serum levels and disease response*
Of the two patients in the cohort, eight patients showed partial or very good partial response to thalidomide treatment. Two patients had progressive disease, Table 5-28. In such a small patient group it is difficult to make any clear statements regarding serum level and disease response. Patients A, B, G and J all had very good partial response, though had difference ranges of thalidomide serum levels, from ~160ng/mL -~1000ng/mL. Of the patients who showed disease progression one had the maximum thalidomide serum concentration found in the study and the other had an average serum level of ~375ng/mL.

One of the considerations when administering chemotherapeutics is the determination of the correct dose for the patient. One of the obvious results of incorrect dose calculations is overdose and excessive toxicity. The key aim of Phase I clinical trials are generally to determine the dose limiting toxicity. To prevent unacceptable toxicity the mean dose is generally aimed to the low range to minimise severe toxicity. As a result of this many cancer patients are inadvertently under dosed[380].

In some tyrosine kinase inhibitors patients who exhibit a skin rash are more likely to respond that those that have no rash. Future studies in the patient pharmacokinetics in multiple myeloma should include increased adverse effect monitoring as well as proteomic studies to monitoring levels of excretion enzymes if possible. It may then be possible to individualise that patient dose to a factor which could avoid under-dosing.

5.6.4. Thalidomide quantification in cells

Given the sensitivity of the method developed, the ability to quantify thalidomide in cell-culture was an objective. The method validated without issue against the biological matrix of cancer cells, Section 5.4.2. DLKP and DLKP-A cell-line models were exposed to 2μM thalidomide and samples taken at 30 minutes internals, as described in Section 2.1.8. The cell pellets were stored in 50μL of citrate buffer. The samples were extracted and data analysed as described, Section 2.2.6.3. Upon analysis of the data, no quantifiable levels of thalidomide were detected in the cell pellets.

Some groups have shown thalidomide activity *in vitro* such as Sung *et al.*[395], who reported that curcumin plus thalidomide increased apoptosis in U266 cells, greater than either agent alone. Keller *et al.*[396], reported that thalidomide inhibited Caspase-1 activity *in vivo* but not *in vitro.* Hideshima *et al.*[397]. examined the activity of thalidomide and three thalidomide analogues, from Celgene, in multiple myeloma cells to discover that high dose thalidomide (100μmol/L) resulted in less than 20% inhibition on DNA synthesis *in vitro,* but the analogues achieved 50% inhibition. DNA synthesis inhibition assays were performed after 48hours incubation of the agent with the cells at 37°C. Thalidomide is noticeably unresponsive in assays *in vitro* with researchers using unfeasibly concentration to achieve results. In our group thalidomide was also determined to be "non-toxic" when examined *in vitro* 7 day toxicity assay, (data not shown).

Given that thalidomide is know to hydrolyse in aqueous conditions at physiological pH, and given that only 8 samples out of 116 samples (~7%) had any detectable level of thalidomide present, an investigation of thalidomide stability in cell-culture media was undertaken. Zhou *et al.*[278], monitored the concentration of thalidomide in HBSS transport buffer for the determination of thalidomide transport in Caco-2 cell monolayers. The stability of thalidomide in HBSS was also monitored. For this reason HBSS was included in this experiment. In cell culture media and HBSS 2μM thalidomide was incubated at 37°C for 24hrs. Two stocks of thalidomide in DMSO were assessed.

Figure 5-32 shows the rate of thalidomide degradation in cell-culture media and HBSS. There is minimal difference between the old and new thalidomide stocks in

either HBSS or cell culture media. This indicates that thalidomide is stable in DMSO at 4°C for at least 7 weeks.

More than 50% of the thalidomide was degraded in HBSS within one hour. In media the rate of degradation was somewhat slower but with only 50% of thalidomide remaining after three hours. This would indicate that thalidomide hydrolysed rapidly in cell culture media and HBSS. This means that thalidomide is not stable in normal cell-culture media and that *in vitro* analysis of the function or response of thalidomide is questionable.

This is not the first time that the hydrolysis of thalidomide has been reported. In 1965 Schumacher et al.,[398, 399] described the products of thalidomide in hydrolysis in the urine, blood and tissues of various species. Despite this however, much data continues to be published on thalidomide *in vitro,* with no mention or reference to the hydrolysis of thalidomide over the course of the assay.

5.6.5. Summary

- In summary an LC-MS/MS was developed and validated for the quantification of thalidomide in human serum from multiple myeloma patients and thalidomide in cells and cell-culture media.

- A liquid-liquid extraction sample clean-up step was optimised. This combination gave a sensitive, accurate, reproducible method which only required 100μL of patient serum. LLE was also applicable for the analysis of thalidomide in cells

- This method was applied to the analysis of thalidomide in multiple myeloma patient serum.

- While no clear relationship between serum level and outcome was seen, it is clear that serum level and dose are directly linked. Also dose reduction decreases peripheral neuropathy.

- However the clearest result from the study was the issue of patient non compliance.

- To the best of our knowledge, this is the only study to report patient non-compliance is terms of thalidomide monitoring in multiple myeloma patients.

- The sensitivity of the LC-MS/MS method also meant that the method could be employed for the quantification of thalidomide in cell-lines.

- Inconsistent results for the quantification of thalidomide in accumulation and efflux assays were shown to be caused by thalidomide instability in media. Thalidomide rapidly breaks down in cell-culture media.

- Even though this rapid break-down of thalidomide has been monitored in HBSS for cell-based transport assays of thalidomide once previously[278], this is the first time these finding have been confirmed in cell-culture media.

Also the attention of the clinical and laboratory based investigator of thalidomide *in vitro* does not seem to have registered the issues of thalidomide in cell-based assays and do not account for thalidomide hydrolysis in their assay.

SECTION 6.0 –Conclusions

6. Conclusions

Over the course of this body of work, two separate sensitive analytical methods have been developed for the analysis of clinically important therapeutic agents. Two classes of anti-cancer agents were investigated; 1) tyrosine kinase inhibitors, specifically dasatinib and lapatinib, and 2) immunomodulatory agents, specifically thalidomide. These methods have been designed to be sensitive, rapid techniques that are easily transferable from one laboratory to another. Using LC-MS/MS as a quantification tool has provided a level of sensitivity which can accurately and precisely determine minute differences in samples both *in vitro* and *in vivo*. The extraction procedure (LLE) employed for the sample clean-up is a low cost, low technology option for the purification of target agents in biological samples. This straightforward approach is applicable to a many biological matrices and can therefore be applied to a variety of cell types, patient serum and other sample types where applicable.

The analytical method for the quantification of tyrosine kinase inhibitors has been applied to *in vitro* cell-line models and used to better understand the resistance mechanisms of dasatinib and lapatinib. Also in conjunction with cell toxicity assays this techniques assists in the teasing apart of complex cross-resistance mechanism. The application of this analytical method for the quantification of erlotinib, gefitinib and imatinib in glioma primary cultures sheds new light on the role of these TKIs in glioma. The greater level of accumulation of these agents in lower grade glioma cultures requires further investigation as to whether this reaction is specific to this cell model or whether this trend is universal for lower grade gliomas.

The application of the LC-MS/MS method for the quantification of thalidomide in patient samples is the result of a pilot study in collaboration with the Mater Hospital, Dublin. This study endeavoured to examine if the collection, the processing and analyses of patient samples was possible with minimum intrusion upon the patient. Although the numbers enrolled were small, a high level of patient non-compliance was detected in this study. Also, the application of this method for the analysis of thalidomide *in vitro* demonstrated the impact of the rapid hydrolysis of thalidomide on *in vitro* assays.

Both of the methods designed within this thesis have further clinical impact beyond the scope of the analysis already undertaken.

The method for the quantification of lapatinib could be employed to quantity the levels of lapatinib in the biopsies tissues of breast cancer patients. By monitoring both the circulating serum levels and the level of lapatinib within the tumour it would be possible to determine the impact of physiological mechanisms of resistance, such as the drug delivery and tumour micro-environment, on patient outcome. As the method developed here is the only method in the literature validated for the quantification of lapatinib in cells it is inherently applicable.

The clinical application of this method for any of the TKIs could be employed to further inform the clinical team and researchers with respect to circulating drug levels and the levels of therapeutic agents at the site of action.

The methods developed here are truly translational in their ability to investigate both *in vivo* and *in vitro* queries.

Detailed below are the specific conclusions of each section investigated.

6.1. The development and validation of a method of the quantification of dasatinib and lapatinib

- A novel and sensitive LC-MS/MS assay has been developed and validated for the determination of cellular levels of the tyrosine kinase inhibitors dasatinib and lapatinib

- The method is as sensitive as those already in the literature but through the use of an isocratic elution this separation method is more straight-forward, lower cost and easier to use.

- The use of one tyrosine kinase inhibitor as the internal standard for the other agent gives excellent results and dual applicability of the method. This avoids the use of expensive deuterated analogues of the analyte of interest as an internal standard.

- The use of a liquid-liquid extraction clean up stage gives simplicity of application making the method accessible to other researchers, as this method does not require the additional equipment or commercial clean-up systems. The extraction solvents and standard laboratory equipment used here are routinely available in most laboratories.

- The LLE method is capable of processing large numbers of samples without the need for extra equipment. Also, the samples obtained from an LLE method are clean, have a low background and generally have excellent recoveries.

- An isocratic elution scheme gives a simple, robust and reproducible chromatographic method.

- Our experimental approach has yielded superior levels of sensitivity and the specificity for the analytical method.

- This LC-MS/MS technique has been successfully employed for the quantification of low dose dasatinib over short time frame in cardiac cells and in cancer cell-line models.

- This LC-MS/MS method has been used to assist the characterisation of dasatinib resistant cell-line model, in collaboration with Dr Brendan Corkery.

- This basic analytical method was applied and partially validated for other TKI molecules, erlotinib, gefitinib, imatinib. This simple method transfer from one TKI to another minimise the time required for method developed and results in a simple and efficient method.

- Using LC-MS/MS quantification techniques, it was possible to quantify the intracellular mass of these TKIs (erlotinib, gefitinib and imatinib) in glioma cell cultures. To the best of our knowledge is the in first time that the accumulation of these agents has been measure in human primary glioma cultures.

- Low grade glioma accumulated more of each TKI compared to higher grade gliomas. While in differences in the level of intracellular TKI accumulated did not directly correlate with the levels of ABC transporters detected in the models, this interesting results requires closer investigation.

6.2. Investigation of dasatinib and lapatinib interaction with MDR over-expressing cell-lines

- Through accumulation and efflux profile of dasatinib in P-gp over-expressing cell-lines, we can conclude that dasatinib is a P-gp substrate. This is a clinically relevant finding as the drug is currently used in the treatment of imatinib-intolerant and imatinib-resistant CML patient. Should an imatinib-resistant patient receiving dasatinib relapse or not respond to treatment this maybe due to the reduced efficacy of dasatinib at the required site of action

due to a lower intracellular concentration associated with intratumoural overexpression of P-gp.

- The efflux of dasatinib by P-gp decreases the intracellular mass, which was seen with decreased the efficacy of dasatinib *in vitro* in resistant cell-line models compared to the parental cell-line models. This was reversible with the inclusion of a P-gp inhibitor, elacridar.

- At pharmacokinetically relevant concentrations, dasatinib is not a P-gp inhibitor.

- Dasatinib is a substrate of the ABC transport BCRP and hence intratumour expression of the transporter may impact efficacy

-

- The active transport of dasatinib by BCRP decreased the efficacy if dasatinib *in vitro.*

- Dasatinib did not appear to inhibit the action of BCRP at clinically relevant concentrations

- Dasatinib is not a substrate of MRP-1.

- Lapatinib is not a substrate of P-gp. The mechanism of P-gp inhibition is not through competitive binding to substrate binding sites.

- In the cell-line model examined, lapatinib is not a substrate of BCRP, though may have some BCRP-inhibitory activity.

- .

- In the cell-line models examined, lapatinib is not substrate of MRP-1.

- The "sister" resistant cell-line models DLKP-Sq/Mitox-BCRP and DLKP-Sq/Mitox-MDR are excellent models for the examination of therapeutic agent transport *in vitro*.

6.3. *The development and validation of a method to quantify thalidomide*

- A sensitive straight-forward method for the quantification of thalidomide by LC-MS/MS has been developed.

- This method is more sensitive, (Section 5.4.3 and Section 5.6.2.2) than methods previously published and the use of an isocratic separation adds simplicity to the analytical method.

- Umbelliferone is an easy, cheap and safe compound to use as an internal standard for the quantification of thalidomide.

- A method has been developed for the chromatographic separation of thalidomide and lenalidomide.

- However, lenalidomide has very different physiochemical properties compared to thalidomide and as such is not appropriate as an internal standard for thalidomide.

- Given the sensitivity of the method developed and the use of a liquid-liquid extraction procedure, this method was validated for the quantification of thalidomide in cells

- However, in cell culture experiments the rate of thalidomide hydrolyses was shown to be detrimental to the quantification of thalidomide in cell efflux and accumulation assay.

- Thalidomide was shown to hydrolyse in cell culture media rapidly, with 50% of thalidomide remaining after three hours at physiological temperature and pH.

- In multiple myeloma patients, the dose administered was shown to be related empirically to the serum concentration levels.

- Non-compliance or partial compliance to the medication protocol was seen to be an issue in 30%-40% of the patient cohort.

- Future clinical trial studies should include more rigorous monitoring and recording of individual patient factors such as medication timings as the rapid pharmacokinetics of thalidomide could be a factor in inter-patient variability following equal doses.

SECTION 7.0 –Future plans

7. Future plans

7.1. LC-MS/MS method for the analysis of TKIs

- To improve the existing separation method of the analysis of lapatinib and dasatinib the effect of reducing the organic component of the mobile phase and increasing the flow should be examined. Theoretically reducing the organic component further should increase the separation of dasatinib from the dead volume and increasing the flow should reduce the time between dasatinib and lapatinib separation

- Rapid resolution LC columns could also be examined for the separation of dasatinib and lapatinib. The decreased particle size (sub 2μm particle size) columns capable of operating at high flow allows for ultra fast separations.

- Investigation into improved separation of multiple TKI mixtures could be used to improve the multiple TKI separation.

- The validation of gefitinib, erlotinib and imatinib should be completed. Also other TKIs such as sorafenib and neratinib could be examined using this extraction and separation method.

- The quantification of dasatinib and lapatinib in serum could be investigated. This would require a partial re-validation in the appropriate matrix (human serum). This could be used for the evaluation of patient samples

- Given that the quantification of erlotinib, gefitinib and imatinib in glioma cell cultures gave such interesting and clear results that showed that the more sensitive and responsive cells had increased TKI accumulation and investigation into other low grade gliomas to further explore this finding would be interesting.

7.2. Investigation of TKIs in MDR expressing cell-lines

- The procedures followed here has given clear information about the MDR status of dasatinib and lapatinib and defined their positions as substrates or inhibitors. This procedure of accumulation/efflux assays, *in vitro* toxicity assay and combination *in vitro* assays could be used to define the MDR status of other TKI agents such as neratinib

7.3. LC-MS/MS methods for the analysis of multiple myeloma drugs

- Given the success of the analysis of serum concentration levels thalidomide in a small group of patient samples this study could be continued and expanded.

- An analytical method for the quantification of lenalidomide could be developed. A method published by Liu *et al.*[400], details the quantification of lenalidomide using a protein precipitation sample preparation stage. This method could be explored and optimised for the analysis of lenalidomide in patient samples in our laboratory.

- An analytical method for the quantification of bortezomib could be developed. Bortezomib is dipeptidyl boronic acid is used in the treatment of multiple myeloma. The quantification of bortezomib both *in vitro* and *in vivo* would be of clinical interest.

SECTION 8.0 – References

8. References

1. **Tsuruo, T., M. Naito, A. Tomida, N. Fujita, T. Mashima, S. Hirosh, and N. Haga**, *Molecular targeting therapy of cancer: drug resistance, apoptosis and survival signal.* Cancer Science, 2003. **94**(1): p. 15-21.

2. **Rosa, D.D., G. Ismael, L.D. Lago, and A. Awada**, *Molecular-targeted therapies: Lessons from years of clinical development.* Cancer Treatment Reviews, 2008. **34**(1): p. 61-80.

3. **O'Connor, R.**, *The pharmacology of cancer resistance.* Anticancer Research, 2007. **27**(3A): p. 1267-1272.

4. **Lage, H.**, *An overview of cancer multidrug resistance: a still unsolved problem.* Cell Mol Life Sci, 2008. **65**(20): p. 3145-67.

5. **Collins, D.M.**, *Docetaxel uptake and modulation of P-gp mediated docetaxel efflux by tyrosine kinase inhibitors in human lung carcinoma cell lines.* National Institute for Cellular Biotechnology (NICB), 2008:

6. **Devery, A.**, *Pharmacological modulation and manipulation of cancer drug resistance.* NICB, 2010:

7. **Dunne, G.**, *Characterisation and Modulation of Drug Resistance in Lung Cancer Cell Lines.* NICB, 2009:

8. **O'Connor, R.**, *A Review of Mechanisms of Circumvention and Modulation of Chemotherapeutic Drug Resistance* Current Cancer Drug Targets, 2009. **9**(3): p. 273-280.

9. **Seeger, M.A. and H.W. van Veen**, *Molecular basis of multidrug transport by ABC transporters.* Biochimica et Biophysica Acta (BBA) - Proteins & Proteomics, 2009. **1794**(5): p. 725-737.

10. **Ambudkar, S.V., S. Dey, C.A. Hrycyna, M. Ramachandra, I. Pastan, and M.M. Gottesman**, *Biochemical, cellular, and pharmacological aspects of the multidrug transporter.* Annu Rev Pharmacol Toxicol, 1999. **39**: p. 361-98.

11. **Dean, M., A. Rzhetsky, and R. Allikmets**, *The human ATP-binding cassette (ABC) transporter superfamily.* Genome Res, 2001. **11**(7): p. 1156-66.

12. **Higgins, C.F.**, *ABC transporters: from microorganisms to man.* Annu Rev Cell Biol, 1992. **8**: p. 67-113.

13. **Walker, J.E., M. Saraste, M.J. Runswick, and N.J. Gay**, *Distantly related sequences in the alpha- and beta-subunits of ATP synthase, myosin, kinases and other ATP-requiring enzymes and a common nucleotide binding fold.* Embo J, 1982. **1**(8): p. 945-51.

14. **Hyde, S.C., P. Emsley, M.J. Hartshorn, M.M. Mimmack, U. Gileadi, S.R. Pearce, M.P. Gallagher, D.R. Gill, R.E. Hubbard, and C.F. Higgins**, *Structural model of ATP-binding proteins associated with cystic fibrosis, multidrug resistance and bacterial transport.* Nature, 1990. **346**(6282): p. 362-5.

15. **Rocchi, E., A. Khodjakov, E.L. Volk, C.H. Yang, T. Litman, S.E. Bates, and E. Schneider**, *The product of the ABC half-transporter gene ABCG2 (BCRP/MXR/ABCP) is expressed in the plasma membrane.* Biochem Biophys Res Commun, 2000. **271**(1): p. 42-6.

16. **Litman, T., T.E. Druley, W.D. Stein, and S.E. Bates**, *From MDR to MXR: new understanding of multidrug resistance systems, their properties and clinical significance.* Cell Mol Life Sci, 2001. **58**(7): p. 931-59.

17. **Loo, T.W. and D.M. Clarke**, *The packing of the transmembrane segments of human multidrug resistance P-glycoprotein is revealed by disulfide cross-linking analysis.* J Biol Chem, 2000. **275**(8): p. 5253-6.

18. **Cragg, G.M. and D.J. Newman**, *Plants as a source of anti-cancer agents.* Journal of Ethnopharmacology, 2005. **100**(1-2): p. 72-79.

19. **Laing, N.M., M.G. Belinsky, G.D. Kruh, D.W. Bell, J.T. Boyd, L. Barone, J.R. Testa, and K.D. Tew**, *Amplification of the ATP-binding cassette 2 transporter gene is functionally linked with enhanced efflux of estramustine in ovarian carcinoma cells.* Cancer Res, 1998. **58**(7): p. 1332-7.

20. **Vulevic, B., Z. Chen, J.T. Boyd, W. Davis, Jr., E.S. Walsh, M.G. Belinsky, and K.D. Tew**, *Cloning and characterization of human adenosine 5'-triphosphate-binding cassette, sub-family A, transporter 2 (ABCA2).* Cancer Res, 2001. **61**(8): p. 3339-47.

21. **Mack, J.T., D.M. Townsend, V. Beljanski, and K.D. Tew**, *The ABCA2 transporter: intracellular roles in trafficking and metabolism of LDL-derived cholesterol and sterol-related compounds.* Curr Drug Metab, 2007. **8**(1): p. 47-57.

22. **Boonstra, R., H. Timmer-Bosscha, J. van Echten-Arends, D.M. van der Kolk, A. van den Berg, B. de Jong, K.D. Tew, S. Poppema, and E.G. de Vries**, *Mitoxantrone resistance in a small cell lung cancer cell line is associated with ABCA2 upregulation.* Br J Cancer, 2004. **90**(12): p. 2411-7.

23. **Steinbach, D., J.P. Gillet, A. Sauerbrey, B. Gruhn, K. Dawczynski, V. Bertholet, F. de Longueville, F. Zintl, J. Remacle, and T. Efferth**, *ABCA3 as a possible cause of drug resistance in childhood acute myeloid leukemia.* Clin Cancer Res, 2006. **12**(14 Pt 1): p. 4357-63.

24. **Lage, H.**, *ABC-transporters: implications on drug resistance from microorganisms to human cancers.* Int J Antimicrob Agents, 2003. **22**(3): p. 188-99.

25. **Szakacs, G., J.K. Paterson, J.A. Ludwig, C. Booth-Genthe, and M.M. Gottesman**, *Targeting multidrug resistance in cancer.* Nat Rev Drug Discov, 2006. **5**(3): p. 219-34.

26. **Riordan, J.R. and V. Ling**, *Purification of P-glycoprotein from plasma membrane vesicles of Chinese hamster ovary cell mutants with reduced colchicine permeability.* J Biol Chem, 1979. **254**(24): p. 12701-5.

27. **Kartner, N., J.R. Riordan, and V. Ling**, *Cell surface P-glycoprotein associated with multidrug resistance in mammalian cell lines.* Science, 1983. **221**(4617): p. 1285-8.

28. **Ueda, K., A. Yoshida, and T. Amachi**, *Recent progress in P-glycoprotein research.* Anticancer Drug Des, 1999. **14**(2): p. 115-21.

29. **Izquierdo, M.A., J.J. Neefjes, A.E. Mathari, M.J. Flens, G.L. Scheffer, and R.J. Scheper**, *Overexpression of the ABC transporter TAP in multidrug-resistant human cancer cell lines.* Br J Cancer, 1996. **74**(12): p. 1961-7.

30. **Lage, H., C. Perlitz, R. Abele, R. Tampe, M. Dietel, D. Schadendorf, and P. Sinha**, *Enhanced expression of human ABC-transporter tap is associated with cellular resistance to mitoxantrone.* FEBS Lett, 2001. **503**(2-3): p. 179-84.

31. **Gottesman, M.M., T. Fojo, and S.E. Bates**, *Multidrug resistance in cancer: role of ATP-dependent transporters.* Nat Rev Cancer, 2002. **2**(1): p. 48-58.

32. **Ruetz, S. and P. Gros**, *Phosphatidylcholine translocase: a physiological role for the mdr2 gene.* Cell, 1994. **77**(7): p. 1071-81.

33. **Chen, K.G., G. Szakacs, J.P. Annereau, F. Rouzaud, X.J. Liang, J.C. Valencia, C.N. Nagineni, J.J. Hooks, V.J. Hearing, and M.M. Gottesman**, *Principal expression of two mRNA isoforms (ABCB 5alpha and ABCB 5beta) of the ATP-binding cassette transporter gene ABCB 5 in melanoma cells and melanocytes.* Pigment Cell Res, 2005. **18**(2): p. 102-12.

34. **Frank, N.Y., A. Margaryan, Y. Huang, T. Schatton, A.M. Waaga-Gasser, M. Gasser, M.H. Sayegh, W. Sadee, and M.H. Frank**, *ABCB5-mediated doxorubicin transport and chemoresistance in human malignant melanoma.* Cancer Res, 2005. **65**(10): p. 4320-33.

35. **Huang, Y., P. Anderle, K.J. Bussey, C. Barbacioru, U. Shankavaram, Z. Dai, W.C. Reinhold, A. Papp, J.N. Weinstein, and W. Sadee**, *Membrane transporters and channels: role of the transportome in cancer chemosensitivity and chemoresistance.* Cancer Res, 2004. **64**(12): p. 4294-301.

36. **Yasui, K., S. Mihara, C. Zhao, H. Okamoto, F. Saito-Ohara, A. Tomida, T. Funato, A. Yokomizo, S. Naito, I. Imoto, T. Tsuruo, and J. Inazawa**, *Alteration in copy numbers of genes as a mechanism for acquired drug resistance.* Cancer Res, 2004. **64**(4): p. 1403-10.

37. **Paterson, J.K., S. Shukla, C.M. Black, T. Tachiwada, S. Garfield, S. Wincovitch, D.N. Ernst, A. Agadir, X. Li, S.V. Ambudkar, G. Szakacs, S. Akiyama, and M.M. Gottesman**, *Human ABCB6 localizes to both the outer mitochondrial membrane and the plasma membrane.* Biochemistry, 2007. **46**(33): p. 9443-52.

38. **Childs, S., R.L. Yeh, D. Hui, and V. Ling**, *Taxol resistance mediated by transfection of the liver-specific sister gene of P-glycoprotein.* Cancer Res, 1998. **58**(18): p. 4160-7.

39. **Gerloff, T., B. Stieger, B. Hagenbuch, J. Madon, L. Landmann, J. Roth, A.F. Hofmann, and P.J. Meier**, *The sister of P-glycoprotein represents the canalicular bile salt export pump of mammalian liver.* J Biol Chem, 1998. **273**(16): p. 10046-50.

40. **Cole, S.P., G. Bhardwaj, J.H. Gerlach, J.E. Mackie, C.E. Grant, K.C. Almquist, A.J. Stewart, E.U. Kurz, A.M. Duncan, and R.G. Deeley**, *Overexpression of a transporter gene in a multidrug-resistant human lung cancer cell line.* Science, 1992. **258**(5088): p. 1650-4.

41. **Haimeur, A., G. Conseil, R.G. Deeley, and S.P. Cole**, *The MRP-related and BCRP/ABCG2 multidrug resistance proteins: biology, substrate specificity and regulation.* Curr Drug Metab, 2004. **5**(1): p. 21-53.

42. **Jedlitschky, G., I. Leier, U. Buchholz, K. Barnouin, G. Kurz, and D. Keppler**, *Transport of glutathione, glucuronate, and sulfate conjugates by the MRP gene-encoded conjugate export pump.* Cancer Res, 1996. **56**(5): p. 988-94.

43. **Taniguchi, K., M. Wada, K. Kohno, T. Nakamura, T. Kawabe, M. Kawakami, K. Kagotani, K. Okumura, S. Akiyama, and M. Kuwano**, *A human canalicular multispecific organic anion transporter (cMOAT) gene is overexpressed in cisplatin-resistant human cancer cell lines with decreased drug accumulation.* Cancer Res, 1996. **56**(18): p. 4124-9.

44. **Materna, V., B. Liedert, J. Thomale, and H. Lage**, *Protection of platinum-DNA adduct formation and reversal of cisplatin resistance by anti-MRP2 hammerhead ribozymes in human cancer cells.* Int J Cancer, 2005. **115**(3): p. 393-402.

45. **Cui, Y., J. Konig, J.K. Buchholz, H. Spring, I. Leier, and D. Keppler**, *Drug resistance and ATP-dependent conjugate transport mediated by the apical multidrug resistance protein, MRP2, permanently expressed in human and canine cells.* Mol Pharmacol, 1999. **55**(5): p. 929-37.

46. **Konig, J., A.T. Nies, Y. Cui, I. Leier, and D. Keppler**, *Conjugate export pumps of the multidrug resistance protein (MRP) family: localization, substrate specificity, and MRP2-mediated drug resistance.* Biochim Biophys Acta, 1999. **1461**(2): p. 377-94.

47. **Borst, P., C. de Wolf, and K. van de Wetering**, *Multidrug resistance-associated proteins 3, 4, and 5.* Pflugers Arch, 2007. **453**(5): p. 661-73.

48. **Kool, M., M. van der Linden, M. de Haas, G.L. Scheffer, J.M. de Vree, A.J. Smith, G. Jansen, G.J. Peters, N. Ponne, R.J. Scheper, R.P. Elferink, F. Baas, and P. Borst**, *MRP3, an organic anion transporter able to transport anti-cancer drugs.* Proc Natl Acad Sci U S A, 1999. **96**(12): p. 6914-9.

49. **de Jong, M.C., J.W. Slootstra, G.L. Scheffer, A.B. Schroeijers, W.C. Puijk, R. Dinkelberg, M. Kool, H.J. Broxterman, R.H. Meloen, and R.J. Scheper**, *Peptide transport by the multidrug resistance protein MRP1.* Cancer Res, 2001. **61**(6): p. 2552-7.

50. **Zeng, H., L.J. Bain, M.G. Belinsky, and G.D. Kruh**, *Expression of multidrug resistance protein-3 (multispecific organic anion transporter-D) in human embryonic kidney 293 cells confers resistance to anticancer agents.* Cancer Res, 1999. **59**(23): p. 5964-7.

51. **Schuetz, J.D., M.C. Connelly, D. Sun, S.G. Paibir, P.M. Flynn, R.V. Srinivas, A. Kumar, and A. Fridland**, *MRP4: A previously unidentified factor in resistance to nucleoside-based antiviral drugs.* Nat Med, 1999. **5**(9): p. 1048-51.

52. **Chen, Z.S., K. Lee, and G.D. Kruh**, *Transport of cyclic nucleotides and estradiol 17-beta-D-glucuronide by multidrug resistance protein 4. Resistance to 6-mercaptopurine and 6-thioguanine.* J Biol Chem, 2001. **276**(36): p. 33747-54.

53. **Chen, Z.S., K. Lee, S. Walther, R.B. Raftogianis, M. Kuwano, H. Zeng, and G.D. Kruh**, *Analysis of methotrexate and folate transport by multidrug resistance protein 4 (ABCC4): MRP4 is a component of the methotrexate efflux system.* Cancer Res, 2002. **62**(11): p. 3144-50.

54. **Wijnholds, J., C.A. Mol, L. van Deemter, M. de Haas, G.L. Scheffer, F. Baas, J.H. Beijnen, R.J. Scheper, S. Hatse, E. De Clercq, J. Balzarini, and P. Borst**, *Multidrug-resistance protein 5 is a multispecific organic anion transporter able to transport nucleotide analogs.* Proc Natl Acad Sci U S A, 2000. **97**(13): p. 7476-81.

55. **Jedlitschky, G., B. Burchell, and D. Keppler**, *The multidrug resistance protein 5 functions as an ATP-dependent export pump for cyclic nucleotides.* J Biol Chem, 2000. **275**(39): p. 30069-74.

56. **Belinsky, M.G., Z.S. Chen, I. Shchaveleva, H. Zeng, and G.D. Kruh**, *Characterization of the drug resistance and transport properties of multidrug resistance protein 6 (MRP6, ABCC6).* Cancer Res, 2002. **62**(21): p. 6172-7.

57. **Kruh, G.D., Y. Guo, E. Hopper-Borge, M.G. Belinsky, and Z.S. Chen**, *ABCC10, ABCC11, and ABCC12.* Pflugers Arch, 2007. **453**(5): p. 675-84.

58. **Hopper-Borge, E., Z.S. Chen, I. Shchaveleva, M.G. Belinsky, and G.D. Kruh**, *Analysis of the drug resistance profile of multidrug resistance protein 7 (ABCC10): resistance to docetaxel.* Cancer Res, 2004. **64**(14): p. 4927-30.

59. **Oguri, T., Y. Bessho, H. Achiwa, H. Ozasa, K. Maeno, H. Maeda, S. Sato, and R. Ueda**, *MRP8/ABCC11 directly confers resistance to 5-fluorouracil.* Mol Cancer Ther, 2007. **6**(1): p. 122-7.

60. **Doyle, L.A., W. Yang, L.V. Abruzzo, T. Krogmann, Y. Gao, A.K. Rishi, and D.D. Ross**, *A multidrug resistance transporter from human MCF-7 breast cancer cells.* Proc Natl Acad Sci U S A, 1998. **95**(26): p. 15665-70.

61. **Allikmets, R., L.M. Schriml, A. Hutchinson, V. Romano-Spica, and M. Dean**, *A human placenta-specific ATP-binding cassette gene (ABCP) on chromosome 4q22 that is involved in multidrug resistance.* Cancer Res, 1998. **58**(23): p. 5337-9.

62. **Miyake, K., L. Mickley, T. Litman, Z. Zhan, R. Robey, B. Cristensen, M. Brangi, L. Greenberger, M. Dean, T. Fojo, and S.E. Bates**, *Molecular cloning of cDNAs which are highly overexpressed in mitoxantrone-resistant cells: demonstration of homology to ABC transport genes.* Cancer Res, 1999. **59**(1): p. 8-13.

63. **Lage, H. and M. Dietel**, *Effect of the breast-cancer resistance protein on atypical multidrug resistance.* Lancet Oncol, 2000. **1**: p. 169-75.

64. **Doyle, L.A. and D.D. Ross**, *Multidrug resistance mediated by the breast cancer resistance protein BCRP (ABCG2).* Oncogene, 2003. **22**(47): p. 7340-58.

65. **Biedler, J.L. and H. Riehm**, *Cellular resistance to actinomycin D in Chinese hamster cells in vitro: cross-resistance, radioautographic, and cytogenetic studies.* Cancer Res, 1970. **30**(4): p. 1174-84.

66. **Juliano, R.L. and V. Ling**, *A surface glycoprotein modulating drug permeability in Chinese hamster ovary cell mutants.* Biochim Biophys Acta, 1976. **455**(1): p. 152-62.

67. **Riehm, H. and J.L. Biedler**, *Cellular resistance to daunomycin in Chinese hamster cells in vitro.* Cancer Res, 1971. **31**(4): p. 409-12.

68. **Dano, K.**, *Cross resistance between vinca alkaloids and anthracyclines in Ehrlich ascites tumor in vivo.* Cancer Chemother Rep, 1972. **56**(6): p. 701-8.

69. **Dano, K.**, *Active outward transport of daunomycin in resistant Ehrlich ascites tumor cells.* Biochim Biophys Acta, 1973. **323**(3): p. 466-83.

70. **Gottesman, M.M. and I. Pastan**, *Biochemistry of multidrug resistance mediated by the multidrug transporter.* Annu Rev Biochem, 1993. **62**: p. 385-427.

71. **Bellamy, W.T.**, *P-glycoproteins and multidrug resistance.* Annu Rev Pharmacol Toxicol, 1996. **36**: p. 161-83.

72. **Garrigues, A., N. Loiseau, M. Delaforge, J. Ferte, M. Garrigos, F. Andre, and S. Orlowski**, *Characterization of two pharmacophores on the multidrug transporter P-glycoprotein.* Mol Pharmacol, 2002. **62**(6): p. 1288-98.

73. **Pleban, K., S. Kopp, E. Csaszar, M. Peer, T. Hrebicek, A. Rizzi, G.F. Ecker, and P. Chiba**, *P-glycoprotein substrate binding domains are located at the transmembrane domain/transmembrane domain interfaces: a combined photoaffinity labeling-protein homology modeling approach.* Mol Pharmacol, 2005. **67**(2): p. 365-74.

74. **Omote, H. and M.K. Al-Shawi**, *A novel electron paramagnetic resonance approach to determine the mechanism of drug transport by P-glycoprotein.* J Biol Chem, 2002. **277**(47): p. 45688-94.

75. **Sharom, F.J., M.R. Lugo, and P.D. Eckford**, *New insights into the drug binding, transport and lipid flippase activities of the p-glycoprotein multidrug transporter.* J Bioenerg Biomembr, 2005. **37**(6): p. 481-7.

76. **Sharom, F.J., R. Liu, Q. Qu, and Y. Romsicki**, *Exploring the structure and function of the P-glycoprotein multidrug transporter using fluorescence spectroscopic tools.* Semin Cell Dev Biol, 2001. **12**(3): p. 257-65.

77. **Loo, T.W. and D.M. Clarke**, *Recent progress in understanding the mechanism of P-glycoprotein-mediated drug efflux.* J Membr Biol, 2005. **206**(3): p. 173-85.

78. **Loo, T.W. and D.M. Clarke**, *Determining the dimensions of the drug-binding domain of human P-glycoprotein using thiol cross-linking compounds as molecular rulers.* J Biol Chem, 2001. **276**(40): p. 36877-80.

79. **Zaman, G.J., J. Lankelma, O. van Tellingen, J. Beijnen, H. Dekker, C. Paulusma, R.P. Oude Elferink, F. Baas, and P. Borst**, *Role of glutathione in the export of compounds from cells by the multidrug-resistance-associated protein.* Proceedings of the National Academy of Sciences of the United States of America, 1995. **92**(17): p. 7690-7694.

80. **Deeley, R.G., C. Westlake, and S.P.C. Cole**, *Transmembrane Transport of Endo- and Xenobiotics by Mammalian ATP-Binding Cassette Multidrug Resistance Proteins.* Physiol. Rev., 2006. **86**(3): p. 849-899.

81. **Nooter, K., G. Brutel de la Riviere, M.P. Look, K.E. van Wingerden, S.C. Henzen-Logmans, R.J. Scheper, M.J. Flens, J.G. Klijn, G. Stoter, and J.A. Foekens**, *The prognostic significance of expression of the multidrug resistance-associated protein (MRP) in primary breast cancer.* Br J Cancer, 1997. **76**(4): p. 486-93.

82. **Arts, H.J., D. Katsaros, E.G. de Vries, M. Massobrio, F. Genta, S. Danese, R. Arisio, R.J. Scheper, M. Kool, G.L. Scheffer, P.H. Willemse, A.G. van der Zee, and A.J. Suurmeijer**, *Drug resistance-associated markers P-glycoprotein, multidrug resistance-associated protein 1, multidrug resistance-associated protein 2, and lung resistance protein as prognostic factors in ovarian carcinoma.* Clin Cancer Res, 1999. **5**(10): p. 2798-805.

83. **Walsh, N., A. Larkin, S. Kennedy, L. Connolly, J. Ballot, W. Ooi, G. Gullo, J. Crown, M. Clynes, and L. O'Driscoll**, *Expression of multidrug resistance markers ABCB1 (MDR-1/P-gp) and ABCC1 (MRP-1) in renal cell carcinoma.* BMC Urol, 2009. **9**: p. 6.

84. **Walsh, N., S. Kennedy, A.M. Larkin, D. Tryfonopoulos, A.J. Eustace, T. Mahgoub, C. Conway, I. Oglesby, D. Collins, J. Ballot, W.S. Ooi, G. Gullo, M. Clynes, J. Crown, and L. O'Driscoll**, *Membrane transport proteins in human melanoma: associations with tumour aggressiveness and metastasis.* Br J Cancer. **102**(7): p. 1157-62.

85. **Borst, P., R. Evers, M. Kool, and J. Wijnholds**, *A Family of Drug Transporters: the Multidrug Resistance-Associated Proteins.* Journal of the National Cancer Institute, 2000. **92**(16): p. 1295-1302.

86. **Xu, J., Y. Liu, Y. Yang, S. Bates, and J.-T. Zhang**, *Characterization of Oligomeric Human Half-ABC Transporter ATP-binding Cassette G2.* Journal of Biological Chemistry, 2004. **279**(19): p. 19781-19789.

87. **Hegedús, C., C. Ozvegy-Laczka, G. Szakacs, and B. Sarkadi**, *Interaction of ABC multidrug transporters with anticancer protein kinase inhibitors: substrates and/or inhibitors?* Curr Cancer Drug Targets, 2009. **9**(3): p. 252-72.

88. **Jonker, J.W., M. Buitelaar, E. Wagenaar, M.A. Van Der Valk, G.L. Scheffer, R.J. Scheper, T. Plosch, F. Kuipers, R.P. Elferink, H. Rosing, J.H. Beijnen, and A.H. Schinkel**, *The breast cancer resistance protein protects against a major chlorophyll-derived dietary phototoxin and protoporphyria.* Proc Natl Acad Sci U S A, 2002. **99**(24): p. 15649-54.

89. **Jonker, J.W., J.W. Smit, R.F. Brinkhuis, M. Maliepaard, J.H. Beijnen, J.H. Schellens, and A.H. Schinkel**, *Role of breast cancer resistance protein in the bioavailability and fetal penetration of topotecan.* J Natl Cancer Inst, 2000. **92**(20): p. 1651-6.

90. **Polgar, O., R.W. Robey, and S.E. Bates**, *ABCG2: structure, function and role in drug response.* Expert Opinion on Drug Metabolism & Toxicology, 2008. **4**(1): p. 1-15.

91. **Honjo, Y., C.A. Hrycyna, Q.W. Yan, W.Y. Medina-Perez, R.W. Robey, A. van de Laar, T. Litman, M. Dean, and S.E. Bates**, *Acquired mutations in the MXR/BCRP/ABCP gene alter substrate specificity in MXR/BCRP/ABCP-overexpressing cells.* Cancer Res, 2001. **61**(18): p. 6635-9.

92. **Volk, E.L., K.M. Farley, Y. Wu, F. Li, R.W. Robey, and E. Schneider**, *Overexpression of wild-type breast cancer resistance protein mediates methotrexate resistance.* Cancer Res, 2002. **62**(17): p. 5035-40.

93. **Sarkadi, B., C. Özvegy-Laczka, K. Német, and A. Váradi**, *ABCG2 - a transporter for all seasons.* FEBS Letters, 2004. **567**(1): p. 116-120.

94. **Sharom, F.J.**, *ABC multidrug transporters: structure, function and role in chemoresistance.* Pharmacogenomics, 2008. **9**(1): p. 105-127.

95. **Shtil, A.A.**, *Signal Transduction Pathways and Transcriptional Mechanisms as Targets for Prevention of Emergence of Multidrug Resistance in Human Cancer Cells.* Current Drug Targets, 2001. **2**(1): p. 57.

96. **Tsuruo, T., H. Iida, S. Tsukagoshi, and Y. Sakurai**, *Overcoming of Vincristine Resistance in P388 Leukemia in Vivo and in Vitro through Enhanced Cytotoxicity of Vincristine and Vinblastine by Verapamil.* Cancer Research, 1981. **41**(5): p. 1967-1972.

97. **Twentyman, P.R., N.E. Fox, and D.J. White**, *Cyclosporin A and its analogues as modifiers of adriamycin and vincristine resistance in a multi-drug resistant human lung cancer cell line.* British Journal of Cancer. 1987 July; 56(1): 55–57., 1987. **56**(1): p. 55–57. .

98. **Wu, C.-P., A.M. Calcagno, and S.V. Ambudkar**, *Reversal of ABC drug transporter-mediated multidrug resistance in cancer cells: Evaluation of current strategies.* Current molecular pharmacology, 2008. **1**(2): p. 93-105.

99. **Benson, A., D. Trump, J. Koeller, M. Egorin, E. Olman, R. Witte, T. Davis, and D. Tormey**, *Phase I study of vinblastine and verapamil given by concurrent iv infusion.* Cancer Treat Reports, 1985. **69**`: p. 795-9.

100. **Bartlett, N.L., B.L. Lum, G.A. Fisher, N.A. Brophy, M.N. Ehsan, J. Halsey, and B.I. Sikic**, *Phase I trial of doxorubicin with cyclosporine as a modulator of multidrug resistance.* Journal of Clinical Oncology, 1994. **12**(4): p. 835-842.

101. **Dhainaut, A., G. Regnier, G. Atassi, A. Pierre, S. Leonce, L. Kraus-Berthier, and J.F. Prost**, *New triazine derivatives as potent modulators of*

multidrug resistance. Journal of Medicinal Chemistry, 1992. **35**(13): p. 2481-2496.

102. **Twentyman, P.R. and N.M. Bleehen**, *Resistance modification by PSC-833, a novel non-immunosuppressive cyclosporin A.* European Journal of Cancer and Clinical Oncology, 1991. **27**(12): p. 1639-1642.

103. **Kuppens, I.E.L.M., E.O. Witteveen, R.C. Jewell, S.A. Radema, E.M. Paul, S.G. Mangum, J.H. Beijnen, E.E. Voest, and J.H.M. Schellens**, *A Phase I, Randomized, Open-Label, Parallel-Cohort, Dose-Finding Study of Elacridar (GF120918) and Oral Topotecan in Cancer Patients.* Clinical Cancer Research, 2007. **13**(11): p. 3276-3285.

104. **Chi, K.N., S.K. Chia, R. Dixon, M.J. Newman, V.J. Wacher, B. Sikic, and K.A. Gelmon**, *A phase I pharmacokinetic study of the P-glycoprotein inhibitor, ONT-093, in combination with paclitaxel in patients with advanced cancer.* Investigational New Drugs, 2005. **23**(4): p. 311-315.

105. **Abraham, J., M. Edgerly, R. Wilson, C. Chen, A. Rutt, S. Bakke, R. Robey, A. Dwyer, B. Goldspiel, F. Balis, O. Van Tellingen, S.E. Bates, and T. Fojo**, *A Phase I Study of the P-Glycoprotein Antagonist Tariquidar in Combination with Vinorelbine.* Clinical Cancer Research, 2009. **15**(10): p. 3574-3582.

106. **Ruff, P., D. Vorobiof, J. Jordaan, G. Demetriou, S. Moodley, A. Nosworthy, I. Werner, J. Raats, and L. Burgess**, *A randomized, placebo-controlled, double-blind phase 2 study of docetaxel compared to docetaxel plus zosuquidar (LY335979) in women with metastatic or locally recurrent breast cancer who have received one prior chemotherapy regimen.* Cancer Chemotherapy and Pharmacology, 2009. **64**(4): p. 763-768.

107. **Baumert, C. and A. Hilgeroth**, *Recent Advances in the Development of P-gp Inhibitors.* Anti-Cancer Agents in Medicinal Chemistry, 2009. **9**(4): p. 415-436.

108. **Gekeler, V., W. Ise, K.H. Sanders, W.R. Ulrich, and J. Beck**, *The Leukotriene LTD4 Receptor Antagonist Mk571 Specifically Modulates MRP Associated Multidrug Resistance.* Biochemical and Biophysical Research Communications, 1995. **208**(1): p. 345-352.

109. **Duffy, C.P., C.J. Elliott, R.A. O'Connor, M.M. Heenan, S. Coyle, I.M. Cleary, K. Kavanagh, S. Verhaegen, C.M. O'Loughlin, R. NicAmhlaoibh, and M. Clynes**, *Enhancement of chemotherapeutic drug toxicity to human tumour cells in vitro by a subset of non-steroidal anti-inflammatory drugs (NSAIDs).* European Journal of Cancer, 1998. **34**(8): p. 1250-1259.

110. **Rabindran, S.K., D.D. Ross, L.A. Doyle, W. Yang, and L.M. Greenberger**, *Fumitremorgin C Reverses Multidrug Resistance in Cells Transfected with the Breast Cancer Resistance Protein.* Cancer Research, 2000. **60**(1): p. 47-50.

111. **Allen, J.D., A. van Loevezijn, J.M. Lakhai, M. van der Valk, O. van Tellingen, G. Reid, J.H.M. Schellens, G.-J. Koomen, and A.H. Schinkel**, *Potent and Specific Inhibition of the Breast Cancer Resistance Protein Multidrug Transporter in Vitro and in Mouse Intestine by a Novel Analogue of Fumitremorgin C* Molecular Cancer Therapeutics, 2002. **1**(6): p. 417-425.

112. **Schlessinger, J.**, *Cell Signaling by Receptor Tyrosine Kinases.* Cell, 2000. **103**(2): p. 211-225.

113. **Özvegy-Laczka, C., J. Cserepes, N.B. Elkind, and B. Sarkadi**, *Tyrosine kinase inhibitor resistance in cancer: role of ABC multidrug transporters.* Drug Resistance Updates, 2005. **8**(1-2): p. 15-26.

114. **Steeghs, N., J.W. Nortier, and H. Gelderblom**, *Small molecule tyrosine kinase inhibitors in the treatment of solid tumors: an update of recent developments.* Ann Surg Oncol, 2007. **14**(2): p. 942-53.

115. **Arora, A. and E.M. Scholar**, *Role of tyrosine kinase inhibitors in cancer therapy.* J Pharmacol Exp Ther, 2005. **315**(3): p. 971-9.

116. **Krause, D.S. and R.A. Van Etten**, *Tyrosine kinases as targets for cancer therapy.* N Engl J Med, 2005. **353**(2): p. 172-87.

117. **Vlahovic, G. and J. Crawford**, *Activation of Tyrosine Kinases in Cancer.* Oncologist, 2003. **8**(6): p. 531-538.

118. **van Erp, N.P., H. Gelderblom, and H.-J. Guchelaar**, *Clinical pharmacokinetics of tyrosine kinase inhibitors.* Cancer Treatment Reviews, 2009. **35**(8): p. 692-706.

119. **Bukowski, R.M., U. Yasothan, and P. Kirkpatrick**, *Pazopanib.* Nat Rev Drug Discov. **9**(1): p. 17-18.

120. *National Cancer Institute.* [cited; Available from: http://www.cancer.gov/.

121. **Druker, B.J.**, *Inhibition of the Bcr-Abl tyrosine kinase as a therapeutic strategy for CML.* Oncogene, 2002. **21**(56): p. 8541-6.

122. **Weisberg, E. and J.D. Griffin**, *Resistance to imatinib (Glivec): update on clinical mechanisms.* Drug Resist Updat, 2003. **6**(5): p. 231-8.

123. **Ozvegy-Laczka, C., T. Hegedús, G. Varady, O. Ujhelly, J.D. Schuetz, A. Varadi, G. Keri, L. Orfi, K. Nemet, and B. Sarkadi**, *High-Affinity Interaction of Tyrosine Kinase Inhibitors with the ABCG2 Multidrug Transporter.* Mol Pharmacol, 2004. **65**(6): p. 1485-1495.

124. **Nimmanapalli, R., E. O'Bryan, M. Huang, P. Bali, P.K. Burnette, T. Loughran, J. Tepperberg, R. Jove, and K. Bhalla**, *Molecular characterization and sensitivity of STI-571 (imatinib mesylate, Gleevec)-resistant, Bcr-Abl-positive, human acute leukemia cells to SRC kinase inhibitor PD180970 and 17-allylamino-17-demethoxygeldanamycin.* Cancer Res, 2002. **62**(20): p. 5761-9.

125. **Campbell, L.J., C. Patsouris, K.C. Rayeroux, K. Somana, E.H. Januszewicz, and J. Szer**, *BCR/ABL amplification in chronic myelocytic leukemia blast crisis following imatinib mesylate administration.* Cancer Genet Cytogenet, 2002. **139**(1): p. 30-3.

126. **Morel, F., M.J. Bris, A. Herry, G.L. Calvez, V. Marion, J.F. Abgrall, C. Berthou, and M.D. Braekeleer**, *Double minutes containing amplified bcr-abl fusion gene in a case of chronic myeloid leukemia treated by imatinib.* Eur J Haematol, 2003. **70**(4): p. 235-9.

127. **Mahon, F.X., F. Belloc, V. Lagarde, C. Chollet, F. Moreau-Gaudry, J. Reiffers, J.M. Goldman, and J.V. Melo**, *MDR1 gene overexpression confers resistance to imatinib mesylate in leukemia cell line models.* Blood, 2003. **101**(6): p. 2368-73.

128. **Hamada, A., H. Miyano, H. Watanabe, and H. Saito**, *Interaction of imatinib mesilate with human P-glycoprotein.* J Pharmacol Exp Ther, 2003. **307**(2): p. 824-8.

129. **Houghton, P.J., G.S. Germain, F.C. Harwood, J.D. Schuetz, C.F. Stewart, E. Buchdunger, and P. Traxler**, *Imatinib mesylate is a potent inhibitor of the ABCG2 (BCRP) transporter and reverses resistance to topotecan and SN-38 in vitro.* Cancer Res, 2004. **64**(7): p. 2333-7.

130. **Gardner, E.R., N.F. Smith, W.D. Figg, and A. Sparreboom**, *Influence of the dual ABCB1 and ABCG2 inhibitor tariquidar on the disposition of oral imatinib in mice.* J Exp Clin Cancer Res, 2009. **28**: p. 99.

131. **Gambacorti-Passerini, C., R. Barni, P. le Coutre, M. Zucchetti, G. Cabrita, L. Cleris, F. Rossi, E. Gianazza, J. Brueggen, R. Cozens, P. Pioltelli, E. Pogliani, G. Corneo, F. Formelli, and M. D'Incalci**, *Role of alpha1 acid glycoprotein in the in vivo resistance of human BCR-ABL(+) leukemic cells to the abl inhibitor STI571.* J Natl Cancer Inst, 2000. **92**(20): p. 1641-50.

132. **Jorgensen, H.G., M.A. Elliott, E.K. Allan, C.E. Carr, T.L. Holyoake, and K.D. Smith**, *alpha 1-Acid glycoprotein expressed in the plasma of chronic myeloid leukemia patients does not mediate significant in vitro resistance to STI571.* Blood, 2002. **99**(2): p. 713-715.

133. **le Coutre, P., K.-A. Kreuzer, I.-K. Na, J. Lupberger, M. Holdhoff, C. Appelt, M. Schwarz, C. Müller, C. Gambacorti-Passerini, U. Platzbecker, R. Bonnet, G. Ehninger, and C.A. Schmidt**, *Determination of [alpha]-1 Acid Glycoprotein in Patients with Ph+ Chronic Myeloid Leukemia during the First 13 Weeks of Therapy with STI571.* Blood Cells, Molecules, and Diseases, 2002. **28**(1): p. 75-85.

134. **Lombardo, L.J., F.Y. Lee, P. Chen, D. Norris, J.C. Barrish, K. Behnia, S. Castaneda, L.A. Cornelius, J. Das, A.M. Doweyko, C. Fairchild, J.T. Hunt, I. Inigo, K. Johnston, A. Kamath, D. Kan, H. Klei, P. Marathe, S. Pang, R. Peterson, S. Pitt, G.L. Schieven, R.J. Schmidt, J. Tokarski, M.L. Wen, J. Wityak, and R.M. Borzilleri**, *Discovery of N-(2-chloro-6-methyl-phenyl)-2-(6-(4-(2-hydroxyethyl)-   piperazin-1-yl)-2-methylpyrimidin-4-ylamino)thiazole-5-carboxamide (BMS-354825), a dual Src/Abl kinase inhibitor with potent antitumor activity in preclinical assays.* J Med Chem, 2004. **47**(27): p. 6658-61.

135. **Ramirez, P. and J.F. DiPersio**, *Therapy options in imatinib failures.* Oncologist, 2008. **13**(4): p. 424-34.

136. **Shah, N.P., C. Tran, F.Y. Lee, P. Chen, D. Norris, and C.L. Sawyers**, *Overriding imatinib resistance with a novel ABL kinase inhibitor.* Science, 2004. **305**(5682): p. 399-401.

137. **Nam, S., D. Kim, J.Q. Cheng, S. Zhang, J.-H. Lee, R. Buettner, J. Mirosevich, F.Y. Lee, and R. Jove**, *Action of the Src Family Kinase Inhibitor, Dasatinib (BMS-354825), on Human Prostate Cancer Cells.* Cancer Res, 2005. **65**(20): p. 9185-9189.

138. **Martin, G.S.**, *The hunting of the Src.* Nat Rev Mol Cell Biol, 2001. **2**(6): p. 467-75.

139. **Manning, G., D.B. Whyte, R. Martinez, T. Hunter, and S. Sudarsanam**, *The protein kinase complement of the human genome.* Science, 2002. **298**(5600): p. 1912-34.

140. **Frame, M.C.**, *Src in cancer: deregulation and consequences for cell behaviour.* Biochim Biophys Acta, 2002. **1602**(2): p. 114-30.

141. **Fizazi, K.**, *The role of Src in prostate cancer.* Ann Oncol, 2007. **18**(11): p. 1765-73.

142. **Summy, J.M. and G.E. Gallick**, *Treatment for advanced tumors: SRC reclaims center stage.* Clin Cancer Res, 2006. **12**(5): p. 1398-401.

143. **Xia, W., R.J. Mullin, B.R. Keith, L.H. Liu, H. Ma, D.W. Rusnak, G. Owens, K.J. Alligood, and N.L. Spector**, *Anti-tumor activity of GW572016:*

a dual tyrosine kinase inhibitor blocks EGF activation of EGFR/erbB2 and downstream Erk1/2 and AKT pathways. Oncogene, 2002. **21**(41): p. 6255-63.

144. **Geyer, C.E., J. Forster, D. Lindquist, S. Chan, C.G. Romieu, T. Pienkowski, A. Jagiello-Gruszfeld, J. Crown, A. Chan, B. Kaufman, D. Skarlos, M. Campone, N. Davidson, M. Berger, C. Oliva, S.D. Rubin, S. Stein, and D. Cameron**, *Lapatinib plus capecitabine for HER2-positive advanced breast cancer.* N Engl J Med, 2006. **355**(26): p. 2733-43.

145. **Hynes, N.E. and G. MacDonald**, *ErbB receptors and signaling pathways in cancer.* Current Opinion in Cell Biology, 2009. **21**(2): p. 177-184.

146. **Graus-Porta, D., R.R. Beerli, J.M. Daly, and N.E. Hynes**, *ErbB-2, the preferred heterodimerization partner of all ErbB receptors, is a mediator of lateral signaling.* Embo J, 1997. **16**(7): p. 1647-1655.

147. **Wada, T., X. Qian, and M.I. Greene**, *Intermolecular association of the p185neu protein and EGF receptor modulates EGF receptor function.* Cell, 1990. **61**(7): p. 1339-1347.

148. **Slamon, D.J., G.M. Clark, S.G. Wong, W.J. Levin, A. Ullrich, and W.L. McGuire**, *Human Breast Cancer: Correlation of Relapse and Survival with Amplification of the HER-2/neu Oncogene.* Science, 1987. **235**(4785): p. 177-182.

149. **Carter, C.A., R.J. Kelly, and G. Giaccone**, *Small-molecule inhibitors of the human epidermal receptor family.* Expert Opinion on Investigational Drugs, 2009. **18**(12): p. 1829-1842.

150. **Spector, N.L., W. Xia, H. Burris, III, H. Hurwitz, E.C. Dees, A. Dowlati, B. O'Neil, B. Overmoyer, P.K. Marcom, K.L. Blackwell, D.A. Smith, K.M. Koch, A. Stead, S. Mangum, M.J. Ellis, L. Liu, A.K. Man, T.M. Bremer, J. Harris, and S. Bacus**, *Study of the Biologic Effects of Lapatinib, a Reversible Inhibitor of ErbB1 and ErbB2 Tyrosine Kinases, on Tumor Growth and Survival Pathways in Patients With Advanced Malignancies.* J Clin Oncol, 2005. **23**(11): p. 2502-2512.

151. **Rusnak, D.W., K. Lackey, K. Affleck, E.R. Wood, K.J. Alligood, N. Rhodes, B.R. Keith, D.M. Murray, W.B. Knight, R.J. Mullin, and T.M. Gilmer**, *The Effects of the Novel, Reversible Epidermal Growth Factor Receptor/ErbB-2 Tyrosine Kinase Inhibitor, GW2016, on the Growth of Human Normal and Tumor-derived Cell Lines in Vitro and in Vivo.* Molecular Cancer Therapeutics, 2001. **1**(2): p. 85-94.

152. **Gazdar, A.F.**, *Activating and resistance mutations of EGFR in non-small-cell lung cancer: role in clinical response to EGFR tyrosine kinase inhibitors.* Oncogene. **28**(S1): p. S24-S31.

153. **Thatcher, N., A. Chang, P. Parikh, J. Rodrigues Pereira, T. Ciuleanu, J. von Pawel, S. Thongprasert, E.H. Tan, K. Pemberton, V. Archer, and K. Carroll**, *Gefitinib plus best supportive care in previously treated patients with refractory advanced non-small-cell lung cancer: results from a randomised, placebo-controlled, multicentre study (Iressa Survival Evaluation in Lung Cancer).* The Lancet, 2005. **366**(9496): p. 1527-1537.

154. **Blackhall, F., M. Ranson, and N. Thatcher**, *Where next for gefitinib in patients with lung cancer?* The Lancet Oncology, 2006. **7**(6): p. 499-507.

155. **Paez, J.G., P.A. Janne, J.C. Lee, S. Tracy, H. Greulich, S. Gabriel, P. Herman, F.J. Kaye, N. Lindeman, T.J. Boggon, K. Naoki, H. Sasaki, Y. Fujii, M.J. Eck, W.R. Sellers, B.E. Johnson, and M. Meyerson**, *EGFR*

Mutations in Lung Cancer: Correlation with Clinical Response to Gefitinib Therapy. Science, 2004. **304**(5676): p. 1497-1500.

156. **Lynch, T.J., D.W. Bell, R. Sordella, S. Gurubhagavatula, R.A. Okimoto, B.W. Brannigan, P.L. Harris, S.M. Haserlat, J.G. Supko, F.G. Haluska, D.N. Louis, D.C. Christiani, J. Settleman, and D.A. Haber**, *Activating Mutations in the Epidermal Growth Factor Receptor Underlying Responsiveness of Non-Small-Cell Lung Cancer to Gefitinib.* N Engl J Med, 2004. **350**(21): p. 2129-2139.

157. **Pao, W., V.A. Miller, K.A. Politi, G.J. Riely, R. Somwar, M.F. Zakowski, M.G. Kris, and H. Varmus**, *Acquired resistance of lung adenocarcinomas to gefitinib or erlotinib is associated with a second mutation in the EGFR kinase domain.* PLoS Med, 2005. **2**(3): p. e73.

158. **Bianco, R., T. Gelardi, V. Damiano, F. Ciardiello, and G. Tortora**, *Mechanisms of resistance to EGFR inhibitors.* Targeted Oncology, 2007. **2**(1): p. 31-37.

159. **Wilhelm, S.M., C. Carter, L. Tang, D. Wilkie, A. McNabola, H. Rong, C. Chen, X. Zhang, P. Vincent, M. McHugh, Y. Cao, J. Shujath, S. Gawlak, D. Eveleigh, B. Rowley, L. Liu, L. Adnane, M. Lynch, D. Auclair, I. Taylor, R. Gedrich, A. Voznesensky, B. Riedl, L.E. Post, G. Bollag, and P.A. Trail**, *BAY 43-9006 Exhibits Broad Spectrum Oral Antitumor Activity and Targets the RAF/MEK/ERK Pathway and Receptor Tyrosine Kinases Involved in Tumor Progression and Angiogenesis.* Cancer Res, 2004. **64**(19): p. 7099-7109.

160. **Chen, F.L., W. Xia, and N.L. Spector**, *Acquired resistance to small molecule ErbB2 tyrosine kinase inhibitors.* Clin Cancer Res, 2008. **14**(21): p. 6730-4.

161. **Steegmann, J.L., M. Michallet, E. Morra, D. Marin, G.J. Ossenkoppele, G. Verhoef, T. Kuhr, M. Bjoreman, M. Sterckx, and K. Cerri**, *Imatinib use in chronic phase CML in clinical practice: the UNIC study.* J Clin Oncol (Meeting Abstracts), 2008. **26**(15_suppl): p. 7077-.

162. **Gorre, M.E., M. Mohammed, K. Ellwood, N. Hsu, R. Paquette, P.N. Rao, and C.L. Sawyers**, *Clinical Resistance to STI-571 Cancer Therapy Caused by BCR-ABL Gene Mutation or Amplification.* Science, 2001. **293**(5531): p. 876-880.

163. **Druker, B.J.**, *Imatinib and chronic myeloid leukemia: validating the promise of molecularly targeted therapy.* European Journal of Cancer, 2002. **38 Suppl 5**: p. S70-6.

164. **Schindler, C.G., T. Armbrust, B. Gunawan, C. Langer, L. Fuzesi, and G. Ramadori**, *Gastrointestinal stromal tumor (GIST) -- single center experience of prolonged treatment with imatinib.* Z Gastroenterol, 2005. **43**(3): p. 267-73.

165. **Mahon, F.X., M.W.N. Deininger, B. Schultheis, J. Chabrol, J. Reiffers, J.M. Goldman, and J.V. Melo**, *Selection and characterization of BCR-ABL positive cell lines with differential sensitivity to the tyrosine kinase inhibitor STI571: diverse mechanisms of resistance.* Blood, 2000. **96**(3): p. 1070-1079.

166. **Hegedús, T., L. Orfi, A. Seprodi, A. Váradi, B. Sarkadi, and G. Kéri**, *Interaction of tyrosine kinase inhibitors with the human multidrug transporter proteins, MDR1 and MRP1.* Biochimica et Biophysica Acta (BBA) - Molecular Basis of Disease, 2002. **1587**(2-3): p. 318-325.

167. **Mukai, M., X.-F. Che, T. Furukawa, T. Sumizawa, S. Aoki, X.-Q. Ren, M. Haraguchi, Y. Sugimoto, M. Kobayashi, H. Takamatsu, and S.-i.**

Akiyama, *Reversal of the resistance to STI571 in human chronic myelogenous leukemia K562 cells.* Cancer Science, 2003. **94**(6): p. 557-563.

168. **Jordanides, N.E., H.G. Jorgensen, T.L. Holyoake, and J.C. Mountford**, *Functional ABCG2 is overexpressed on primary CML CD34+ cells and is inhibited by imatinib mesylate.* Blood, 2006. **108**(4): p. 1370-1373.

169. **Houghton, P.J., G.S. Germain, F.C. Harwood, J.D. Schuetz, C.F. Stewart, E. Buchdunger, and P. Traxler**, *Imatinib Mesylate Is a Potent Inhibitor of the ABCG2 (BCRP) Transporter and Reverses Resistance to Topotecan and SN-38 in Vitro.* Cancer Res, 2004. **64**(7): p. 2333-2337.

170. **Burger, H., H. van Tol, A.W.M. Boersma, M. Brok, E.A.C. Wiemer, G. Stoter, and K. Nooter**, *Imatinib mesylate (STI571) is a substrate for the breast cancer resistance protein (BCRP)/ABCG2 drug pump.* Blood, 2004. **104**(9): p. 2940-2942.

171. **Brendel, C., C. Scharenberg, M. Dohse, R.W. Robey, S.E. Bates, S. Shukla, S.V. Ambudkar, Y. Wang, G. Wennemuth, A. Burchert, U. Boudriot, and A. Neubauer**, *Imatinib mesylate and nilotinib (AMN107) exhibit high-affinity interaction with ABCG2 on primitive hematopoietic stem cells.* Leukemia, 2007. **21**(6): p. 1267-1275.

172. **Artursson, P., K. Palm, and K. Luthman**, *Caco-2 monolayers in experimental and theoretical predictions of drug transport.* Advanced Drug Delivery Reviews, 2001. **46**(1-3): p. 27-43.

173. **Kamath, A.V., J. Wang, F.Y. Lee, and P.H. Marathe**, *Preclinical pharmacokinetics and in vitro metabolism of dasatinib (BMS-354825): a potent oral multi-targeted kinase inhibitor against SRC and BCR-ABL.* Cancer Chemother Pharmacol, 2008. **61**(3): p. 365-76.

174. **Hiwase, D.K., V. Saunders, D. Hewett, A. Frede, S. Zrim, P. Dang, L. Eadie, L.B. To, J. Melo, S. Kumar, T.P. Hughes, and D.L. White**, *Dasatinib cellular uptake and efflux in chronic myeloid leukemia cells: therapeutic implications.* Clin Cancer Res, 2008. **14**(12): p. 3881-8.

175. **Lagas, J.S., R.A. van Waterschoot, V.A. van Tilburg, M.J. Hillebrand, N. Lankheet, H. Rosing, J.H. Beijnen, and A.H. Schinkel**, *Brain accumulation of dasatinib is restricted by P-glycoprotein (ABCB1) and breast cancer resistance protein (ABCG2) and can be enhanced by elacridar treatment.* Clin Cancer Res, 2009. **15**(7): p. 2344-51.

176. **White, D.L., V.A. Saunders, P. Dang, J. Engler, A.C.W. Zannettino, A.C. Cambareri, S.R. Quinn, P.W. Manley, and T.P. Hughes**, *OCT-1-mediated influx is a key determinant of the intracellular uptake of imatinib but not nilotinib (AMN107): reduced OCT-1 activity is the cause of low in vitro sensitivity to imatinib.* Blood, 2006. **108**(2): p. 697-704.

177. **Polli, J.W., J.E. Humphreys, K.A. Harmon, S. Castellino, M.J. O'Mara, K.L. Olson, L.S. John-Williams, K.M. Koch, and C.J. Serabjit-Singh**, *The role of efflux and uptake transporters in [N-{3-chloro-4-[(3-fluorobenzyl)oxy]phenyl}-6-[5-({[2-(methylsulfonyl)ethy l]amino}methyl)-2-furyl]-4-quinazolinamine (GW572016, lapatinib) disposition and drug interactions.* Drug Metab Dispos, 2008. **36**(4): p. 695-701.

178. **Molina, J.R., S.H. Kaufmann, J.M. Reid, S.D. Rubin, M. GÃ¡lvez-Peralta, R. Friedman, K.S. Flatten, K.M. Koch, T.M. Gilmer, R.J. Mullin, R.C. Jewell, S.J. Felten, S. Mandrekar, A.A. Adjei, and C. Erlichman**, *Evaluation of Lapatinib and Topotecan Combination Therapy: Tissue Culture,*

Murine Xenograft, and Phase I Clinical Trial Data. Clinical Cancer Research, 2008. **14**(23): p. 7900-7908.

179. **Collins, D.M., J. Crown, N. O'Donovan, A. Devery, F. O'Sullivan, L. O'Driscoll, M. Clynes, and R. O'Connor**, *Tyrosine kinase inhibitors potentiate the cytotoxicity of MDR-substrate anticancer agents independent of growth factor receptor status in lung cancer cell lines.* Invest New Drugs, 2009.

180. **Dunne, G., L. Breen, D. Collins, S. Roche, M. Clynes, and R. O'Connor**, *Modulation of P-gp expression by lapatinib.* Investigational New Drugs, 2010: p. 1-10.

181. **Kuang, Y.-H., T. Shen, X. Chen, K. Sodani, E. Hopper-Borge, A.K. Tiwari, J.W.K.K. Lee, L.-W. Fu, and Z.-S. Chen**, *Lapatinib and erlotinib are potent reversal agents for MRP7 (ABCC10)-mediated multidrug resistance.* Biochemical Pharmacology, 2010. **79**(2): p. 154-161.

182. **Kitazaki, T., M. Oka, Y. Nakamura, J. Tsurutani, S. Doi, M. Yasunaga, M. Takemura, H. Yabuuchi, H. Soda, and S. Kohno**, *Gefitinib, an EGFR tyrosine kinase inhibitor, directly inhibits the function of P-glycoprotein in multidrug resistant cancer cells.* Lung Cancer, 2005. **49**(3): p. 337-343.

183. **Nakamura, Y., M. Oka, H. Soda, K. Shiozawa, M. Yoshikawa, A. Itoh, Y. Ikegami, J. Tsurutani, K. Nakatomi, T. Kitazaki, S. Doi, H. Yoshida, and S. Kohno**, *Gefitinib ("Iressa", ZD1839), an Epidermal Growth Factor Receptor Tyrosine Kinase Inhibitor, Reverses Breast Cancer Resistance Protein/ABCG2-Mediated Drug Resistance.* Cancer Res, 2005. **65**(4): p. 1541-1546.

184. **Azzariti, A., L. Porcelli, G.M. Simone, A.E. Quatrale, N.A. Colabufo, F. Berardi, R. Perrone, M. Zucchetti, M. D'Incalci, J.M. Xu, and A. Paradiso**, *Tyrosine kinase inhibitors and multidrug resistance proteins: interactions and biological consequences.* Cancer Chemother Pharmacol, 2009.

185. **de Vries, N., T. Buckle, J. Zhao, J. Beijnen, J. Schellens, and O. van Tellingen**, *Restricted brain penetration of the tyrosine kinase inhibitor erlotinib due to the drug transporters P-gp and BCRP.* Investigational New Drugs: p. 1-7.

186. **Li, J., G. Cusatis, J. Brahmer, A. Sparreboom, R.W. Robey, S.E. Bates, M. Hidalgo, and S. Baker**, *Association of variant ABCG2 and the pharmacokinetics of epidermal growth factor receptor tyrosine kinase inhibitors in cancer patients.* Cancer and Biology Therapy, 2007. **6**(3).

187. **Shi, Z., X.-X. Peng, I.-W. Kim, S. Shukla, Q.-S. Si, R.W. Robey, S.E. Bates, T. Shen, C.R. Ashby, L.-W. Fu, S.V. Ambudkar, and Z.-S. Chen**, *Erlotinib (Tarceva, OSI-774) Antagonizes ATP-Binding Cassette Subfamily B Member 1 and ATP-Binding Cassette Subfamily G Member 2–Mediated Drug Resistance.* Cancer Research, 2007. **67**(22): p. 11012-11020.

188. **Alnaim, L.**, *Therapeutic drug monitoring of cancer chemotherapy.* Journal of Oncology Pharmacy Practice, 2007. **13**(4): p. 207-221.

189. **McLeod, H.L.**, *Therapeutic drug monitoring opportunities in cancer therapy.* Pharmacology & Therapeutics, 1997. **74**(1): p. 39-54.

190. **Liu, Y., Y. Yang, X. Liu, and T. Jiang**, *Quantification of pegylated liposomal doxorubicin and doxorubicinol in rat plasma by liquid chromatography/electrospray tandem mass spectroscopy: Application to preclinical pharmacokinetic studies.* Talanta, 2008. **74**(4): p. 887-895.

191. **Jain, K.K.**, *Personalised medicine for cancer: from drug development into clinical practice.* Expert Opinion on Pharmacotherapy, 2005. **6**(9): p. 1463-1476.

192. **Chatelut, E., X. Pivot, J. Otto, C. Chevreau, A. Thyss, N. Renée, G. Milano, and P. Canal**, *A limited sampling strategy for determining carboplatin AUC and monitoring drug dosage.* European Journal of Cancer, 2000. **36**(2): p. 264-269.

193. **Rousseau, A. and P. Marquet**, *Application of pharmacokinetic modelling to the routine therapeutic drug monitoring of anticancer drugs.* Fundam Clin Pharmacol, 2002. **16**(4): p. 253-62.

194. **McMahon, G.**, *Analytical Instrumentation, A Guide to Laboratory, Portable and Miniaturized Instruments.* First ed. 2007: John Wiley & Sons Ltd.

195. **Kealey, D. and P. Haines**, *Analytical Chemistry.* Instant Notes, ed. B.D. Haines. 2002, Leeds, UK: BIOS Scientific Publishers Ltd.

196. **Ardrey, R.E.**, *Liquid Chromatography –Mass Spectrometry: An Introduction*, ed. D.J. Ando. 2003: John Wiley & Sons Ltd,.

197. **Gates, P.** *Mass Spectrometry Resource -Electrospray Ionisation* 2004 [cited; Available from: http://www.chm.bris.ac.uk/ms/theory/esi-ionisation.html.

198. **Agilent**. *Agilent 6410 Triple Quadrupole LC/MS.* [cited; Available from: http://www.chem.agilent.com/Library/brochures/5989-4894EN_Lo.pdf.

199. **Shin, K.-H., B.-H. Kim, T.-E. Kim, J.W. Kim, S. Yi, S.-H. Yoon, J.-Y. Cho, S.-G. Shin, I.-J. Jang, and K.-S. Yu**, *The effects of ketoconazole and rifampicin on the pharmacokinetics of mirodenafil in healthy Korean male volunteers: An open-label, one-sequence, three-period, three-treatment crossover study.* Clinical Therapeutics, 2009. **31**(12): p. 3009-3020.

200. **Bai, F., B.B. Freeman, 3rd, C.H. Fraga, M. Fouladi, and C.F. Stewart**, *Determination of lapatinib (GW572016) in human plasma by liquid chromatography electrospray tandem mass spectrometry (LC-ESI-MS/MS).* J Chromatogr B Analyt Technol Biomed Life Sci, 2006. **831**(1-2): p. 169-75.

201. **Owen, L.J., S. Haslam, J.E. Adaway, P. Wood, C. Glenn, and B.G. Keevil**, *A simplified liquid chromatography tandem mass spectrometry assay, using on-line solid-phase extraction, for the quantitation of cortisol in saliva and comparison with a routine DELFIA method.* Ann Clin Biochem, 2010: p. acb.2009.009053.

202. **Phillip, A.S., D.S. Kelsie, and K. Sarah**, *Quantitative Analysis of Gamma-Hydroxybutyrate at Endogenous Concentrations in Hair using Liquid Chromatography Tandem Mass Spectrometry.* Journal of Forensic Sciences. **9999**(9999).

203. **de Bruijn, P., I.M.G. Moghaddam-Helmantel, M.J.A. de Jonge, T. Meyer, M.-H. Lam, J. Verweij, E.A.C. Wiemer, and W.J. Loos**, *Validated bioanalytical method for the quantification of RGB-286638, a novel multi-targeted protein kinase inhibitor, in human plasma and urine by liquid chromatography/tandem triple-quadrupole mass spectrometry.* Journal of Pharmaceutical and Biomedical Analysis, 2009. **50**(5): p. 977-982.

204. **Chang, M.S., Q. Ji, J. Zhang, and T.A. El-Shourbagy**, *Historical review of sample preparation for chromatographic bioanalysis: pros and cons.* Drug Development Research, 2007. **68**(3): p. 107-133.

205. **Hsieh, S., T. Tobien, K. Koch, and J. Dunn**, *Increasing throughput of parallel on-line extraction liquid chromatography/electrospray ionization tandem mass spectrometry system for GLP quantitative bioanalysis in drug*

development. Rapid Communications in Mass Spectrometry, 2004. **18**(3): p. 285-292.

206. **Scorrano, S., L. Longo, and G. Vasapollo**, *Molecularly imprinted polymers for solid-phase extraction of 1-methyladenosine from human urine.* Analytica Chimica Acta. **659**(1-2): p. 167-171.

207. **Pérez-Moral, N. and A.G. Mayes**, *Direct rapid synthesis of MIP beads in SPE cartridges.* Biosensors and Bioelectronics, 2006. **21**(9): p. 1798-1803.

208. **Anderson, R.A., M.M. Ariffin, P.A.G. Cormack, and E.I. Miller**, *Comparison of molecularly imprinted solid-phase extraction (MISPE) with classical solid-phase extraction (SPE) for the detection of benzodiazepines in post-mortem hair samples.* Forensic Science International, 2008. **174**(1): p. 40-46.

209. **Little, J.L., M.F. Wempe, and C.M. Buchanan**, *Liquid chromatography-mass spectrometry/mass spectrometry method development for drug metabolism studies: Examining lipid matrix ionization effects in plasma.* Journal of Chromatography B, 2006. **833**(2): p. 219-230.

210. **Jemal, M.**, *High-throughput quantitative bioanalysis by LC/MS/MS.* Biomed Chromatogr, 2000. **14**(6): p. 422-9.

211. **Hopfgartner, G. and E. Bourgogne**, *Quantitative high-throughput analysis of drugs in biological matrices by mass spectrometry.* Mass Spectrom Rev, 2003. **22**(3): p. 195-214.

212. **De Francia, S., A. D'Avolio, F. De Martino, E. Pirro, L. Baietto, M. Siccardi, M. Simiele, S. Racca, G. Saglio, F. Di Carlo, and G. Di Perri**, *New HPLC-MS method for the simultaneous quantification of the antileukemia drugs imatinib, dasatinib, and nilotinib in human plasma.* J Chromatogr B Analyt Technol Biomed Life Sci, 2009. **877**(18-19): p. 1721-6.

213. **Haouala, A., B. Zanolari, B. Rochat, M. Montemurro, K. Zaman, M.A. Duchosal, H.B. Ris, S. Leyvraz, N. Widmer, and L.A. Decosterd**, *Therapeutic Drug Monitoring of the new targeted anticancer agents imatinib, nilotinib, dasatinib, sunitinib, sorafenib and lapatinib by LC tandem mass spectrometry.* J Chromatogr B Analyt Technol Biomed Life Sci, 2009.

214. **dell'Adulto, G.I.M.E.** *Ph+/Bcr-Abl+ ALL Imatinib and Nilotinib Rotational Study (LAL1408).* 2010 [cited; Available from: http://clinicaltrials.gov/ct2/show/NCT01025505?term=TKI&rank=31.

215. **dell'Adulto, G.I.M.E.**, *Nilotinib and Imatinib Mesylate in Treating Patients With Early Chronic Phase Chronic Myelogenous Leukemia.* 2009(NCT00769327).

216. **Roche, S., G. McMahon, M. Clynes, and R. O'Connor**, *Development of a high-performance liquid chromatographic-mass spectrometric method for the determination of cellular levels of the tyrosine kinase inhibitors lapatinib and dasatinib.* J Chromatogr B Analyt Technol Biomed Life Sci, 2009. **877**(31): p. 3982-90.

217. **Hsieh, Y., G. Galviz, Q. Zhou, and C. Duncan**, *Hydrophilic interaction liquid chromatography/tandem mass spectrometry for the simultaneous determination of dasatinib, imatinib and nilotinib in mouse plasma.* Rapid Commun Mass Spectrom, 2009. **23**(9): p. 1364-70.

218. **Honeywell, R., K. Yarzadah, E. Giovannetti, N. Losekoot, E.F. Smit, M. Walraven, J.S.W. Lind, C. Tibaldi, H.M. Verheul, and G.J. Peters**, *Simple and selective method for the determination of various tyrosine kinase*

inhibitors used in the clinical setting by liquid chromatography tandem mass spectrometry. Journal of Chromatography B, 2010. **878**(15-16): p. 1059-1068.

219. **Masters, A.R., C.J. Sweeney, and D.R. Jones**, *The quantification of erlotinib (OSI-774) and OSI-420 in human plasma by liquid chromatography-tandem mass spectrometry.* J Chromatogr B Analyt Technol Biomed Life Sci, 2007. **848**(2): p. 379-83.

220. **Lepper, E.R., S.M. Swain, A.R. Tan, W.D. Figg, and A. Sparreboom**, *Liquid-chromatographic determination of erlotinib (OSI-774), an epidermal growth factor receptor tyrosine kinase inhibitor.* Journal of Chromatography B, 2003. **796**(1): p. 181-188.

221. **Zhao, M., C. Hartke, A. Jimeno, J. Li, P. He, Y. Zabelina, M. Hidalgo, and S.D. Baker**, *Specific method for determination of gefitinib in human plasma, mouse plasma and tissues using high performance liquid chromatography coupled to tandem mass spectrometry.* J Chromatogr B Analyt Technol Biomed Life Sci, 2005. **819**(1): p. 73-80.

222. **Guetens, G., H. Prenen, G. De Boeck, W. Van Dongen, E. Esmans, F. Lemiere, A.T. van Oosterom, P. Schoffski, and E.A. de Bruijn**, *Sensitive and specific quantification of the anticancer agent ZD1839 (Gefitinib) in plasma by on-column focusing capillary liquid chromatography-tandem mass spectrometry.* J Chromatogr A, 2005. **1082**(1): p. 2-5.

223. **Jones, H.K., L.E. Stafford, H.C. Swaisland, and R. Payne**, *A sensitive assay for ZD1839 (Iressa) in human plasma by liquid-liquid extraction and high performance liquid chromatography with mass spectrometric detection: validation and use in Phase I clinical trials.* J Pharm Biomed Anal, 2002. **29**(1-2): p. 221-8.

224. **Widmer, N., A. Béguin, B. Rochat, T. Buclin, T. Kovacsovics, M.A. Duchosal, S. Leyvraz, A. Rosselet, J. Biollaz, and L.A. Decosterd**, *Determination of imatinib (Gleevec®) in human plasma by solid-phase extraction-liquid chromatography-ultraviolet absorbance detection.* Journal of Chromatography B, 2004. **803**(2): p. 285-292.

225. **Micová, K., D. Friedecký, E. Faber, A. Polýnková, and T. Adam**, *Flow injection analysis vs. ultra high performance liquid chromatography coupled with tandem mass spectrometry for determination of imatinib in human plasma.* Clinica Chimica Acta. **411**(23-24): p. 1957-1962.

226. **Roth, O., O. Spreux-Varoquaux, S. Bouchet, P. Rousselot, S. Castaigne, S. Rigaudeau, V. Raggueneau, P. Therond, P. Devillier, M. Molimard, and B. Maneglier**, *Imatinib assay by HPLC with photodiode-array UV detection in plasma from patients with chronic myeloid leukemia: Comparison with LC-MS/MS.* Clinica Chimica Acta. **411**(3-4): p. 140-146.

227. **Titier, K., S. Picard, D. Ducint, E. Teilhet, N. Moore, P. Berthaud, F.X. Mahon, and M. Molimard**, *Quantification of imatinib in human plasma by high-performance liquid chromatography-tandem mass spectrometry.* Ther Drug Monit, 2005. **27**(5): p. 634-40.

228. **Masatomo, M., T. Naoto, and S. Ken-ichi**, *High-performance liquid chromatography with solid-phase extraction for the quantitative determination of nilotinib in human plasma.* Biomedical Chromatography, 2009. **9999**(9999): p. n/a.

229. **Davies, A., A.K. Hayes, K. Knight, S.J. Watmough, M. Pirmohamed, and R.E. Clark**, *Simultaneous determination of nilotinib, imatinib and its main*

metabolite (CGP-74588) in human plasma by ultra-violet high performance liquid chromatography. Leukemia Research, 2010. **34**(6): p. 702-707.

230. **Zhao, M., M.A. Rudek, P. He, F.T. Hafner, M. Radtke, J.J. Wright, B.D. Smith, W.A. Messersmith, M. Hidalgo, and S.D. Baker**, *A rapid and sensitive method for determination of sorafenib in human plasma using a liquid chromatography/tandem mass spectrometry assay.* J Chromatogr B Analyt Technol Biomed Life Sci, 2007. **846**(1-2): p. 1-7.

231. **Minkin, P., M. Zhao, Z. Chen, J. Ouwerkerk, H. Gelderblom, and S.D. Baker**, *Quantification of sunitinib in human plasma by high-performance liquid chromatography-tandem mass spectrometry.* J Chromatogr B Analyt Technol Biomed Life Sci, 2008.

232. **Blanchet, B., C. Saboureau, A.S. Benichou, B. Billemont, F. Taieb, S. Ropert, A. Dauphin, F. Goldwasser, and M. Tod**, *Development and validation of an HPLC-UV-visible method for sunitinib quantification in human plasma.* Clinica Chimica Acta, 2009. **404**(2): p. 134-139.

233. **Barattè, S., S. Sarati, E. Frigerio, C.A. James, C. Ye, and Q. Zhang**, *Quantitation of SU11248, an oral multi-target tyrosine kinase inhibitor, and its metabolite in monkey tissues by liquid chromatograph with tandem mass spectrometry following semi-automated liquid-liquid extraction.* Journal of Chromatography A, 2004. **1024**(1-2): p. 87-94.

234. **Zirrolli, J.A., E.L. Bradshaw, M.E. Long, and D.L. Gustafson**, *Rapid and sensitive LC/MS/MS analysis of the novel tyrosine kinase inhibitor ZD6474 in mouse plasma and tissues.* J Pharm Biomed Anal, 2005. **39**(3-4): p. 705-11.

235. **Kyle, R.A. and S.V. Rajkumar**, *Multiple Myeloma.* New England Journal of Medicine, 2004. **351**(18): p. 1860-1873.

236. **Kumar, S. and S.V. Rajkumar**, *Thalidomide and lenalidomide in the treatment of multiple myeloma.* European journal of cancer (Oxford, England : 1990), 2006. **42**(11): p. 1612-1622.

237. **Voet, D. and J.G. Voet**, *Biochemistry*. 1990. 1099-1100.

238. **Kumar, S.K., S.V. Rajkumar, A. Dispenzieri, M.Q. Lacy, S.R. Hayman, F.K. Buadi, S.R. Zeldenrust, D. Dingli, S.J. Russell, J.A. Lust, P.R. Greipp, R.A. Kyle, and M.A. Gertz**, *Improved survival in multiple myeloma and the impact of novel therapies.* Blood, 2008. **111**(5): p. 2516-2520.

239. **Winslow, T.** *Hematopoietic Tree Plasma Cell*. 2008 [cited; Available from: http://www.cancer.gov/Common/PopUps/popImage.aspx?imageName=/images/cdr/live/CDR596562-750.jpg&caption=Blood%20cell%20development.%20A%20blood%20stem%20cell%20goes%20through%20several%20steps%20to%20become%20a%20red%20blood%20cell,%20platelet,%20or%20white%20blood%20cell.

240. **Kyle, R.A. and S.V. Rajkumar**, *Multiple myeloma.* Blood, 2008. **111**(6): p. 2962-2972.

241. **Kumar, S.**, *Multiple myeloma - current issues and controversies.* Cancer Treatment Reviews, 2010. **36**: p. S3-S11.

242. **Palumbo, A., S. Bringhen, T. Caravita, E. Merla, V. Capparella, V. Callea, C. Cangialosi, M. Grasso, F. Rossini, M. Galli, L. Catalano, E. Zamagni, M.T. Petrucci, V. De Stefano, M. Ceccarelli, M.T. Ambrosini, I. Avonto, P. Falco, G. Ciccone, A.M. Liberati, P. Musto, and M. Boccadoro**, *Oral melphalan and prednisone chemotherapy plus thalidomide compared with melphalan and prednisone alone in elderly patients with multiple*

myeloma: randomised controlled trial. The Lancet, 2006. **367**(9513): p. 825-831.

243. **Facon, T., J.Y. Mary, C. Hulin, L. Benboubker, M. Attal, B. Pegourie, M. Renaud, J.L. Harousseau, G. Guillerm, C. Chaleteix, M. Dib, L. Voillat, H. Maisonneuve, J. Troncy, V. Dorvaux, M. Monconduit, C. Martin, P. Casassus, J. Jaubert, H. Jardel, C. Doyen, B. Kolb, B. Anglaret, B. Grosbois, I. Yakoub-Agha, C. Mathiot, and H. Avet-Loiseau**, *Melphalan and prednisone plus thalidomide versus melphalan and prednisone alone or reduced-intensity autologous stem cell transplantation in elderly patients with multiple myeloma (IFM 99-06): a randomised trial.* The Lancet, 2007. **370**(9594): p. 1209-1218.

244. **Hulin, C., T. Facon, P. Rodon, B. Pegourie, L. Benboubker, C. Doyen, M. Dib, G. Guillerm, B. Salles, J.-P. Eschard, P. Lenain, P. Casassus, I. Azaïs, O. Decaux, L. Garderet, C. Mathiot, J. Fontan, I. Lafon, J.M. Virion, and P. Moreau**, *Efficacy of Melphalan and Prednisone Plus Thalidomide in Patients Older Than 75 Years With Newly Diagnosed Multiple Myeloma: IFM 01/01 Trial.* Journal of Clinical Oncology, 2009. **27**(22): p. 3664-3670.

245. **Mateos, M.-V., J.M. Hernandez, M.T. Hernandez, N.C. Gutierrez, L. Palomera, M. Fuertes, P. Garcia-Sanchez, J.J. Lahuerta, J. de la Rubia, M.-J. Terol, A. Sureda, J. Bargay, P. Ribas, A. Alegre, F. de Arriba, A. Oriol, D. Carrera, J. Garcia-Larana, R. Garcia-Sanz, J. Blade, F. Prosper, G. Mateo, D.-L. Esseltine, H. van de Velde, and J.F. San Miguel**, *Bortezomib plus melphalan and prednisone in elderly untreated patients with multiple myeloma: updated time-to-events results and prognostic factors for time to progression.* Haematologica, 2008. **93**(4): p. 560-565.

246. **Palumbo, A., P. Falco, P. Corradini, A. Falcone, F. Di Raimondo, N. Giuliani, C. Crippa, G. Ciccone, P. Omedè, M.T. Ambrosini, F. Gay, S. Bringhen, P. Musto, R. Foà, R. Knight, J.B. Zeldis, M. Boccadoro, and M.T. Petrucci**, *Melphalan, Prednisone, and Lenalidomide Treatment for Newly Diagnosed Myeloma: A Report From the GIMEMA—Italian Multiple Myeloma Network.* Journal of Clinical Oncology, 2007. **25**(28): p. 4459-4465.

247. **Eriksson, T., S. Björkman, and P. Höglund**, *Clinical pharmacology of thalidomide.* European Journal of Clinical Pharmacology, 2001. **57**(5): p. 365-376.

248. **Kunz, W.**, *N-Phthalyl glutaminsäure-imid.* Arzneimittelforschung, 1956(6): p. 426-430.

249. **Bartlett, J.B., K. Dredge, and A.G. Dalgleish**, *The evolution of thalidomide and its IMiD derivatives as anticancer agents.* Nat Rev Cancer, 2004. **4**(4): p. 314-22.

250. **Lenz, W., R.A. Pfeiffer, W. Kosenow, and D.J. Hayman**, *THALIDOMIDE AND CONGENITAL ABNORMALITIES.* The Lancet, 1962. **279**(7219): p. 45-46.

251. **McBride, W.G.**, *THALIDOMIDE AND CONGENITAL ABNORMALITIES.* The Lancet, 1961. **278**(7216): p. 1358-1358.

252. **Melchert, M. and A. List**, *The thalidomide saga.* The International Journal of Biochemistry & Cell Biology, 2007. **39**(7-8): p. 1489-1499.

253. **Sheskin, J.**, *Thalidomide in the treatment of lepra reactions.* Clinical Pharmacology and Theraputics, 1965(6): p. 303–306

254. **Iyer, C.G.S., J. Languillon, K. Ramanujam, G. Tarabini-Castellani, J.T.d.l. Aguas, L.M. Bechelli, K. Uemura, V.M. Dominguez, and T. Sundaresan**, *WHO co-ordinated short-term double-blind trial with thalidomide in the treatment of acute lepra reactions in male lepromatous patients.* Bull World Health Organ, 1971. **45.** (6): p. 719–732.

255. **Olson, K., T. Hall, J. Horton, C. Khung, and H. Hosley**, *Thalidomide (N-phthaloylglutamimide) in the treatment of advanced cancer.* Clin Pharmacol Ther., 1965. **6**: p. 292-7.

256. **Grabstald, H. and R. Golbey**, *Clinical experiences with thalidomide in patients with cancer.* Clin Pharmacol Ther., 1965. **6**: p. 298-302.

257. **Singhal, S., J. Mehta, R. Desikan, D. Ayers, P. Roberson, P. Eddlemon, N. Munshi, E. Anaissie, C. Wilson, M. Dhodapkar, J. Zeldis, D. Siegel, J. Crowley, and B. Barlogie**, *Antitumor Activity of Thalidomide in Refractory Multiple Myeloma.* New England Journal of Medicine, 1999. **341**(21): p. 1565-1571.

258. **Rajkumar, S.V., E. Blood, D. Vesole, R. Fonseca, and P.R. Greipp**, *Phase III Clinical Trial of Thalidomide Plus Dexamethasone Compared With Dexamethasone Alone in Newly Diagnosed Multiple Myeloma: A Clinical Trial Coordinated by the Eastern Cooperative Oncology Group.* Journal of Clinical Oncology, 2006. **24**(3): p. 431-436.

259. **Eriksson, T., S. Bjöurkman, B. Roth, Å. Fyge, and P. Höuglund**, *Stereospecific determination, chiral inversion in vitro and pharmacokinetics in humans of the enantiomers of thalidomide.* Chirality, 1995. **7**(1): p. 44-52.

260. **Kenyon, B.M., F. Browne, and R.J. D'Amato**, *Effects of Thalidomide and Related Metabolites in a Mouse Corneal Model of Neovascularization.* Experimental Eye Research, 1997. **64**(6): p. 971-978.

261. **Reist, M., P.-A. Carrupt, E. Francotte, and B. Testa**, *Chiral Inversion and Hydrolysis of Thalidomide:Mechanisms and Catalysis by Bases and Serum Albumin, and Chiral Stability of Teratogenic Metabolites.* Chemical Research in Toxicology, 1998. **11**(12): p. 1521-1528.

262. **D'Amato, R.J., M.S. Loughnan, E. Flynn, and J. Folkman**, *Thalidomide is an inhibitor of angiogenesis.* Proceedings of the National Academy of Sciences of the United States of America, 1994. **91**(9): p. 4082-4085.

263. **Bellamy, W.T., L. Richter, D. Sirjani, C. Roxas, B. Glinsmann-Gibson, Y. Frutiger, T.M. Grogan, and A.F. List**, *Vascular endothelial cell growth factor is an autocrine promoter of abnormal localized immature myeloid precursors and leukemia progenitor formation in myelodysplastic syndromes.* Blood, 2001. **97**(5): p. 1427-1434.

264. **Gupta, D., S.P. Treon, Y. Shima, T. Hideshima, K. Podar, Y.T. Tai, B. Lin, S. Lentzsch, F.E. Davies, D. Chauhan, R.L. Schlossman, P. Richardson, P. Ralph, L. Wu, F. Payvandi, G. Muller, D.I. Stirling, and K.C. Anderson**, *Adherence of multiple myeloma cells to bone marrow stromal cells upregulates vascular endothelial growth factor secretion: Therapeutic applications.* Leukemia, 2001. **15**(12): p. 1950-1961.

265. **Haslett, P.A.J., L.G. Corral, M. Albert, and G. Kaplan**, *Thalidomide Costimulates Primary Human T Lymphocytes, Preferentially Inducing Proliferation, Cytokine Production, and Cytotoxic Responses in the CD8+ Subset.* The Journal of Experimental Medicine, 1998. **187**(11): p. 1885-1892.

266. **Celgene** (2010) *System for Thalidomide Education and Prescribing Safety.*

267. **Zeldis, J.B., B.A. Williams, S.D. Thomas, and M.E. Elsayed**, *S.T.E.P.S.(TM): A comprehensive program for controlling and monitoring access to thalidomide.* Clinical Therapeutics, 1999. **21**(2): p. 319-330.

268. **Mateos, M.-V.**, *Management of treatment-related adverse events in patients with multiple myeloma.* Cancer Treatment Reviews, 2010. **36**(Supplement 2): p. S24-S32.

269. **Teo, S.K., P.J. Sabourin, K. O'Brien, K.A. Kook, and S.D. Thomas**, *Metabolism of thalidomide in human microsomes, cloned human cytochrome P-450 isozymes, and Hansen's disease patients.* J Biochem Mol Toxicol, 2000. **14**(3): p. 140-7.

270. **Lu, J., B.D. Palmer, P. Kestell, P. Browett, B.C. Baguley, G. Muller, and L.M. Ching**, *Thalidomide metabolites in mice and patients with multiple myeloma.* Clin Cancer Res, 2003. **9**(5): p. 1680-8.

271. **Chung, F., J. Lu, B.D. Palmer, P. Kestell, P. Browett, B.C. Baguley, M. Tingle, and L.M. Ching**, *Thalidomide pharmacokinetics and metabolite formation in mice, rabbits, and multiple myeloma patients.* Clin Cancer Res, 2004. **10**(17): p. 5949-56.

272. **Haque, A. and J.T. Stewart**, *Determination of Racemic Thalidomide in Human Plasma by use of an Avidin Column and Solid Phase Extraction.* Journal of Liquid Chromatography & Related Technologies, 1998. **21**(14): p. 2151 - 2163.

273. **Teo, S.K., R.S. Chandula, J.L. Harden, D.I. Stirling, and S.D. Thomas**, *Sensitive and rapid method for the determination of thalidomide in human plasma and semen using solid-phase extraction and liquid chromatography-tandem mass spectrometry.* J Chromatogr B Analyt Technol Biomed Life Sci, 2002. **767**(1): p. 145-51.

274. **Toraño, J.S., A. Verbon, and H.J. Guchelaar**, *Quantitative determination of thalidomide in human serum with high-performance liquid chromatography using protein precipitation with trichloroacetic acid and ultraviolet detection.* J Chromatogr B Biomed Sci Appl, 1999. **734**(2): p. 203-10.

275. **Murphy-Poulton, S.F., F. Boyle, X.Q. Gu, and L.E. Mather**, *Thalidomide enantiomers: Determination in biological samples by HPLC and vancomycin-CSP.* Journal of Chromatography B, 2006. **831**(1-2): p. 48-56.

276. **Saccomanni, G., V. Turini, C. Manera, G. Placanica, E.O. Salè, C. Jemos, M. Giorgi, and M. Macchia**, *High performance liquid chromatographic determination of thalidomide in patients affected by hepatocellular carcinoma.* Journal of Pharmaceutical and Biomedical Analysis, 2008. **48**(2): p. 447-451.

277. **Yang, X., Z. Hu, S.Y. Chan, P.C. Ho, E. Chan, W. Duan, B.C. Goh, and S. Zhou**, *Determination of thalidomide by high performance liquid chromatography: Plasma pharmacokinetic studies in the rat.* Journal of Pharmaceutical and Biomedical Analysis, 2005. **39**(1-2): p. 299-304.

278. **Zhou, S., Y. Li, P. Kestell, and J.W. Paxton**, *Determination of thalidomide in transport buffer for Caco-2 cell monolayers by high-performance liquid chromatography with ultraviolet detection.* Journal of Chromatography B, 2003. **785**(1): p. 165-173.

279. **Teo, S.K., W.A. Colburn, and S.D. Thomas**, *Single-dose oral pharmacokinetics of three formulations of thalidomide in healthy male volunteers.* J Clin Pharmacol, 1999. **39**(11): p. 1162-8.

280. **Simmons, B.R., R.M. Lush, and W.D. Figg**, *A reversed-phase high performance liquid chromatography method using solid phase extraction to*

quantitate thalidomide in human serum. Analytica Chimica Acta, 1997. **339**(1-2): p. 91-97.

281. **Delon, A., S. Favreliere, W. Couet, P.H. Courtois, and S. Bouquet**, *Rapid and Sensitive Determination of Thalidomide in Human Plasma by High-Performance Liquid-Chromatography.* Journal of Liquid Chromatography, 1995. **18**(2): p. 297-309.

282. **Eriksson, T., S. Bjorkman, A. Fyge, and H. Ekberg**, *Determination of thalidomide in plasma and blood by high-performance liquid chromatography: avoiding hydrolytic degradation.* J Chromatogr, 1992. **582**(1-2): p. 211-6.

283. **Law, E., U. Gilvarry, V. Lynch, B. Gregory, G. Grant, and M. Clynes**, *Cytogenetic comparison of two poorly differentiated human lung squamous cell carcinoma lines.* Cancer Genet Cytogenet, 1992. **59**(2): p. 111-8.

284. **Clynes, M., A. Redmond, E. Moran, and U. Gilvarry**, *Multiple drug-resistance in variant of a human non-small cell lung carcinoma cell line, DLKP-A.* Cytotechnology, 1992. **10**(1): p. 75-89.

285. **McBride, S., P. Meleady, A. Baird, D. Dinsdale, and M. Clynes**, *Human lung carcinoma cell line DLKP contains 3 distinct subpopulations with different growth and attachment properties.* Tumour Biol, 1998. **19**(2): p. 88-103.

286. **Breen, L., L. Murphy, J. Keenan, and M. Clynes**, *Development of taxane resistance in a panel of human lung cancer cell lines.* Toxicol In Vitro, 2008. **22**(5): p. 1234-41.

287. **Collins, S.J., R.C. Gallo, and R.E. Gallagher**, *Continuous growth and differentiation of human myeloid leukaemic cells in suspension culture.* Nature, 1977. **270**(5635): p. 347-9.

288. **Marsh, W., D. Sicheri, and M.S. Center**, *Isolation and characterization of adriamycin-resistant HL-60 cells which are not defective in the initial intracellular accumulation of drug.* Cancer Res, 1986. **46**(8): p. 4053-7.

289. **Liang, Y., P. Meleady, I. Cleary, S. McDonnell, L. Connolly, and M. Clynes**, *Selection with melphalan or paclitaxel (Taxol) yields variants with different patterns of multidrug resistance, integrin expression and in vitro invasiveness.* European Journal of Cancer, 2001. **37**(8): p. 1041-52.

290. **Hooijberg, J.H., H.J. Broxterman, M. Kool, Y.G. Assaraf, G.J. Peters, P. Noordhuis, R.J. Scheper, P. Borst, H.M. Pinedo, and G. Jansen**, *Antifolate Resistance Mediated by the Multidrug Resistance Proteins MRP1 and MRP2.* Cancer Research, 1999. **59**(11): p. 2532-2535.

291. **Akiyama, S., A. Fojo, J. Hanover, I. Pastan, and M. Gottesman**, *Isolation and genetic characterization of human KB cell lines resistant to multiple drugs.* Somatic Cell Molecular Genetics, 1985. **11**: p. 117-126.

292. **Ma, J., M. Maliepaard, H.J. Kolker, J. Verweij, and J.H. Schellens**, *Abrogated energy-dependent uptake of cisplatin in a cisplatin-resistant subline of the human ovarian cancer cell line IGROV-1.* Cancer Chemother Pharmacol, 1998. **41**(3): p. 186-92.

293. **Wall, R., G. McMahon, J. Crown, M. Clynes, and R. O'Connor**, *Rapid and sensitive liquid chromatography-tandem mass spectrometry for the quantitation of epirubicin and identification of metabolites in biological samples.* Talanta, 2007. **72**(1): p. 145-54.

294. **Chandler, B., M. Detsika, A. Owen, S. Evans, R.C. Hartkoorn, P.A. Cane, D.J. Back, and S.H. Khoo**, *Effect of transporter modulation on the*

emergence of nelfinavir resistance in vitro. Antivir Ther, 2007. **12**(5): p. 831-4.

295. **Dolan, J.W.** *LC resources - definitions.* [cited; Available from: http://www.lcresources.com/resources/TSWiz/hs150.htm.

296. **Hendriks, G., D.R.A. Uges, and J.P. Franke**, *Reconsideration of sample pH adjustment in bioanalytical liquid-liquid extraction of ionisable compounds.* Journal of Chromatography B, 2007. **853**(1-2): p. 234-241.

297. **IUPAC**, *Compendium of Chemical Terminology.* 2nd ed. 1997.

298. **Buhrman, D.L., P.I. Price, and P.J. Rudewicz**, *Quantitation of SR 27417 in Human Plasma Using Electrospray Liquid Chromatography-Tandem Mass Spectrometry: A Study of Ion Suppression.* Journal of the American Society for Mass Spectrometry, 1996. **7**(11): p. 1099-1105.

299. **Ermer, J.**, *Validation in pharmaceutical analysis. Part I: an integrated approach.* J Pharm Biomed Anal, 2001. **24**(5-6): p. 755-67.

300. **Shah, V.P., K.K. Midha, S. Dighe, I.J. McGilveray, J.P. Skelly , A. Yacobi, T. Layloff, C.T. Viswanathan, C.E. Cook, R.D. McDowall, K.A. Pittman, and S. Spector**, *Analytical methods validation: Bioavailability, bioequivalence, and pharmacokinetic studies.* J Pharm Sci, 1992. **81**(3): p. 309-312.

301. **Corkery, B., J. Crown, S. Roche, R. O'Connor, D. Tryfanopoulos, M. Clynes, and N. O'Donovan**. *Constitutive Activation of Src Kinase as a Mechanism of Acquired Resistance to Dasatinib in Triple Negative Breast Cancer*. in *San Antonio Breast Cancer Symposium 2009*. 2009.

302. **Corkery, B.**, *Tyrosine kinase inhibitors in triple negative breast cancer.* NICB, 2010:

303. **Balasubramanian, S., S.K. Mani, H. Kasiganesan, C.C. Baicu, and D. Kuppuswamy**, *Hypertrophic stimulation increases beta-actin dynamics in adult feline cardiomyocytes.* PLoS One. **5**(7): p. e11470.

304. **Porter, K.E. and N.A. Turner**, *Cardiac fibroblasts: at the heart of myocardial remodeling.* Pharmacol Ther, 2009. **123**(2): p. 255-78.

305. **Kleihues, P.**, *Pathology and Genetics of tumours of the Nervous System.* 1997.

306. **Adamson, C., O.O. Kanu, A.I. Mehta, C. Di, N. Lin, A.K. Mattox, and D.D. Bigner**, *Glioblastoma multiforme: a review of where we have been and where we are going.* Expert Opinion on Investigational Drugs, 2009. **18**(8): p. 1061-1083.

307. **Bidros, D.S. and M.A. Vogelbaum**, *Novel Drug Delivery Strategies in Neuro-Oncology.* Neurotherapeutics, 2009. **6**(3): p. 539-546.

308. **Omuro, A.M.P., S. Faivre, and E. Raymond**, *Lessons learned in the development of targeted therapy for malignant gliomas.* Molecular Cancer Therapeutics, 2007. **6**(7): p. 1909-1919.

309. **Huang, T.T., S.M. Sarkaria, T.F. Cloughesy, and P.S. Mischel**, *Targeted Therapy for Malignant Glioma Patients: Lessons Learned and the Road Ahead.* Neurotherapeutics : the journal of the American Society for Experimental NeuroTherapeutics, 2009. **6**(3): p. 500-512.

310. **Kinsella, P.**, *The investigation of targets for therapy in brain tumours.* NICB, School of Biotechnology, 2010:

311. *HPLC Troubleshooting Guide*: Waters. 55-56.

312. **Picó, Y., G. Font, M.J. Ruiz, and M. Fernández**, *Control of pesticide residues by liquid chromatography-mass spectrometry to ensure food safety.* Mass Spectrometry Reviews, 2006. **25**(6): p. 917-960.

313. **Kraemer, T. and L.D. Paul**, *Bioanalytical procedures for determination of drugs of abuse in blood.* Anal Bioanal Chem, 2007. **388**(7): p. 1415-35.

314. **Shephard, G.S.**, *Determination of mycotoxins in human foods.* Chem Soc Rev, 2008. **37**(11): p. 2468-77.

315. **Wieling, J.**, *LC-MS-MS experiences with internal standards.* Chromatographia, 2002. **55**: p. S107-S113.

316. **Stokvis, E., H. Rosing, and J.H. Beijnen**, *Stable isotopically labeled internal standards in quantitative bioanalysis using liquid chromatography/mass spectrometry: necessity or not?* Rapid Communications in Mass Spectrometry, 2005. **19**(3): p. 401-407.

317. **Brockman, A.H., P. Hatsis, M. Paton, and J.-T. Wu**, *Impact of Differential Recovery in Bioanalysis: The Example of Bortezomib in Whole Blood.* Analytical Chemistry, 2006. **79**(4): p. 1599-1603.

318. **Jemal, M., A. Schuster, and D.B. Whigan**, *Liquid chromatography/tandem mass spectrometry methods for quantitation of mevalonic acid in human plasma and urine: method validation, demonstration of using a surrogate analyte, and demonstration of unacceptable matrix effect in spite of use of a stable isotope analog internal standard.* Rapid Communications in Mass Spectrometry, 2003. **17**(15): p. 1723-1734.

319. **Dolan, J.W.** *Getting started in HPLC*. [cited; Available from: http://www.lcresources.com/resources/getstart/2f01.htm.

320. **Snyder, L.R. and J.J. Kirkland**, *Introduction to Modern Liquid Chromatogrpahy*. 2nd ed. 1979: John Wiley & Sons, Inc.

321. **ACD/Labs), C.u.A.C.D.A.L.S.V.f.S.-.** [cited.

322. **Calderoli, S., E. Colombo, E. Frigerio, C.A. James, and M. Sibum**, *LC-MS-MS determination of brostallicin in human plasma following automated on-line SPE.* Journal of Pharmaceutical and Biomedical Analysis, 2003. **32**(4-5): p. 601-607.

323. **Amini, N., M. Shariatgorji, C. Crescenzi, and G. Thorsen**, *Screening and Quantification of Pesticides in Water Using a Dual-Function Graphitized Carbon Black Disk.* Anal Chem, 2009.

324. **van Beek, T.A. and P. Montoro**, *Chemical analysis and quality control of Ginkgo biloba leaves, extracts, and phytopharmaceuticals.* J Chromatogr A, 2009. **1216**(11): p. 2002-32.

325. **Zhou, Q. and J.M. Gallo**, *Quantification of sunitinib in mouse plasma, brain tumor and normal brain using liquid chromatography-electrospray ionization-tandem mass spectrometry and pharmacokinetic application.* J Pharm Biomed Anal, 2009.

326. **Koichi, I., Y. Yukiko, H. Tomoaki, and O. Hisao**, *Simultaneous determination of avermectins in bovine tissues by LC-MS/MS.* Journal of Separation Science, 2009. **9999**(9999): p. NA.

327. **Jemal, M. and X. Yuan-Qing**, *LC-MS Development Strategies for Quantitative Bioanalysis.* Current Drug Metabolism, 2006. **7**(5): p. 491-502.

328. **Giuseppe, C., C. Bruno, S. Sara, V. Emanuela, and T. Giuseppe**, *Rapid and sensitive analysis of vincristine in human plasma using on-line extraction combined with liquid chromatography/tandem mass spectrometry.* Rapid Communications in Mass Spectrometry, 2008. **22**(4): p. 519-525.

329. **Brunen, S., R. Kruger, S. Finger, F. Korf, F. Kiefer, K. Wiedemann, K.J. Lackner, and C. Hiemke**, *Determination of naltrexone and 6beta-naltrexol in human blood: comparison of high-performance liquid chromatography with*

spectrophotometric and tandem-mass-spectrometric detection. Anal Bioanal Chem, 2009.

330. **Oostendorp, R.L., J.H. Beijnen, J.H. Schellens, and O. Tellingen**, *Determination of imatinib mesylate and its main metabolite (CGP74588) in human plasma and murine specimens by ion-pairing reversed-phase high-performance liquid chromatography.* Biomed Chromatogr, 2007. **21**(7): p. 747-54.

331. **Matuszewski, B.K., M.L. Constanzer, and C.M. Chavez-Eng**, *Strategies for the Assessment of Matrix Effect in Quantitative Bioanalytical Methods Based on HPLCâ^'MS/MS.* Analytical Chemistry, 2003. **75**(13): p. 3019-3030.

332. **Huber, L.**, *Validation of Analytical Methods:Review and Strategy.* LC-GC International, 1998(Feb): p. 95-105.

333. **Brooks, H.D., B.S. Glisson, B.N. Bekele, L.E. Ginsberg, A. El- Naggar, K.S. Culotta, N. Takebe, J. Wright, H.T. Tran, and V.A. Papadimitrakopoulou**, *Phase 2 study of dasatinib in the treatment of head and neck squamous cell carcinoma.* Cancer: p. n/a-n/a.

334. **Storniolo, A.M., M.D. Pegram, B. Overmoyer, P. Silverman, N.W. Peacock, S.F. Jones, J. Loftiss, N. Arya, K.M. Koch, E. Paul, L. Pandite, R.A. Fleming, P.F. Lebowitz, P.T.C. Ho, and H.A. Burris**, *Phase I Dose Escalation and Pharmacokinetic Study of Lapatinib in Combination With Trastuzumab in Patients With Advanced ErbB2-Positive Breast Cancer.* Journal of Clinical Oncology, 2008. **26**(20): p. 3317-3323.

335. **Kondo, T., T. Tasaka, F. Sano, K. Matsuda, Y. Kubo, Y. Matsuhashi, H. Nakanishi, Y. Sadahira, H. Wada, T. Sugihara, and K. Tohyama**, *Philadelphia chromosome-positive acute myeloid leukemia (Ph + AML) treated with imatinib mesylate (IM): A report with IM plasma concentration and bcr-abl transcripts.* Leukemia Research, 2009. **33**(9): p. e137-e138.

336. **Vessman, J.**, *Selectivity or specificity? Validation of analytical methods from the perspective of an analytical chemist in the pharmaceutical industry.* Journal of Pharmaceutical and Biomedical Analysis, 1996. **14**(8-10): p. 867-869.

337. **Christian, G.D.**, *Analytical Chemistry.* 5th ed. 1994, New York: John Wiley.

338. **Jinno, K.**, *Encyclopedia of Chromatography.* Detection Principles, ed. J. Cazes. 2004, New York: Marcel Dekker, Inc.

339. **Papadoyannis, I.N. and G.A. Theodoridis**, *Encyclopedia of Chromatogrpahy.* Liquid Chromatography–Mass Spectrometry, ed. J. Cazes. 2004, New York: Marcel Dekker, Inc.

340. **Snyder, L.R., J.J. Kirkland, and J.L. Glajch**, *Practical HPLC Method Development.* 2nd ed. 1997: John Wiley & Sons.

341. **Dadgar, D. and P.E. Burnett**, *Issues in evaluation of bioanalytical method selectivity and drug stability.* J Pharm Biomed Anal, 1995. **14**(1-2): p. 23-31.

342. **Karnes, H.**, *Validation and Control of Bioanalytical Methods.* Handbook of Anti-Cancer Pharmacokinetics and Pharmacodynamics–Cancer Drug Discovery and Development ed. H.M. WD Figg 2004, New Jersey: Humana Press. 91-111.

343. **Trissel, L.A.**, *Avoiding common flaws in stability and compatibility studies of injectable drugs.* Am J Hosp Pharm, 1983. **40**(7): p. 1159-60.

344. **Marchetti, S., N.A. de Vries, T. Buckle, M.J. Bolijn, M.A.J. van Eijndhoven, J.H. Beijnen, R. Mazzanti, O. van Tellingen, and J.H.M. Schellens**, *Effect of the ATP-binding cassette drug transporters ABCB1,*

ABCG2, and ABCC2 on erlotinib hydrochloride (Tarceva) disposition in in vitro and in vivo pharmacokinetic studies employing Bcrp1â˘′/â˘′/Mdr1a/1bâ˘′/â˘′ (triple-knockout) and wild-type mice. Molecular Cancer Therapeutics, 2008. **7**(8): p. 2280-2287.

345. **Kinsella, P., M. Clynes, and V. Amberger-Murphy**, *Imatinib and docetaxel in combination can effectively inhibit glioma invasion in an in vitro 3D invasion assay.* Journal of Neuro-Oncology, 2010: p. 1-10.

346. **Razis, E., P. Selviaridis, S. Labropoulos, J.L. Norris, M.-J. Zhu, D.D. Song, T. Kalebic, M. Torrens, A. Kalogera-Fountzila, G. Karkavelas, S. Karanastasi, J.A. Fletcher, and G. Fountzilas**, *Phase II Study of Neoadjuvant Imatinib in Glioblastoma: Evaluation of Clinical and Molecular Effects of the Treatment.* Clinical Cancer Research, 2009. **15**(19): p. 6258-6266.

347. **Carcaboso, A.M., M.A. Elmeliegy, J. Shen, S.J. Juel, Z.M. Zhang, C. Calabrese, L. Tracey, C.M. Waters, and C.F. Stewart**, *Tyrosine Kinase Inhibitor Gefitinib Enhances Topotecan Penetration of Gliomas.* Cancer Research, 2010. **70**(11): p. 4499-4508.

348. **Agarwal, S., R. Sane, J.L. Gallardo, J.R. Ohlfest, and W.F. Elmquist**, *Distribution of Gefitinib to the Brain Is Limited by P-glycoprotein (ABCB1) and Breast Cancer Resistance Protein (ABCG2)-Mediated Active Efflux.* Journal of Pharmacology and Experimental Therapeutics, 2010. **334**(1): p. 147-155.

349. **Liang, Y., L. O'Driscoll, S. McDonnell, P. Doolan, I. Oglesby, K. Duffy, R. O'Connor, and M. Clynes**, *Enhanced in vitro invasiveness and drug resistance with altered gene expression patterns in a human lung carcinoma cell line after pulse selection with anticancer drugs.* International Journal of Cancer, 2004. **111**(4): p. 484-493.

350. **Chen, W.S., K.E. Luker, J.L. Dahlheimer, C.M. Pica, G.D. Luker, and D. Piwnica-Worms**, *Effects of MDR1 and MDR3 P-glycoproteins, MRP1, and BCRP/MXR/ABCP on the transport of 99mTc-tetrofosmin.* Biochemical Pharmacology, 2000. **60**(3): p. 413-426.

351. **Stordal, B., M. Clynes, M. Gottesman, and J.-P. Gillet**. *Mechanisms of cross resistance between cisplatin and paclitaxel in IGROV-1CDDP ovarian cancer cells.* in *TP-Binding Cassette (ABC) Proteins: From Multidrug Resistance to Genetic Diseases,* . 2010. Innsbruck, Austria.

352. **Law, E., U. Gilvarry, V. Lynch, B. Gregory, G. Grant, and M. Clynes**, *Cytogenetic comparison of two poorly differentiated human lung squamous cell carcinoma lines.* Cancer Genetics and Cytogenetics, 1992. **59**(2): p. 111-118.

353. **Shen, D.W., C. Cardarelli, J. Hwang, M. Cornwell, N. Richert, S. Ishii, I. Pastan, and M.M. Gottesman**, *Multiple drug-resistant human KB carcinoma cells independently selected for high-level resistance to colchicine, adriamycin, or vinblastine show changes in expression of specific proteins.* Journal of Biological Chemistry, 1986. **261**(17): p. 7762-7770.

354. **Hiss, D., G. Gabriels, P. Jacobs, and P. Folb**, *Tunicamycin potentiates drug cytotoxicity and vincristine retention in multidrug resistant cell lines.* European Journal of Cancer, 1996. **32**(12): p. 2164-2172.

355. **Richert, N., S. Akiyama, D. Shen, M.M. Gottesman, and I. Pastan**, *Multiply drug-resistant human KB carcinoma cells have decreased amounts of*

a 75-kDa and a 72-kDa glycoprotein. Proceedings of the National Academy of Sciences of the United States of America, 1985. **82**(8): p. 2330-2333.

356. **Hyafil, F., C. Vergely, P. Du Vignaud, and T. Grand-Perret**, *In Vitro and In Vivo Reversal of Multidrug Resistance by GF120918, an Acridonecarboxamide Derivative.* Cancer Res, 1993. **53**(19): p. 4595-4602.

357. **Stordal, B., M. Hamon, J.-P. Gillet, S. Roche, M. Gottesman, and M. Clynes**, *Cross resistance to paclitaxel in a cisplatin resistant ovarian cell line IGROV-1CDDP-2 is mediated by P-glycoprotein.* Manuscript in preparation, 2011.

358. **Porkka, K., P. Koskenvesa, T. Lundan, J. Rimpilainen, S. Mustjoki, R. Smykla, R. Wild, R. Luo, M. Arnan, B. Brethon, L. Eccersley, H. Hjorth-Hansen, M. Hoglund, H. Klamova, H. Knutsen, S. Parikh, E. Raffoux, F. Gruber, F. Brito-Babapulle, H. Dombret, R.F. Duarte, E. Elonen, R. Paquette, C.M. Zwaan, and F.Y.F. Lee**, *Dasatinib crosses the blood-brain barrier and is an efficient therapy for central nervous system Philadelphia chromosome-positive leukemia.* Blood, 2008. **112**(4): p. 1005-1012.

359. **Giri, N., S. Agarwal, N. Shaik, G. Pan, Y. Chen, and W.F. Elmquist**, *Substrate-Dependent Breast Cancer Resistance Protein (Bcrp1/Abcg2)-Mediated Interactions: Consideration of Multiple Binding Sites in in Vitro Assay Design.* Drug Metabolism and Disposition, 2009. **37**(3): p. 560-570.

360. **Holló, Z., L. Homolya, T. Hegedüs, and B. Sarkadi**, *Transport properties of the multidrug resistance-associated protein (MRP) in human tumour cells.* FEBS Letters, 1996. **383**(1-2): p. 99-104.

361. **O'Connor, R., M. Clynes, P. Dowling, N. O'Donovan, and L. O'Driscoll**, *Drug resistance in cancer - searching for mechanisms, markers and therapeutic agents.* Expert Opinion on Drug Metabolism & Toxicology, 2007. **3**(6): p. 805-817.

362. **Ozvegy-Laczka, C., J. Cserepes, N.B. Elkind, and B. Sarkadi**, *Tyrosine kinase inhibitor resistance in cancer: role of ABC multidrug transporters.* Drug Resist Updat, 2005. **8**(1-2): p. 15-26.

363. **Qiang, F., B.-J. Lee, I. Ha, K.W. Kang, E.-R. Woo, and H.-K. Han**, *Effect of maceligan on the systemic exposure of paclitaxel: In vitro and in vivo evaluation.* European Journal of Pharmaceutical Sciences, 2010. **41**(2): p. 226-231.

364. **Shannon, K.M.**, *Resistance in the land of molecular cancer therapeutics.* Cancer Cell, 2002. **2**(2): p. 99-102.

365. **Hegedus, C., C. Ozvegy-Laczka, A. Apáti, M. Magócsi, K. Német, L. Orfi, G. Kéri, M. Katona, Z. Takáts, A. Váradi, G. Szakács, and B. Sarkadi**, *Interaction of nilotinib, dasatinib and bosutinib with ABCB1 and ABCG2: implications for altered anti-cancer effects and pharmacological properties.* Br J Pharmacol, 2009. **158**(4): p. 1153-64.

366. **Chen, Y., S. Agarwal, N.M. Shaik, C. Chen, Z. Yang, and W.F. Elmquist**, *P-glycoprotein and Breast Cancer Resistance Protein Influence Brain Distribution of Dasatinib.* J Pharmacol Exp Ther, 2009. **330**(3): p. 956-963.

367. **Dohse, M., C. Scharenberg, S. Shukla, R.W. Robey, T. Volkmann, J.F. Deeken, C. Brendel, S.V. Ambudkar, A. Neubauer, and S.E. Bates**, *Comparison of ATP-Binding Cassette Transporter Interactions with the Tyrosine Kinase Inhibitors Imatinib, Nilotinib, and Dasatinib.* Drug Metabolism and Disposition. **38**(8): p. 1371-1380.

368. **Shapiro, A.B. and V. Ling**, *Extraction of Hoechst 33342 from the Cytoplasmic Leaflet of the Plasma Membrane by P-Glycoprotein.* European Journal of Biochemistry, 1997. **250**(1): p. 122-129.

369. **Shapiro, A.B. and V. Ling**, *Transport of LDS-751 from the cytoplasmic leaflet of the plasma membrane by the rhodamine-123-selective site of P-glycoprotein.* European Journal of Biochemistry, 1998. **254**(1): p. 181-188.

370. **Shapiro, A.B., K. Fox, P. Lam, and V. Ling**, *Stimulation of P-glycoprotein-mediated drug transport by prazosin and progesterone.* European Journal of Biochemistry, 1999. **259**(3): p. 841-850.

371. **Ceppi, P., M. Papotti, V. Monica, M.L. Iacono, S. Saviozzi, M. Pautasso, S. Novello, S. Mussino, E. Bracco, M. Volante, and G.V. Scagliotti**, *Effects of Src kinase inhibition induced by dasatinib in non-small cell lung cancer cell lines treated with cisplatin.* Molecular Cancer Therapeutics, 2009. **8**(11): p. 3066-3074.

372. **Eustace, A.**, *Investigation of response and resistance to dasatinib in melanoma cells.* NICB, 2010:

373. **Imai, Y., K. Ohmori, S.i. Yasuda, M. Wada, T. Suzuki, K. Fukuda, and Y. Ueda**, *Breast cancer resistance protein/ABCG2 is differentially regulated downstream of extracellular signal-regulated kinase.* Cancer Science, 2009. **100**(6): p. 1118-1127.

374. **Théou, N., S. Gil, A. Devocelle, C. Julié, A. Lavergne-Slove, A. Beauchet, P. Callard, R. Farinotti, A. Le Cesne, A. Lemoine, L. Faivre-Bonhomme, and J.-F. Emile**, *Multidrug Resistance Proteins in Gastrointestinal Stromal Tumors: Site-Dependent Expression and Initial Response to Imatinib.* Clinical Cancer Research, 2005. **11**(21): p. 7593-7598.

375. **Medina, P.J. and S. Goodin**, *Lapatinib: A dual inhibitor of human epidermal growth factor receptor tyrosine kinases.* Clinical Therapeutics, 2008. **30**(8): p. 1426-1447.

376. **Dai, C.-l., A.K. Tiwari, C.-P. Wu, X.-d. Su, S.-R. Wang, D.-g. Liu, C.R. Ashby, Jr., Y. Huang, R.W. Robey, Y.-j. Liang, L.-m. Chen, C.-J. Shi, S.V. Ambudkar, Z.-S. Chen, and L.-w. Fu**, *Lapatinib (Tykerb, GW572016) Reverses Multidrug Resistance in Cancer Cells by Inhibiting the Activity of ATP-Binding Cassette Subfamily B Member 1 and G Member 2.* Cancer Res, 2008. **68**(19): p. 7905-7914.

377. **Staud, F. and P. Pavek**, *Breast cancer resistance protein (BCRP/ABCG2).* The International Journal of Biochemistry & Cell Biology, 2005. **37**(4): p. 720-725.

378. **Perry, J., E. Ghazaly, C. Kitromilidou, E. Nsubuga-McGrowder, S.P. Joel, and T. Powles**, *A synergistic interaction between lapatinib and chemotherapy agents in a panel of cell lines is due to inhibition of the efflux pump BCRP.* Molecular Cancer Therapeutics.

379. **Cavo, M., E. Zamagni, P. Tosi, P. Tacchetti, C. Cellini, D. Cangini, A. de Vivo, N. Testoni, C. Nicci, C. Terragna, T. Grafone, G. Perrone, M. Ceccolini, S. Tura, and M. Baccarani**, *Superiority of thalidomide and dexamethasone over vincristine-doxorubicin dexamethasone (VAD) as primary therapy in preparation for autologous transplantation for multiple myeloma.* Blood, 2005. **106**(1): p. 35-9.

380. **Gurney, H.**, *Defining the starting dose.* Handbook of Anticancer Pharmacokinetics and Pharmacodynamics, ed. W.D. Figg and M. H.L., Totowa, NJ: Humana Press Inc.

381. **Tohnya, T.M., K. Hwang, E.R. Lepper, H.A. Fine, W.L. Dahut, J. Venitz, A. Sparreboom, and W.D. Figg**, *Determination of CC-5013, an analogue of thalidomide, in human plasma by liquid chromatography-mass spectrometry.* J Chromatogr B Analyt Technol Biomed Life Sci, 2004. **811**(2): p. 135-41.

382. **Meyring, M., D. Strickmann, B. Chankvetadze, G. Blaschke, C. Desiderio, and S. Fanali**, *Investigation of the in vitro biotransformation of R-(+)-thalidomide by HPLC, nano-HPLC, CEC and HPLC--APCI-MS.* J Chromatogr B Biomed Sci Appl, 1999. **723**(1-2): p. 255-64.

383. **Durie, B.G.M., J.L. Harousseau, J.S. Miguel, J. Blade, B. Barlogie, K. Anderson, M. Gertz, M. Dimopoulos, J. Westin, P. Sonneveld, H. Ludwig, G. Gahrton, M. Beksac, J. Crowley, A. Belch, M. Boccadaro, I. Turesson, D. Joshua, D. Vesole, R. Kyle, R. Alexanian, G. Tricot, M. Attal, G. Merlini, R. Powles, P. Richardson, K. Shimizu, P. Tosi, G. Morgan, and S.V. Rajkumar**, *International uniform response criteria for multiple myeloma.* Leukemia, 2006. **20**(9): p. 1467-1473.

384. (1999) *National Cancer Insitute, Cancer Therapy Evaulation Program, Common Toxicity Criteria, Version 2.0.*

385. **Swartz, M. and I. Krull**, *Validation of Bioanalytical Methods —Highlights of FDA's Guidance.* LCGC NORTH AMERICA, 2003. **21**(2): p. 136.

386. **Teo, S.K.**, *Properties of thalidomide and its analogues: implications for anticancer therapy.* Aaps J, 2005. **7**(1): p. E14-9.

387. **NCI**. *FDA Approval for Thalidomide*. 2006 [cited; Available from: http://www.cancer.gov/cancertopics/druginfo/fda-thalidomide.

388. **Figg, W.D., S. Raje, K.S. Bauer, A. Tompkins, D. Venzon, R. Bergan, A. Chen, M. Hamilton, J. Pluda, and E. Reed**, *Pharmacokinetics of thalidomide in an elderly prostate cancer population.* Journal of Pharmaceutical Sciences, 1999. **88**(1): p. 121-125.

389. **Skirvin, J.A. and S.M. Lichtman**, *Pharmacokinetic Considerations of Oral Chemotherapy in Elderly Patients with Cancer.* Drugs & Aging, 2002. **19**(1): p. 25-42.

390. **Ruddy, K., E. Mayer, and A. Partridge**, *Patient adherence and persistence with oral anticancer treatment.* CA Cancer J Clin, 2009. **59**(1): p. 56-66.

391. **O'Neill, V.J. and C.J. Twelves**, *Oral cancer treatment: developments in chemotherapy and beyond.* Br J Cancer, 2002. **87**(9): p. 933-937.

392. **Partridge, A.H., J. Avorn, P.S. Wang, and E.P. Winer**, *Adherence to Therapy With Oral Antineoplastic Agents.* Journal of the National Cancer Institute, 2002. **94**(9): p. 652-661.

393. **Palumbo, A., S. Bringhen, A.M. Liberati, T. Caravita, A. Falcone, V. Callea, M. Montanaro, R. Ria, A. Capaldi, R. Zambello, G. Benevolo, D. Derudas, F. Dore, F. Cavallo, F. Gay, P. Falco, G. Ciccone, P. Musto, M. Cavo, and M. Boccadoro**, *Oral melphalan, prednisone, and thalidomide in elderly patients with multiple myeloma: updated results of a randomized controlled trial.* Blood, 2008. **112**(8): p. 3107-3114.

394. **Rajkumar, S.V., L. Rosiñol, M. Hussein, J. Catalano, W. Jedrzejczak, L. Lucy, M. Olesnyckyj, Z. Yu, R. Knight, J.B. Zeldis, and J. Bladé**, *Multicenter, Randomized, Double-Blind, Placebo-Controlled Study of Thalidomide Plus Dexamethasone Compared With Dexamethasone As Initial Therapy for Newly Diagnosed Multiple Myeloma.* Journal of Clinical Oncology, 2008. **26**(13): p. 2171-2177.
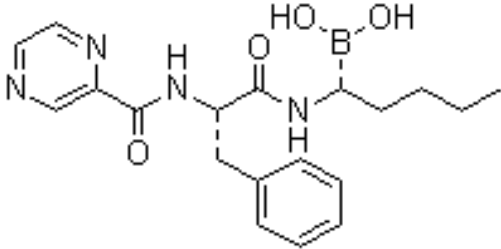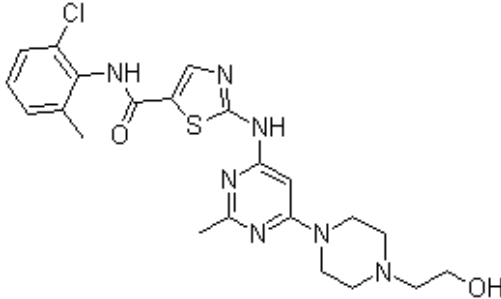
395. **Sung, B., A.B. Kunnumakkara, G. Sethi, P. Anand, S. Guha, and B.B. Aggarwal**, *Curcumin circumvents chemoresistance in vitro and potentiates the effect of thalidomide and bortezomib against human multiple myeloma in nude mice model.* Molecular Cancer Therapeutics, 2009. **8**(4): p. 959-970.

396. **Keller, M., G. Sollberger, and H.-D. Beer**, *Thalidomide Inhibits Activation of Caspase-1.* J Immunol, 2009. **183**(9): p. 5593-5599.

397. **Hideshima, T., D. Chauhan, Y. Shima, N. Raje, F.E. Davies, Y.-T. Tai, S.P. Treon, B. Lin, R.L. Schlossman, P. Richardson, G. Muller, D.I. Stirling, and K.C. Anderson**, *Thalidomide and its analogs overcome drug resistance of human multiple myeloma cells to conventional therapy.* Blood, 2000. **96**(9): p. 2943-2950.

398. **Schumacher, H., R.L. Smith, and R.T. Williams**, *The metabolism of thalidomide: the fate of thalidomide and some of its hydrolysis products in various species.* British journal of pharmacology and chemotherapy, 1965. **25**(2): p. 338–351.

399. **Schumacher, H., R.L. Smith, and R.T. Williams**, *The metabolism of thalidomide: the spontaneous hydrolysis of thalidomide in solution.* British journal of pharmacology and chemotherapy, 1965. **25**: p. 324-337.

400. **Liu, Q., K.L. Farley, A.J. Johnson, N. Muthusamy, C.C. Hofmeister, K.A. Blum, L.J. Schaaf, M.R. Grever, J.C. Byrd, J.T. Dalton, and M.A. Phelps**, *Development and validation of a highly sensitive liquid chromatography/mass spectrometry method for simultaneous quantification of lenalidomide and flavopiridol in human plasma.* Ther Drug Monit, 2008. **30**(5): p. 620-7.
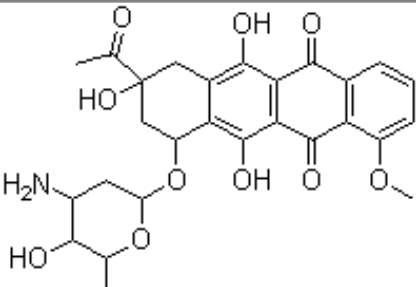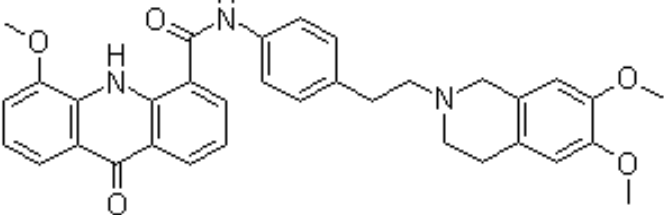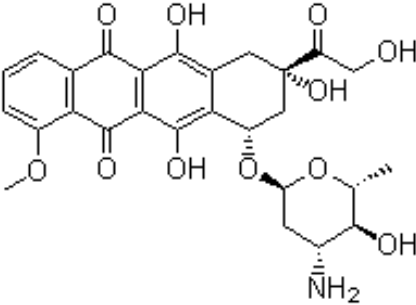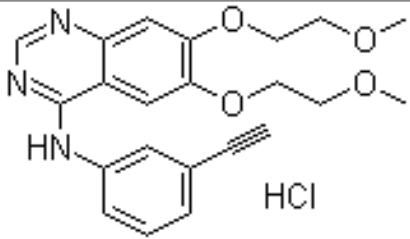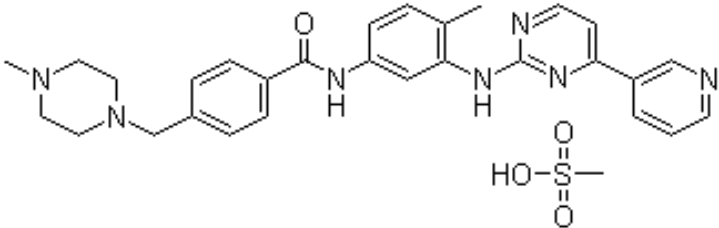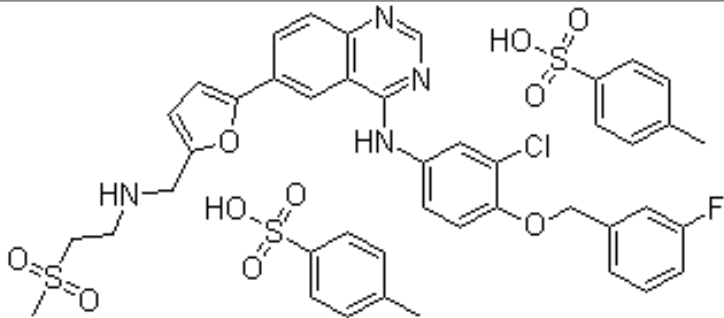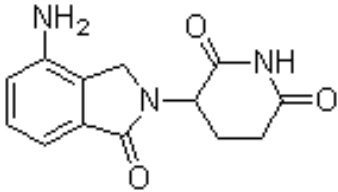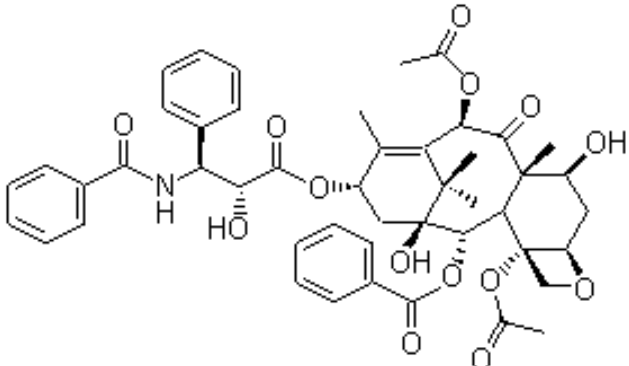
SECTION 9.0 – Appendices
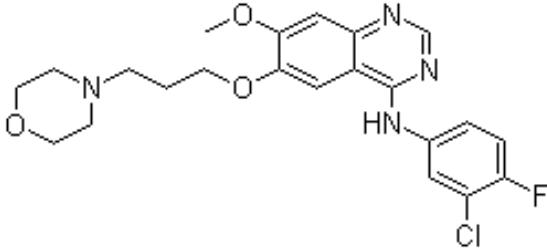
9. Appendices

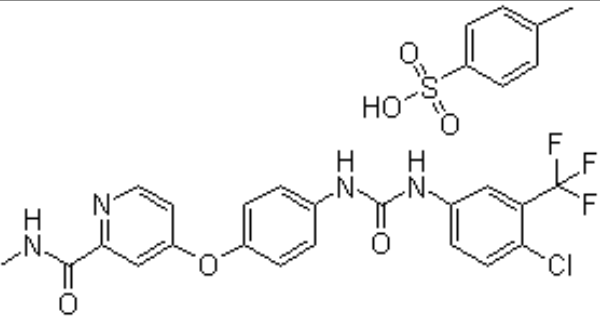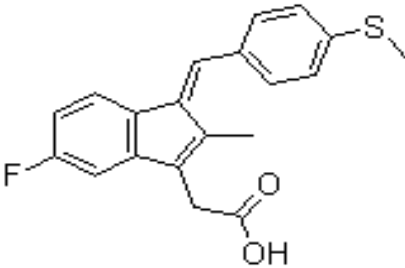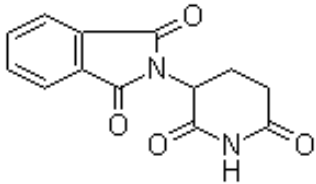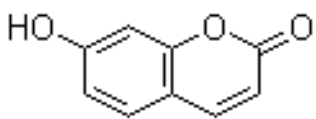## *Appendix 1-Details of drugs*

This table contains a list of all drugs used in this project. All drugs were disposed of by incineration

Drug	Mr (g/mol)	Structure	Source	Storage
Bortezomib	384.24		Sequoia Research Chemicals	Room temperature in the dark
Dasatinib	506		Sequoia Research Chemicals	Room temperature in the dark

Drug	Mr (g/mol)	Structure	Source	Storage
Daunorubicin	527.52		St Vincent's University Hospital	4°C
Elacridar (GF120918)	600.1		Sigma-Aldrich	-20°C
Epirubicin*	543.52		St Vincent's University Hospital	4°C

Drug	Mr (g/mol)	Structure	Source	Storage
Erlotinib (HCl)	429.9		Sequoia Research Chemicals	Room temperature in the dark
Gefitinib	446.9		Sequoia Research Chemicals	Room temperature in the dark
Imatinib (Mesylate)	589.72		Sequoia Research Chemicals	Room temperature in the dark

Drug	Mr (g/mol)	Structure	Source	Storage
Lapatinib (Ditosylate Monohydrate)	943.5		Sequoia Research Chemicals	Room temperature in the dark
Lenalidomide	259.3		Sequoia Research Chemicals	Room temperature in the dark
Paclitaxel (Taxol)*	853.9		St Vincent's University Hospital	Room temperature in the dark

Drug	Mr (g/mol)	Structure	Source	Storage
Sorafenib (Tosylate)	464.825		Sequoia Research Chemicals	Room temperature in the dark
Sulindac Sulfide	340.4		Sigma-Aldrich	4°C
Thalidomide	464.825		Sigma-Aldrich	-20°C
Umbelliferone	162.14		Sigma-Aldrich	-20°C

* Clinical formulation

All structures were taken from http://www.chemblink.com/

Appendix 2: Lapatinib matrix sample

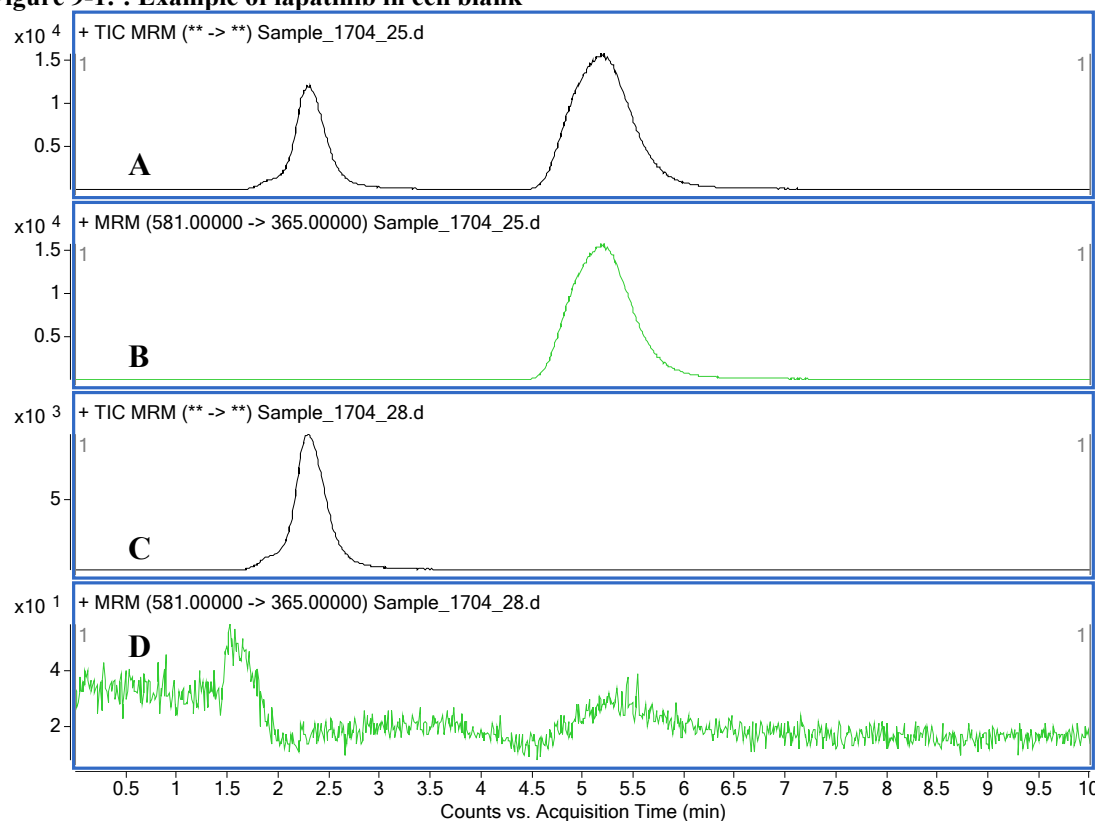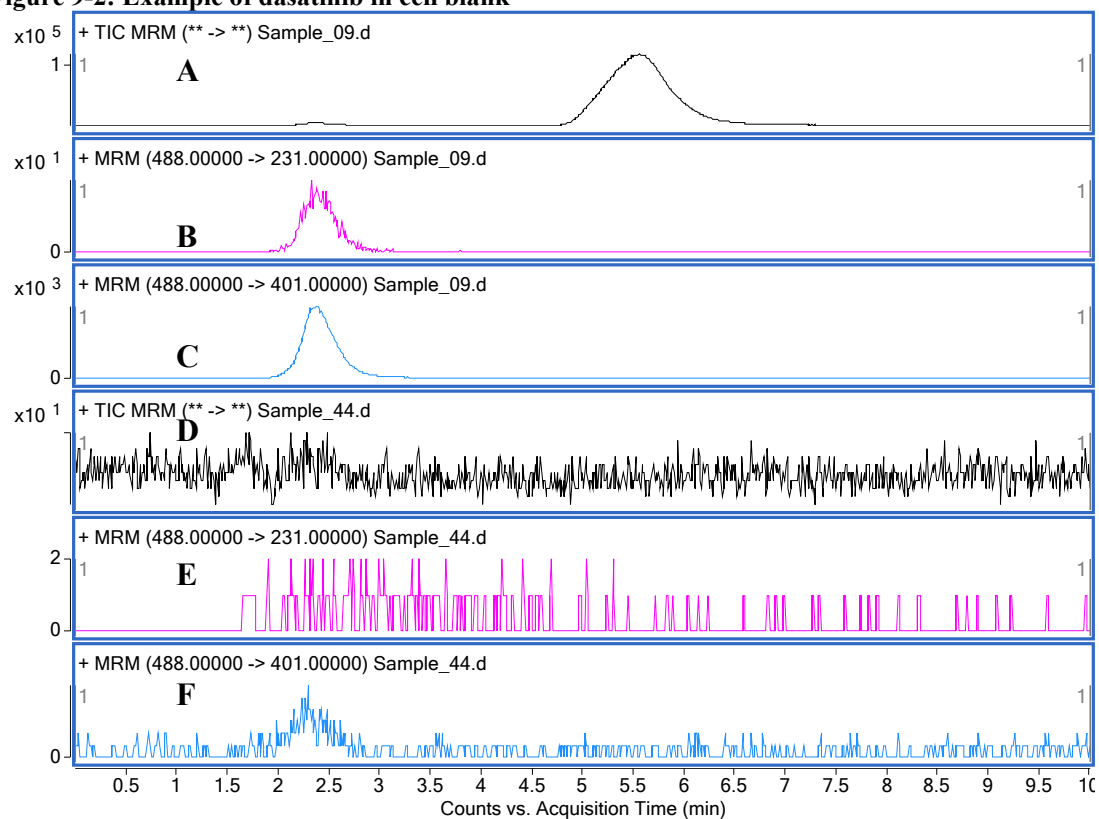**Figure 9-1: : Example of lapatinib in cell blank**

Figure 9-1 shows a quantification of lapatinib in an extracted cell sample in comparison to the quantification of lapatinib in a treated cell sample, where A indicates the TIC for the treated sample and B is the extracted MRM for lapatinib in the treated sample. C shows the TIC for the untreated cell sample with dasatinib internal standard added, while D shows the extracted MRM of lapatinib in the untreated cell sample

Appendix 3: Dasatinib matrix sample

Figure 9-2: Example of dasatinib in cell blank

Figure 9-2 shows a quantification of dasatinib in an extracted cell sample in comparison to the quantification of dasatinib in a treated cell sample, where A indicates the TIC for the treated sample, B and C are the extracted MRM for dasatinib in the treated sample. D shows the TIC for the untreated cell sample, E and F show the extracted MRM from the untreated cell sample.

Appendix 4- Thalidomide blank chromatogram

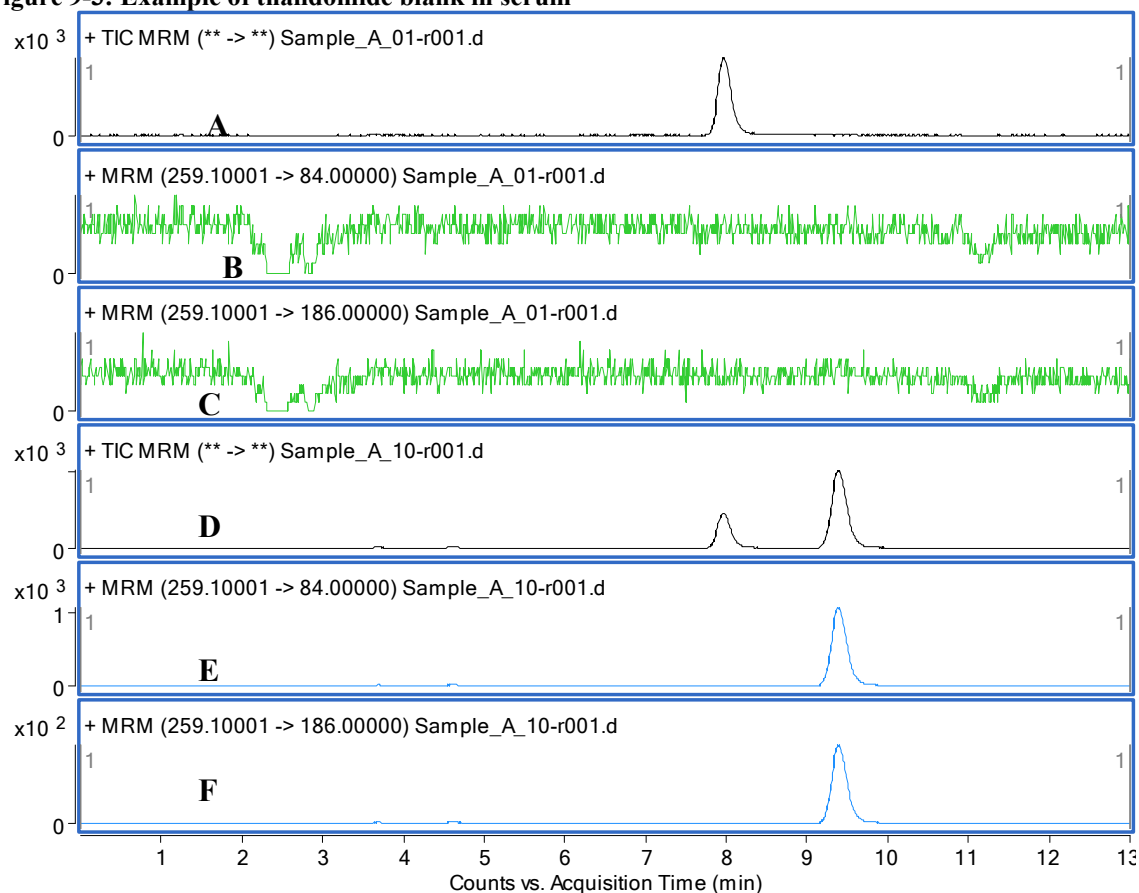**Figure 9-3: Example of thalidomide blank in serum**

Figure 9-3 shows a quantification of thalidomide in a serum samples.

The TIC A is shown for a patient sample with no thalidomide, though internal standard has been added and D is a patient receiving thalidomide. B and C are the extracted MRM for thalidomide in a thalidomide negative patient while E and F show the extracted MRM transitions for thalidomide in the samples of patient receiving thalidomide.

Figure 9-4: Expanded viewed of Figure 9-3
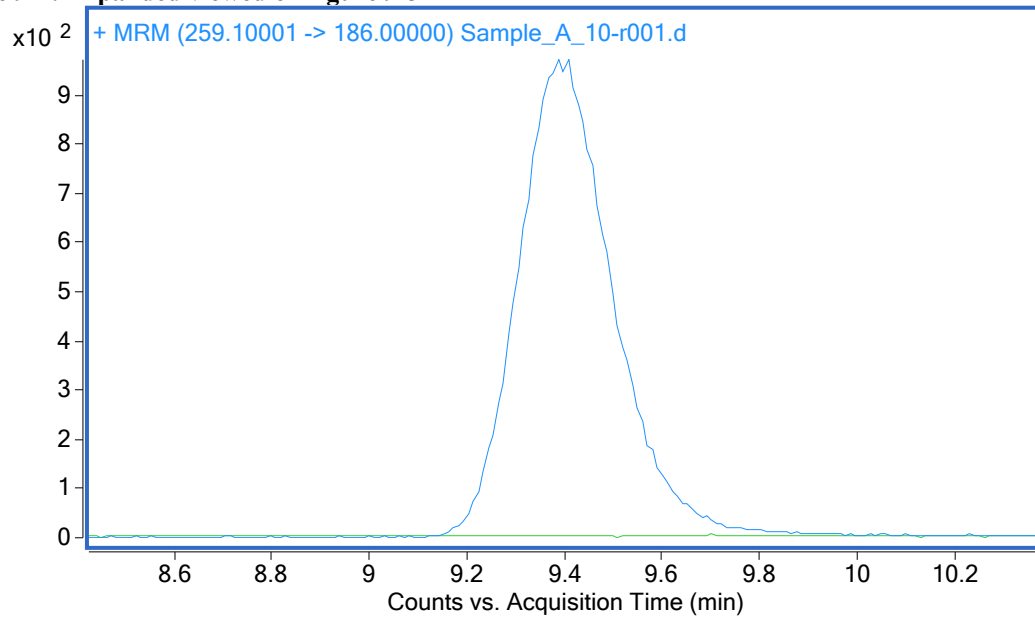
Shown here is a zoom of the overlay of the extracted MRM chromatograms C and F above, where the green trace is for the blank and the blue trace is the thalidomide measured in a patient sample.

Appendix 5 – Project Outputs

Publications

- **Roche S., McMahon G., Clynes M., O'Connor R,** Development of a high-performance liquid chromatographic–mass spectrometric method for the determination of cellular levels of the tyrosine kinase inhibitors lapatinib and dasatinib, *Journal of Chromatography B, Volume 877, Issue 31, 1 December 2009, Pages 3982-3990*

- **Dunne G., Breen L., Collins D.M., Roche S., Clynes M., O'Connor R.,** Modulation of P-gp expression by lapatinib. *Investigational New Drugs, 2010 Jul 6*

Oral Presentation

- "LC-MS in the Analysis of Tyrosine Kinases Inhibitors in Cancer Cell-Lines" presented at The Irish Mass Spectrometry Society, Dublin, Ireland, May 2009

Posters

- **Roche S., Clynes M., O' Connor R**., "The Uptake of Tyrosine Kinase Inhibitors in MDR Cell Lines" presented at the Irish Association for Cancer Research, Athlone, Ireland, March 2009

- **Roche S., Clynes M., O' Connor R.,** "The Quantitative Analysis of Tyrosine Kinase Inhibitor Levels In Biological Samples by LC-MS" presented at Analytical Research Forum, Hull, UK, June, 2008